M.P. Bendsøe
O. Sigmund

Topology Optimization

Theory, Methods and Applications

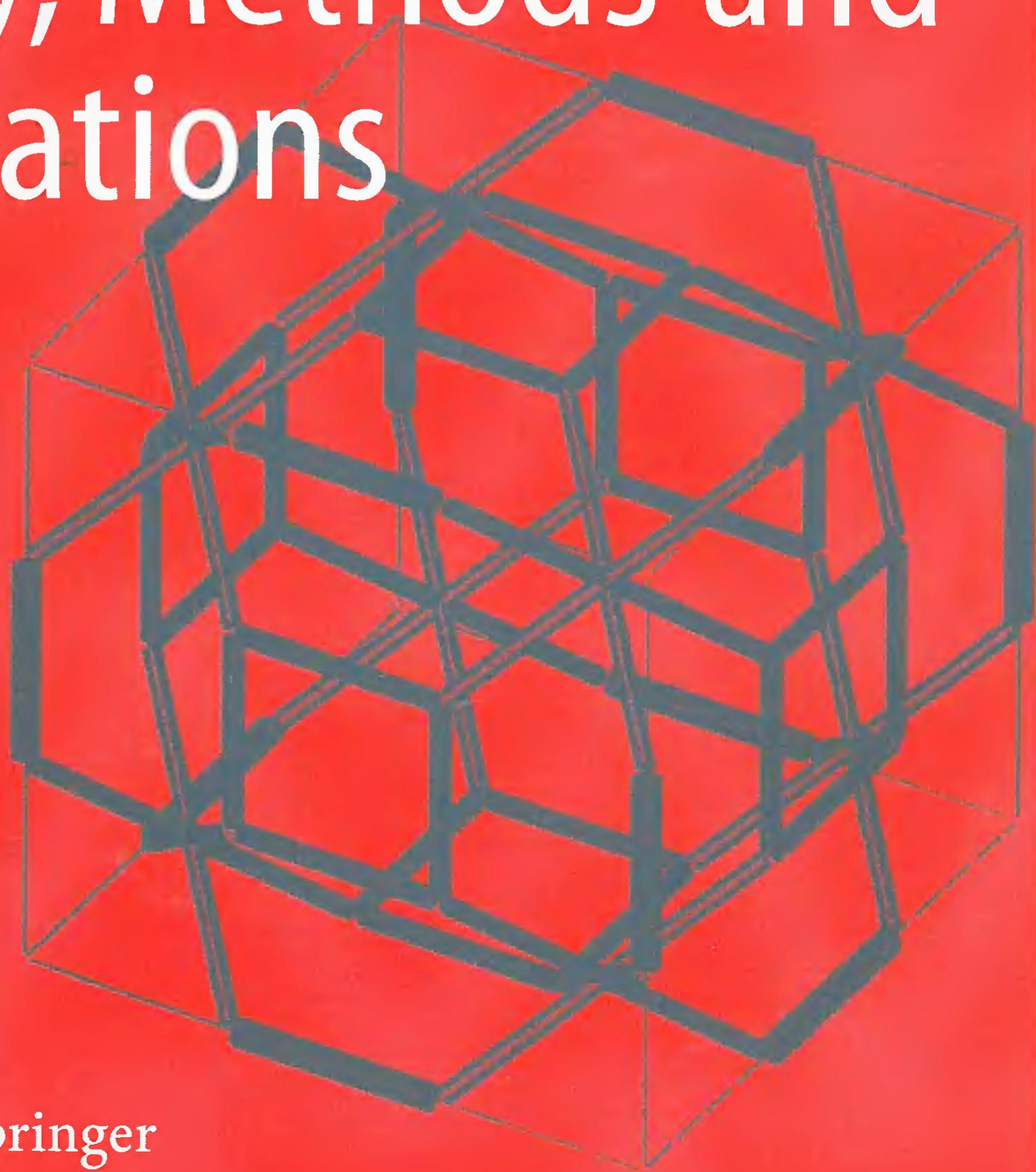

Springer

Springer

Berlin
Heidelberg
New York
Barcelona
Hong Kong
London
Milan
Paris
Tokyo

Engineering ONLINE LIBRARY

http://www.springer.de/engine/

M. P. Bendsøe, O. Sigmund

Topology Optimization

Theory, Methods and Applications

With 140 Figures

Springer

Prof. Dr. techn. Martin P. Bendsøe

Technical University of Denmark
Department of Mathematics
2800 Lyngby
Denmark

Prof. Dr. techn. Ole Sigmund

Technical University of Denmark
Department of Mechanical Engineering,
Solid Mechanics
2800 Lyngby
Denmark

ISBN 3-540-42992-1 Springer-Verlag Berlin Heidelberg New York

CIP data applied for

Die Deutsche Bibliothek – CIP-Einheitsaufnahme
Bendsøe, Martin P. : Topology optimization : theory, methods and applications /
M. P. Bendsøe ; O. Sigmund. – Berlin ; Heidelberg ; New York ; Barcelona ;
Hong Kong ; London ; Milan ; Paris ; Tokyo : Springer, 2003
(Engineering online library)
ISBN 3-540-42992-1

Springer-Verlag Berlin Heidelberg New York
a member of BertelsmannSpringer Science+Business Media GmbH

http://www.springer.de

Typesetting: Camera ready by authors
Cover-design: Medio, Berlin
Printed on acid-free paper SPIN: 10859778 62 / 3020 hu – 5 4 3 2 1 0 –

To the women of our lives:

Susanne, Charlotte, Anne

and

Birgitte

Preface

"The art of structure is where to put the holes"
Robert Le Ricolais, 1894-1977

This is a completely revised, updated and expanded version of the book titled "Optimization of Structural Topology, Shape and Material" (Bendsøe 1995). The field has since then developed rapidly with many new contributions to theory, computational methods and applications. This has meant that a simple editing of Bendsøe (1995) had to be superseded by what is to a large extent a completely new book, now by two authors.

This work is an attempt to provide a unified presentation of methods for the optimal design of topology, shape and material for continuum and discrete structures. The emphasis is on the now matured techniques for the topology design of continuum structures and its many applications that have seen the light of the day since the first monograph appeared. The technology is now well established and designs obtained with the use of topology optimization methods are in production on a daily basis.

The efficient use of materials is important in many different settings. The aerospace industry and the automotive industry, for example, apply sizing and shape optimization to the design of structures and mechanical elements. Shape optimization is also used in the design of electromagnetic, electrochemical and acoustic devices. The subject of non-linear, finite-dimensional optimization for this type of problem is now relatively mature. It has produced a number of successful algorithms that are widely used for structural optimization. However, these methods are unable to cope with the problem of topology optimization, for either discrete or continuum structures.

The optimization of the geometry and topology of structural lay-out has great impact on the performance of structures, and the last decade has seen a great amount of work in this important area of structural optimization. This has mainly been spurred by the success of the material distribution method for generating optimal topologies of structural elements. This defines shape in terms of a material density and geometry is described by what amounts to a raster representation as seen in computer graphics. Today one naturally distinguishes between the search for "classical" designs made from a given material, and methods that allow for a broader range of material usage. When considering materials in the large, the method unifies two subjects, each of intrinsic interests and previously considered distinct. One is structural optimization at the level of macroscopic design, using a macroscopic definition

of geometry given by for example thicknesses or boundaries. The other subject is micromechanics, the study of the relation between microstructure and the macroscopic behaviour of a composite material. Moreover, the introduction of composite material in the shape design context leads naturally to the design of materials themselves, widening the field of applications of structural design techniques.

Materials with microstructure enter naturally in problems of optimal structural design, be it shape or sizing problems. This was for example clearly demonstrated in the paper by Cheng & Olhoff (1981) on optimal thickness distribution for elastic plates. Their work led to a series of works on optimal design problems introducing microstructure in the formulation of the problem. The material distribution method for topology design first introduced as a computational tool in Bendsøe & Kikuchi (1988) can be seen as a natural continuation of these studies and has lead to the capability to reliably predict optimal topologies of continuum structures.

For thin structures, that is, structures with a low fraction of available material compared to the spatial dimension of the structure, the material distribution method predicts grid- and truss-like structures. Thus the material distribution method supplements classical analytical methods for the study of fundamental properties of grid like continua, as first treated by Michell. Applications of numerical methods to truss problems and other discrete models were first described in the early sixties but now we see that these challenging large-scale problems can be solved with specialized algorithms that use the most recent developments in mathematical programming.

In its most general setting shape optimization of continuum structures should consist of a determination for every point in space if there is material in that point or not. Alternatively, for a FEM discretization every element is a potential void or structural member. In this setting the topology of the structure is not fixed a priori, and the general formulation should allow for the prediction of the layout of a structure. Similarly, the lay-out of a truss structure can be found by allowing all connections between a fixed set of nodal points as potential structural or vanishing members. Topology design problems formulated this way are inherently discrete optimization problems. For truss problems it is natural to avoid this by using the continuously varying cross-sectional bar areas as design variables, allowing for zero bar areas. For continuum structures one can apply an interpolation scheme that works with a density of isotropic materials together with methods that steer the optimized designs to "classical" black and white designs or one can use a relaxation of the problem that introduces anisotropic composites such as layered periodic media, also leading to a description of shape by a density of material. In both cases the density can take on all values between zero and one, and one can also make physical sense of intermediate density values.

The approach to topology design outlined above is sometimes known as the ground structure approach. This means that for an initially chosen layout

of nodal points in the truss structure or in the finite element mesh, the optimum structure connecting the imposed boundary conditions and external loads is found as a subset of all the elements of the initially chosen set of connections between the truss nodal points or the initially chosen set of finite elements. The positions of nodal points are not used as design variables, so a high number of nodal points should be used in the ground structure to obtain efficient topologies. Also, the number of nodal points is not used as design variables, so the approach appears as a standard sizing problem and for continuum structures, the topology design problem has been cast as a problem of finding the optimal density distribution of material in a fixed domain, modelled with a fixed FEM mesh. This is of major importance for the implementation of topology optimization methods.

The field of structural optimization combines mechanics, variational calculus and mathematical programming to obtain better designs of structures. This places any author in a somewhat problematic position on how to present the material at hand. Here we take an operational approach, with strict mathematical formalism reserved for situations where this is crucial for a precise statement of results. The monograph falls in two parts. The first part (Chaps. 1 and 2) deals with the topology design within the framework of searching for optimum "classical designs" made from isotropic materials, covering theory and computational procedures and describing the broad range of applications that have appeared in recent years. The second part concentrates on compliance design and emphasizes the use of composites and materials in the large for optimal structural design (Chap. 3). Here the particular format of the compliance functional plays a significant role, and this is also exploited for trusses, where much fundamental understanding can be obtained from a series of problem statements that can be devised (Chap. 4).

The monograph also contains a substantial bibliography together with bibliographical notes[1] covering the main subjects of this exposition as well as related background material the reader may want to consult (Chap. 6). Finally, appendices (Chap. 5) cover various more technical aspects of the area, and Matlab codes that can be used for initial experiments in the field are included.

It is the aim of this monograph to demonstrate the importance of topology and material design for structural optimization and that effective and mature means for handling such design problems do exist. Structural optimization enforces rather than removes the creative aspect of designing and the final design must be a product of creativity rather than availability or lack of analysis facilities. A topology design methodology is an important brick in providing such facilities.

[1] To avoid long lists of references in the text, use is made of bibliographical notes for a survey of the literature. Reference to the notes is by numbers in square brackets, e.g., [36].

We close this brief introduction by remarking that the material distribution method for topology design has demonstrated its potential in a large number of case studies. Also, commercial design software has now been available for a number of years and the method is standard technology in many industries. While compliance design for structures was the state-of-the-art in the early nineties, we see today that topology design is used for a broad range of structural problems (free and forced vibrations, buckling, snap, stress constraints, pressure loads, compliant mechanisms, material design, design of supports, crashworthiness, bio-mechanics, etc.) with both linear and nonlinear analysis modelling. Moreover, new areas are today included in the problem types that can be handled, encompassing for example electrothermal actuators, MEMS, Stokes flow problems, piezoelectric transducers, electromagnetic, and band gap structures. We expect the number of application areas to grow even more in the coming years.

The findings and methods presented in this monograph are very much the result of an international research effort and we wish to thank W. Achtziger, I.A. Aksay, A. Ben-Tal, S. Bouwstra, T. Bruns, T. Buhl, A.R. Díaz, P. Duysinx, L.V. Gibiansky, R.B. Haber, R.T. Haftka, V.B. Hammer, L.V Hansen, J.M. Guedes, J.S. Jensen, C. Jog, J. Jonsmann, N. Kikuchi, M. Kocvara, U.D. Larsen, R. Lipton, M.M. Neves, N. Olhoff, C.B.W. Pedersen, P. Pedersen, J. Petersson, S. Plaxton, J. Rasmussen, H.C. Rodrigues, G.I.N. Rozvany, J. Sokolowski, J.E. Taylor, D. Tcherniak, S. Torquato, N. Triantafyllidis, and J. Zowe for the research collaborations that have provided the bases for the material described in this book. Also, we would like to acknowledge G. Allaire, M. Bagge, T. Borrvall, B. Bourdin, G. Buttazzo, L. Trabucho de Campos, A.V Cherkaev, G. Francfort, J. Gravesen, J.M. Hansen, J. Kofoed, R.V Kohn, E. Lund, K.A. Lurie, G.W Milton, P. Papalambros, N.L. Pedersen, E. Petersen, U. Raitums, U. Ringertz, , O. da Silva Smith, C.A. Soto, M. Stolpe, K. Svanberg, and D. Tortorelli for many very fruitful discussions on the subjects of this book. Special thanks go to V.B. Hammer, M. Kocvara and C.A. Soto for providing texts for a number of sections of the book; C.A. Soto has also kindly given us much useful feedback from readings of the manuscript at various stages. For the typing of the manuscript and the compilation of the bibliography we have had invaluable help from master students M.H. Søndergård, C.L. Felter, and B. Rasmussen. Finally, we are indebted to our colleagues at the Departments of Mathematics and of Mechanical Engineering (Solid Mechanics), Technical University of Denmark, for providing scientifically and socially inspiring working conditions.

Lyngby, June 2002

Martin Philip Bendsøe

Ole Sigmund

Table of Contents

1 Topology optimization by distribution of isotropic material

In this chapter we present an overview of the basic ingredients of what we will denote as the *material distribution method* for finding the optimum lay-out of a linearly elastic structure. In this context the "lay-out" of the structure includes information on the topology, shape and sizing of the structure and the material distribution method allows for addressing all three problems simultaneously.

Sizing, shape, and topology optimization problems address different aspects of the structural design problem. In a typical *sizing* problem the goal may be to find the optimal thickness distribution of a linearly elastic plate or the optimal member areas in a truss structure. The optimal thickness distribution minimizes (or maximizes) a physical quantity such as the mean compliance (external work), peak stress, deflection, etc. while equilibrium and other constraints on the state and design variables are satisfied. The design variable is the thickness of the plate and the state variable may be its deflection. The main feature of the sizing problem is that the domain of the design model and state variables is known *a priori* and is fixed throughout the optimization process. On the other hand, in a *shape* optimization problem the goal is to find the optimum shape of this domain, that is, the shape problem is defined on a domain which is now the design variable. *Topology* optimization of solid structures involves the determination of features such as the number and location and shape of holes and the connectivity of the domain.

1.1 Problem formulation and parametrization of design

The lay-out problem that shall be defined in the following combines several features of the traditional problems in structural design optimization. The purpose of topology optimization is to find the optimal lay-out of a structure within a specified region. The only known quantities in the problem are the applied loads, the possible support conditions, the volume of the structure to be constructed and possibly some additional design restrictions such as the location and size of prescribed holes or solid areas. In this problem the physical size and the shape and connectivity of the structure are unknown.

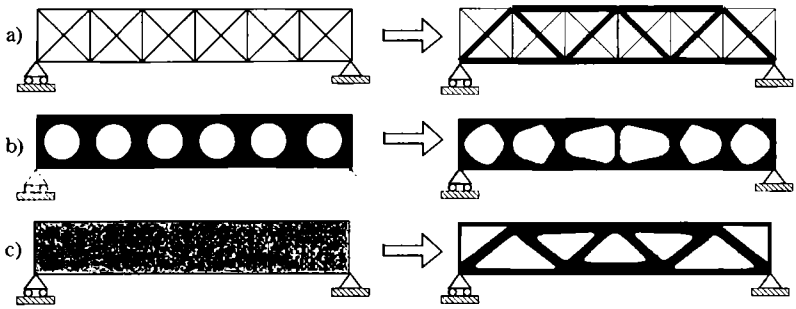

Fig. 1.1. Three categories of structural optimization. a) Sizing optimization of a truss structure, b) shape optimization and d) topology optimization. The initial problems are shown at the left hand side and the optimal solutions are shown at the right

The topology, shape, and size of the structure are not represented by standard parametric functions but by a set of distributed functions defined on a *fixed design domain.* These functions in turn represent a parametrization of the stiffness tensor of the continuum and it is the suitable choice of this parametrization which leads to the proper design formulation for topology optimization.

1.1.1 Minimum compliance design

In the following, the general set-up for optimal shape design formulated as a *material distribution problem* is described. The set-up is analogous to well known formulations for sizing problems for discrete and continuum structures [1], and to truss topology design formulations that are described later in this monograph. It is important to note that the problem type we will consider is from a computational point of view inherently large scale, both in state and in the design variables. For this reason the first problems treated in this area employed the simplest type of design problem formulation in terms of objective and constraint, namely designing for minimum compliance (maximum global stiffness) under simple resource constraints. This is also conceptually a natural starting point for this exposition as its solution reflects many of the fundamental issues in the field.

Consider a mechanical element as a body occupying a domain Ω^{mat} which is part of a larger reference domain Ω in $\mathbf{R}^2$ or $\mathbf{R}^3$ The reference domain Ω is chosen so as to allow for a definition of the applied loads and boundary conditions and the reference domain is sometimes called the ground structure, in parallel with terminology used in truss topology design. Referring to the reference domain Ω we can define the optimal design problem as the problem

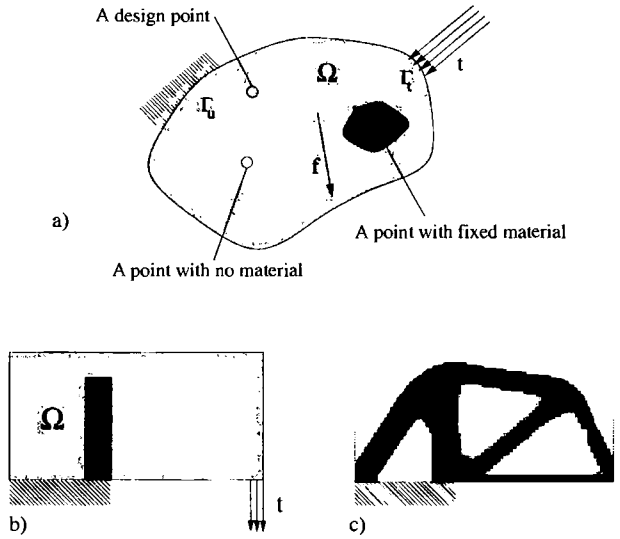

Fig. 1.2. a) The generalized shape design problem of finding the optimal material distribution in a two-dimensional domain. b) Example rectangular design domain and c) topology optimized solution based on a 3200 element discretization and 50% material volume.

of finding the optimal choice of stiffness tensor $E_{ijkl}(x)$ [1] which is a variable over the domain. Introducing the energy bilinear form (i.e., the internal virtual work of an elastic body at the equilibrium u and for an arbitrary virtual displacement v):

$$a(u,v) = \int_\Omega E_{ijkl}(x)\varepsilon_{ij}(u)\varepsilon_{kl}(v)\mathrm{d}\Omega \ ,$$

with linearized strains $\varepsilon_{ij}(u) = \frac{1}{2}\left(\frac{\partial u_i}{\partial x_j} + \frac{\partial u_j}{\partial x_i}\right)$ and the load linear form

$$l(u) = \int_\Omega f u \mathrm{d}\Omega + \int_{\Gamma_T} t u \mathrm{d}s \ ,$$

the minimum compliance (maximum global stiffness) problem takes the form

$$\begin{aligned} &\min_{u\in U, E} \ l(u) \\ &\text{s.t.} \quad a_E(u,v) = l(v), \quad \text{for all } v \in U \\ &\qquad E \in \mathsf{E}_{\mathsf{ad}} \end{aligned} \tag{1.1}$$

[1] In what follows we use a standard tensor notation consistent with a Cartesian reference frame; this does not imply a loss of generality.

Here the equilibrium equation is written in its weak, variational form, with U denoting the space of kinematically admissible displacement fields, f are the body forces and t the boundary tractions on the traction part $\Gamma_T \subset \Gamma \equiv \partial\Omega$ of the boundary. Note that we use the index E to indicate that the bilinear form a_E depends on the design variables.

In problem (1.1), E_{ad} denotes the set of admissible stiffness tensors for our design problem. In the case of topology design, E_{ad} could, for example, consist of all stiffness tensors that attain the material properties of a given isotropic material in the (unknown) set Ω^{mat} and zero properties elsewhere, the limit of resource being expressed as $\int_{\Omega^{\mathrm{mat}}} 1 \mathrm{d}\Omega \leq V$ The various possible definitions of E_{ad} is the subject of the following section.

When solving problems of the form (1.1) by computational means a typical approach, and the one used throughout this monograph, is to discretize the problem using finite elements. It is here important to note that there are *two* fields of interest in (1.1), namely both the displacement u and the stiffness E. If we use the same finite element mesh for both fields, and discretize E as constant in each element, we can write the discrete form of (1.1) as

$$\begin{aligned} &\min_{\mathbf{u}, E_e} \ \mathbf{f}^T \mathbf{u} \\ &\text{s.t.} \quad \mathbf{K}(E_e)\mathbf{u} = \mathbf{f} \\ &\qquad E_e \in \mathsf{E}_{\mathsf{ad}} \end{aligned} \tag{1.2}$$

Here $\mathbf{u}$ and $\mathbf{f}$ are the displacement and load vectors, respectively. The stiffness matrix $\mathbf{K}$ depends on the stiffness E_e in element e, numbered as $e = 1, \ldots, N$, and we can write $\mathbf{K}$ in the form

$$\mathbf{K} = \sum_{e=1}^{N} \mathbf{K}_e \left(E_e\right)$$

where $\mathbf{K}_e$ is the (global level) element stiffness matrix.

1.1.2 Design parametrization

In the design of the topology of a structure we are interested in the determination of the optimal placement of a given isotropic material in space, i.e., we should determine which points of space should be material points and which points should remain void (no material). That is, we think of the geometric representation of a structure as similar to a black-white rendering of an image. In discrete form this then corresponds to a black-white raster representation of the geometry, with "pixels" (or "voxels") given by the finite element discretization.

Restricting our spatial extension to the reference domain Ω, we are thus seeking to determine the optimal subset Ω^{mat} of material points. For the

optimization problem defined above, this approach implies that the set E_{ad} of admissible stiffness tensors consists of those tensors for which[2]:

$$
\begin{aligned}
&E_{ijkl} = 1_{\Omega^{\text{mat}}} E^0_{ijkl}, \; 1_{\Omega^{\text{mat}}} = \begin{cases} 1 \text{ if } x \in \Omega^{\text{mat}} \\ 0 \text{ if } x \in \Omega \setminus \Omega^{\text{mat}} \end{cases}, \\
&\int_\Omega 1_{\Omega^{\text{mat}}} \mathrm{d}\Omega = \mathrm{Vol}(\Omega^{\text{mat}}) \leq V
\end{aligned}
\tag{1.3}
$$

Here the last inequality expresses a limit, V, on the amount of material at our disposal, so that the minimum compliance design is for a limited (fixed) volume. The tensor E^0_{ijkl} is the stiffness tensor for the given *isotropic* material and one normally writes $E_{ijkl} \in L^\infty(\Omega)$ to indicate the relevant function-space for our problem. Note that this definition of E_{ad} means that we have formulated a distributed, discrete valued design problem (a 0-1 problem).

The most commonly used approach to solve this problem is is to replace the integer variables with continuous variables and then introduce some form of penalty that steers the solution to discrete 0-1 values[3] The design problem for the fixed domain is then formulated as a sizing problem by modifying the stiffness matrix so that it depends continuously on a function which is interpreted as a density of material [6]. This function is then the design variable. The requirement is that the optimization results in designs consisting almost entirely of regions of material or no material. This means that intermediate values of this artificial density function should be penalized in a manner analogous to other continuous optimization approximations of 0-1 problems.

One possibility which has proven very popular and extremely efficient is the so-called penalized, proportional stiffness model (the SIMP-model [4]):

$$
\begin{aligned}
&E_{ijkl}(x) = \rho(x)^p E^0_{ijkl}, \quad p > 1 \,, \\
&\int_\Omega \rho(x) \mathrm{d}\Omega \leq V; \quad 0 \leq \rho(x) \leq 1, \quad x \in \Omega \,,
\end{aligned}
\tag{1.4}
$$

Here the "density" $\rho(x)$ is the design function and E^0_{ijkl} represents the material properties of a given isotropic material. One refers to ρ as a density of material by the fact that the volume of the structure is evaluated as $\int_\Omega \rho(x)\mathrm{d}\Omega$. The density interpolates between the material properties 0 and and E^0_{ijkl}:

$$
E_{ijkl}(\rho = 0) = 0, \qquad E_{ijkl}(\rho = 1) = E^0_{ijkl}
$$

[2] We consider isotropic materials only, as for anisotropic materials the placement of the principal directions of the material should also be considered as a design variable.

[3] Methods that deals directly with the integer problem are briefly discussed in Sect. 1.5.6.

[4] SIMP: Solid Isotropic Material with Penalization.

meaning that if a final design has density zero or one in all points, this design is a black-and-white design for which the performance has been evaluated with a correct physical model. In SIMP one will choose to use $p > 1$ so that intermediate densities are unfavourable in the sense that the stiffness obtained is small compared to the cost (volume) of the material. In other words, by specifying a value of p higher than one makes it "uneconomical" to have intermediate densities in the optimal design. Thus the penalization is achieved without the use of any explicit penalization scheme. For problems where the volume constraint is active, experience shows that optimization does actually result in such designs if one chooses p sufficiently big (in order to obtain true "0-1" designs, $p \geq 3$ is usually required). Moreover, it has been proven for the minimum compliance problem in *discrete* form (cf., problem (1.2)) that for p large enough there exists a globally optimal solution of 0-1 form, provided the volume constraint is compatible with such a design (Rietz 2001) (see also section 1.5.4). The SIMP interpolation is the basis for most computational results in the first half of this monograph.

We note that the original "0-1" problem is defined on a fixed reference domain and this together with the SIMP-interpolation means that the optimal topology problem takes on the form of a standard sizing problem on a fixed domain.

It has often been questioned if the SIMP-model can be interpreted in physical terms (the term "material" is part of the acronym!). That is, can one find a material, for example as a composite, which realizes the interpolation model. It is important to point out that this comparison of an interpolation scheme like SIMP with micromechanical models is significant mainly for the benefit of understanding the nature of such computational measures. If a numerical scheme leads to black-and-white designs one can in essence choose to ignore the physical relevance of intermediate steps which may include "grey" However, the question of physical relevance is often raised, especially as most computational schemes involving interpolations do give rise to designs which are not *completely* clear of "grey" Also, the physical realization of all feasible designs plays a role when interpreting results from a premature termination of an optimization algorithm that has not converged fully to a 0-1 design.

We will return later in section 2.10 to the construction of a material model that mimics the SIMP interpolation model. Central in such considerations is a comparison with the Hashin-Shtrikman bounds for two-phase materials, which expresses the limits of possible *isotropic* material properties one can achieve by constructing composites (materials with microstructure) from two given, linearly elastic, isotropic materials [4]. Without further elaboration (and referring the reader to section 1.5.4) we remark here that the SIMP-model can indeed be considered as a material model if the power p satisfies that:

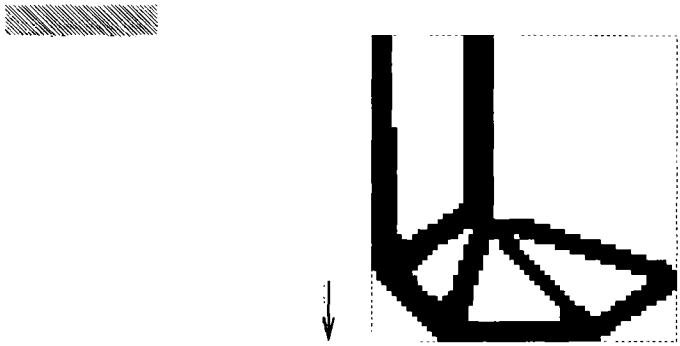

Fig. 1.3. A black-and-white minimum compliance design for a loaded knee structure obtained with the SIMP interpolation scheme. The discretization is 60 by 60 elements and the material volume is limited to 47% of the design domain.

$$
\begin{aligned}
p &\geq \max\left\{\frac{2}{1-\nu^0} \quad \frac{4}{1+\nu^0}\right\} \qquad \text{(in 2 - D)}\,, \\
p &\geq \max\left\{15\frac{1-\nu^0}{7-5\nu^0}\,,\ \frac{3}{2}\frac{1-\nu^0}{1-2\nu^0}\right\} \text{(in 3 - D)}\,,
\end{aligned}
\tag{1.5}
$$

where ν^0 is the Poisson ratio of the given base material with stiffness tensor E^0_{ijkl} (Bendsøe & Sigmund 1999). In dimension 2 this implies that the smallest p is 3, which is admissible for $\nu^0 = 1/3$. In dimension 3 the smallest admissible p is 2, but for $\nu^0 = 1/3$ one should also in 3-D choose p greater than 3.

The use of the SIMP interpolation scheme addresses the integer format of the original setting of the topology design problem with designs given as in (1.3). It converts this integer problem to a sizing problem that typically results in what for all practical purposes can be considered as 0-1 designs. Another serious problem associated with the 0-1 problem statement, and a problem SIMP does not resolve, is the now well established lack of existence of solutions to the distributed problem [3], [25], [34]. This is not only a serious theoretical drawback. It also has the effect of making the computational results sensitive to the fineness of the finite element mesh discretization. As mentioned, the interpolation scheme does not directly resolve this problem, and further considerations are in place to assure a well-posed distributed design problem that also is benign in terms of mesh-refinement of the finite element model. This aspect will be covered in some detail in 1.3.1.

The role of composites The initial work on numerical methods for topology design of continuum structures was based on using composite materials as the basis for describing varying material properties in space [3], [6]. This approach has been named the *homogenization method* and its development was strongly inspired by theoretical studies on generalized shape design in

conduction and torsion problems and by numerical and theoretical work related to plate design (see, e.g., [25], [29]). The homogenization approach to topology design can also be viewed as an interpolation model and many of the developments in the area of topology design of structures are based on this type of interpolation schemes. However, composites in topology design has deeper roots than this and composites play a key role for providing insight in the optimal use of materials in the large and for understanding the mathematics and the physics of the "0-1" design problem.

We have here chosen to base the first part of this monograph on the use of the somewhat simpler SIMP-type interpolation schemes (see also section 1.5.4). This allows for a concentration on issues related to computational implementations and developments related to the consideration of more elaborate optimal design settings than the minimum compliance design problem. In the second half of the monograph we will return to discuss issues related to the optimal use of material in general and the details of the homogenization based method in particular.

1.1.3 Alternative problem forms

For the developments in the following it is important to note that problem (1.1) can be given a number of equivalent formulations. These reformulations use the special structure of the minimum compliance problem and they are extremely useful for analysis and the development of specialized computational procedures for this type of problem. For this purpose we note that the equilibrium condition of problem (1.1) can be expressed in terms of the principle of minimum potential energy. That is, the displacement field u is a minimizer of the functional $F(v) = \frac{1}{2}a_{\bar{E}}(v,v) - l(v)$ on U (the total potential energy). Then note that the value $F(u)$ of the potential energy at equilibrium equals $-\frac{1}{2}l(u) < 0$. Thus problem (1.1) can be written as

$$\max_{E\in\mathsf{E}_{\mathrm{ad}}} \min_{u\in U} \left\{ \frac{1}{2}a_E(u,u) - l(u) \right\} \tag{1.6}$$

Problem (1.6) can also be formulated in terms of stresses. Expressing the inner equilibrium problem of (1.6) in terms of the (dual) principle of minimum complementary energy, we have the formulation

$$\min_{E\in\mathsf{E}_{\mathrm{ad}}} \min_{\sigma\in S} \left\{ \frac{1}{2}\int_\Omega C_{ijkl}\sigma_{ij}\sigma_{kl}\mathrm{d}\Omega \right\} \tag{1.7}$$

of the minimum compliance design problem. Here $C_{ijkl} = (E^{-1})_{ijkl}$ is the compliance tensor, and the minimization with respect to the stresses σ is taken over the set S of statically admissible stress fields, i.e.

$$S = \left\{ \sigma \middle| \ \mathrm{div}\sigma + f = 0 \,\mathrm{in}\,\Omega,\ \sigma\cdot n = t \,\mathrm{on}\,\Gamma_T \right\}.$$

From the problem statement (1.6) we see that if the displacement field in an optimal structure is known, then the optimal distribution of the stiffness is such that the strain energy is maximized. Likewise, for a known stress distribution in the optimal structure the complementary energy is minimized, cf., (1.7). This characterization plays an important role in understanding the nature of the design problem, both theoretically and computationally.

1.2 Solution methods

The use of an interpolation scheme like SIMP allows us to convert the optimal topology problem into a *sizing* problem on a *fixed* domain. Compared to many traditional sizing problems for, e.g., frames and built-up structures of plates, stringers, etc., the present problem differs in that the number of design variables is typically very large (the number of design parameters and the number of analysis variables is of the same order of magnitude). Thus efficiency of the optimization procedure is crucial and one typically has to adopt optimization settings that trade number of constraints for number of design variables. The compliance design problem is an example of this. One can here work with many variables, as the optimization problem (seen as a problem in the density only) has just one constraint in addition to the simple box-constraints giving upper and lower limits on the density variable.

1.2.1 Conditions of optimality

In the following we shall derive the necessary conditions of optimality for the density ρ of the minimum compliance design problem that employs the SIMP interpolation scheme.

Following standard optimality criteria methods used in structural optimization [7], the simple structure of the continuum, single load problem (1.1) can be utilized to generate extremely efficient computational update schemes for solving the problems we address here. The key is to devise iterative methods which, for a previously computed design and its associated displacements, update the design variables at each point (or rather at each element of a finite element discretization) independently from the updates at other points, based on the necessary conditions of optimality. To this end, we first recapitulate the form of the minimum compliance problem (1.1) written for the case of the SIMP interpolation. In the continuum setting this is

$$\begin{aligned} &\min_{u\in U,\rho} \; l(u) \\ &\text{s.t.} \quad a_E(u,v) = l(v), \quad \text{for all } v \in U \\ &\qquad E_{ijkl}(x) = \rho(x)^p E^0_{ijkl} \\ &\qquad \int_\Omega \rho(x)\mathrm{d}\Omega \le V; \quad 0 < \rho_{\min} \le \rho \le 1 \,. \end{aligned} \tag{1.8}$$

Note that we here have introduced a lower bound $\rho_{\min}$ on the density in order to prevent any possible singularity of the equilibrium problem. In typical applications we set $\rho_{\min} = 10^{-3}$

With Lagrange multipliers $\Lambda, \lambda^-(x), \lambda^+(x)$ for the constraints of (1.8), the necessary conditions for optimality for the sizing variable ρ are a subset of the stationarity conditions for the Lagrange function

$$\mathcal{L} = l(u) - \left\{ a_E(u, \bar{u}) - l(\bar{u}) \right\} + \Lambda(\int_\Omega \rho(x) \mathrm{d}\Omega - V) + \int_\Omega \lambda^+(x)(\rho(x) - 1)\mathrm{d}\Omega + \int_\Omega \lambda^-(x)(\rho_{\min} - \rho(x))\mathrm{d}\Omega$$

where $\bar{u}$ is the Lagrange multiplier for the equilibrium constraint. Note that $\bar{u}$ belongs to the set U of kinematically admissible displacement fields. Under the assumption that $\rho \geq \rho_{\min} > 0$ (so that displacement fields are unique), the conditions for optimality with respect to variations of the displacement field u give that $\bar{u} = u$ while the condition for ρ becomes:

$$\frac{\partial E_{ijkl}}{\partial \rho} \varepsilon_{ij}(u)\varepsilon_{kl}(u) = \Lambda + \lambda^+ - \lambda^- \tag{1.9}$$

with the switching conditions

$$\lambda^- \geq 0,\ \lambda^+ \geq 0,\ \lambda^-(\rho_{\min} - \rho(x)) = 0,\ \lambda^+(\rho(x) - 1) = 0 \tag{1.10}$$

For intermediate densities ($\rho_{\min} < \rho < 1$) the conditions (1.9), can be written as

$$p\rho(x)^{p-1} E^0_{ijkl} \varepsilon_{ij}(u)\varepsilon_{kl}(u) = \Lambda\ , \tag{1.11}$$

which expresses that the strain energy density-like left-hand side term [5] is constant and equal to Λ for all intermediate densities. This is thus a condition that is similar to the fully stressed design condition in plastic design. As we expect areas with high energy to be too low on stiffness, we devise the following fix-point type update scheme for the density [7]:

$$\rho_{K+1} = \begin{cases} \max\{(1-\zeta)\rho_K, \rho_{\min}\} & \text{if } \rho_K B_K^\eta \leq \max\{(1-\zeta)\rho_K, \rho_{\min}\}\ , \\ \min\{(1+\zeta)\rho_K, 1\} & \text{if } \min\{(1+\zeta)\rho_K, 1\} \leq \rho_K B_K^\eta \\ \rho_K B_K^\eta & \text{otherwise} \end{cases} \tag{1.12}$$

Here ρ_K denotes the value of the density variable at iteration step K , and B_K is given by the expression

[5] This term is in many circumstances called the *mutual energy density* – "mutual" since it involves the two fields u and $\bar{u}$. For compliance, $u = \bar{u}$, and the mutual energy density equals the strain energy density.

$$B_K = \Lambda_K^{-1} p\rho(x)^{p-1} E^0_{ijkl}\varepsilon_{ij}(u_K)\varepsilon_{kl}(u_K) \tag{1.13}$$

where u_K is the displacement field at at the iteration step K, determined from the equilibrium equation and dependent on ρ_K. Note that a (local) optimum is reached if $B_K \quad 1$ for densities ($\rho_{\min} < \rho < 1$). The update scheme (1.12) adds material to areas with a specific strain energy that is higher than Λ (that is, when $B_K > 1$) and removes it if the energy is below this value; this only takes place if the update does not violate the bounds on ρ. From integrating (1.11) one can see that Λ is proportional (by a factor p) to the average strain energy density of the part of the structure that is given by intermediate values of the density.

The variable η in (1.12) is a tuning parameter and ζ a move limit. Both η and ζ controls the changes that can happen at each iteration step and they can be made adjustable for efficiency of the method. Note that the update ρ_{K+1} depends on the present value of the Lagrange multiplier Λ, and thus Λ should be adjusted in an inner iteration loop in order to satisfy the active volume constraint. It is readily seen that the volume of the updated values of the densities is a continuous and decreasing function of the multiplier Λ. Moreover, the volume is strictly decreasing in the interesting intervals, where the bounds on the densities are not active in all points (elements of a FEM discretization). This means that we can uniquely determine the value of Λ, using a bisection method or a Newton method. The values of η and ζ are chosen by experiment, in order to obtain a suitable rapid and stable convergence of the iteration scheme. A typical useful value of η and ζ is 0.5 and 0.2, respectively.

It is noted above that the optimality criteria method is closely related to the concept of fully stressed design. However, it is important to note that the conditions (1.9, 1.10) only imply that the specific strain energy is constant in areas of *intermediate* density, while it is lower in regions with a density $\rho = \rho_{\min}$ and higher in regions with a density equal to 1.

The type of algorithm described above has been used to great effect in a large number of structural topology design studies and is well established as an effective (albeit heuristic) method for solving large scale problems [6], [7]. The effectiveness of the algorithm comes from the fact that each design variable is updated independently of the update of the other design variables, except for the rescaling that has to take place for satisfying the volume constraint. The algorithm can be generalized to quite a number of structural optimization settings (see for example Rozvany (1989), Rozvany (1992)), but it is not always straightforward. For cases where for example constraints of a non-structural nature should be considered (e.g., representing geometry considerations), when non-self-adjoint problems are considered or where physical intuition is limited, the use of a mathematical programming method can be a more direct way to obtain results. Typically, this will be computationally more costly, but a careful choice of algorithm can make this approach as efficient as the optimality criteria method (see section 1.2.3).

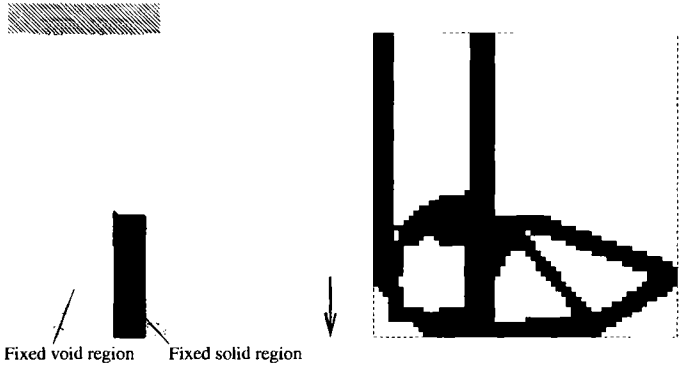

Fig. 1.4. The possibility of letting the design area be a sub-area of the reference domain. Same design domain as in Fig. 1.3 but with a square area fixed to be void and a rectangular area fixed to be solid. The compliance of the optimized topology is 25% lower than in Fig. 1.3 due to the restricted design domain.

1.2.2 Implementation of the optimality criteria method

In sections 1.1.2 and 1.2.1 we have outlined the basic ingredients of the optimality criteria method for implementing the material distribution procedure for topology design. These consist of the basic parametrization of design through the design-stiffness relation given by an appropriate interpolation scheme and the update scheme for the density based on the optimality conditions. Finally, this update scheme is based on the ability to solve the equilibrium equations, and here we presume this to be performed by the finite element method.

Computational procedure The direct method of topology design using the material distribution method is based on the numerical calculation of the globally optimal distribution of the density of material ρ which is the design variable. For an interpolation scheme that properly penalizes intermediate densities (cf., discussion in section 1.1.2) the resulting 0-1 (or black and white) design is actually the primary target of our scheme. The optimality criteria method for finding the optimal topology of a structure constructed from a single isotropic material then consists of the following steps:

Pre-processing of geometry and loading:

- Choose a suitable reference domain (the ground structure) that allows for the definition of surface tractions, fixed boundaries, etc. (see Fig. 1.4).
- Choose the parts of the reference domain that should be designed, and what parts of the ground structure that should be left as solid domains or voids (see Fig. 1.4).

Construct a finite element mesh for the ground structure. This mesh should be fine enough in order to describe the structure in a reasonable resolution bit-map representation. Also, the mesh should make it possible to define the a priori given areas of the structure by assigning fixed design variables to such areas. The mesh is unchanged through-out the design process.
- Construct finite element spaces for the independent fields of displacements and the design variables.

Optimization:
Compute the optimal distribution over the reference domain of the design variable ρ. The optimization uses a displacement based finite element analysis and the optimality update criteria scheme for the density. The structure of the algorithm is:

- Make initial design, e.g., homogeneous distribution of material. The iterative part of the algorithm is then:
- For this distribution of density, compute by the finite element method the resulting displacements and strains.
- Compute the compliance of this design. If only marginal improvement (in compliance) over last design, stop the iterations. Else, continue. For detailed studies, stop when necessary conditions of optimality are satisfied.
- Compute the update of the density variable, based on the scheme shown in section 1.2.1. This step also consists of an inner iteration loop for finding the value of the Lagrange multiplier Λ for the volume constraint.
  Repeat the iteration loop.

For a case where there are parts of the structure which are fixed (as solid and/or void) the updating of the design variables should only be invoked for the areas of the ground structure which are being redesigned (reinforced).

Post-processing of results:

Interpret the optimal distribution of material as defining a shape, for example in the sense of a CAD representation.

For the method above, one should at an initial stage decide on a choice of a basic interpolation scheme, for example SIMP. It is interesting to note that topology optimization using for example SIMP with a suitable high value of the power p gives rise to very well defined designs consisting almost entirely of areas with material or no material and very little area with intermediate density of material, i.e. very little grey.

It is important to underline that the algorithm just described can be implemented on any type of finite element mesh and any type of reference domain Ω (ground structure). This gives a significant flexibility to the method in terms of defining boundary conditions and non-design parts of the structure. Nevertheless, in many cases one works with rectangular (in 2-D) or

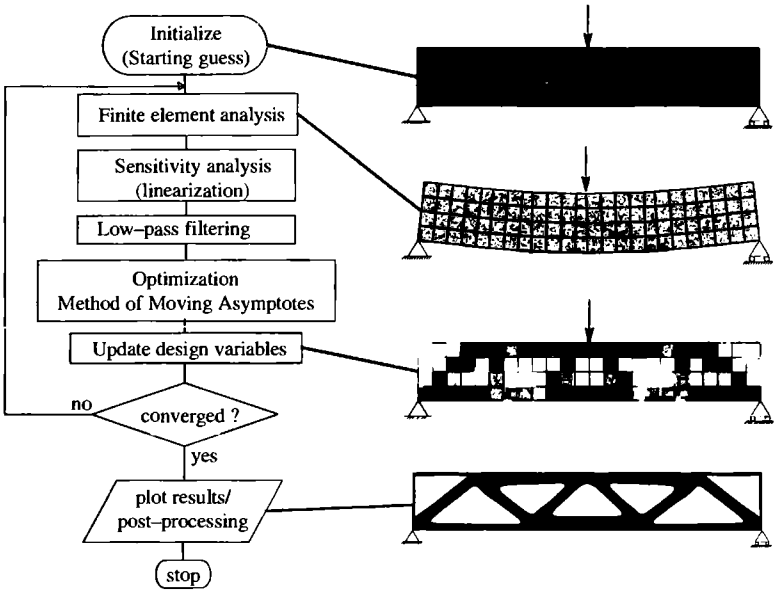

Fig. 1.5. The flow of computations for topology design using the material distribution method and the Method of Moving Asymptotes (MMA) for optimization. The low-pass filter step (filtering of sensitivities) is discussed in Sec. 1.3.1.

box-like (in 3-D) domains, and with a mesh consisting of squares or cubes. This simplifies implementation and can be employed to speed up the analysis part of the procedure, see section 1.2.4.

On programming complexity The procedure described above does not require any great programming efforts in order to solve the compliance topology design problem. When access to a FEM code is provided, only a few lines of extra code is required for the update scheme and for the computation of the energies involved. If for example a rectangular design domain is considered and one uses square elements and a Q4 interpolation of displacements and element wise constant densities, a complete program *including* FE analysis and plotting of the resulting designs can be written in 99 lines of Matlab code (see appendix 5.1.1). This actually also includes a filtering procedure that caters for the so-called checkerboard and mesh-dependency problems associated with our design problem (see section 1.3.2 for further details).

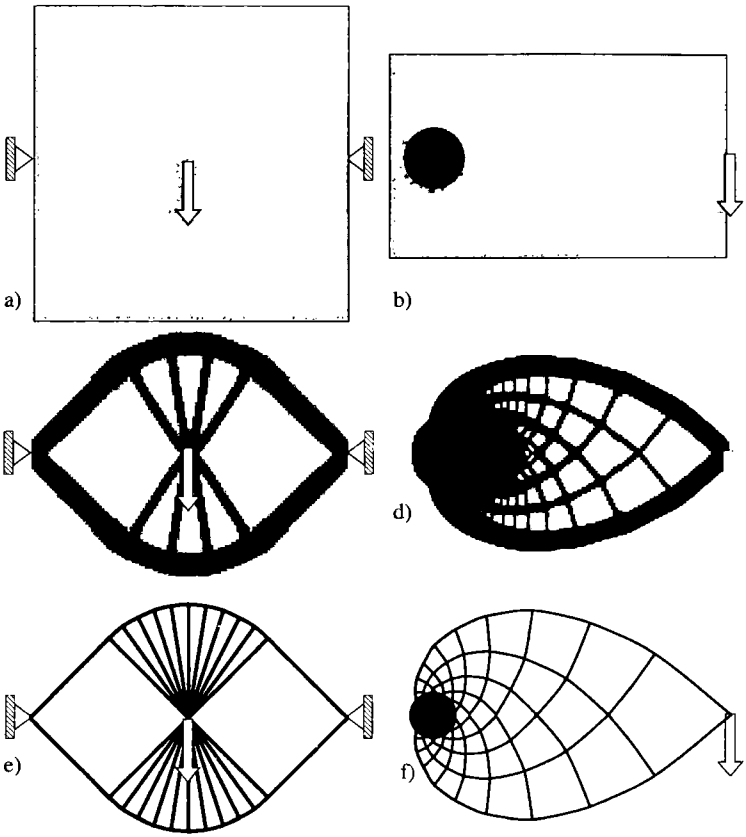

Fig. 1.6. Two examples of topology design for minimum compliance compared with optimal Michell type structures (Michell 1904). a) and b) design domains, c) and d) topology optimized solutions and e) and f) corresponding Michell type optimal solutions (from Sigmund 2000a).

1.2.3 Sensitivity analysis and mathematical programming methods

The use of mathematical programming algorithms for solving problems in structural optimization is well established and described in detail in the literature, for sizing as well as shape design problems [1]. The standard procedure is to consider the design problem as an optimization problem in the design variables *only*, and with the displacement field regarded as a function of these design variables. The displacement fields are given *implicitly* in terms of the

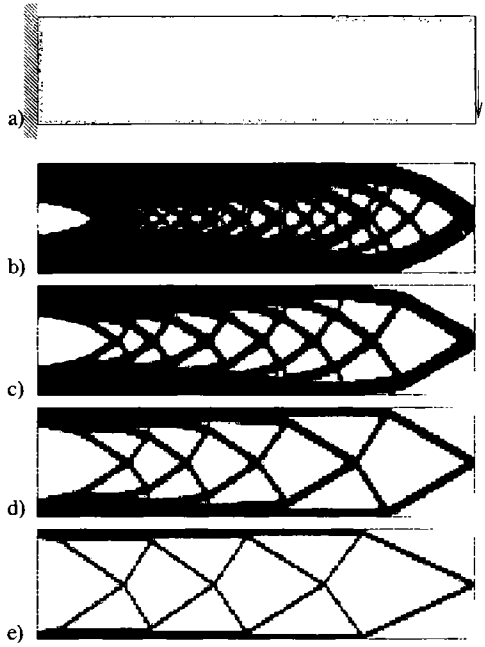

Fig. 1.7. The influence of volume fraction. A long cantilever beam discretized by 6400 square elements and optimized for volume fractions of b) 80%, c) 60%, d) 40% and e) 20%. For low amounts of volume, truss-like structures are predicted.

design variables through the equilibrium equation and finding the derivatives of the displacements with respect to the design variables is termed *sensitivity analysis* [1].

The basic idea of the material distribution technique for topology design is to rephrase the problem as a sizing problem for the density ρ on a fixed domain. Thus the technique outlined above carries over to topology design as well. The major challenge, though, is to apply mathematical programming software that is well geared to cope with many variables and typically a moderate number of constraints. Here and in the following we will rely on the MMA algorithm, with "MMA" being the acronym for Method of Moving Asymptotes (Svanberg 1987, Svanberg 2002). This algorithm has proven itself to be versatile and well suited for large scale topology optimization problems.

Sensitivity analysis In order to complement the presentation of the optimality criteria method, we will here work with the FEM form of the minimum compliance problem, that is the problem (cf., (1.2)):

$$\begin{aligned} &\min_{\mathbf{u},\rho_e} \mathbf{f}^T\mathbf{u} \\ &\text{s.t.} \quad \left(\sum_{e=1}^{N} \rho_e^p \mathbf{K}_e\right)\mathbf{u} = \mathbf{f} \\ &\qquad \sum_{e=1}^{N} v_e\rho_e \le V, \quad 0 < \rho_{\min} \le \rho_e \le 1, \quad e = 1,\ldots,N \end{aligned} \tag{1.14}$$

When solving this by a mathematical programming algorithm we first rewrite the problem as a problem in the design variables only:

$$\begin{aligned} &\min_{\rho_e} c(\rho_e) \\ &\text{s.t.} \quad \sum_{e=1}^{N} v_e\rho_e \le V, \quad 0 < \rho_{\min} \le \rho_e \le 1, \quad e = 1,\ldots,N \end{aligned} \tag{1.15}$$

where the equilibrium equation is considered as part of a function-call:

$$c(\rho_e) = \mathbf{f}^T\mathbf{u}\,, \quad \text{where } \mathbf{u} \text{ solves} \quad \sum_{e=1}^{N} \rho_e^p \mathbf{K}_e\mathbf{u} = \mathbf{f} \tag{1.16}$$

When gradients are required by the optimization algorithm employed to solve (1.15), these are easily derived for the objectives and constraints involving only ρ. For functions that depend on the displacements also, derivatives can be obtained by the chain-rule. These expressions will then contain derivatives of the displacement, which in turn can be obtained by taking the derivative of the equilibrium equation $\mathbf{K}\mathbf{u} = \mathbf{f}$. In topology design we typically work with a moderate number of constraints, so the most effective method for calculating derivatives is to use the *adjoint* method, where the derivatives of the displacement are not calculated explicitly. For the minimum compliance problem (1.15) at hand we rewrite the function $c(\rho)$ by adding the zero function:

$$c(\rho) = \mathbf{f}^T\mathbf{u} - \tilde{\mathbf{u}}^T(\mathbf{K}\mathbf{u} - \mathbf{f})$$

where $\tilde{\mathbf{u}}$ is any arbitrary, but *fixed* real vector. From this, after rearrangement of terms, we obtain that

$$\frac{\partial c}{\partial \rho_e} = \left(\mathbf{f}^T - \tilde{\mathbf{u}}^T\mathbf{K}\right)\frac{\partial \mathbf{u}}{\partial \rho_e} - \tilde{\mathbf{u}}^T\frac{\partial \mathbf{K}}{\partial \rho_e}\mathbf{u}$$

This can in turn be written as

$$\frac{\partial c}{\partial \rho_e} = -\tilde{\mathbf{u}}^T\frac{\partial \mathbf{K}}{\partial \rho_e}\mathbf{u}\,,$$

when $\tilde{\mathbf{u}}$ satisfies the adjoint equation:

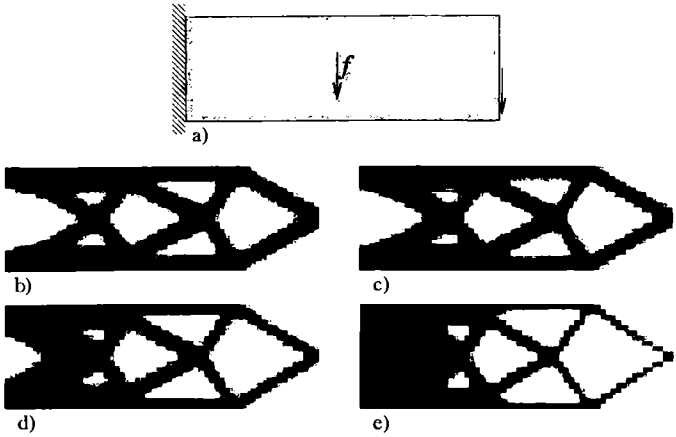

Fig. 1.8. Influence of self-weight on the topology optimized cantilever beam. Here, the load vector is design dependent (i.e. $\mathbf{f} = \mathbf{f}(\rho)$) and the sensitivity of compliance including self-weight can be found as $\frac{\partial c}{\partial \rho_e} = -\mathbf{u}_e^T \frac{\partial \mathbf{K}_e}{\partial \rho_e} \mathbf{u}_e + \frac{\partial \mathbf{f}_e^T}{\partial \rho_e} \mathbf{u}_e$. a) Design domain and loads, b) resulting topology for zero self weight, c) resulting topology for self weight equal to 1.2 times the non-structural load, d) resulting topology for self weight equal to 6 times the non-structural load and e) resulting topology for self weight equal to 24 times the non-structural load.

$$\mathbf{f}^T - \tilde{\mathbf{u}}^T \mathbf{K} = 0$$

This latter equation is in the form of an equilibrium equation and for compliance we see that we obtain directly that $\tilde{\mathbf{u}} = \mathbf{u}$ (normally the adjoint equation requires additional computations). Moreover, the form of the stiffness matrix means that the derivatives of the compliance $c(\rho)$ for problem (1.15) is of the particularly simple form:

$$\frac{\partial c}{\partial \rho_e} = -p\rho_e^{p-1} \mathbf{u}^T \mathbf{K}_e \mathbf{u} \tag{1.17}$$

Thus derivatives for the minimum compliance problem are extremely easy to compute. Also, one notices that the derivative is "localized" in the sense that the derivative only involves information at the element level; however, there is an effect from other design variables hidden in the displacement $\mathbf{u}$. Finally, we see that the sensitivity is negative for all elements, so physical intuition is confirmed in that additional material in any element decreases compliance, that is, makes the structure stiffer.

The basics of MMA The Method of Moving Asymptotes (MMA) and its "mother" method CONLIN are mathematical programming algorithms

well suited for topology design[6] They are in nature similar to methods like Sequential Linear Programming (SLP) and Sequential Quadratic Programming (SQP) for solving smooth, non-linear optimization problems, in the sense that they work with a sequence of simpler approximate subproblems of given type. For MMA and CONLIN these subproblems are separable and convex and are constructed based on sensitivity information at the current iteration point as well as some iteration history. At each iteration point this subproblem is solved by for example a dual method or by an interior point algorithm (primal-dual algorithm) , and the solution to the subproblem is then used as the next design in the iterative procedure.

In MMA the approximation of a function F of n real variables $\mathbf{x}$ $(x_1, \ldots, x_n)$ around a given iteration point $\mathbf{x}^0$ has the form

$$F(\mathbf{x}) \approx F(\mathbf{x}^0) + \sum_{i=1}^{n} \left(\frac{r_i}{U_i - x_i} + \frac{s_i}{x_i - L_i} \right)$$

where the numbers r_i, s_i are chosen as

$$\text{if } \frac{\partial F}{\partial x_i}(x^0) > 0 \text{ then } r_i = \left(U_i - x_i^0\right)^2 \frac{\partial F}{\partial x_i}(x^0) \quad \text{and} \quad s_i = 0 \,,$$
$$\text{if } \frac{\partial F}{\partial x_i}(x^0) < 0 \text{ then } r_i = 0 \quad \text{and} \quad s_i = -\left(x_i^0 - L_i\right)^2 \frac{\partial F}{\partial x_i}(x^0) \,,$$

and where, loosely speaking, the positive numbers U_i, L_i control the range for which the approximation of F can generate reasonable answers for our optimization problem (the parameters U_i, L_i give vertical asymptotes for the approximations of F and is the source of the name of the algorithm). In the optimization algorithm, the values of U_i, L_i for each function of the problem are updated in each iteration, depending on the iteration history so far.

A central aspect of MMA and CONLIN is the use of such *separable* and convex approximations. The former property means that the necessary conditions of optimality of the subproblems do not couple the primary variables (the design variables) while the convexity means that dual methods or primal-dual methods can be used. Together this has an immense effect on reducing the computational effort needed to solve the subproblems, especially for problems with only a few constraints.

Experience over the last couple of years have shown that the convex approximation methods are very efficient for topology optimization. Typically in these problems one chooses to work with a large number of design variables (for the raster representation of the design, one operates with one or more density variables per element in the finite element mesh) and try to formulate the optimization problem with a fairly limited number of constraints. Compared to optimality criteria methods, the use of a mathematical programming tool does provide an added flexibility to topology design. One

[6] The use of convex and separable approximations was first introduced with CONLIN (see, e.g. Fleury (1993) and references therein).

avoids the development and coding of new algorithms for each new problem that is to be solved, and it is also possible to handle geometry considerations and situations where physical intuition is limited.

We close this discussion by noting that for the minimum compliance problem the use of the optimality criteria method or the use of MMA in essence involves the same type of computations (see also Borrvall & Petersson (2001a)). We found in (1.17) that the sensitivity of compliance is negative for any element density ρ_e. Thus an MMA approximation of the compliance gives a subproblem after iteration step K in the form

$$\begin{aligned} &\min_{\rho_e} \left\{ c(\rho^K) - \sum_{e=1}^{N} \frac{\left(\rho_e^K - L_e\right)^2}{\rho_e - L_e} \frac{\partial c}{\partial \rho_e}(\rho^K) \right\} \\ &\text{s.t.} \quad \sum_{e=1}^{N} v_e \rho_e \leq V, \quad 0 < \rho_{\min} \leq \rho_e \leq 1, \quad e = 1, \ldots, N \end{aligned} \tag{1.18}$$

Solving this problem by a dual method now involves steps similar to the ones performed in section 1.2.1 for the optimality criteria method. First one minimizes the Lagrange functional

$$\mathcal{L} = c(\rho^K) - \sum_{e=1}^{N} \frac{\left(\rho_e^K - L_e\right)^2}{\rho_e - L_e} \frac{\partial c}{\partial \rho_e}(\rho^K) + \Lambda(\sum_{e=1}^{N} v_e \rho_e - V)$$

with respect to densities satisfying $\rho_{\min} \leq \rho_e \leq 1$, $e = 1, \ldots, N$. Using convexity and that $\mathcal{L}$ is separable, this optimization can easily be performed, element by element. For the case where $L_e = 0$ this results in exactly the optimality criteria update scheme given in (1.12), with move limit $\zeta = \infty$ and tuning parameter $\eta = 0.5$. The second step of the dual method is to maximize the resulting functional with respect to Λ, and as for the optimality criteria method this corresponds to adjusting the value of Λ so that the update scheme gives a density $\rho^{(K+1)}$ that satisfies the volume constraint. In the actual implementation of MMA, one chooses the asymptote parameters L_e more cleverly, improving speed of convergence.

In conclusion, we note that MMA is an invaluable tool for topology optimization problems. For simple compliance optimization problems it may be a bit slower than the OC method but for more complicated problems involving several constraints MMA stands for excellent convergence properties. Also, the advanced versions of the program caters for more complex problems formulations including min-max formulations etc. Contestants to MMA may be Sequential Linear Programming (SLP) method, CONLIN and other first order methods. Unless otherwise noted, we use either OC or MMA for all the applications shown in this book.

1.2.4 Implementation - the general concept

The use of mathematical programming techniques does not change the general flow of a topology design procedure. Thus, compared to the optimality criteria based method for topology design described in section 1.2.2, it only influences the optimization step of the scheme. This iterative loop becomes:

Optimization with, for example, MMA:

- Make initial design, e.g., homogeneous distribution of material. The iterative part of the algorithm is then:
  For this distribution of density, compute by the finite element method the resulting displacements.
  Compute the compliance of this design and the associated sensitivity with respect to design changes. If only marginal improvement (in compliance) over last design, stop the iterations. Else, continue.
- Compute the update of the density variable, based on the MMA approximate subproblem solved by a dual or a primal-dual method.
  Repeat the iteration loop.

The flow of computations sketched above shows the general concept, but programming details may be somewhat different, depending on how the specific mathematical programming software is structured. What is shown here is what is typically called an externally controlled optimization loop. In some cases an alternative structure is used, where the user provides subroutines that compute function values and sensitivity information, and the optimization software runs the loops "internally"

For the compliance problem the use of for example MMA does not change significantly the programming effort required to implement the topology design procedure, and it can also be easily implemented in the 99 line Matlab code mentioned earlier (see appendix 5.1.1)[7]

With this general outline of computations it is possible to generalize the concept to many other design settings of interest. This is the subject of Chap. 2.

A publicly available topology optimization software The topology optimization procedure as described in the preceding subsections has been implemented as an interactive design program made available to the public at the internet address `http://www.topopt.dtu.dk`. The program which is described in detail in Tcherniak & Sigmund (2001) solves a standard 3-load case compliance optimization problem. The topology optimization code is written in FORTRAN77 and the Graphical User Interface (GUI) and the

[7] The MMA-code is available both in FORTRAN and MATLAB versions from K. Svanberg. The codes are free for academic use.

file-transfer system is written in JAVA. The structures are independently of aspect ratio always discretized by approximately 1000 elements[8]

Screen-dumps of the Graphical User Interface of the TOPOPT program is shown in Fig. 1.9 together with a plot of the output. By pressing the left panel buttons and using the mouse and the delete key, the user can define the design domain, passive and active areas, load-cases and supports. After choosing the volume fraction and hitting the submit button, a sequence of GIF-files illustrating the iteration history appears on the screen. Depending on network load and connection, the solution of the problem may take from 10 seconds and up to a minute. As an extra feature, the animation sequences may be downloaded after running the program.

Implementation details The apparent simplicity of computing minimum compliance optimal topologies is somewhat betrayed by certain details that one has to cater for if a generally useful and applicable tool is to be constructed. For example, as already mentioned, the scheme described till now needs to be supplemented with some computational device that controls the range of allowable density distributions, especially the so-called checkerboard patterns that are numerical artifacts related to the discretization of displacements and densities. Also, the problem is inherently mesh-dependent as formulated and will generally not converge with mesh-refinement. Rather, finer and finer structure of the designs will arise. These aspects are the subject of the following section 1.3.

Another topic which is relevant to discuss here is the effect of the power p of the SIMP interpolation. As mentioned, to obtain black and white (0-1) topologies one has to work with a fairly large value of p, say, above 3. Moreover, to eventually be able to interpret appearance of grey in the final design as composite material, one also requires p be at least 3 (cf., (1.5), and the discussion in 1.5.4). However, in implementations it is often seen that a too severe penalization of the intermediate density can lead to designs which are local minima and which are very sensitive to choice of the initial design for the iterative optimization procedure (one "jumps" too fast to a 0-1 design). Thus a continuation method is often advisable, which means that the power p is slowly raised through the computations, until the final design is arrived at (for a power satisfying our requirements). The scheme is not guaranteed to give a fully 0-1 design (see Stolpe & Svanberg (2001b)). Nonetheless, it works well in most cases, especially when combined with a filtering of sensitivities as described in section 1.3.1. It is advisable to use such a continuation scheme as the standard procedure.

It is here important to underline that for the minimum compliance problem the by far most time-consuming part of the computations is spent on solving the equilibrium equations (Borrvall & Petersson (2001a) report this

[8] The current version of the web-program has been updated and additional features added by Lars Voxen Hansen and Thomas Buhl (DTU) in the spring of 2002.

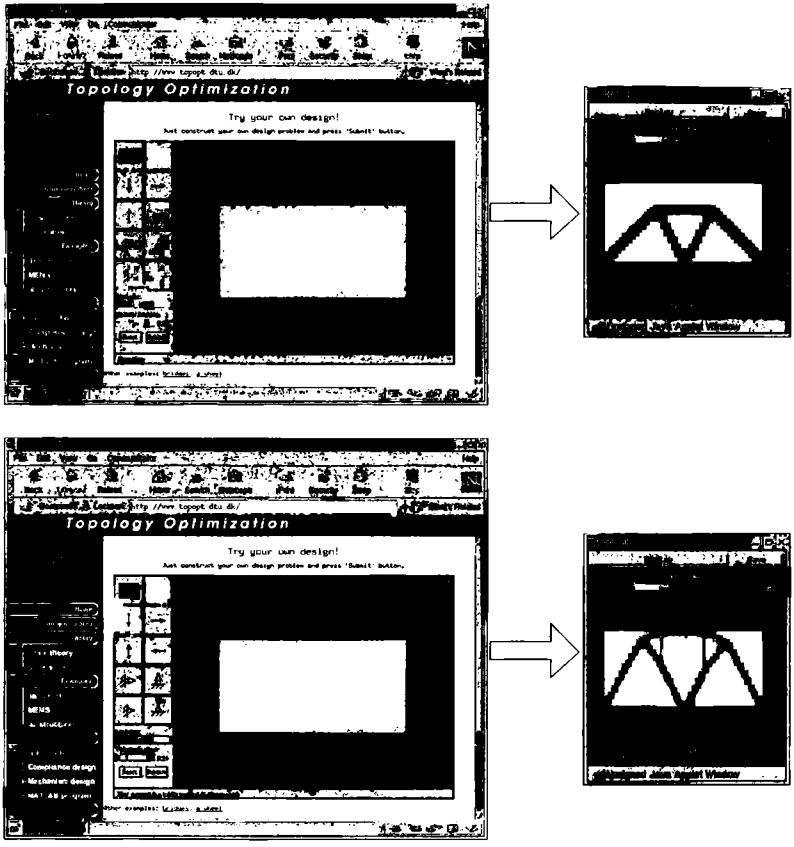

Fig. 1.9. A web-based topology optimization program (http://www.topopt.dtu.dk) for stiffness design of arbitrary two dimensional structures. The pictures demonstrate an investigation of the influence of boundary conditions on the optimal topology (from Tcherniak & Sigmund 2001).

share as up to 97%, in a parallel implementation). Thus it is critical for large problems, especially in 3-D, to improve on the efficiency of the analysis capability. Here the utilization of homogeneous meshes on rectangular or box-like domains is useful, as it removes the necessity for the repeated computation of local stiffness matrices. Also, the use of iterative solvers is useful in large scale problems, and may be required for storage reasons. The ultimate tool is to use vector computations and parallel computing, as for example reported in Borrvall & Petersson (2001a), where also the MMA-based optimization is

parallellized - solutions to 3-D problems with up to 220.000 brick elements have been obtained (c.f., Figs. 1.11 and 1.12). Solutions to similar-sized problems have also been reported in DeRose Jr. & Díaz (2000) (c.f. Fig. 1.10), but here the paradigm for the analysis part of the problem is fundamentally changed. Instead of finite elements, a mesh-less, fictitious domain method is used, based on using wavelets in a Galerkin scheme. The advantage here is that an iterative, preconditioned conjugate gradient scheme exhibits a performance that is insensitive to the discretization level.

In the future we may also see new approaches to solving the topology optimization problem, based for example on developments in computational mechanics. One possibility is to solve the original combined optimization problem in one optimization routine and break with the tradition of viewing the equilibrium statement as a function call. This means that analysis becomes part of the iterative procedure and for example a Newton scheme will solve simultaneously the necessary conditions of optimality for the density as well as for the displacements (the latter being the equilibrium equations). This is what has been named a SAND approach (Simultaneous ANalysis and Design). It has for example been tested for topology design in a multigrid framework in Maar & Schulz (2000) and in the setting of free material design and truss design where for example semi-definite programming can be applied due to special problem structure (see Sects. 4.3 and 5.5). From a practical point of view this approach has the weakness that a premature termination of the procedure does not provide any analysis results for the current design, and the method also requires full integration of optimal design and analysis in one software system, i.e., optimization will no longer be an "add-on" to existing FE software.

1.2.5 Topology optimization as a design tool

In the following we will try to illustrate some basic features of the material distribution method when used for design, dealing for the moment only with compliance design. In a later section 1.4 of this chapter we shall describe the possible use of the topology design method as a pre-processor in an integrated design process where boundary variation techniques are employed for refining a design created by the topology design method.

In Chap. 2 we shall see that the topology design methodology over the last decade has matured immensely and that one can today cater for a broad range of structural objectives and constraints. Also, aspects of controlling geometric features can be handled, as illustrated in section 1.3.1. Moreover, a broad range of physics can be included in the modelling. This combined with progress in algorithms and computational power means that the topology design methodology is today much closer to being able to provide the user with a final design than just a few years ago, and for example in the design and manufacturing of MEMS (MicroElectroMechanical Systems, see section 2.6) case studies have shown that one can go directly from the topology

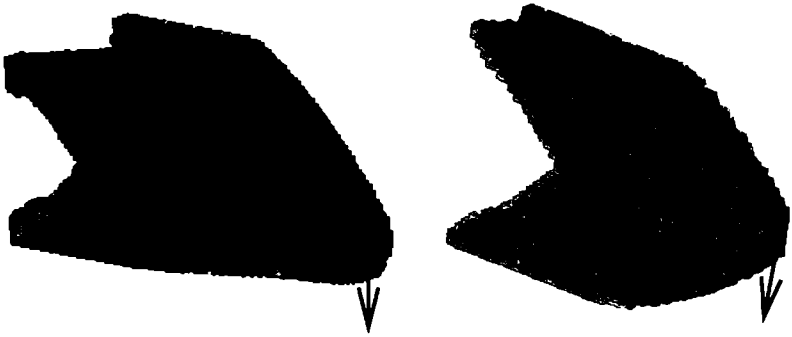

Fig. 1.10. Optimized 3D cantilever beams. Left: discretization by 221.184 design elements in a fictitious domain consiting of $128^3 = 1.097.152$ voxels. By courtesy of De Rose and A. Díaz (from DeRose Jr. & Díaz 2000).

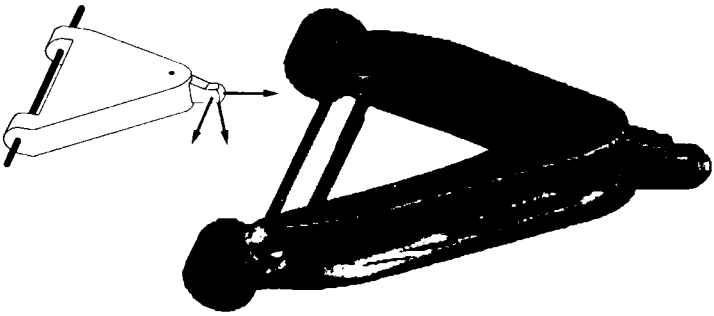

Fig. 1.11. Optimal design of a wishbone. Multiple load design using a very fine FE model (260.000 elements). Note that post-processing is basically not needed. By courtesy of T. Borrvall.

design output to manufacturing. In many other circumstances the practical use of topology design is often at the level of a creative sparring partner in the *initial* phase of a design process. Thus the output of the topology design method is used to identify potentially good designs, the completion of the design being based on traditional skills of the design office. One effect of the topology method that cannot be underestimated is the efficient testing of the appropriateness of the model of loads and supports. As the *topology* is very sensitive to a proper modelling of the load environment, one can immediately discover discrepancies or inaccuracies in this modelling.

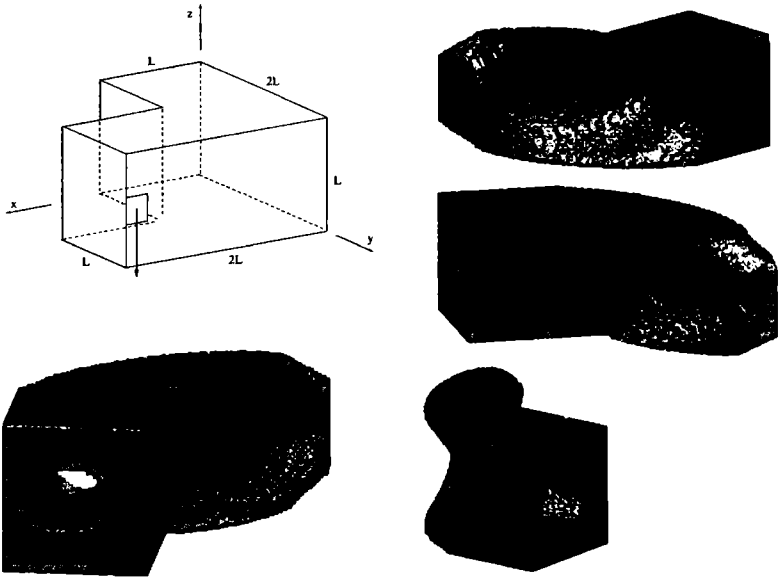

Fig. 1.12. Optimal design of cantilevered torsional beam in 3D. Design domain and different views of the optimized topology. Discretized using 128000 elements for one half of the problem and solved using parallel processing. By courtesy of T. Borrvall and J. Petersson (from Borrvall & Petersson 2001a).

Examples of topology design The material distribution method for topology design has been tested on a large number of examples, a few being illustrated in this and the preceding sections. The method allows for an efficient prediction of the optimal topology, the optimal shape and the optimal use of the prescribed possible support conditions. Also, it has proven to be a flexible and reliable design tool. The methodology has over the last decade become a fairly widespread tool in industrial applications, especially among some major car manufacturers (see section 2.12.4), and the appearance of commercial software has had an immense impact on the utilization of topology design methods in practise [23].

For an efficient use of topology design, the problem should be formulated on a ground structure (a reference domain) that is chosen as simple as possible to reduce the size of the analysis problem. The domain should, as described in section 1.2.2, allow for definition of loads and tractions and of boundary condition. The use of an automatic mesh generator will, of course, simplify the treatment of problems with complicated geometry such as non-simply connected reference domains. Complicated reference domains are needed for

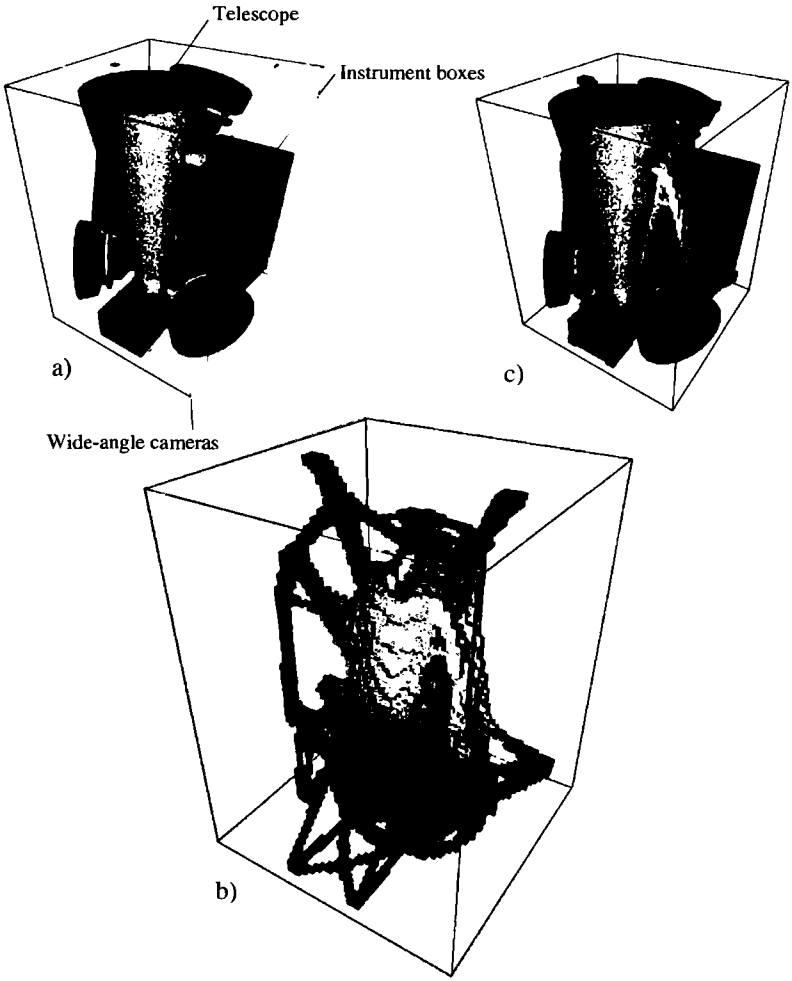

Fig. 1.13. Optimal design of frame for a satellite. Multiple load design using a 3-D model. The structure is discretized by 288.000 cubic finite elements. a) Design domain showing instruments around which the frame is to be designed. b) Optimized topology and c) optimized topology with instruments (from Sigmund 2000a).

cases where design requirements imply the exclusion of certain parts of space as parts of the structure. If the precise shapes of inner holes in a non-simply connected reference domain are unimportant, it is advisable to cater for such holes by fixing the density of material to be zero for the elements defining the

hole (or parts of it). These considerations have led to most examples being treated in rectangular reference domains, but the use of the method is of course not restricted to such domains.

For very low volume fractions, very fine discretization meshes are required when dealing with 0-1 designs, as the structures break up if coarse meshes are used. However, for high volume fractions, even coarse meshes give a very good indication of shape and topology and a good estimate of the optimal compliance. Note that for comparatively small volume fractions, the method predicts the lay-out of truss like structures and Michell frames (Fig. 1.2.2), thus supplementing lay-out theory and truss topology methods (see Chap. 4) for cases with a large, dense set of nodes; the material distribution method not only predicts the optimal connectivities, but also the optimal location of nodal points.

The application of interpolation schemes like SIMP that penalizes the designs to become of a 0-1 nature results in what one could classify as classically useful structures. One may argue that with present day technology for producing advanced composite materials one should certainly *not* remain limited by a wish to predict black and white designs only, but composites should also be part of the "structural universe" This is the theme of Chap. 3.

Here and in the remainder of the monograph we show only a restricted number of examples of optimal topologies. Many more examples of topology designs from academia and industry can be found in the literature and on the web.

1.3 Complications

In the following we will discuss two important issues that significantly influences the computational results that can be obtained with the material distribution based topology design procedure. These are the appearance of checkerboards and the mesh-dependency of results. The former refers to the formation of regions of alternating solid and void elements ordered in a checkerboard like fashion and is related to the discretization of the original continuous problem. Mesh-dependence concerns the effect that qualitatively different optimal solutions are reached for different mesh-sizes or discretizations and this problem is rooted in the issue of existence of solutions to the continuous problem.

1.3.1 Mesh-refinement and existence of solutions

It is well-established that the 0-1 and the SIMP topology optimization problem formulated in section 1.1 lacks existence of solutions in its general con-

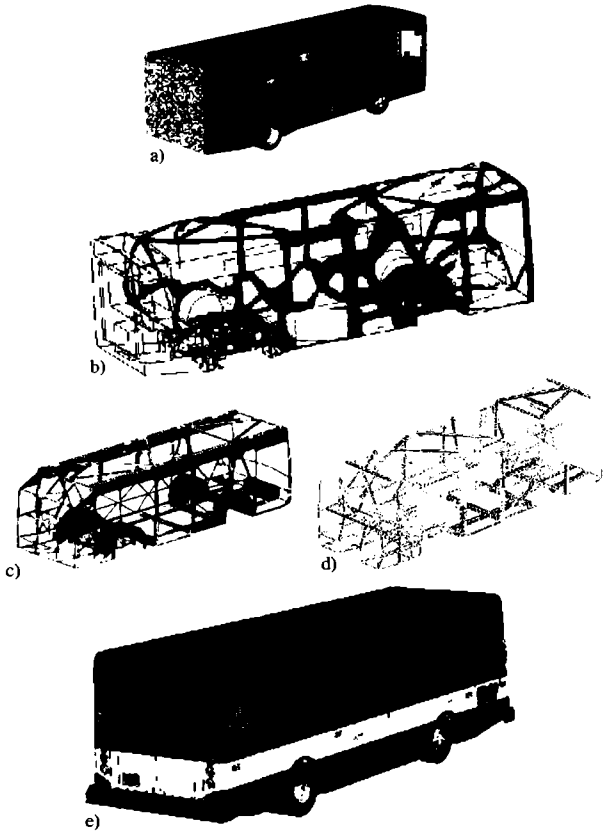

Fig. 1.14. Design of a lightweight city bus from preliminary design to final structural design. This example is courtesy of Altair Engineering, Inc., and has appeared in the Altair OptiStruct users manual and in (Thomas et al. 2002). At first, topology optimization is used to generate the optimum structural lay-out concept. The design space is shown in a) as the gray colored panels. b) The results of the topology optimization. c) CAD representation of the interpretation of the results of the topology optimization. d) Sizing optimization is performed on the hollow rectangular bar members of the bus structure. e) Final bus design. The shape of the windows was decided by the results of the structural needs identified by the topology optimization.

tinuum setting[9] The reason is that the introduction of more holes, without

[9] In any discretized version of the 0-1 problem, existence is trivial, as one has a design space with finitely many different design options.

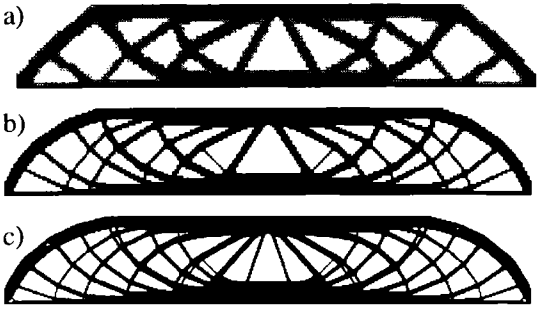

Fig. 1.15. Dependence of the optimal topology on mesh refinement for the MBB-beam example. Solution for a discretization with a) 2700, c) 4800 and d) 17200 elements.

changing the structural volume, will generally increase the efficiency of a given structure. In the limit of this process one obtains structural variations in the form of microstructures that have an improved use of the material. Such microstructures are typically not isotropic and cannot be represented within the original design description of only isotropic material; one says that there is a lack of closedness of the admissible set of designs. In computational implementations this effect is seen as a numerical instability where a larger number of holes appear when a finer finite element mesh is employed. That is, refining the finite element mesh for the reference domain ultimately leads to a generation of a fine-scale internal structural lay-out similar in nature to the microstructures that theory predicts. Thus the *non-existence* of solutions is indeed a problem for the numerical solutions of the topology optimization problem. This dependence of the solutions on mesh-refinement is illustrated in figure 1.15, where an improved finite element discretization results in a much more detailed structure. Ideally, mesh-refinement should result in a better finite element modelling of the same optimal structure and a better description of boundaries – not in a more detailed and qualitatively different structure. As we shall show, there are actually efficient and uncomplicated ways to achieve mesh-independent procedures for obtaining 0-1 designs, so there is no reason to accept results that are inherently mesh-dependent.

The approach to generate macroscopic and mesh-independent 0-1 solutions is to reduce the space of admissible designs by some sort of global or local restriction on the variation of density, thus effectively ruling out the possibility for fine scale structures to formate. The techniques that have been suggested for enforcing such a restriction fall into three generic classes of methods. These consists of either adding constraints to the optimization problem, reducing directly the parameter space for the designs, or applying filters in the optimization implementation. For most of these methods, exis-

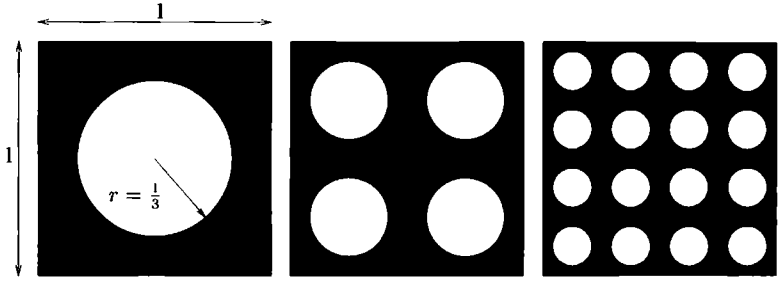

$V = 1 - 1 \cdot \pi \frac{1}{3^2} = 0.65$ $\quad$ $V = 1 - 4 \cdot \pi \frac{1}{6^2} = 0.65$ $\quad$ $V = 1 - 16 \ \pi \frac{1}{12^2} = 0.65$

$P = 1 \ \ 2\pi \frac{1}{3} = 2.09$ $\quad$ $P = 4 \cdot 2\pi \frac{1}{6} = 4.19$ $\quad$ $P = 16 \cdot 2\pi \frac{1}{12} = 8.38$

Fig. 1.16. An example of how smaller holes increase the perimeter, for a fixed volume. V is the volume and P is the perimeter of internal holes.

tence of solutions and also convergence of the FE approximations have been proved, providing a solid foundation [8].

We close this brief discussion by noting that the alternative to a restriction of the design space is to extend the space by allowing composites as admissible designs (see Chap. 3). For minimum compliance this lives up to our requirement of independence of mesh refinement, but also gives designs with large areas of "grey" This is thus not an option if 0-1 designs are the goal[10]

Perimeter control The *perimeter* of a mechanical element Ω^{mat} is, vaguely speaking, the sum of the lengths/areas of all inner and outer boundaries. Constraining the perimeter clearly limits the number of holes that can appear in the domain, (cf. figure 1.16) and existence of solutions to the perimeter controlled topology optimization is actually assured for both the discrete 0-1 setting and the interpolated version using SIMP Also, it has been implemented for both situations and for 2-D as well as 3-D problems [8]. For the SIMP method, one can impose a constraint that mimics such a perimeter bound in the form of an upper bound on the *total variation*, $TV(\rho)$, of the density ρ. In case the function ρ is smooth, the total variation constraint is a L^1 bound on its gradient:

$$TV(\rho) = \int_{\mathbf{R}^n} \|\nabla \rho\| \, \mathrm{d}x \leq P^* \tag{1.19}$$

[10] In order to force the composite solutions to a 0-1 design, an explicit penalty on intermediate densities can be added - but this destroys the existence as one reverts to the ill-posed 0-1 problem.

For a 0-1 design, the total variation of ρ coincides with the perimeter of Ω^{mat} when ρ is 1 in Ω^{mat} and 0 elsewhere (in $\mathbf{R}^n, n \quad 2(3)$). In this case the constraint is expressed as

$$TV(\rho) = \sup\left\{\int_{\mathbf{R}^n} \rho \text{div}\varphi \mathrm{d}x \middle| \varphi \in C_c^1(\mathbf{R}^n, \mathbf{R}^n),\ \|\varphi\| \leq 1\right\} \leq P^* \tag{1.20}$$

where $C_c^1(\mathbf{R}^n, \mathbf{R}^n)$ denotes compactly supported vector valued C^1 functions.

For an element wise constant finite element discretization of the density the total variation can in 2-D be calculated as

$$P = \sum_{k=1}^{K} l_k \left(\sqrt{\langle\rho\rangle_k^2 + \epsilon^2} - \epsilon\right) \tag{1.21}$$

where $\langle\rho\rangle_k$ is the jump of material density through element interface k of length l_k and K is the number of element interfaces (here one should also count interfaces at the boundary of the domain Ω – else there will be bias towards having material at the borders of Ω). The parameter ϵ is a small positive number which is used to convert the non-differentiable absolute value into a differentiable term. This expression is exactly the total variation of the element-wise constant density when $\epsilon = 0$.

It should be mentioned that there is an inherent problem of assuring isotropy in an implementation of a discretized perimeter measure (this effect is also known from work in image segmentation, cf. , Chambolle (1995)). Thus, in a regular 2-D mesh of squares, a bound on the discretized expression (1.21) will tend to favour structural edges parallel to those of the finite element mesh. This is caused by the effect that a straight edge of length 1 that is angled 45 degrees to the directions of the finite element mesh will be approximated by a jagged edge that has the perimeter $\sqrt{2}$. In contrast, the same edge has perimeter 1 when it is parallel to the mesh directions. In the limit of mesh refinement for a FE-mesh directed along the x_i-axes, the discretized perimeter measure (1.21) is thus rather the proper discretization of what is referred to a "taxi-cab" perimeter measure(cf., Petersson (1999b)):

$$TV_{\text{taxicab}}(\rho) = \int_{\mathbf{R}^2} \left(|\frac{\partial\rho}{\partial x_1}| + |\frac{\partial\rho}{\partial x_2}|\right) \mathrm{d}x \tag{1.22}$$

This means that the numerical results will approach solutions of a continuum topology optimization problem statement that includes a "perimeter bound" that actually measures the "length" of the boundary of the structure by projecting this onto the coordinate axes. This in turn implies that even though the perimeter constraint (1.21) assures convergence with respect to mesh refinement, a dependence on the choice of mesh will nonetheless be seen. This effect, however, does not change with mesh refinement. This directional bias of the results can be reduced considerably by considering more involved discrete versions of the perimeter measure, see Petersson, Beckers & Duysinx

(2000) and Borrvall (2001); in the latter reference more refined discretization schemes are also discussed.

The perimeter bound adds one extra constraint to the topology optimization problem and thus does not create any substantial problems for the use of an algorithm like MMA. However, it has been reported that the perimeter constraint can be quite difficult to approximate resulting in fluctuations in the design variables (this relates to the choice of the asymptotes of MMA). However, this can be solved by an internal loop procedure for the perimeter approximation which is computationally inexpensive compared to the equilibrium analysis (see Duysinx (1997)). Finally, one should note that choosing the bounding value of the perimeter constraint can be rather tricky, see below.

Other methods of restricting gradients One can also consider other types of gradient constraints for the SIMP method that ensure existence of solutions and convergence with mesh-refinement. These presuppose that ρ is sufficiently smooth for the bound to make sense and do not seem to have any equivalent for the discrete-valued 0-1 setting, in contrast to the perimeter measure discussed above.

One possibility is to constrain the local density variation by imposing pointwise bounds on the derivatives of the function ρ:

$$\left|\frac{\partial \rho}{\partial x_i}\right| \leq G, \ (i = 1, 2, (3)) \tag{1.23}$$

This scheme, which in essence constrains the L^∞ norm of the gradient of ρ, does assure existence of solutions and convergence of the finite element scheme (Petersson & Sigmund 1998). The advantage of this gradient constraint is that it gives a well-defined local length scale. The constraint in (1.23) implies that a transition from void to void through full material has to take place over a distance that is longer than $2/G$, which is thus the width of the thinnest features of a feasible design. Unfortunately, an implementation results in a huge number of extra constraints in the optimization problem and the method must therefore be considered to be too slow for practical design problems, if implemented directly as constraints. However, if one approximates the L^∞ constraint (1.23) by a L^q constraint for suitable large q one can alternatively operate with just one global constraint (but choosing the constraint value can be tricky and requires experimentation for each design case) (see Borrvall (2001)).

The basic concept of a slope constraint can also be enforced by an adaptive constraint strategy in the optimization algorithm that is similar to adding move limits (Zhou, Shyy & Thomas 2001). This means that one only works with the values of the box-constraints on the density ρ, which at the $(K+1)$-th iteration step are modified to restrict the variations in the design

$$\rho_i^{K+1} \geq \max\{\rho_{\min}, \rho_{j(i)}^K - D_{i,\ j(i)} G\} \ . \tag{1.24}$$

Here $j(i)$ is the element number of the element with the highest density value among all elements adjacent to the element i at the prior iteration step, and $D_{i,\,j(i)}$ is the distance between the centers of the elements i and $j(i)$. This strategy does not add to the computational complexity of the optimization procedure. However, it does require that the applied optimization algorithm can handle (temporary) violations of the box constraints. Furthermore, it is unclear whether "playing" with the move-limits will jeopardize convergence of the algorithm.

Another option is to implement a "global gradient constraint" by which we mean the norm of the function ρ in the Sobolov space $H^1(\Omega)$:

$$||\rho||_{H^1} = \left(\int_\Omega \left(\rho^2 + ||\nabla\rho||^2\right)\, \mathrm{d}\Omega\right)^{\frac{1}{2}} \leq M \tag{1.25}$$

Proof of existence when including this bound in the minimum compliance problem can be found in appendix 5.2.2 (for three dimensional problems the proof requires that the power in SIMP satisfies $p < 3$). Note that we for any finite element discretization of the ground structure Ω can choose a large enough bound M on the norm of ρ so that the norm constraint remains inactive, thus seemingly returning to the original formulation for this discretization. Thus implementation of (1.25) also requires utmost care and should involve experimenting with a range of values of the bound M. A global gradient constraint can also be formulated with the term ρ^2 removed from (1.25), so that the constraint becomes a L^2 constraint on the gradient of ρ. Numerical experiments with global gradients in the setting of topology optimization can be found in Borrvall (2001), where also L^q constraints in general are considered.

Filtering the density The techniques above impose explicit limitations on the allowable density distributions that can appear in the optimal design, and as such have to be catered for as constraints in the optimization formulation. An alternative to this is to directly limit the variations of the densities that appear in the set of admissible stiffness tensor E_{ad} by only admitting *filtered* densities in the stiffness [8]. Thus the SIMP method is modified to the following reduced design space:

$$\begin{aligned}
&E_{ijkl}(x) = ((\rho * K)(x))^p\, E^0_{ijkl}, \;\; \rho \in L^\infty(\Omega)\,, \\
&(\rho * K)(x) = \int_\Omega \rho(y) K(x-y)\, \mathrm{d}y\,, \\
&\int_\Omega \rho(x)\mathrm{d}\Omega \leq V; \quad 0 \leq \rho(x) \leq 1, \quad x \in \Omega\,,
\end{aligned} \tag{1.26}$$

where K is a convolution kernel, for example

$$K_r(x) = \begin{cases} 1 - \dfrac{||x||}{r} & \text{if} \quad ||x|| \leq r\,, \\ 0 & \text{otherwise}\,. \end{cases}$$

The filter radius r is fixed in the formulation and implies the enforcement of a fixed length-scale in the stiffness distribution. The filtering means that the stiffness in a point x depends on the density $\rho(x)$ in all points of a neighborhood of x. This implies a smoothing of the stiffness fields in a fashion similar to a filtering of an image. The smoothing and the fixed scale means that this method gives existence of solutions and convergence with refinement of the FE mesh. Loosely speaking, the reason that the filter removes any fine scale behaviour of the density ρ is that such variations in the mechanical analysis (via the filtering $(\rho * K)$) appears like a grey which is penalized by SIMP. Generally this method results in density fields ρ that are bi-valued, but the stiffness distribution $(\rho * K)^p$ is more "blurred" with grey boundaries. In a sense this is an ambiguity, as the mechanical analysis is done on the filtered density[11] For implementation, the differences compared to the standard procedure described in section 1.2 are that the element stiffness matrices in the finite element analysis are defined by weighted averages of the stiffnesses of neighbouring elements, and the sensitivity information should be modified to cater for the redefined stiffness tensor (this means that the sensitivity of the compliance with respect to $\rho(x)$ will involve the mutual energy of a neighborhood of x).

Filtering the sensitivities Computational experience has shown that filtering of the sensitivity information of the optimization problem is a highly efficient way to ensure mesh-independency [8]. This means modifying the design sensitivity of a specific element, based on a weighted average of the element sensitivities in a *fixed* neighborhood. Such a filter is purely heuristic but it produces results very similar to for example those obtained by a local gradient constraint, it requires little extra CPU-time and it is very simple to implement as it does not add to the complexity of the optimization problem (no extra constraints need to be considered). Similar ideas of weighted averages have been used to ensure mesh-independence for simulations of bone-remodelling and for analysis with plastic-softening materials (Mullender, Huiskes & Weinans. 1994, Leblond, Perrin & Deveaux 1994).

The scheme works by modifying the element sensitivities of the compliance as follows:

$$\widehat{\frac{\partial f}{\partial \rho_k}} = \frac{1}{\rho_k \sum_{i=1}^{N} \hat{H}_i} \sum_{i=1}^{N} \hat{H}_i \, \rho_i \, \frac{\partial f}{\partial \rho_i} \,, \tag{1.27}$$

where N is the total number of elements in the mesh and where the *mesh-independent* convolution operator (weight factor) $\hat{H}_i$ is written as

$$\hat{H}_i = r_{\min} - \mathrm{dist}(k,i), \quad \{i \in N \mid \mathrm{dist}(k,i) \leq r_{\min}\}\,, \; k = 1, \ldots, N \tag{1.28}$$

[11] In contrast, a non-filtered version of SIMP evaluates a 0-1 design with the same distribution of stiffness as represented by the density.

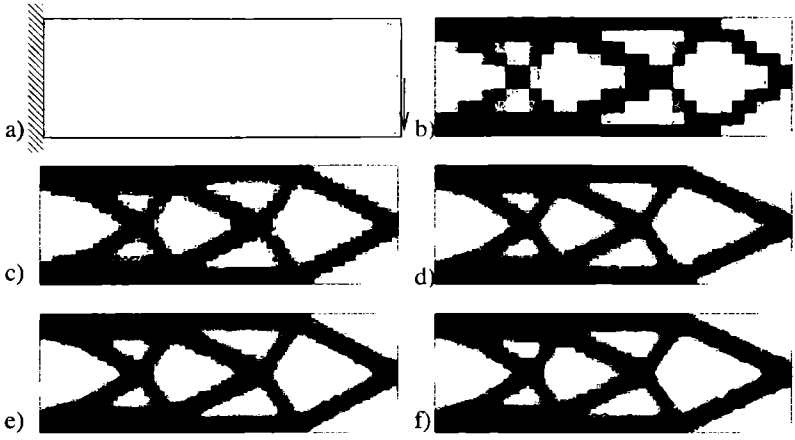

Fig. 1.17. Mesh-independent solutions of the cantilever problem using filtering of sensitivities. a) Design domain and load, b) 300, c) 600, d) 4800, e) 10.800 and f) 19.200 element discretization. Filter radius is 8.2% of the height of the design domain.

In this expression, the operator $\text{dist}(k, i)$ is defined as the distance between the center of the element k and the center of an element i. The convolution operator $\hat{H}_i$ is zero outside the filter area. The convolution operator for element i is seen to decay linearly with the distance from element k. It is worthwhile noting that the sensitivity (1.27) converges to the original sensitivity when the filter radius $r_{\min}$ approaches zero and that all sensitivities will be equal (resulting in an even distribution of material) when $r_{\min}$ approaches infinity. This filter is implemented in the Matlab code of appendix 5.1.1.

Unfortunately, the theoretical basis for the method is not yet understood. Also, it is unclear exactly what problem we are solving. However, numerous applications, many of which are shown in this monograph are based on this filtering method. It has been applied to 2 and 3 dimensional problems, to problems with up to 20 structural or other constraints, to problems involving multiple areas of physics and it has been an invaluable tool in designing extremal material structures (c.f. Sect. 2.10). Furthermore, it gives results that are stable under mesh-refinement and maintain a minimum length-scale that is controlled by the filter radius $r_{\min}$. Also, experience shows that the filter somehow improves the computational behaviour of the topology design procedures as it delays the tendency of the SIMP scheme to get "stuck" in 0-1 designs (this is discussed in more detail in Chap. 2). Fig. 1.17 shows an example of mesh-independent designs obtain by the filter. In the following we will refer to this filtering as the *mesh-independence filter*.

Monotonicity based length scale control In some recent work a scheme called the MOLE method (*MOnotonicity based minimum LEngth scale*) has been proposed for the control of length-scale (Poulsen 2001a). As for the perimeter and global gradient control it adds one extra constraint to the optimization problem, but in this case the non-negative constraint function should have value *zero* for the minimum length scale restriction to be satisfied. Moreover, one can explicitly specify the desired minimum width d of material parts and void inclusions. Thus it provides similar exact control as when using local gradients, but within just one constraint.

The idea is to pass a circular "filter" window over the design and measure if the density ρ along four equally spaced diagonals[12] is monotonic or not. The reason for testing over four diagonals is that a test only along the horizontal and vertical directions would not be able to detect the fine-scale variation of a corner to corner "hinge" in a regular mesh, while testing along the diagonals only would prevent checkerboard detection. On the other hand testing along more directions would make almost any design infeasible (see below).

The monotonicity of the density can be measured by applying the functional

$$\mathcal{M}(F) = \int_a^b |F'(x)|\, dx - \left| \int_a^b F'(x)\, dx \right| \geq 0\,, \tag{1.29}$$

which is *zero* if the smooth function F of one variable is monotonic on the interval $[a, b]$, and strictly positive otherwise. As the length scale criterion is violated if the design at any point and at any of the test directions is non-monotonic, one obtains a constraint function $\mathcal{M}_d(\rho)$ with the required properties by "summing" the values of $\mathcal{M}(\rho|_\gamma)$ over all points and all directions γ. We write this as

$$\mathcal{M}_d(\rho) = \int_\Omega \left(\sum_{\gamma \in \Lambda(x,d)} \mathcal{M}(\rho|_\gamma) \right)^q \mathrm{d}\Omega\,, \tag{1.30}$$

where $\Lambda(x, d)$ is the set of four diagonals of length d that we test over. The exponent q is used to assure good numerical behaviour of the constraint $\mathcal{M} = 0$ and experiments have shown that $q = 4$ is a good choice in implementations[13]

In the discrete formulation of the constraint one works with differences of element values of the density ρ and, as for the perimeter constraint, one has to use a smoothed approximation to the absolute value (cf., (1.21). We note that the computational effort in evaluating the constraint is linear in the number of elements, and that derivatives can be computed directly (and analytically). The idea also extends to 3-D, where the window is a ball and where one will check along 13 diagonals.

[12] Horizontal, vertical and at $\pm\pi/4$ from the horizontal.

[13] In the actual implementation one uses $\mathcal{M} \leq \delta$, where δ is decreased during the iterative procedure.

We remark that, as we consider only four directions for checking the minimum length scale, it is clear that there will be some directional dependence of the minimum allowed width of a strip of either material or void. Even in the continuous formulation, the constraint $\mathcal{M} = 0$ only allows piecewise straight lines as boundaries between solid and void. It also restricts the angle between these piecewise straight lines where they meet and the angle between the boundary lines at a kink will be less than $\pi/4$. This shows that more test directions will restrict the boundary curves even further and in the limit of testing along all diagonals only straight lines would be possible as boundaries between solid and void. Finally, we note that, as we cannot make angles sharper than $\frac{\pi}{4}$, the smallest inscribed polygon of a hole is an octagon which for a minimum length d gives the minimum (approximate) radius of curvature $\frac{1+\sqrt{2}}{2} d \approx 1.2\, d$.

Comparison of methods The perimeter, local gradient and filter methods produce very similar designs, but there are some differences. The perimeter control and the global gradient control schemes are global constraints and will allow the formation of locally very thin bars (albeit in limited numbers). The local gradient and filtering schemes are local constraints and will generally remove thin bars.

Predicting the value of the perimeter constraint for a new design problem must be determined by experiments, since there is no direct relation between local scale in the structure and the perimeter bound. If the perimeter bound is too tight, there may be no solution to the optimization problem. This problem is particularly difficult for three-dimensional problem. In contrast, the gradient and filtering schemes define a local length scale under which structural variation is filtered out. This local length scale corresponds to a lower limit on bar/beam widths. Such a possibility of imposing a minimum length scale is not only of importance for obtaining methods that are stable under mesh-refinement. Almost of greater importance is the possibility this gives for taking manufacturing considerations (machining constraints) into account. This can be in the form of minimum member size requirements for the material phase. This is important for the fabrication of MEMS (Micro-ElectroMechanical Systems, see section 2.6), where mechanisms are etched or deposited by chemical processes. Also, minimum size of a void inclusion is crucial if a structure is machined out by milling processes.

Finally, we remark that the use of a *fixed, finite dimensional set* of designs is a direct way of assuring existence of solutions as well as stability with respect to mesh-refinement – the latter here then *only* means improving the *analysis* grid. The geometric resolution cannot be improved beyond what is contained in the initial design description.

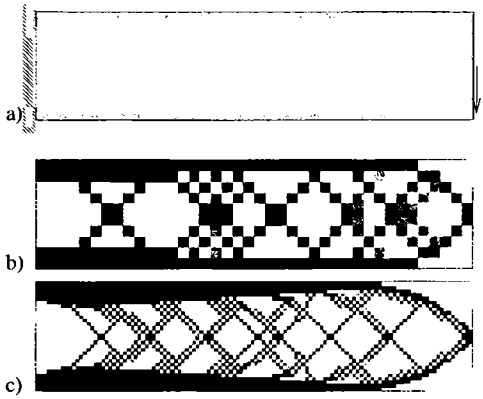

Fig. 1.18. The checkerboard problem demonstrated on a long cantilever beam. a) Design problem, b) solution for 400 element discretization and c) solution for 6400 element discretization.

1.3.2 The checkerboard problem

Patches of checkerboard patterns appear often in solutions obtained by a direct implementation of the material distribution method that use the displacement based finite element method, cf., figure 1.18. Within a checkerboard patch of the structure the density of the material assigned to contiguous finite elements varies in a periodic fashion similar to a checkerboard consisting of alternating solid and void elements. Such patterns are also observed in the spatial distribution of the pressure in some finite element analyses of Stokes flows. It is now well understood that also for topology design the origin of the checkerboard patterns is related to features of the finite element approximation, and more specifically is due to bad numerical modelling that overestimates the stiffness of checkerboards [9].

The restriction methods already described also has the effect that checkerboarding is reduced or removed The reason for this is that when one enforces a constraint on geometry (generally speaking in terms of the length of the boundary or in terms of gradient variation) that assure that solutions exist, one also obtains FE-convergence and checkerboards cannot be present for a fine enough mesh (more precisely, they can be made arbitrarily weak).

There are situations where one does *not* wish to enforce a fixed scale geometric restriction on the designs. This is the case when one uses numerical methods to obtain an understanding of the behaviour of optimal topologies at a fairly fine scale, but in a macroscopic representation. This is of theoretical interest for obtaining insight in for example solutions to problems involving Michell type continua. Moreover, it has great practical interest when designing low volume fraction structures, where one can gain very useful insight

for the design of truss and frame structures – here the continuum topology design methodology can predict both member sizes and nodal positions. Another situation where geometric restriction is unwanted is in the computational implementation of the relaxed form of the topology optimization problem, where composites are used to achieve existence of solutions. Also, when studying variable thickness sheets and problems where all possible elasticity tensors are part of the design space, checkerboard control should be achieved by other means than by geometric restriction.

In the following we shall for 2-D problems outline explanations for the appearance of checkerboards and describe a number of methods that can be used to avoid them for cases where geometric scale is not restricted.

The stiffness of checkerboards The most direct explanation as to why checkerboards appear in topology design is that such lay-outs of material have an artificially high stiffness when analyzed in certain discretized formulations. Thus it turns out that a checkerboard of material in a uniform grid of square Q4 elements has a stiffness which is comparable to the stiffness of a $\rho = 1/2$ *variable thickness* sheet, for any applied loads (or prescribed strains) (see Fig. 1.19 and section 3.3.5). For the minimum compliance problem of an infinite medium, this means that for a Q4 discretization of displacements and any discrete as well as the continuum description of ρ, the corresponding optimization problem has the checkerboard version (matched to the Q4 mesh) as an optimal design. Thus it is not surprising that one in general sees that optimization generates these non-physical checkerboards when Q4-displacement elements are used.

Checkerboards and choice of FE spaces The problem of finding the optimal topology by the material distribution method is a *two* field problem. It involves finding the optimal distribution of material described by the density ρ (or stiffness tensor E) as well as the displacement field u of this optimal design. It is in this connection useful to remember that the displacement based minimum compliance problem we consider can be cast in the form

$$\max_{E\in\mathbf{E}_{\mathrm{ad}}} \min_{v\in U} \left\{ \frac{1}{2}\int_\Omega E_{ijkl}\varepsilon_{ij}(v)\varepsilon_{kl}(v)\mathrm{d}\Omega - l(v) \right\} \tag{1.31}$$

and a numerical implementation operates on a discretized version of this min-max type problem for a functional of two variables. It is well-known (cf., Stokes flow), that the finite element analysis of such problems can cause problems, being unstable and being prone to the development of checkerboard patterns for one of the fields. The so-called Babuska-Brezzi (B-B) condition has been developed as a criterion that will guarantee that a a finite element discretization results in a stable numerical scheme, see Brezzi & Fortin (1991). Unfortunately, the functional (1.31) of the topology design problem is not quadratic in the *two* fields and it is also not concave-convex. Thus one cannot directly apply standard saddle point theory and the related

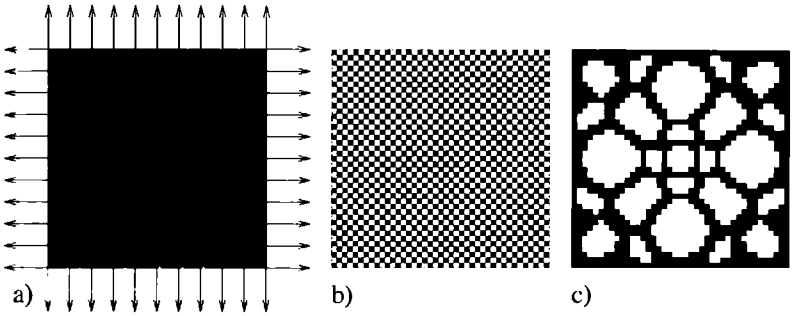

Fig. 1.19. The checkerboard problem demonstrated on a square structure subject to biaxial stress and modelled by Q4 elements. a) Design problem, b) solution without checkerboard control and c) solution with sensitivity filtering. All volume fractions are 50% and the resulting compliances for a variable thickness plate ($p = 1$ in SIMP) (a) is 2.67; for the checkerboard structure (b) 2.81; and for the non-checkerboard structure (c) it is 6.16. Even in this finite lay-out the non-physical checkerboard – modelled by Q4 elements – is almost as stiff as the sheet.

application of the Babuska-Brezzi condition to the present situation. However, these problems aside, taking a direct analogy to the similar problem in Stokes flow indicates nonetheless that certain combinations of finite element discretizations will be unstable and some stable. This has been confirmed by numerical experiments for both the SIMP model, for cases with composites and for variable thickness sheets [9]. The analogy suggests that the use of higher order finite elements for the displacement function is a viable method to avoid the checkerboard problem and checkerboards are typically prevented when using 8 or 9-node quadrilaterals for the displacements in combination with an element wise constant discretization of density. An analysis based on a patch test of the finite element models substantiates this finding (Jog & Haber 1996). These patch tests are based on a B-B type analysis of a linearized, incremental form of the necessary conditions, corresponding to an incremental, quadratic approximation of the saddle point problem (1.31), and the tests give information on the performance of various combinations of finite element approximations of the two field problem at hand. We also note that it is possible to extend the full mathematical analyses of mixed FE developed for the Stokes' flow problem to the variable thickness sheet problem (cf., Petersson (1999a)).

The use of higher order finite elements in topology design results in a substantial increase in CPU-time, even though this is not today a serious problem for 2-D problems. But it is still productive to employ alternative and computationally more economical methods. Many such methods have been proposed and typically include some flavour of a mesh related filtering

of the densities. A series of such methods will be described below. Before we turn our attention to these concepts, it is worth mentioning some very recent ideas that work with modifications of the typical element density based parametrization.

One is to change the discretization of the density field to be given by the nodal values of the squares that define the mesh for the displacements; the element density is then the *average* of the nodal values (Hammer 2001). A sensitivity of compliance with respect to one of these densities will then depend on the energies in the four neighboring elements, and the design description is in nature similar to filtering methods (see sections 1.3.1). It can be shown that for a finite element discretization based on square elements, this idea corresponds to imposing a local gradient constraint as in 1.23, where G is equal to two times the element size. This means that there always will be a rim of at least one grey element between solid and void elements. Obviously, this also means that this nodal based averaging technique does not imply mesh-independence. An example of the scheme applied to compliant mechanism design is shown in Fig. 2.27 Note that a scheme that uses a density interpolation of nodal values does *not* have the desired effect.

Another idea is to use non-conforming elements for the displacement fields, effectively giving correct zero stiffness to an infinite checkerboard also in the discretized problem (Jang, Kim, Kim, Kim, Park & Shin 2001).

Finally, we remark that theoretical studies of the appearance of checkerboards in three-dimensional problems are yet to be carried out. However numerical experience shows that checkerboards also appear for this case.

Removing checkerboards in a patch In order to save CPU-time, but still obtain checkerboard free designs, it has been suggested to employ a patch technique inspired by a method applied for the similar problems in Stokes flow (cf., Johnson & Pitkäranta (1982)). This technique has in practical tests shown an ability to damp the appearance of checkerboards. The strategy controls the formation of checkerboards in meshes of 4-node quadrilateral displacement elements coupled with constant material properties within each element. Thus one maintains the use of low order elements. However, the end result is the introduction of some type of element with a higher number of nodes, as the method in effect results in a"super-element" for the density and displacement functions in 4 neighbouring elements. In what follows we will assume that the design domain Ω is rectangular. It is discretized using a uniform mesh of square, 4-node iso-parametric elements K_{ij}, $i = 1, \ldots, 2M$, $j = 1, \ldots, 2N$ where $2M$ and $2N$ are the (even) number of elements per side. Consider now, for odd i and j, a patch P_{ij} of four contiguous elements $\mathrm{K}_1 = \mathrm{K}_{i,j}$, $\mathrm{K}_2 = \mathrm{K}_{i+1,j}$, $\mathrm{K}_3 = \mathrm{K}_{i,j+1}$ and $\mathrm{K}_4 = \mathrm{K}_{i+1,j+1}$, as shown in Fig. 1.20, i.e.,

$$\mathrm{P}_{ij} = \mathrm{K}_1 \cup \mathrm{K}_2 \cup \mathrm{K}_3 \cup \mathrm{K}_4 \ .$$

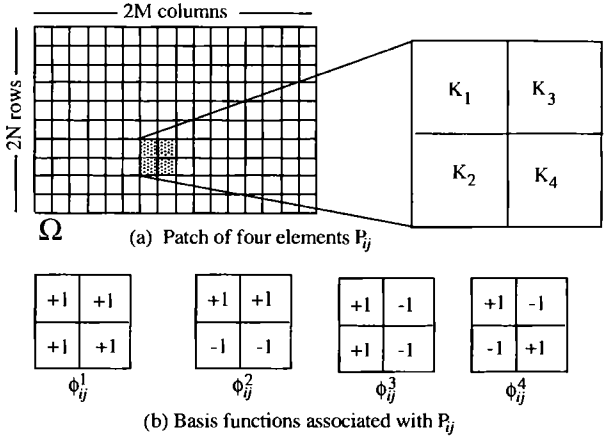

Fig. 1.20. Patches and basis functions used for checkerboard control.

Associated with P_{ij} we introduce basis functions ϕ^1_{ij}, ϕ^2_{ij}, ϕ^3_{ij} *and* ϕ^4_{ij} which take the values ± 1 in P_{ij} according to the pattern shown in Fig. 1.20 and are zero outside P_{ij}. Here we note that:

– The functions $\{\phi^k_{ij}\}$ constitute an orthogonal basis,
  A "pure" checkerboard pattern is of the form $u = \sum_{P_{ij}} u_{ij}\phi^4_{ij}$

This suggests that in order to avoid the formation of checkerboard patterns we need to restrict ρ to lie within the more restricted, checkerboard-free space

$$\bar{V} = \left\{ v \middle| \begin{array}{l} v(x) = \sum_{P_{ij}} (v^1_{ij}\phi^1_{ij} + v^2_{ij}\phi^2_{ij} + v^3_{ij}\phi^3_{ij}),\ (v^1_{ij}, v^2_{ij}, v^3_{ij}) \in \mathbf{R}^3, \\ i = 1, 3, \ldots 2N-1,\ j = 1, 3,\ ..2M-1 \end{array} \right\}$$

This restriction on ρ links the four elements in a patch, and the amount of material in $K_1 \cup K_4$ equals that of $K_2 \cup K_3$ and each is half of the total volume of the patch.

The coupling of the density distribution makes it difficult to apply the usual iterative optimality condition method. In MMA one can work directly with the design space $\bar{V}$ by using the $3MN$ parameters $(v^1_{ij}, v^2_{ij}, v^3_{ij})$ as design variables. This, however, changes the simple bound constraints $0 \le \rho \le 1$ into a huge number of linear constraints on the parameters v, making this option impractical. Instead, the following simpler procedure, which has been applied in a variety of problems, can be employed for both algorithms:

1. At each iteration of the optimization algorithm the cell size parameters within each element K_{ij} are updated using the usual update method (optimality criteria approach or an MMA step).
2. For each patch P_{ij} let $\{\rho_1, \rho_2, \rho_3, \rho_4\}$ be the be the updated densities in the

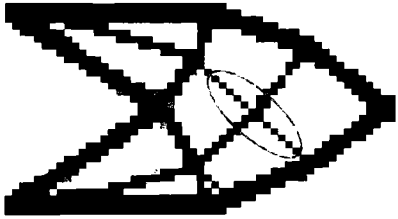

Fig. 1.21. Single checkerboard-patterns may form within the patch control scheme. But no extended checkerboard patterns can be present (from Poulsen 2002).

four quadrants of the patch associated with the updated cell sizes (using the numbering of 1.20). We then seek, as the starting point for the next iteration, a new piece-wise constant and *checkerboard-free* density distribution within the patch, say $\bar{\rho}$, written as

$$\bar{\rho}(x) = \frac{1}{4}(\rho_1 + \rho_2 + \rho_3 + \rho_4)\phi^1 + \bar{v}_2\phi^2 + \bar{v}_3\phi^3, \; x \in \mathrm{P}_{ij}$$

Here $\bar{\rho}$ is *checkerboard-free* (as $\bar{v}_4 = 0$) and it preserves material in the patch (as the coefficient of ϕ^1 is set as $\bar{v}_1 = \frac{1}{4}(\rho_1 + \rho_2 + \rho_3 + \rho_4)$). To determine the parameters $\bar{v}_2, \bar{v}_3$, we select $\bar{\rho}$ as the best L^2 approximation to ρ in P_{ij} under the constraints that $0 \leq \bar{\rho}_i \leq 1, i = 1, 2, 3, 4$. This corresponds to a QP problem in two variables, with linear constraints. The solution can be found analytically, and is given as

$$\bar{\rho}_1 = \frac{1}{4}(3\rho_1 + \rho_2 + \rho_3 - \rho_4)\,, \qquad \bar{\rho}_3 = \frac{1}{4}(\rho_1 - \rho_2 + 3\rho_3 + \rho_4)\,,$$
$$\bar{\rho}_2 = \frac{1}{4}(\rho_1 + 3\rho_2 - \rho_3 + \rho_4)\,, \qquad \bar{\rho}_4 = \frac{1}{4}(-\rho_1 + \rho_2 + \rho_3 + 3\rho_4)\,,$$

if these values satisfies $0 \leq \bar{\rho}_i \leq 1$. If a $\bar{\rho}_i$ in these expressions is above 1, it is set to 1 and the corresponding diagonal density is adjusted to maintain the volume of the patch; negative values are handled likewise and are set to 0. The modification of the density outlined here has the flavour of a filtering in a post-processing step that is invoked at each step of the optimization procedure and should therefore be used with some caution. We note that it does not disturb areas of the domain where no checkerboard control is needed, and also remark again that the method corresponds to introducing a "super-element" of four Q4 elements with a total of 9 displacements nodal points and with 3 degrees of freedom for the density approximation. Thus the method maintains more resolution in densities, as compared to, say, the approach of using Q9 elements for displacements and element-wise constant density ρ.

An alternative to the procedure above is to perform a change of variables that allows one to work directly with checkerboard free designs. Inspired by

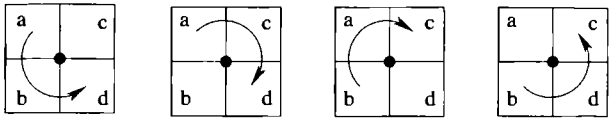

Fig. 1.22. A check for monotonicity along four paths around an interior node.

work in wavelet-based parametrization of the design (see section 1.5.5), we introduce a checkerboard free space of auxiliary variables $\bar{W} = \{w \in \bar{V}\}$. We do not impose any side constraints on $w(x)$ and convert it into to a density satisfying the bounds $0 < \rho < 1$ by a transformation:

$$\rho(x) = h(w(x)), \text{ with } h(w) = \frac{\arctan(w)}{\pi} + \frac{1}{2},$$

where h is a strictly increasing function[14] that will map checkerboard free patches of the auxiliary variable w to checkerboard free patches of the density ρ.

In the optimization, the variables $(w^1_{ij}, w^2_{ij}, w^3_{ij})$ then become the design variables. For implementation, sensitivity information with respect to these variables are needed, but this information can be gained from sensitivities wrt. $\rho(x)$ by an application of the chain-rule. The volume constraint becomes a non-linear function in the auxiliary variables, but this does not create any difficulties. Finally one notes that box constraints on the auxiliary variables are a requirement of MMA (as in most mathematical programming algorithms) and these can be chosen big enough as not to affect the results; also, one can use an imposed $w_{\min}$ to match a desired value of $\rho_{\min}$, but this is not critical [11].

We note here that the schemes proposed above depend on the build-up of the mesh in 2 by 2 patches of quadrilaterals. In each such patch checkerboards are removed, but checkerboards between patches are still possible if the row or column number of the upper left corner of a checkerboard is even. This also means that corner to corner patterns of the single elements can occur, but no large areas of checkerboards are possible. This is discussed in further detail in section 2.6 that deals with design of mechanisms.

NoHinge: A checkerboard constraint In section 1.3.1 geometry control was achieved by defining one extra constraint for the optimization problem. This idea can also be implemented for checkerboard control, i.e., one defines a non-negative constraint function that should have value *zero* for the design to be free of checkerboards.

Consider the patch of square elements in figure 1.22. Defining the function

$$m(x, y, z) = |y - x| + |z - y| - |z - x|,$$

[14] A function $S(w) = \frac{1}{2}\frac{1-e^{-kw}}{1+e^{-kw}} + \frac{1}{2}$ is also a choice among many other possibilities.

that is zero if the sequence of real numbers x, y, z is monotonic (increasing, decreasing or constant) and strictly positive otherwise, we can determine that the patch is free of checkerboard patterns, if just one of the numbers $m(a,b,d)$, $m(a,c,d)$, $m(b,a,c)$ or $m(b,d,c)$ is zero. This can be in turn be expressed as the condition that the number

$$h(a,b,c,d) = m(a,b,d)\, m(a,c,d)\, m(b,a,c)\, m(b,d,c) \ ,$$

is zero. A design defined by a density ρ that is element wise constant on a mesh of quadrilaterals with N interior nodes will thus be free of checkerboards if it satisfies the constraint

$$\sum_{k=1}^{N} h(\rho_{k,a}, \rho_{k,b}, \rho_{k,c}, \rho_{k,d}) = 0 \ , \tag{1.32}$$

where $\rho_{k,e}$, $e = a, b, c, d$ are the material densities in the elements connected to the node k. This constraint can thus be added to our optimization problem to assure checkerboard free solutions. It can also be used to remove "artificial" hinges in mechanism design, see section 2.6. As we have seen in other situations, an implementation using gradient based optimization techniques requires a replacement of the absolute value by a smooth substitute, for example $|x| \simeq \sqrt{x^2 + \epsilon^2} - \epsilon$ with $\epsilon = 0.1$. With this modification a sensitivity analysis of the constraint is straightforward, but rather tedious (Poulsen 2001b). For an example of the use of this scheme, see Fig. 2.25.

Checkerboard control by filtering of sensitivities The filtering technique for gradients described in 1.3.1 can also be cast in a version that only constrains checkerboards, without imposing a mesh independent length scale. This just requires that one adjusts the filter in (1.27) to exactly making the design sensitivity of a specific element depend on a weighted average over the element itself and its *eight* direct neighbours. This is a is very efficient method for removing checkerboards [9].

1.3.3 Non-uniqueness, local minima and dependence on data

It is important to observe that most problems in topology design (as in structural problems in the large) are not convex. Moreover, many problems have multiple optima, i.e. *non-unique solutions*. An example of the latter is the design of a structure in uni-axial tension. Here a structure consisting of one thick bar will be just as good as a structure made up of several thin bars with the same overall area. The non-convexity typically means that one can find several different local minima (which is what the gradient based algorithms locate) and one can obtain different solutions to the same discretized problem when choosing different starting solutions and different parameters of the algorithms. Most global optimization methods seem to be unable to handle

problems of the size of a typical topology optimization problem. Based on experience, it seems that continuation methods must be applied to ensure some sort of stable convergence towards reliably good designs.

The idea of *continuation methods* is to gradually change the optimization problem from an (artificial) convex (or quasiconvex) problem to the original (non-convex) design problem in a number of steps. In each step a gradient-based optimization algorithm is used until convergence. This is useful in many types of problems. Examples are the use of a continuation method were the structure first is optimized allowing regions consisting of composites (see Chap. 3), and after convergence, a penalization scheme is gradually introduced to obtain a 0-1 design. Likewise (as mentioned in section 1.2.4), for SIMP it is advisable to start out with $p = 1$ and then slowly raise the value of p through the computations until the final design is arrived at. For the perimeter constraint it is also beneficial to perform a gradual decrease of value of the constraint on the perimeter. For the mesh-independence filter (see section 1.3.1) it is normally recommended to start with a large value of the filter size r_{min} (which gives designs with blurry edges) and to gradually decrease it, to end up with a well-defined 0-1 design.

Finally, it is extremely important to observe that the results that one obtains with topology design of course depends on the data that one decides on using before applying the optimization procedure. Thus a change of the geometry of the design domain, the choice of load and boundary conditions can result in drastical changes in the"optimal design" that an algorithm may produce. Similar effects can be seen from variations of perimeter constraint values or filter parameters, etc. This is actually not that surprising as we are dealing with very "nasty" optimization problems, but in topology design this effect is just much more noticeable than in many other types of structural optimization problems.

1.4 Combining topology and shape design

Traditionally, in shape design of mechanical bodies, a shape is defined by the oriented boundary curves or boundary surfaces of the body and in shape optimization the optimal form of these boundaries is computed. This approach is very well established and the literature is extensive [2], [35]. On the other hand, we have just seen how the material distribution formulation can give a good estimate of the boundary of a structure, but here a reasonable prediction of the finer details of the boundaries requires very large FEM models. Also, the inherent large scale nature of the topology optimization method is such that the objectives used for the optimization should be global criteria, e.g. compliance, volume, average stress, etc., so that the effectiveness of the dual optimizers can be maintained by treating problems with a moderate number of constraints. For example, the focal point in the presentation so far has been the minimization of the compliance of a structure subject to a

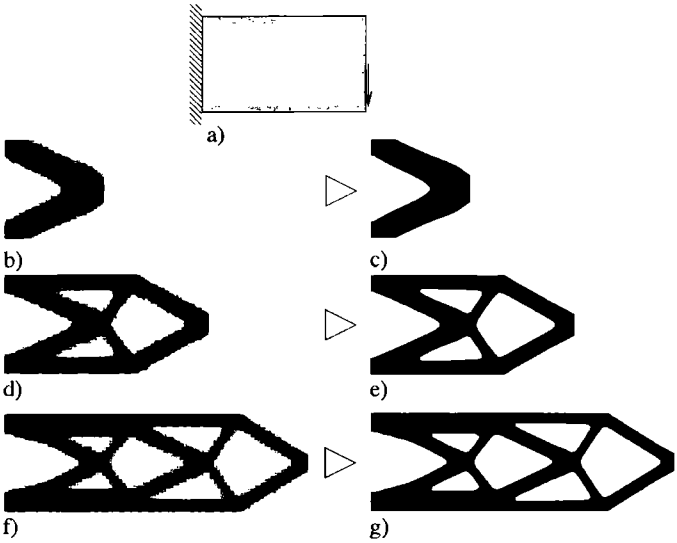

Fig. 1.23. Postprocessing of grey-scale pictures by automatic (MATLAB) contour-plotting. Cantilever beam for different aspect ratios. b), d) and f): optimized topologies based on SIMP and filtering of sensitivities and c), e) and g): contour plots based on the grey-scale pictures.

constraint on the volume of the structure. On the other hand, the description of the body by boundary curves and surfaces allows the finer details of the body to be controlled by a moderate number of design variables (e.g., spline control points) so this setting is better suited for studying problems such as the minimization of the maximum value of the displacements or of the Von Mises equivalent stress in the body[15]

It is thus for this type of situations natural to integrate the material distribution method and the boundary variations approach into one design tool, employing the topology optimization techniques as a pre-processor for boundary shape optimization. The possibility of generating the optimal topology for a body can be used by the designer to select the shape of the initial proposed form of the body for the boundary variations technique. This is usually left entirely to the designer, but the material distribution method gives the designer a rational basis for his choice of initial form. As to be expected, the topology is of great importance for the performance of the structure, and it has turned out that - not unexpectedly - the compliance optimized topologies generated using topology design are very good starting points for optimiza-

[15] The handling of local stress constraints for continuum topology design problems is described in section 2.3.

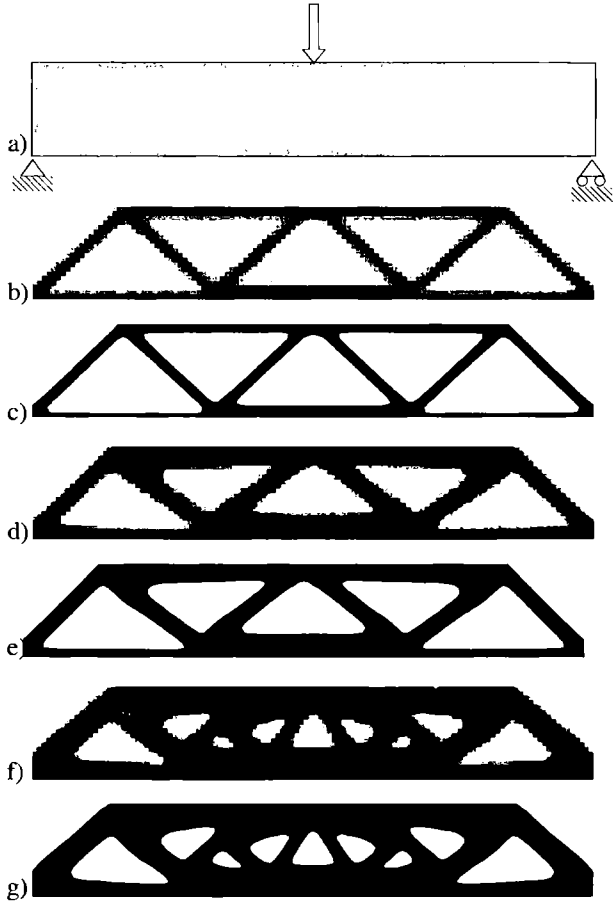

Fig. 1.24. Postprocessing of grey-scale pictures by automatic (MATLAB) contour-plotting. MBB-beam for volume fractions of 30%, 50% and 70%, respectively. b), d) and f): optimized topologies based on SIMP and filtering of sensitivities and c), e) and g): contour plots based on the grey-scale pictures. Only moderate modifications (smoothing of corners etc.) seems to be needed before manufacturing.

tion concerning several other criteria such as maximum stress, maximum deflection, etc.

The direct integration of topology optimization and shape design methods is made difficult by the fact that the description of a structure by a density function is fundamentally different from a description by boundary curves or

surfaces, as used in boundary variations shape optimization methods. In a CAD integrated shape optimization system, it is perhaps natural that the integration is based on the designer drawing the initial shape for the boundary variations technique directly on the top of a picture of the topology optimized structure, allowing for designer interaction [10]. This also creates a design situation where the ingenuity of the designer is put to use for generating a "good" initial form from the topology optimization results. The term "good" in this context covers considerations such as ease of production, aesthetics, etc. that may not have a quantified form. However, automatic interfacing between the topology optimization method and other structural optimization methods is no doubt more productive. Here image processing and smooth surface generation are key technologies [10]. Such techniques are especially important for an effective integration of topology design methodology in general purpose 3-D Computer Aided Optimal Design (CAOD) systems. We note that any integration of the two design methods is simplified by the fact that the integration can be based on a common FEM mesh generator and analysis module and a common CAD input-output facility. The requirements on the mesh generator are mainly governed by the boundary variations technique, as mesh distortions and mesh non-uniformities for that problem can become critical due to the shape changes of the analysis domain.

An important aspect of shape design is adaptivity of the FE mesh. Likewise, for topology design on can work with a sequence of design situations where the groundstructure (the reference domain) as well as the FE mesh is subject to adaptation; for further details consult [10].

It should be emphasized that the boundary variation method in essence is computationally significantly more involved than the topology design method. Also, the mathematical technicalities of formulating the problem and computing sensitivity information are more daunting, as is indicated in appendix 5.3. On the other hand, the material distribution method is a large scale optimization problem. Describing boundaries by for example spline control points requires a much lower number of design variables, meaning that standard mathematical programming techniques can be used also for problems with a substantial number of constraints. Note also that the basic approach to topology design is of equal complexity for two and three dimensional structures, but that the description of geometry for boundary shape design is much more complicated in dimension three.

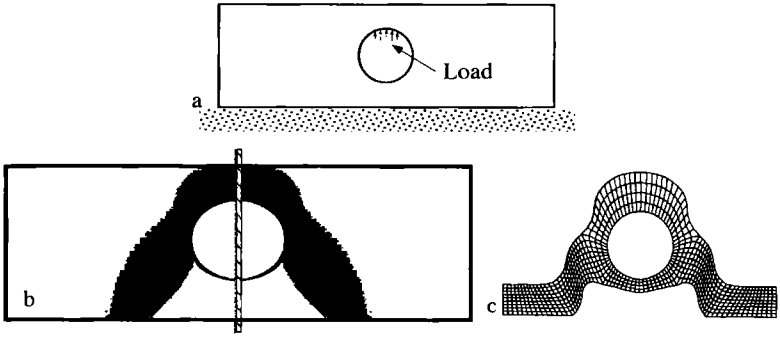

Fig. 1.25. The optimal design of a bearing pedestal, using the homogenization approach (see Chap. 3) integrated with the boundary shape design system CAOS (see Rasmussen et al. (1993)). a) The reference domain, with loading. The rim of the inner hole was kept as a solid in the topology optimization. b) The result of the homogenization approach. c) The final design, after boundary shape design for minimum maximal Von Mises stress and after adding outer parts to the structure for fastening. Utilizing symmetry only one half of the structure was analysed, as indicated in b) (from Olhoff et al. 1992a).

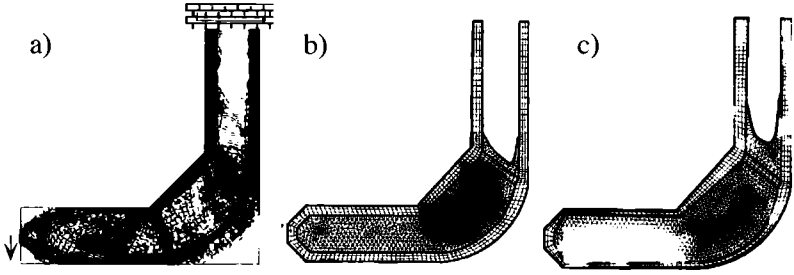

Fig. 1.26. Optimized topology and shape design of a structure made of two materials, resulting in a sandwich structure. a) Optimized two-material topology computed using rank-3 layered materials (see Chap. 3). b) Initial design for a refinement using boundary shape optimization. All boundaries between skin and core are restricted to be piecewise straight lines. For the boundary design the weight is minimized without increasing the compliance relative to the optimal topology. c) Final shape optimized structure. By courtesy of Rasmussen, Thomsen and Olhoff.

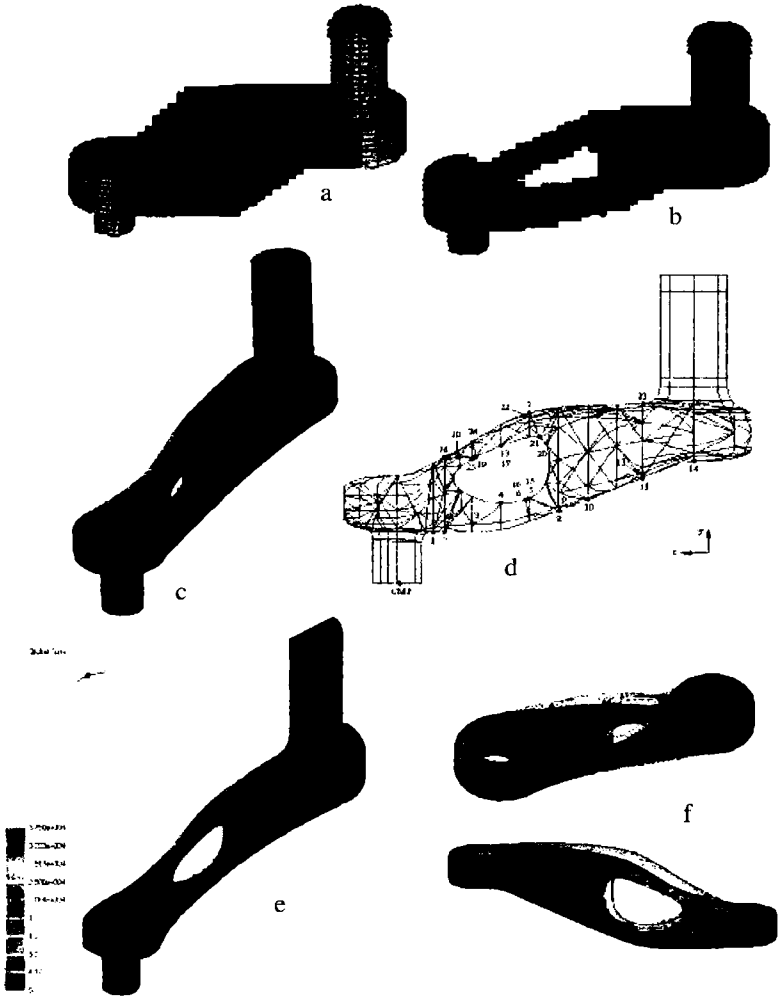

Fig. 1.27. Inegrated optimal design of a vehicle roadarm. a) Initial Finite Element Model, b) topology optimized roadarm, c) reconstructed solid model, d) Finite Element mesh for shape design e) Von Mises stress of the shape optimized design and f) comparison of the 3D Roadarm before and after shape design (Light grey: initial design, dark grey: optimized design) (from Tang & Chang 2001).

1.5 Variations of the theme

1.5.1 Multiple loads

The framework described for minimum compliance design for a single load case generalizes easily to the situation where design for multiple load conditions is formulated as a minimization of a weighted average of the compliances for each of the load cases. We here obtain a simple multiple load formulation as:

$$\begin{aligned} &\min_{u^k \in U, E} \sum_{k=1}^{M} w^k l^k(u^k) \\ &\text{s.t.} \quad a_E(u^k, v) = l^k(v), \quad \text{for all } v \in U,\ k = 1, \ldots, M \\ &\qquad E \in \mathsf{E}_{\text{ad}} \ , \end{aligned} \tag{1.33}$$

for a set $w^k, f^k, t^k, l^k,\ k = 1, \ldots, M$, of weighting factors, loads and tractions, and corresponding load linear forms given as

$$l^k(u) = \int_\Omega f^k u \, \mathrm{d}\Omega + \int_{\Gamma_T^k} t^k u \, \mathrm{d}s \ ,$$

for the M load cases we consider.

In this formulation the displacement fields for each individual load case are independent, thus implying that the multiple load formulation for the displacement based case has the equivalent form

$$\begin{aligned} &\max_{E \in \mathsf{E}_{\text{ad}}} \min_{\substack{\hat{u} = \{u^1, \ldots, u^M\} \\ u^k \in U,\ k=1,\ldots,M}} \left\{ \int_\Omega W(E, \hat{u}) \mathrm{d}\Omega - l(\hat{u}) \right\} \\ &W\big(E, \hat{u} = \{u^1, \ldots, u^M\}\big) = \frac{1}{2} \sum_{k=1}^{M} w^k E_{ijpq}(x) \varepsilon_{ij}(u^k) \varepsilon_{pq}(u^k) \ , \\ &l\big(\hat{u} = \{u^1, \ldots, u^M\}\big) = \sum_{k=1}^{M} w^k l^k(u^k) \end{aligned} \tag{1.34}$$

Likewise, we have a stress based formulation

$$\min_{E \in \mathsf{E}_{\text{ad}}} \min_{\substack{\operatorname{div} \sigma^k + f^k = 0 \text{ in } \Omega, \\ \sigma^k \cdot n = t^k \text{ on } \Gamma_T^k \\ k=1,\ldots,M}} \left\{ \frac{1}{2} \int_\Omega \sum_{k=1}^{M} w^k C_{ijkl} \sigma_{ij}^k \sigma_{pq}^k \mathrm{d}\Omega \right\} \tag{1.35}$$

For the stiffness modelled as in the SIMP model, the optimality criteria method developed for the single load case generalizes directly and we obtain an update scheme for ρ_K at iteration step K which is exactly the same as given in (1.12) of section 1.2.1, but with a modified "energy" expression

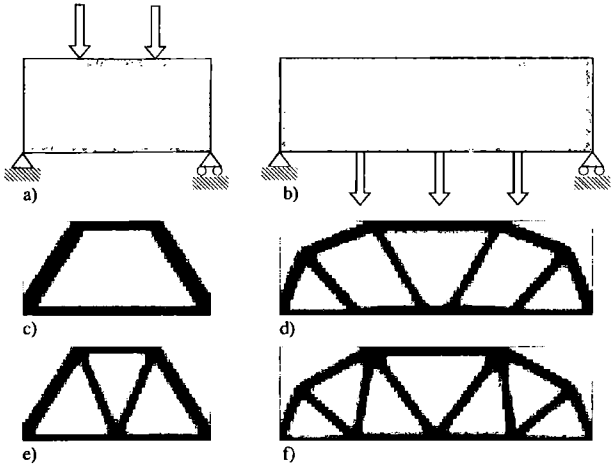

Fig. 1.28. Example of differences in using one or more load cases. a) and b) Design domains. c) and d) Optimized topologies for all loads in one load case. e) and f) Optimized topologies for multiple loading cases. It is seen that single load problems result in instable structures based on square frames whereas multi load case problems results in stable structures based on triangular frames.

$$B_K = \Lambda_K^{-1} p\rho(x)^{(p-1)} E^0_{ijkl} \sum_{k=1}^{M} w^k \varepsilon_{ij}(u_K^k)\varepsilon_{pg}(u_K^k)$$

Similarly, for use of an algorithm like MMA, the sensitivity of the weighted average of compliances just becomes the weighted average of the sensitivities of each of the compliances. Also, the similarity of the iterations in MMA and in the the optimality criteria method remains. Finally, it may be remarked that the inclusion of extra load cases is very cheap since the stiffness matrix already has been factorized.

1.5.2 Variable thickness sheets

For planar problems, the stiffness tensors given by the SIMP method reduces to the setting of the well-known variable thickness sheet design problem if we set $p = 1$; in this circumstance the density function ρ is precisely the thickness h of the sheet. The minimum compliance problem then becomes

$$
\begin{aligned}
&\min_{u,\rho} \quad l(u) \\
&\text{s.t.}: a_h(u,v) \equiv \int_\Omega h(x) E^0_{ijkl} \varepsilon_{ij}(u) \varepsilon_{kl}(v) \mathrm{d}\Omega = l(v), \ \text{for all } v \in U \\
&\int_\Omega h(x) \mathrm{d}\Omega \leq V, \ h_{\min} \leq h \leq h_{\max} < \infty
\end{aligned}
\tag{1.36}
$$

Problem (1.36) can also be written as (cf., (1.6))

$$
\begin{aligned}
&\min_{\substack{h \in L^\infty(\Omega), \\ h_{\min} \leq h \leq h_{\max} < \infty \\ \int_\Omega h(x) \mathrm{d}\Omega \leq V}} \quad c(h) \\
&c(h) = \min_{v \in U} \left\{ 2l(v) - \int_\Omega h(x) E^0_{ijkl} \varepsilon_{ij}(v) \varepsilon_{kl}(v) \mathrm{d}\Omega \right\}
\end{aligned}
\tag{1.37}
$$

As the stiffness is linear in h, the compliance c is convex, as it is given as a maximization of convex functions. Also, the complete problem statement (1.37) is a convex-concave saddle point problem that (as noted earlier) lends itself to a complete FE convergence analysis (see Petersson (1999b)) within the framework of the theory developed for the Stokes' flow problem. The variable thickness sheet design problem also corresponds very closely to truss design problems in the sense that the stiffness of the structure as well as the volume of the structure depend linearly on the design variable for both models. This implies that a discrete version of the problem can be solved using some very efficient algorithms that have been developed for truss topology design (cf. Chap. 4). These algorithms do not require that $h_{\min} > 0$, and the setting thus allows for a prediction of the the optimal topology of the sheet without the ambiguity inherent in the chosen value of $h_{\min}$; this is especially important here as we do not force the design towards a 0-1 design.

The linear dependence of the stiffness on the design function h has an even more significant implication for the continuum problem, as one can prove existence of solutions (see appendix 5.2.1). Thus there is no need for restriction methods or the introduction of materials with micro structure (this holds for minimization of compliance and optimization of the fundamental frequency). Finally, we remark that the variable thickness sheet problem also plays a significant role when considering optimal design within a completely free parametrization of the stiffness tensors over all positive definite tensors in 2-D as well as 3-D. Here the problem form (1.36) arises after a reduction of the original full formulation; this will be discussed in detail in Chap. 3.

Explicit penalization of thickness The variable thickness design problem has been used as the inspiration for topology design methods where one seeks the optimum over all isotropic materials with given Poisson ratio and linearly varying Young's modulus [11]. This formulation results in designs with large domains of "grey" and modifications are necessary to obtain 0-1 designs. This can be accomplished by adding to the objective an explicit penalty of

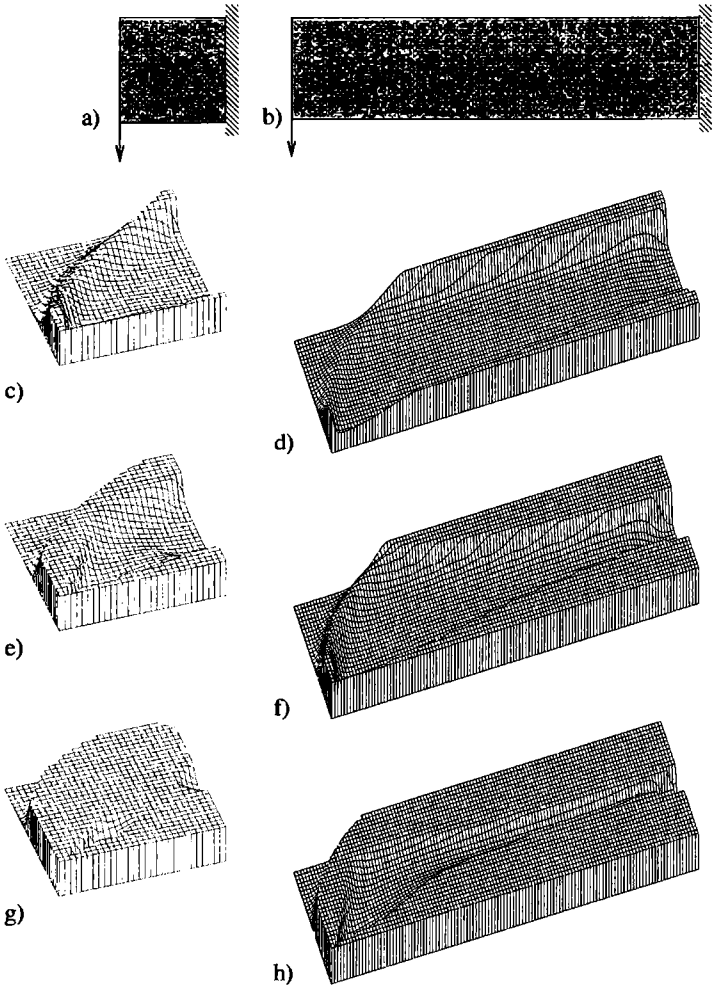

Fig. 1.29. The design of a variable thickness sheet for two cantilever-like ground structures with aspect ratios a) 1:1 and b) 1:4. c) – h): The optimal designs for a volume constraint c) and d) 30%, e) and f) 60% and g) and h) 90%, respectively, of the volume of a design with uniform thickness $h_{\max}$ (cf. constraints on thickness). Notice that the areas of intermediate thickness is considerable, especially for low amounts of available material. Thus the variable thickness design does not predict the topology of the structure as a true 2-dimensional object, but utilizes that the structure is in effect a 3-dimensional object.

intermediate densities, for example in the form of functionals (we revert to using a density ρ as the design variable):

$$\mathcal{W}(\rho) = \int_\Omega \rho(x)(1-\rho(x))\mathrm{d}\Omega,\ \hat{\mathcal{W}}(\rho) = \int_\Omega \rho(x)^2(1-\rho(x))^2\mathrm{d}\Omega \tag{1.38}$$

Alternatively, the penalty function can be used as a constraint $\mathcal{W}(\rho) \leq \delta$ for some small $\delta \geq 0$.

The use of a penalty function such as $\mathcal{W}$ (or $\hat{\mathcal{W}}$) has a detrimental effect on the very nice mathematical properties of the original variable thickness sheet problem. For one, existence of solutions is no longer true. However, existence of solutions can be recovered (Borrvall & Petersson 2001b) by modifying the penalty function (1.38) to the form

$$\widetilde{\mathcal{W}}(\rho) = \int_\Omega (\rho * K)(x)(1-(\rho * K)(x))\mathrm{d}\Omega\ , \tag{1.39}$$

where one evaluates the original penalty function on a *filtered* version of the density ρ (we use here the notation introduced in section 1.3.1). The filter smoothes the density before penalization and as such provides for a more severe penalization than does $\mathcal{W}$ (for details, consult Borrvall & Petersson (2001b)). Thus using $\widetilde{\mathcal{W}}$, the designs become almost entirely black and white (a 0-1 design) if the penalty factor is large enough (see Fig. 1.12).

The penalty approach just outlined maintains the existence of solutions for the problem of minimum compliance and the maximization of the fundamental frequency. If a broader range of problems is to be considered the restriction techniques, as described in section 1.3.1, should be applied. Note also that the use of the penalty $\widetilde{\mathcal{W}}$ makes it impossible to use the efficient truss-type algorithm mentioned above (but an MMA inspired optimality criterion method is an efficient alternative (Borrvall & Petersson 2001a)).

In order to maintain the structure of the original computational problem it has been suggested instead to consider a sequence of problems where the volume constraint in each step K of the sequence is modified as (see for example Guedes & Taylor (1997), Rodrigues, Soto & Taylor (1999))

$$\int_\Omega w_K(x)\rho(x)\mathrm{d}\Omega \leq V$$

where the weight function w_K is fixed and determined from the optimal solution ρ_{K-1} to the prior step so as to penalize low density regions:

$$w_K(x) = \begin{cases} T_K & \text{if} \rho_{K-1} \leq \delta \\ 0 & \text{otherwise} \end{cases}$$

With suitable big values of T_k and a small value of δ this scheme generates 0-1 designs and each step is computationally equivalent to the original variable thickness sheet problem. In implementation, the tuning of the penalization becomes an issue. Also note that as above, the advantages of this idea is closely linked to the properties of the minimum compliance problem.

1.5.3 Plate design

Studies of the problem of variable thickness plate design and the appearance of stiffeners in such design problems have played a crucial role in the developments in optimal structural design [29]. Thus topology design and especially design with materials with microstructure can be seen as a natural extension of the original work by Cheng and Olhoff on plates. In this sense this exposition of topology design methods is reversed relative to history, but it is today more natural to consider plate design as a special variation of the general framework.

The design of variable thickness Kirchhoff plates or Mindlin plates is at first glance just another sizing problem of finding the optimal continuously varying thickness of the plate. The close connection with the 0-1 topology design problems is not entirely evident, but the cubic dependence of plate bending stiffness on the thickness of the plate implies that the optimal design prefers to achieve either of the bounds on the thickness, in essence a plate with integral stiffeners. This in turn implies non-existence of solutions unless the gradient of the thickness function is constrained or the problem is extended to include fields of infinitely many stiffeners; this latter concept is dealt with in Chap. 3.

Variable thickness design of Kirchhoff plates The minimum potential energy statement for a Kirchhoff plate is of the form[16]

$$\min_w \left\{ \frac{1}{2} \int_\Omega \frac{h^3}{12} E^0_{ijkl} \kappa_{ij}(w) \kappa_{kl}(w) \mathrm{d}\Omega - \int_\Omega f w \mathrm{d}\Omega \right\}$$

where f is the transverse load. The thickness of the plate is denoted by h and we assume that the mid-plane is a plane of symmetry. The deformation of the plate is described by the transverse displacement of the mid-plane w, with associated (linearized) curvature tensor $\kappa_{ij} = \frac{\partial^2 w}{\partial x_i \partial x_j}$, and the relationship between the curvature tensor and moment tensor M is given as

$$M_{ij} = D_{ijkl} \kappa_{kl} \qquad \text{with} \quad D_{ijkl} = \frac{h^3}{12} E^0_{ijkl}$$

where E^0_{ijkl} is the plane stress elasticity tensor of the given material. The similarity between the curvature-moment relation for plates and the strain-stress relation in elasticity hides the fundamental difference that the Kirchhoff plate is governed by a fourth order scalar equation, while standard linear elasticity is governed by a system of second order equations. As for the variable thickness sheet problem, the thickness of the plate also here automatically provides the plate design problem with a continuous design variable. Considering the minimization of compliance the most natural problem to consider is thus

[16] Here and elsewhere in this section (section 1.5.3) all indices range over 1 and 2.

$$\max_{D\in \mathsf{PE}_{ad}} \min_{w} \left\{ \frac{1}{2}\int_\Omega D_{ijkl}\kappa_{ij}(w)\kappa_{kl}(w)\mathrm{d}\Omega - \int_\Omega fw\mathrm{d}\Omega \right\} \tag{1.40}$$

with the set $\mathsf{PE}_{\mathrm{ad}}$ of bending stiffnesses given as

$$\begin{aligned} D_{ijkl} &= \tfrac{h^3}{12}E^0_{ijkl}, \quad h \in L^\infty(\Omega)\,, \\ 0 \le h_{\min} \le h \le h_{\max} &< \infty, \quad \textstyle\int_\Omega h\mathrm{d}\Omega \le V \end{aligned} \tag{1.41}$$

which looks like a SIMP interpolation scheme! Also in the plate setting, problem (1.40) with the design set (1.41) is not well posed, and the existence of solution is not always assured. This was first vividly demonstrated by Cheng & Olhoff (1981), who discovered the formation of stiffeners in numerically computed "optimal" solutions for high ratios of $h_{\max}/h_{\min}$ and $h_{\max}/h_{\mathrm{unif}}$, where $h_{\mathrm{unif}} = V/\int_\Omega \mathrm{d}\Omega$, see Fig. 3.21 in Chap. 3. The number of stiffeners increase when the discretization of design is refined, with a resulting (substantial) decrease in compliance, a situation completely similar to the behaviour of the 0-1 topology design setting. Compared to the variable thickness design problem for sheets, this is caused by the cubic dependence of the stiffness of the plate on the thickness. Physically, this dependence makes it advantageous to move as much material as possible away from the mid-plane of the plate, for example in the form of integral stiffeners. A method to obtain mesh-independence and existence of solutions is analogous to what has been described in section 1.3.1, by restricting the variation of the thickness function, for example in the form of a constraint on the slope (gradient) of the thickness function. Example solutions with a point wise bound on the slope of the thickness of a rotational symmetric plate were first shown in Niordson (1983).

The computational procedure for computing optimal plate designs is completely analogous to the procedure described earlier in this chapter and the optimality criteria and sensitivity calculations carry over ad verbatim, with strains and stresses interpreted as curvatures and moments, respectively.

Topology design for Mindlin plates We close this brief discussion on plate design by considering some models for the design of Mindlin plates.

The minimum potential energy statement for a *constant thickness* Mindlin plate constructed from one material is of the form

$$\min_u \left\{ \begin{array}{c} \frac{1}{2}\int_\Omega hE^0_{ijkl}\varepsilon_{ij}(u)\varepsilon_{kl}(u)\mathrm{d}\Omega + \frac{1}{2}\int_\Omega \frac{h^3}{12}E^0_{ijkl}\kappa_{ij}(u)\kappa_{kl}(u)\mathrm{d}\Omega \\ +\frac{1}{2}\int_\Omega hD^S_{ij}\gamma_i(u)\gamma_j(u)\mathrm{d}\Omega - \left(\int_\Omega fu\mathrm{d}\Omega + \int_{\Gamma_t} tu\mathrm{d}\Gamma\right) \end{array} \right\}$$

where f is the transverse and t the in-plane load. The thickness of the plate is denoted by h and we assume that the mid-plane is a plane of symmetry Also, E^0_{ijkl} is the plane stress elasticity tensor and D^S is the transverse shear stiffness matrix. In Mindlin plate theory generalized displacements of the plate $u = (u_1, u_2, w, \theta_1, \theta_2)$ consist of the in-plane displacements (u_1, u_2), the fibre

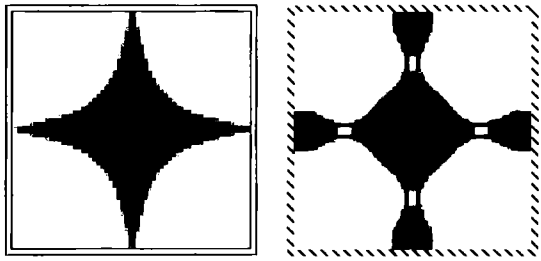

Fig. 1.30. Resulting topologies for compliance minimization of square Mindlin plates. The material volumes are restricted to 25% of the filled plates and the plates are loaded with a force at the center. a) Simply supported and b) clamped plate (from Pedersen 2001).

rotations (θ_1, θ_2) and the transverse displacement of the mid-plane w The associated membrane, bending, and transverse shear strains are, respectively,

$$\varepsilon_{ij} = \frac{1}{2}(\frac{\partial u_i}{\partial x_j} + \frac{\partial u_j}{\partial x_i}), \quad \kappa_{ij} = \frac{1}{2}(\frac{\partial \theta_i}{\partial x_j} + \frac{\partial \theta_j}{\partial x_i}), \quad \text{and} \quad \gamma_i = \frac{\partial w}{\partial x_i} - \theta_i$$

For plates there are several options for performing topology design, connected to the possibility to also consider out-of-plane variations of the build-up of the plate. For the design of a perforated plate one would thus use thickness functions that attain values 0 or $\bar{h}$, for example implemented with the help of a density function ρ and a SIMP interpolation:

$$h = \rho^p \bar{h} \ , \quad \text{Vol} = \int_\Omega \rho \bar{h} \mathrm{d}\Omega$$

Other possibilities is to consider *reinforcement* of a given plate or to consider the design of a sandwich structure, where two outer skins are given and the topology design deals with the topology design of the inner core [29].

1.5.4 Other interpolation schemes with isotropic materials

The use of SIMP or the penalized variable thickness formulation have in the last few years been supplemented by some alternative interpolation schemes that have certain theoretical or computationally advantageous features for specific problems. As they fall within the class of interpolation models with isotropic materials we briefly discuss them in this chapter. The use of composites is the theme of Chap. 3.

Hashin-Shtrikman bounds The so-called Hashin-Shtrikman bounds for two-phase materials express the limits of *isotropic* material properties that

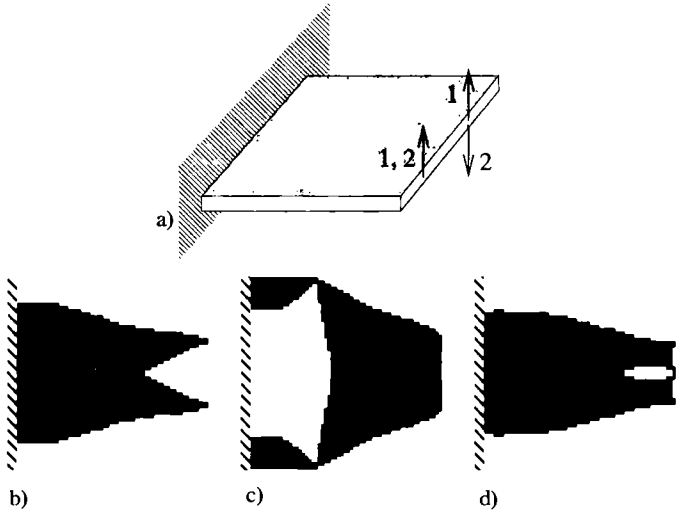

Fig. 1.31. Resulting topologies for compliance minimization of square Mindlin cantilever plates. a) Design problem with loads for the first and the second load case. b) Solution to one-load case problem with two upward oriented forces, c) solution to one-load case problem with one force upwards and one downwards and d) solution to two load case problem. The volume fraction is 50% (by Niels L. Pedersen).

one can possibly achieve by constructing composites (materials with microstructure) from two (or more) given, linearly elastic, isotropic materials [4]. These bounds give expressions of material parameters as functions of volume fraction, or for our purposes as functions of density ρ of material, and can thus be employed as interpolation schemes (all material laws involved will be isotropic). For our purposes we work with two materials, one with a low stiffness $E^{\min}$ and one with high stiffness E^0 The corresponding values of the Poisson ratios are $\nu^{\min}$ and ν^0

The Hashin-Shtrikman bounds are typically expressed in terms of the bulk and shear moduli of the materials , κ and μ (corresponding to the eigenvalues of the stiffness tensor). Restricting ourselves here to 2-D plane elasticity, we have for isotropic materials that

$$\kappa = \frac{E}{2(1-\nu)}; \quad \mu = \frac{E}{2(1+\nu)} \qquad (\text{in } 2-D) \ .$$

The bounds are then in terms of these parameters (in 2-D)[17] (we assume here that $\kappa^0 \geq \kappa^{\min}$ and $\mu^0 \geq \mu^{\min}$):

$$\kappa^{HS}_{\text{upper}} = (1-\rho)\kappa^{\min} + \rho\kappa^0 - \frac{(1-\rho)\rho(\kappa^{\min}-\kappa^0)^2}{(1-\rho)\kappa^0 + \rho\kappa^{\min} + \mu^0}\,, \tag{1.42}$$

$$\mu^{HS}_{\text{upper}} = (1-\rho)\mu^{\min} + \rho\mu^0 - \frac{(1-\rho)\rho(\mu^{\min}-\mu^0)^2}{(1-\rho)\mu^0 + \rho\mu^{\min} + \frac{\kappa^0\mu^0}{\kappa^0+2\mu^0}} \tag{1.43}$$

$$\kappa^{HS}_{\text{lower}} = (1-\rho)\kappa^{\min} + \rho\kappa^0 - \frac{(1-\rho)\rho(\kappa^{\min}-\kappa^0)^2}{(1-\rho)\kappa^0 + \rho\kappa^{\min} + \mu^{\min}}\,, \tag{1.44}$$

$$\mu^{HS}_{\text{lower}} = (1-\rho)\mu^{\min} + \rho\mu^0 - \frac{(1-\rho)\rho(\mu^{\min}-\mu^0)^2}{(1-\rho)\mu^0 + \rho\mu^{\min} + \frac{\kappa^{\min}\mu^{\min}}{\kappa^{\min}+2\mu^{\min}}} \tag{1.45}$$

Each combination of formulas $\kappa^{HS}_{\text{upper}}, \mu^{HS}_{\text{upper}}$ and $\kappa^{HS}_{\text{lower}}, \mu^{HS}_{\text{lower}}$ represents an interpolation of the material properties of the two materials, and any convex combination is also and interpolation scheme, which then satisfies the bounds. Thus a whole range of schemes can be generated. Here the *lower* bound interpolation penalizes intermediate densities most. Note that the Hashin-Shtrikman bounds represent materials that have both a Young's modulus *and* a Poisson ratio that vary with density (even if the two base materials have the same Poisson ratio).

If both materials have Poisson ratio equal to 1/3, then the upper and lower bounds (and all convex combinations) also represent a material law with Poisson ratio $\nu = 1/3$, and the bound can be expressed in terms of the Young's modulus only:

$$\text{for } \nu = 1/3 \quad \begin{cases} E^{HS}_{\text{upper}} = E^0 \dfrac{\rho E^0 + (3-\rho)E^{\min}}{(3-2\rho)E^0 + 2\rho E^{\min}}\,, \\ E^{HS}_{\text{lower}} = E^{\min} \dfrac{(2+\rho)E^0 + (1-\rho)E^{\min}}{2(1-\rho)E^0 + (1+2\rho)E^{\min}} \end{cases} \tag{1.46}$$

This reduces further if the weak material is void ($E^{\min} = 0$):

$$E_{\text{upper}} = \frac{\rho E^0}{3-2\rho} \qquad E_{\text{lower}} = \begin{cases} 0 & \text{for } \rho < 1\,, \\ E^0 & \text{for } \rho = 1\,, \end{cases} \tag{1.47}$$

which is then an interpolation with void and with a material with $\nu = 1/3$ and Young's modulus E^0 For many test cases in topology design one works within this framework of $\nu = 1/3$.

[17] The bounds are *necessary conditions*. It is known that not all combinations of numbers κ and μ that satisfy the bounds actually represent the bulk and shear moduli of a realizable material - see Chap. 2.

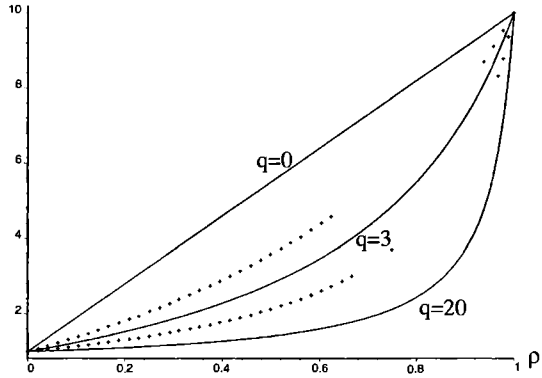

Fig. 1.32. The interpolation using RAMP (solid curves) compared with the Hashin-Shtrikman bounds (dotted curves).

SIMP and the Hashin-Shtrikman bound If we require that an interpolation model in any sense can be related to a composite made of the given materials, then we should demand that the model satisfies the Hashin-Shtrikman bounds stated above. For SIMP one of the material phases is zero, i.e., $E^{\min} = 0$. Then the only relevant Hashin-Shtrikman bound (1.42) simplify somewhat and it is possible to show that SIMP satisfies the bounds if the power of the model satisfies the inequalities stated in (1.5) (Bendsøe & Sigmund 1999). As already noted, this does not assure that a composite can actually be constructed. But we shall in Chap. 2 see how topology design (sic!) can be used to construct microstructures that realizes the SIMP interpolation scheme.

An approach with rational functions In the section on the variable thickness sheet problem it was seen how the expression of the compliance c via the potential energy makes it possible to conclude that the compliance in that situation is convex. On the other hand, if c is derived in terms of the complementary energy (cf., (1.7), we have that

$$c = \min_{\sigma \in S} \left\{ \int_\Omega C_{ijkl}\sigma_{ij}\sigma_{kl} \mathrm{d}\Omega \right\} \tag{1.48}$$

This shows that if one can make the compliance tensor C_{ijkl} a concave function of the design, then c, as a minimization of concave functions, becomes concave. And this is advantageous if we want 0-1 designs that are on the "border" of the space of densities (this will be made precise below). For interpolating the compliance we cannot work with vanishing stiffness, but instead operate with a low stiffness $E^{\min}$ and interpolate between this and the properties E^0 (we assume constant Poisson ratio). The simplest concave

interpolation of the inverse of the Young's modulus E is then the linear one (as proposed in Stolpe & Svanberg (2001b) and Rietz (2001)), which is

$$\frac{1}{E(\rho)} = \frac{1}{E^{\min}} + \rho\left(\frac{1}{E^0} - \frac{1}{E^{\min}}\right)$$

This, in turn, corresponds to the following rational expression for E:

$$E(\rho) = E^{\min} + \frac{\rho}{1+q(1-\rho)}\left(E^0 - E^{\min}\right) \tag{1.49}$$

where $q = \bar{q}$, $\bar{q} \equiv (E^0 - E^{\min})/E^{\min}$ (the corresponding expression for SIMP is $E = E^{\min} + \rho^p\left(E^0 - E^{\min}\right)$). The relation given in (1.49) can also be used for other values of q; the scheme has in certain circumstances been given the acronym RAMP for Rational Approximation of Material Properties.

The interpolation (1.49) makes, by construction, the compliance a concave function of ρ if q is chosen as $q = \bar{q}$ (or bigger). Moreover, $q \quad 0$ gives the linear interpolation (which makes compliance convex), and for materials with Poisson ratio 1/3 the interpolation equals the Hashin-Shtrikman *upper* bound for $q = 2(E^0 - E^{\min})/(E^0 - 2E^{\min})$ and the Hashin-Shtrikman *lower* bound for $q = \frac{2}{3}\bar{q}$. The intermediate densities are thus severely penalized for larger values of q, cf., figure 1.5.4. A natural continuation method using this interpolation scheme is then to begin the optimization procedure with $q = 0$ and then increase q until $q \geq \bar{q}$. The concavity of compliance for such large values of q implies the existence of a globally optimal 0-1 solution for a FE discretized version of the problem, for example where we use element wise constant densities in a mesh of squares, only the simple bounds $0 \leq \rho \leq 1$ and a volume constraint that is an integer times the volume of the base element (Stolpe & Svanberg 2001b). This has the added side effect that one can conclude similarly for the SIMP interpolation[18]provided we choose $p \geq (\bar{q} + 1)$ If for example a perimeter constraint is added to the problem statement this property does not hold any longer; however, the intrinsic penalization of the interpolation still results in designs that are almost free of grey, if q is large enough. It is also worth noting that if $E^{\min}$ is much smaller than E^0 (as typical for finding the topology of a structure made from one material), then the "magic" value $\bar{q}$ becomes large (and infinite for the limit of $E^{\min} = 0$).

We remark here that if design of two-material structures is the goal of the topology optimization, the RAMP model is in a sense more physical than SIMP. The latter will always violate the Hashin-Shtrikman bounds for small density values, while RAMP has a whole range of q values for which the bound is satisfied (for a Poisson ratio 1/3). However, RAMP does not satisfy these bounds for the range of q where the compliance becomes concave.

[18] This follows from the property that for a given ρ, the SIMP interpolation gives a higher compliance than the RAMP interpolation, when $p \geq q + 1$.

A Reuss-Voigt interpolation scheme The Voigt upper bound for the effective properties of a mixture of two materials state that for any strain field ε we have that the strain energy W of the composite is bounded from above by the expression

$$W \leq \left[\rho E^0_{ijkl} + (1-\rho)E^{\min}_{ijkl}\right]\varepsilon_{ij}\varepsilon_{kl} \ ,$$

where the two materials have elasticity tensors E^0 and $E^{\min}$, respectively, and where the volume fraction of the material E^0 is ρ. Likewise, the Reuss lower bound states that the energy W is bounded from below by the expression

$$W \geq \left[\rho C^0_{ijkl} + (1-\rho)C^{\min}_{ijkl}\right]^{-1}\varepsilon_{ij}\varepsilon_{kl} \ ,$$

where C denotes the compliance tensors of the materials.

These two bounds can be combined to a convex combination to what has been named a Reuss-Voigt interpolation scheme (Swan & Arora 1997, Swan & Kosaka 1997a)

$$E^{VR}_{ijkl}(\rho) = \alpha\left[\rho E^0_{ijkl} + (1-\rho)E^{\min}_{ijkl}\right] + (1-\alpha)\left[\rho C^0_{ijkl} + (1-\rho)C^{\min}_{ijkl}\right]^{-} \tag{1.50}$$

Here α is a parameter which weighs the contributions from the Voigt and Reuss bounds. If one of the materials is void, the interpolation introduces a jump (discontinuity) at $\rho = 1$ which is not present if both materials have some stiffness. In that case, for two materials that both have a Poisson's ratio of $\nu = 1/3$ we have that the Hashin-Shtrikman bounds are satisfied if and only if $\alpha = 1/3$ (Bendsøe & Sigmund 1999).

Spline-based approach The SIMP interpolation scheme has zero slope at zero density. Thus the stiffness converges to zero orders of magnitude faster than mass and this has proven to be a difficulty when considering vibration problems. For benign computational behaviour in these problems (see section 2.1) one needs an interpolation scheme where the ratio of mass to stiffness ($\rho/E(\rho)$) remains finite in the limit of vanishing density ρ. The RAMP scheme and the Hashin-Shtrikman bound schemes have this feature. Another way to secure this property is to construct a Bézier curve interpolation in the (ρ, E)–plane that connects the two points $(0,0)$ and $(1, E^0)$ and has tangents $(1, k_1)$ and $(1, k_2)$, respectively, at the endpoints. As shown in Pedersen (2002e), such a Bézier curve with four control points can be given a parametrization as

$$\left.\begin{aligned} \rho(t) &= \frac{1-k_1}{k_1-k_2}(3t-3t^2)+t^3 \\ E(t) &= k_1\frac{1-k_1}{k_1-k_2}(3t-3t^2)+t^3 \end{aligned}\right\}, \quad t \in [0,1] \ . \tag{1.51}$$

For a given density, the first equation gives the corresponding parameter value t, and this in turns gives the stiffness E. For (1.51) to satisfy the Hashin-Shtrikman bounds for (Poisson ratio 1/3) one needs to choose the slopes so that $k_1 \leq 1/3$ and $k_2 \geq 3$, and as for the other schemes, almost 0-1 designs are best achieved through a continuation method. Here that means working with decreasing values of k_1 and increasing values of k_2.

1.5.5 Design parametrization with wavelets

The possibility of controlling geometric features of the designs that are obtained from topology design has already been a central theme in section 1.3.1. There such control is basically achieved by filtering techniques or by imposing constraints on the pixel (voxel) based description of design. Another possibility should be to work with alternative design descriptions that inherently allows for some form of control of geometric complexity. This means that one will express the density function ρ in terms of basis functions where the coefficients will govern aspects of the geometry. A natural choice for such a representation is *wavelets*, as these can represent data that is localized in space as well as in frequency [11].

The general framework of wavelet representation of image data will not be treated here. Instead we will indicate how one from a pixel representation can construct an alternative design description that directly works with data at different scales[19] We take as the starting point the setting of the patch-based checkerboard control described in section 1.3.2. As a first step of changing the design representation one chooses to describe the density distribution in the domain as

$$\rho(x) = \sum_{\mathrm{P}_{ij}} (v_{ij}^1 \phi_{ij}^1 + v_{ij}^2 \phi_{ij}^2 + v_{ij}^3 \phi_{ij}^3 + v_{ij}^4 \phi_{ij}^4) \ ,$$

where the basis functions ϕ_{ij}^k, $k = 1, 2, 3, 4$, are illustrated in Fig. 1.20. In this expansion the coefficients v_{ij}^1 represents the average value of the densities in the patch, and the other coefficients express the local variations from this average. One can now consider the larger scale mesh consisting of the patches P_{ij} and the corresponding average values v_{ij}^1, which can be likened to standing back from a picture so that local variations are averaged out. Here we can again repeat this procedure of expanding in terms of basis functions $\tilde{\phi}_{ij}^k$, $k = 1, 2, 3, 4$, at this larger scale of working with 4-patches of the the patches P_{ij} (and the values v_{ij}^1). This procedure is possible to perform if the number of elements per side is 2^M by 2^N, and it can be continued until the last patch consists of the full domain divided into four "super-elements" In terms of a design representation, we now have parameters that at different levels of

[19] This is based on the discrete Haahr-wavelet and the associated Mallat decomposition.

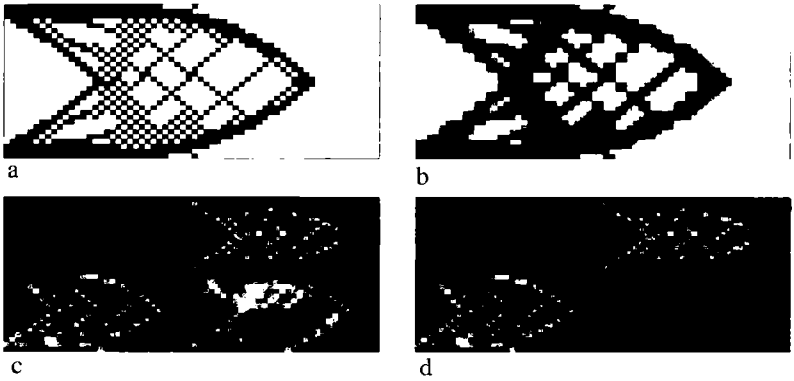

Fig. 1.33. A design with checkerboards, here shown in terms of its a) pixel values and c) in terms of the basis functions ϕ_{ij}^k, $k = 1, 2, 3, 4$: the top left quarter of c) is the design in a spatial resolution which is half the original one, and the three other quarters represent the difference from this to the original design in various ways. The original design in a) can be obtained by combining the four parts. In b), checkerboards have been removed by setting the lower right corner of c) equal to zero, as shown in d) (from Poulsen 2002).

fineness describe the density in terms of averages and variations from the averages.

The alternative parametrization of design just outlined gives a direct way to control the overall length scale from the level of fineness of the basis functions that are applied. Moreover, it makes it possible to systematically do the design process from coarse scale to fine scale (Kim & Yoon 2000). Finally, it makes it possible to work directly with a checkerboard-free design space, as seen in section 1.3.2. However, the wavelet representation should not be used directly in topology optimization, as it introduces a huge number of constraints associated with the condition $0 \leq \rho \leq 1$ which regretfully reduces computational efficiency. Instead, it is recommended to use intermediate variables as described in section 1.3.2 (Kim & Yoon (2000), Poulsen (2002)).

We close this brief sketch by noting that wavelet based methods have also been used as an alternative to finite elements for the analysis part of topology design, see DeRose Jr. & Díaz (1999), DeRose Jr. & Díaz (2000). Moreover, it is expected that use of more advanced wavelet bases than the Haahr-wavelet should potentially lead to more refined methodologies to control geometry.

1.5.6 Alternative approaches

The technique for topology design of continuum structures that is described in this monograph is based on the concept of optimal distribution of material, using interpolation of material properties together with mathematical programming. As we shall see in Chap. 2, this is a universally efficient approach for a broad range of problems in engineering design. In parallel with the development of this methodology, other schemes have also evolved [13]. Some of these work within the same modelling framework using algorithms for *discrete* optimization or various types of growth/shrinking procedures, but a completely different modelling paradigm can also be found in for example the *bubble method*. We will here only briefly mention some of these concepts, and refer to Eschenauer & Olhoff (2001) for a survey.

Solving the discrete problem The introduction of the interpolation schemes for the 0-1 design problem is extremely useful as it allows for the use of mathematical programming methods for continuous (smooth) problems. However, it would be very useful if one could attack the original formulation directly[20] [13]. This has been done for the compliance design problem using dual methods, that have been shown to be effective in the absence of local constraints. Methods like simulated annealing or genetic algorithms have also been tested for more general settings, but their need for many function evaluations is computationally prohibitive, but for rather small scale examples (each call involves a costly finite element analysis on a grid at least as fine as the raster representation of the design).

It has been shown recently (Stolpe & Svanberg 2001a) that for a broad class of problems one can formulate the 0-1 topology design problem as a *linear* mixed continuous-integer programming problem and this will no doubt be useful for generating more efficient methods for treating the discrete format in the future.

Growing and shrinking a structure; Bone remodelling Numerous methods have been proposed for dealing with topology design without the use of mathematical programming [13]. They are typically named as "evolutionary" methods, but they are *not* in any way connected to the use of genetic algorithms. On the contrary, these methods typically work with concepts that are similar to the idea of *fully stressed design*, i.e., material is added to highly stressed areas of a design and removed from understressed areas of the design, typically implemented by an addition or removal of elements from the FE model.

Some implementations of such concepts are very similar to an optimality criteria type algorithm, but the removal and adding of elements can lead to erroneous results. This is basically because gradient information is used to

[20] In a well-posed form, for example with a perimeter constraint.

perform changes of variables between zero and one, as illustrated in Zhou & Rozvany (2001) for the case of minimum compliance design.

It is interesting to note that many models used in bio-mechanics for bone adaptation have a form which is similar to the optimality criteria algorithm described in section 1.2.1 [7]. These models are usually based on energy arguments and are not derived from an optimization principle. This similarity in approach to material redistribution updates has also lead to bone adaptation models being proposed as topology redesign methods.

Topological variations and level sets The concepts of *topological derivatives* and the *bubble method* is based on utilizing ideas from the boundary variations technique for shape design as a basis for topology design [13].

The topological derivative of a functional as compliance expresses the sensitivity with respect to the opening of a small (infinitesimal) hole at a certain position in the analysis domain. Likewise, in the bubble method a criterion is developed that allows for the prediction of the most effective location for creating a hole and this information is used to perform a boundary variations shape optimization of the resulting topology. The hole placement is then repeated in this shape optimized structure leading to good designs with smooth boundaries. A direct application of the topological derivative in a mathematical programming technique is presently not possible, as there is no evident underlying parametrization available; implementations have thus been based on techniques reminiscent of element removal techniques.

The application of level-set techniques for topology design have also been proposed recently [13]. The contours of a parametrized family of level-set functions are here used to generate the boundaries of a structure, and the topology can change with changes in the level-set function. This technique is in an initial stage of development.

2 Extensions and applications

In Chapter 1 we discussed the basics of the topology optimization method applied to compliance minimization. Due to the simple form of the compliance minimization problem, this problem was used as the fundamental test case in the initial developments of the topology optimization method. Despite its simplicity, the compliance minimization problem gives rise to non-trivial theoretical and numerical problems such as checkerboards, mesh-dependency and existence issues, and convergence to local minima. These problems have to be dealt with before one can proceed to more advanced applications and objective functions.

This chapter describes a range of advanced applications, emphasizing problem formulations and solution procedures. New numerical and theoretical problems like for example localized modes in low-density regions, one-node connected hinges, instability of low density elements for geometrical non-linear modelling, etc., appear for the more advanced applications, and we here discuss methods to avoid them.

One of the most challenging and difficult parts of applying the topology optimization method to new areas is to develop prudent choices and combinations of objective functions and constraints. This is mostly based on many experiments before arriving at "good" formulations that make physical sense and which can be handled by the modelling and the optimization algorithms. For example, structures that have been optimized with respect to a certain load case may be useless when subjected to another load case. Therefore, both (or more) load cases must be taken into account when formulating the optimization problem. During the process it is important to interpret the resulting topologies not only visually but also quantitatively. New methods and formulations should if possible be compared with analytical results and estimates. One should also check that the obtained results are better or at least as good as intuitive solutions.

In this chapter we mainly use the SIMP approach (1.4) to interpolate between solid and void material since this approach has proven to generalize easily to alternative applications. Unless otherwise stated we use filtering of sensitivities (1.27) to obtain checkerboard-free and mesh-independent designs. Also, the solution procedure follows the methodology described in section 1.2. This means that the optimization is based on the use of den-

sity as the primary variable, with state equations and associated sensitivity analysis being treated as a function call. For this reason we write all optimization problems with only the density as a free variable. Nonetheless, for easy identification of problem structure we still include the state equations in the formulation. Finally note that we throughout this chapter base all formulations on a discretized FE format.

The chapter is not meant as a comprehensive review of the area of advanced applications of topology design methods (see the bibliographical notes). Rather, we quite naturally orient the developments toward projects in which we have personally been involved.

2.1 Problems in dynamics

One of the first applications of the topology optimization method outside of compliance minimization was in eigenvalue optimization for free vibrations. This problem is relevant for the design of machines and structures subjected to dynamic loads [14]. For example, one may wish to keep the eigenfrequencies of a structure away from the driving frequency of an attached engine or one may wish to keep the fundamental eigenfrequencies well above possible disturbance frequencies. Also, structures with high fundamental eigenfrequency tend to be reasonable stiff for all conceivable loads and therefore maximization of the fundamental frequency results in designs that are also good for static loads.

In specialized cases, one may wish to maximize the dynamic response of a structure. This may be the case in sensors where the output signal is dependent on the vibration amplitude, in actuators where resonance phenomena may increase performance or in musical instruments and loudspeakers where the radiated sound power (over a wide spectrum of frequencies) should be maximized.

2.1.1 Free vibrations and eigenvalue problems

A commonly used design goal for dynamically loaded structures is the maximization of the fundamental eigenvalue λ_{min}. The problem formulation may be written as

$$\begin{aligned} &\max_{\boldsymbol{\rho}} \left\{ \lambda_{min} = \min_{i=1,\ldots,N_{dof}} \lambda_i \right\} \\ &\text{s.t.} \quad (\mathbf{K} - \lambda_i \mathbf{M})\boldsymbol{\Phi}_i = \mathbf{0}, \quad i = 1, \ldots, N_{dof} \\ &\qquad \sum_{e=1}^{N} v_e \rho_e \leq V, \qquad 0 < \rho_{min} \leq \rho_e \leq 1, \quad e = 1, \ldots, N \end{aligned} \tag{2.1}$$

where $\mathbf{K}$ and $\mathbf{M}$ are the system stiffness and mass matrices, respectively and $\boldsymbol{\Phi}_i$ is the eigenvector associated with the i'th eigenvalue. In practice one does

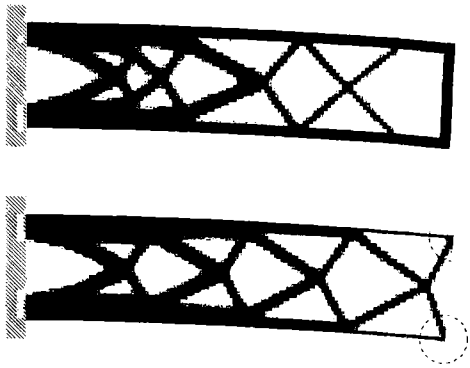

Fig. 2.1. Top: A reinforcement problem. Maximization of the fundamental eigenvalue of a 5-bay tower structure where the outer frame structure is fixed to be solid. Below: Maximization of the fundamental eigenvalue of a structure with non-structural masses (each with a mass of 10% of the distributable mass) attached on the rightmost corners. The structures are shown in their fundamental mode of vibrations.

not solve for all N_{dof} modes of the eigenvalue problem. Only the first up to 10 modes will usually play a role in determining the dynamical response of a structure.

Note that the problem (2.1) *as stated* has a trivial solution: one can in principle obtain an infinite eigenvalue by removing the entire structure. Therefore, the eigenvalue problem (2.1) is often used in "reinforcement" problems where parts of the structure are fixed to be solid (see Fig. 2.1) or there is a finite minimum thickness of the structure like a fixed shell thickness in the reinforcement optimization of an engine hood. Alternatively, non-structural masses may be added to parts of the design domain (see Figs. 2.1, 2.2 and 2.3).

An alternative to the formulation (2.1) is to apply the so-called bound-formulation

$$\begin{aligned} \max_{\boldsymbol{\rho}} \quad & \beta \\ \text{s.t.} \quad & \lambda_i \geq \beta, \quad i = 1, \ldots, N_{dof} \\ & (\mathbf{K} - \lambda_i \mathbf{M})\boldsymbol{\Phi}_i = \mathbf{0}, \quad i = 1, \ldots, N_{dof} \\ & \sum_{e=1}^{N} v_e \rho_e \leq V, \qquad 0 < \rho_{min} \leq \rho_e \leq 1, \quad e = 1, \ldots, N \end{aligned} \tag{2.2}$$

The sensitivities of a *single* modal eigenvalue are simply found as

$$\frac{\partial \lambda_i}{\partial \rho_e} = \boldsymbol{\Phi}_i^T \left[\frac{\partial \mathbf{K}}{\partial \rho_e} - \lambda_i \frac{\partial \mathbf{M}}{\partial \rho_e} \right] \boldsymbol{\Phi}_i \ ,$$

where it is assumed that the eigenvector has been normalized with respect to the kinetic energy, i.e. $\mathbf{\Phi}_i^T \mathbf{M} \mathbf{\Phi}_i = 1$

For a solution where the optimum eigenvalue is *single* modal, the implementation of (2.1) is straight forward although one should note that the sensitivities of eigenvalues, as opposed to the sensitivities of the compliance objective, may take negative as well as positive values. This is not a problem when using mathematical programming methods for the optimization but it requires a small modification for an application of the optimality criteria algorithm. The density update (1.13) used in compliance minimization

$$\rho_{K+1} = \rho_K [B_K]^\eta = \rho_K \left[\frac{-\frac{\partial c}{\partial \rho_e}}{\Lambda \, v_e} \right]^\eta \tag{2.3}$$

must for eigenvalue maximization be changed to

$$\rho_{K+1} = \rho_K [B_K]^\eta = \rho_K \left[\frac{\max(0, \; -\frac{\partial \lambda_{min}}{\partial \rho_e})}{\Lambda \, v_e} \right]^\eta \tag{2.4}$$

The bound-formulation problem (2.2) may be solved using mathematical programming solvers like for example MMA.

In the case of repeated eigenvalues, the eigenvalues are non-differentiable and ignoring this usually results in bad or wrong convergence of the algorithm. Nonetheless, many results and algorithms can be found in the literature that completely ignores this possibility of repeated eigenvalues. The problem is actually well understood; thus the sensitivity analysis for repeated eigenvalue problems should be performed as suggested in (Seyranian 1993, Seyranian, Lund & Olhoff 1994), while the non-smoothness can be handled in a number of ways [14] (see also Sect. 4.4.3).

For the formulations above, the optimized structures will often have a multi-modal eigenvalue and this may be critical for stability. In order to prevent multiple eigenmodes, one may require that the second eigenvalue is some percent bigger than the first, the third is some percent bigger than the second and so on. These constraints may easily be applied by rewriting the bound formulation (2.2) to the format:

$$\begin{aligned} \max_{\boldsymbol{\rho}} \quad & \beta \\ \text{s.t.} \quad & [\alpha]^i \, \lambda_i \geq \beta, \quad i = 1, \ldots, N_{dof} \\ & (\mathbf{K} - \lambda_i \mathbf{M}) \mathbf{\Phi}_i = \mathbf{0}, \quad i = 1, \ldots, N_{dof} \\ & \sum_{e=1}^{N} v_e \rho_e \leq V, \qquad 0 < \rho_{min} \leq \rho_e \leq 1, \quad e = 1, \ldots, N \end{aligned} \tag{2.5}$$

where e.g. $\alpha = 0.95$ (in (2.5) each eigenvalue is multiplied with α in the power i). In this way one also eliminates the problem of non-differentiability at the

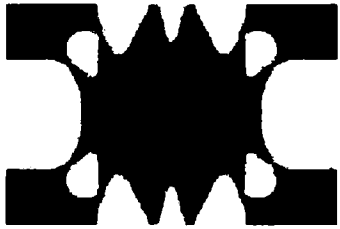

Fig. 2.2. Optimized topology for maximization of the fundamental eigenfrequency. The design domain is a simply supported Mindlin plate with a 10% non-structural mass at the center and volume constraint of 60% of the total volume (from Pedersen 2000b).

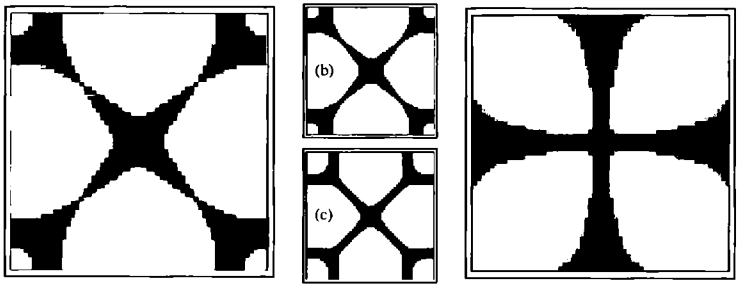

Fig. 2.3. Maximization of the fundamental eigenfrequency for pre-stressed Mindlin plates. The plates are clamped at all edges, there is a 10% non-structural mass attached to the center and the distributable amount of material is 25% of the total volume. The pre-stress levels are a) $\sigma_{11} = \sigma_{22} = 0$, b) $\sigma_{11} = \sigma_{22} = 10$, c) $\sigma_{11} = \sigma_{22} = 25$ and d) $\sigma_{11} = \sigma_{22} = 100$ (from Pedersen 2001).

optimum for a multiple eigenvalue solution. However, one should be careful when using this method since the constraints may prevent the eigenmodes in switching during the optimization. Therefore convergence to better solutions may be jeopardized.

Another pitfall in eigenvalue optimization is the use of symmetry to reduce problem sizes. Since eigenmodes may be asymmetric or totally non-symmetric even for symmetric structures, the use of problem reduction by modelling and optimizing only parts of the domain with symmetric boundary conditions should be avoided, or at least, the results should be validated by analysing the full problem after a design process that has forced symmetry. Problem reduction by use of design variable symmetries and not analysis symmetries is recommended and may in certain cases eliminate the problem of non-differentiability of repeated eigenvalues (Kosaka & Swan 1999).

For topology design based on interpolation models (isotropic or not) another issue becomes significant in eigenvalue optimization (both for vibration and buckling problems). This is the appearance of "artificial modes" in low density regions. For vibration problems, artificial modes appear as very localized modes (groups of a few elements) in regions with relatively large mass to stiffness ratio. For the SIMP interpolation, this happens for the density going to zero. If the element mass is linearly dependent on the element density ρ_e and the element stiffness depends on the power of the element density $(\rho_e)^p$, the ratio of the stiffness and the mass will go towards zero when the density goes to zero. This gives rise to very low eigenfrequencies in low density regions. The problem may be avoided by modifying the stiffness interpolation using one of the methods described in Sect. 1.5.4; the key is to provide for a ratio of mass to stiffness that remains finite in the limit of vanishing density.

An alternative way to solve eigenvalue optimization is by interior point methods for mathematical programming problems with matrix inequalities [14]. This is discussed for truss structures in Sect. 4.4.3. However, one should bear in mind that the truss example is more benign than the general case, as the problem there is a *convex* so-called SDP (semi-definite programming) problem. However, recently developed algorithms for non-convex SDPs should also be able to cater for the general eigenvalue problem (see Sect. 4.4.2).

2.1.2 Forced vibrations

In some situations one may want to minimize or maximize the dynamical response of a structure for a given driving frequency or frequency range. An example of the former could be for an airplane where the vibrations in the structure should be minimized at the frequency of the propeller. For the latter, examples are a sensor which should give a large output for a certain driving frequency or a clock frequency generator that should vibrate at a certain frequency for least possible input.

For solving this type of design problem we define the dynamic compliance as driving force times magnitude of the displacement and express the goal for the dynamical response in terms of this compliance. An optimization problem solving the problem of minimizing the dynamic compliance of a structure subject to periodic forces, $\mathbf{f}(\Omega)$, with frequency Ω, can then be written as

$$\begin{aligned} \min_{\boldsymbol{\rho}} \quad & \{c = (\mathbf{f}^T \mathbf{u})^2\} \\ \text{s.t.} \quad & (\mathbf{K} - \Omega^2 \mathbf{M})\, \mathbf{u} = \mathbf{f} \\ & \sum_{e=1}^{N} v_e \rho_e \leq V, \qquad 0 < \rho_{min} \leq \rho_e \leq 1, \quad e = 1, \ldots, N \end{aligned} \tag{2.6}$$

The sensitivities of the objective function may by use of the adjoint method be found as

$$\frac{\partial c}{\partial \rho_e} = \boldsymbol{\lambda}^T \left[\frac{\partial \mathbf{K}}{\partial \rho_e} - \Omega^2 \frac{\partial \mathbf{M}}{\partial \rho_e} \right] \mathbf{u} \ ,$$

where $\boldsymbol{\lambda}$ is the solution to the adjoint problem

$$(\mathbf{K} - \Omega^2 \mathbf{M})\ \boldsymbol{\lambda} = -2(\mathbf{f}^T \mathbf{u})\ \mathbf{f}$$

We readily see from (2.6) that for low driving frequencies Ω, the results obtained should correspond roughly to the results of solving static problems (the term $\Omega^2\mathbf{M}$ is a small perturbation to the stiffness matrix). However, for higher driving frequencies we should expect different resulting topologies. It can be shown that this formulation corresponds to forcing the closest eigenfrequency away form the driving frequency. An interesting result obtained using this formulation is seen in Fig. 2.4c. Here a tuned mass damper is vibrating out of phase with the input point, resulting in an almost complete damping of the vibrations at the input point.

Other interesting results may be obtained when the driving force is located at another point than the point where the amplitude should be minimized. Such problems are considered in Sect. 2.11.

2.2 Buckling problems

Another important problem in structural optimization is the maximization of the fundamental bucklingload of a structure [15]. The solution of the buckling problem and its associated numerical problems have many features in common with the dynamical problems discussed in the previous section.

Limiting ourselves to considering only linear modelling, i.e. small displacements, the standard objective is to maximize the minimum critical load P_{crit} (or equivalently to minimize $1/P_{crit}$). Typically the optimization problem is formulated as[1]

$$\begin{aligned} \min_{\boldsymbol{\rho}} \quad & \left\{ \frac{1}{P_{crit}} = \max_{i=1,\ldots,N_{dof}} \frac{1}{P_i} \right\} \\ \text{s.t.} \quad & \left[\mathbf{G}(\mathbf{u}) - \frac{1}{P_i}\mathbf{K} \right] \boldsymbol{\Phi}_i = \mathbf{0}, \quad i = 1, \ldots, N_{dof} \\ & \sum_{e=1}^{N} v_e \rho_e \leq V, \qquad 0 < \rho_{min} \leq \rho_e \leq 1, \quad e = 1, \ldots, N \end{aligned} \tag{2.7}$$

where $\boldsymbol{\Phi}_i$ is the eigenvector associated with the i'th critical load and $\mathbf{G}(\mathbf{u})$ is the so-called geometric stiffness matrix which depends on the displacements obtained from the linear, static equilibrium problem $\mathbf{K}\mathbf{u} = \mathbf{f}$

[1] As $\mathbf{K}$ is positive definite and as $\mathbf{G}$ may not be positive definite, it is most natural to work with $1/P_{crit}$ as an eigenvalue.

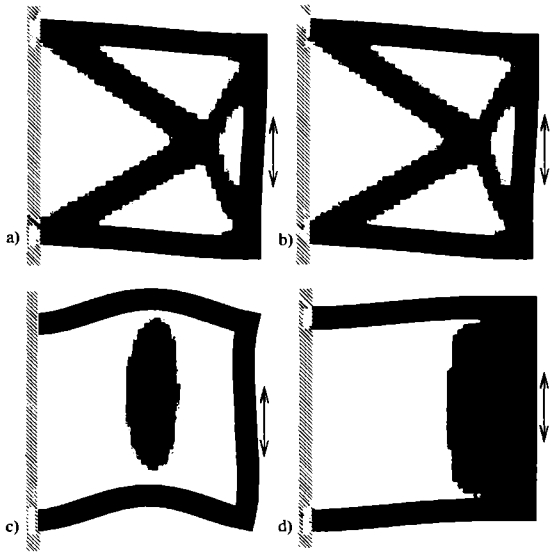

Fig. 2.4. Optimized topologies for different driving frequencies. a) A zero driving frequency gives a statically stiff structure. b) while a small driving frequency forces the first eigenfrequency upwards resulting in a statically stiff structure. c) A larger driving frequency results in a tuned mass damper, d) and an even larger driving frequency forces the first eigenfrequency downwards and away from the driving frequency. All four examples where solved as reinforcement problems for a given outer frame and a stiffness ratio between black and white areas of 100:1. The structures are shown in their deformed states corresponding to the forced vibration mode.

In practice one does not solve for all N_{dof} modes of the eigenproblem in (2.7). In the beginning of the design iterations there is usually only one or two critical eigenvalues whereas towards the end, up to 10 eigenvalues may cluster above the most critical eigenvalue. The number of eigenvalues close to the most critical eigenvalue should be monitored during the iterations.

Alternatively, one may reformulate (2.7) to a bound-formulation

$$
\begin{aligned}
\min_{\boldsymbol{\rho}} \quad & \beta \\
\text{s.t.} \quad & \frac{1}{P_i} \leq \beta, \qquad = 1, \ldots, N_{dof} \\
& \left[\mathbf{G}(\mathbf{u}) - \frac{1}{P_i}\mathbf{K}\right] \boldsymbol{\Phi}_i = \mathbf{0}, \quad i = 1, \ldots, N_{dof} \\
& \sum_{e=1}^{N} v_e \rho_e \leq V, \qquad 0 < \rho_{min} \leq \rho_e \leq 1, \quad e = 1, \ldots, N \ .
\end{aligned}
\tag{2.8}
$$

The sensitivities of a *single* modal eigenvalue are found as

$$\frac{\partial \lambda_{min}}{\partial \rho_e} = \mathbf{\Phi_1}^T \left[\frac{\partial \mathbf{G}}{\partial \rho_e} - \frac{1}{P_1} \frac{\partial \mathbf{K}}{\partial \rho_e} \right] \mathbf{\Phi}_1 + \mathbf{v}^T \frac{\partial \mathbf{K}}{\partial \rho_e} \mathbf{u}, \tag{2.9}$$

where $\mathbf{v}$ is the solution to the adjoint load problem

$$\mathbf{K}\mathbf{v} = \mathbf{\Phi}_1^T \frac{\partial \mathbf{G}(\mathbf{u})}{\partial \mathbf{u}} \mathbf{\Phi}_1 .$$

In the literature one can sometimes find that the last term of (2.9) is ignored, but this should of course be avoided. We also remark that the issues associated with multiple eigenvalues discussed for vibration problems are also important for buckling problems.

As was the case for dynamical problems, artificial modes may also here appear in low density regions where the (non-linear) geometrical stiffness is high compared to the linear stiffness. To avoid the problem of artificial local modes one can ignore the geometrical stiffness of low-density elements (Neves, Rodrigues & Guedes 1995). This approach corresponds to ignoring the mass of low-density elements in the vibration problem. This cut-off method seems to stabilize the problem but may cause oscillations of the algorithm due to abrupt changes in the values of the objective function and sensitivities. However, a smooth version of this approach can be obtained by writing the interpolation schemes in a slightly different way for the two stiffness matrices:

For matrix $\mathbf{K}$ $\quad E_{\mathbf{K}} = [\rho_{\min} + (1 - \rho_{\min})\, \rho^p]\, E^0$

For matrix $\mathbf{G}$ $\quad E_{\mathbf{G}} = [\rho^p]\, E^0$

where $\rho_{\min}$ is the minimum density normally imposed in the topology design problems. This method seems to eliminate the problem for our test cases.

Solutions to a buckling problem are shown in Fig. 2.5. All the three towers are optimized within a formulation that corresponds to (2.5) combined with (2.8). With α 0.99, the second buckling load was thus required to be 1% higher than the first, etc. For the low tower (Fig. 2.5a), the first five eigenvalues of the resulting topology are governed by the buckling constraint. During the optimization process these five critical modes take turns in being the most critical mode. This means that convergence is very slow since only very small steps can be taken in order not to violate the bound constraints. For the higher towers (Fig. 2.5b and c), initial convergence is faster since only the first global buckling mode is active. For the "almost optimal" structure a local mode in the top vertical parts of the structure becomes just as critical as the global mode and convergence again becomes slow.

2.3 Stress constraints

Imposing stress constraints on topology optimization problems is an extremely important topic. However, several challenges must be overcome in

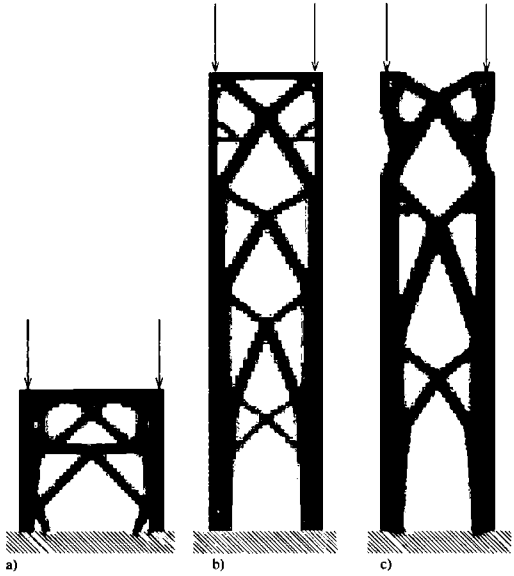

Fig. 2.5. Optimal re-enforcement of portal frames for maximum fundamental buckling load. a) 40 by 40 elements discretization. b) and c) 120 by 30 element discretizations where b) is a re-enforcement problem where the outer frame is fixed to be solid and c) allows a free distribution of 50% material. The buckling load for the second tower c) is 1% lower than for the first tower b).

order to solve the problem efficiently. This section discusses some possible solution methods. However, the best way to solve stress constrained problems has probably yet to be suggested. Literature relevant for the stress problem is found in literature section [16].

2.3.1 A stress criterion for the SIMP model

For the 0-1 formulation of the topology design problem a stress constraint is well-defined, but when a material of intermediate density is introduced, the form of the stress constraint is not a priori given.

A stress criterion for the SIMP model should be as simple as possible (like for the stiffness-density relation), and the isotropy of the stiffness properties should be extended to the stress model. Moreover, for physical relevance it is reasonable that the criterion should mimic consistent microstructural considerations as for example illustrated in appendix 5.4.4. This leads one to apply a stress constraint for the SIMP model (with exponent p) that is expressed as a constraint of the the von Mises equivalent stress σ_{VM}:

$$\sigma_{\mathrm{VM}} \leq \rho^p \, \sigma_l \quad \text{if } \rho > 0 \, . \tag{2.10}$$

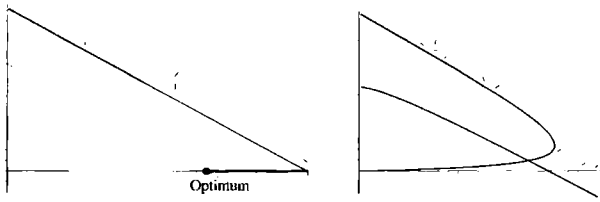

Fig. 2.6. The stress singularity problem. Left: a typical feasible set of design variables for a minimum weight stress constrained problem with two variables. The optimum solution is only connected to the interior of the feasible set by a line. Right: relaxed design problem that enhances the chance of finding the right optimum.

This constraint reflects the strength attenuation of a porous medium that arises when an average stress is distributed in the local microstructure, meaning that "local" stresses remain finite and non zero at zero density (cf. appendix 5.4.4). This results in a reduction of strength domain by the factor ρ^p We see that the same exponents are used for the stiffness interpolation and the stress constraint. Choosing another exponent is not consistent with physics and using an exponent that is less than p can for example lead to an artificial removal of material (see Duysinx & Bendsøe (1998)).

The classical stress-constrained optimization problem consists of finding the minimum weight structure that satisfies the stress constraint and which is in elastic equilibrium with the external forces, that is, we have a design problem in the form

$$\begin{aligned}
&\min_{\boldsymbol{\rho}} \sum_{e=1}^{N} v_e \rho_e \\
&\text{s.t.} \quad \mathbf{K}\mathbf{u} = \mathbf{f}, \\
&\qquad (\sigma_e)_{\mathrm{VM}} \leq \rho_e^p \, \sigma_l \text{ if } \rho > 0\,, \qquad 0 < \rho_{min} \leq \rho_e \leq 1, \quad e = 1, \ldots, N
\end{aligned}$$

where the stress for example is evaluated at the center-node of the individual FE elements.

2.3.2 Solution aspects

Constraint relaxation The so-called "singularity" problem associated with stress constraints requires special care when dealing with topology design problems [16]. It was first identified for truss problems and arises from a "degeneracy" or an "irregularity" of the design space. The key effect is that the feasible set in the *design space* contains degenerated appendices where constraint qualification (the Slater condition) does not hold. This means that

classical optimization algorithms based on Kuhn-Tucker conditions are unable to reach the optima that are located in these regions. In other words, a standard optimization algorithm is not able to completely remove some low density regions and to find the true optimal topologies.

One approach to circumvent this complication is to reformulate the problem as a sequence of problems that have nicer properties and which can give solutions that converge to the true design (like a continuation method). First, we note that in a topology design problem, the stress constraints should *only* be imposed if material is present. To eliminate the condition $\rho > 0$ from the constraint, one considers a modified formulation:

$$\rho \left(\frac{\sigma_{\mathrm{VM}}}{\rho^p \sigma_l} - 1 \right) \leq 0 \tag{2.11}$$

For bars in a truss, this is equivalent to considering forces instead of stresses [16]. Unfortunately, this reformulation does not change the problems with constraint qualification, and additional measures are required. One method is to rewrite the stress constraints using the ϵ-relaxation approach proposed in Cheng & Guo (1997). This relaxation[2] is a perturbation of the original problem where the original stress constraints are replaced by the following relaxed stress constraints and associated side constraints:

$$\rho \left(\frac{\sigma_{\mathrm{VM}}}{\rho^p \sigma_l} - 1 \right) \leq \epsilon(1-\rho) \qquad \epsilon^2 = \rho_{min} \leq \rho \ , \tag{2.12}$$

where ϵ is given. For any $\epsilon > 0$, the ϵ-relaxed problem with the constraints (2.12) is characterized by a design space that is not any longer degenerate, and the factor $(1-\rho)$ on ϵ assures that the real stress constraint is imposed for $\rho = 1$. It is thus possible to reach a *local* optimum with optimization algorithms based on Karush-Kuhn-Tucker conditions. If we can find the global optimum ρ_ϵ^*, then for $\epsilon \to 0$, the sequence of feasible domains and their optimal solutions $\{\rho_\epsilon^*\}$ converge continuously towards the original degenerate problem and its associated optimal solution (see [16]).

The solution procedure thus now consists in solving a sequence of optimization problems, for decreasing ϵ , in a *continuation* approach similar to what is done with barrier and penalty functions. The implementation process is here driven by the minimum density $\rho_{min} = \epsilon^2$ and choosing a quite large initial minimum density is necessary to obtain reasonable results. We remark here that the method may fail if the problem is such that there are many local minima for the relaxed problems; as shown in Stolpe & Svanberg (2001c) this may happen even for rather simple truss examples. An alternative approach is to not rely on gradient based techniques, see the discussion in Achtziger (2000).

[2] Relaxation in the sense of mathematical programming.

Implementation aspects The local stress criterion adds a large number of constraints to what is already a large scale optimization problem. Thus it is important to apply an active set strategy which at each iteration step preselects the potentially dangerous stress constraints to be considered. At the beginning of the optimization process, the selection is large, but at the end of the optimization the set of active constraints is stable and it can be restricted to a fraction of the elements.

For working with MMA (or CONLIN) it is also important to treat the stress constraint in a form which is suited for the approximation strategies of these methods (Duysinx & Bendsøe 1998). Thus the stress constraints should be written as (observe that the density variables are strictly positive for $\epsilon > 0$):

$$\frac{\sigma_{\mathrm{VM}}}{\rho^p \sigma_l} - \frac{\epsilon}{\rho} + \epsilon \leq 1.$$

A global stress constraint An alternative to working with the local constraints is to use global L^q constraints that for large q approximates the local constraints. This can be implemented in the form (Duysinx & Sigmund 1998):

$$\left[\sum_{e=1}^{N} \max\left(\left\{ 0 \,,\, \frac{\sigma_{\mathrm{VM}}}{\rho^p \sigma_l} - \frac{\epsilon}{\rho} + \epsilon \right\} \right)^q \right]^{1/q} \leq 1.$$

This is just one constraint, so the savings in computational effort is immense. The difficulty is the numerical problems associated with using large q. Computational experiments shows that $q = 4$ is a good choice; however, for problems with very localized high stresses (like an L-shape) one cannot assure that the stress is below the critical value in all areas. Nonetheless, the designs one can obtain are quite reasonable compared to using the very cumbersome local constraint.

Example The MBB beam problem is here first optimized within a minimum weight and stress constrained formulation, and the result of Fig. 2.7a was produced with a finite element mesh of 45 by 15 nine node finite elements. This design has a compliance value of $306.3Nm$ and a volume of material of $1.0632m^3$, which is approximatively 33 percents of the volume of the total design area. This compliance value is used for a new problem where the volume is minimized while the compliance is bounded to the same level as that of the stress design. As one can see in Fig. 2.7b, this compliance design is different from the stress constrained one. The volume of the design is lower, at $0.9177m^3$, and the topology as well as the thicknesses of the bar-like members are different. This demonstrates that stress constraints have a non-trivial influence on the topology design even for simple problems. Note that the results here do not apply any mesh independency constraints. Thus if we refine the mesh, see Fig. 2.7c, we see changes in the design.

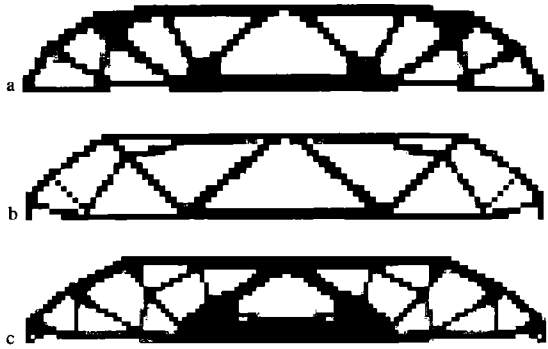

Fig. 2.7. The MBB beam. a) stress design and b) compliance design with 45x15 finite elements, and c) stress design with 60x20 finite elements (from Duysinx & Bendsøe 1998)

As demonstrated in Pedersen (1998), compliance design and stress design are equivalent if the stress criterion is consistent with the elastic energy measure. However, we consider here the von Mises criterion, which is not consistent with the energy criterion, except if the material is incompressible i.e. if the Poisson's ratio is 0.5. Therefore it is not surprising to observe a deviation between stress and compliance topology predictions for cases where the stress state is characterized by hydrostatic pressure in some areas.

Stress concentration For stress constraints one has to pay special attention to domains or problems that introduce a stress singularity (like in the inner corner of an L-shaped domain). The real difficulty for such situations is not so much in the optimization part but more the numerical problem of capturing the high stress at the corner. The optimization solution is of course strongly dependent on the quality of the analysis, and for most applications the stress constrained design optimization should be coupled with a much more refined analysis, using for example mesh adaptation.

2.4 Pressure loads

An example of design dependent loads is pressure loads. Since the direction as well as the position of attack of the pressure loads depend on the boundary between solid and void and because the boundaries are not well defined in topology optimization problems, topology design with pressure loads is a highly challenging problem [22].

The optimization problem is the classical one of compliance minimization of a structure where the design parameters are the volumetric material

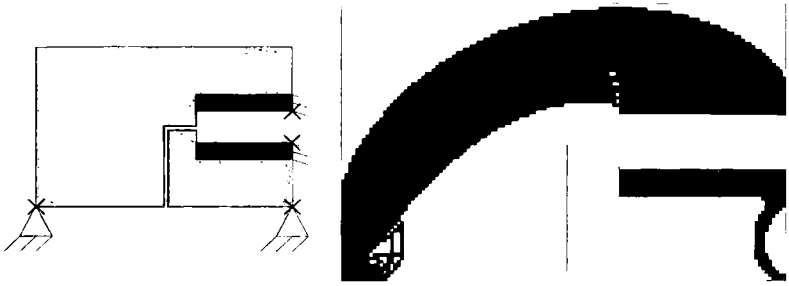

Fig. 2.8. Optimization of an inlet. Two separate parts of the structural surface are subjected to pressure loads. The design domain with the pressure initially distributed to narrow white internal channel is shown to the left. To the right is shown the optimized topology for a volume fraction of 40%. The pressurized surfaces are marked with grey lines (from Hammer & Olhoff 2000).

densities throughout the design domain. The novel aspect here lies in the type of loading considered which occurs if free structural surface domains are subjected to forces where both the direction, the location, and the size can change with the material distribution. Examples are pressure and fluid flow loading with the direction and location of the load changing with and following the structural surface.

The compliance of the structure is written as

$$c(u) = \int_{\Omega} fu \mathrm{d}\Omega + \int_{\Gamma_t} tu \mathrm{d}\Gamma + \int_{\Gamma_p} pu \mathrm{d}\Gamma,$$

where an extra term representing the design dependent load – here a pressure p – acting on parts of the boundary Γ_p of the *material domain.*

In the work of Hammer & Olhoff (2000), (2001) the optimization process is performed by successive iterations making use of the finite element analysis model with fixed mesh on the one hand, and the design model with the parametrized iso-volumetric density surface for the pressure loading on the other. The load surfaces in the design model are controlled by the density distribution in the finite element model and in turn fully determine the global load vector on the finite element model. Thus the sensitivity analysis is based on both the analysis model and the design model. In the sensitivity analysis also the sensitivities of the load vector with respect to a design change must be evaluated, and this is done analytically. The problem is solved by an optimality criteria method.

The example in Fig. 2.8 models the inlet from a channel to a larger pressure chamber. The material around the inlet is prescribed to be solid and non-changeable. Here, two domains of the structural surface are subjected to pressure, and the initial pressure distribution is shown along with the de-

sign domain in figure 2.8(a). The value for the iso-volumetric density line ρ_c was initially chosen to be 0.25, and then gradually increased to $\rho_c = 0.85$. Other shapes of the initial small channel leading the pressure from the inlet to the chamber could of course have been chosen, but the final design seems unaffected thereof.

2.5 Geometrically non-linear problems

For compliance minimization problems displacements are typically small and the problems may be modelled using linear finite element theory. For soft structures, slender structures and mechanisms, however, it is imperative that the problems are modelled using geometrically non-linear finite element analysis. This section discusses objective functions and modelling issues related to stiffness optimization of structures undergoing finite displacements [17]. Later sections will discuss compliant mechanism design, crashworthiness design and other design problems involving geometrical non-linearities.

Structures undergoing large displacements may or may not be subject to large strains. In this section, we assume that strains are small and hence material non-linearity can be ignored.

2.5.1 Problem formulation and objective functions

The general topology optimization problem for situations with geometrical non-linearities can in broad terms be written as

$$\begin{aligned} &\min_{\boldsymbol{\rho}} \; c(\boldsymbol{\rho}) \\ &\text{s.t.} \quad \mathbf{r} = \mathbf{0} \; , \\ &\qquad \sum_{e=1}^{N} v_e \rho_e \leq V, \qquad 0 < \rho_{min} \leq \rho_e \leq 1, \quad e = 1, \ldots, N \end{aligned} \tag{2.13}$$

where $\mathbf{r}$ is the residual in obtaining the structural equilibrium, $c(\boldsymbol{\rho})$ is the objective functions to be defined later and all other symbols have been defined previously.

This topology optimization problem only differs from the standard topology optimization problems in that the equilibrium $\mathbf{r} = \mathbf{0}$ must be found using an iterative procedure. For the linear analysis problems discussed in Chap. 1, the equilibrium is found from the solution of a linear system of (finite element) equations.

In the following we use the (non-linear) Green-Lagrange strain measure to model the strain-displacement relations, that is

$$\eta_{ij} = \frac{1}{2}(u_{i,j} + u_{j,i} + u_{k,i}\, u_{k,j}) \; ,$$

where u is the point-wise displacement and subscript "$_{,j}$" means differentiation with respect to coordinate j. For later use we define the displacement dependent matrix $\mathbf{B}$ as the matrix that transforms a change in displacement $d\mathbf{u}$ into a change in strain, i.e.

$$d\eta = \mathbf{B}(\mathbf{u})\, d\mathbf{u} \ ,$$

where $\mathbf{u}$ is the finite element displacement vector.

The (linear) Hooke's law for Piola-Kirchhoff stresses and Green-Lagrange strains with SIMP interpolations is written as

$$s_{ij} = \rho^p \, E^0_{ijkl} \, \eta_{kl}$$

where E^0_{ijkl} is the constitutive tensor for a solid, linear, isotropic material.

The residual is defined as the error in obtaining the equilibrium

$$\mathbf{r}(\mathbf{u}) = \mathbf{f} - \int_V \mathbf{B}(\mathbf{u})^T \mathbf{s}(\mathbf{u}) \, dV \tag{2.14}$$

where $\mathbf{f}$ is the external force vector and $\mathbf{s}$ is the Piola-Kirchhoff stress written in vector form. Following a Total Lagrangian approach, the integration is performed over the undeformed volume. The equilibrium has been found when the residual vector is equal to the zero vector. This finite element equilibrium may be found incrementally or in one load step using the iterative Newton-Raphson method. Both kinds of methods require the determination of the tangent stiffness matrix

$$\mathbf{K}_T = -\frac{\partial \mathbf{r}}{\partial \mathbf{u}}.$$

For further details on the derivations of the finite element matrices for geometrically non-linear systems, the reader is referred to standard books on non-linear finite element theory (see e.g. Zienkiewicz & Taylor (2000) or Crisfield (1997)).

2.5.2 Choice of objective function for stiffness optimization

The first goal we consider is to maximize the stiffness of a structure undergoing large deformations. Several different objective functions may be considered in order to solve this task and we will here deal with three possibilities, namely: minimization of end-compliance, minimization of a weighted sum of end-compliances and minimization of the complementary elastic work (Buhl, Pedersen & Sigmund 2000). These objective functions are discussed in the following.

Minimization of end-compliance The natural choice of objective function with regards to an efficient numerical implementation is the minimization of the compliance in the deflected configuration here denoted "end-compliance" The calculation of the end-compliance is simple since it only requires the finding of one equilibrium, i.e. no incremental procedure is necessary. Obviously the draw-back of this objective function is that the structure may break down or collapse for loads lower than the design load, see below.

Defining end-compliance as the compliance of a structure in its equilibrium configuration, the objective function can be written as

$$c(\rho) = \mathbf{f}^T \mathbf{u} \ ,$$

where $\mathbf{u}$ is the displacement vector for the structure in its equilibrium position. Assuming design independent loads, the sensitivity of the end-compliance with respect to a change in element density may be found by the adjoint method to be

$$\frac{dc}{d\rho_e} = \boldsymbol{\lambda}^T \frac{\partial \mathbf{r}}{\partial \rho_e}$$

where the adjoint field $\boldsymbol{\lambda}$ is the solution to the linear adjoint problem $\mathbf{K}_T \boldsymbol{\lambda} = \mathbf{f}$

The sensitivity of the residual with respect to design changes $\frac{\partial \mathbf{r}}{\partial \rho_e}$ is found by differentiation of (2.14)[3] Solving the adjoint system is computationally cheap because the factorized tangent stiffness matrix already has been found during the equilibrium iterations and a solution only requires one extra forward/backward substitution.

Multiple loading cases For multiple loading cases the objective function is simply a weighted sum of end-compliances

$$c(\rho) = \sum_{i=1}^{M} w_i \ \mathbf{f}_i^T \ \mathbf{u}_i \tag{2.15}$$

where M is the number of loading cases, $\mathbf{f}_i$ and $\mathbf{u}_i$ are the load and displacement vectors of loading case i, respectively and w_i are weighting factors ($\sum_{i=1}^{M} w_i = 1$). The sensitivity analysis corresponds to a simple weighting of the sensitivities of the individual loading cases.

Minimization of complementary work The last objective we consider is the minimization of the complementary elastic work. Using the trapezoidal

[3] Note that for a linear system, the partial derivative of the residual (assuming design independent loads) is $-\frac{\partial \mathbf{K}}{\partial \rho_e}\mathbf{u}$ and the adjoint equals the original displacement vector $\mathbf{u}$; thus the sensitivity of the compliance becomes $\frac{dc}{d\rho_e} = -\mathbf{u}^T \frac{\partial \mathbf{K}}{\partial \rho_e}\mathbf{u}$ as derived in Section 1.2.3

method for numerical integration, the complementary work of the external forces can be calculated as

$$c(\rho) = W^C \approx \Delta \mathbf{f}^T \left[\frac{1}{2}\, \mathbf{u}(\mathbf{f}_0) \;+\; \sum_{i=1}^{n-1} \mathbf{u}(\mathbf{f}_i) \;+\; \frac{1}{2}\, \mathbf{u}(\mathbf{f}_n) \right] \tag{2.16}$$

where n is the number of increments in the load vector. The size of the increments is determined by $\Delta \mathbf{f} = (\mathbf{f}_n - \mathbf{f}_0)/n$, where $\mathbf{f}_0$ and $\mathbf{f}_n$ is the zero and maximum load vectors, respectively. The sensitivity analysis for the complementary work is again found using the adjoint method as described for the end compliance. This results in

$$\frac{dc}{d\rho_e} = \Delta \mathbf{f}^T \left[\frac{1}{2}\, \boldsymbol{\lambda}_0^T \frac{\partial \mathbf{r}_0}{\partial \rho_e} \;+\; \sum_{i=1}^{n-1} \boldsymbol{\lambda}_i^T \frac{\partial \mathbf{r}_i}{\partial \rho_e} \;+\; \frac{1}{2}\, \boldsymbol{\lambda}_n^T \frac{\partial \mathbf{r}_n}{\partial \rho_e} \right] \tag{2.17}$$

where $\boldsymbol{\lambda}_i$ and $\mathbf{r}_i$ are the vectors of adjoint and residuals, respectively, for the load increment i This means that for the sensitivity analysis we simply have to perform one extra forward/backward substitution for each load step and sum the results in Eq. 2.17.

2.5.3 Numerical problems and ways to resolve them

In the non-linear finite element analysis, we save computational time by reusing the displacement solution from a previous topology iteration in the new Newton-Raphson equilibrium iteration. This saves a considerable number of finite element iterations, especially when the topology changes get smaller near convergence. The computational time highly depends on the size of the applied force. For relatively small forces, obtaining the optimal solution takes 1.5 to 2 times the time to obtain a solution using linear modelling. For larger loads where local buckling can be observed, the time in which the optimal solution is found can be 5 to 10 times higher than for the linear case.

When the finite element analysis is based on the Green-Lagrange or other non-linear strain measures, large displacements may cause the tangent stiffness matrix to become indefinite or even negative definite. This phenomena is observed frequently during the topology optimization process and results in non-convergence of the equilibrium iterations. Numerical experiments show that the problem occurs in low-density elements with minimum or close to minimum stiffness (see Fig. 2.9). The problem is "artificial" since the elements with minimum stiffness represent void and therefore their behaviour should not influence the structural response. Since the problem is an artefact of the numerical model, different schemes may be devised to circumvent the problem.

Ignoring convergence in low density elements Usually, the Newton-Raphson iterative scheme is stopped when the changes in nodal displacements get below a certain value. For the topology optimization case, non-convergence occurs when the displacements oscillate in nodes surrounded by

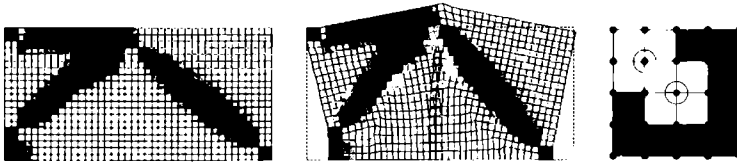

a) b) c)

Fig. 2.9. a) Original mesh, b) distortion of finite element mesh causing ill-convergence of Newton-Raphson procedure and c) prevention of ill-convergence by ignoring "low-density" nodes (indicated by circles) in the convergence criterion.

"void" (minimum density) elements. Since these nodes should have no structural importance one can circumvent the problem by relaxing the convergence criterion for these nodes in the equilibrium iterations, that is, those nodes surrounded by void elements are eliminated from the convergence criterion (see Figure 2.9c) (Buhl et al. 2000). This solution to the problem is efficient and seldomly causes convergence problems. In the few cases where the procedure does not converge after 20 iterations, the displacement vector is reset to zero and the equilibrium iterations are restarted.

Element removal Another way to circumvent the problem is to remove elements with minimum density from the design domain. Element removal may jeopardize convergence to the right minimum since re-appearance of material in the removed elements is impossible. Examples show that the "re-appearance" of material is crucial for the design process. Therefore one should include a criterion for the "re-appearance" of elements. This can be based on the same type of filtering techniques that are used to ensure mesh-independency (Bruns & Tortorelli 2001).

2.5.4 Examples

It is not typical that structures optimized for stiffness undergo large displacements. Nonetheless it may happen for very slender structures or for structures built from very soft materials such as Nylon.

Optimal topologies for maximum stiffness Results from minimizing the end-compliance of a cantilever beam for three different load magnitudes are shown in the right column of Fig. 2.10. The left column shows the topologies obtained using linear modelling which are independent of the load magnitude. We notice that the topology obtained for the large displacement modelling and the smallest load is equal to the topology obtained with a small displacement modelling. We also see that the non-linear topologies become less symmetric for larger loads. Finally, we notice that the optimized topologies become increasingly degenerated for larger loads.

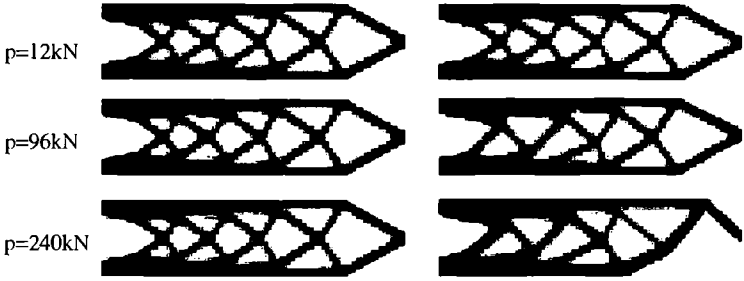

Fig. 2.10. Optimized topologies for end-loaded cantilever example. Left column: Optimized topology for small displacement FE-modelling. Right column: Optimized topologies for large displacement FE-modelling (from Buhl et al. 2000).

Fig. 2.11. Deformed configuration of the topology optimized for 144 kN (see Fig. 2.10). Note that the right-most bar supporting the load is un-bent in the deformed configuration (from Buhl et al. 2000).

The deformed state of the structure optimized for the largest load is shown in Fig. 2.11. It is seen that the bar in the right side of the structure (which supports the load) is vertical in the deformed configuration. In this configuration the bar is un-bent. For any other load the bar will bend, resulting in a bad compliance for the structure. This example therefore demonstrates, that *minimization of the end-compliance may result in degenerated structures which only can support the load they are designed for.* However, the problem is worse for the non-linear case. Here the structure may not only collapse for a load having another *direction* than the design load, but it may also collapse for a load which just in *magnitude* is different from the design load.

One can partially circumvent the problem of degenerated topologies by applying a minimization of a weighted sum of end-compliances (cf. (2.15)). Figure 2.12 shows a design optimized for two loadings, one pointing upwards and one pointing downwards. As expected, the optimal topology is symmetric and in fact cannot be differentiated in topology nor in compliance from the results obtained for small displacement theory (see Fig. 2.10, left). It is interesting to note that the compliance of the symmetric structure is only 2.5% lower than for the non-symmetric one shown in Fig. 2.10(right).

In other situations the results are not so convincing, and one may obtain structures that still become unstable due to buckling at a load which is not

Fig. 2.12. A two-load case problem with two large loads acting in opposite vertical directions (from Buhl et al. 2000).

Fig. 2.13. Optimized topology for minimization of complementary elastic work (from Buhl et al. 2000).

a design load; this depends very intricately on the choice of loads. The most effective way to prevent this is to operate with the complementary elastic work (cf., (2.16)). In this way, we can make sure that the structure is stable for any load up to the maximum design load. An example topology obtained for a load of 144 kN and 12 load steps is shown in Figure 2.13 and this is a structure seemingly without degeneracies.

A force-displacement diagram for the results obtained for a) small displacement modelling, b) end-compliance and c) complementary work minimization is shown in Figure 2.14a-c. Notice that the topology optimized for end-compliance has minimum deflection at the design load as expected, but for smaller loads, it has the maximum deflection. The curves for the designs obtained with linear modelling and with minimization of complementary work are almost coinciding, with the latter designs being slightly stiffer for most of the interval. It is also interesting to note that the topology obtained for linear modelling has a higher maximum load than the two others. This means that obtaining a slightly higher stiffness by using non-linear modelling is achieved at the cost of a more critical response to load perturbations.

Optimization of a structure with snap-through effect The examples above show that the inclusion of large displacements in the topology optimization process does not significantly affect the resulting topologies. Also, the force-displacement curves obtained for small displacement optimization and complementary work minimization only differ by a few percent. However, in some cases the difference can be extremely large as will be seen in this example.

Thus, for the design problem sketched in Figure 2.15 we obtain the solutions shown in Figure 2.16a and b, using linear and non-linear analysis, respectively. It is seen that the two topologies are totally different due to the buckling effects. The topology obtained using linear modelling (Fig-

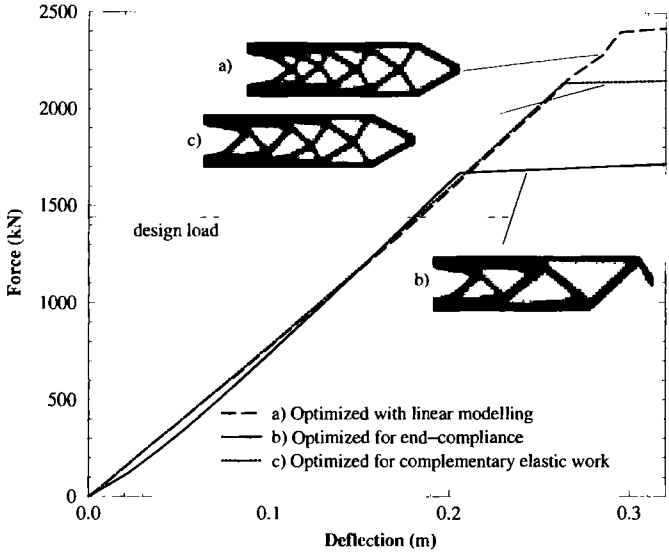

Fig. 2.14. Force-displacement diagram for the topologies optimized for a) minimum compliance using small displacement finite element analysis, b) minimum end-compliance for large displacement analysis and loading of 144 kN and c) minimum complementary elastic work and end-loading of 144 kN (from Buhl et al. 2000).

ure 2.16a) consists of two long beams under compression and when using non-linear modelling the compressed beams buckle and the whole structure snaps through. Using non-linear modelling in the design process, the resulting topology consists of two longer beams in tension and two short beams in compression as seen in Figure 2.16b.

Obviously, the topology in Figure 2.16a is optimal also in the non-linear case if the force is applied in the upward direction instead of in the downward direction. To obtain a structure that is stiff for loads in both directions, the topology can be optimized using non-linear modelling and two load-cases, one acting upwards and the other acting downwards. The resulting topology is shown in Figure 2.16c and is seen to be a hybrid of the two single-load topologies.

The non-linear responses for the three topologies are shown in Figure 2.17. It is seen that the topology which is optimized using linear modelling buckles just below the design load, whereas the buckling load of the design optimized using non-linear modelling is well above the design load. Moreover, the buckling load for the two-load structure is also seen to be higher than the design load.

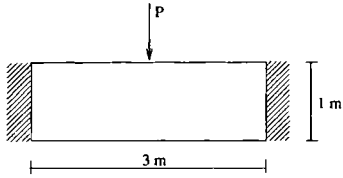

Fig. 2.15. Design problem with snap-through effect.

Fig. 2.16. Optimal topologies for the design problem in Figure 2.15. a) optimized topology for small displacement finite element modelling and b) optimized topology for large displacement modelling and c) optimized topology for large displacement modelling and two load-cases (from Buhl et al. 2000).

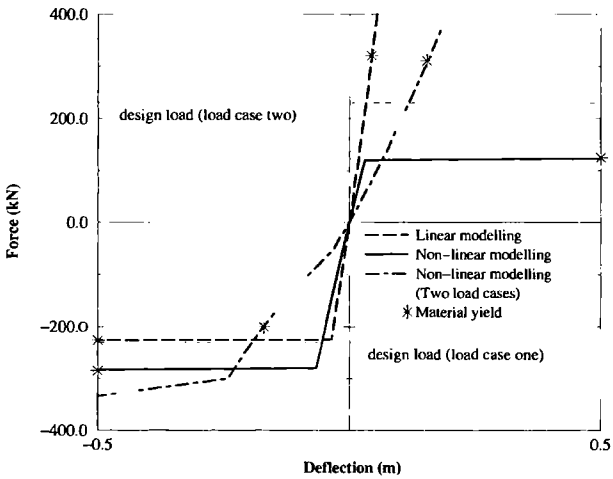

Fig. 2.17. Force-displacement diagram for the optimized topologies in Fig. 2.16 found using linear, non-linear and two-load non-linear finite element modelling (from Buhl et al. 2000).

2.6 Synthesis of compliant mechanisms

Compliant mechanisms attain their mobility from flexibility of their constituents as opposed to their rigid body counterparts that attain their mobility from hinges, bearings and sliders. The main advantages of compliant

mechanisms are that they can be built using fewer parts, require fewer assembly processes and need no lubrication. Special care must be taken, however, in designing compliant mechanisms in order to obtain sufficient mobility and safety against failure due to fatigue. An important application of compliant mechanisms lies in MicroElectroMechanical Systems (MEMS) which cannot be manufactured using typical assembly processes and may not make use of hinges and bearings since friction dominates at the small (typically submilimeter) scale (Petersen 1982).

One of the most important objectives in compliant mechanism synthesis (and rigid-body mechanism synthesis for that sake) is to be able to control the ratios between output and input displacements or output and input forces which are described by the geometrical and mechanical advantages, respectively. It is also important to be able to synthesize mechanisms with prescribed output paths for given inputs.

Topology optimization of compliant mechanisms can be performed based on continuum as well as truss and frame discretizations [18]. Each discretization has advantages and disadvantages. The truss and frame formulations may have crossing members which cannot be manufactured in microscale. On larger scales, however, overlaps are allowed and may result in mechanisms with larger displacement ranges. Here we concentrate on the continuum discretization but the basic procedures apply to truss and frame discretizations as well.

As an example of a compliant mechanism design problem we consider the displacement inverter in Fig. 2.18(left). The goal of the topology optimization problem is to design a structure that converts an input displacement on the left edge to a displacement in the opposite direction on the right edge. In order to be able to transfer work from the input port to the output port, the inversion must be performed in a structurally efficient way. Also, it must be possible to control the displacement amplification of the mechanism. Finally, the modelling of the input force and displacements should model physical actuators that may have limited strokes, actuation and blocking forces. In the following, we discuss a formulation that satisfies all of these requirements.

Since it is extremely important to use large displacement theory in compliant mechanism design, this section is based on geometrically non-linear modelling. The simplified problem for linear analysis, which may be used as a first step into compliant mechanism design is discussed at the end of this section.

2.6.1 Problem setting

Assuming that the input actuator is a linear strain based actuator it can be modelled by a spring with stiffness k_{in} and a force f_{in}. Examples of strain based actuation principles are piezoelectric, thermal or electrothermal heating, shape memory alloys, etc., which are characterized by their blocking force (f_{in}) and their free (un-loaded) displacement (f_{in}/k_{in}). An alternative to the

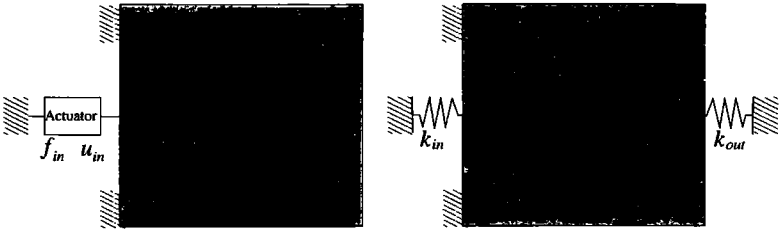

Fig. 2.18. A basic compliant mechanism design problem: the displacement inverter. Left: the basic design problem and Right: spring and load model for the input actuator and workpiece. Example solutions are shown in Fig. 2.23.

linear strain based actuator could be a constant force actuator with a limited stroke. Such an actuator can be modelled by a force f_{in} and a non-linear spring which has a very small stiffness up to the maximum stroke value u_{in} and a very high stiffness after u_{in} so that further displacement is prevented.

The goal of the optimization problem is to maximize the displacement u_{out} (or force or work) performed on a workpiece modelled by a spring with stiffness k_{out}. By specifying different values of k_{out} we can control the displacement amplification. If we specify a low value of k_{out} we get large output displacements and vice versa. In order to maximize the work on the output spring, the available material must be distributed in the structurally most efficient way. An optimization problem incorporating these ideas can be written as

$$\begin{aligned} &\max_{\boldsymbol{\rho}} \quad u_{out} \\ &\text{s.t.} \quad \mathbf{r} = \mathbf{0} \\ &\qquad \sum_{e=1}^{N} v_e \rho_e \leq V, \qquad 0 < \rho_{min} \leq \rho_e \leq 1, \quad e = 1, \ldots, N \end{aligned} \tag{2.18}$$

where $\mathbf{r}$ is the finite element residual for the analysis problem with the applied load f_{in}. This optimization problem is very similar to the minimization problem (2.13) formulated for the minimization of end-compliance.

We now express the displacement at the output point as $u_{out} = \mathbf{l}^T\mathbf{u}$, where $\mathbf{l}$ is a vector with the value 1 at the degree of freedom corresponding to the output point and with zeros at all other places. Then sensitivity of the output displacement can be found to be given as

$$\frac{\partial u_{out}}{\partial \rho_e} = \boldsymbol{\lambda}^T \frac{\partial \mathbf{r}}{\partial \rho_e} ,$$

where $\boldsymbol{\lambda}^T$ is the solution to the adjoint load problem

$$\mathbf{K_T}\boldsymbol{\lambda} = -\mathbf{l} .$$

The simple compliant mechanism optimization problem (2.18) is of the same form as the compliance minimization problems discussed in Chapter 1, in the sense that a simple objective function is to be minimized within the limitation of a single linear constraint on volume. Therefore, we may also use an optimality criteria approach to solve it. However, the fixed-point type density update (2.3) has to be modified since the sensitivity of the objective function may take both positive and negative signs. A (heuristic) modification that results in a fairly stable convergence is

$$\rho_e^{K+1} = \rho_e^K \left[\frac{\max(0, \; -\frac{\partial u_{out}}{\partial \rho_e})}{\lambda \; v_e} \right]^{\eta}$$

Whereas the damping coefficient η for linear compliance minimization problems was chosen as 0.5 in order to ensure stable convergence, it sometimes has to be chosen a bit lower to ensure stable convergence in compliant mechanism design problems. The best convergence, however, is obtained using a mathematical programming algorithm like MMA.

The problem formulation for compliant mechanism synthesis described so far is very simple and does not allow for multiple inputs or outputs or for a very detailed control of the output ports[4] The following sections discuss extensions that cater for such aspects.

2.6.2 Output control

Control of output direction Example solutions to the inverter example in Fig. 2.18 are shown in Fig. 2.23. It is here assumed that the structure is symmetric and therefore the output displacement is a horizontal movement. In other cases where the output displacement does not coincide with a line of symmetry or if an inclined output displacement is specified, the problem formulation (2.18) does not ensure an output displacement along the desired direction. It only ensures that the component of the output displacement along the desired direction is maximized. This effect is clearly seen in the example of Fig. 2.19b where the output displacement is maximized in the negative horizontal direction. However, the vertical displacement of the resulting topology is actually bigger than the horizontal displacement.

This problem can be handled by adding an extra constraint to the optimization problem (2.18). The constraint ensures that the relative displacement $\hat{u}_{out}$ perpendicular to the output displacement u_{out} is below a small number ϵ, i.e.

$$\frac{\hat{u}_{out}^2}{u_{out}^2} \leq \epsilon^2 \tag{2.19}$$

[4] A Matlab implementation of the basic compliant mechanism design problem for *linear modelling* and based on OC is found in Appendix 5.1.5.

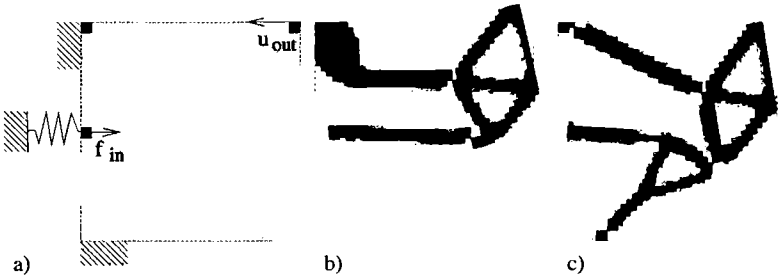

Fig. 2.19. Example with (b) and without (c) cross-sensitivity constraint.

where ϵ is decreased during the design process. Adding an extra constraint to the topology optimization problem is not problematic if one uses mathematical programming (like the MMA) for solving the design problem. Nevertheless, one finds that much work in the area operates with all requirements formulated in one objective function (with weighted multiple objectives) in order to use simple algorithms. This has the disadvantage that it is difficult to have precise control of the behaviour of the resulting mechanisms.

That the constraint (2.19) manages to control the output displacement as desired is shown in Fig. 2.19c. This topology is obtained with $\epsilon = 0.01$, that is, a maximum cross-sensitivity between the two perpendicular output directions of 1%. The added constraint results in a mechanism with an entirely different topology that ensures that the output point moves horizontally. It is interesting to note that the extra constraint only penalizes the horizontal output by 2% compared to the mechanism in (Fig. 2.19b) that has an extremely high cross-sensitivity.

Multiple outputs Figure 2.20b shows an example design of a gripping mechanism. Here the problem is formulated so that the vertical displacements of the outer "jaws" is maximized, resulting in jaws that open like a pair of scissors. In some cases one may require a parallel movement of the jaws. This can be obtained by reformulating the objective function to a min-max problem

$$\max_{\rho} \min \{u_{out,1},\ u_{out,2}\}$$

where $u_{out,i}$ is the displacement of the i'th output point. This problem may be solved using a bound formulation for the two objectives $u_{out,1}$, $u_{out,2}$, and gives results as shown in 2.20c.

2.6.3 Path generating mechanisms

An important problem in compliant mechanism design is the synthesis of path-generating mechanisms. Here, the output point of the mechanism is

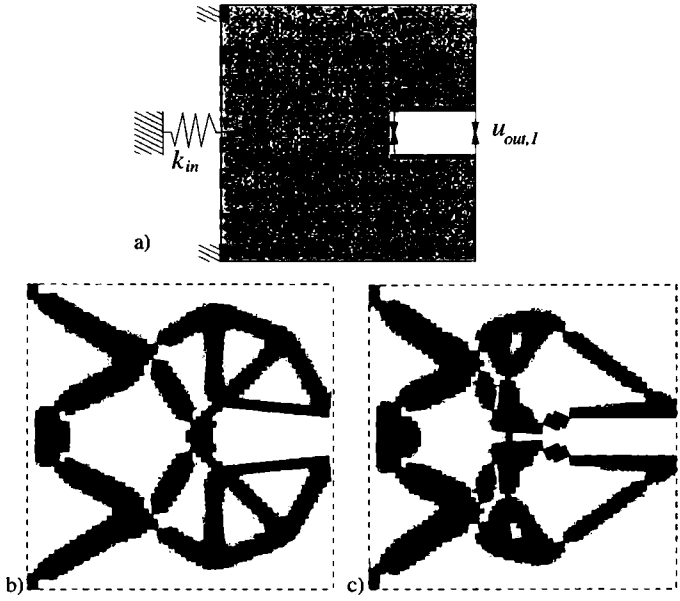

Fig. 2.20. Example with parallel and non-parallel output displacements. a) Design domain, b) the use of one output point results in a non-parallel opening of the 'jaws', while c) the max-min formulation results in a parallel movement of the jaws.

required to pass through a number M of precision points defined by given displacement vectors $\mathbf{u}^*_{out,m}$. An objective function formulated as the sum of errors may then be written as

$$c(\rho) = \sum_{k=1}^{K} (\mathbf{u}_{out,k} - \mathbf{u}^*_{out,k})^2 \tag{2.20}$$

where $\mathbf{u}_{out,k}$ is the k'th output displacement corresponding to the input load step k.

For complicated output paths it does not make sense to attach a spring at the output point in order to ensure an efficient force transfer, as done in the previous subsections. Instead, apart from (2.20), we also require the output point to pass through the precision points when loaded with counter loads $p_{k,1}$ and $p_{k,2}$, corresponding to counter-loads against the path and counter loads perpendicular to the path at the points k, respectively. The objective function may then be reformulated to

$$c(\rho) = \sum_{i=0}^{K} \alpha_i \sum_{k=1}^{K} (\mathbf{u}_{out,k,i} - \mathbf{u}^*_{out,k})^2, \tag{2.21}$$

where α_i are weighting factors and $\mathbf{u}_{out,k,i}$, corresponds to the output displacement vectors for no counter load (i=0), for the counter load against the output path (i=1) and for the counter load perpendicular to the output path (i=2). For further discussions on this scheme, the reader is referred to Pedersen, Buhl & Sigmund (2001).

With the extended optimization formulation (2.21) which requires the output point to pass through a number of precession points, it is possible to synthesize mechanisms like the ones shown in Fig. 2.21. Here, the same input displacement can be converted to a straight horizontal output, a straight slanted output and an arch following output, respectively. It is not possible to synthesize such path-generating mechanisms using linear (small displacement) modelling.

An example of generating mechanisms that exhibits snap-through and bistable behaviour is shown in Fig. 2.22. This is a highly complex topology optimization problem and involves an arch-length-type finite element solver and a lot of experiments in formulating objective functions and constraints (Bruns, Sigmund & Tortorelli 2002, Bruns & Sigmund 2001).

2.6.4 Linear modelling

A linear version of the compliant mechanism design problem discussed above may be used as an exercise and introduction to compliant mechanism design. However, one must be aware of the severe limitations that such modelling imposes (see Sect. 2.6.5). The linear optimization problem may be written as

$$\begin{aligned} &\max_{\boldsymbol{\rho}} u_{out} \\ &\text{s.t.} \quad \mathbf{K}\mathbf{u} = \mathbf{f} \\ &\qquad \sum_{e=1}^{N} v_e \rho_e \leq V, \qquad 0 < \rho_{min} \leq \rho_e \leq 1, \quad e = 1, \ldots, N \end{aligned} \tag{2.22}$$

If the load vector $\mathbf{f}$ is design independent the sensitivities can be found as

$$\frac{\partial u_{out}}{\partial \rho_e} = \boldsymbol{\lambda}^T \frac{\partial \mathbf{K}}{\partial \rho_e} \mathbf{u} \tag{2.23}$$

where (as for the non-linear case) $\boldsymbol{\lambda}^T$ is found as the solution to the adjoint load problem $\mathbf{K}\boldsymbol{\lambda} = -\mathbf{l}$

Compared to the implementation of the minimum compliance problem only small changes are required for solving the linear mechanism design problem. Compared to the 99 line Matlab code needed for compliance design (cf., appendix 5.1.1), 105 lines of Matlab code can solve the linear mechanism design problem; we need to add six lines and change another 12 lines to adapt the 99 line code into a code for compliant mechanism synthesis (see Appendix 5.1.5).

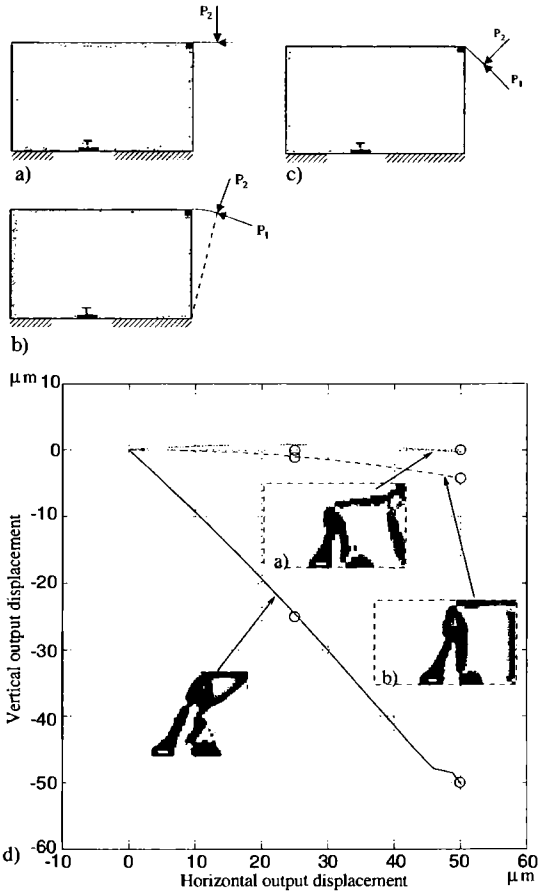

Fig. 2.21. Path generating mechanisms with linear inputs. a) Design problem where the output is required to follow a straight horizontal path, b) a straight slanted path and c) an arch. d) Plots of the output paths of the synthesized mechanisms. Path-generating mechanisms cannot be synthesized using linear modelling (from Pedersen et al. 2001).

2.6.5 Linear vs. non-linear modelling

The mechanism designs obtained using linear analysis typically behave differently when modelled using large displacement analysis. In the best of situations one merely has inaccurate results but in the worst cases the results are useless as large displacement mechanisms. Therefore, the use of geometrically non-linear finite element modelling is absolutely essential for mechanism

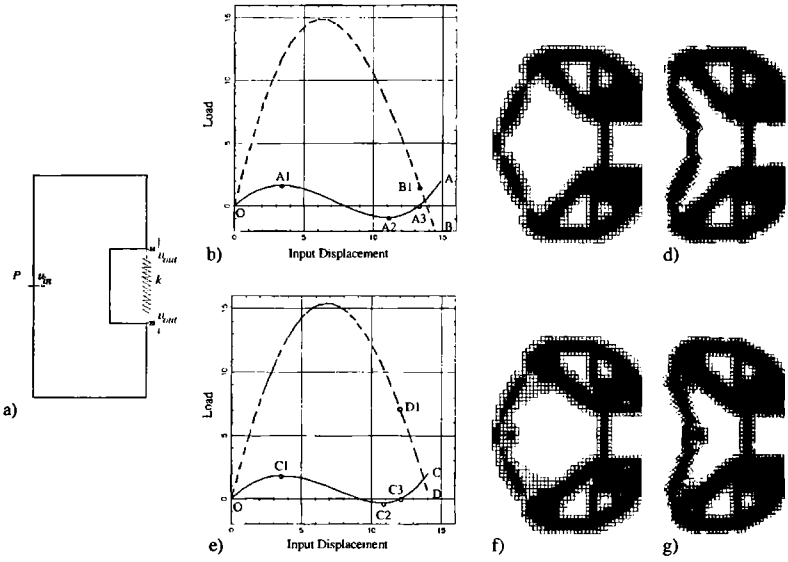

Fig. 2.22. Two-phase design process to generate a gripper mechanism that exhibits snap-through and bistable behavior. In phase I, the goal is to generate a topology that exhibits snap-through and bistable behavior from an initial design with uniform material distribution. In phase II, the goal is to retain the bistable behavior of phase I and maximize the gripping force on the workpiece while in its deformed bistable configuration. a) Design domain. b/e) Optimal phase I/II load-displacement trajectories (path O-A/path O-C) and clamping force histories (path O-B/path O-D). Optimal phase I/II topology plots of the gripper mechanism in c/f) their undeformed bistable configurations (point O/point O) and d/g) their deformed bistable configurations (point A3/point C3). Note that the phase I topology exhibits bistable behavior, a nonzero clamping force (point B1) is applied to the mechanism when the gripper is in its deformed bistable configuration (point A3), the phase II topology retains its phase I bistable behavior, and the clamping force (point D1) is improved by a factor of 4 when the gripper is in its deformed bistable configuration (point C3) (from Bruns & Sigmund 2001).

synthesis. The inverter example in Figure 2.23 illustrates this. The goal in this synthesis problem is to maximize the work performed on a spring in the negative horizontal direction for an input force in the positive horizontal direction as sketched in Fig. 2.18. The mechanism obtained for linear modelling is shown in Figure 2.23a. When modelled using small displacement theory it deflects as shown in Figure 2.23c. When modelled using large displacement theory it deflects as seen in Figure 2.23d. We see that linear theory ignores the locking of the two right-most bars when they reach the vertical position.

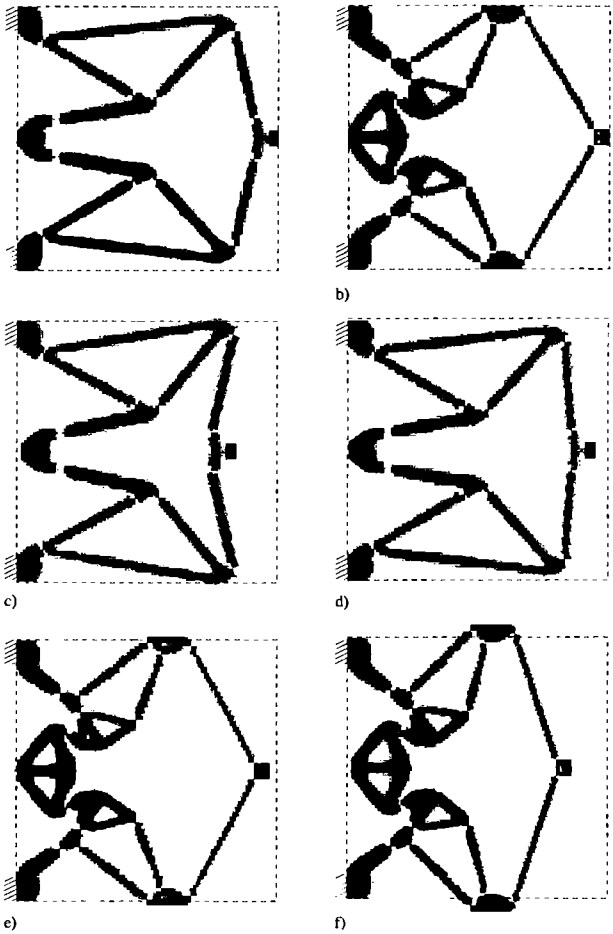

Fig. 2.23. Inverter synthesis. Design domain is seen in Fig. 2.18. a) Optimized topology using linear modelling, b) optimized topology using non-linear modelling, c) and d) deflection of a) using linear and non-linear modelling, respectively and e) and f) deflection of b) using linear and non-linear modelling, respectively (from Pedersen et al. 2001).

The mechanism topology obtained using non-linear modelling Figure 2.23b does not have this problem (Fig. 2.18f) and its output displacement is, in the large displacement setting, therefore more than two times higher than for the linearly optimized mechanism in Fig. 2.18a.

2.6.6 Design of thermal actuators

In the applications of compliant mechanism design discussed so far the input load was design independent. However, when designing for example thermally dependent structures or thermal actuators the applied load depends on the design. Example design problems are optimization of thermal circuit breakers or minimization of displacements and stresses due to thermal mismatch. Here the temperature field is considered as uniform and the loads arise due to a uniform change in the temperature.

The main difference in the design problem as compared to above is that the sensitivity analysis has to take the dependent loads into account. We will here just write the sensitivity expression for the linear case, were we have

$$\frac{\partial u_{out}}{\partial \rho_e} = \boldsymbol{\lambda}^T \left[\frac{\partial \mathbf{K}}{\partial \rho_e} \mathbf{u} - \frac{\partial \mathbf{f}}{\partial \rho_e} \right]$$

Here $\boldsymbol{\lambda}^T$ is again found as the solution to the adjoint load problem

$$\mathbf{K}\boldsymbol{\lambda} = -\mathbf{l}.$$

while the load vector is found as

$$\mathbf{f} = \sum_e \int_{V^e} \mathbf{B}\mathbf{E}\boldsymbol{\alpha}\Delta T dV$$

where $\mathbf{B}$ is the finite element strain displacement matrix, $\mathbf{E}$ is the constitutive matrix, $\boldsymbol{\alpha}$ is the vector of thermal expansion coefficients and ΔT is the (uniform) temperature change.

An example of thermal actuator design is shown in Fig. 2.24. The effect of varying output springs is clearly seen. Note that topology optimized thermal actuators have been manufactured and tested in microscale by Jonsmann, Sigmund & Bouwstra (1999c).

2.6.7 Computational issues

Mechanism design should, as we have seen, preferably be carried out within the framework of large displacement, non-linear analysis. Compared to stiffness optimization (Sect. 2.5), the problems with excessive distortions of low density elements and ill-convergence of equilibrium iterations are even more pronounced for mechanism design. The methods of ignoring convergence in low density elements or entirely removing low density elements as discussed in section 2.5.3 must therefore be implemented.

One-node connected hinges In the examples of compliant mechanism design shown so far, one notices that the resulting mechanisms are not truly compliant but rather tend to have what amounts to almost moment-free one-node connected hinges. This is especially the case for examples with large

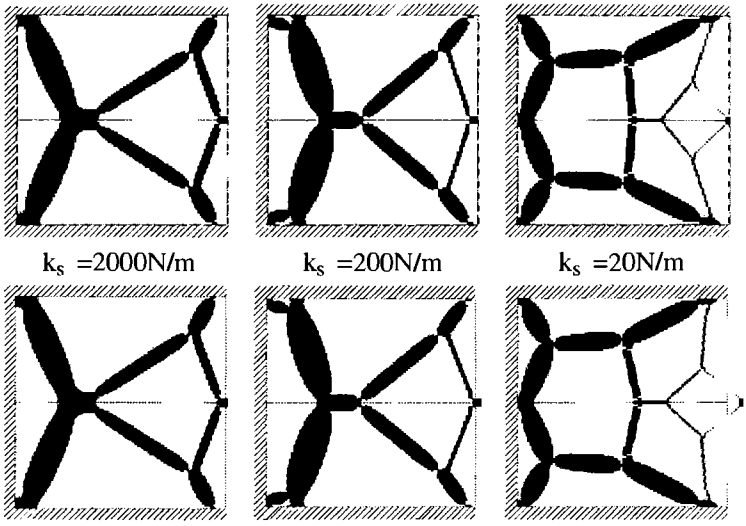

Fig. 2.24. Design of compliant thermal actuators with actuation caused by a uniform rise in temperature (linear modelling). Top row: Optimized topologies for output spring stiffnesses of 2000, 200 and 20 N/m, respectively. Bottom row: Displacements patterns of the optimized actuators.

output displacements, i.e., small transfer of forces. In reality the stress in a sharp hinge would approach infinity and the structure would break, so techniques to avoid them are required.

Like the checkerboard problem, one-node connected hinges are caused by bad computational modelling that the optimization procedure exploits. In the numerical model, the hinge is modelled by an artificially stiff corner to corner connection of two Q4 elements. Moreover, the stress variations are very badly modelled. The use of *higher order elements* only partly alleviates the problem, and local stress constraint should probably be added to the formulation. This is computationally prohibitive, so instead other methods have been devised.

Only some of the checkerboard and mesh-independency schemes described in Sect. 1.3 prevent the non-physical one-node connected hinges. For example, the *filter method* which has been applied in all the examples shown so far is based on a weighted averaging of neighbouring sensitivities. This means that if the gain (sensitivity) in building a hinge is big enough, it will dominate the average and cause hinges to appear. Also, the *perimeter constraint* will not prevent the hinge since only a global constraint is imposed on the design. The *local gradient control* will partly eliminate the problem but will result in "grey" (intermediate density) hinges.

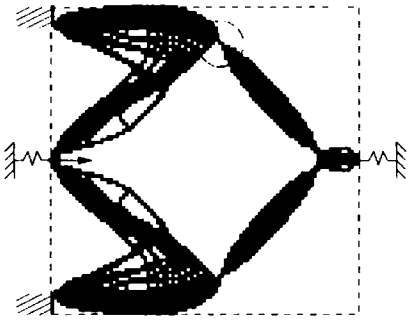

Fig. 2.25. Hinge prevention by the NoHinge constraint (1.32) (from Poulsen 2001b).

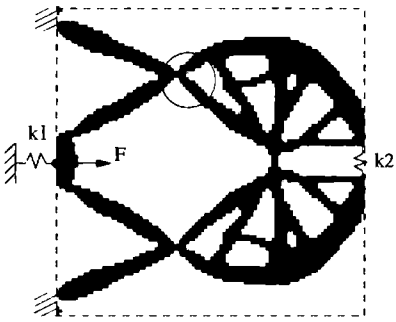

Fig. 2.26. Hinge prevention by MOLE constraint (1.30) (from Poulsen 2001a).

The *MOLE* constraint (1.30) as well as the checkerboard (NoHinge) constraint (1.32) described in section 1.3 were developed precisely with the hinge problem in mind and they do actually prevents hinges. The former method furthermore imposes a minimum width of the hinge.

An alternative, but somewhat questionable, solution is to perform a *post-processing* of the resulting topology and substitute the one-node connected hinges with long slender compliant hinges. The post-processing may be based on a contour plot of the topology as seen in Fig. 2.27.

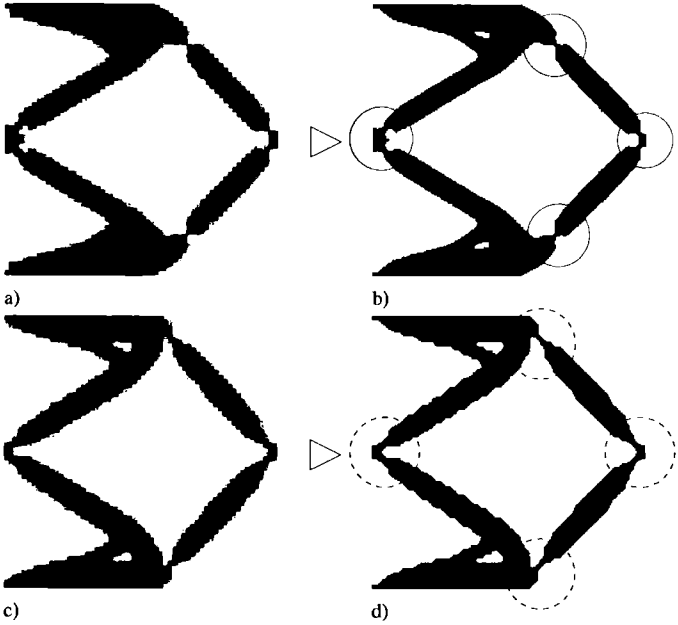

Fig. 2.27. Post-processing of topology optimization results for the inverter problem from Fig. 2.18. a) Optimized inverter topology obtained using conventional element based densities and c) optimized inverter topology obtained using the nodal based approach. b) and d) are 200 by 100 element structures based on an automatic (one level) contour plot of a) and c), respectively. The originals have output displacements of -1.18 and -1.11, respectively. The contour based structures have output displacements of -1.09 and -1.12, respectively. Hinge stresses in the nodal based structure (d) are approximately 80% lower than for (b). Full circles indicate highly stressed hinges and dashed circles indicate better compliant and lowly stressed hinges.

The recently suggested *nodal variable method* discussed in Sect. 1.3.2 actually makes the post-processing easier. Although the method is closely related to the gradient constraint method, the method has the advantage that nodal values in most cases takes the discrete 0-1 values whereas the element values still take intermediate density values. However, basing a post-processing on the nodal values results in nice, well-defined, and slender hinges. Figure 2.27 compares the post-processing step for the conventional FE schemes and the nodal variable method. The resulting structure for the former case has some very compact and highly stressed hinges, while the latter method gives a topology with long and slender hinges. A disadvantage of the nodal variable

method is the zig-zag interpolation of the boundary curves; however, this may be removed by combining it with a filtering scheme.

2.7 Design of supports

Hitherto, we have only considered optimum structural design by material distribution. However, the positions and amounts of supports in a structure also play a major role in structural optimization, and substantial gains from introducing design of supports is obtained for especially compliant mechanism design [19].

If one can place supports anywhere in the design domain, the optimum position of supports in a compliance minimization problem would be directly under the load, causing zero compliance. Therefore, a judicious choice of the possible location of the supports and their cost is in place.

The support design formulation consists in assigning rigid or no supports to each element in a support design domain which may be a subset of the normal (material) design domain (cf., Buhl (2002)). As in material distribution problems we convert this integer type problem into a continuous problem by introducing an element support design variable ξ_e. The model of the variable support of an element in the FE mesh is sketched in Fig. 2.28. All the nodes of the element are supported by variable stiffness springs and for high spring stiffnesses this corresponds to fixing the element (as also used in the penalization approach for imposing prescribed boundary conditions). We may then introduce a diagonal element support stiffness matrix

$$\mathbf{K}_s(\xi_e) = \xi_e^q \mathbf{K}_{s,e}, \quad \xi_e \in [\xi_{min}; 1]$$

where $\mathbf{K}_{s,e}$ is a diagonal matrix with "high" values compared to the diagonals of the original stiffness matrix and q is a penalization factor corresponding to the power p for stiffness variables in the SIMP approach. The global stiffness matrix may thus be assembled as

$$\mathbf{K} = \sum_{e=1}^{N} \rho_e^p \mathbf{K}_e + \sum_{e=1}^{N} \xi_e^q \mathbf{K}_s,$$

To reduce the possibility of the design being forced into a local optimum, a small lower bound ξ_{min} is imposed on the support design variables. This assures that the sensitivities always are non-zero making a re-introduction of supports possible[5]

As for the material distribution part of the topology design problem, we introduce a bound on the total support area S. For mechanism design this bound is not very important but for stiffness problems the objective function

[5] This effect may alternatively be obtained by using the RAMP or the spline interpolation schemes (cf., Sect. 1.5.4) which have non-zero sensitivities for $\xi = 0$.

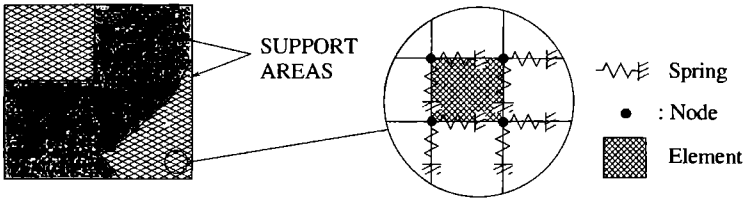

Fig. 2.28. Each node is supported by a horizontal and a vertical spring. Thus a 4-node element is supported by 8 springs.

will obviously be improved if more supports are added. In order to encourage or discourage the forming of supports in certain areas or along certain boundaries, we introduce an element support cost factor f_e. The constraint on support area thus becomes $\sum_{e=1}^{N} f_e \xi_e \leq S$. If all $f_e = 1$, the cost of supports is uniform, whereas if some support cost factors are set to higher values (e.g. $f_e = 10$), supports appearing in these elements will be discouraged. The example in Fig. 2.29 demonstrates this aspect.

For compliance minimization (the linear case) , the optimization problem can now be written as

$$
\begin{aligned}
&\min_{\boldsymbol{\rho}} \ \{c(\boldsymbol{\rho}) = \mathbf{f}^T\mathbf{u}\} \\
&\text{s.t.} \quad \left(\sum_{e=1}^{N} \rho_e^p \mathbf{K}_e + \sum_{e=1}^{N} \xi_e^q \mathbf{K}_{s,e}\right)\mathbf{u} = \mathbf{f} \\
&\qquad \sum_{e=1}^{N} v_e \rho_e \leq V, \qquad 0 < \rho_{min} \leq \rho_e \leq 1, \quad e = 1, \ldots, N \\
&\qquad \sum_{e=1}^{N} f_e \xi_e \leq S, \qquad 0 < \xi_{min} \leq \xi_e \leq 1, \quad e = 1, \ldots, N
\end{aligned}
\tag{2.24}
$$

Here, the sensitivity of the compliance with respect to the support design variable is simply

$$
\frac{dc}{d\xi_e} = -q\xi_e^{q-1}\mathbf{u}^T\mathbf{K}_{s,e}\mathbf{u}
$$

As an example of compliance minimization including costs of supports, we consider the design of the bridge structure sketched in Fig. 2.29a. Gradually making the cost of supports more expensive at the bottom of the design domain results in bridge structures with three columns (Fig. 2.29b), two columns (Fig. 2.29c) and no columns (Fig. 2.29d). Correspondingly, the compliances of the three structures increase.

An example of the possible gains in using variable supports in compliant mechanism design is shown in Fig. 2.30. The goal is to design a gripping

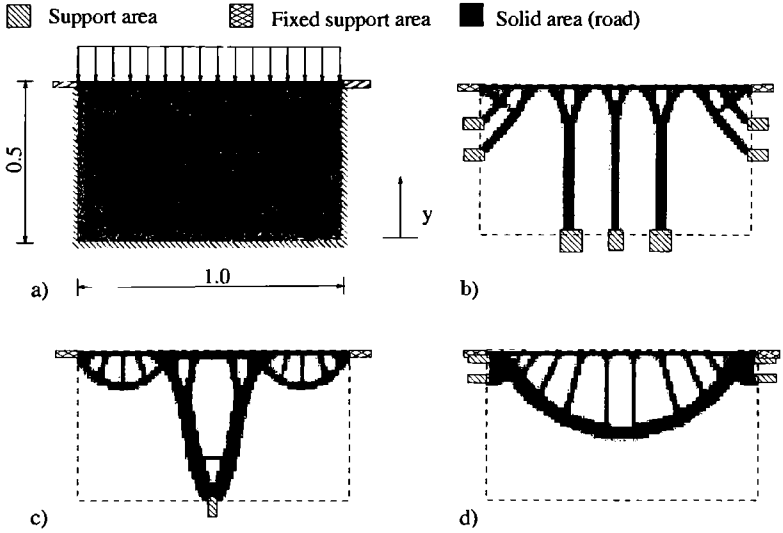

Fig. 2.29. Examples of design of supports combined with compliance minimization. a) Design domain with possible support areas at the all edges except the top edge. b) Optimized topology for equal support cost in the design domain ($c = 1.12 \cdot 10^{-4}$). c) Optimized topology for support cost varying linearly from 1.0 at the top edge to 10.0 at the bottom edge ($c = 2.38 \cdot 10^{-4}$). d) Optimized topology for support cost varying linearly from 1.0 at the top edge to 20.0 at the bottom edge ($c = 3.79 \cdot 10^{-4}$) (from Buhl 2002).

mechanism that maximizes the gripping motion for a given input actuation. A limited amount of support may be located in the top and bottom parts of the design domain. Fig. 2.30b shows the optimized gripper obtained with fixed supports at the left edge and Fig. 2.30c shows the optimized gripper including support design. The output displacement of the latter is 77% higher than for the former, demonstrating the importance of including support design in mechanism synthesis problems.

2.8 Alternative physics problems

The computational procedures for topology optimization were originally developed for the design of elastic structures, but its theoretical inspiration came to a large extend from work carried out for plates and for scalar problems such as conduction problems (heat or electricity). The application of numerical methods for topology optimization for these problems is with todays knowledge rather straightforward, and the computations are typically

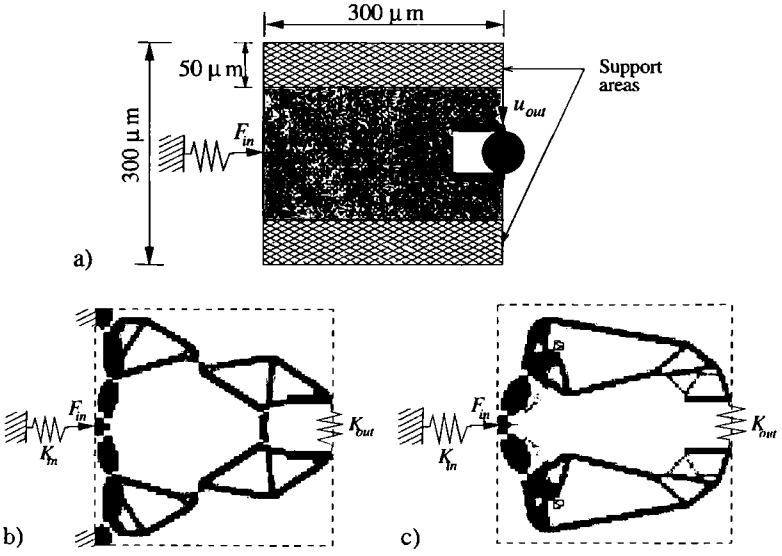

Fig. 2.30. Design of a micro-gripper including design of supports. b) Optimized topology without support design ($u_{out} = 10.8\mu m$) and c) Optimized topology including support design ($u_{out} = 19.1\mu m$). The gain in output displacement is 77% (from Buhl 2002).

less time consuming due to the simpler FE analysis models. We note here that all the theoretical considerations required for the elasticity case (mesh-dependence, the role of composites, etc.) have parallels for the scalar situation; actually much more theoretical insight has been gained for this setting.

In recent years, topology design methods have also been expanded to for example electro-magnetic problems, coupled problems, fluid problems, and wave propagation problems. Here and in later sections of this chapter we illustrate some of these settings.

2.8.1 Multiphysics problems

The phrase "multiphysics problems" covers optimization problems that require modelling in several areas of physics [18], [22]. Apart from making the modelling more complicated due to coupling effects, it also complicates the sensitivity analysis. However, with the help of the adjoint method, it is always possible to perform the sensitivity analysis in an efficient way as long as the objective function is a global description of the response.

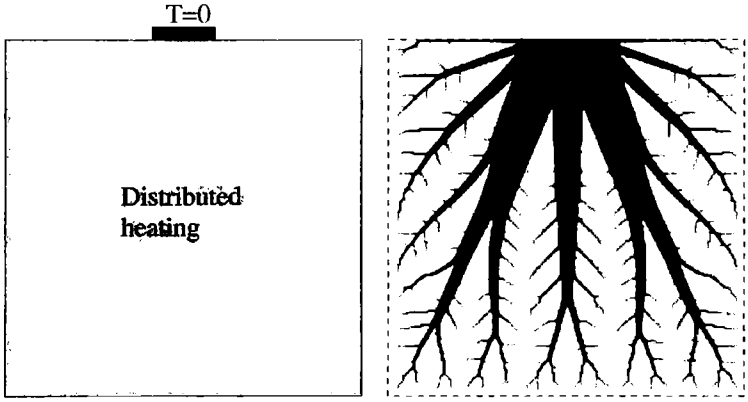

Fig. 2.31. Topology optimization for a heat conduction problem of minimum resistance between input and output points. Left: The design domain isolated at all edges except for the heat sink at the center of the upper edge. The plate is subjected to distributed heating all over the plate. Right: Optimized topology obtained using a 91 line Matlab (cf., Appendix 5.1.6). The discretization consists of 40.000 elements.

We will demonstrate the sensitivity analysis for multiphysics problems on a simple weakly coupled linear problem involving two fields (for example heat conduction and elasticity).

The FE-equations of the two systems are given by

$$\mathbf{K}_1\mathbf{u}_1 = \mathbf{f}_1 \qquad \text{and} \qquad \mathbf{K}_2\mathbf{u}_2 = \mathbf{f}_2(\mathbf{u}_1) \tag{2.25}$$

where it is assumed that system 2 (the elastic problem) is weakly dependent on system 1 (the thermal field) and that both system matrices depend on the design variables. This means that we have to solve system 1 and insert the solution in the load vector of system 2. Physically, it means that the temperature field gives rise to a thermal expansion that influences the elastic field. The aim is to find the sensitivity of a component of the second response vector (a displacement at a point) which can (as done previously) be written as

$$u_{out} = \mathbf{l}^T\mathbf{u}_2$$

Using the adjoint method (cf., 1.2.3), we proceed as follows. We start by adding two null terms to the original expression

$$u_{out} = \mathbf{l}^T\mathbf{u}_2 + \boldsymbol{\lambda}_1\left[\mathbf{K}_1\mathbf{u}_1 - \mathbf{f}_1\right] + \boldsymbol{\lambda}_2\left[\mathbf{K}_2\mathbf{u}_2 - \mathbf{f}_2(\mathbf{u}_1)\right]$$

where $\boldsymbol{\lambda}_1$ and $\boldsymbol{\lambda}_2$ are arbitrary, fixed vectors. The sensitivity of this augmented expression is

$$\frac{\partial u_{out}}{\partial \rho_e} = \mathbf{l}^T \frac{\partial \mathbf{u}_2}{\partial \rho_e} + \boldsymbol{\lambda}_1^T (\frac{\partial \mathbf{K}_1}{\partial \rho_e}\mathbf{u}_1 - \frac{\partial \mathbf{f}_1}{\partial \rho_e}) + \boldsymbol{\lambda}_2^T (\frac{\partial \mathbf{K}_2}{\partial \rho_e}\mathbf{u}_2 - \frac{\partial \mathbf{f}_2}{\partial \rho_e}) + \boldsymbol{\lambda}_1^T \mathbf{K}_1 \frac{\partial \mathbf{u}_1}{\partial \rho_e} + \boldsymbol{\lambda}_2^T \mathbf{K}_2 \frac{\partial \mathbf{u}_2}{\partial \rho_e} - \boldsymbol{\lambda}_2^T \frac{\partial \mathbf{f}_2}{\partial \mathbf{u}_1} \frac{\partial \mathbf{u}_1}{\partial \rho_e}$$

To remove the field sensitivity terms $\frac{\partial \mathbf{u}_i}{\partial \rho_e}$, the following expressions should be zero

$$\left[\mathbf{l}^T + \boldsymbol{\lambda}_2^T \mathbf{K}_2\right] \frac{\partial \mathbf{u}_2}{\partial \rho_e} = 0 \quad \text{and} \quad \left[-\boldsymbol{\lambda}_2^T \frac{\partial \mathbf{f}_2}{\partial \mathbf{u}_1} + \boldsymbol{\lambda}_1^T \mathbf{K}_1\right] \frac{\partial \mathbf{u}_1}{\partial \rho_e} = 0$$

This can be achieved by selecting the adjoint vectors $\boldsymbol{\lambda}_i$ as the solution to the two adjoint problems

$$\mathbf{K}_2 \boldsymbol{\lambda}_2 = -\mathbf{l} \quad \text{and} \quad \mathbf{K}_1 \boldsymbol{\lambda}_1 = \boldsymbol{\lambda}_2^T \frac{\partial \mathbf{f}_2}{\partial \mathbf{u}_1} \tag{2.26}$$

With solutions to these equations, the sensitivity expression becomes

$$\frac{\partial u_{out}}{\partial \rho_e} = \boldsymbol{\lambda}_1^T (\frac{\partial \mathbf{K}_1}{\partial \rho_e}\mathbf{u}_1 - \frac{\partial \mathbf{f}_1}{\partial \rho_e}) + \boldsymbol{\lambda}_2^T (\frac{\partial \mathbf{K}_2}{\partial \rho_e}\mathbf{u}_2 - \frac{\partial \mathbf{f}_2}{\partial \rho_e})$$

It is now seen that the complete analysis and associated sensitivity calculation requires that one first solves system 1, then system 2 (2.25), and then for the sensitivity analysis one solves system 2 with a new (unit) load case and finally system 1 is solved with a modified load that depends on $\boldsymbol{\lambda}_1$ (see (2.26)).

This scheme immediately applies also to systems that involve three weakly coupled fields. This has been utilized for the results that are illustrated in the next section.

2.8.2 MicroElectroMechanical Systems (MEMS)

In the introduction to section 2.6, we discussed the advantages of compliant mechanism in connection with MEMS applications [18]. Modelling of MEMS typically involves simulations in multiple physical domains, for example coupled electrostatics and elasticity or coupled electric, thermal and elastic fields. The latter is required for the analysis and design of an electrothermal micro actuator. Electrothermal actuation is based on Joule's (resistive) heating and thereby thermal expansion and therefore requires modelling of three physical fields, namely electric, thermal and elastic fields. Electrothermal actuation is attractive for micro-systems due to its large displacement and force potential but the drawbacks are that it requires a strong electric field and that the operating temperature may disturb its environment.

A typical MEMS synthesis problem is to come up with a two-degree-of-freedom device with zero cross-axis sensitivity for scanning purposes. A design problem for such an application is sketched in Fig. 2.32a. The synthesis

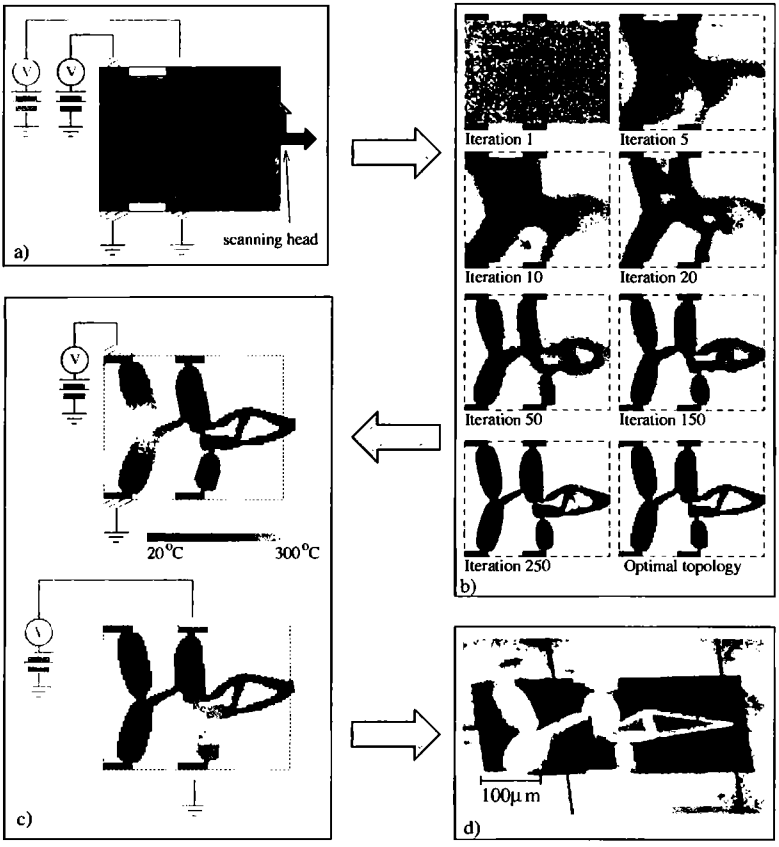

Fig. 2.32. Two degree-of-freedom electrothermomechanical actuator synthesis. a) design problem with two electrical inputs, b) iteration history, c) actuation modes and d) micro-fabricated actuator (from Jonsmann et al. 1999c).

problem here consists in finding a scanning mechanism where the scanning head (output point) moves in the horizontal direction for one electric input and in the vertical direction for another electrical input. The optimization problem involves 16 "load cases", 8 constraints and 8000 design variables. The iteration history is shown in Figure 2.32b, the two modes of actuation are shown in Figure 2.32c, and an actuator built in Nickel (size 500μm by 400μm) which was fabricated and tested at MIC, DTU is shown in Fig. 2.32d.

2.8.3 Stokes flow problems

A new and very interesting application of the topology optimization method is optimization for Stokes flow problems (Borrvall & Petersson 2002).

The finite element equations for general Stokes flow in three dimensions can be written as

$$\begin{bmatrix} \mathbf{K} & -\mathbf{G}_F \\ -\mathbf{G}_F^T & \mathbf{0} \end{bmatrix} \begin{Bmatrix} \mathbf{u} \\ \mathbf{p} \end{Bmatrix} = \begin{Bmatrix} \mathbf{f} \\ \mathbf{0} \end{Bmatrix} \tag{2.27}$$

where $\mathbf{u}$ is the velocity vector, $\mathbf{p}$ the pressure vector, and

$$\mathbf{K} = \int_V \mu \mathbf{B}^T \mathbf{I}_0 \mathbf{B} dV, \quad \mathbf{G}_F = \int_V (\nabla \mathbf{N}_\mathbf{u})^T \mathbf{N}_p dV, \quad \mathbf{f} = \int_{\Gamma_t} \mathbf{N}_\mathbf{u}^T \, \bar{t} \, d\Gamma$$

and μ is the dynamic viscosity. $\mathbf{N}_\mathbf{u}$ and $\mathbf{N}_p$ are the usual finite element shape matrices for the velocity and pressure fields, respectively, and $\mathbf{I}_0$ is a diagonal (6 by 6) matrix with 2's on the first three diagonal entries and 1's on the last three diagonal entries (e.g. Zienkiewicz & Taylor 2000).

The key question is now how to optimize such kinds of problems using topology optimization. For 2d problems, Borrvall & Petersson (2002) suggest to model the flow as a Couette flow, i.e. a flow between plates with a distance of 2ρ. This means that the components of the flow vector can be written as

$$u_1(x_1, x_2, x_3) = \hat{u}_1 (1 - \left(\frac{x_3}{\rho}\right)^2)$$

$$u_2(x_1, x_2, x_3) = \hat{u}_2 (1 - \left(\frac{x_3}{\rho}\right)^2)$$

$$u_3(x_1, x_2, x_3) = 0$$

Re-deriving the finite element equations with these assumptions and dropping the hats, one gets the following matrices to insert in the general FE-equation (2.27) which now is 2-dimensional

$$\mathbf{K} = \int_V \mu \mathbf{B}^T \mathbf{I}_0 \mathbf{B} dV + \int_V \alpha(\rho) \mathbf{N}^T \mathbf{N} dV = \sum_e \mu \mathbf{K}_e^\mu + \sum_e \alpha(\rho) \mathbf{K}_e^\alpha$$

$$\mathbf{G}_F = \int_V (\nabla \mathbf{N}_\mathbf{u})^T \mathbf{N}_p dV \qquad \mathbf{f} = \int_{\Gamma_t} \mathbf{N}_\mathbf{u}^T \, \bar{t} \, d\Gamma$$

where $\alpha(\rho) = \frac{5\mu}{2\rho^2}$.

The second term in $\mathbf{K}$ is interesting. For big ρ and therefore small α, we have an undisturbed Stokes flow. For small ρ (narrow channel) the term becomes large and may be interpreted as a large "damping" term that stops the flow. Another way to interpret the second term is to see it as a penalization term that ensures zero velocities at the penalized points just as for the support design problem in Sect. 2.7.

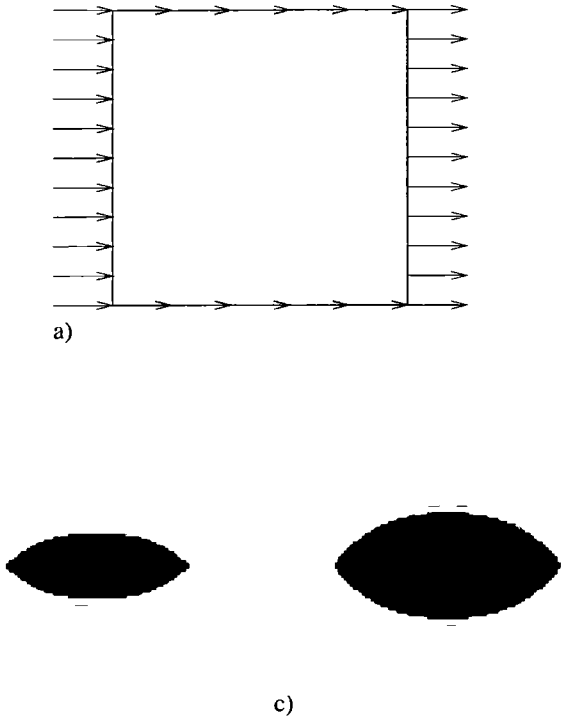

Fig. 2.33. Topology optimization of Stokes flow problem. The minimum drag profiles for b) 80% and c) 90% fluid volume, respectively. The results are obtained using bi-linear 4-node elements for modelling of the velocity field and 4-node constant pressure elements for the pressure field.

Although this formulation was derived for two-dimensional problems, the idea generalizes to three dimensions although the physical explanation in this case is lost.

We are now ready to formulate the optimization problem. We will take $\rho_e \in]0,1]$ as the design variable and we are allowed to use a prescribed amount of fluid in the design domain, i.e. the sum of the ρ_e's is constrained. We want to minimize the energy dissipation in the system. This corresponds to maximizing the "flow compliance" $c = \mathbf{f}^T\mathbf{u}$.

The optimization problem may now be stated as

$$
\begin{aligned}
\min_{\boldsymbol{\rho}} \quad & -\mathbf{f}^T\mathbf{u} \\
\text{s.t.} \quad & \begin{bmatrix} \mathbf{K} & -\mathbf{G}_F \\ -\mathbf{G}_F^T & \mathbf{0} \end{bmatrix} \begin{Bmatrix} \mathbf{u} \\ \mathbf{p} \end{Bmatrix} = \begin{Bmatrix} \mathbf{f} \\ \mathbf{0} \end{Bmatrix} \\
& \sum_{e=1}^{N} v_e \rho_e \leq V, \qquad 0 \leq \rho_e \leq 1, \quad e = 1, \ldots, N
\end{aligned}
\tag{2.28}
$$

The sensitivities of the objective function are simply

$$
\frac{\partial c}{\partial \rho_e} = \mathbf{u}^T \frac{\partial \mathbf{K}}{\partial \rho_e} \mathbf{u} = \frac{\partial \alpha(\rho_e)}{\partial \rho_e} \mathbf{u}^T \mathbf{K}_e^{\alpha} \mathbf{u}
$$

The optimization problem (2.28) is closely related to compliance minimization problems and may therefore be solved easily using an Optimality Criteria based algorithm.

Interestingly, Borrvall & Petersson (2002) prove existence of solutions to this problem without any additional relaxation or restriction. This can be explained by the fact that contrary to elasticity problems where smaller and smaller microstructures give better an better designs, smaller microstructures in Stokes flow will cause increased drag and will therefore not appear.[6]

We show two examples of topology optimization in Stokes flow. The first is the minimum drag profile (Fig. 2.33) and the second is flow in a structure with two parallel inlets and outlets (Fig. 2.34). Both examples are inspired by Borrvall & Petersson (2002) and compare favourably to examples that can be found in Pironneau (1973).

2.9 Optimal distribution of multiple material phases

In Chapter 1 we discussed different ways to interpolate the stiffness of elements with intermediate densities for solid void (one material and void) compliance minimization problems. We concluded that the choice of interpolation scheme plays a role in being able to interpret intermediate variables but otherwise, many different schemes have proven equally useful in obtaining good topological solutions. When considering distribution of multiple material phases in a design domain, the choice of interpolation function becomes more critical. For stiffness interpolation there is again the risk of ending up with intermediate design elements that cannot be represented by physical materials. Worse however, there is a risk that the optimization algorithm will make use of these non-physical properties to produce artificially good structures. An example of this could be a non-physically high thermal expansion coefficient for an intermediate density element.

[6] In mathematical terms, the existence issue is simplified by the fact that the design variable ρ now appears in the low-order terms of the analysis problem.

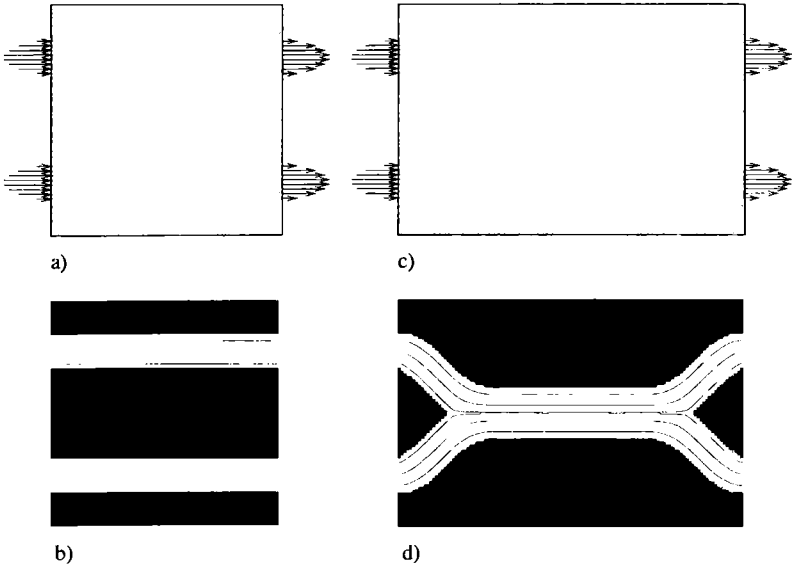

Fig. 2.34. Minimization of flow resistance in a structures with two parallel inlets and outlets for 30% fluid volume. a) Design domain with aspect ratio 1:1 and solution b). c) Design domain with aspect ratio 3:2 and solution d). The flow resistance of d) is 22% lower than for a topology with two straight pipes as in b) due to the lower resistance of the single wide channel.

In the following, we first discuss alternative ways to write the stiffness interpolation for one material and void structures. Then we discuss the extensions to two material structures and finally to two material and void structures.

2.9.1 One material structures

Considering structures built from one material and void, the SIMP interpolation for stiffness can be written in either of the following ways

$$E(\rho_e) = \rho_e^p E^0 \quad \left(E_{ijkl}(\rho_e) = \rho_e^p E_{ijkl}^0\right) \tag{2.29}$$

$$\left.\begin{aligned} \kappa(\rho_e) &= \rho_e^p\ \kappa^0 \\ \mu(\rho_e) &= \rho_e^p\ \mu^0 \end{aligned}\right\} \tag{2.30}$$

where superscript ^{0} signifies a property of the solid material, and κ and μ are the bulk and shear moduli, respectively,. Also, it is assumed in (2.29) that the Poisson's ratio is constant and equal to ν^0 As discussed earlier (see Sect. 1.1.2) the power p must be larger than a certain number dependent on

the Poisson's ratio of the material (cf., (1.5)) in order to satisfy the Hashin-Shtrikman bounds on elastic material behaviour (see Appendix 5.4.6).

For an interpolation of scalar problems like electrical or thermal conduction we can use an interpolation as

$$\zeta(\rho_e) = \rho_e^p \zeta^0$$

where likewise p must be bigger or equal to 2 to ensure physical realizability of intermediate density elements (Bendsøe & Sigmund 1999).

2.9.2 Two material structures without void

Considering structures composed of two materials, the interpolation laws must be modified. A modification of the power-law approach is to express the elasticity tensor of element e as

$$E_{ijkl}(\rho_e) = \rho_e^p \; E^1_{ijkl} + (1-\rho_e)^p \; E^2_{ijkl} \tag{2.31}$$

where E^1_{ijkl} and E^2_{ijkl} are the elasticity tensors of material 1 and 2, respectively. Although this interpolation has been used with success, it suffers a number of drawbacks. First, it violates the Hashin-Shtrikman bounds for low values of ρ_e and for large values of the power p. Furthermore, for the case of two materials with equal Young's moduli but *different* Poisson's ratios, it gives a strangely acting interpolation scheme. Finally, the scheme (2.31) changes behaviour if the phases are interchanged.

Instead of (2.31) one can use an interpolation that works with a weighted average of the Hashin-Shtrikman upper and lower bounds for each material property independently (cf., Sect. 1.5.4). The interpolated values for bulk, shear and conductivity moduli, respectively, are then written as

$$\left.\begin{aligned} \kappa(\rho_e) &= (1-\psi)\; \kappa^{HS}_{lower}(\rho_e) \; + \psi \; \kappa^{HS}_{upper}(\rho_e) \\ \mu(\rho_e) &= (1-\psi)\; \mu^{HSW}_{lower}(\rho_e) + \psi \; \mu^{HSW}_{upper}(\rho_e) \\ \zeta(\rho_e) &= (1-\psi)\; \zeta^{HS}_{lower}(\rho_e) \; + \psi \; \zeta^{HS}_{upper}(\rho_e) \end{aligned}\right\}, \tag{2.32}$$

where $(\kappa^{HS}_{lower}, \; \kappa^{HS}_{upper})$, $(\zeta^{HS}_{lower}, \; \zeta^{HS}_{upper})$ are the lower and upper Hashin-Shtrikman bounds on bulk and conductivity moduli, respectively, and $(\mu^{HSW}_{lower}, \mu^{HSW}_{upper})$ are the lower and upper Hashin-Shtrikman-Walpole bounds on shear modulus for two-phase composites [7] In (2.32), $\psi \in [0,1]$ interpolates between the lower and upper bounds. If we choose $\psi = 0$, the use of intermediate densities is made uneconomical just as in the power-law approach.

For design of two-phase composite involving the thermal expansion coefficient, one does not need an interpolation scheme as it is directly given

[7] The upper and lower Hashin-Strikhman bounds are given in (1.42), (1.44) and in Appendix 5.4.6.

in terms of the effective (interpolated) bulk modulus (Levin 1967, Rosen & Hashin 1970)

$$\alpha(\rho_e) = \frac{\alpha^1\kappa^1(\kappa^2 - \kappa(\rho_e)) - \alpha^2\kappa^2(\kappa^1 - \kappa(\rho_e))}{\kappa(\rho_e)(\kappa^1 - \kappa^2)}, \tag{2.33}$$

where κ^1 and κ^2 are the bulk moduli of material 1 and 2, respectively.

2.9.3 Two material structures with void

The two-phase power-law interpolation scheme can also be extended to a scheme for three material phases (two materials and void) with two design variables ρ_e^1 and ρ_e^2

$$E_{ijkl}(\rho_e^1, \rho_e^2) = (\rho_e^1)^{p_1}\left((\rho_e^2)^{p_2}\ E_{ijkl}^1 + (1-\rho_e^2)^{p_2}\ E_{ijkl}^2\right),$$

where the penalization powers p_1 and p_2 can be chosen independently. This modified SIMP scheme performs very well for pure stiffness problems. For use in multiphysics, however, one should apply a hybrid of the power-law and the Hashin-Shtrikman interpolation scheme, making use of the best features of both. By interpolating between material (any of the two materials) and void using the power-law approach, problems with jumps in properties are avoided and by using the Hashin-Shtrikman bounds to interpolate between the two material phases, a consistent interpolation is obtained.

The scheme is invoked for each property independently as

$$\left.\begin{aligned}
\kappa(\rho_e^1,\ \rho_e^2) &= (\rho_e^1)^p\left[(1-\psi)\ \kappa_{lower}^{HS}(\rho_e^2) + \psi\ \kappa_{upper}^{HS}(\rho_e^2)\right]\\
\mu(\rho_e^1,\ \rho_e^2) &= (\rho_e^1)^p\left[(1-\psi)\ \mu_{lower}^{HSW}(\rho_e^2) + \psi\ \mu_{upper}^{HSW}(\rho_e^2)\right]\\
\zeta(\rho_e^1,\ \rho_e^2) &= (\rho_e^1)^p\left[(1-\psi)\ \zeta_{lower}^{HS}(\rho_e^2) + \psi\ \zeta_{upper}^{HS}(\rho_e^2)\right]
\end{aligned}\right\} \tag{2.34}$$

The interpolation law for the thermal expansion coefficient is just a slight modification of (2.33) and is given by

$$\alpha(\rho_e^2) = \frac{\alpha^1\ \kappa^1\ (\kappa^2 - \kappa(\rho_e^2)) - \alpha^2\ \kappa^2\ (\kappa^1 - \kappa(\rho_e^2))}{\kappa(\rho_e^2)\ (\kappa^1 - \kappa^2)}. \tag{2.35}$$

Note that the thermal expansion coefficient depends on the bulk modulus of the two-phase composite only (which is found by setting $\rho_1^e = 1$ in (2.34)).

The material interpolation scheme, defined by (2.34) and (2.35), is controlled by the two penalization parameters p and Ψ. If these parameters are selected according to the criterion

$$p \geq \max\left(\frac{\kappa^1+\mu^1}{\mu^1}, \frac{\kappa^1+\mu^1}{\kappa^1}, \frac{\kappa^2+\mu^2}{\mu^2}, \frac{\kappa^2+\mu^2}{\kappa^2}\right) \qquad 0 \leq \Psi \leq 1 \tag{2.36}$$

then it can be shown that the interpolated parameters always will satisfy the Hashin-Shtrikman bound. Usually we choose $p = 3$ and $\Psi = 1$, corresponding to the usual power-law penalization and the upper Hashin-Shtrikman

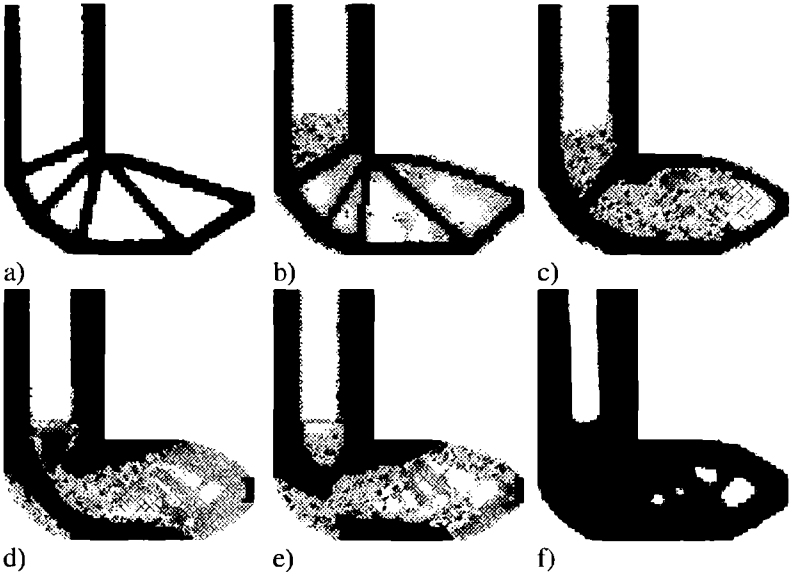

Fig. 2.35. Optimal distribution of two material phases for compliance minimization of the L-shaped structure from Fig. 1.3. Different ratios between the stiff (black) and the soft phase (hatched). a) Optimal distribution of 25% volume fraction of only one phase. b-e) Optimal distributions of two materials with each a volume fraction of 25%. Ratio between material stiffnesses: b) 0.01, c) 0.2, d) 0.5 and e) 0.8. f) Optimal distribution of 50% volume fraction of only one phase.

bound for the two material composite. In the cases where the upper Hashin-Shtrikman bound interpolation results in intermediate values of the second design variable, i.e. we have a two-material composite, the value of Ψ is lowered towards zero, resulting in a non-composite (and manufacturable) topology.

2.9.4 Examples of multiphase design

An example of distribution of two material phases in an L-shaped design domain is shown in Fig. 2.35. Depending on the stiffness of the second material it will act as core material (Figs. 2.35b and c) or as a structural material (Figs. 2.35d and e).

In the thermal actuator design problem shown in Figure 2.24a one may introduce a second material with alternative thermomechanical properties to compete in the material distribution process. However, if only the total volume fraction is prescribed rather than the volume fractions of the individual

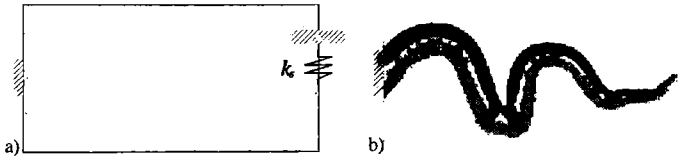

Fig. 2.36. a) Two-material thermal actuator design problem and b) topology optimized bi-metal actuator with small support (from Sigmund 2001c).

phases and the design has lots of possible supports, experience shows that the synthesis algorithm prefers only to make use of the material with the highest product of Young's modulus and the squared thermal expansion coefficient. This numerical observation has also been verified analytically. In these cases, the two-material synthesis problem would results in one-material actuators like the ones shown in Figure 2.24 (see Sigmund (2001c) for details).

If there are only few and small supports (insufficiently grounded), the synthesis algorithm can not make use of the type of amplification mechanisms that are shown in Figure 2.24. Rather, the design procedure makes use of the so-called bi-material or bimorph principle, see Figure 2.36. The efficiency of the optimized actuator is here only 14% of an actuator with ample supports (as shown in Figure 2.24). This underlines that bimorph actuation is extremely inefficient due to the loss of mechanical energy in the interface between the two material phases. Consequently, they will only appear in topology optimized two-material actuators if supports are small or rare (cf., Sigmund (2001c)).

More examples of design of multiphase material structures are given in section 2.10.3 that deals with design of materials.

2.10 Material design

The response of structures depends on the materials they are built from. If one can design materials with tailored or extreme properties one may be able to design better structures. This aspect is central also in topology design where the role of composites in the homogenization approach and other optimization models operating with general material tensors underlines such an aspect of *local optimal use of material.* This is the theme of Chap. 3.

In this section we will deal with methods that apply the ideas of topology optimization, originally developed for structural optimization problems, to the design of material design as well [21]. The fundamental idea is that *any material is a structure if you look at it through a sufficiently strong microscope.*

Assuming that the material one considers is periodic, its effective properties may be fully described by an analysis of the smallest repetitive unit,

the *base cell.* The design problem then consists in assigning a material type to each point in the base cell. In the discretized topology optimization setting this corresponds to assigning a material type to each element used to discretize the base cell. The material type may be selected from two or more constituent phases of which one may be void. For example, a porous honeycomb material may be designed from a void and a solid material phase.

The effective properties of a material are found by homogenization of the microstructure. In our case the microstructure does not exist ab initio but we seek to come up with a microstructure with prescribed or extreme homogenized properties. Therefore the material design method has also been called *the inverse homogenization method.*

Before we proceed to define objective functions for material design, we briefly discuss how to find the effective properties and the sensitivities thereof using the homogenization method.

There is, as indicated above, a very strong interrelation between the developments that follows and the content of Chap. 3. Thus this section would equally well fit in the framework of that Chapter. However, as the emphasis in the following is on modelling and computational issues that have been discussed so far in this Chapter, the application of topology design to material design is treated here and not in Chap. 3.

2.10.1 Numerical homogenization and sensitivity analysis

If a structure is built from periodic materials it is often too cumbersome or even impossible to model it taking every detail of the micro-structure into consideration. Therefore, one substitutes the microstructure with some average or smeared out properties that model the material behaviour seen on a global scale. The process of finding representative or effective properties of microstructured materials is called homogenization [20]. In Chap. 3 and in appendix 5.4 we discuss analytical procedures for the homogenization of simple layered microstructures and their more complicated off-springs, the so-called rank-N microstructures. If we want to model (and design) microstructures with more general micro-geometries we have to perform the homogenization by numerical means. In the following we describe the homogenization equations and briefly discuss their discretization in the finite element formulation.

The homogenized stiffness tensor is by integration over the base cell area Y found as

$$E^H_{ijkl} = \frac{1}{|\mathrm{Y}|}\int_Y \left[E_{ijkl} - E_{ijpq}\frac{\partial \chi^{kl}_p}{\partial y_q}\right] \mathrm{d}y \tag{2.37}$$

where the Y-periodic test fields χ^{kl}_p are found as the solutions to the equilibrium equations

$$\int_{\mathrm{Y}} E_{ijpq}\frac{\partial \chi^{kl}_p}{\partial y_q}\frac{\partial \phi_i}{\partial y_j}\mathrm{d}y = \int_{\mathrm{Y}} E_{ijkl}\frac{\partial \phi_i}{\partial y_j}\mathrm{d}y \quad \text{for all Y} - \text{periodic } \phi\ , \tag{2.38}$$

and Y is the area of the unit cell.

In a somewhat simpler notation, (2.37) may be written as

$$E^H_{ijkl} = \frac{1}{|\mathrm{Y}|}\int_{\mathrm{Y}} E_{pqrs}(\varepsilon^{0(ij)}_{pq} - \varepsilon^{*(ij)}_{pq})(\varepsilon^{0(kl)}_{rs} - \varepsilon^{*(kl)}_{rs})\ \mathrm{d}y\ ,$$

where $\varepsilon^{*(kl)}_{pq} = \frac{1}{2}(\frac{\partial \chi^{kl}_p}{\partial y_q} + \frac{\partial \chi^{kl}_q}{\partial y_p})$ and ε^0_{ij} corresponds to the three (2D) or six (3D) unit test strain fields.

In practice, the equilibrium equations (2.38) are solved as a finite element problem with three or six load cases

$$\mathbf{K}\chi^{kl} = \mathbf{f}^{kl}$$

where the displacements χ^{kl} are constrained to be Y-periodic by either a penalty approach or by assigning equal node numbers to opposing boundary nodes. The force vector is found from

$$\mathbf{f}^{kl} = \sum_e \int_{\mathrm{Y}_e} \mathbf{B}^T_e \mathbf{E}_e(\rho_e)\ \boldsymbol{\varepsilon}^{0(kl)} \mathrm{d}y$$

and the global stiffness matrix is calculated as the usual assembly of element stiffness matrices $\mathbf{K} = \sum_e \mathbf{K_e}$ plus corrections for periodicity. In FE-notation, the effective properties may then be found as

$$\begin{aligned} E^H_{ijkl} =& \frac{1}{|\mathrm{Y}|}\sum_e (\chi^{0(ij)} - \chi^{ij})^T \int_{\mathrm{Y}_e} \mathbf{B}^T\ \mathbf{E}(\rho_e)\ \mathbf{B}\ \mathrm{d}y\ (\chi^{0(kl)} - \chi^{kl}) = \\ & \frac{1}{|\mathrm{Y}|}\sum_e (\chi^{0(ij)} - \chi^{ij})^T\ \mathbf{K}_e(\rho_e)\ (\chi^{0(kl)} - \chi^{kl}), \end{aligned}$$

where $\mathbf{E}$ is the constitutive matrix, $\mathbf{B}$ is the finite element strain-displacement matrix and $\chi^{0(ij)}$ is the nodal displacement vector corresponding to the test strain field $\boldsymbol{\varepsilon}^{0(ij)}$

The sensitivity of a component of the constitutive tensor with respect to the density design variable ρ_e can again be found by the adjoint method. The resulting sensitivity expression in FE-notation is

$$\frac{\partial E^H_{ijkl}}{\partial \rho_e} = \frac{1}{|\mathrm{Y}|}(\chi^{0(ij)} - \chi^{ij})^T\ \frac{\partial \mathbf{K}_e(\rho_e)}{\partial \rho_e}\ (\chi^{0(kl)} - \chi^{kl}).$$

2.10.2 Objective functions for material design

The goal of material design may be to synthesize a material with prescribed constitutive properties or it may be to synthesize materials with extreme constitutive properties. An example of the former could be the need for designing a material with a specific Young's modulus and a specific isotropic

thermal expansion coefficient. This material could be used to neutralize thermal mismatch in a heat generating structure. An example of synthesis of an extremal material could be to maximize the bulk modulus of a material for a given volume fraction of solid material. This would result in a material with an extreme stiffness to weight ratio.

For now, we consider the design of materials composed of a solid and a void phase. Therefore, the element stiffness may be interpolated by the SIMP interpolation $E(\rho_e) = \rho_e^p E_0$ as we did for structural design problems.

If we want to obtain a material with prescribed elastic tensor E^*_{ijkl}, an objective function to be minimized could be the error between the homogenized elasticity tensor E^H_{ijkl} and the wanted stiffness tensor E^*_{ijkl}. An optimization problem with this goal can be written as

$$\begin{aligned} \min_{\boldsymbol{\rho}} \quad & \sum_{i,j,k,l=1}^{d} (E^*_{ijkl} - E^H_{ijkl}(\boldsymbol{\rho}))^2 \\ \text{s.t.} \quad & \mathbf{K}\boldsymbol{\chi}^{kl} = \mathbf{f}^{kl}, \quad k,l = 1,\ldots,d\,, \\ & \frac{1}{|Y|}\sum_{e=1}^{N} v_e\rho_e \le \vartheta, \\ & 0 < \rho_{min} \le \rho_e \le 1, \quad e = 1,\ldots,N \end{aligned} \tag{2.39}$$

where ϑ is the bound on the volume fraction and d is the spatial dimension.

If a material with the wanted properties E^*_{ijkl} cannot be obtained for the given constituent materials and volume fractions, the problem formulation (2.39) may give useless results. On the other hand, if the wanted properties E^*_{ijkl} are easy to obtain, it means that one could take out material of the base cell and still obtain the wanted properties. This superfluous material tends to cloak the design process and prevent convergence of the optimization algorithm. Also, it paralyses the SIMP scheme since the volume constraint is not active, in turn producing pictures with lots of grey elements.

Alternatively one my turn the problem upside down and minimize the volume fraction for prescribed constitutive properties. This may be formulated as

$$\begin{aligned} \min_{\boldsymbol{\rho}} \quad & \frac{1}{|Y|}\sum_{e=1}^{N} v_e\rho_e \\ \text{s.t.} \quad & \mathbf{K}\boldsymbol{\chi}^{kl} = \mathbf{f}^{kl}, \quad k,l = 1,\ldots,d\,, \\ & E^*_{ijkl} - E^H_{ijkl}(\boldsymbol{\rho}) = 0, \quad ,j,k,l = 1,\ldots,d\,, \\ & 0 < \rho_{min} \le \rho_e \le 1, \quad e = 1,\ldots,N \end{aligned} \tag{2.40}$$

For a continuum model[8] of the unit cell not every positive definite stiffness tensor is realizable [25], and theoretical bounds on the material parameters

[8] Using trusses for the unit cell is discussed in section 3.4.5.

for isotropic, square or cubic symmetric composite material are known. This means that the problem formulation (2.40) may in some cases suffer from lack of any feasible designs. To circumvent this and in order to be able to synthesize extreme materials, i.e. materials with properties that reach the limits of the bounds, we write a new problem formulation as

$$
\begin{aligned}
&\min_{\boldsymbol{\rho}} c(E^H_{ijkl}(\boldsymbol{\rho})) \\
&\text{s.t.} \quad \mathbf{K}\chi^{kl} = \mathbf{f}^{kl}, \quad k,l = 1,\ldots,d\,, \\
&\qquad \frac{1}{|\mathrm{Y}|}\sum_{e=1}^{N} v_e\rho_e \le \vartheta, \\
&\qquad g_i(E^H_{ijkl}(\boldsymbol{\rho})) \le g_i^*, \quad i = 1,\ldots,M \\
&\qquad 0 < \rho_{min} \le \rho_e \le 1, \quad e = 1,\ldots,N
\end{aligned}
\tag{2.41}
$$

where the objective function $c(E^H_{ijkl})$ and constraints $g_i(E^H_{ijkl})$ are functions of the homogenized tensor and M is the number of constraints.

The constraints in (2.41) may take different forms. For example minimum Poisson's ratio is obtained for very soft structures and to prevent too flimsy materials a lower bound constraint on the effective bulk modulus κ_{min} may therefore be added, i.e. $g_1 = -\kappa^H$ and $g_1^* = -\kappa_{min}$. Also, it may be desired to impose a constraint that ensures symmetries in the resulting material properties. Orthotropy (i.e. $E^H_{1112} = E^H_{2212} = 0$) may be obtained by imposing one or more lines of symmetry in the base cell. Square symmetry may for example be obtained by imposing one line of symmetry and adding the constraint $g_2 = (E^H_{1111} - E^H_{2222})^2/(E^H_{1111} + E^H_{2222})^2$ with $g_2^* = \epsilon^2$, where ϵ is a small tolerance number.

The problem formulation (2.41) was first suggested in Sigmund & Torquato (1997) and has since then been used successfully in the design of material with extremal elastic, thermoelastic, piezoelectric and other physical properties [21]. As will be seen in the following subsections, the results are very close to theoretical limits and have in fact in some cases inspired the improvement of theoretical limits.

2.10.3 Material design results

Extremal elastic properties A basic material design problem is to find a structure with maximum bulk modulus for a given volume fraction. This is a highly non-unique optimization problem. Four types of microstructures are now known to have extreme bulk moduli, i.e. they have bulk moduli equal to the upper Hashin-Shtrikman bounds. These microstructures are sketched in Fig. 2.37.

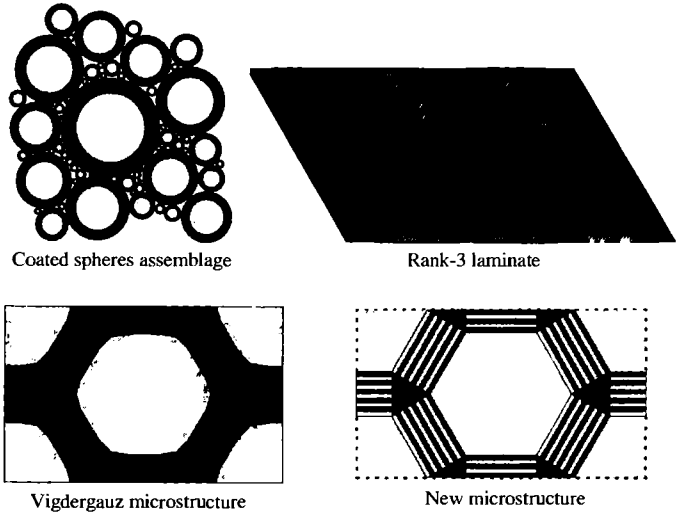

Fig. 2.37. The four known classes of extremal isotropic microstructures. The isotropy requires special geometries of the different unit cells.

Topology optimization results for the maximization of bulk modulus of two-dimensional microstructures and a one-length-scale constraint[9] are shown in Fig. 2.38. All four microstructures have effective bulk moduli within a few percent of each other and the known analytical bound. By control of starting guesses, objective functions, base cell geometry and/or isotropy type, one may obtain one structure or another. The results in Fig. 2.38 were obtained for an initial filter radius of 10% of the base cell. The filter size was gradually decreased to zero during the design process. The obtained structures may be denoted one-length-scale microstructures and correspond to the known optimal so-called Vigdergauz structures (Vigdergauz 1994, Vigdergauz 1999). Note that the bulk optimized microstructures are closed walled cells.

Figure 2.39 shows two examples of maximization of bulk modulus of 3D structures. Again, the two structures that were obtained without and with isotropy constraint have effective bulk moduli extremely close to the theoretical Hashin-Shtrikman bounds.

[9] One length scale materials are here defined as microstructures that do not make use of several length scales in the base cell. One length scale materials are obtained by specifying rather big sizes of the sensitivity filter (e.g. 10% of the base cell) in the initial topology optimization iterations.

b) c) d)

Fig. 2.38. Four microstructures with extremal bulk moduli obtained by the inverse homogenization procedure. a) Isotropic hexagonal microstructure (maximization of bulk modulus for rectangular base cell with isotropy constraint), b) isotropic triangular microstructure (maximization of product of bulk and shear modulus for rectangular base cell with isotropy constraint), c) isotropic octagonal microstructure (maximization of bulk modulus with isotropy constraint) and d) square symmetric microstructure (maximization of bulk modulus) (from Sigmund 2000b).

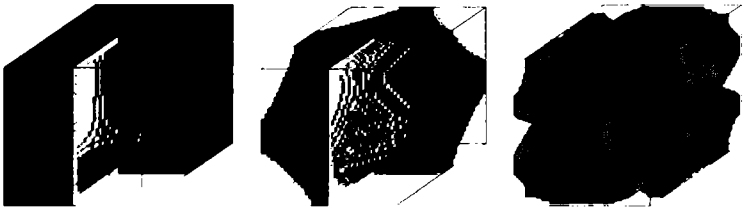

Fig. 2.39. Three optimized three-dimensional microstructures. Left: cubic-symmetric maximum bulk modulus microstructure. Center: Isotropic maximum bulk modulus microstructure. Right: Isotopic negative Poisson's ratio material (from Sigmund 2000b).

A realization of the SIMP model We have continually compared the SIMP and other interpolation models with the Hashin-Shtrikman bounds for isotropic composites. These bounds gives *necessary* conditions for the interpolation models. However, it is the material design methodology of the inverse homogenization method that allows us to construct concrete realizations of the SIMP model, as seen in Figs. 2.40 and 2.41. Note that, in itself, the inverse homogenization is based on a SIMP interpolation in the unit cell, making the dog bite its tail.

Negative Poisson's ratio materials An extremely interesting application of the material design method is the search for negative Poisson's ratio materials. A number of such structures have been suggested in the literature (cf. [21]), but here we apply topology optimization to obtain the behaviour we are looking for. If (2.41) is formulated so as to minimize the Poisson's ratio with a constraint on bulk modulus and isotropy, the inverse homogenization method gives results as shown for 2D in Fig. 2.42 and for 3D in Fig. 2.39.

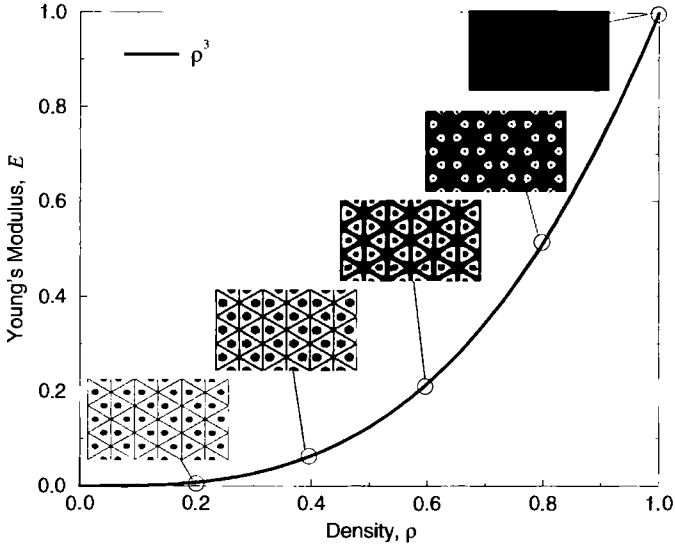

Fig. 2.40. Microstructures of material and void realizing the material properties of the SIMP model with $p = 3$, for a base material with Poisson's ratio $\nu = 1/3$. As stiffer material microstructures can be constructed from the given densities, non-structural areas are seen at the cell centers (from Bendsøe & Sigmund 1999).

The isotropic and negative Poisson's ratio structure has been manufactured in micro-scale (Larsen, Sigmund & Bouwstra 1997). The 40 by 8 cell testbeam was built using surface micromachining with a unit-cell size of 60 μm as shown in Fig. 2.42c. The Poisson's ratio of the test-beam was measured to -0.9±0.1 in experiments; this compares favourably to the theoretical value of -0.8. Recently, manufacturing of the topology optimized negative Poisson's ratio materials by extrusion techniques have been performed at University of Michigan (http://msewww.engin.umich.edu:81/people/halloran).

Optimizing the thermal expansion coefficient For two-phase composites made from solid and void, the effective thermal expansion coefficient will always be the same as for the solid phase, unless the material is disconnected. For two-phase mixtures of two non-void materials, the effective thermal expansion coefficient for any square or cubic symmetric mixture of the materials will always take values between the maximum and the minimum thermal expansion coefficients of the two phases. However, for three-phase composites, it becomes more interesting. According to theory (Schapery 1968, Rosen & Hashin 1970, Gibiansky & Torquato 1997) it is possible to synthesize three-phase materials with effective thermal expansion coefficients that exceed

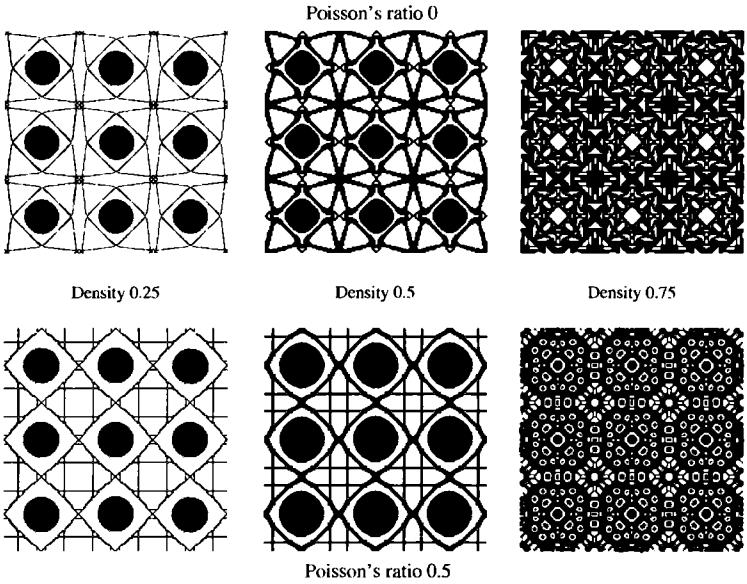

Fig. 2.41. Microstructures of material and void realizing the material properties of the SIMP model with $p = 4$ for a base material with Poisson's ratio $\nu = 0$ (top row) and $\nu = 0.5$ (bottom row), respectively. As in Fig. 2.40, non-structural areas are seen at the centers of the cells (from Bendsøe & Sigmund 1999).

those of the individual phases. In particular, it should be possible to synthesize negative thermal expansion materials from mixtures of two positive expansion phases and a void phase. The extreme thermal expansion is obtained at the cost of a decrease in the effective bulk modulus. The theoretical bounds on the range of attainable combinations of thermal coefficients and bulk modulus for a particular case are shown in Fig. 2.43a.

For the design of extremal thermal expansion coefficients it is necessary to extend the previous problem formulation to include an extra load case. This extra load case corresponds to subjecting the base cell to a uniform temperature increase. The new problem formulation may be written as

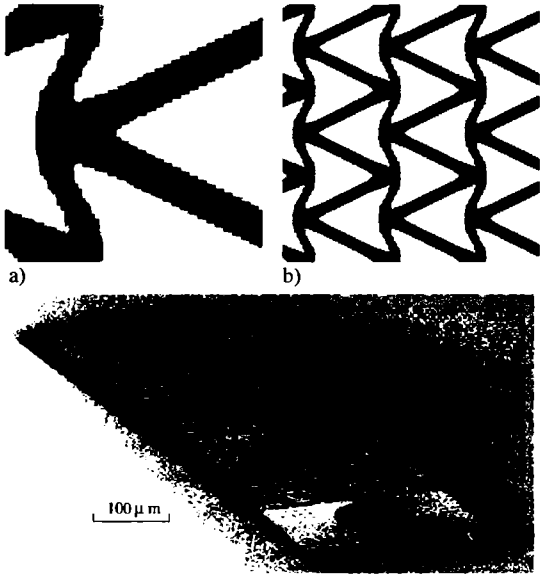

Fig. 2.42. Material microstructure with negative Poisson's ratio. a) one unit cell discretized by 60 by 60 elements, b) repeated unit cell and c) micromachined test beam built at MIC, DTU, DK (from Larsen et al. 1997).

$$
\begin{aligned}
&\max_{\boldsymbol{\rho}} \; c(E^H_{ijkl}(\boldsymbol{\rho}^1,\boldsymbol{\rho}^2),\; \alpha^H_{ij}(\boldsymbol{\rho}^1,\boldsymbol{\rho}^2)) \\
&\text{s.t.} \quad \mathbf{K}\boldsymbol{\chi}^{kl} = \mathbf{f}^{kl}, \quad k,l = 1,\ldots,d\,, \\
&\qquad \mathbf{K}\boldsymbol{\chi}^{\alpha} = \mathbf{f}^{\alpha} \\
&\qquad \frac{1}{|\mathrm{Y}|}\sum_e v_e \rho^1_e \rho^2_e \le \vartheta_1, \quad 0 < \rho_{min} \le \rho^1_e \le 1, \quad e = 1,\ldots,N \\
&\qquad \frac{1}{|\mathrm{Y}|}\sum_e v_e \rho^1_e (1-\rho^2_e) \le \vartheta_2, \quad 0 \le \rho^2_e \le 1, \quad e = 1,\ldots,N \\
&\qquad g_i(E^H_{ijkl}(\boldsymbol{\rho}^1,\boldsymbol{\rho}^2)) \le g^*_i, \quad i = 1,\ldots,M
\end{aligned}
\tag{2.42}
$$

where the thermal test field $\boldsymbol{\chi}^{\alpha}$ is again Y-periodic and the thermal finite element load vector is defined as

$$
\mathbf{f}^{\alpha} = \sum_e \int_{Y_e} \mathbf{B}^T_e \mathbf{E}_e(\rho^1_e,\rho^2_e)\; \boldsymbol{\alpha}(\rho^2_e) dY.
$$

Here, the element thermal expansion coefficient $\alpha(\rho_e^2)$ is interpolated by the expression given in (2.35). The examples shown in the following are all based on the three phase SIMP interpolation scheme (2.31).

Figure 2.43a shows a graph of the thermal expansion coefficients as a function of the bulk moduli for some numerically obtained microstructures compared with the theoretical bounds. The design problem consists in extremizing the thermoelastic properties of a composite consisting of 25% of a material with thermal expansion coefficient 10 (normalized value) and 25% of a material with thermal expansion coefficient 1. A resulting composite with a negative thermal expansion coefficient of -4.02 is shown in Figure 2.43b. This shows that it is actually possible to design materials with *negative* thermal expansion coefficients from constituent phases with *positive* thermal expansion coefficients. Actual manufacturing of three-phase composites has been difficult but recent reports from researchers at University of Michigan show that it is indeed possible to manufacture the suggested composites but test results are not yet publicly available (http://msewww.engin.umich.edu:81/people/halloran).

In Figure 2.43a one notes that the numerically obtained effective values are far away from the old bounds (Schapery 1968, Rosen & Hashin 1970) but very close to the newer bounds (Gibiansky & Torquato 1997). In fact, the substantial improvement of the new bounds compared to the old bounds was inspired by the numerical results by Sigmund & Torquato (1997). Using the translation method, Gibiansky & Torquato (1997) managed to make the theoretical bounds match the numerical results!

A new class of extremal two-phase composites Existing bounds on the possible range of the bulk and shear moduli of isotropic two-phase composites composed of isotropic constituents (Hashin & Shtrikman 1963, Cherkaev & Gibiansky 1993) have only been proven optimal (in the sense that there exist microstructures that attain them) for certain cases. In order to investigate the optimality of these bounds in further detail, a study based on the inverse homogenization was performed in (Sigmund 2000b). The study resulted in numerically obtained bounds for one-length-scale structures, proof of optimality of the bounds in a wider range than previously known and a new class of extremal composites. Thus, use of the topology design methodology has lead to new understanding in the area of theoretical material science. This symbiosis is strongly present when one considers topology design with composites where design has benefited immensely from work in material science, see Chap. 3.

Limiting the microstructural variation to one length-scale by fixing the value of the mesh-independency filter, one-length-scale bounds on bulk and shear moduli of isotropic two-phase composites shown in Figure 2.44a are obtained. These bounds shall not be taken formally but more as bounds based on experience and trust in that the inverse homogenization procedure produces reliable results.

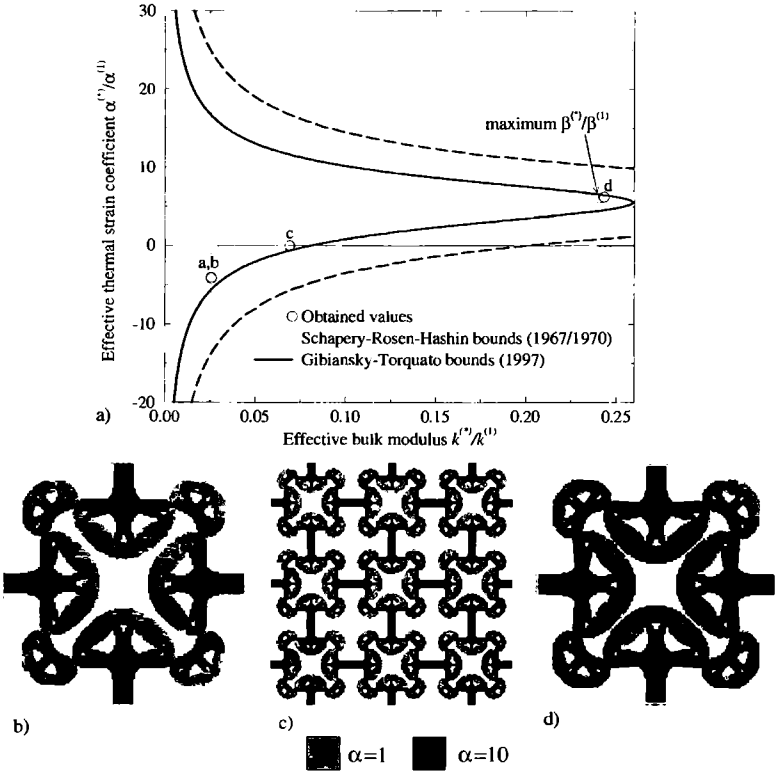

Fig. 2.43. Design of materials with extreme thermoelastic properties using topology optimization a) Thermal expansion coefficient-bulk modulus graph for specific thermoelastic composite including theoretical bounds and numerically obtained properties, b), c) and d) material microstructure with negative thermal expansion coefficient (single base cell, 3 by 3 array and heated single cell). When heated, the cell contracts resulting in an effective negative thermal expansion coefficient (from Sigmund & Torquato 1997).

Studying the bounds based on the one-length-scale structures in Figure 2.44a, one notes that no structures get close to the lower right corner of the bounds, also called the Walpole point (i.e. maximum bulk modulus and minimum shear modulus corresponding to the lower right corner of the bounds). Allowing finer variation in the microstructures by decreasing the filter size, a sequence of designs with properties getting closer and closer to the Walpole point (see Figure 2.44a) may be obtained. Inspired by these numeri-

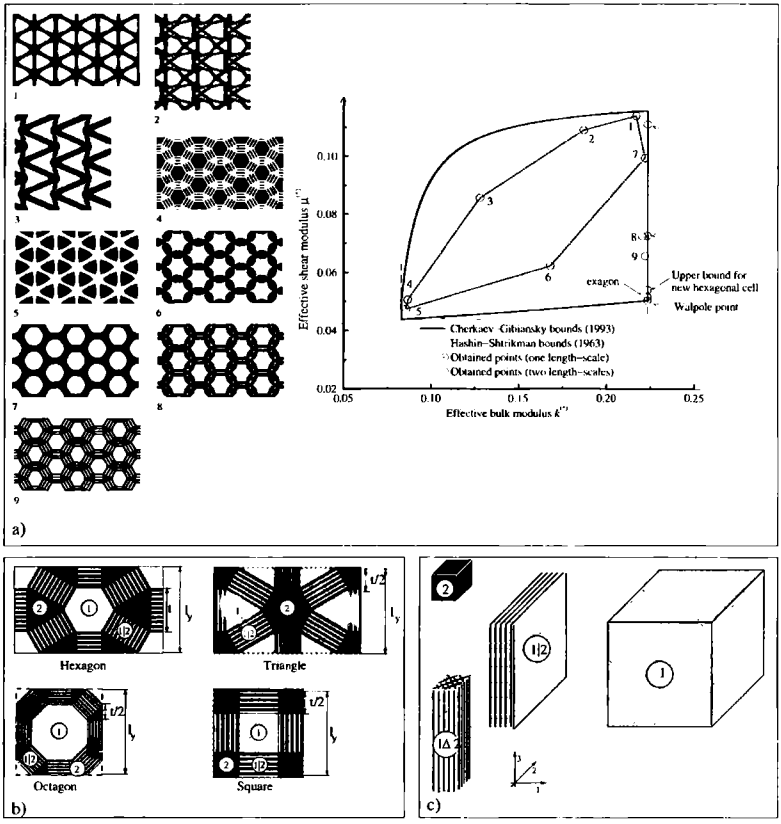

Fig. 2.44. Design of extremal two-phase composites. a) Bound for one-length-scale composites and numerically obtained microstructures and allowing finer variation in the microstructure results in a new microstructure with properties close to the Walpole point (maximum bulk modulus and minimum shear modulus, b) two-dimensional members of the new class of extremal microstructures consisting of solid convex polygonal regions connected by laminated bars and c) three-dimensional members of the new class of extremal microstructures (from Sigmund 2000b).

cally obtained results, a parametrized hexagonal microstructure consisting of convex polygonal regions of solid material phases connected by *layers* of equal proportions was investigated analytically (see Figure 2.44b). Surprisingly, it was possible to calculate the effective properties exactly and the bulk modulus of the composite corresponded to the Hashin-Shtrikman bounds. Even more surprising, exact solutions and proof of extremity could be obtained

for a whole class of similar microstructures in two and three dimensions (see Fig. 2.44b and c). The investigation thus resulted in a new class of extremal isotropic microstructures which constitutes an alternative to the three previously known classes, namely Composite Spheres assemblages, Vigdergauz structures and rank-N layered materials (see Fig. 2.37). One member of this class of materials (the hexagonal microstructure) has maximum bulk modulus and lower shear modulus than any previously known composite. Although no member of the new class of materials attains the Walpole point exactly, the Walpole point can be considered attainable for all practical means and the Hashin-Shtrikman/Cherkaev-Gibiansky bounds have been proven optimal for a wider range of properties than was previously known.

A new class of extremal three-phase composites Inspired by the two-phase results in the previous subsection the same type study consisting of analytical methods combined with numerical experiments may be performed for three-phase materials. When considering three material phases the equations become much more complicated, and a large number of special cases must be considered for the large number of possible material combinations (e.g. bulk and shear moduli may be well-ordered or not). Nevertheless, the existence of a new class of three-phase composites with extremal bulk moduli can be proved (Gibiansky & Sigmund 2000). The three phase microstructures are closely related to the two-phase class from the previous subsection. For example, the three-phase structures converge to the two-phase structures when the volume fraction of one phase approaches zero. For the three-phase case, the new class of structures also expands the ranges of previously known attainable properties and optimality of bounds. Figure 2.45a shows some numerically obtained three-phase microstructures and Figure 2.45b shows schematics of members of the new class of three-phase extremal microstructures. Note how *layered* regions again play a significant role.

Piezoelectric sensors Another three-phase material design example is the design of hydrophones based on piezoelectric sensing. A piezoelectric material responds with an electric output when strained. For a typical ceramical piezoelectric rod, the electric field depends on the elongation of the rod. Simply said, this means that the electric output for a horizontal compression will have the negative sign of a that for a longitudinal compression. For hydrophones which should detect changes in hydrostatic pressures, this is a problem. Compression in all directions simultaneously will almost cancel the electrical output. In order to circumvent this problem it has been suggested to embed piezoelectric rods in a matrix material with tailored properties. A negative Poisson's ratio matrix material will for example convert transverse pressure to a compression of the rod instead of extension, in turn causing a much larger output signal.

The inverse homogenization method may be used to identify the matrix microstructure that maximizes the electric output of hydrophones. The prob-

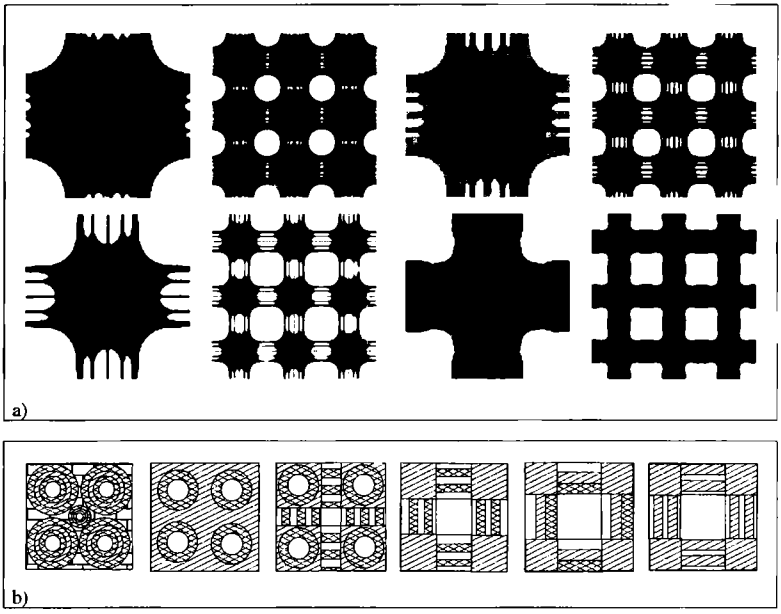

Fig. 2.45. Design of extremal three-phase composites. a) Numerically obtained three-phase microstructures with extremal bulk modulus, b) schematics of the new class of extremal microstructures (from Gibiansky & Sigmund 2000).

lem corresponds to a three-phase material design problem of distributing a piezoelectric, a polymer and a void phase in a periodic base cell. However, for various reasons, the periodicity of the matrix microstructure will often be much smaller than for the embedded rods. Therefore one may model the problem partly by effective medium theory and partly by numerical homogenization. This means that the effective properties of the matrix material may be found by numerical homogenization whereas the effective properties of the mixture of the matrix material and the piezoelectric rods may be found analytically (Avellaneda & Swart 1998). The effective piezoelectric properties may thus be determined directly as functions of the effective matrix properties E^H_{ijkl}. The optimization problem may then be solved by the extremal material design formulation given in (2.41).

Figure 2.46b shows one base cell of the matrix material of a hydrophone optimized for maximum piezoelectric charge coefficient (Sigmund, Torquato & Aksay 1998). One observes that this matrix material is a transversely isotropic material with negative Poisson's ratio. The improvement compared to a solid polymer matrix is a factor of 11. Figure 2.46c shows a base cell (5 mm cubed) manufactured at Princeton Materials Institute using stereolithography.

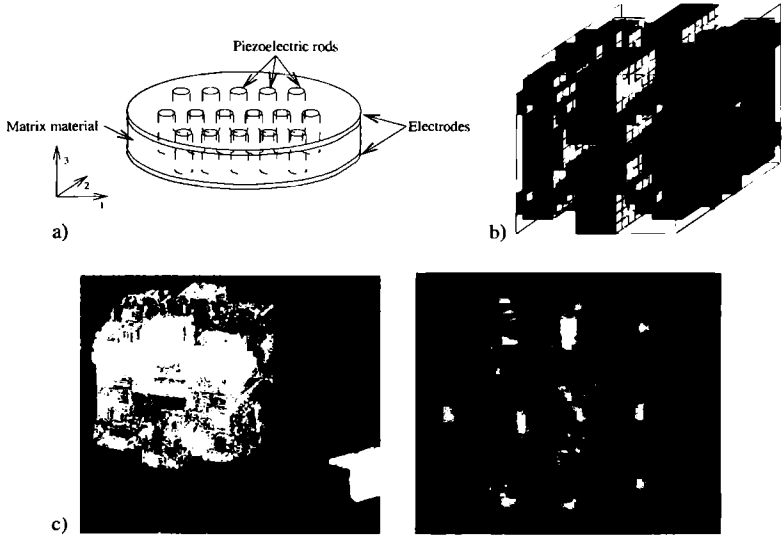

Fig. 2.46. Design of hydrophones using topology optimization. a) Schematic of a 1-3 piezoelectric hydrophone, b) one base cell of hydrophone matrix optimized for piezoelectric charge coefficient and c) one base cell manufactured at Princeton Material Institute using stereo-lithography (from Sigmund et al. 1998).

An investigation of bone microstructures If a 3D material is optimized for stiffness (e.g. maximum bulk modulus), the resulting microstructures are close-walled (c.f. Fig. 2.39), while it has been observed that most bone structures are built up as open walled cells (Gibson & Ashby 1988). This indicates that bone structure is not optimal with respect to stiffness and that other requirements also govern the growth of bone.

Bone is a material that can be considered quasi periodic and thus we can apply homogenization. In many cases the material is orthotropic and physical observations indicate that orthotropic directions of bone follow the principal stress in loaded bone (Wolff's law)[10]

In order to open up the cell walls of high stiffness microstructures, a constraint on the permeability of the cell could be imposed. Permeability is essential for the flow of nutritients that is necessary for maintaining the steadily active bone growth or degradation. Instead of setting up a complicated flow model (like the Stokes flow model in section 2.8.3) we add an extra constraint to the material optimization problem related to the conductivity of the base cell. Here a void element should have a high conductivity and

[10] This is consistent with results on the optimal rotation of orthotropic materials, see Sect. 3.1.4.

a solid element should have a low (zero conductivity). The interpolations of Young's modulus E and the conductivity ζ, respectively, may thus be written as

$$E(\rho_e) = \rho_e^p E_0 \quad \text{and} \quad \zeta(\rho_e) = (1-\rho_e)^p \zeta_0$$

The optimization problem is then be written as

$$\begin{aligned} &\max_{\boldsymbol{\rho}} \ \kappa(\boldsymbol{\rho}) \\ &\text{s.t.} \quad \mathbf{K}\boldsymbol{\chi}^{kl} = \mathbf{f}^{kl}, \quad k,l = 1,\ldots,d\,, \\ &\qquad \frac{1}{|\mathrm{Y}|}\sum_e v_e \rho_e \le \vartheta \\ &\qquad \zeta^H(\rho) \ge \zeta^* \\ &\qquad 0 < \rho_{min} \le \rho_e \le 1, \quad e = 1,\ldots,N \end{aligned} \tag{2.43}$$

where ζ^* is the lower bound constraint on the effective conductivity. Obviously, this optimization problem only makes sense for 3D problems where both phases may be connected from cell to cell.

By specifying a lower bound on the conductivity of respectively 0%, 10% and 20% of the conductivity of a totally void cell, the open-walled microstructures shown in Fig. 2.47 are obtained. Comparisons of the objective functions (bulk moduli) for the closed and the open-walled structures show that the close-walled microstructures are significantly stiffer than the open-walled structures (Sigmund 1999). Thus stiffness cannot be the only objective of bone microstructures. Here a conductivity constraint for allowing flow of nutrition has been applied, but many other objectives of biological or mechanical nature may also play a role; for the latter minimum size constraints and buckling sensitivity (Sect. 2.12.1) may well be significant.

2.11 Wave propagation problems

An interesting new application of the topology optimization method is the design of structures and materials subject to wave propagation. The waves may be elastic, acoustic or electromagnetic, and the phenomenon to be exploited is that for some frequency bands it is possible to construct periodic structures or materials that hinder propagation. This is called a band gap.

The phenomenon of band gaps in structures subject to periodic loads is illustrated in Fig. 2.48a and b. Here a two dimensional square domain is subjected to a periodic loading at the left edge and it has absorbing boundary conditions along all four edges. The frequency of excitation of the structure in Fig. 2.48a is lower than for Fig. 2.48b. It is seen that waves propagate through the structures from left to right and that the absorbing boundary conditions damp the waves at the top and bottom. These are perfectly normal situations

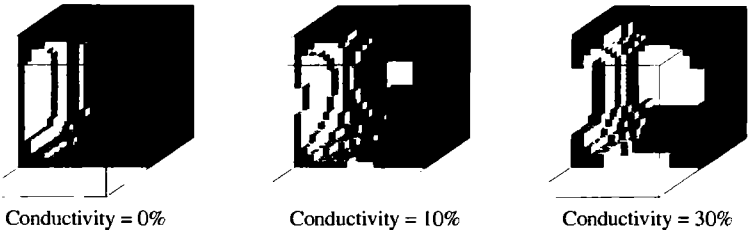

Fig. 2.47. Investigation of "bone" microstructures. All pictures show one half of the resulting base cell topologies. Left: close-walled cell obtained from stiffness optimization without conductivity constraint and center right: open-walled cells obtained from stiffness optimization with conductivity constraints. The local conductivity is inversely proportional to the local stiffness (from Sigmund 1999).

and could model surface waves on water, acoustic waves through air, out-of plane waves in an elastic structure, polarized electromagnetic waves, etc.

Now, if we introduce a periodic distribution of inclusions with different propagation speeds than in the original structures, the situation changes. For the structure subjected to the lower excitation frequency (Fig. 2.48c), there is still propagation although the waves have different shapes. However, for the structure subjected to a higher excitation frequency (Fig. 2.48d) there seems to be no propagation at all. This illustrates the band gap phenomenon. A band gap material is defined as a material that does not allow wave propagation for certain frequency ranges. For elastic and acoustic waves the materials are called phononic band gap materials, for electromagnetic wave propagation the materials are called photonic band gap materials and the same principle on the atomic scale lies behind semiconductors. The length scale of the periodic structure in band gap materials is typically close to the wavelengths of the forbidden frequencies.

Band gap materials may be used for many purposes, for example for waveguides. The idea is illustrated in Figs. 2.48e and f. If we introduce a defect in the periodic structures from Figs. 2.48c and d, waves with frequencies outside the band gap may still propagate through the whole structure (Fig. 2.48e) but waves with frequencies within the band gap may now only propagate through the defect, resulting in a wave guide as seen in Fig. 2.48f. It is seen that it is actually possible to guide waves around a corner. This is especially interesting for light waves since it may allow for the manufacturing and design of so-called photonics based microchips which have much higher clock frequencies than conventional microchips based on electrical conduction.

Apart from semiconductors and wave guides, band gap materials may be used to generate frequency filters with control of pass or stop bands, as beam

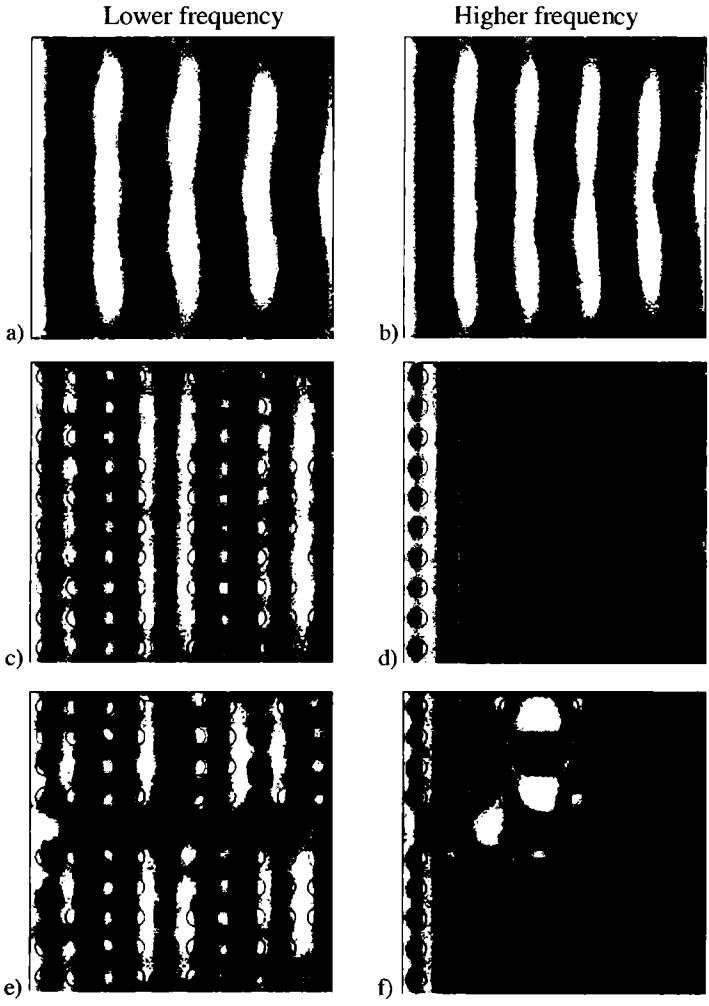

Fig. 2.48. Scalar wave propagation in 2D domains with absorbing boundary conditions and forced vibrations at the left edge. a) Wave propagation through homogeneous structure, b) wave propagation with higher frequency through homogeneous structure, c) wave propagation through structure with periodic inclusions, d) (no) wave propagation with higher frequency through periodic structure, e) wave propagation through periodic structure with defect and f) wave guiding at higher frequency through a periodic structure with defect.

splitters, as sound or vibration protection devices, as perfect mirrors and in many other applications.

2.11.1 Modelling of wave propagation

Elastic wave propagation in a homogeneous material is governed by the Navier vector equation

$$(\lambda + \mu)\nabla(\nabla \quad \mathbf{u}) + \mu\nabla^2\mathbf{u} - \tilde{\rho}\ddot{\mathbf{u}} = \mathbf{0} \ ,$$

where λ and μ are Lamé's coefficients, $\tilde{\rho}$ is material mass density and $\mathbf{u}$ is the point wise (vectorial) displacement.

For planar problems, the Navier equation may be split into an in-plane equation (transverse and longitudinal modes) coupled to an out-of-plane equation (also called the acoustic mode)

$$(\lambda + \mu)\nabla(\nabla \quad \mathbf{u}_T) + \mu\nabla^2\mathbf{u}_T - \tilde{\rho}\ddot{\mathbf{u}}_T = \mathbf{0} \ , \tag{2.44}$$

$$\mu\nabla^2 u_3 - \tilde{\rho}\ddot{u}_3 = 0 \ , \tag{2.45}$$

where subscripts $_T$ and $_3$ stand for transverse and out-of-plane components, respectively.

For an inhomogeneous structure, the acoustic or out-of-plane problem (2.45) may be written as

$$\nabla \quad (\mu\nabla u) - \tilde{\rho}\ddot{u} = 0 \ , \tag{2.46}$$

where the subscript $_3$ has been omitted. This equation has the same form as one of the in-plane modes for electromagnetic wave propagation (Maxwell's equations), i.e.

$$\nabla \quad \left(\frac{1}{\epsilon}\nabla\psi\right) - \frac{1}{c^2}\ddot{\psi} = 0 \ ,$$

the so-called Transverse Electric TE-polarization mode and is closely related to the equation

$$\nabla^2\psi - \frac{\epsilon}{c^2}\ddot{\psi} = 0$$

governing the so-called Transverse Magnetic TM-polarization mode. Here, ϵ is the electric permitivity and c is the speed of light in vacuum.

In the following, we just consider the scalar problem (2.46). The wave equation (2.46) may be solved for a structure subject to forced periodic loading or it may be solved as a cell problem assuming an infinite periodic structure.

For the structural problem we assume that the waves are harmonic and described by $u_3 = \hat{u}_3 e^{(i\Omega t)}$, where Ω is the driving frequency and $\hat{u}_3$ is the amplitude. Substituting this into (2.46) and dropping the hats we get

$$\nabla \ (\mu \nabla u) + \Omega^2 \tilde{\rho} u = 0$$

This equation may be written in finite element notation as

$$\left(\mathbf{K} + i\Omega\mathbf{C} - \Omega^2\mathbf{M}\right)\mathbf{u} = \mathbf{f} \tag{2.47}$$

where we have added (harmonic) boundary forces $\mathbf{f}$ and a damping matrix $\mathbf{C}$ that models absorbing boundary conditions and/or structural damping. This equation has a form which is very similar to the one used for forced structural vibration (cf., Sect. 2.1.2).

For periodic structures (i.e. materials) the wave equation may also be treated as an eigenvalue problem. As for the homogenization problem (Sect. 2.10.1), we may solve the global problem by analysing the base cell Y In contrast to usual homogenization problems, however, the modes may not be cell periodic and therefore we cannot just impose the usual periodic boundary conditions. Instead we assume that the modes can be described by the expression

$$u(\mathbf{y}, \mathbf{k}) = v(\mathbf{y}) e^{i\mathbf{k}^T\mathbf{y}} e^{i\omega t} \tag{2.48}$$

where v is a Y-periodic displacement field, $\mathbf{y}$ is the spatial coordinate and $\mathbf{k}$ is the wave vector. For $\mathbf{k} = \mathbf{0}$, the solution mode $u(\mathbf{y})$ will be Y-periodic. For $\mathbf{k} = \pi$, the solution mode will be 2Y-periodic. For other $\mathbf{k}$, the solution modes can take any kind of periodicity in all directions. This kind of modelling is based on the so-called Floquet-Bloch wave theory (Kittel 1986, Mathews & Walker 1964).

Inserting (2.48) in (2.46) we get the eigenvalue problem

$$(\nabla \ (\mu \nabla v) + \omega^2 \tilde{\rho} v) \ e^{\mathbf{k}^T\mathbf{y}} \ = 0, \tag{2.49}$$

which in principle should be solved for any wave vector $\mathbf{k}$. However, due to symmetry we may restrict the wave vector to the first Brillouin zone $\mathbf{k} \in [-\pi, \ \pi]^d$ (d is the dimension) (e.g. Brillouin 1946). This corresponds to analysing the structural response to incident waves of any possible wave length and direction. If we furthermore assume that the base cell is square symmetric (i.e. is quadratic and symmetric around horizontal, vertical and diagonal lines), we may restrict the range of wave vectors to the triangular region indicated in Fig. 2.49, left. It is generally accepted (but to the authors knowledge, not proved) that one only has to search the borders of the triangular region to obtain a description of the band gap structure of a periodic material. This means that the wave equation (2.49) only has to be solved for a number of wave vectors along the lines $\Gamma \to X$, $X \to M$ and $M \to \Gamma$ (see Fig. 2.49, left).

In finite element notation (2.49) may be written as

$$\left(\mathbf{K}(\mathbf{k}) - \omega^2\mathbf{M}\right)\mathbf{v} = \mathbf{0} \ , \tag{2.50}$$

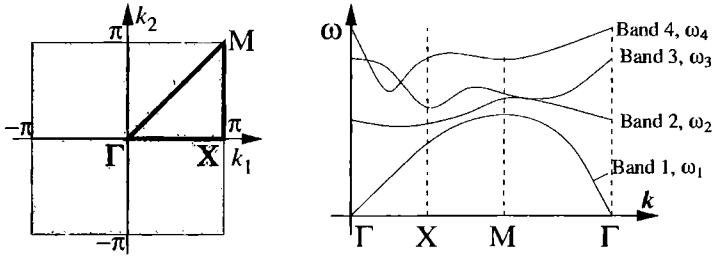

Fig. 2.49. Left: The irreducible Brillouin zone indicating the wave vectors to be searched for the general 2D case (grey area). For square symmetry, the wave equation only has to be calculated for **k**-vector values along the curve $\Gamma - X - M - \Gamma$ Right: Sketch of band structure indicating lowest four eigenvalues for wave vectors along the line $\Gamma - X - M - \Gamma$ in the irreducible Brillouin zone.

which is a standard eigenvalue problem. Since **K** is a Hermitian matrix and M is real, symmetric and positive definite, the eigenvalues of (2.50) will all be real and positive.

If one solves for the first few eigenvalues of (2.50) for a number of **k**, the results can be plotted as a band diagram as sketched in Fig. 2.49, right. From the curves one may read the propagation modes for given frequencies.

Real band diagrams for out-of-plane polarized waves are shown in Fig. 2.50a and b for pure epoxy and duralumin, respectively (data from (Vasseur, Deymier, Frantziskonis, Hong, Djafari-Rouhani & Dobrzynski 1998)). It is seen that for these homogeneous materials there exist eigenmodes for any frequency, i.e. there are no band gaps. Fig. 2.50c shows the band structure of duralumin cylinders (radius equal to 30% of cell size) in an epoxy matrix. It is seen that there are ranges of frequencies with no corresponding eigenmodes. This means that no modes will propagate for these frequencies. There is a large band gap between the first and the second band (from 31 kHz to 43 kHz corresponding to a relative gap size of $\Delta f/f_0 = 0.32$) and a small gap ($\Delta f/f_0 = 0.11$) between the second and the third band. This means that no elastic waves with frequencies within the band gaps may propagate through the structure. The band gap zones are indicated with hatched regions in the diagram.

We may now consider two kinds of optimization problems. Either we optimize the *material problem* modelled by (2.50) or we optimize the *structural problem* modelled by (2.47).

2.11.2 Optimization of band gap materials

An obvious goal for the optimization of band gap materials is to maximize the relative band gap size. In this way the range of prohibited frequencies

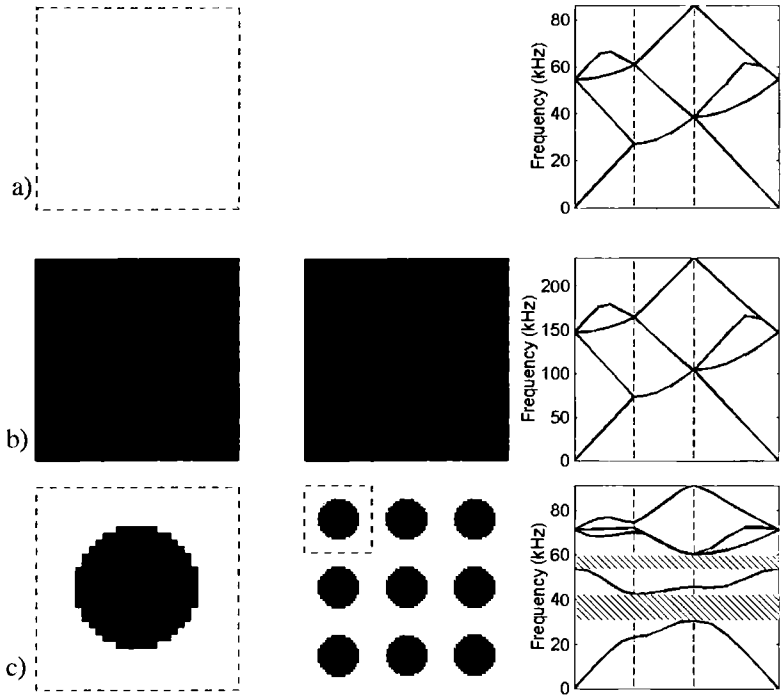

Fig. 2.50. Left: single cell, middle: 3 by 3 arrays of cells and right: band structure of a) pure epoxy, b) pure duralumin and c) duralumin cylinders (radius 30% of cell size) in epoxy. Hatched areas denote band gaps. The horizontal axes denote values of the wave vector **k** on the boundary of the irreducible Brillouin zone. The band diagrams are based on the solution of 15 eigenvalue problems with varying **k**.

will be wider and more signals may be sent through a waveguide based on defects in the band gap material.

The design problem is a two material problem. We want to distribute two non-void phases in the design domain (base cell). For reasons that will become clear later, we here choose a linear material interpolation between the phases, i.e. the wave shear modulus and mass density are interpolated as

$$\mu(\rho_e) = (1-\rho_e)\mu_1 + \rho_e\mu_2 \quad \text{and} \quad \tilde{\rho}(\rho_e) = (1-\rho_e)\tilde{\rho}_1 + \rho_e\tilde{\rho}_2$$

where μ_1 and μ_2 are the shear moduli of material one and two, respectively, $\tilde{\rho}_1$ and $\tilde{\rho}_2$ are the mass densities, and the interpolation density ρ_e belongs to $[0,\ 1]$.

The objective is to maximize the relative band gap size between to bands j and $j+1$, i.e. maximizing the lowest value of the overlying bands and

minimizing the maximum value of the underlying bands. This can be written as a (double) max-min problem

$$\max_{\boldsymbol{\rho}} \left\{ c(\boldsymbol{\rho}) = \frac{\Delta\omega^2(\boldsymbol{\rho})}{\omega_0^2(\boldsymbol{\rho})} = 2\,\frac{\min\limits_{\mathbf{k}} \omega_{j+1}^2(\mathbf{k},\boldsymbol{\rho}) - \max\limits_{\mathbf{k}} \omega_j^2(\mathbf{k},\boldsymbol{\rho})}{\min\limits_{\mathbf{k}} \omega_{j+1}^2(\mathbf{k},\boldsymbol{\rho}) + \max\limits_{\mathbf{k}} \omega_j^2(\mathbf{k},\boldsymbol{\rho})} \right\} \tag{2.51}$$

This is a "dirty" objective function in the sense that it is a max-min problem with varying critical points (the $\mathbf{k}$-vector(s) for the critical frequencies may change during the optimization) and it may have several multiple eigenvalues. Interestingly, however, there is no need for a volume fraction constraint in the problem since neither a pure phase one structure produces a band gap (see e.g. Fig. 2.50a) and nor does a pure phase two structure (see e.g. Fig. 2.50b). Somewhere in between there must be a volume fraction that results in the biggest band gap. Another interesting observation is that due to the missing volume constraint, the usual SIMP interpolation becomes useless in ensuring black-and-white designs. However, this is not a big problem since by experience, the optimized designs tend to be mostly black and white anyway. Finally, the mesh-independent filtering techniques works badly due to the missing volume constraint. Therefore, the regularized penalty function method (1.39) is used to ensure black-and-white and mesh-independent designs for this design problem.

The optimization problem may then now be written as

$$\begin{aligned} \max_{\boldsymbol{\rho}} \quad & \frac{\Delta\omega^2(\boldsymbol{\rho})}{\omega_0^2(\boldsymbol{\rho})} \\ \text{s.t.} \quad & \left[\mathbf{K}(\mathbf{k}) - \omega^2\mathbf{M}\right]\mathbf{u} = \mathbf{0}, \quad \mathbf{k} \in [\Gamma - X - M - \Gamma]\,, \\ & 0 \le \rho_e \le 1, \quad e = 1, \quad , N \end{aligned} \tag{2.52}$$

and may be rewritten in the more convenient bound formulation

$$\begin{aligned} \max_{\boldsymbol{\rho}} \quad & = \beta \\ \text{s.t.} \quad & [\omega_{j+1}(\mathbf{k})]_m \ge \beta, \quad m = 1, \ldots, M \\ & [\omega_j(\mathbf{k})]_m \le \beta \qquad m = 1, \ldots, M \\ & \left[\mathbf{K}(\mathbf{k}) - \omega^2\mathbf{M}\right]\mathbf{u} = \mathbf{0}, \quad \mathbf{k} \in [\Gamma - X - M - \Gamma]\,, \\ & 0 \le \rho_e \le 1, \quad e = 1, \ldots, N, \end{aligned} \tag{2.53}$$

where the two first constraints take the M most critical values into account. This problem may efficiently be solved using MMA.

Results from optimizing the epoxy/duraluminum structures from Fig. 2.50 are shown in Fig. 2.51. The first example maximizes the relative band gap size between the first and the second band. The result is an almost square inclusion of a duraluminum in the epoxy matrix. The relative band gap size has increased from 0.32 for the circular inclusion in Fig. 2.50c to 0.65 for

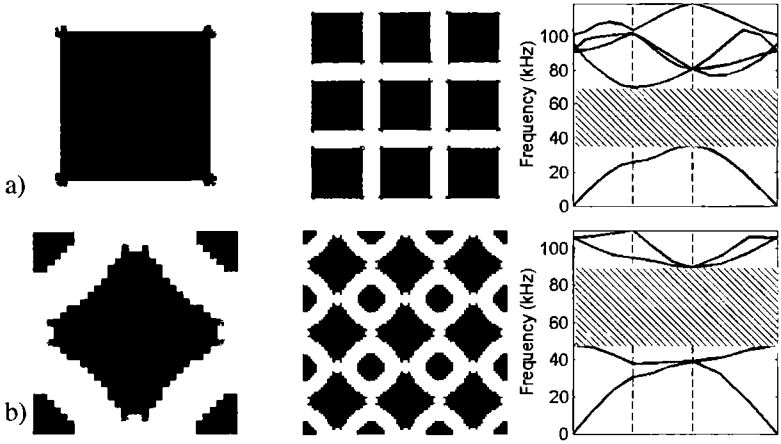

Fig. 2.51. Maximization of relative band gap size between a) first and second band and b) second and third band.

the square inclusion structure in Fig. 2.51a. The second example maximizes the relative band gap size between the second and the third band. In this case, the resulting structure consists of diamond and circular inclusion of duraluminum inclusions in the epoxy matrix. The relative size of the second band gap has increased from 0.11 for the circular inclusion in Fig. 2.50c to 0.61 for the structure in Fig. 2.51b.

2.11.3 Optimization of band gap structures

The material design problem in the previous sub-section assumed infinite periodicity of the material. This means that the influence of boundaries as well as the influence of defects in the periodic structure can not be modelled. In order to model finite domains we use the wave equation (2.47) and the objective function here may be to minimize the magnitude of the wave at the boundaries (hinder wave propagation) or to maximize the wave at certain points in the structure (wave-guiding).

The optimization problem looks very much like the one defined for structures subjected to forced vibrations (Sect. 2.1.2) (Sigmund & Jensen 2002b, Sigmund & Jensen 2002a). Here, however, the input point and the point to be damped are not coincident. The difference may be seen as the difference in optimizing for minimum compliance (Chap. 1) and in optimizing compliant mechanisms (section 2.6).

An optimization problem solving the problem of minimizing the wave magnitude at a point, a line or an area of a structure subjected to forced

vibrations with frequency Ω can be written as

$$\begin{aligned} &\min_{\rho} \quad c = \bar{\mathbf{u}}^T \mathbf{L} \mathbf{u} \\ &\text{s.t.} \quad (\mathbf{K} + i\ \Omega\ \mathbf{C} - \Omega^2 \mathbf{M})\ \mathbf{u} = \mathbf{f} \\ &\qquad \sum_{e=1}^{N} v_e \rho_e \leq V, \qquad 0 < \rho_{min} \leq \rho_e \leq 1, \quad e = 1, \ldots, N \end{aligned} \tag{2.54}$$

where $\mathbf{L}$ is a zero matrix with ones at the diagonal elements corresponding to the degrees of freedom of the nodes, lines or areas to be damped. Due to the complex damping term, the solution of (2.47) is complex and we use overbar $\bar{(\cdot)}$ for the complex conjugate. This formulation corresponds to (2.6) with an added damping term and a slightly modified objective function.

The sensitivities of the objective function can by the adjoint method be found as

$$\frac{\partial c}{\partial \rho_e} = 2\Re\left(\boldsymbol{\lambda}^T \left[\frac{\partial \mathbf{K}}{\partial \rho_e} + i\Omega \frac{\partial \mathbf{C}}{\partial \rho_e} - \Omega^2 \frac{\partial \mathbf{M}}{\partial \rho_e}\right] \mathbf{u}\right)$$

where $\Re(\cdot)$ means real part and $\boldsymbol{\lambda}$ is the solution to the adjoint equation

$$(\mathbf{K} + i\mathbf{C} - \Omega^2 \mathbf{M})\ \boldsymbol{\lambda} = -\mathbf{L}\bar{\mathbf{u}}$$

Figure 2.52 shows an example where the suggested optimization procedure is used to minimize wave propagation through a square plate. The left edge if subjected to forced vibrations with frequency $\Omega = 200$, the left and right edges have absorbing boundary conditions and the top and bottom edges are free. The size of the plate is 0.12, the shear moduli are $\mu_1 = 0.384$ and $\mu_2 = 0.769$ and the specific densities are $\tilde{\rho}_1 = \tilde{\rho}_2 = 1$ (all data is normalized). The objective is to minimize the average amplitude at the right edge. The resulting structure is not unexpected a grid of alternating phase one and phase two material corresponding to a Bragg grating. This structure is known to reflect one dimensional waves. Compared to un-damped wave propagation, the magnitude of the outgoing wave has been decreased by almost 3 orders of magnitude.

The problem formulation (2.54) may also be used to design wave guides as shown in Fig. 2.53. Here, all edges have absorbing boundary conditions. The centerpart of the left edge is subjected to forced vibrations and the objective function is to *maximize* the wave magnitude at the center of the lower edge. The resulting structure is intriguing. Apparently, the wave is bent by a wave guide based on curved Bragg gratings. It is seen from the wave picture (Fig. 2.53c) that the mode at the output port is almost as strong as at the input port.

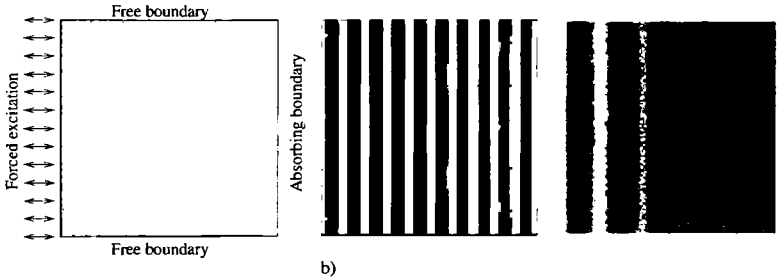

Fig. 2.52. Damping of wave propagation in a quadratic plate. a) Design domain and boundary conditions, b) optimized structure and c) the wave field (from Sigmund & Jensen 2002b).

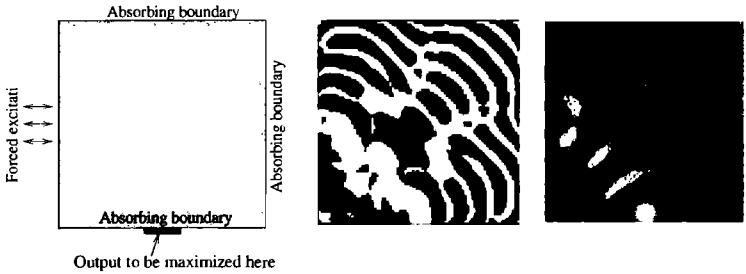

Fig. 2.53. Optimization of waveguidance in a quadratic plate. a) Design domain and boundary conditions, b) optimized structure and c) the wave field (from Sigmund & Jensen 2002b).

2.12 Various other applications

This section discusses various recent applications of the topology optimization method [22].

2.12.1 Material design for maximum buckling load

In Sect. 2.10.3 we discussed a new class of materials with extremal elastic properties. This material class makes use of infinitely fine laminations of the constituent material phases so-called rank-1 laminates (c.f. Appendix 5.4). Such materials are from a practical point of view not very useful since they have very low critical buckling loads when the softer phase has close to zero stiffness. Therefore, it makes sense to optimize material structures for buckling load rather than for normal linear loads. As we also discussed in Sect. 2.10.3 under bone-remodelling, a buckling load criterion may very well

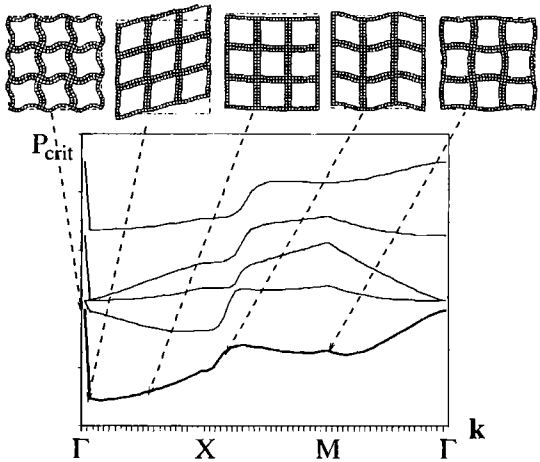

Fig. 2.54. Modelling of non-local buckling using Floquet-Bloch wave theory (from Neves et al. 2002a).

be the reason for why bone structure is a stiffness sub-optimal open-walled cell structure.

In order to eliminate lamination type structures in the periodic cell, one may introduce a local buckling load constraint on the cell problem, just as we did for structural buckling problems in Section 2.2 (Neves, Sigmund & Bendsøe 2002b). However, there is no guaranty that a cell periodic buckling mode is the most critical one, and therefore we should include also non-cell periodic buckling modes when we search for the most critical buckling load. This can be done by Floquet-Bloch wave analysis just as we did in Sect. 2.11 for wave propagation problems. Figure 2.54 shows a buckling load diagram for varying wave-vectors **k** (see Sect. 2.11 for the theory) and some of the associated buckling modes for a specific square microstructure. It is seen that the most critical buckling mode is the shear mode which has a buckling load that is less than a third of the cell periodic mode. This demonstrates the importance of using Floquet-Bloch wave theory for modelling the problem.

Figure 2.55 shows another example of a critical load diagram for square microstructures. The material structures are subject to uniaxial horizontal loading and we allow a total volume fraction of 0.52 to be filled with stiff material. In the first case (Fig. 2.55a), the outer square frame is fixed to be solid and the rest of the material is evenly distributed in the interior of the cell. This results in a non-dimensionalized buckling load of 0.029. Now we maximize the minimum buckling load over all wave vectors along the lines $\Gamma - X - M - \Gamma$ in the Brillouin zone. The optimized topology and its associated buckling diagram is shown in Fig. 2.55a. The buckling load for the

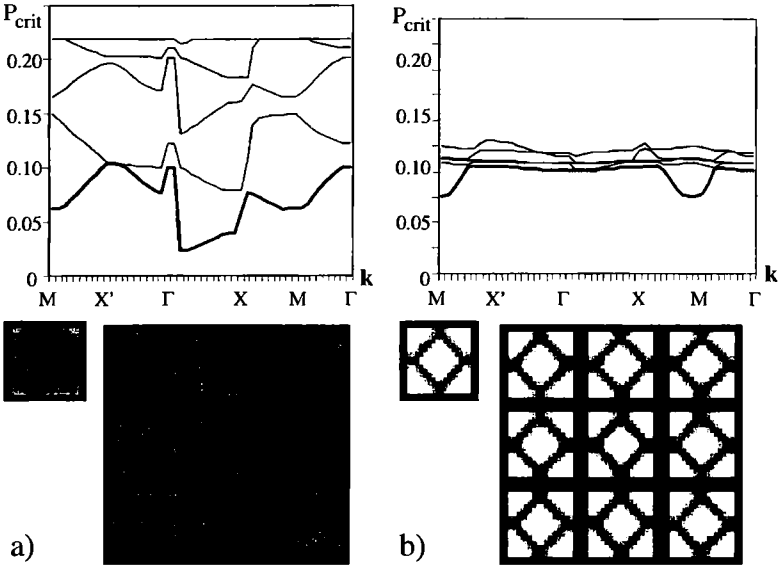

Fig. 2.55. Maximization of microstructural buckling load. a) Initial design with buckling load 0.029 and b) topology optimized design with buckling load 0.061 (from Neves et al. 2002a).

optimized material structure is 0.061 – an increase of more than a factor of two.

2.12.2 Crashworthiness

One of the most complicated optimization problem we can think of is the optimization of transport vehicles for crashworthiness. First, the modelling is extremely complicated, involving geometric and material non-linearities, contact and very complex geometries. Second, especially for automotive structures, the load conditions are unknown since a crash between two cars or a crash of a single car against a wall, a tree or a roll-over may happen in infinitely many ways. Third, the sensitivity analysis for path-dependent and dynamic problems is rather involved.

These complications may be the reason why not much work has been done in applying topology optimization methods to crashworthiness design problems. Further problems that are expected in the applications of topology optimization methods to crashworthiness problems is how to model the response for intermediate density materials and internal contact. Ford Motor Company has built up an in-house software for crashworthiness design

based on the RADIOSS software for modelling (Soto 2001). The topology optimization can be categorized as a re-enforcement optimization problem and is performed based on heuristic criteria without sensitivity analysis (see also Sect. 2.12.4).

A short description of recent work (Pedersen 2002b, Pedersen 2002c, Pedersen 2002a, Pedersen 2002d) on topology optimization of frame structures for crashworthiness is given in the following. The work considers simplified planar models ignoring contact between elements. However, the sensitivity analysis is derived analytically which makes the algorithm very efficient. The modelling is based on plastic beam elements and an implicit dynamic Newmark time-stepping algorithm for obtaining the transient response.

The formulation of the optimization problem must accommodate conflicting criteria such as a maximum acceleration constraint to avoid driver and passenger injuries due to too high g-forces (e.g. whip-lash) and a maximum deformation constraint to avoid passenger and driver injuries due to penetration of the passenger cabin. These requirements are best met by a structure with constant high acceleration (for example just below the head injury criteria (HIC) acceleration) throughout the crash. Therefore the optimization problem is formulated as a min-max problem where the error in obtaining the prescribed acceleration $\ddot{u}_m^*$ in M design points is minimized. This optimization problem may be written as

$$\begin{aligned} \min_{\mathbf{h}} \quad & \max_{m=1,2\ldots,M} |\ddot{u}_m(\mathbf{h}) - \ddot{u}_m^*| \\ \text{s.t.} \quad & \mathbf{r}(t,\mathbf{h}) = \mathbf{0}, \\ & \sum_{e=1}^{N} h_e b_e l_e \leq V, \\ & 0 < h_{min} \leq h_e \leq h_{max}, \quad e = 1,\ldots,N \end{aligned} \tag{2.55}$$

where b_e is the thickness of element e, l_e its length and h_e is the design variable (height of the beams). The residual $\mathbf{r}(t,\mathbf{h}) = \mathbf{0}$ describes the dynamic equilibrium where t is the time.

An example of the design of a car-front for frontal crash is shown in Figs. 2.56 and 2.57.

Other applications of topology optimization to damage problems are discussed in Sect. 3.6 and an overview of literature on material non-linearities and damage related problems are found in [22] and [31].

2.12.3 Bio-mechanical simulations

Models for bone remodelling and optimal design have mutually provided inspiration for new developments in either area (see Pedersen & Bendsøe (1999) for a collection of papers dealing with such aspects [7]). It thus turns out that there is a close similarity between the optimality criteria algorithm

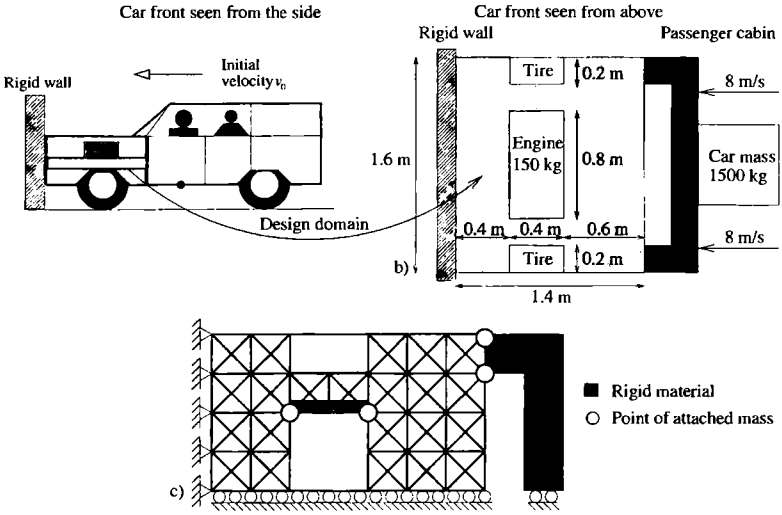

Fig. 2.56. Sketch of the design domain for crashworthiness design of a car. The front part of the car is modelled by 272 plastic beam elements (c).

and schemes for bone remodelling. Also, in many *isotropic* remodelling algorithms, the relationship between density and the elasticity modulus of cancellous bone is modelled exactly like in the SIMP model. Furthermore, when orthotropy is taken into account, Wolff's law for bone predicts that stresses and material axes are aligned, exactly as for minimum compliance design, see Sect. 3.1.4. Even though it is commonly agreed that the bone does not attain, from a structural optimization point of view, a stable optimal configuration with respect to any given static loads, the similarity between the two types of modelling has suggested that optimal *remodelling* will provide a framework for simulating the adaptation of bone structure that is subject to external loading. We will not elaborate further on this here, but refer to the vast literature on the subject [7].

2.12.4 Applications in the automotive industry

Since the introduction of the idea of treating structural topology optimization as a material distribution problem this subject has evolved substantially and it has changed the design process in the automotive industry[11] by providing better structures, not only in the early stages of the process, but also as a technique to improve component designs in subsequent phases.

[11] This section is based on a text kindly provided to us by Ciro A. Soto, Ford Motor Co., Dearborn, MI.

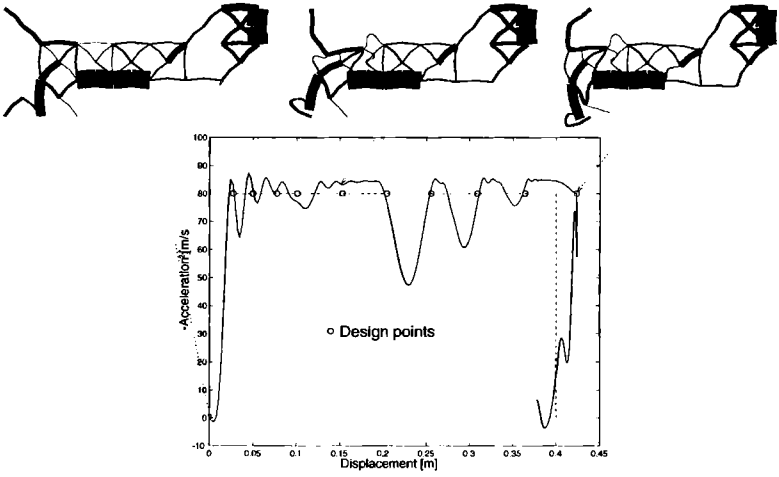

Fig. 2.57. Topology optimized frame structure. Response curve and snapshots of the deformations. The goal was to obtain a constant acceleration throughout the crash.

Fig. 2.58. Bone remodelling simulation for multiple loads. Femur longitudinal cuts. Two sets of results depending on cost of bone creation. By courtesy of P. A. Fernandes, J. M. Guedes and H. C. Rodrigues.

Among the first publications on topology optimization applications in the automotive industry are Huang, Walsh, Mancini, Wlotkowski, Yang & Chuang (1993) and Yang & Chuang (1994). They implemented a topology optimization software that used a commercial finite element method code to perform the structural analysis, and solved automotive design problems with a large number of degrees of freedom.

Structural topology optimization is an important tool for structural designers in the automotive industry. In the first half of the 20th century, new structural designs were obtained using much of the experience of the de-

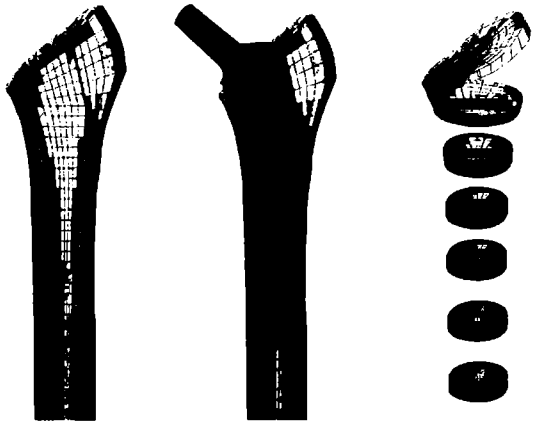

Fig. 2.59. Bone remodelling with tapered hip prosthesis, contact conditions, for multiload case and with bone ingrowth modelling. By courtesy of J. Folgado, J. M. Guedes and H. C. Rodrigues.

signer. However, with the introduction of structural optimization in the early 1960s, plus the advances in topology optimization in the 1990s, design processes have changed dramatically in the industry. Nowadays, computers help to create new topological designs in a matter of minutes using commercially available structural topology optimization software. The applications of such tools in the design cycle have had a tremendous impact on the final product and in the design process as well. There are many types of structural problems that can be encountered in the automotive industry, from simple linear static problems like a bracket design, to non-linear transient problems like designing for crashworthiness.

Software for topology optimization In 1989 a company in Japan, Quint Co., released Optishape, a commercial software to perform topology optimization using the approach of Bendsøe & Kikuchi (1988). Since then many other CAE-software companies have developed similar packages for applications in the aerospace and automotive industry. Among them there are Optistruct (from Altair Computing, USA), Construct (from MSC Software, USA) and Catopo (from CES Eckard GmbH, Germany). Ford Motors developed its own topology optimization software in 1992 called TOP (Huang et al. (1993), Yang & Chuang (1994), Soto, Yang & DeVries (1996), Soto & Yang (1999)) and integrated it into a more comprehensive structural optimization software called Optcom which is also able to do shape and size optimization, plus sensitivity analysis based on simulations done with MSC/Nastran structural analysis software. Thanks to the availability of such software since

the early 1990s the automotive industry has included the use of topology optimization techniques in their structural design processes.

Challenges in vehicle design A vehicle can be succinctly described as a payload box (cabin and trunk) on a suspension system (wheels and suspension) propelled by an engine (power train). This three-element description interacts with the rest of the world through three other elements: human beings (conductor and passengers), road (in contact with tires) and environment (wind, temperature, pressure, obstacles, pedestrians). This simplified view will be used to quickly review three challenges engineers face during the design process. The first challenge is the number of loading conditions that a vehicle structure is subject to during its entire life. The second challenge of vehicle design is the variability within each design condition. Roads are not perfectly flat; tires do not wear uniformly; steel quality varies from batch to batch, etc. Finally, engineers also have to deal with multidisciplinary aspects.

Stiffness maximization of vehicle structures The structural body of a vehicle is required to provide a stiffness in bending and torsional directions beyond some lower limits prescribed by the design team based on previous experiences and/or competitive vehicles. Maximization of the stiffness is equivalent to minimization of the mean compliance of the structure under a given load. This type of problem can be solved not only for components, but also for vehicle structural skeletons (body structures). In its multiload format (see Sect. 1.5.1), more than 80% of structural topology design optimization problems in industry can be addressed by solving compliance minimization problems. Here one often seeks the Pareto curve by solving several optimization problems for different sets of weights. This is a very common situation in automobile design, where two or more responses go through a trade-off analysis to determine the final design.

Figure 2.60 shows a compliance optimized body structure (also known as"the body in white") of a sedan vehicle. The finite element meshes used for such structures can easily reach 200,000 or more finite elements. The design objective is to maximize the torsional and bending stiffness. These two stiffnesses are important for static loading, for ride and handling and also from the vibrational point of view.

Noise, vibration and harshness (NVH) NVH is a vehicle response that passengers feel and judge continuously when the car is running. Vibrations from 20 Hz up to 5000 Hz must be minimized in a vehicle design to reduce discomfort on passengers. There are three main sources of vibrations: power train (engine and transmission), wind, and road-tire interaction. Each one of them has its own frequency range and are resolved in different ways. Power train vibrations are well defined in terms of their frequency spectrum since they come at known rpm values. In such cases, the optimization problem has the design objective of preventing structural natural frequencies to coincide

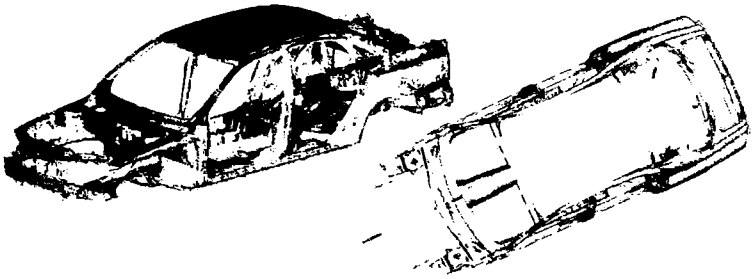

Fig. 2.60. A compliance optimized body structure of a sedan vehicle. Dark areas indicate where more material improves the performance in torsional and bending stiffness simultaneously. By courtesy of Ciro Soto and Ford Research Laboratory.

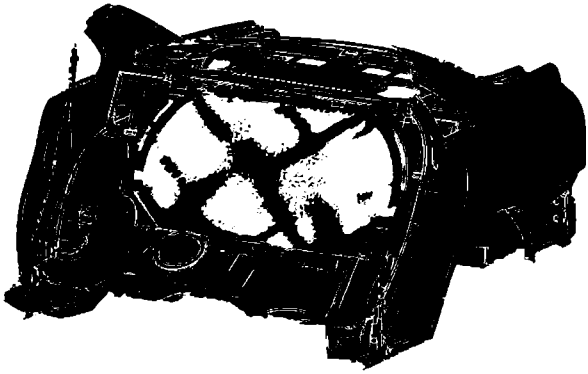

Fig. 2.61. Reinforcement of the back-plate of a sedan. Dark areas indicate where more material improves the performance in torsional and bending stiffness simultaneously. By courtesy of Ciro Soto and Ford Research Laboratory.

with the power train frequencies. Wind vibration and noise are caused by vibratory pressure of the wind on windshield, window glasses and other external panels. These vibrations are usually reduced by changes in the contour and finish of the vehicle external surfaces. Vibrations coming from road-tire interaction (harshness) are more difficult to treat because the range of frequencies is very wide and sometimes it is impossible to provide a structure with low vibration for the entire range. There are two main approaches to deal with structural vibration problems. If the frequency spectrum of loads

is very well defined with distinguishable frequencies, the manipulation of the natural frequency spectrum is the better approach. Moving up or down natural frequencies can be achieved using topology optimization techniques. However, if the frequency spectrum of loads is very dense, with almost white noise characteristics, the reduction of the magnitude of vibrations is the better approach. This can be done when the simulation is performed as a forced frequency vibration problem (cf., Sect. 2.1.2, [14]), rather than a free (eigenvalue) vibration problem (cf., Sect. 2.1.1, [14]). The former approach works on the cause of the problem, while the latter works on the symptoms.

Design for stress reduction - durability Durability is the term used to describe the fatigue phenomena in the automotive industry. The goal is to build a vehicle with a useful life span of several hundred thousands kilometers without experiencing any fatigue problems. The main difficulty lies in the prediction of life (number of loading cycles) for the random loads acting during the life time of the vehicle. Even more difficult is to compute sensitivity coefficients of life with respect to changes in the thickness of panels or changes in curvature. In addition, there has always been a controversy about including local constraints in topology optimization problems. One side of the argument is that topology is a global property of the structure and should not be subject to point-wise constraints. On the other hand, local topology features (such as holes) are often dominated by local structural behavior (e.g., stresses). Nevertheless, there has been several attempts to include local stresses into the problem formulation (cf., Sect. 2.3, [16]).

Topology of embossed ribs in structural shells One technique used to increase local stiffness of structural shells is the addition of embossed ribs (also knows as beading). These are stamped indentations with given length, depth and separation to provide directional rigidity to the shell. The difference between doing the standard topology optimization and embossed rib optimization is that the goal is not to look for isotropic material layout, but for a layout and orientation of a fixed orthotropic stiffness property. More specifically, when the design variable is close to zero, the local stiffness property (membrane and bending components) must be of an isotropic material plate of given thickness; and when the design variable is close to one, the local stiffness properties must be that of an orthotropic ribbed plate. In order to achieve this a new model is needed to simulate the structural behavior of embossed ribs (see Soto & Yang (1999)) based on orthotropic plate modelling (cf., Chap. 3). Since the local stiffness properties then depend on the amount and location of the embossed ribs and also depend on their orientation, the optimization problem is posed with two design variables, namely local rib-amount and orientation. See the paper (Soto 2002) for examples.

Topology optimization for crashworthiness In crashworthiness analysis of transportation vehicles there is a long list of complex phenomena:

non-linear materials (plasticity, hardening, etc.); non-linear geometry (large deformations and displacements, buckling); dynamics (inertial forces); surface contacts (including self-contact of members); and strain rate effect due to the speed of the crash, just to mention some of them. One of the main difficulties in the crashworthiness design is the simulation of the phenomena. A single simulation may take 24 to 30 hours on a supercomputer, and days in a 2002-model workstation, hence, any attempt to do topology optimization, where each finite element has at least one design variable, must carefully consider the use of more CPU time. See also the discussion in Sect. 2.12.2.

3 Design with anisotropic materials

In Chapters 1 and 2 we have concentrated on the generation of optimal topologies based on the use of *isotropic* materials within the framework of "classical" black-white (or 0-1) structures. Early developments in topology optimization were build around the employment of *composite materials* as an interpolation of void and full material. This was founded on theoretical work that had lead to the understanding that the issue of existence of solutions can be resolved by extending the design space to include relaxed designs, here in the form of composites.

When introducing composites as part of the solution method in topology design one has to deal with a number of aspects of materials science and specifically methods for computing the effective material parameters of composites. Thus *homogenization* is an intrinsic part of topology design together with the area of material science which is concerned with bounds on the properties of composites. The latter deals with the limits on the possible effective material behaviour and directly gives information on the optimal use of local material properties.

What is thus named the *homogenization approach* for topology design constitutes the basis for many studies in topology design. One can here distinguish between the use of the methodology mainly as a tool for interpolation of properties and studies where existence of solutions is a central aspect. One will find that many of the developments in Chap. 2 have a counterpart based on the homogenization method as an interpolation tool. On the other hand, the complete theoretical insight of the existence issue has presently only been gained for problems involving compliance and fundamental frequency optimization [4].

Design with composite materials is, of course, an important area in its own right [24]. This involves such issues as the optimal choice of orientation of an orthotropic material and especially the optimal layup of laminates. Moreover, one can choose to work with a completely free parametrization of the stiffness tensor in order to find the optimal design where any material can be used. The homogenization method and such aspects of the optimal use of material in a broad sense is the topic of this Chapter.

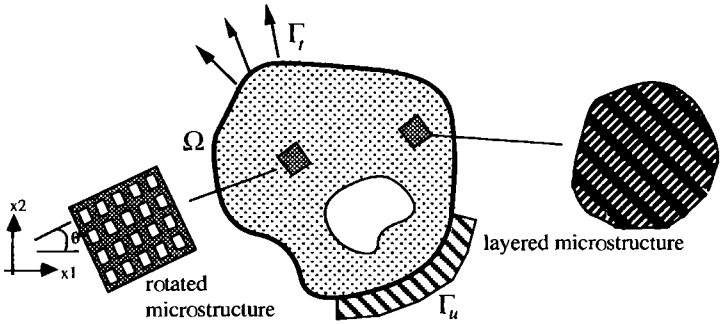

Fig. 3.1. A structure made of materials with micro structure. Notice how the micro structure is rotated by a rotation of the unit cells.

3.1 The homogenization approach

3.1.1 Parametrization of design

We have already noted that the original 0-1 problem statement of topology design lacks existence of solutions in the continuum setting (the distributed problem) [34], [25]. We have hitherto used a *restriction* method to assure existence of solutions. On the other hand, existence studies shows that non-convergent, minimizing sequences of admissible designs with finer and finer geometrical details that can be found for the original "0-1" problem and that these limits should be interpreted as designs where composites made from the original material (and void) are integral parts of the optimal structure.

If we decide to work with an *extension* of the design space, the key to assuring the existence of solutions to our basic shape optimization problem with unknown topology is thus the introduction of composite materials constructed from the given isotropic material (as defined by F^0_{ijkl} of (1.3)) [4], [5], [34], [25]. The design variable is then the continuous density of the base material in these composites. We immediately note that such a *relaxation* of the problem in itself provides an interpolation for use in computations, as the composites allows for a density of material, i.e., a definition of "grey" Introducing a composite material consisting of an infinite number of infinitely small holes periodically distributed through the base material, the topology problem is consequently transformed to the form of a sizing problem where the sizing variable is the material density ρ. As in SIMP, the on-off nature of the problem is avoided through the introduction of this density, with $\rho = 0$ corresponding to a void, $\rho = 1$ to material and $0 < \rho < 1$ to the porous composite with voids at a micro level. We thus in this situation have a set of admissible E_{ad} stiffness tensors given in the form:

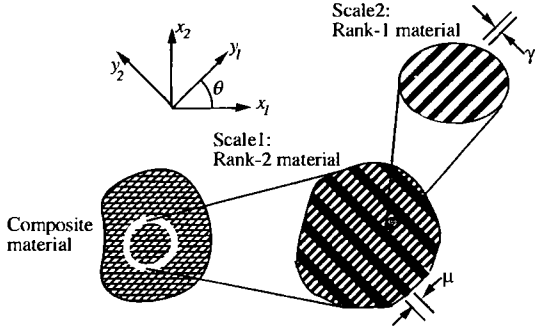

Fig. 3.2. Layered materials for single load cases in dimension 2. The build-up of a second rank layered material, by successive layering of mutual orthogonal layers, resulting in an orthotropic material.

$$
\begin{aligned}
&\text{Geometric variables } \mu, \gamma, .. \in L^\infty(\Omega), \text{ angle } \theta \in L^\infty(\Omega) \\
&E_{ijkl}(x) = \tilde{E}_{ijkl}(\mu(x), \gamma(x), .. \ , \theta(x)), \\
&\text{density of material } \rho(x) = \rho(\mu(x), \gamma(x), \ldots) \\
&\int_\Omega \rho(x) \mathrm{d}\Omega \leq V \cdot \ 0 \leq \rho(x) \leq 1, \ x \in \Omega \ ,
\end{aligned}
\tag{3.1}
$$

where $\tilde{E}_{ijkl}(x)$ are the effective material parameters for the composite. These quantities can be obtained analytically or numerically through a suitable micro mechanical modelling (cf., Sect. 2.10 on material design; see also below). The composite material will, in general, be anisotropic (or orthotropic) so the angle of rotation θ of the directions of orthotropy enters as a design variable, via well-known transformation formulas for frame rotations. Observe that the density of material ρ is, in itself, a function of a number of design variables which describe the geometry of the holes at the micro level and it is these variables that should be optimized. This means that one typically will have more than one design variable per spatial point (or mesh element).

Note that for any material consisting of a given linearly elastic material with microscopic inclusions of void, intermediate values of the density of the base material will provide the structure with strictly less than proportional stiffness (see Fig. 3.4). In an optimal structure one could then expect to find ρ-values of 0 and 1 in large areas. On the contrary, the optimal application of the microstructures (see later) usually results in a very efficient use of intermediate densities of material and the resulting designs have large areas of "grey" One central aspect of this optimal employment of composites is the possibility to adapt to the directions of strain/stress – in a manner of speech, isotropic materials "waste" material also on non-loaded directions.

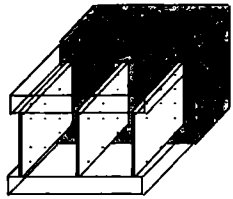

Fig. 3.3. A 3-dimensional cell of a rank-3 layering, with orthogonal layerings at three different scales. This microstructure is useful for single load problems in 3 dimensions.

In the initial studies of the homogenization approach, composites consisting of square or rectangular holes in periodically repeated square cells were used for planar problems, and these still play a central role in many applications. Later so-called ranked laminates (layers) have also become popular, both because analytical expressions of their effective properties can be given and because existence of solutions to the minimum compliance problem for both single and multiple load cases in this case can be formally proved (without any additional constraints on the design space).

Figure 3.1 shows a two-dimensional continuum structure made of a material with microstructure and illustrates how the rotation of the unit *cells* influences a microscopic view of the material. Figures 3.2, and 3.3 show layered microstructures that are regularly used for optimal design[1].The figures show the unit cells for a material with a periodically distributed microstructure, so the cells in the structure are considered as being infinitely small, but infinitely many. Finally, Fig. 3.4 shows the non-linear density-stiffness relation for a composite with square holes aligned with the axes of reference. Also shown in this figure is the dependence of the effective properties on the angle of rotation of the cells.

3.1.2 The homogenization formulas

The "homogenization approach" to topology design of continuum structures as described above relies on the ability to model a material with microstructure, thus allowing for the description of a structure by a density of material. Here one takes an approach where the porous material with microstructure is constructed from a basic unit cell, consisting at a macroscopic level of material and void. The composite, porous medium then consists of infinitely many of such cells, now infinitely small, and repeated periodically through the medium. At this limit, we can also have continuously varying density of

[1] It is common in the theoretical materials science literature to see these structures denoted as laminates. However, to avoid confusion with the use of this word in a structures context we call these structures "layerings".

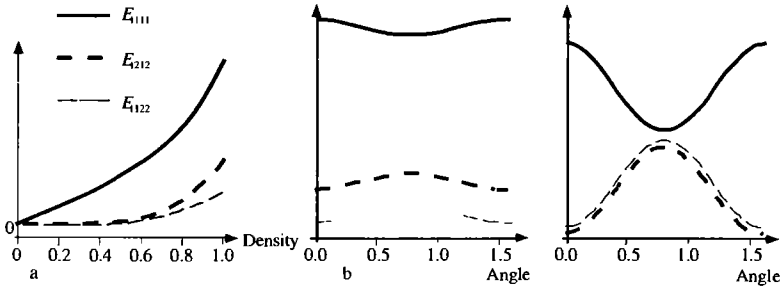

Fig. 3.4. The dependence of the effective material properties of a periodic composite with square holes in square cells on the size of hole and the angle of rotation of the cell. a): The effective properties in a frame aligned with the directions of the sides of the cell. Dependence on material density ρ. The dependence on cell rotation (seen from a fixed frame), b) for a small sized hole with density of material in the cell of 0.91 and c) for a large sized hole with density of material 0.36 (from Bendsøe & Kikuchi 1988).

material through the structure. The resulting medium can be described by effective, macroscopic material properties which depend on the geometry of the basic cell, and these properties can be computed by invoking the formulas of homogenization theory.

The computation of these effective properties play a key role for the topology optimization. Also, the formulas are central for comparing the different choices of cell structure and they form the basis for the topology design of the materials themselves, cf., Sect. 2.10 where the formulas have already been presented. However, for the sake of completeness of the presentation in this Chapter, the formulas of homogenization will again be briefly presented here for the case of dimension 2. For details, the reader is referred to the references quoted in the bibliographical notes [4], [20]. Suppose that a periodic micro structure is assumed in the neighbourhood of an arbitrary point x of a given linearly elastic structure (cf., Fig. 3.1). The length of periodicity is represented by a parameter δ which is very small and the elasticity tensor E^{δ}_{ijkl} is given in the form

$$E^{\delta}_{ijkl}(x) = E_{ijkl}(x, \frac{x}{\delta})$$

where $y \to E_{ijkl}(x,y)$ is Y-periodic, with cell $Y = [Y_{1R}, Y_{1L}] \times [Y_{2R}, Y_{2L}]$ of periodicity. Here x is the macroscopic variation of material parameters, while x/δ gives the microscopic, periodic variations. Now, suppose that the structure is subjected to a macroscopic body force and a macroscopic surface traction. The resulting displacement field $u^{\delta}(x)$ can then be expanded as

$$u^{\delta}(x) = u_0(x) + \delta u_1(x, \frac{x}{\delta}) + \dots\dots\dots$$

where the leading term $u_0(x)$ is a macroscopic deformation field that is independent of the microscopic variable y. It turns out that this effective displacement field is the macroscopic deformation field that arises due to the applied forces when the stiffness of the structure is assumed given by the effective stiffness tensor

$$E^{\mathbf{H}}_{ijkl}(x) = \frac{1}{|\mathrm{Y}|}\int_{\mathrm{Y}}\left[E_{ijkl}(x,y) - E_{ijpq}(x,y)\frac{\partial\chi^{kl}_p}{\partial y_q}\right]\mathrm{d}y \tag{3.2}$$

Here χ^{kl} is a microscopic displacement field that is given as the Y-periodic solution of the cell-problem (in weak form):

$$\int_{\mathrm{Y}}\left[E_{ijpq}(x,y)\frac{\partial\chi^{kl}_p}{\partial y_q}\right]\frac{\partial\varphi_i}{\partial y_j}\mathrm{d}y = \int_{\mathrm{Y}} E_{ijkl}(x,y)\frac{\partial\varphi_i}{\partial y_j}\mathrm{d}y \text{ for all } \varphi \in U_{\mathrm{Y}} \tag{3.3}$$

where U_{Y} denotes the set of all Y-periodic virtual displacement fields.

With y^{11} $(y_1, 0)$, $y^{12} = (y_2, 0)$, $y^{21} = (0, y_1)$ and y^{22} $(0, y_2)$, the variational form for the definition of the effective properties is:

$$E^{H}_{ijkl}(x) = \min_{\varphi\in U_{\mathrm{Y}}}\frac{1}{|\mathrm{Y}|}a_{\mathrm{Y}}(y^{ij} - \varphi, y^{kl} - \varphi) \tag{3.4}$$

while the form of the equations (3.2) and (3.3) in compact notation is

$$E^{H}_{ijkl}(x) = \frac{1}{|\mathrm{Y}|}a_{\mathrm{Y}}(y^{ij} - \chi^{ij}, y^{kl} - \chi^{kl}) \tag{3.5}$$

$$a_{\mathrm{Y}}(y^{ij} - \chi^{ij}, \varphi) = 0 \quad \text{for all } \varphi \in U_{\mathrm{Y}} \tag{3.6}$$

From Equations (3.2) and (3.3) we see that the effective moduli for plane problems can be computed by solving three analysis problems for the unit cell Y For most geometries this has to be done numerically using finite element methods [20] or, as can be advantageous, by use of boundary element methods or spectral methods. For use in a design context the homogenization process should be implemented as an easy-to-use pre-processor (Guedes & Kikuchi 1991). Equations (3.2) and (3.3) hold for mixtures of linearly, elastic materials and for materials with voids (Cioranescu & Paulin 1979). Figure 3.4 shows the variation of the effective moduli for a material consisting of square cells with square holes.

It is important here to underline that the use of homogenized material coefficients is consistent with a basic property of the minimum compliance problem as formulated in (1.1). To this end, consider a minimizing sequence of designs in the set of 0-1 designs defined in (1.3) and assume that this sequence of designs consists of microcells given by a scaling parameter $\delta > 0$. In the limit of $\delta \to 0$, the sequence of designs has a response governed by the homogenized coefficients. It is a fundamental property of the homogenization process that the displacements $u^{\delta}(x)$ of the sequence of designs will converge

weakly to the displacement $u_0(x)$ of the homogenized design (cf., [4]). As the compliance functional is a weakly continuous functional of the displacements this implies the convergence of the compliance values. We can thus conclude that inclusion of homogenized materials in the design formulation does not provide for a jump in performance, but rather provides (some) closure of the design space. Moreover, at the same time we achieve a design description by continuous variables, and can avoid the recourse to any additional interpolation scheme.

We remark that layered materials have analytical expressions for the effective moduli (see below) and this is a distinct advantage for optimization. For other types of micro voids the effective moduli have to be computed numerically for a number of dimensions of the voids in the unit cell, and for other values of densities the effective moduli can be interpolated using for example Legendre polynomials or splines; this gives an easy method for computing design derivatives as well. Note that the interpolation only needs to be carried out for different values of Poisson's ratio, as Young's modulus enters as a scaling factor. The plot in Fig. 3.4 was generated this way.

Layered material We now consider a layered material (cf., scale 2 of Fig. 3.2 rotated 90°) with layers directed along the y_2-direction and repeated periodically along the y_1-axis. The unit cell is $[0,1] \times \mathbf{R}$, and it is clear that the unit cell fields χ^{kl} are independent of the variable y_2. Also note that in Equation (3.2), the term involving the cell deformation field χ^{kl} is of the form $E_{ijpq}(x,y)\frac{\partial \chi_p^{kl}}{\partial y_q}$, so an explicit expression for χ^{kl} is not needed. Using periodicity and appropriate test functions and assuming that the direction of the layering coalesces with the directions of orthotropy of the materials involved, the only non-zero elements E_{1111}, E_{2222}, $E_{1212}(= E_{1221} = E_{2121} = E_{2112})$, $E_{1122}(= E_{2211})$ of the tensor E_{ijkl} can be calculated as shown in Appendix 5.4. Specifically, for a layering of two isotropic materials with the same Poisson ratio ν, with different Young's moduli E^+ and E^- and with layer thicknesses γ and $(1-\gamma)$, respectively, the layering formulas (in plane stress) reduce to the following simple expressions:

$$\begin{aligned} &E_{1111}^H = I_1,\ E_{2222}^H = I_2 + \nu^2 I_1,\ E_{1212}^H = \frac{1-\nu}{2} I_1,\ E_{1122}^H = \nu I_1 \\ &I_1 = \frac{1}{1-\nu^2}\frac{E^+E^-}{\gamma E^- + (1-\gamma)E^+},\ I_2 = \gamma E^+ + (1-\gamma)E^- \end{aligned} \tag{3.7}$$

It has been noted earlier that layered materials (so-called rank-N layered materials) play an important role as a class of composites for use in the homogenization approach. Such materials are created by successive layering of one material with composites already constructed. For example, the construction of a rank-2 layering is as follows. First, a (first order) layering of the strong and the weak material (void in the following) is constructed (see scale 2 of Fig. 3.2). This resulting composite material is then used as one

of two components in a new layered material, with layers of the isotropic, strong material and of the composite just constructed; the layers of this composite material are placed at an angle to the direction of the new layering. The effective material properties of the resulting material can be computed by recursive use of the effective material parameters for a layering and the moduli are computed as the material is constructed, bottom up. The rank-N construction is analogous, and just includes more steps. For a rank-2 layering of material and void, with *perpendicular* layerings and with primary layerings of density μ in the 2-direction and the secondary layer of density γ in direction 1 (as in Fig. 3.2), the resulting material properties are:

$$\begin{aligned} E^H_{1111} &= \frac{\gamma E}{\mu\gamma(1-\nu^2)+(1-\mu)}, \quad E^H_{1122} = \mu\nu E^H_{1111}, \\ E^H_{2222} &= \mu E + \mu^2\nu^2 E^H_{1111}, \quad E^H_{1212} = 0\ , \end{aligned} \tag{3.8}$$

where E is Young's modulus and ν is Poisson's ratio of the base material. Also,the total density of the strong material in the unit cells of this rank-2 layered material is

$$\rho = \mu + (1-\mu)\gamma = \mu + \gamma - \mu\gamma$$

A detailed derivation of the layer formulas is described in Appendix 5.4, where the relation of the homogenization theory to traditional engineering smear-out techniques is also underlined.

The importance of the layered materials not only hinges on the analytical formulas for the effective material parameters. Of equal significance, studies on bounds on the effective material properties of composite mixtures made of two isotropic materials have shown that for elasticity the stiffest (or softest) material for a single load or multiple load problem can be obtained by a layered medium, with layering at several microscales[2] [4], [25]. For single load problems the stiffest material consists of orthogonal layers, with no more than 2 layers for dimension 2 and no more than 3 layers for dimension 3. For multiple load problems the stiffest material (for the weighted average formulation) consists of layers that are not necessarily orthogonal, up to 3 for dimension 2 and up to 6 for dimension 3. The rank-2 materials are not the only composites which in 2-D achieves the upper bound on stiffness of a mixture of two materials [25]. The layered materials are thus not special in the sense of being uniquely optimal, but they are special in the sense that their effective material properties can be expressed analytically.

Parametrization by moments The formulas presented above become very cumbersome if one employs rank-N layerings with many non-perpendicular layers. In this case it is more convenient to work with the so-called *moment* formulation for the effective material properties [25].

[2] It is known that *single scale* microstructures cannot generate the stiffest structure in all situations (Allaire & Aubry 1999).

It turns out that the full range of effective material properties for *all* rank-N layerings in 2-D can be described by just 5 parameters (see Appendix 5.4). These are the bulk density ρ of material together with four moments (m_1, m_2, m_3, m_4) that are parameters of the form

$$\left.\begin{array}{l} m_1 = \sum_{r=1}^{m} \mu_r \cos(2\theta^r),\ m_2 = \sum_{r=1}^{m} \mu_r \cos(4\theta^r) \\ m_3 = \sum_{r=1}^{m} \mu_r \sin(2\theta^r),\ m_4 = \sum_{r=1}^{m} \mu_r \sin(4\theta^r)\ , \end{array}\right\} \text{ with } \sum_{r=1}^{m} \mu_r = 1$$

In terms of these moments and the density ρ, the effective compliance tensor can for example be written as (in plane stress and for layerings of material and void)

$$C^H = C^+ + \frac{(1-\rho)}{\rho E}[D]^{-1} \tag{3.9}$$

where the entries of the tensor D are

$$\begin{aligned} &D_{1111} = \tfrac{1}{8}(3 + m_2 - 4m_1) \qquad D_{2222} = \tfrac{1}{8}(3 + m_2 + 4m_1) \\ &D_{1122} = D_{2211} = \tfrac{1}{8}(1 - m_2) \\ &D_{1112} = D_{1121} = D_{2111} = \tfrac{1}{8}(m_3 - m_4)\ , \\ &D_{1222} = D_{2221} = D_{2122} = D_{2212} = \tfrac{1}{8}(m_3 + m_4) \\ &D_{1212} = D_{1221} = D_{2112} = D_{2121} = \tfrac{1}{8}(1 - m_2) \end{aligned}$$

When considering all possible layer combinations as well as layer directions, the tensor C^H will be parametrized by (m_1, m_2, m_3, m_4) belonging to the convex set $\mathcal{M}$ given as

$$\mathcal{M} = \left\{ \mathbf{m} \in \mathbf{R}^4 \left| \begin{array}{l} m_1^2 + m_3^2 \le 1,\ -1 \le m_2 \le 1, \\ 2m_1^2(1 - m_2) + 2m_3^2(1 + m_2) + \\ +(m_2^2 + m_4^2) - 4m_1 m_3 m_4 \le 1 \end{array} \right. \right\} \tag{3.10}$$

This convex set also encompasses the material tensors of rank-2 and rank-3 layerings. However, compared to a rank-3 layering described by 2 relative densities and 3 directions of layerings, by introduction of the *moments* (m_1, m_2, m_3, m_4) there is one less variable to worry about. If optimization is carried out using these moments one may wish to recover a composite from the optimal moments – it turns out that for any given set of moments, a composite with at most three layers can be can be constructed analytically, see Lipton (1994a). For 3-D a parametrization in terms of moments can also be given. Here one has to work with 15 moments and a characterization of the set of moments in terms of matrix-inequalities, see Díaz & Lipton (2000).

3.1.3 Implementation of the homogenization approach

The homogenization approach to design of a structure with composites can be implemented using the same flow of computations as for the material

distribution method with isotropic materials, see sections 1.2.2 and 1.2.3. However, two additional aspects have to be considered. First, a database of material properties as functions of the design variables should be generated, with one set of data for each allowed value of Poisson ratio. For layered materials no database is required, only a suitable subroutine. Second, the optimization routine should also cater for angles of rotations of the unit cells. Finally, the implementation should be able to remove checkerboard patterns as these also appear in this setting.

The homogenization approach has been used as the basis for many design studies, encompassing many of the problems dealt with in Chaps. 1 and 2. Compared to use of for example SIMP, the homogenization approach requires additional design variables to describe the structure. On the other hand, one always works with microstructures of a given type, giving a direct physical understanding and in many cases a formal framework (homogenization theory [4]) for computing the behaviour for intermediate densities when more involved physical situations are involved.

In many cases the homogenization approach is actually used as a basis for computing black and white designs, and the extended design space that encompasses composites is not employed to obtain information about the optimal micro-scale use of material as well. Also, to obtain such "classical" designs, explicit penalties on the density (as discussed in Sect. 1.5.2) is typically needed to steer the design to a 0-1 format; in some circumstances neglecting the rotation angle of the cells in the composite constitutes a sufficient penalization that results in such designs. For compliance design it is also known that the use of such sub-optimal microstructures consiting of square holes in square cells give rise to rather well defined designs consisting almost entirely of areas with material or no material and very little area with intermediate density of material, i.e. very little composite material. This favours the use of this micro geometry for obtaining 0-1 designs and the success of the material distribution method in applications would probably never have come about if such sub-optimal microstructures had not been used in the initial numerical studies of the method (this was before the optimality of the layered materials had been proven).

On the other hand, one of the main interest in using composites in the design formulation is to see how this can influence the effectiveness of a structure, and ultimately, to understand what constitutes the best structure. That composites have a big part to play in such design studies can be seen when computing minimum compliance designs with layered materials where the result usually consists of large areas of intermediate densities ("grey" areas of composite).

Fig. 3.5. Optimal design using a rank-2 material. Left: The optimal design using an element wise constant density function and a 8-node displacement model. Right: The unstable checkerboard solution obtained when using a 4-node displacement model (from Jog et al. 1994).

Fig. 3.6. Optimal design using a rank-2 material strain energy density with penalties on intermediate densities and on perimeter. a) shows the density distribution for the unpenalized case. In b) intermediate densities are penalized. In c) and d) intermediate densities and perimeter are penalized, with d) being a fine mesh variant of c) (from Jog et al. 1994).

3.1.4 Conditions of optimality for compliance optimization - rotations and densities

In the following we shall derive the necessary conditions of optimality for the *minimum compliance design* problem that employs *composite* materials in the parametrization of design. For this design formulation there are now *two* distinct types of design variables. First, the composite material is an anisotropic (normally orthotropic) material for which the angle of rotation of the unit cell is an important unconstrained design variable, and second, the sizes describing the unit cells constitute a different type of variables which are globally constrained through the volume constraint. For the latter, the derivation of the conditions of optimality follows directly from the developments in Sect. 1.2.1, so we will here concentrate on the problem for the directions of orthotropy.

Optimal rotation of orthotropic materials The composites with cell symmetry described in the preceding sections are orthotropic, and the angle of rotation of the material axes of this material will influence the value of the compliance of the structure. It turns out that the optimal rotation can be found analytically and this is of great importance for computations and

it is interesting in its own right. Thus the optimal rotation of an orthotropic material is not only of importance for the present setting, but is equally significant in the design of composite structures, laminates, etc. For this reason we will here derive the conditions of optimality for material rotations in plane stress/strain problems (i.e. 2-D) [24].

Assume an orthotropic material as given. Then in the frame of reference given by the material axes of this material we have a stress-strain relation

$$\sigma_{ij} = E_{ijkl}\varepsilon_{kl}$$

with E_{1111}, E_{2222}, E_{1122}, E_{1212} being the only non-zero components of the stiffness tensor E_{ijkl}. We assume that $E_{1111} \geq E_{2222}$, and assume that a given set ε_{ij}^k, $k = 1, \ldots, M$, of strain fields for a number of load cases are specified. With compliance design in mind, we see from the formulations (1.6) and (1.34) of the minimum compliance problem that our interest is to maximize the weighted sum of a number of strain energy densities:

$$W = \frac{1}{2}\sum_{k=1}^{M} w^k \left[E_{1111}{\varepsilon_{11}^k}^2 + E_{2222}{\varepsilon_{22}^k}^2 + 2E_{1122}\varepsilon_{11}^k\varepsilon_{22}^k + 4E_{1212}{\varepsilon_{12}^k}^2\right]$$

We now express the strains in terms of the principal strains ε_I^k, ε_{II}^k, where we choose $|\varepsilon_I^k| \geq |\varepsilon_{II}^k|$ for convenience:

$$\begin{aligned}
\varepsilon_{11}^k &= \frac{1}{2}\left[(\varepsilon_I^k + \varepsilon_{II}^k) + (\varepsilon_I^k - \varepsilon_{II}^k)\cos 2\psi^k\right] \\
\varepsilon_{22}^k &= \frac{1}{2}\left[(\varepsilon_I^k + \varepsilon_{II}^k) - (\varepsilon_I^k - \varepsilon_{II}^k)\cos 2\psi^k\right] \\
\varepsilon_{12}^k &= -\frac{1}{2}(\varepsilon_I^k - \varepsilon_{II}^k)\sin 2\psi^k
\end{aligned}$$

Here ψ^k is the angle of rotation of the material frame relative to the frame of the k'th principal strains. We are interested in the angle Θ of rotation of the material relative to a chosen frame of reference which maximizes the function W Each angle ψ^k is thus written as $\psi^k = \Theta - \alpha^k$, where α^k is the angle of rotation of the k'th strain field (see Fig. 3.7).

Inserting the expressions for the strains expressed in terms of the reference principal strains into the equation for W and differentiating, we get the condition of stationarity as:

$$\begin{aligned}
&\sum_{k=1}^{M} w^k \left[A^k \sin 2(\Theta - \alpha^k) + B^k \sin 2(\Theta - \alpha^k)\cos 2(\Theta - \alpha^k)\right] = 0 \ , \\
&A^k = ({\varepsilon_I^k}^2 - {\varepsilon_{II}^k}^2)(E_{1111} - E_{2222}) \\
&B^k = (\varepsilon_I^k - \varepsilon_{II}^k)^2(E_{2222} + E_{1111} - 2E_{1122} - 4E_{1212})
\end{aligned}$$

Stationarity is thus achieved if the following fourth order polynomial in $\sin 2\Theta$ is zero:

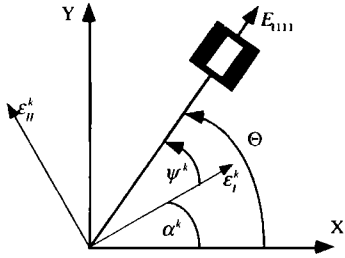

Fig. 3.7. The definition of angles of rotation of material and principal strain axes.

$$
\begin{aligned}
P(\sin 2\Theta) =& a_4 \sin^4 2\Theta + a_3 \sin^3 2\Theta + a_2 \sin^2 \Theta + a_1 \sin 2\Theta + a_0 \\
a_4 =& z_3^2 + z_4^2 \quad a_3 = 2z_1 z_4 - 2z_3 z_2 \\
a_2 =& z_1^2 + z_2^2 - z_3^2 - z_4^2 \quad a_1 = z_2 z_3 - 2z_1 z_4, \quad a_0 = \frac{z_3^2}{4} - z_1^2 \\
z_1 =& \sum_{k=1}^{M} w^k A^k \sin 2\alpha^k \quad z_2 = \sum_{k=1}^{M} w^k A^k \cos 2\alpha^k \\
z_3 =& 2\sum_{k=1}^{M} w^k B^k \sin 4\alpha^k \quad z_4 = 2\sum_{k=1}^{M} w^k B^k \cos 4\alpha^k
\end{aligned}
\tag{3.11}
$$

The energy W is periodic so there exist at least two real roots of P Also, as the order of P is four, the roots of P can be given analytically. The actual minimizer of the compliance is found by evaluating W for the four or eight stationary rotations. This feature is of great importance for the numerical implementation of the homogenization approach for optimal topology design, as the iterative optimization of a periodic function with several local minima and maxima is very likely to give the wrong result. Also, the analytical derivation of the optimal angles saves considerably in computational time.

For the single load case we can express directly the stationary angle ψ (using the principal strain axes as the reference system):

$$
\begin{aligned}
&\sin 2\psi = 0 \ , \quad \text{or} \quad \cos 2\psi = -\gamma, \text{ with } \gamma = \frac{\alpha}{\beta}\frac{\varepsilon_I + \varepsilon_{II}}{\varepsilon_I - \varepsilon_{II}}, \text{ and} \\
&\alpha = (E_{1111} - E_{2222}) \geq 0 \ , \quad \beta = (E_{2222} + E_{1111} - 2E_{1122} - 4E_{1212})
\end{aligned}
$$

Inserting these values in the second variation of W with respect to ψ (Pedersen 1989), it can be seen that the maximizing ψ (i.e. the compliance minimizer) depends on the sign of the parameter β. The parameter β is a measure of the shear stiffness of the orthotropic material. For low shear stiffness, that is, $\beta \geq 0$, the globally minimal compliance is achieved for $\psi = 0$,

i.e. the intuitive result that the numerically largest principal strain is aligned with the stiffer material axis; also, from the stress-strain relation, we see that in this case these axes are aligned with the axes of principal stresses. The materials used in topology design (as described in Sect. 3.1.1) are weak in shear i.e., $\beta \geq 0$. For certain (engineering) laminates with ply-angle $\pm\phi$, $22,5^\circ \leq \phi \leq 45^\circ$, we can have the situation of high shear stiffness, i.e. $\beta \leq 0$ (Pedersen 1989). In this case, $\cos 2\psi = -\gamma$ is the global minimum for compliance as long as $-1 < \gamma < 0$ (γ has the sign of β), and for $\gamma \leq -1$, $\psi = 0$ is again the global minimum. Note that a similar analysis can be carried out based on given stresses (here the complementary energy should be minimized, c.f., (1.7), (1.35)).

For three dimensional elasticity we have three angles of rotations possible for the axes of orthotropy (e.g. using Euler angles) and the expressions above for first variations with respect to angles become much more complicated. For the materials used for design, it is possible to show stationarity of the alignment of material axes, principal strain axes and principal stress axes. The full answer to the 3-D cases is still open [24].

For the materials involving multi-layered media (the rank-N laminates or layerings) the result on the optimal rotation follows by alternative means from the studies on optimal bounds on effective moduli of materials [25]. For these materials it is thus proven that for the single load case, the optimal rotation of the material is consistent with an alignment of the layerings with the principal stresses/strains and this holds in dimension two *and* three.

We remark here that the problem of optimal design of the spatially varying angle of rotation of a fixed orthotropic material is not, in itself, well-posed in general. Relaxation is needed for this case also, as the introduction of for example layered materials consisting of the orthotropic material at various rotations extends the range of available materials. This is discussed in Fedorov & Cherkaev (1983); see also Thomsen (1991).

Optimality conditions for density The conditions of optimality for the density parameters describing the stiffness of a composite can be derived exactly along the lines of Sect. 1.2.1. For the problems at hand we note that the tensor E_{ijkl} now depends on geometric quantities which define the microstructure. For a square, 1 by 1, micro cell with a *rectangular* hole of dimension $(1-\mu)$ times $(1-\gamma)$ the density of material is given as $\rho = \mu+\gamma-\mu\gamma$ and the constraints on the design variables μ, γ are

$$\int_\Omega (\mu + \gamma - \mu\gamma)(x)\mathrm{d}\Omega = V, \quad 0 \leq \mu(x) \leq 1 \ , \ 0 \leq \gamma(x) \leq 1 \tag{3.12}$$

This relation also holds for the rank-2 layered material with layers of density μ and γ. For the present setting the optimality criterion update derived in Sect. 1.2.1 then has the format:

$$\mu_{K+1} = \begin{cases} \max\{(1-\zeta)\mu_K, 0\} \text{ if } \mu_K B_K^\eta \leq \max\{(1-\zeta)\mu_K, 0\} \\ \mu_K B_K^\eta \text{ if } \max\{(1-\zeta)\mu_K, 0\} \leq \mu_K B_K^\eta \leq \min\{(1+\zeta)\mu_K, 1\} \\ \min\{(1+\zeta)\mu_K, 1\} \text{ if } \min\{(1+\zeta)\mu_K, 1\} \leq \mu_K B_K^\eta \end{cases},$$

$$\gamma_{K+1} = \begin{cases} \max\{(1-\zeta)\gamma_K, 0\} \text{ if } \gamma_K E_K^\eta \leq \max\{(1-\zeta)\gamma_K, 0\} \\ \gamma_K E_K^\eta \text{ if } \max\{(1-\zeta)\gamma_K, 0\} \leq \gamma_K E_K^\eta \leq \min\{(1+\zeta)\gamma_K, 1\} \\ \min\{(1+\zeta)\gamma_K, 1\} \text{ if } \min\{(1+\zeta)\gamma_K, 1\} \leq \gamma_K E_K^\eta \end{cases},$$

Here μ_K, γ_K denotes the variables at iteration step K , and B, E are

$$B_K = [\Lambda_K(1-\gamma_K)]^{-1} \sum_{k=1}^{M} w^k \frac{\partial E_{ijpq}}{\partial \mu}(\mu_K, \gamma_K)\varepsilon_{ij}(u_K^k)\varepsilon_{pg}(u_K^k)$$

$$E_K = [\Lambda_K(1-\mu_K)]^{-1} \sum_{k=1}^{M} w^k \frac{\partial E_{ijpq}}{\partial \gamma}(\mu_K, \gamma_K)\varepsilon_{ij}(u_K^k)\varepsilon_{pg}(u_K^k)$$

Also here, Λ is a Lagrange multiplier that should be adjusted in an inner iteration loop in order to satisfy the active volume constraint.

In an implementation, the density update above can be combined with a parallel, but separate update that caters for the optimization of the rotations of the composites, using the roots of the polynomial (3.11). For stability of such a scheme it is typically best to rely on the use of the principal stresses.

The parametrization (3.9) in terms of moments, together with the constraints (3.10) is not suited for use of the optimality criterion method. Also, for a straightforward application of for example MMA it is troublesome that the constraints (3.10) adds two extra constraints per element that are not simple bounds. However, as the effective tensor is concave in the moments (Lipton 1994c) this parametrization is perfectly suited for a hierarchical approach where locally optimal material properties are found (numerically) as solutions to a set of inner optimization problems. Such an approach will described in the following section.

3.2 Optimized energy functionals

The introduction of composite materials as part of the design formulation signifies that the goal of the optimization is both to determine the optimal spatial distribution of material as well as the optimal local use of this material. If we allow the material variables to vary from point to point it seems reasonable to accentuate this local optimal choice of microstructure, and this perspective gives the inspiration for some alternative formulations of optimization problems involving composites [26].

3.2.1 Combining local optimization of material properties and spatial optimization of material distribution

In the following, we will consider the material distribution method for general anisotropic materials where an extra set of local variables (for example cell rotation and some geometric parameters) define the material tensor E of the problem. In turn the local variables also determine the pointwise density ρ of material (the bulk density), or rather, the density ρ determines the volume of material available for the pointwise (local) construction of E. Within this framework we can then write the minimum compliance design problems (1.6) and (1.7) as

$$\max_{\substack{\text{density} \\ \rho(x),\, x\in\Omega, \\ \int_\Omega \rho \mathrm{d}\Omega \le V}} \; \max_{\substack{E \text{ for} \\ \text{microstructure} \\ \text{of density } \rho(x)}} \; \min_{u\in U} \left\{ \frac{1}{2}\int_\Omega E_{ijkl}(x)\varepsilon_{ij}(u)\varepsilon_{kl}(u)\mathrm{d}\Omega - l(u) \right\} \tag{3.13}$$

$$\min_{\substack{\text{density} \\ \rho(x),\, x\in\Omega, \\ \int_\Omega \rho \mathrm{d}\Omega \le V}} \; \min_{\substack{E \text{ for} \\ \text{microstructure} \\ \text{of density } \rho(x)}} \; \min_{\substack{\sigma \\ \mathrm{div}\sigma + f = 0 \\ \sigma\cdot n = t}} \left\{ \frac{1}{2}\int_\Omega C_{ijkl}(x)\sigma_{ij}\sigma_{kl}\mathrm{d}\Omega \right\} \tag{3.14}$$

The basic idea is then to interchange the optimization over the design of the microstructure and the optimization over stresses or displacement. This interchange gives valuable insight in problem structure and provides us with a basis for constructing some alternative solution procedures and computational schemes.

The interchange of min-min in the stress formulation (3.14) results in an equivalent problem as the constraint sets for the two operators in the inf-inf problem are given entirely in terms of the variable over which each individual infimum is sought. Introduction of, for example, stress constraints at the outer design level of problem (3.14) would destroy this feature. For the displacement formulation (3.13) the interchange will in general not result in an equivalent problem. Nonetheless, as we have that

$$\sup_x \inf_y \phi(x,y) \le \inf_y \sup_x \phi(x,y) \,,$$

for any function of two parameters, the interchange will provide us with an upper bound on the optimal objective in (1.6) and thus a lower bound for the compliance of the optimal structure. In situations where the problem satisfies conditions for the existence of a saddle value (saddle point), the interchange will result in an equivalent problem also for the strain case this holds if we work in the framework of layered materials (see Sect. 3.3), for a free parametrization of the tensor E (see section 3.4), and for laminated plates (see Sect. 3.5.2).

The interchange of equilibrium analysis and optimization of local material properties results in a reformulated displacement based problem

$$\max_{\substack{\rho(x),\, x\in\Omega,\\ \int_\Omega \rho \mathrm{d}\Omega \le V}} \min_{u\in U} \left\{ \int_\Omega \overline{W}(\rho, \varepsilon_{ij}(u)) \mathrm{d}\Omega - l(u) \right\} \tag{3.15}$$

where $\overline{W}(\rho, \varepsilon)$ denotes the pointwise optimal strain energy density expression given by

$$\overline{W}(\rho, \varepsilon) = \max_{\substack{E \text{ for}\\ \text{microstructure}\\ \text{of density } \rho(x)}} \left\{ \frac{1}{2} E_{ijkl} \varepsilon_{ij} \varepsilon_{kl} \right\} \tag{3.16}$$

Here we have used that the optimization of microstructure is pointwise, so that one can move this extremization under the integration over the domain.

In the stress based case we have a problem form

$$\min_{\substack{\rho(x),\, x\in\Omega,\\ \int_\Omega \rho \mathrm{d}\Omega \le V}} \min_{\substack{\sigma\\ \mathrm{div}\,\sigma + f = 0\\ \sigma\cdot n = t}} \left\{ \int_\Omega \overline{\Pi}(\rho, \sigma_{ij}) \mathrm{d}\Omega \right\} \tag{3.17}$$

with an optimized complementary energy density

$$\overline{\Pi}(\rho, \sigma_{ij}) = \min_{\substack{E \text{ for}\\ \text{microstructure}\\ \text{of density } \rho(x)}} \left\{ \frac{1}{2} C_{ijkl} \sigma_{ij} \sigma_{kl} \right\} \tag{3.18}$$

For the optimization problems consisting of (3.15)-(3.16) and (3.17)-(3.18) we have two coupled optimization problems, which we label the *local anisotropy* and the *material distribution* optimization problems, respectively. The material distribution problems are the problems (3.15), (3.17). These are the "master" problems (the outer problems) of this hierarchical formulation and they deal with the spatial distribution of resource/material (a global problem). The local anisotropy problems are the problems (3.16) and (3.18). These inner "slave" problems address the question of optimal choice of material (a local problem).

The local anisotropy problems (3.16) and (3.18) correspond to finding the pointwise stiffest material for a given fixed strain or fixed stress field and a given density of material. This is a standard problem setting in the theory of variational bounds on effective moduli of anisotropic materials. It is of great importance in its own right and has been the subject of intense studies in material science.

The equilibrium problem in (3.15) seeks kinematically admissible equilibrium displacements for the locally optimum energy functional, for a given distribution of resource ρ, while the equilibrium problem in (3.17) seeks statically admissible equilibrium stress fields which minimize the locally optimum

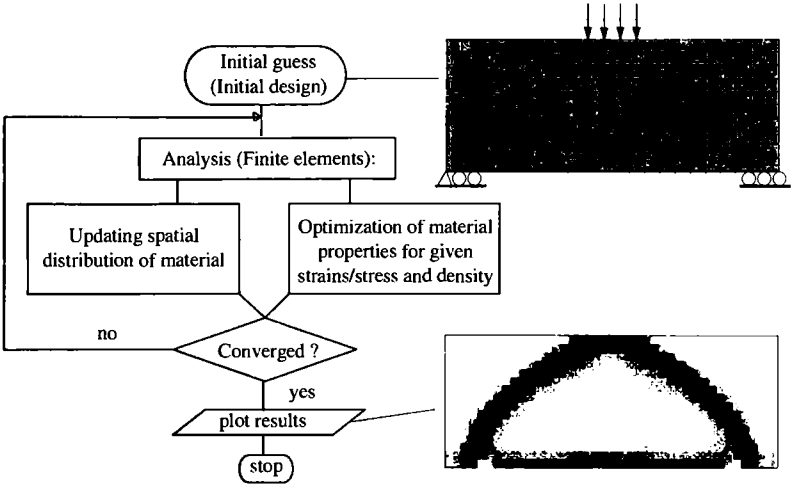

Fig. 3.8. Optimal design using a hierarchical approach. The resulting structure is here a low volume solution to the problem shown in Fig. 3.5.

energy functional, again for a given distribution of resource ρ. It should be noted that, since the locally optimum energies depend on the displacement and stress fields in a complex fashion via the optimization problems (3.16) and (3.18), the inner equilibrium statements of the problems (3.15) and (3.17) are in fact constitutively non-linear and non-smooth elasticity problems, except in very special cases. However, as we shall see in the coming sections, there are important cases of material modelling where these equilibrium problems become problems in linear elasticity or where the non-smoothness is isolated to unimportant strain/stress values. For the strain based problem, it is worth remarking that the equilibrium problem remains a convex problem after the optimization over local material properties. The optimal strain energy density $\overline{W}(\rho, \varepsilon)$ is derived as a maximization of convex functions in the strains and is thus in itself convex in these variables.

3.2.2 A hierarchical solution procedure

The problem separation described above naturally leads one to consider a different computational implementation as compared to the procedure described in Sect. 3.1.3. Such an implementation can for example work with problem (3.15) in the displacements and density only. We accordingly consider the solution to (3.16) as given, either through an analytical or a computational procedure. Then (3.15) has exactly the format of the compliance problem dealt with in Chap. 1 for the SIMP model, that is, the compliance

is a function of the density and is given by the solution of a minimum potential energy problem. This problem can then be solved for example by an optimality criterion method or by MMA. Here one needs sensitivity information of the compliance, i.e., derivative information for the equilibrium problem of (3.15), which is given by the derivative of the optimized strain energy $\overline{W}$ with respect to the density. For an analytically derived optimal strain energy functional this derivative is straightforward to obtain, while for a computationally derived optimal strain energy functional this derivative is given simply as the Lagrange multiplier for the volume constraint of problem (3.16), i.e., the derivative is given directly from the computation of the optimal energy. The equilibrium problem in (3.15) is in general a non-linear problem, so the equilibrium problem requires an inner iteration loop at this point, but computational experience has shown that, as the optimization over the bulk density is in itself iterative, only one (or a few) equilibrium iterations need to be used for each design update.

One of the advantages of the computational program just described is that the main flow of the procedure is *independent* of the modelling of the material used for the description of design. This latter information is added as an external module (the solution of (3.16)). This feature makes it possible to generate flexible procedures, where the material model can be changed easily.

In many implementations the non-linear analysis iterations are avoided [26]. Thus linear analysis is applied for the equilibrium problem with *fixed* material parameters and problem (3.16) is used to generate the parameters of the optimal stiffness tensor for each displacement iteration. The direct coupling between the material parameters and the displacements is therefore ignored in the implementation of the *linear* equilibrium analysis. This computational procedure is especially attractive for multiple load problems where the use of the linear analysis also circumvents the coupling between the displacements for the different loads that is introduced via (3.16).

The procedure described here has been implemented for a broad variety of models [26]. It is particularly well suited for the parametrization by moments (3.9) of the effective parameters for rank-N layered materials needed for multiple load cases. Here the inner problem (3.16) becomes a convex problem that can be solved efficiently by computational means. In other situations, as we shall see in the following sections, this inner problem can actually be solved analytically. One can go one step further and solve the inner anisotropy problem by the material design method described in Sect. 2.10. In this situation one uses only microstructures which involve one length-scale, and the microstructure is designed by a topology design method as described in Sect. 2.10. The computations involved in this approach are quite massive: the number of local topology design problems equals the number of finite elements in the mesh defining the material distribution ρ. However, all these

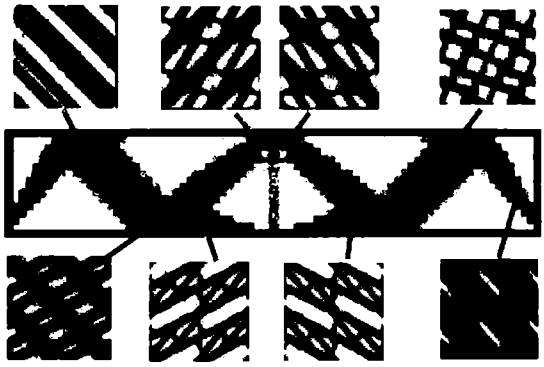

Fig. 3.9. The MBB beam. The optimal distribution of material and associated microstructures obtained from a hierarchical approach. The local material anisotropy problem (3.16) has here been solved numerically, using topology design of the unit cell of a composite. The cell is not rotated – the necessary rotation arises from the material design (from Rodrigues et al. 2002).

local problems are independent and can be solved simultaneously using parallel processing methodologies.

Additional problem reduction In the development above we could have performed one further interchange for the stress case[3] namely the interchange of the optimization over density and the extremum form of the equilibrium problem. Such an interchange results in the problem

$$\min_{\substack{\sigma \\ \mathrm{div}\sigma+f=0 \\ \sigma\cdot n=t}} \left\{\widehat{\Pi}(\sigma)\right\}, \qquad \widehat{\Pi}(\sigma) = \min_{\substack{\text{density} \\ \rho(x),\, x\in\Omega, \\ \int_\Omega \rho \mathrm{d}\Omega \leq V}} \left[\int_\Omega \overline{\Pi}(\rho, \sigma_{ij})\mathrm{d}\Omega\right] \tag{3.19}$$

We have written problem (3.19) in a form which underlines that this reduced problem should be interpreted as an equilibrium *only* problems for a globally optimized complementary energy expression. The optimized energy is non-smooth and couples all degrees of freedom through the volume constraint. This latter complication can be circumvented by considering the volume constraint of the original problem (3.14) in the form of a penalization and not a constraint (Allaire & Kohn 1993, Allaire & Francfort 1993). With this interpretation problem (3.19) becomes

$$\min_{\substack{\sigma \\ \mathrm{div}\sigma+f=0 \\ \sigma\cdot n=t}} \left\{\widehat{\Pi}_\Lambda(\sigma)\right\}, \quad \widehat{\Pi}_\Lambda(\sigma) = \min_{\substack{\text{density} \\ \rho(x),\, x\in\Omega}} \left[\overline{\Pi}(\rho, \sigma_{ij}) + \Lambda\rho\right] \mathrm{d}\Omega\,, \tag{3.20}$$

[3] Examples show that this typically does not make sense for the strain based setting.

where Λ is now a fixed penalty factor. For a computational procedure for problem (3.20) one could solve the inner problem by analytical or computational means and implement a non-smooth optimization method for solving the equilibrium problem. Such a procedure for layered microstructures is described in Allaire & Kohn (1993), while Allaire & Francfort (1993) have implemented a method, as outlined above, based on linear analysis, where both the material properties *and* the density is updated based on the algebraic solution of the optimization of the complementary energy (see section 3.3 for the derivation of these expressions). Further details can also be found in Allaire (2002).

3.3 Optimized energy functionals for the homogenization modelling

In the following we will compute the optimal strain and complementary energies for rank-2 layered materials in 2-D, corresponding to the *local anisotropy* optimization problem for single load minimum compliance design. That is, we will develop the solution to problems (3.16) and (3.18) for the class of composites that are rank-2 layered materials.

We use here the parametrization of the stiffness of the rank-2 material by the two layer-thicknesses μ and γ, see Sect. 3.1.2. If the primary layerings of density μ are placed in the 2-direction of our reference frame, the effective material properties in plane stress are (cf., (3.8))

$$E^H_{1111} = \frac{\gamma E}{\mu\gamma(1-\nu^2)+(1-\mu)}, \qquad E^H_{1122} = \mu\nu E^H_{1111},$$
$$E^H_{2222} = \mu E + \mu^2\nu^2 E^H_{1111}, \qquad E^H_{1212} = 0$$

when the weak material is void, i.e. $E^- \to 0$. It is straightforward to verify that such a material is weak in shear, i.e. that the material parameters satisfy $E^H_{1111} + E^H_{2222} - 2E^H_{1122} - 4E^H_{1212} \geq 0$ (cf., definition in Sect. 3.1.4).

3.3.1 The stress based problem of optimal layered materials

The results on optimal rotation of orthotropic materials shows that for the minimum compliance problem with a material which is weak in shear, the axes of orthotropy should be aligned with the axes of principal stresses σ_I, σ_{II} This gives a complementary energy of the form

$$\Pi = \frac{1}{2}C^H_{ijkl}\sigma_{ij}\sigma_{kl} = \frac{1}{2|D|}\left[E^H_{1111}\sigma_{II}^2 + E^H_{2222}\sigma_I^2 - 2E^H_{1122}\sigma_I\sigma_{II}\right]$$

with $|D| = E^H_{1111}E^H_{2222} - (E^H_{1122})^2$ Here, we have the well-known relations between principal stresses and stresses in an arbitrary frame:

$$\sigma_I = \frac{1}{2}\left(\sigma_{11} + \sigma_{22} + \sqrt{(\sigma_{11} - \sigma_{22})^2 + 4\sigma_{12}^2}\right)$$
$$\sigma_{II} = \frac{1}{2}\left(\sigma_{11} + \sigma_{22} - \sqrt{(\sigma_{11} - \sigma_{22})^2 + 4\sigma_{12}^2}\right)$$

We see that the alignment of axes is consistent with the fact that $E^H_{1212} = 0$ for the layered material; the vanishing shear stiffness for the layered material plays no role as the material automatically rotates to a frame of zero shear.

Note that the material law described by the energy expression above represents a non-linear material, by virtue of the optimal rotation and the fact that $E^H_{1111} \neq E^H_{2222}$. Here and in the following we use the term "material law" to describe the characteristics of the optimized energy expressions. This should not be interpreted as properties of the layered materials in a physical sense, but expresses the peculiarity of the energy of a structure which automatically assigns the real material in accordance with the applied load (stress/strain field).

We now fix the density ρ and express γ in terms of μ from the relation $\rho = \mu + \gamma - \mu\gamma$ Stationarity of the energy with respect to the layer density μ can now be found by standard but fairly lengthy calculations. We find the stationary layer density μ and corresponding layer density γ given as

$$\mu = \frac{\rho|\sigma_{II}|}{|\sigma_{II}| + (1-\rho)|\sigma_I|}, \quad \gamma = \frac{\rho|\sigma_I}{|\sigma_I| + |\sigma_{II}|}$$

These values turn out to represent minimizing values if the value of μ satisfy the constraints $0 < \mu < \rho$. This implies that the stresses should satisfy $\sigma_I\sigma_{II} \neq 0$ and for such values of stress the optimal layering is a true rank-2 layering. If $\sigma_I\sigma_{II} = 0$ we have a region with an unidirectional, single layering or a solid region corresponding to $\mu = 0, \gamma = \rho$ or $\mu = \rho, \gamma = 0$. The numerical values of stresses in the formula above indicate that there for the rank-2 regions are two distinct types of layerings depending on the sign of the quantity $\sigma_I\sigma_{II}$. We denote the two types of stationary layerings as mode I ($\sigma_I\sigma_{II} < 0$) and mode II ($\sigma_I\sigma_{II} > 0$) materials, and the rank-1 materials as mode III materials. Note that the expressions above were derived under the assumption that the direction of the outer layer of the rank-2 layering (corresponding to μ) is aligned with σ_{II}, and that no restrictions where imposed on the relative sizes of σ_I and σ_{II} The analysis shows that the optimization over layer densities automatically assures that the axis of maximal stiffness is aligned with the axis of the largest stress, in accordance with the result on optimal rotations. Also note that a second, equally optimal layering can be obtained by aligning the outer layerings with the stress σ_I; the formulas above now hold with σ_I and σ_{II} interchanged. The effective complementary energy for both optimal microstructures is given by the expressions

$$\begin{aligned}
&\text{Mode I} \quad \overline{\Pi} = \frac{1}{2E\rho}\left[\sigma_I^2 + \sigma_{II}^2 - 2(1-\rho+\rho\nu)\sigma_I\sigma_{II}\right] \\
&\text{Mode II} \quad \overline{\Pi} = \frac{1}{2E\rho}\left[\sigma_I^2 + \sigma_{II}^2 + 2(1-\rho-\rho\nu)\sigma_I\sigma_{II}\right] \\
&\text{Mode III} \quad \overline{\Pi} = \frac{\sigma_I^2}{2E\rho} \ \text{ if } \ \sigma_{II} = 0\,, \quad \overline{\Pi} = \frac{\sigma_{II}^2}{2E\rho} \ \text{ if } \ \sigma_I = 0
\end{aligned} \tag{3.21}$$

The material properties of the now optimized microstructure are completely given in terms of the density and the principal stresses. Noting that

$$\sigma_I^2 + \sigma_{II}^2 = \sigma_{11}^2 + \sigma_{22}^2 + 2\sigma_{12}^2\,, \quad \sigma_I\sigma_{II} = \sigma_{11}\sigma_{22} - \sigma_{12}^2$$

we observe the surprising fact that the optimized energy corresponds to a material law which for the regions with two layerings is linearly elastic and quasi isotropic. For the single layering regions the material law is non-linear. Note that the isotropy of the optimized material law is natural in view of the rotation of the rank-2 material. The linearity and isotropy of this extremal material law can be understood in a broader context from the so-called translation method for obtaining optimal bounds on effective moduli of composite materials (Cherkaev 1993, Milton 1990).

The expression (3.21) is the solution to the problem (3.18) for the single load case we consider. For the stress based problem (3.17) a further reduction to a design-free problem is possible, cf., problem (3.19) defined in Sect. 3.2.2. To this end we should optimize with respect to the density of material also. Taking the volume constraint into account for the inner problem of (3.19), we minimize with respect to the bulk density ρ the expression $\overline{\Pi}+\Lambda\rho$, where $\Lambda \geq 0$ is a Lagrange multiplier for the volume constraint. By fairly straightforward algebraic manipulations, we get the following optimality condition for the bulk density ρ:

$$\rho = \frac{|\sigma_I| + |\sigma_{II}|}{\sqrt{2\Lambda E}} \quad \text{in all modes} \tag{3.22}$$

In (3.22) the absolute value operators indicate that we have different expressions for mode-I and mode-II. The corresponding densities γ and μ are

$$\mu = \frac{|\sigma_{II}|}{\sqrt{\Lambda E} - |\sigma_I|}, \quad \gamma = \frac{|\sigma_I|}{\sqrt{\Lambda E}}$$

and the optimal distribution of the bulk density should satisfy the volume constraint

$$\int_\Omega \rho \mathrm{d}\Omega = \int_\Omega \min\left\{\frac{|\sigma_I| + |\sigma_{II}|}{\sqrt{2\Lambda E}}, 1\right\} \mathrm{d}\Omega = V \tag{3.23}$$

This constraint determines the value of the Lagrange multiplier Λ for any relevant volume constraint. Thus the volume constraint implies that we can

consider Λ as a function of the principal stresses, given via the equation (3.23). Taking this feature into consideration, the optimal complementary energy density can be expressed in terms of *stresses* only, and we have reduced the stress based *design* problem (1.7) to a *design independent* non-linear, non-smooth elasticity problem of the form

$$\min_{\substack{\sigma \\ \mathrm{div}\sigma+f=0 \\ \sigma\cdot n=t}} \left\{ \int_\Omega \widehat{\Pi}(\sigma)\mathrm{d}\Omega \right\} \tag{3.24}$$

Details of a numerical procedure for solving the stress based problem (3.24) can be found in Allaire & Kohn (1993) and Allaire (2002).

3.3.2 The strain based problem of optimal layered materials

The algebra involved in optimizing the microstructure for the strain based formulation is much more complicated than for the stress case and for simplification of presentation in this case, it turns out to be convenient to impose the choice $|\varepsilon_I| \geq |\varepsilon_{II}|$ for the principal strain directions. The steps of the analysis are all analogous to the procedure for the stress case, but the algebraic manipulations now become very involved, and the use of symbolic manipulations is recommended.

The optimal density μ and corresponding density γ are again given by different expressions, depending on the relative values of the principal strains ε_I, ε_{II} as well as the size of the bulk density ρ. We again denote the different expressions as Mode-I, Mode-II and Mode-III regions (there is a one-to-one correspondence with the stress energy modes). The optimal values are

$$\text{Mode I} \quad \left\{ \begin{array}{l} \mu = \frac{\varepsilon_I(1+\nu\rho-\rho)+\varepsilon_{II}}{\nu\varepsilon_I+(2-\rho-\nu+\nu\rho)\varepsilon_{II}} \\ \gamma = \frac{\varepsilon_I+\varepsilon_{II}(1+\nu\rho-\rho)}{(1-\nu)(\varepsilon_I-\varepsilon_{II})} \end{array} \right\} \quad \text{if} \quad \frac{\varepsilon_I+\varepsilon_{II}}{(1-\nu)\varepsilon_I} < \rho < 1\,,$$

$$\text{Mode II} \quad \left\{ \begin{array}{l} \mu = \frac{\varepsilon_I(\nu\rho+\rho-1)+\varepsilon_{II}}{\nu\varepsilon_I+(2-\rho+\nu-\nu\rho)\varepsilon_{II}} \\ \gamma = \frac{\varepsilon_I+\varepsilon_{II}(\nu\rho+\rho-1)}{(1+\nu)(\varepsilon_I+\varepsilon_{II})} \end{array} \right\} \quad \text{if} \quad \frac{\varepsilon_I-\varepsilon_{II}}{(1+\nu)\varepsilon_I} < \rho < 1\,,$$

$$\text{Mode III} \quad \left\{ \begin{array}{l} \mu = 0 \\ \gamma = \rho \end{array} \right\} \quad \text{if} \quad 0 \leq \rho \leq \frac{\varepsilon_I-\varepsilon_{II}}{(1+\nu)\varepsilon_I} \quad \text{or} \quad 0 \leq \rho \leq \frac{\varepsilon_I+\varepsilon_{II}}{(1-\nu)\varepsilon_I}$$

The effective strain energy corresponding to either optimal layering is given by the expressions

$$\text{I} \quad \overline{W}(\rho,\varepsilon) = \frac{E}{2(1-\nu)(2-\rho+\nu\rho)}\left[\varepsilon_I^2+\varepsilon_{II}^2+2(1-\rho+\rho\nu)\varepsilon_I\varepsilon_{II}\right]$$

$$\text{II} \quad \overline{W}(\rho,\varepsilon) = \frac{E}{2(1+\nu)(2-\rho-\nu\rho)}\left[\varepsilon_I^2+\varepsilon_{II}^2-2(1-\rho-\rho\nu)\varepsilon_I\varepsilon_{II}\right]$$

$$\text{III} \quad \overline{W}(\rho,\varepsilon) = \frac{\rho E\varepsilon_I^2}{2} \text{ if } |\varepsilon_I| \geq |\varepsilon_{II}|, \quad \overline{W}(\rho,\varepsilon) = \frac{\rho E\varepsilon_{II}^2}{2} \text{ if } |\varepsilon_I| \leq |\varepsilon_{II}|$$

In the Mode-III regions with single layers, the material law is non-linear and, as for the stress based analysis, the rank-2 layered regions of Modes I and

Fig. 3.10. Optimal design using an optimized rank-2 material strain energy density. Optimized designs computed using element wise constant density function and a 8-node displacement model. Center: the optimal density distribution, and Right: the associated principal stress distribution for a volume fraction of 20%. Note that grey area is not limited to biaxial response. The bicycle wheel like design has an area with radial uniaxial stress as well as a rim of circumferential uniaxial stress (the rim of a 'wheel') (from Jog et al. 1994).

II correspond to a linearly elastic material law which has the same stiffness matrix as the optimal material obtained in the stress case. This is consistent with a duality principle for the optimized strain and complementary energies

$$\min_{\substack{\mathrm{div}\sigma+f=0\\ \sigma\cdot n=t}} \left\{ \int_\Omega \overline{\Pi}(\rho,\sigma)\mathrm{d}\Omega \right\} = \max_{u\in U} \left\{ l(u) - \int_\Omega \overline{W}(\rho,\varepsilon(u))\mathrm{d}\Omega \right\}$$

that holds when the bulk density ρ is kept fixed (Lipton 1994c).

The optimization of the strain energy with respect to layer directions as well as layer densities results in an optimized strain energy $\overline{W}$ which is convex in the density ρ; this is readily checked by examining the second derivative of the energy for the different modes. This excludes the possibility of interchanging min and the max in the reduced problem

$$\max_{\substack{\text{density } \rho\\ \int_\Omega \rho\mathrm{d}\Omega=V}} \min_{u\in U} \left\{ \int_\Omega \overline{W}(\rho,\varepsilon(u))\mathrm{d}\Omega - l(u) \right\} \tag{3.25}$$

and this is thus the final reduced form of the strain based formulation (compare with (3.24)).

3.3.3 The limiting case of Michell's structural continua

The lay-out theory of Michell frames and its extensions to flexural systems is the classical approach to topology and lay-out design of structures [3], [27]. It has been illustrated earlier that the material distribution method predicts structures that resemble truss-type lay-outs and Michell continua type lay-outs, when constrained to small volumes of available material. We show here that this limiting process can be formalized through an asymptotic expansion of the problem under rescaling of the geometric and load data.

A Michell frame is a continuum in dimension two consisting of two mutually orthogonal fields of tension/compression only members that are directed along the principal strain. The total amount of material used is described by two independent densities of material, constrained to satisfy some volume constraint. The problem is a continuum analogue to the single-load truss optimal design problem, and there are a number of equivalent stress or strain based problem statements. The frame is described by a specific strain energy of the form

$$W = \frac{E}{2}\left[\alpha\varepsilon_I^2 + \beta\varepsilon_{II}^2\right]$$

where α, ε_I and β, ε_{II} are the densities and corresponding principal strains in the two directions of the continua, and the optimization problem is the one of minimizing compliance for a given volume of material, or equivalently, maximizing of compliance for given constraints on the strains in each bar, cf., Hemp (1973), Bendsøe, Ben-Tal & Zowe (1994). Lay-out theory for grid-type structures in general, as treated by Prager and Rozvany, deals with problems with a wider scope of objectives and constraints, but with basically the same energy definition as above.

The Michell frame is usually understood as a limiting case for low densities of material, where the interaction of thin members in a planar frame can be ignored. Thus, we are concerned with the limiting situation where the layers in a layered material become "thin" relative to the cell size of the problem. This can be modelled by letting the density of material tend to zero in an asymptotic expansion. Taking the limit of zero density of material requires a complementary rescaling of the loads and tractions to make the energy limit well posed. We thus introduce a scaling parameter ξ which reduces the layer densities by rescaling the dimensions of the microstructure relative to the unit cell (see Fig. 3.11). The rescaled densities are

$$\hat{\mu} = \xi^2\mu, \quad \hat{\gamma} = \xi^2\gamma, \quad \hat{\rho} = \xi^2\rho$$

We now use the rescaled densities together with an expansion of the stresses and strains in the expressions for the optimized energies described above, using only the terms of zero order in ξ and requiring that the energies remain finite in the limit of $\xi \to 0$. For the stress based case the stress expansion reads

$$\hat{\sigma}_{ij} = \quad + \xi^{-2}\sigma_{ij}^{-2} + \xi^{-1}\sigma_{ij}^{-1} + \sigma_{ij}^{0} + \xi\sigma_{ij} + \xi^2\sigma_{ij}^{2} +$$

For the energy to remain finite in the limit, the expansion in stresses must be of order greater than or equal to 1. The zero-order part of the optimized complementary energy $\overline{\Pi}$ (see Sect. 3.3.1) then becomes (for all modes)

$$\Pi_M = \frac{1}{2E\rho}(|\sigma_I| + |\sigma_{II}|)^2 \ ,$$

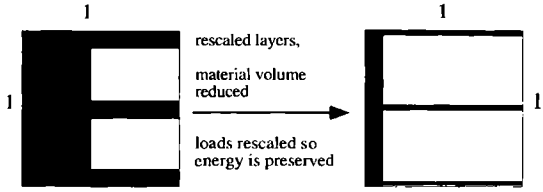

Fig. 3.11. The rescaling of the layerings that leads to the Michell frame limit.

corresponding to a rescaling of stress given by $\xi\sigma_{ij}$ This is expected from equilibrium considerations for the unit cell.

The rescaling at the limit of $\xi \to 0$ implies that the upper constraint on bulk density ρ is not active. Thus the optimization over ρ under the volume constraint results in the stress based problem (3.17) reducing to the form

$$\min_{\substack{\sigma \\ \mathrm{div}\sigma+f=0 \\ \sigma\cdot n=t}} \left\{ \int_\Omega (|\sigma_I| + |\sigma_{II}|)\mathrm{d}\Omega \right\}$$

This is the classical Michell problem formulated in stresses. Here the specific reference to the volume constraint is not present, as the Lagrange multiplier for this constraint only enters as a scaling parameter which has no influence on the form of the optimal solution. The problem corresponds to a lay-out problem, where the cost of carrying the principal stresses is minimized over all statically admissible stress fields. This corresponds directly to the classical stress-based truss optimization problem stated as

$$\begin{aligned} &\min_{\mathbf{q}^+,\mathbf{q}^-} \sum_{i=1}^{m} \frac{l_i}{\overline{\sigma}_i}(q_i^+ + q_i^-) \\ &\text{s.t.} \quad \mathbf{B}(\mathbf{q}^+ - \mathbf{q}^-) = \mathbf{f}, \quad q_i^+ \geq 0,\ q_i^- \geq 0,\ i = 1,\ldots,m\ , \end{aligned}$$

which is a problem in plastic design. Here, q_i^+, q_i^- are the truss bar member forces in compression and tension, respectively, $\mathbf{B}$ is the compatibility matrix, l_i the lengths of the bars and $\overline{\sigma}_i$ the yield limit for bar number i. This problem is equivalent to the problem of fixed volume, minimum compliance design of an elastic truss structure with Young's moduli $E_i = \overline{\sigma}_i^2$ and a volume equal to the optimal volume for the plastic problem, thus taking the development "full circle" Truss topology design is treated in detail in Chap. 4.

One can also perform an analysis as above for the strain based case where the relevant scaling of strain is $\frac{1}{\xi}\varepsilon_{ij}$, consistent with the stress scaling (see Bendsøe & Haber (1993)). Also, an alternative to the development above is to consider the stress-based formulation (3.24). Here one obtains that the limiting case of infinitely large Lagrange multiplier Λ for the volume constraint (i.e. small density) corresponds to the stress-based Michell frame lay-out problem formulation (Allaire & Kohn 1993).

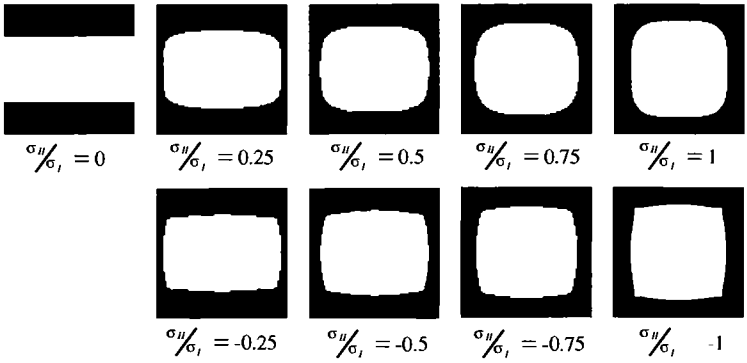

Fig. 3.12. The shape of single inclusions of void in a cell of a homogenized, periodic medium minimizing complementary energy (Vigdergauz-like structures for $\nu = 1/3$ and a density $\rho = 0.5$). Results for a range of principal stress ratios of a macroscopic stress field (from Bendsøe & Sigmund 1999).

3.3.4 Comparing optimal energies

A key question for understanding the nature of the results that can be obtained from optimization of material distribution is a comparison of the stiffness parameters of various microstructures at hand. For compliance design the local anisotropy problems (3.16) and (3.18) give the relevant measures to consider, i.e., one works in terms of strain or complementary energies.

It is known from work in the theoretical materials science [25] that the optimal complementary energy (3.21) derived in Sect. 3.3.1 for rank-2 layered materials constitutes the attainable *lower bound* on the complementary energy of *any* composite constructed from void and an isotropic, linearly elastic material with Young's modulus E and Poisson's ratio ν. This means that any elasticity tensor E^H_{ijkl} related to the given material satisfies that

$$\left[E^H_{ijkl}\right]^{-1}\sigma_I\sigma_{II} \geq \begin{cases} \frac{1}{2E\rho}\left[\sigma_I^2+\sigma_{II}^2-2(1-\rho+\rho\nu)\sigma_I\sigma_{II}\right] \text{ if } \sigma_I\sigma_{II}\leq 0\ , \\ \frac{1}{2E\rho}\left[\sigma_I^2+\sigma_{II}^2+2(1-\rho-\rho\nu)\sigma_I\sigma_{II}\right] \text{ if } \sigma_I\sigma_{II}\geq 0\ , \end{cases} \tag{3.26}$$

for any stress tensor σ with principal stresses σ_I, σ_{II}. We have seen in Sect. 3.3.2 that this upper bound on the stiffness of a composite can also be expressed in terms of strain energy. As we have seen, the bound (3.26) can be attained by a rank-2 layering that have *two* length scales. For stresses with $\sigma_I\sigma_{II} \geq 0$, *single scale*, single inclusion microstructures which attain the bounds have been presented in Vigdergauz (1989), Grabovsky & Kohn (1995). For illustration, Fig. 3.12 shows a range of single inclusion Vigdergauz-like

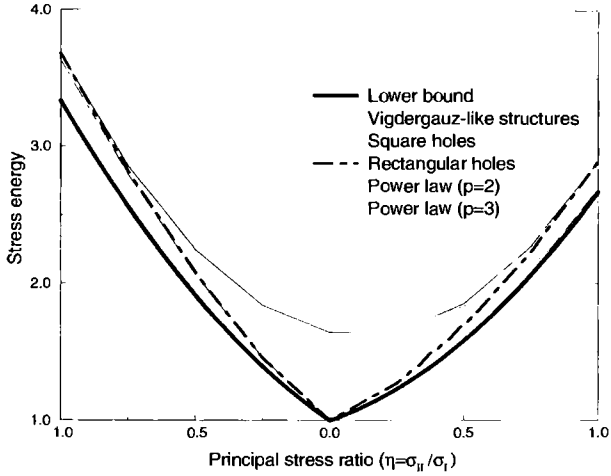

Fig. 3.13. Comparison of the optimal (minimal) complementary energy as a function of the ratio of the principal stresses, for a density $\rho = 0.5$, and for various types of microstructures and interpolation schemes (material and void mixtures). The Vigdergauz-like structures are shown in Fig. 3.12 (from Bendsøe & Sigmund 1999).

microstructures for a range of positive as well as negative values of $\frac{\sigma_I}{\sigma_{II}}$; these structures have been computed by the inverse homogenization methodology described in Sect. 2.10. Note, however, that for $\sigma_I \sigma_{II} < 0$ no single scale periodic composite can obtain the bounds, and any composite obtaining the bound (in 2-D) must be degenerate (i.e. has a singular stiffness tensor) (see Allaire & Aubry (1999)); this effect is also seen in Fig. 3.13.

For their use in optimal topology design it is useful to compare energies attainable by other microstructures and interpolation schemes with the bound (3.26). Figure 3.13 thus shows (for $\rho = 0.5$) a comparison of the optimal bound, achievable by the ranked layered materials, with the range of *minimal* complementary energies[4] which can be obtained by the SIMP interpolation, by microstructures with square holes, by microstructures with rectangular holes, and by the Vigdergauz microstructures. What is noticeable is how close the various energies are for stress fields close to pure dilation, while shearing stress fields demonstrates a considerable difference. In the latter case, the microstructural based models are considerably stiffer than the SIMP model. Moreover, the microstructure with square holes is notably less stiff for uni-axial stresses compared to the other microstructures, since

[4] We compare complementary energies as this gives more informative plots.

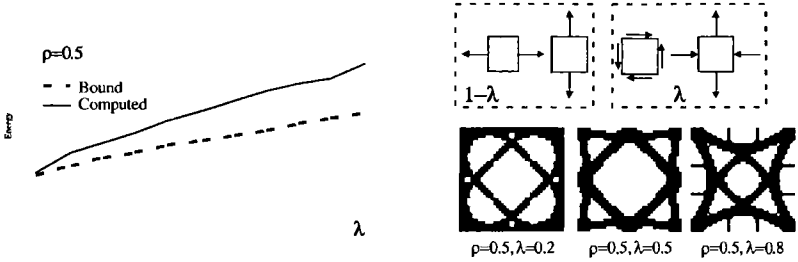

Fig. 3.14. Comparison of the complementary energy of optimized base cells for a multiload situation with $\rho = 0.5$ (see text). The single scale composites are obtained with square base cells (from Guedes et al. 2001).

the imposed symmetry of this microstructure here hinders an efficient use of material.

The plots of the complementary energy explains many features of computational experience with the various interpolation schemes. For compliance optimization, the complementary energy should be minimized. As ranked laminates are efficient also at intermediate densities, optimal design with this material model leads to designs with typically rather large areas of intermediate density. This is also the case when using the microstructures with rectangular holes and the Vigdergauz microstructures. Thus if such materials are used for obtaining black-and-white designs, some other form of penalization of intermediate density has to be introduced, as discussed earlier. On the other hand, the SIMP model and the microstructure with square holes usually lead to designs with very little "grey", as intermediate values of density tend to give poor performance in comparison with cost.

The multiload case For the local anisotropy problems for multiple loads one works with a weighted average of strain or complementary energies. Also here the optimal bound (i.e., the lowest average complementary energy) can be found by using rank-N layered materials [25]. This situation is studied in detail in Cherkaev, Krog & Kucuk (1998), and one can here benefit by working with the moment-based parametrization of stiffness by moments (see Sect. 3.1.2). As above, it is instructive for this situation also to compare this optimal energy with computational results (inverse homogenization) that approximate the energy bounds by use of single scale microstructures.

The example in Fig. 3.14 considers four load cases. The same weight factor is used for each pair of load cases, where the first pair gives tension and the second pair gives shear. The weighting factors on the energies are written as $w^1 = \lambda$ and $w^2 = (1 - \lambda)$ where λ varies from zero to one, where zero corresponds to the tension load situations and λ equal to one corresponds to shear.

3.3.5 Optimal energies and the checkerboard problem

In Sect. 1.3.2 we showed by example that a checkerboard of material in a uniform grid of square Q4 elements has a stiffness which is comparable to the stiffness of a $\rho = 1/2$ *variable thickness* sheet. Let us here formalize this in light of the energy considerations carried out so far, following the ideas of Díaz & Sigmund (1995).

For exemplification, consider the optimal design of a planar, infinite and periodic medium with an average density of material equal to 1/2 and subject to an average, macroscopic strain $\bar{\varepsilon}$. The minimization of compliance then corresponds to the problem

$$\begin{aligned} &\max_{\rho, <\rho>=0.5} \ \min_{u,\ \text{periodic}} \Psi(\rho, u) \\ &\text{with } \Psi(E, \rho, u) = \int_\Omega \rho^p E^0_{ijkl} \left(\bar{\varepsilon} - \varepsilon(u)\right)_{ij} \left(\bar{\varepsilon} - \varepsilon(u)\right)_{kl} \mathrm{d}\Omega \ , \end{aligned} \tag{3.27}$$

where we use a SIMP interpolation. Assuming now that the displacement is restricted to the space of Q4 discretizations for a square mesh we first note that if ρ is distributed in a 0-1 checkerboard pattern in this mesh (denoted as ρ_P), then (this can be derived analytically, see Díaz & Sigmund (1995))

$$\min_{u \in \text{Q4},\ \text{periodic}} \Psi(\rho_P, u) = \frac{1}{2} E^0_{ijkl} \bar{\varepsilon}_{ij} \bar{\varepsilon}_{kl}$$

This can also be understood as follows: the Q4-homogenized properties of a checkerboard pattern is $\frac{1}{2}E^0$ By Q4-homogenized we mean the homogenized properties that one obtains if the displacement fields are restricted to Q4 discretizations at the level of the checkerboard.

For the design problem (3.27) we also have:

$$\begin{aligned} \min_{u \in \text{Q4},\ \text{periodic}} \Psi(\rho, u) &\leq \int_\Omega \rho^p E^0_{ijkl} \bar{\varepsilon}_{ij} \bar{\varepsilon}_{kl} \mathrm{d}\Omega \\ &= E^0_{ijkl} \bar{\varepsilon}_{ij} \bar{\varepsilon}_{kl} \int_\Omega \rho^p \mathrm{d}\Omega \leq \frac{1}{2} E^0_{ijkl} \bar{\varepsilon}_{ij} \bar{\varepsilon}_{kl} \end{aligned}$$

Thus the checkerboard pattern is an optimal design, for the model with Q4-displacements. This is unphysical for several reasons. First, the *true* homogenized material parameters for a checkerboard of material and void is actually *zero* (Berlyand & Kozlov 1992). Second, the stiffest material that can be constructed is the rank-2 layered composite, which has a strain energy $\overline{W}$ given in Sect. 3.3.2. Comparing, we obtain that

$$\overline{W}(\rho = 0.5, \bar{\varepsilon}) \leq \frac{1}{2} E^0_{ijkl} \bar{\varepsilon}_{ij} \bar{\varepsilon}_{kl}$$

where equality *only* holds if the principal strains satisfy $\frac{\bar{\varepsilon}_I}{\bar{\varepsilon}_{II}} = -\nu$ (with the convention $|\bar{\varepsilon}_I| \geq |\bar{\varepsilon}_{II}|$). This means that a Q4-checkerboard grossly overestimates the stiffness, to the extend that it is "stiffer" than the stiffest lay-out

of material (the stiffness corresponds to the Voigt bound, which cannot be realized by a composite).

If one carries out a similar analysis for displacements in a Q9 discretization, the checkerboards instead have a stiffness which is *smaller* than that of a rank-2 material, so here these patterns are not advantageous; see Díaz & Sigmund (1995) for details.

3.4 Design with a free parametrization of material

The goal of this section is to formulate a structural optimization problem in a form that encompasses the design of structural material in a *broad sense*, while also encompassing the provision of predicting the structural topologies and shapes associated with the optimum distribution of the optimized materials. This is accomplished by representing as design variables the material properties in the most general form possible for a (locally) linear elastic continuum namely as the *unrestricted* set of positive semi-definite constitutive tensors [28].

In the modelling of the optimization problem the parameters which describe the structure are, as in the preceding sections of this chapter divided into two sets: the parameters defining the local material tensor and those that describe the specific cost of the material. In parallel with the developments for layered materials, see Sect. 3.3, it can be shown that the minimum compliance optimization of a structure with respect to these two sets of parameters can be performed independently. Furthermore, the optimization with respect to the local material tensor parameters can be performed analytically. This derivation is fairly simple for both the single load case and the multiple load problem and for any dimension of the spatial domain. Thus the more general problem statement is considerably simpler as compared to the homogenization topology problem (see Sect. 3.3).

The very general framework of optimizing directly on a free parametrization of the material tensor results in developments which provide an attainable global lower bound on the performance of any structure designed for the same loads, boundary conditions and ground structure. At the same time, it provides an attainable global upper variational bound on the effective moduli of any elastic material, within the cost measures defined. Also, the considerable simplifications that can be demonstrated indicate that the broader form of a material design problem, as described and analyzed in this section, constitutes effective means for studying the global structural optimization problem involving sizing, shape, topology and material selection.

The results that we can obtain within the assumption of a locally unconstrained configuration of material are informative towards gaining insight into the nature of efficient local structures. This is useful for theoretical as well as practical purposes. As an example of the latter, recent work has thus employed the framework of free material design to generate procedures for

tape-lay-up in composites. Also, the original theoretical work on the subject laid the seeds for the very successful use of topology design methodology for design of materials, as described in Sect. 2.10. Here one tries, for practical reasons, to understand how to match a particular local microstructure to the specific form of a elasticity tensor, for example the ones predicted here.

3.4.1 Problem formulation for a free parametrization of design

Modelling considerations In the homogenization method, the total volume of material, defined at the micro level, provides a natural cost function for the optimization problem. There is not at first glance a natural cost function for the general material design formulation we consider here, where we allow for all possible positive semi-definite constitutive tensors. Instead, we use certain invariants of the stiffness tensor as the measure of cost, thus ensuring that the optimal design solutions are independent of the choice of reference frame.

For physical reasons, the possible stiffness tensors in the design formulation are restricted to the set of positive semi-definite, symmetric tensors. Also, suitable cost functions must have the property of frame indifference. Since the goal is to optimize the local material properties as well as the global structural response, we choose to consider cost in terms of invariants of the constitutive tensor itself. Specifically, we choose for the developments in the following two invariants as examples of local cost (Bendsøe, Guedes, Haber, Pedersen & Taylor 1994)

$$\text{Case A} \quad \Psi_{\mathrm{A}}(E) = E_{ijij} \qquad \text{Case B} \quad \Psi_{\mathrm{B}}(E) = [E_{ijkl}E_{ijkl}]^{\frac{1}{2}}$$

i.e., respectively, the trace and the Frobenius norm of the 4-tensor E. Note that these measures are homogeneous of degree one. Thus comparing to the conventional 2D problem for the design of material distribution in a sheet (where total cost is proportional to the volume of material), the above "cost measures" correspond in their role to the sheet thickness. More general considerations are also possible, combining several invariants of the tensor to provide for *generalized cost measures* which can be varied to cater for specific design goals, for example governed by available fiber composites (see [28]).

Problem statement The problem we consider is the multiple load minimum compliance problem (1.33) (cf., Sect. 1.5.1) generalized to the situation where the material properties themselves appear in the role of design variables. This means that we consider a design parametrization (a definition of E_{ad}) in the form[5]

$$E \succeq 0 \text{ in } \Omega\ , \quad E_{ijkl} \in L^{\infty}(\Omega), \text{ for all } ijkl\ , \quad \int_{\Omega} \Psi(E)\mathrm{d}\Omega \leq V \tag{3.28}$$

[5] We use the notation $E \succeq 0$ to signify that E is positive semidefinite.

Thus we take the minimization over all positive, semi-definite stiffness tensors E_{ijkl} (with the usual symmetry properties) and use the integral over the domain of some invariant $\Psi(E_{ijkl})$ of the stiffness tensor as the measure of cost. For the the sake of simplifying the derivation, we introduce the resource density functions, $\rho_{\mathrm{A}} = \Psi_{\mathrm{A}}(E)$ and $\rho_{\mathrm{B}} \quad \Psi_{\mathrm{B}}(E)$ and state the minimum compliance problem for a multiple load setting in terms of potential energy as

$$\max_{\substack{\text{density } \rho \\ 0\le\rho_{\min}\le\rho\le\rho_{\max}<\infty \\ \int_\Omega \rho \mathrm{d}\Omega\le V}} \quad \max_{\substack{\text{stiffness } E\succeq 0 \\ \Psi(E)\le\rho}} \quad \min_{\substack{\hat{u}=\{u^1,\ldots,u^M\} \\ u^k\in U,\, k=\ \ldots,M}} \int_\Omega W(E,\hat{u})\mathrm{d}\Omega - l(\hat{u})$$

$$W(E,\hat{u}) = \frac{1}{2}\sum_{k=1}^{M} w^k E_{ijpq}(x)\varepsilon_{ij}(u^k)\varepsilon_{pq}(u^k) \tag{3.29}$$

$$l(\hat{u}) = \sum_{k=1}^{M} w^k l^k(u^k), \qquad \hat{u} = \{u^1,\ldots\ ,u^M\}$$

with M load cases (body forces f^k, boundary traction t^k, and weighting factors w^k). Here we have, as in Sect. 3.2.1, provided a separation between the properties of the tensor E that can be optimized locally (at each point in the structure) and those that must be treated as a distributed parameter problem over the full domain.

In the max-min problems above we have introduced an upper bound on the resource densities in order to ensure that the problem is well posed. A possible non-zero lower bound is also catered for. Note that the resource constraints are convex for both case A and B.

In the developments to follow, we show that an analytical optimization actually can reduce the number of free design variables from 6 in dimension two and 21 in dimension three to only *one* in both dimensions (in any dimension that is).

Splitting the problem into a series of sub-problems Analogous to the developments in Sect. 3.2.1 we can rearrange problem (3.29) and split it into two coupled optimization subproblems (the *local anisotropy problem*, and the *material distribution problem*). The interchange of the min and max for the inner problems of (3.29) here gives an *equivalent* problem as (3.29) satisfies the conditions for existence of a saddle point: the objective function is concave (linear) in E and convex in the displacements u^k and the set $\{E|\Psi(E) \le \rho,\ E \succeq 0\}$ is closed, convex and weak*-compact in $L^\infty(\Omega)$ (see also Appendix 5.2).

3.4.2 The solution to the optimum local anisotropy problems

In this section we study the solution to the local anisotropy optimization problem. To this end we define the positive semi-definite, symmetric 4-tensor

A as

$$A_{ijpq} = \sum_{k=1}^{M} w^k A^k_{ijpq}, \quad A^k_{ijpq} = \varepsilon_{ij}(u^k)\varepsilon_{pq}(u^k)$$

and write the optimization of the energy $W(E, \hat{u})$ of (3.29) as

$$\max_{\substack{E \succeq 0 \\ \Psi(E) \leq \rho}} \frac{1}{2} E_{ijpq} A_{ijpq} \tag{3.30}$$

The Frobenius norm case. For the norm resource measure, problem (3.30) corresponds to finding the tensor E of given norm that has the largest standard inner product with the given tensor A. The optimal stiffness tensor is thus proportional to A and because of the resource constraint it is (uniquely) given as

$$E^B_{ijpq} = \rho \frac{A_{ijpq}}{\sqrt{A_{mnrs} A_{mnrs}}}$$

The corresponding extremal energy functional is

$$\overline{W}_B(\rho, \hat{u}) = \rho \check{W}_B(\hat{u}) = \frac{\rho}{2}\sqrt{A_{ijpq} A_{ijpq}} = \frac{\rho}{2}\sqrt{\sum_{k,l=1}^{M} w^k w^l [\varepsilon_{ij}(u^k)\varepsilon_{ij}(u^l)]^2}$$

We have denoted by $\check{W}$ the optimum energy density function per unit amount of resource ρ. Here and elsewhere we embellish with an upper inverted "hat" ($\check{W}$) quantities per unit amount of resource.

Note that the optimized material properties represented by E^B_{ijpq} do not possess any specific symmetry properties and the material is thus generally anisotropic for all but very special cases. The optimized material tensor can have zero eigenvalues, and this happens always if the number of load cases that we consider is one or two in dimension 2 or one to five in dimension 3. For more than this number of load cases, the material will generically be stable, with zero eigenvalues only appearing if the strain fields are linearly dependent.

The trace case. For the trace resource measure, problem (3.30) corresponds to solving a linear programming problem, with objective given by the tensor A In order to find the solution to this problem, introduce the spectral decompositions of E and A. Now let $0 \leq \eta_1 \leq \quad \leq \eta_N$, $\sum_{i=1}^{N} \eta_i = \rho$, and $0 \leq \lambda_1 \leq \quad \leq \lambda_N$ be the ordered eigenvalues of E and A, respectively ($N = 3$ in dimension 2 and $N = 6$ in dimension 3). From a result on the eigenvalues of positive symmetric matrices (Mirsky 1959), it follows that

$$E_{ijpq} A_{ijpq} \leq \sum_{i=1}^{N} \eta_i \lambda_i \leq \sum_{i=1}^{N} \eta_i \overline{\lambda} = \rho \overline{\lambda} \ ,$$

where $\overline{\lambda}$ denotes the largest eigenvalue of the tensor A, with orthonormal eigentensors $\varepsilon_{ij}^{\alpha}$, $\alpha = 1, \ldots, P$ We observe that the right hand side of these inequalities is achieved by any stiffness tensor E of the form

$$E_{ijpq}^{A} = \rho \sum_{\alpha=1}^{P} \mu^{\alpha} \varepsilon_{ij}^{\alpha} \varepsilon_{pq}^{\alpha}, \quad \text{with} \sum_{\alpha=1}^{P} \mu^{\alpha} = 1$$

so we conclude that the optimal energy in the trace case is

$$\overline{W}_A(\rho, \hat{u}) = \rho \check{W}_A(\hat{u}) = \frac{\rho}{2}\overline{\lambda} = \frac{\rho}{2} \max \operatorname{eig} \left\{ \sum_{k=1}^{M} w^k \varepsilon_{ij}(u^k) \varepsilon_{pq}(u^k) \right\}$$

If $\overline{\lambda}$ is a simple eigenvalue, E^A is unique and it corresponds to an orthotropic material, but in the generic case the form of an optimal E^A is only determined when the full problem is solved (the parameters μ^{α} of the expansion of E^A is found from this "outer" problem).

The single load case For the case of a single load case ($M = 1$), the optimal energy in the trace and norm case reduce to the same expression, namely

$$\rho \check{W}_0(u^1) = \frac{1}{2}\rho \varepsilon_{ij}(u^1)\varepsilon_{ij}(u^1) = \frac{1}{2}\rho I_{ijkl}\varepsilon_{ij}(u^1)\varepsilon_{kl}(u^1)$$

corresponding the energy of an isotropic, zero-Poisson-ratio material, with stiffness tensor ρI, which is ρ times the identity tensor. This matrix has norm $\Psi_B(\rho I) = \sqrt{N}\rho$ and trace $\Psi_A(\rho I) = N\rho$ ($N = 3$ in dimension 2 and $N = 6$ in dimension 3). Note however, that the bound $\check{W}_0$ is achieved with the (unique) tensor

$$E_{ijkl}^{*} = E_{ijkl}^{A} = E_{ijkl}^{B} = \rho \frac{\varepsilon_{ij}(u^1)\varepsilon_{kl}(u^1)}{\varepsilon_{pq}(u^1)\varepsilon_{pq}(u^1)}$$

which has norm as well as trace equal to ρ. The optimized material represented by E^* is orthotropic, with axes of orthotropy given by the axes of principal strains (and stresses) for the field $\varepsilon_{ij}(u^1)$, in analogy to the results on optimal rotations of orthotropic materials as described in Sect. 3.1.4.

For completeness of presentation, we write for dimension 2 the resulting optimal stiffnesses in terms of and in the frame of the principal strains ε_I, ε_{II} of the single strain field $\varepsilon_{ij}(u)$ (for convenience we have dropped the index "1" for this load case)

$$(E^*)_{\text{matrix}} = \frac{\rho}{\varepsilon_I^2 + \varepsilon_{II}^2} \begin{bmatrix} \varepsilon_I^2 & \varepsilon_I\varepsilon_{II} & 0 \\ \varepsilon_I\varepsilon_{II} & \varepsilon_{II}^2 & 0 \\ 0 & 0 & 0 \end{bmatrix}$$

Note again that the optimized material is indeed orthotropic, and that the material stiffness tensor has *two* zero eigenvalues. Thus, the extremization

of the strain energy density results in a material which is at the utmost limit of feasibility for satisfying the positivity constraint, and the material can only carry strain fields which are direct scalings of the given strain field for which the optimization was undertaken. This underlines the true optimal nature of the material. Such behaviour of extremized materials was also seen in the homogenization method for topology design with one given material, as described in Sect. 3.3; in that case the optimized material has *one* zero eigenvalue corresponding to vanishing shear stiffness.

For the single load case, we have for both resource measures obtained the reduced equivalent problem statement in the form

$$\max_{\substack{\text{density } \rho \\ 0\le\rho_{\min}\le\rho\le\rho_{\max} \\ \int_\Omega \rho \mathrm{d}\Omega\le V}} \quad \min_{u\in U} \left\{ \frac{1}{2}\int_\Omega \rho\varepsilon_{ij}(u)\varepsilon_{ij}(u)\mathrm{d}\Omega - l(u) \right\}$$

which not only gives the optimal distribution of material, but also the displacements, strains, stresses and material properties of the optimal structure. For this problem we can return to the original form of the minimum compliance problem as stated in (1.6) taking the development "full circle"

$$\begin{aligned} &\min_{u,\,\rho}\ l(u) \\ &\text{s.t.} \quad \int_\Omega \rho\varepsilon_{ij}(u)\varepsilon_{ij}(v)\mathrm{d}\Omega = l(v) \quad \text{for all } v\in U \\ &\qquad 0\le\rho_{\min}\le\rho\le\rho_{\max}, \quad \int_\Omega \rho\mathrm{d}\Omega\le V \end{aligned}$$

This reduced problem is exactly equivalent to the variable-thickness design problem for a sheet made of an isotropic zero-Poisson-ratio material, with the density ρ playing the role of the thickness of the sheet. This problem is discussed in detail in Sect. 5.2.1, and in Appendix 5.2 where the existence of optimal solutions is proved by a fairly straightforward development.

Let us briefly for the single load case consider the stress based formulation (1.7) for the design parametrization used here. This problem can be stated as

$$\inf_{\substack{E\succ 0 \\ \int_\Omega \Psi(E)\mathrm{d}\Omega\le V}} \quad \min_{\substack{\mathrm{div}\sigma+f=0 \\ \sigma\cdot n=t \text{ on } \Gamma_T}} \left\{ \frac{1}{2}\int_\Omega E^{-1}_{ijkl}\sigma_{ij}\sigma_{kl}\mathrm{d}\Omega \right\} \tag{3.31}$$

where we take the infimum with respect to all *positive definite* stiffness tensors, in order to give meaning to $E^{-1}_{ijkl}\sigma_{ij}\sigma_{kl}$ Interchanging the equilibrium minimization with the local minimization of complementary energy (cf. Sect. 3.2.1) and using that we from a spectral decomposition can derive that

$$\inf_{E\succ 0,\,\Psi(E)=\rho} E^{-1}_{ijkl}\sigma_{ij}\sigma_{kl} = \frac{1}{\rho}\sigma_{ij}\sigma_{ij}\ , \tag{3.32}$$

for both of our resource measures, we see that the stress based case has a reduced formulation

$$\inf_{\substack{\text{density } \rho \\ 0<\rho\leq\rho_{\max} \\ \int_\Omega \rho \mathrm{d}\Omega\leq V}} \min_{\substack{\mathrm{div}\sigma+f=0 \text{ in } \Omega \\ \sigma\cdot n=t \text{ on } \Gamma_T}} \left\{ \frac{1}{2}\int_\Omega \frac{1}{\rho}\sigma_{ij}\sigma_{kl}\mathrm{d}\Omega \right\}$$

as expected in light of the form of the displacements based formulation above.

3.4.3 Analysis of the reduced problems

The equilibrium problem for the optimized energy The solution to the local anisotropy problems has shown that the equilibrium problem with the optimized strain energy functions for both cases we consider can be written as

$$\min_{\substack{\hat{u}=\{u^1,\ldots,u^M\} \\ u^k\in U,\, k=1,\ldots,M}} \left\{ \int_\Omega \rho\check{W}(\hat{u})\mathrm{d}\Omega - l(\hat{u}) \right\} \tag{3.33}$$

This is a coupled, non-linear problem for all the load cases at once, the coupling arising through the optimized strain energy functional.

We note here that the function $\check{W}(u^1,\ldots,u^M)$ of the displacements is homogeneous of degree two, that is, under proportional loading the optimized material behaves as a linearly elastic material. Moreover, $\check{W}$ is a convex function. This follows from the fact that $\check{W}$ is given as a maximization of convex functions of the displacements. For the Frobenius norm resource measure, we note that $\check{W}_B$ is a smooth function, except at the origin $(u^1,\ldots,u^M) = (0,\ldots,0)$ when all displacements are zero. For the trace resource measure the optimized strain energy functional involves an eigenvalue problem, which implies that the functional $\check{W}_A$ is only differentiable at sets of displacements for which the maximal eigenvalue of the tensor A is not repeated, and it is non-differentiable at displacements for which the maximal eigenvalue is multiple. This includes the origin $(u^1,\ldots,u^M) = (0,\ldots,0)$ where all displacements are zero. Remark that for the single load case, the equilibrium problem (3.33) is just a single linear equilibrium problem for a structure made of a zero-Poisson-ratio material with varying Young moduli, as described through the variable ρ.

The optimization problem in resource density The reduced optimization problem is as described earlier

$$\max_{\substack{\text{density } \rho \\ 0\leq\rho_{\min}\leq\rho\leq\rho_{\max} \\ \int_\Omega \rho\mathrm{d}\Omega\leq V}} \left[\Phi(\rho) = \min_{\substack{\hat{u}=\{u^1,\ldots,u^M\} \\ u^k\in U,\, k=1,\ldots,M}} \left\{ \int_\Omega \rho\check{W}(\hat{u})\mathrm{d}\Omega - l(\hat{u}) \right\} \right] \tag{3.34}$$

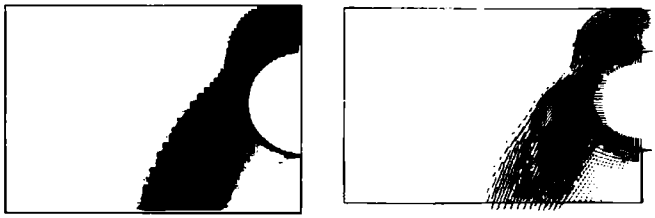

Fig. 3.15. The design of a bearing pedestal using optimal materials. The single load, boundary conditions etc. are described in Fig. 1.25. Left: Distribution of resource. Right: Directions and sizes of principal strains. Compare with Fig. 1.25 (from Bendsøe & Guedes 1994).

This is of the form of a variable thickness sheet problem for a sheet made of a non-linear elastic material. Here the function $\Phi(\rho)$ of the density distribution ρ is defined through the non-linear equilibrium problem discussed in the previous section. Since $\Phi(\rho)$ is given as a minimization of concave (linear) functions in ρ, $\Phi(\rho)$ is in itself concave. Thus (3.34) is a convex minimization problem in the density variable ρ, where the condition of optimality is that the energy $W(u^1, \ldots, u^M)$ is constant in the region of intermediate density.

The reduced problem (3.34) is also a saddle point problem in the resource density ρ and displacements $\{u^k\}$ The existence of a saddle point is also here assured and we can thus find an optimal solution of the optimization problem (3.34) by solving

$$\min_{\substack{\hat{u}=\{u^1,\ldots,u^M\} \\ u^k \in U,\, k=1,\ldots,M}} \left\{ \widehat{W}(\hat{u}) - l(\hat{u}) \right\}, \quad \widehat{W}(\hat{u}) = \max_{\substack{\text{density } \rho \\ 0 \le \rho_{\min} \le \rho \le \rho_{\max} \\ \int_\Omega \rho \mathrm{d}\Omega \le V}} \int_\Omega \rho \check{W}(\hat{u}) \mathrm{d}\Omega \tag{3.35}$$

Using a Lagrange multiplier Λ for the resource constraint, the globally optimized weighted strain energy functional $\widehat{W}(\hat{u})$ can then be expressed as

$$\widehat{W}(\hat{u}) = \min_{\Lambda \ge 0} \left\{ \int_\Omega \max \left\{ \rho_{\min}[\check{W}(\hat{u}) - \Lambda],\, \rho_{\max}[\check{W}(\hat{u}) - \Lambda] \right\} \mathrm{d}\Omega + \Lambda V \right\} \tag{3.36}$$

This implies that the design variables can be removed entirely from the problem, and the resulting problem becomes a non-linear and non-smooth, convex, analysis-only problem. Similar results are also developed for truss design in Chap. 4.

An extension to contact problems It is clear from the analysis above that all steps can be performed without restriction for problems that include

design independent, convex displacement constraints in the equilibrium statement. Thus design problems including unilateral contact can be treated by a similar analysis.

Now let Γ_C denote the boundary of potential contact and let $u \cdot n \geq 0$ on Γ_C be the unilateral contact condition; this is a convex constraint. Then the design problem for minimum compliance under multiple loads can be stated as (see also Sect. 4.2.3)

$$\max_{\substack{\text{stiffness } E \succeq 0 \\ \int_\Omega \Psi(E)\mathrm{d}\Omega \leq V}} \min_{\substack{\hat{u}=\{u^1,\ldots,u^M\} \\ u^k \in U,\, u^k \cdot n \geq 0 \text{ on } \Gamma_C}} \left\{ \int_\Omega W(E,\hat{u})\mathrm{d}\Omega - l(\hat{u}) \right\}$$

where the inner problem is the minimum potential energy principle expressed for a contact problem. For both resource measures this problem can be reduced to the forms seen earlier, the only change being the addition of the contact condition on the admissible displacements. Also, the optimal materials are given by the same expressions.

Materials with piecewise linear elastic behaviour The general framework of free material optimization can also be extended to cover the design of a structure and associated material properties for a system composed of a generic form of *nonlinear softening material.* Here the optimal distribution of material properties depends on the magnitude of load, in contrast to the case with linear material.

The relevant mechanics is now represented in terms of a generalized complementary energy principle and the design objective is likewise based on complementary energy. Net material properties of the softening medium reflect a superposition of properties associated with each of a number of material constituents, and the collection of these properties, expressed through the stiffness tensors for each of these constituents, provides the problem with a set of design parameters. It is the availability of an extremum problem formulation for the analysis part of the problem that makes it possible to treat the design of nonlinear materials conveniently. The formulation used amounts to a generalized form of the complementary energy principle, and is stated here in stresses alone (a mixed formulation in terms of stress and deformation fields is in other situations convenient, see Taylor (1993)). With the superposition of M softening components and one purely elastic basis component to make up the total stress, the analysis problem has the form:

$$\max_{\alpha,\sigma^k,\gamma} \alpha$$

$$\text{s.t.} \quad \operatorname{div}(\gamma_{ij} + \sum_{k=1}^{M} \sigma_{ij}^k) + \alpha f = 0 \ ,$$

$$(\gamma_{ij} + \sum_{k=1}^{M} \sigma_{ij}^k) \cdot n = \alpha t \text{ on } \Gamma_T$$

$$\sigma^k \in \mathcal{K}_k \ , k = 1, \ \ldots, M$$

$$\frac{1}{2} \int_\Omega (D_{ijrs}\gamma_{ij}\gamma_{rs} + \sum_{k=1}^{M} C_{ijrs}^k \sigma_{ij}^k \sigma_{rs}^k) \mathrm{d}\Omega \leq \Pi$$

Here $C_{ijrs}^k = [E_{ijrs}^k]^{-1}$ are the compliance tensors for the M softening components and $D_{ijrs} = [F_{ijrs}]^{-1}$ is the compliance tensor for the basis component. The stresses for the softening components are denoted σ^k and the stress of the basis component is γ. The convex sets of admissible stresses for the softening components are denoted by $\mathcal{K}_k$. This problem statement is a parametrized complementary energy formulation for the general softening material. The solution to this problem predicts a bound to the equilibrium load within the limit Π on total complementary energy.

The formulation above leads one naturally to consider the design of the nonlinear material for maximization of load carrying capacity within the framework of free material design. Up to a rescaling factor on the load this problem is equivalent to the convex problem:

$$\inf_{E^k,F} \min_{\sigma^k,\gamma} \frac{1}{2} \int_\Omega ([F_{ijrs}]^{-1} \gamma_{ij}\gamma_{rs} + \sum_{k=1}^{M} [E_{ijrs}^k]^{-1} \sigma_{ij}^k \sigma_{rs}^k) \mathrm{d}\Omega$$

$$\text{s.t.} \quad \operatorname{div}(\gamma_{ij} + \sum_{k=1}^{M} \sigma_{ij}^k) + \bar{\alpha} f = 0 \ ,$$

$$(\gamma_{ij} + \sum_{k=1}^{M} \sigma_{ij}^k) \ \ n = \bar{\alpha} t \text{ on } \Gamma_T$$

$$\sigma^k \in \mathcal{K}_k \ , k = 1, . \quad , M$$

$$F \succ 0 \ \ E^k \succ 0 \ , k = 1, \ldots \ , M$$

$$\int_\Omega \Psi(F) \mathrm{d}\Omega \leq V_0 \quad \int_\Omega \Psi(E^k \mathrm{d}\Omega \leq V_k \ , k = 1, \ldots, M$$

where each phase has a limited total amount of resource. This is a generalized complementary energy formulation of the design of structures with piecewise linear behaviour.

In the formulation above it is assumed that the softening constraints for the softening components σ^k of total stress are design independent. Thus the

solution predicts the optimal distribution of stiffnesses within these specified softening limits. With this assumption we can now perform the minimization with respect to the pointwise variation of the stiffness tensors, using the result (3.32). With the introduction of these optimal local energy expression, the problem can be reduced to the convex problem:

$$
\begin{aligned}
&\inf_{\rho_k,\rho_0} \min_{\sigma^k,\gamma} \tfrac{1}{2} \int_\Omega \Big(\frac{1}{\rho_0}\gamma_{ij}\gamma_{rs} + \sum_{k=1}^{M} \frac{1}{\rho_k}\sigma^k_{ij}\sigma^k_{rs}\Big)\mathrm{d}\Omega \\
&\quad \text{s.t.} \quad \mathrm{div}(\gamma_{ij} + \sum_{k=1}^{M} \sigma^k_{ij}) + \bar{\alpha} f = 0 \,, \\
&\qquad\quad (\gamma_{ij} + \sum_{k=1}^{M} \sigma^k_{ij}) \cdot n = \bar{\alpha} t \text{ on } \Gamma_T \\
&\qquad\quad \sigma^k \in \mathcal{K}_k \;, k = 1, \ldots, M \\
&\qquad\quad F \succ 0 \;\; E^k \succ 0 \;, k = 1, \ldots, M \\
&\qquad\quad \int_\Omega \rho_0 \mathrm{d}\Omega \le V_0 \quad \int_\Omega \rho_k \mathrm{d}\Omega \le V_k \;, k = 1, \ldots, M
\end{aligned}
$$

where the energy measure for each constituent corresponds to the complementary energy of a linear elastic, zero-Poisson-ratio material of density equal to the locally assigned resource value.

The analysis above can also be performed for an analogous problem of designing a structure made of a general type of elastic/stiffening material (see Bendsøe, Guedes, Plaxton & Taylor (1996); here computational examples can also be found). The analysis model in this case is a displacement based equivalent to the models used above. A detailed description of the analysis model can be found in Taylor (1994). For further discussions on analysis models and sizing and shape design for elasto-plastic problems we refer to the bibliographical notes [31] and the references of the literature mentioned there.

3.4.4 Numerical implementation and examples

Computational procedure for the single load case For the single load case, both the trace and Frobenius norm resource measures lead to the same reduced problem of what amounts to a variable thickness sheet problem for a sheet made of a zero-Poisson-ratio material. In this case we have a design problem that shares important features with minimum compliance problems for trusses, and the problem can be efficiently solved using one of the algorithms presented in Sect. 4.3 on truss topology optimization (Zowe, Kocvara & Bendsøe 1997). This is based on the format of the problem formulation (3.36), which in discretized FE form can be rewritten as a smooth and

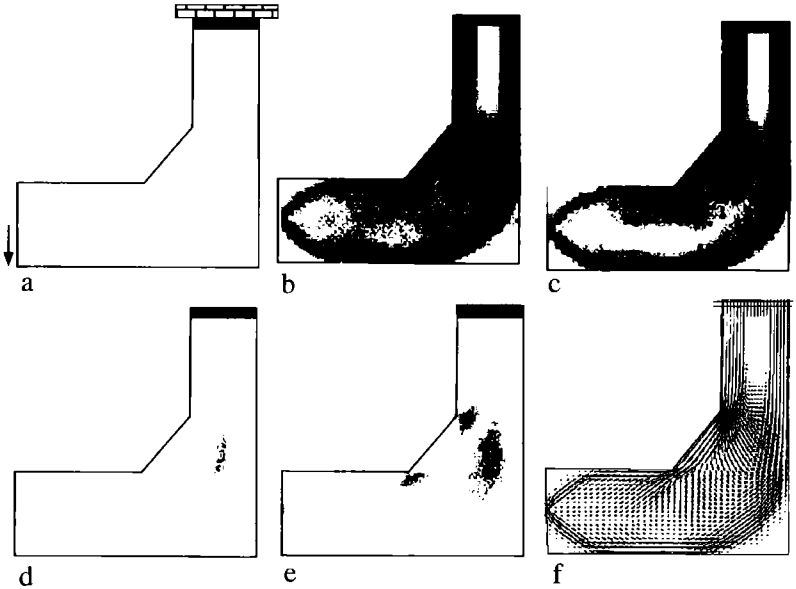

Fig. 3.16. The design of a L-shaped cantilever a) using optimal materials. Single load case. The upper, black part at the support is considered as fixed. b): Distribution of resource. c): Distribution of E_{1111} d): Distribution of E_{2222} e): Distribution of $|E_{1122}|$. f) Directions and sizes of principal strains; directions correspond to direction of material axes (from Bendsøe & Guedes 1994).

convex optimization problem in displacements only (with the notation of, e.g., (1.14)):

$$\begin{aligned} &\min_{\mathbf{u},\Lambda,\tau} \ \{\tau - \mathbf{f}^T\mathbf{u} + \Lambda V\} \\ &\text{s.t.} \quad \rho_{\min}[\tfrac{1}{2}\mathbf{u}^T\mathbf{K}_e\mathbf{u} - \Lambda] \le \tau \quad e = 1,\ldots,N \\ &\qquad\ \ \rho_{\max}[\tfrac{1}{2}\mathbf{u}^T\mathbf{K}_e\mathbf{u} - \Lambda] \le \tau \quad e = 1,\ldots,N \end{aligned} \tag{3.37}$$

This format is well-suited for solution by the so-called PBM interior point methods (see Appendix 5.5). Note that (3.37) only involves the displacement variables (and two auxiliary variables), that it is a linear optimization problem with quadratic constraints, and that the Lagrange multipliers for the constraints determines the values of the density ρ (see Ben-Tal & Bendsøe (1993) and Achtziger, Bendsøe, Ben-Tal & Zowe (1992)).

Computational procedure for the general case The presence of multiple load cases introduces significant complications if the reduced energy

expressions are applied. These complications arise because the locally optimal material couples deformations associated with the different load cases in a complex way that, as we have already seen, involves non-linear, non-smooth energy functionals which depend on all the load cases simultaneously. This stands in sharp contrast with the solution of the problem of design for a single load case. Early numerical work for the multiple load scenario employed an iterative secant method method for solving the inner non-linear equilibrium problem and an optimality criteria method for the density optimization (Bendsøe, Díaz, Lipton & Taylor 1995). This can be applied for the Frobenius norm case, but experience has shown that the complicated non-smoothness for the trace resource case prevents the use of this approach.

An efficient alternative is to apply the formulation (3.35) also in the multiple load case. Limiting ourselves to the *trace* case, a reformulation in the spirit of (3.37) is also possible, but it now involves constraints stating that certain matrices are positive definite; in the trace case the optimal specific energy $\check{W}_A$ is the largest eigenvalue of the tensor A and this can be expressed as

$$\check{W}_A = \inf_{kI_{ijpq} - A_{ijpq} \succeq 0} \tau$$

This also means that $\check{W}_A$ is bounded by a constant k if and only if $kI_{ijpq} - A_{ijpq} \succeq 0$. This can, as A is the sum of dyadic products, be rewritten as a condition that a certain matrix, which is linear in the strains $\varepsilon(u^k)$, is positive semidefinite (see Sect. 5.5.4 for details). Based on (3.35) it is thus possible to write a FE discretized version of the problem as a *semidefinite program* in the displacements only (see Ben-Tal, Kocvara, Nemirovski & Zowe (1999) where also contact conditions are treated). The advantage of this reformulation is that such problems can be solved very efficiently by modern mathematical programming methods, see Appendix 5.5.

3.4.5 Free material design and composite structures

The result of the free parametrization of material is in a sense the ultimately best physically attainable material and it is natural to utilize the full information obtained in the results in an attempt to design an attainable advanced material. This obviously depends on the type of the advanced material available and on the manufacturing technology.

Realization by tape-lay-up First we consider a procedure that relies on the free material optimization for design of composite materials manufactured by the so-called tape-laying technology. In a post-processing phase one can here generate curves which indicate how to lay the tapes and how to organize the thickness of the tapes. This gives a good initial approximation for an optimization procedure that also takes into consideration all the technological restrictions of the tape-laying process.

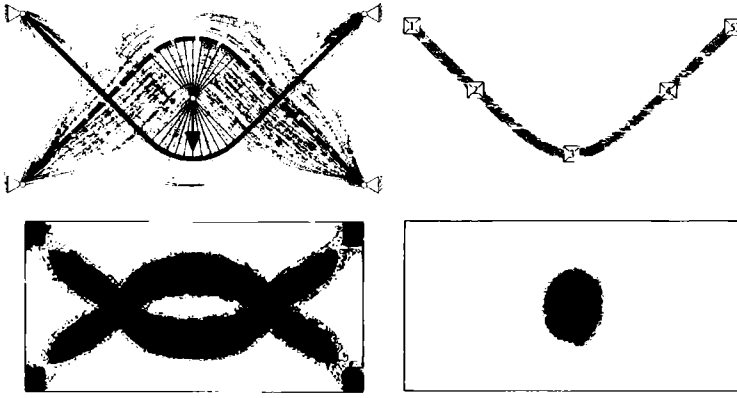

Fig. 3.17. Tape-laying example. Top left is the stress directions from the free material optimization and a super-posed Michell solution. Top right shows the laying of the first tape. Bottom pictures show two tape layers obtained by post-processing of the top left design. By courtesy of M. Kocvara and H.R.E.M. Hörnlein.

The post-processing uses that the optimal material for the single load free material design is orthotropic and that the axes of orthotropy correspond point-wise to the orthogonal directions of principal strains or stresses. This allows an interpretation where this governs the direction of fibres in a (weak) resin material. To get an impression of the lay-out of these fibres and the thickness, a graphical post-processing tool can be employed that plots the vector fields of principal strain direction by means of *smooth* curves. The optimal load path is interpreted as that of a fibre reinforced material, for example in the form of pre-pregs of Carbon Fibre Reinforced Plastic (CFRP) tapes. Tape-laying is thus a way to bridge the gap between free material design and the preliminary design phases for structures constructed from such tapes. Further details can be found in Hörnlein, Kocvara & Werner (2001).

Realization by materials with microstructure Alternatively, skeletal bar structures could be used to generate microstructures that mimic the behaviour of the optimized material tensors, see figures below. These results are obtained numerically by an inverse homogenization operation (see Sect. 2.10) that works with unit cells constructed from truss elements (Sigmund 1994b, Sigmund 1995). The results substantiates the theoretical finding ((Milton & Cherkaev 1995)) that any stiffness tensor can be constructed from layered materials made from an infinitely strong phase and an infinitely weak phase.

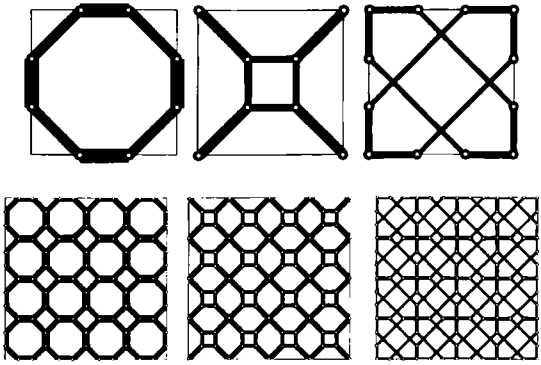

$$E^* = \begin{bmatrix} 1 & 1 & 0 \\ 1 & 1 & 0 \\ 0 & 0 & 0 \end{bmatrix}$$

Fig. 3.18. Minimum weight 2-D microstructures (upper row shows the unit cells, lower row an assemblage of cells) for obtaining materials with the indicated stiffness in the axis of the cell, corresponding the optimal material for a single strain field $\varepsilon = (1, 1, 0)$. This is an isotropic material with Poisson's ratio 1.0. The three designs all have the same weight and are obtained using a 4 by 4 equidistant nodal lay-out in a square cell. All 120 possible connections between the nodal points are considered as potential members. Members not shown for the optimum cell (and structure) are at the minimum gauge which is 10^5 times smaller than the maximum gauge. The different designs are obtained by penalization of the lengths of the bars (from Sigmund 1994b).

3.5 Plate design with composite materials

3.5.1 The homogenization approach for Kirchhoff plates

In analogy with the topology design problem treated so far, a relaxation of the Kirchhoff plate design problem[6] requires that one considers plates with infinitely many, infinitely thin integral stiffeners ([29]). This can be in the form of a rank-2 structure of stiffeners of height $h_{\max}$ on a solid plate of variable thickness h, i.e. a planar rank-2 layering of the weak tensor $\frac{h^3}{12} E^0_{ijkl}$ and the strong tensor $\frac{h^3_{\max}}{12} E^0_{ijkl}$ (see Fig. 3.20).

For the relaxed design problem we thus need to state the homogenization formulas for Kirchhoff plates, more specifically the effective material parameters for rib-stiffened plates. With these formulas at hand (see Sect. 5.4.5 of Appendix 5.4), the computational procedure for computing optimal designs is completely analogous to the procedure described in Sect. 3.1.3. The optimality criteria for the densities are equivalent to those derived in Sect. 3.1.4, with strains and stresses interpreted as curvatures and moments. However, extra care is required for use of the result on optimal rotations.

[6] We refer to Sect. 1.5.3 for notation.

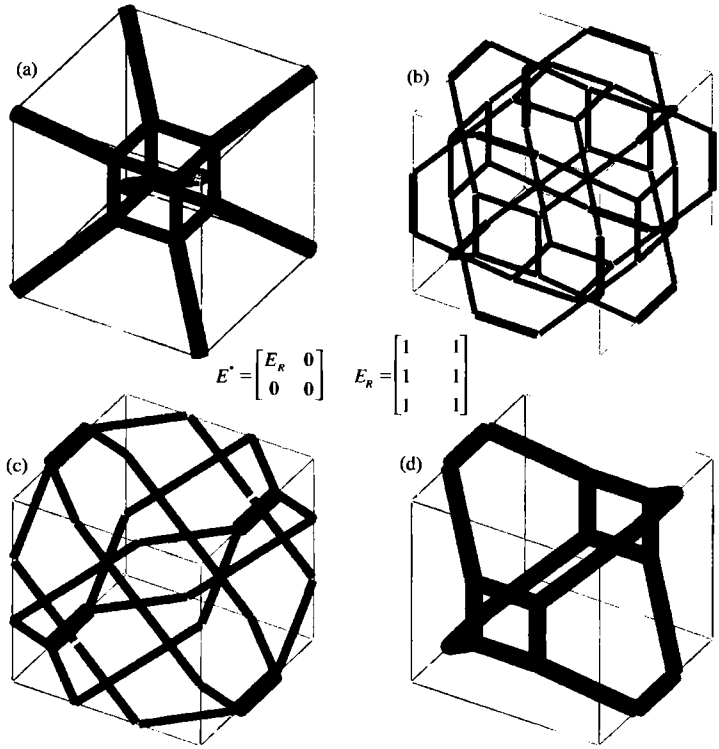

Fig. 3.19. Minimum weight microstructures in dimension 3 for obtaining materials which corresponds to the optimal material for a single strain field $\varepsilon = (1, 1, 1, 0, 0, 0)$. The three designs all have the same weight and are obtained using a 4 by 4 by 4 equidistant nodal lay-out in a cubic cell. All 2016 possible connection between the nodal points are considered as potential members. Members not shown for the optimum cell (and structure) are at the minimum gauge. The different designs are obtained by penalization of members with certain lengths. The topologies in a) and b) have full cubic symmetry. The topology in c) has bars on the surface of the cell only and is not cubic symmetric, even though the effective parameters are isotropic. Notice the similarity between the 3-D microstructures and the 2-D microstructures shown in Fig. 3.18 (from Sigmund 1995).

In order to exemplify the difference to the plane stress situation, consider a constant thickness, perforated plate with an orthogonal rank-2 system of stiffeners. The effective bending stiffness is then $D = \frac{h_{\max}^3}{12}\tilde{D}$, with (see Appendix 5.4)

Fig. 3.20. Cross-section of the upper half of a rib-stiffened plate with one field of stiffeners running along the normal of the cutting plane.

$$\begin{aligned} \tilde{D}_{1111} &= \frac{\gamma E}{\mu\gamma(1-\nu^2)+(1-\mu)}, \quad \tilde{D}_{1122} = \mu\nu E_{1111}, \\ \tilde{D}_{2222} &= \mu E + \mu^2\nu^2 E_{1111}, \quad \tilde{D}_{1212} = (\gamma+\mu+\mu\gamma)\frac{E}{2(1+\nu)} \end{aligned} \tag{3.38}$$

where the primary layering of density μ is in the 2-direction and the secondary layer has density γ. This material law satisfies that $D_{1111} + D_{2222} - 2D_{1122} - 4D_{1212} < 0$ (see discussion in section 3.1.4), meaning that the analysis of the minimum compliance plate problem is more tricky than the plane stress case. As an example, there may be regions in a plate where an optimal, orthogonal rank-2 layering is not aligned with the principal curvatures. We will not treat the plate problem in further detail, as this is a major subject (see the monograph by Lewiński & Telega (2000) and [29]).

We do mention, however, that the optimal design of plates takes an extra twist when the analysis modelling is taken into account. The design problem and its associated relaxation can be viewed as a purely mathematical question of achieving well-posedness, but as any plate model is an approximate model, it is natural to question the validity of the relaxation in relation to the modelling restrictions/assumptions made to achieve the plate model under consideration [29]. Thus the use of thin, high stiffeners in a Kirchhoff plate model is in fact a violation of the assumptions under which this model can be derived from 3-D elasticity. This means that the developments above should be seen in the framework of achieving regularization strictly within the Kirchhoff plate framework, ignoring eventual modelling restrictions. The modelling problem should by no means be dismissed but lies outside the scope of this presentation. The reader is referred to the literature [29] for further information on this problem as well as to studies of optimal thickness design of Mindlin plates within the framework of the homogenization modelling.

3.5.2 Minimum compliance design of laminated plates

This section is concerned with the optimal design of the lay-up of *laminated* plates for maximum stiffness. We consider optimization with respect to the ply thicknesses, fiber orientations and the stacking sequence of the laminates, keeping the ply material properties and the shape of the plate fixed. Instead of working directly with this mix of integer and real design parameters we

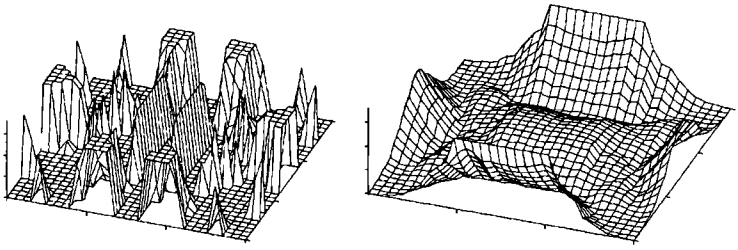

Fig. 3.21. Plate design of a clamped Kirchhoff plate subject to uniform transverse load. Left: Optimal thickness design (ill-posed). Right: Optimal distribution of material with two fields of stiffeners. The design data is $h_{\min}/h_{\max} = 5.0$ and $h_{\max}/h_{\text{unif}} = 2.84$. In both illustrations only the variation over the minimum gauge $h_{\min}$ is shown.

employ a design parametrization through the so-called lamination parameters [30]. These represent the effective, integrated properties of the laminate and are given as moments relative to the plate mid-plane of the trigonometric functions entering in the frame rotation formulas for stiffness matrices. In this way the properties related to the stiffness of the laminates are emphasized in the optimization model, while the realization of the optimal effective properties is postponed for subsequent post-processing.

The developments below are strongly related to the free material design and to the homogenization approach discussed earlier, and also here we can carry out an analytical derivation of the optimal local properties of material. Moreover, we choose to extend the design space to include "chattering" designs, thereby allowing infinitely many small variations of the fiber orientation in each point through the thickness for each design domain of the plate (Hammer, Bendsøe, Lipton & Pedersen 1996). This corresponds to the introduction of periodic composites for topology design and the use of rib-reinforced plates in plate design.

Parametrization by lamination parameters Before defining the lamination parameters we first need to express the constitutive relations for a single ply of material in convenient form. Thus the elasticity tensor E_{ijkl} will for convenience be written as a matrix

$$\mathbf{E}_X = \begin{bmatrix} E_{1111} & E_{1122} & \sqrt{2}E_{1112} \\ E_{1122} & E_{2222} & \sqrt{2}E_{2212} \\ \sqrt{2}E_{1112} & \sqrt{2}E_{2212} & 2E_{1212} \end{bmatrix}_X \tag{3.39}$$

The index indicates that the constitutive parameters are given in the coordinate system X. In another coordinate system x rotated the angle ψ positive anti-clockwise relative to the X-system, $\mathbf{E}_x$ is most easily expressed using

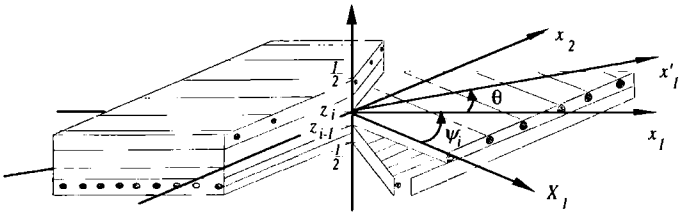

Fig. 3.22. Sketch of a laminate with the global coordinate systems x and x', a material system X and orientations of the plies shown.

the material parameters E_{1-7}, (Tsai & Hahn 1980). To ease the formulations later on, the constitutive matrix $\mathbf{E}_x$ is written in terms of five symmetric matrices containing the material parameters as:

$$\mathbf{E}_x = \boldsymbol{\Upsilon}_0 + \boldsymbol{\Upsilon}_1 \cos 2\psi + \boldsymbol{\Upsilon}_2 \cos 4\psi + \boldsymbol{\Upsilon}_3 \sin 2\psi + \boldsymbol{\Upsilon}_4 \sin 4\psi \ , \tag{3.40}$$

$$\boldsymbol{\Upsilon}_0 = \begin{bmatrix} E_1 & E_4 & 0 \\ E_4 & E_1 & 0 \\ 0 & 0 & 2E_5 \end{bmatrix} \quad \boldsymbol{\Upsilon}_1 = \begin{bmatrix} E_2 & 0 & \sqrt{2}E_6 \\ 0 & -E_2 & \sqrt{2}E_6 \\ \sqrt{2}E_6 & \sqrt{2}E_6 & 0 \end{bmatrix}$$

$$\boldsymbol{\Upsilon}_2 = \begin{bmatrix} E_3 & -E_3 & \sqrt{2}E_7 \\ -E_3 & E_3 & -\sqrt{2}E_7 \\ \sqrt{2}E_7 & -\sqrt{2}E_7 & -2E_3 \end{bmatrix} \quad \boldsymbol{\Upsilon}_3 = \begin{bmatrix} 2E_6 & 0 & -\frac{1}{\sqrt{2}}E_2 \\ 0 & -2E_6 & -\frac{1}{\sqrt{2}}E_2 \\ -\frac{1}{\sqrt{2}}E_2 & -\frac{1}{\sqrt{2}}E_2 & 0 \end{bmatrix}$$

$$\boldsymbol{\Upsilon}_4 = \begin{bmatrix} E_7 & -E_7 & -\sqrt{2}E_3 \\ -E_7 & E_7 & \sqrt{2}E_3 \\ -\sqrt{2}E_3 & \sqrt{2}E_3 & -2E_7 \end{bmatrix}$$

where the material parameters E_{1-7} are expressed as

$$E_1 = \tfrac{1}{2}\left(E_{1111} + E_{2222}\right)_X - E_3 \quad E_2 = \tfrac{1}{2}\left(E_{1111} - E_{2222}\right)_X$$
$$E_3 = \tfrac{1}{8}\left(E_{1111} + E_{2222} - 2E_{1122} - 4E_{1212}\right)_X$$
$$E_4 = \left(E_{1122}\right)_X + E_3 \quad E_5 = \left(E_{1212}\right)_X + E_3 = \tfrac{1}{2}\left(E_1 - E_4\right)$$
$$E_6 = \tfrac{1}{2}\left(E_{1112} + E_{2212}\right)_X \quad E_7 = \tfrac{1}{2}\left(E_{1112} - E_{2212}\right)_X$$

If the material is orthotropic in the X-system $E_6 = E_7 = 0$ and in the case of an isotropic material $E_2 = E_3 = 0$ as well.

We consider a laminate of the *fixed* thickness h made from several plies. Here the orientation of the i'th ply with respect to a suitable, fixed frame of reference is specified by ψ_i and z_i gives the location (dimensionless) of the interface between ply i and $i+1$, see Fig. 3.22. All the plies consist of the same anisotropic material.

In the classical plate theory the global relation between the membrane forces and moments per unit length $\{N\}$, $\{M\}$ and the mid-plane strains $\{\varepsilon^0\}$ and curvatures $\{\kappa\}$ is

$$\begin{bmatrix} \{N\} \\ \{M\} \end{bmatrix} = \begin{bmatrix} \mathbf{A} & \mathbf{B} \\ \mathbf{B} & \mathbf{D} \end{bmatrix} \begin{bmatrix} \{\varepsilon^0\} \\ \{\kappa\} \end{bmatrix}$$

where a $\sqrt{2}$-notation is used ($\{N\} = \{N_{11},\ N_{22},\ \sqrt{2}N_{12}\}^T$ etc. see e.g. (Pedersen 1995b). The stiffness matrices for the whole laminate can be expressed in a very similar way as the constitutive matrix in equation (3.40). The symmetric membrane, coupling and bending stiffness matrices **A**, **B** and **D**, respectively are in terms of the material parameters E_{1-7} and the lamination parameters $\xi_{1-4}^{A,B,D}$ given as

$$\begin{aligned} \mathbf{A} &= h\left(\boldsymbol{\Upsilon}_0 + \boldsymbol{\Upsilon}_1\xi_1^A + \boldsymbol{\Upsilon}_2\xi_2^A + \boldsymbol{\Upsilon}_3\xi_3^A + \boldsymbol{\Upsilon}_4\xi_4^A\right) \\ \mathbf{B} &= h^2\left(\boldsymbol{\Upsilon}_1\xi_1^B + \boldsymbol{\Upsilon}_2\xi_2^B + \boldsymbol{\Upsilon}_3\xi_3^B + \boldsymbol{\Upsilon}_4\xi_4^B\right) \\ \mathbf{D} &= h^3\left(\tfrac{1}{12}\boldsymbol{\Upsilon}_0 + \boldsymbol{\Upsilon}_1\xi_1^D + \boldsymbol{\Upsilon}_2\xi_2^D + \boldsymbol{\Upsilon}_3\xi_3^D + \boldsymbol{\Upsilon}_4\xi_4^D\right) \end{aligned} \tag{3.41}$$

The *lamination parameters* in a global coordinate-system x are defined as the weighted trigonometric integrals over the thickness (compare with the definition of the moments used for parametrization of the stiffness rank-N layered materials, see Sect. 3.1.2):

$$\xi_{[1,2,3,4]}^{A,B,D} = \int_{-}^{\frac{1}{2}} z^{0,1,2}\left[\cos 2\psi(z), \cos 4\psi(z), \sin 2\psi(z), \sin 4\psi(z)\right] \mathrm{d}z$$

This compact notation implies for instance that ξ_3^B is given as

$$\xi_3^B = \int_{--}^{\frac{1}{2}} z \sin 2\psi(z)\, \mathrm{d}z$$

Generalized lamination parameters In the following we will consider lamination parameters arising from any arbitrary variations of the ply angles through the thickness of the plate, including limits of rapidly varying oscillations. We thus extend the definition of the lamination parameters to

$$\xi_{[1,2,3,4]}^{A,B,D} = \int_{-\frac{1}{2}}^{\frac{1}{2}} z^{0,1,2} P_{[1,2,3,4]}(z)\, \mathrm{d}z \tag{3.42}$$

where P is the vector

$$P_{[1,2,3,4]}(z) = \int_0^{\pi} \left[\cos 2\psi, \cos 4\psi, \sin 2\psi, \sin 4\psi\right] \mathrm{d}\theta_z(\psi) \tag{3.43}$$

corresponding to a microscopic lay-up defined by a probability measure $\theta_z(\psi)$ with support in $[0, \pi]$.

The set of lamination parameters $\mathcal{D}$ constitutes a convex and compact set in $\mathbf{R}^{12}$, (Grenestedt & Gudmundson 1993), and this property is expressed in the representation given by equations (3.42) and (3.43); convexity, for

example, follows from the possible use of a chattering design with a density of two laminate angles (see also below).

The advantage of expressing laminate plate design in terms of the lamination parameters is that one obtains a reduction in the number of variables to twelve (per point or per design area), irrespective of the number of plies. Moreover, one avoids a troublesome optimization over periodic functions of the rotation angles, as well as working with a discrete number of plies. In the sense of topology design of choosing between plies, the lamination parameters thus constitute the basis for an interpolation model. Also, the convexity of the set of lamination parameters together with the linear dependence of the stiffnesses on these parameters also leads to further simplifications as seen also for the free material optimization problem.

The lamination parameters are obviously not independent, as there exist trigonometric relations between the functions over which the weights are taken. This is completely equivalent to the situation for the moments used in the expression (3.9) for layered materials. Also here the the range of admissible weights $P(z)$ are given by the solution to the geometric moment problem as developed in Krein & Nudelman (1977). We thus have that $P(z)$ is an L^∞-map from the interval $\left[-\frac{1}{2}, \frac{1}{2}\right]$ to the set $\mathcal{M}$ defined by (cf., (3.10))

$$\mathcal{M} = \left\{ \mathbf{y} \in \mathbf{R}^4 \left| \begin{array}{l} y_1^2 + y_3^2 \leq 1, \quad -1 \leq y_2 \leq 1 \\ 2y_1^2(1-y_2) + 2y_3^2(1+y_2) + \\ +y_2^2 + y_4^2 - 4y_1y_3y_4 \leq 1 \end{array} \right. \right\} \tag{3.44}$$

The set $\mathcal{M}$ is the convex hull (bounded by the supporting hyperplanes) of the closed curve $(\cos 2\psi, \cos 4\psi, \sin 2\psi, \sin 4\psi)$, $\psi \in [0, \pi]$ in $\mathbf{R}^4$ We can thus conclude that the set $\mathcal{D}$ is also compact as well as convex in $\mathbf{R}^{12}$

The constraints on $P(z)$ are inherited directly by the lamination parameters $\xi^A_{[1,2,3,4]}$ governing the *membrane* stiffnesses, so we have that $\boldsymbol{\xi}^A \in \mathcal{M}$. The same conditions hold for the four bending parameters ξ^D_{1-4} when pure bending is considered. Various necessary conditions for different combinations of ξ's can be found in the literature, but the complete set of sufficient conditions for all twelve parameters is still not known [30].

In general the solution to the problem of finding a combination of ply thicknesses t_i's and ply angles ψ_i's for prescribed lamination parameters ξ's is *not* unique. The problem can therefore be formulated and solved as an inverse optimization problem with the possibility of adding additional constraints as for example on the total thickness and/or on the variation of the orientation from ply to ply [30]. This is similar to the use of an inverse homogenization problem for finding specific material properties of a material with microstructure. Regarding the number of plies, it can be shown that when only the coefficients ξ^A_{1-4} governing the membrane stiffness are considered, all points within the feasible domain given by $\mathcal{M}$ can be realized by a laminate with at most three plies (see Lipton (1994a) for a possible algorithm).

Minimum compliance of laminated plates The problem of minimizing the compliance of a laminated plate can now be analyzed along the lines used previously for free material design and for layered media. The design variables are the lamination parameters varying from point to point throughout the plate and we will base the developments on the multiple load case. As the stiffness matrices $\mathbf{A}$, $\mathbf{B}$ and $\mathbf{D}$ are all linear in the lamination parameters, the strain energy is linear (and thus concave) in the lamination parameters. As seen for the free material case the problem thus satisfies the conditions for existence of a saddle point and we can perform our analysis by solving the local anisotropy problem together with the equilibrium problem. Here there is no material distribution problem, unless one chooses also to consider a variable thickness h as a design variable.

The local anisotropy problem for laminates The local anisotropy problem of finding the pointwise best use of material is for laminates of the form

$$\begin{aligned} &\max_{\xi \in \mathbf{D}} \sum_{k=1}^{M} w^k W_k \qquad \text{with} \\ &W_k = \frac{1}{2h}\left(\left\{\varepsilon^0\right\}_k^T \mathbf{A}\left\{\varepsilon^0\right\}_k + 2\left\{\varepsilon^0\right\}_k^T \mathbf{B}\left\{\kappa\right\}_k + \left\{\kappa\right\}_k^T \mathbf{B}\left\{\kappa\right\}_k\right) \end{aligned} \tag{3.45}$$

Here the displacement field at equilibrium u^k for the load case k enters via the strain energy density W_k (w^k is the weight factor for this load case). We note here that the objective function of problem (3.45) is linear and that the constraint set is convex and compact. There thus exists a solution among the extreme points of the convex set $\mathcal{D}$.

The energy density can also be written directly in terms of the total strains $\{\varepsilon(z)\}_k \quad \{\varepsilon^0\}_k + zh\{\kappa\}_k$ as (setting $P_0 = 1$ and using the matrix definitions in equation (3.40))

$$W_k = \frac{1}{2}\int_{-\frac{1}{2}}^{\frac{1}{2}} \left(\sum_{i=0}^{4} \{\varepsilon(z)\}_k^T \boldsymbol{\Upsilon}_i \{\varepsilon(z)\}_k P_i(z)\right) \mathrm{d}z \tag{3.46}$$

As we also will allow for any variation of the ply lay-up through the thickness of the plate, we see that in order to solve (3.45) we have for each position z through the thickness to maximize the expression

$$\sum_{l=1}^{L} w^k \left(\sum_{i=0}^{4} \{\varepsilon(z)\}_k^T \boldsymbol{\Upsilon}_i \{\varepsilon(z)\}_k P_i(z)\right) \tag{3.47}$$

over the parameters P_i. Thus the optimal lay-up of the laminate (for maximum stiffness) for each position (x_1, x_2, z) in the plate domain can be found by solving the problem

$$\max_{\mathbf{y} \in \mathcal{M}} \sum_{l=1}^{L} w^k \left(\sum_{i=1}^{4} \{\varepsilon(z)\}_k^T \boldsymbol{\Upsilon}_i \{\varepsilon(z)\}_k y_i\right) \tag{3.48}$$

over the well-known set $\mathcal{M}$ given earlier. Problem (3.48) is also, like problem (3.45), a linear optimization problem with convex and compact constraint set. There thus exists a solution among the extreme points of the convex set $\mathcal{M}$ which is the convex hull of the curve $(\cos 2\psi, \cos 4\psi, \sin 2\psi, \sin 4\psi)$, $\psi \in [0, \pi]$, so we conclude that for each position (x_1, x_2, z) in the plate there exist a solution to (3.48) which corresponds to a single ply rotated at a given angle. However, as this solution is *not* unique, we cannot make this conclusion about the optimal design. This will be elaborated in the following.

The pure membrane case Let us now consider the situation of designing the lay-up for a situation of only in-plane loading, i.e. the pure membrane case. In that setting the strain energy density of the plate reduces to

$$W_k = \frac{1}{2}\int_{-\frac{1}{2}}^{\frac{1}{2}} \left(\sum_{i=0}^{4} \{\varepsilon^0\}_k^T \boldsymbol{\Upsilon}_i \{\varepsilon^0\}_k P_i(z)\right) \mathrm{d}z \tag{3.49}$$

Thus the optimization over the variables P_i gives the same result at any cross-sectional position z of the plate. Together with the fact that the stacking sequence is of no consequence for the membrane stiffness and the fact that any element of the set $\mathcal{M}$ can be constructed as a convex combination of at most three points on the curve $(\cos 2\psi, \cos 4\psi, \sin 2\psi, \sin 4\psi)$, $\psi \in [0, \pi]$ (see e.g., Lipton (1994b), Lipton (1994b)), this implies that the optimal plate can be constructed from at most *three* plies. This holds for the single as well as the multiple load case. In the single load case this can be reduced to at most two plies, as will be shown below.

Let us now for exemplification of the use of lamination parameters solve (3.48) for the case of a single load case and an orthotropic material. For simplicity, we use the directions of principal strains, $\varepsilon_I, \varepsilon_{II}$, as a local frame of reference, while for the ply material we assume that the directions of orthotropy are ordered so $E_2 \geq 0$, i.e. so $E_{1111} \geq E_{2222}$. Problem (3.48) then reduces to

$$\max_{\mathbf{y}\in\mathcal{M}} \left(E_2\left(\varepsilon_I^2 - \varepsilon_{II}^2\right) y_1 + E_3\left(\varepsilon_I - \varepsilon_{II}\right)^2 y_2\right) \tag{3.50}$$

Furthermore, as the third and fourth lamination parameters do not enter in (3.50), we can reduce the constraint set to the range of the trigonometric averages P_1, P_2, that is, to the set

$$\widehat{\mathcal{M}} = \left\{\mathbf{y} \in \mathbf{R}^2 \,\middle|\, -1 \leq y_1 \leq 1, -1 \leq y_2 \leq 1, 2y_1^2(1 - y_2) + y_2^2 \leq 1, \right\}$$

so that (3.50) is reduced to

$$\max_{(y_1, y_2)\in\widehat{\mathcal{M}}} \left(E_2\left(\varepsilon_I^2 - \varepsilon_{II}^2\right) y_1 + E_3\left(\varepsilon_I - \varepsilon_{II}\right)^2 y_2\right) \tag{3.51}$$

Assume first that $E_3 \geq 0$; this is a material which has low shear stiffness, cf. Sect. 3.1.4 and Pedersen (1990). As $E_3(\varepsilon_I - \varepsilon_{II})^2 \geq 0, E_2 \geq 0$, the optimal

energies will depend on the sign of $(\varepsilon_I^2 - \varepsilon_{II}^2)$ and will be given by the energies obtained from the lamination parameters $(y_1, y_2]) = (1,1)$ (if $(\varepsilon_I^2 - \varepsilon_{II}^2) \geq 0$) and $(y_1, y_2) = (-1,1)$ (if $(\varepsilon_I^2 - \varepsilon_{II}^2) \leq 0$). If $(\varepsilon_I^2 - \varepsilon_{II}^2) \neq 0$, the design is unique and corresponds to a single ply rotated so the numerically largest principal strain is aligned with the material axis corresponding to E_{1111} (we have assumed $E_{1111} \geq E_{2222}$). The optimal energy (i.e. the optimal value of (3.51)) becomes

$$\Phi(\{\varepsilon\}) = \max \left\{ \begin{array}{l} E_2 \left(\varepsilon_I^2 - \varepsilon_{II}^2\right) + E_3 \left(\varepsilon_I - \varepsilon_{II}\right)^2, \\ -E_2 \left(\varepsilon_I^2 - \varepsilon_{II}^2\right) + E_3 \left(\varepsilon_I - \varepsilon_{II}\right)^2 \end{array} \right\} \tag{3.52}$$

which is non-smooth at strains which satisfy $\varepsilon_1^2 = \varepsilon_{II}^2$, i.e. uniform dilation or pure shear (in terms of strains). The resulting reduced minimum potential energy problem (the reduced equilibrium problem, cf., (3.15)) is then a non-smooth, convex problem, for which the necessary conditions of optimality at points with $\varepsilon_1^2 = \varepsilon_{II}^2$ will involve a convex combination of the gradients of the two smooth branches of Φ. This implies that at points where the strains of the optimal plate satisfy $\varepsilon_1^2 = \varepsilon_{II}^2$, the optimal design can consist of some cross-ply consisting of two plies rotated at 0 and 90 degrees relative to the principal strain axes, with thicknesses decided through the conditions of equilibrium.[7] The relative thicknesses of the two plies can actually be determined by considering the complementary energy formulation of the compliance problem. In terms of principal *membrane forces* N_I, N_{II} (with $|N_I| \geq |N_{II}|$) one gets (see Hammer (1999a)) that the optimal $[0_t^\circ/90_{1-t}^\circ]$ laminate has a relative thickness t ($t \in [\frac{1}{2}, 1]$) of the zero degree ply given as:

$$2t - 1 = \begin{cases} \frac{N_I + N_{II}}{N_I - N_{II}} \frac{E_{1111} + E_{2222} - 2E_{1122}}{E_{1111} - E_{2222}} & \text{for } \frac{N_{II}}{N_I} \leq -\frac{E_{2222} - E_{1122}}{E_{1111} - E_{1122}} \\ \frac{N_I - N_{II}}{N_I + N_{II}} \frac{E_{1111} + E_{2222} + 2E_{1122}}{E_{1111} - E_{2222}} & \text{for } \frac{N_{II}}{N_I} \geq \frac{E_{2222} + E_{1122}}{E_{1111} + E_{1122}} \\ 1 & \text{otherwise} \end{cases} \tag{3.53}$$

Then consider the case $E_3 \leq 0$ (a material with high shear stiffness). Here the algebra becomes somewhat messier. In this case we get unique solutions to (3.51) if $\varepsilon_1 \neq \varepsilon_{II}$, with the solution corresponding to a single ply rotated at an angle ψ given by $\cos 2\psi = -\frac{E_2}{4E_3} \frac{\varepsilon_1 + \varepsilon_{II}}{\varepsilon_1 - \varepsilon_{II}}$ if $\left| \frac{E_2}{4E_3} \frac{\varepsilon_1 + \varepsilon_{II}}{\varepsilon_1 - \varepsilon_{II}} \right| \leq 1$ and given as $\psi = 0$ if $\left| \frac{E_2}{4E_3} \frac{\varepsilon_1 + \varepsilon_{II}}{\varepsilon_1 - \varepsilon_{II}} \right| \geq 1$. In the case $\varepsilon_I = \varepsilon_{II}$ we have a non-unique solution and the optimal energy becomes non-smooth, resulting in an optimal design which also in this case must consist of some cross-ply at 0 and 90 degrees relative to the principal axes (formulas similar to (3.53) can be found in Hammer (1999a)).

[7] We remark here that the displacement field of the optimal plate is unique; this follows from the strict convexity of each energy appearing in the inner maximization of (3.52).

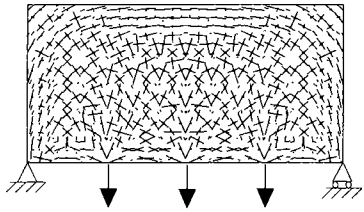

Fig. 3.23. Optimal three ply laminate for a plate with three *independent* single loads applied.

The analysis above is consistent with the result on the optimal rotation of an orthotropic material derived by different means in Sect. 3.1.4. It was remarked there that this problem does not have existence of solutions in general and that some type of additional microstructure is necessary. Here we use lamination parameters, and find that just *two* plies are required as part of the optimal solution that we know exists. This simpler situation is possible as we work with effective material parameters given directly as a summation of stiffness via the out-of-plane stacking of the different plies ("materials").

Computational example The computational procedure used here for a multiple load problem follows the algorithm outlined in Sect. 3.2.2. That is, one iterates between the inner local anisotropy problem and the outer equilibrium problem. The deformations and strains of the plate are determined using the finite element method in which a set of lamination parameters is related to each finite element. Based on fixed strains the local anisotropy problem (3.48) is then solved in each finite element using a standard SQP algorithm (Schittkowski 1985).

The example here is a "bridge"-structure with three independent loads all given the same weight factors. It is a laminate built of graphite/epoxy plies and the total plate thickness is kept constant. The method described in Lipton (1994a) is applied after the iteration process to find a three ply laminate with the optimal properties. The final three ply design is shown in Fig. 3.23. The hatch direction in each element marks the orientation of each of the three plies, the density of the hatching varying as the ply thickness. The more dense, the thicker the ply. As the loading is in-plane, the order of the plies is non-important.

3.6 Optimal topology design with a damage related criterion

In this section we discuss an attempt at introducing damage related criteria in topology design of continuum structures. We use an interpretation of con-

tinuum damage models from Francfort & Marigo (1993), where a variational statement is adopted to replace the standard internal variable representation pioneered by Kachanov (see, e.g., Krajcinovic (1996), Lemaitre (1996)). The model is represented in the form of an *optimal remodelling* problem, where a damaged material of reduced stiffness is distributed in a healthy structure so as to maximize the compliance, i.e., to minimize overall stiffness, for a given set of damage loads. Thus the treatment of the damage model is in itself a study of optimal structural design. Evolution would be described as a time-series of such static remodelling models, but we accept here the limitation of only considering the onset of damage.

3.6.1 A damage model of maximizing compliance

The damage model takes the form of a design problem involving the layout of a structure made from two materials, a stiff material and a flexible, damaged material. The structure we consider is made of a linearly elastic material with elasticity tensor E^+ Under the action of the damage loads the material is damaged in some parts of the structure, leaving there a more compliant material with elasticity tensor E^- By more flexible, it is meant here simply that we in terms of tensors have that $E^+ - E^- \succ 0$, i.e., for any strains, the specific strain energy of the flexible material is strictly less than that of the stiffer material. When damage occurs, energy is released, and we denote by K the energy release per unit volume. Interpreting the distribution of damage as a material distribution design problem, we impose that for a certain load, the damage is distributed so that the compliance of the structure is *maximized*, making the structure as *flexible* as possible among all distributions of damage.

The damage problem is thus formulated as

$$\min_{E\in\mathsf{E}_{ad}} \min_{u\in U} \left\{ \frac{1}{2}\int_\Omega E_{ijkl}(x)\varepsilon_{ij}(u)\varepsilon_{kl}(u)\mathrm{d}\Omega - l(u) + K\int_\Omega 1_{\Omega^-}\mathrm{d}\Omega \right\} \tag{3.54}$$

where Ω^- is the damaged zone, and where the set of admissible tensors E_{ad} is given by the relations:

$$E_{ijkl} = 1_{\Omega^-}E^-_{ijkl} + (1-1_{\Omega^-})E^+_{ijkl} = \begin{cases} E^+_{ijkl} & \text{if } x\in\Omega\setminus\Omega^- \\ E^-_{ijkl} & \text{if } x\in\Omega^- \end{cases} \tag{3.55}$$

We note that (3.54) could alternatively be written as a fixed volume *maximum* compliance problem, where K is the Lagrange multiplier for the volume constraint. Thus our problem is just a variant of the 0-1 topology design problem, now with an objective of minimizing stiffness.

Here, we will not go into details on the relation between model (3.54) and other types of models used in continuum damage mechanics. However, the close relationship is evident if one solves in (3.54) for the minimization over

stiffness tensors. One then obtains a minimum potential energy principle for the damaged structure in the form

$$\min_{u \in U} \left\{ \frac{1}{2} \int_\Omega \Phi(u) \mathrm{d}\Omega - l(u) \right\} \tag{3.56}$$

where the specific strain energy $\frac{1}{2}\Phi(u)$ in the damaged structure is given by

$$\Phi = \begin{cases} E^+_{ijkl}\varepsilon_{ij}(u)\varepsilon_{kl}(u) & \text{if } \Delta_{ijkl}\varepsilon_{ij}(u)\varepsilon_{kl}(u) \leq 2K \\ E^-_{ijkl}\varepsilon_{ij}(u)\varepsilon_{kl}(u) + 2K & \text{if } \Delta_{ijkl}\varepsilon_{ij}(u)\varepsilon_{kl}(u) > 2K \end{cases}$$

where $\Delta = E^+ - E^-$ In an internal variable representation of damage, in the spirit of the equivalent stress principle of Kachanov (Krajcinovic 1996, Lemaitre 1996), one represents the reduced stiffness of a partially damaged material as

$$E_{ijkl}(t) = (1-t)E^+_{ijkl} + tE^-_{ijkl} = E^+_{ijkl} - t\Delta_{ijkl}, \quad 0 \leq t \leq 1$$

Here t is interpreted as a volume fraction of the damaged state. The reduced problem (3.56) then also appears from a damage model in the form

$$\min_{\substack{t(x) \\ 0 \leq t(x) \leq 1}} \min_{u \in U} \left\{ \tfrac{1}{2} \int_\Omega E_{ijkl}(t)\varepsilon_{ij}(u)\varepsilon_{kl}(u)\mathrm{d}\Omega - l(u) + K \int_\Omega t(x)\mathrm{d}\Omega \right\}$$

when one solves for the internal parameter t.

Note that the model (3.54) as stated does not distinguish between tension and compression, but it is fairly straightforward to also include such effects in the model (Allaire, Aubry & Jouve 1997, Achtziger, Bendsøe & Taylor 1998).

We finish by noting that model (3.54) lacks any notion of history of the development of damage. As such, the model is in philosophy related to holonomic elasto-plastic models for proportional loading. A notion of history dependence and time dependency can be introduced through a time-stepping procedure where a sequence of problems is considered (as in semi-static, elasto-plastic modelling). A sequence of loads $f_1, f_2, \quad , f_n,$ can model a time dependent load, while the irreversibility of damage requires the introduction of an additional constraint for the $(i+1)$'th problem of the form $\left[\Omega_i^-\right]^* \subseteq \Omega_{i+1}^-$, where $\left[\Omega_i^-\right]^*$ is the domain of damage for the i'th problem. Thus history dependence is achieved through the formulation of a series of optimal remodelling problems in the spirit of Olhoff & Taylor (1979).

Relaxed problem statement Just as for the minimum compliance topology design problem, the damage models (3.54) and (3.56) are not well-posed and we have to relax the problem by introducing composite mixtures of the two phases in a development that is completely parallel to that for the minimum compliance problem (Allaire & Kohn 1994, Bendsøe & Díaz 1998). Thus

rank-2 materials also provide for a realization of the most flexible composites, and the corresponding "optimal" energy can be derived as in section 3.3.

We will write these expressions for a case where the healthy material and the damaged material have the same Poisson's ratio ν, and only the Young moduli E^+, E^- are distinct. For given principal strains $\varepsilon_I, \varepsilon_{II}$ (ordered so that $|\varepsilon_I| \geq |\varepsilon_{II}|$) and a local volume fraction of damage ϑ, the relaxed specific strain energy $\frac{1}{2}\hat{\Phi}(u,\vartheta)$, including here the released energy due to damage, is given through the formulas [31]:

$$\hat{\Phi}(u,\vartheta) = \begin{cases} \hat{\Phi}_1(u,\vartheta) + 2K\vartheta & \text{if } \varepsilon_I\varepsilon_{II} \leq 0 \\ \hat{\Phi}_2(u,\vartheta) + 2K\vartheta & \text{if } \varepsilon_I\varepsilon_{II} \geq 0 \text{ and } \vartheta \leq \bar{\vartheta} \\ \hat{\Phi}_3(u,\vartheta) + 2K\vartheta & \text{if } \varepsilon_I\varepsilon_{II} \geq 0 \text{ and } \vartheta \geq \bar{\vartheta} \end{cases} \tag{3.57}$$

$$\hat{\Phi}_1 = \frac{1}{1-\nu^2}\frac{E^+E^-}{(1-\vartheta)E^- + \vartheta E^+}(\varepsilon_I^2 + \varepsilon_{II}^2 + 2\nu\varepsilon_I\varepsilon_{II})$$

$$\hat{\Phi}_2 = \frac{(1-\vartheta)E^+ + \vartheta E^-}{1-\nu^2}(\varepsilon_I^2 + \varepsilon_{II}^2 + 2\nu\varepsilon_I\varepsilon_{II}) - \frac{\vartheta(1-\vartheta)}{(1-\vartheta)E^- + \vartheta E^+}\frac{(E^+ - \vartheta E^-)^2}{2(1-\nu^2)} \times$$
$$\times \left((1+\nu^2)(\varepsilon_I^2 + \varepsilon_{II}^2) + 4\nu\varepsilon_I\varepsilon_{II} + (1-\nu^2)|\varepsilon_I - \varepsilon_{II}|\right)$$

$$\hat{\Phi}_3(u,\vartheta) = \frac{E^-}{2(1+\nu)}(\varepsilon_I - \varepsilon_{II})^2 + \frac{E^-}{2(1-\nu)}\frac{2E^+ - \vartheta(1-\nu)(E^+ - E^-)}{2E^- + \vartheta(1+\nu)(E^+ - E^-)}(\varepsilon_I + \varepsilon_{II})^2$$

where

$$\bar{\vartheta} = \frac{2E^-}{(1-\nu)(E^+ - E^-)}\left(\frac{|\varepsilon_I + \varepsilon_{II}|}{|\varepsilon_I - \varepsilon_{II}|} - 1\right)$$

The first and second regimes of the strain energy correspond to the use of an optimal rank 1 material consisting of one system of layers of the two materials, at one microscale. The third regime corresponds to an orthogonal rank-2 layering, consisting of two systems of layerings, at two scales. The inner layering consists of the stiff and damaged material, the outer layering of this material layered with the damaged material. Thus in the rank-2 structure the stiff material is surrounded by flexible material, shielding this material in order to weaken the material as much as possible (for the fixed volume fraction) (thus, in Fig. 3.2 the weak material constitutes in this case the black areas). Moreover, the energy is minimized when the angle ψ between the principal strain directions and the material coordinate system (layering directions) is $\pm\pi/2$ in regimes 2 and 3 and $\pm\frac{1}{2}\arccos(1-\gamma)$, $\gamma = \frac{|\varepsilon_1 + \varepsilon_{11}|}{|\varepsilon_1 - \varepsilon_{11}|}$ in regime 1. This is in accordance with the well-known results on rotation of an orthotropic material for maximum flexibility (this can be seen as in Sect. 3.1.4, cf., Pedersen (1989)). Finally note that $\hat{\Phi}$ is convex as a function of ϑ.

The functional above constitutes the relaxed form for the problem (3.54). Here we can go one step further (compare with the developments in Sect. 3.2.1)

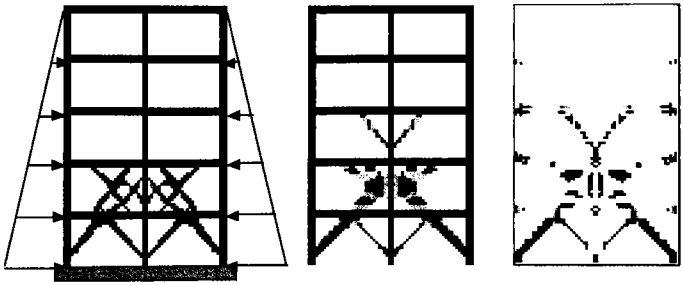

Fig. 3.24. Optimal reinforcement of a frame. Left: The frame and loads, etc. with the standard minimum compliance solution. Mid: the solution of the design problem with damage taken into consideration, Right: the corresponding distribution of damage $\vartheta(x)$ (from Bendsøe & Díaz 1998).

and compute the final relaxed specific strain energy for the damaged structure, i.e., the relaxed form of the energy appearing in (3.56). It is obtained by minimizing $\hat{\Phi}$ with respect to the volume fraction ϑ. This can be solved analytically (use of symbolic manipulation software is strongly recommended). Its solution provides the optimum value of ϑ for the given strain field, along with details of the optimum material orientation, and provides an analytical form of the effective, relaxed strain energy density $\tilde{\Phi}(\varepsilon)$ of the damaged structure, with no reference to ϑ. Thus (3.54) becomes the non-linear and non-smooth problem

$$\min_{u \in U} \left\{ \frac{1}{2} \int_{\Omega} \tilde{\Phi}\big(\epsilon(u)\big) \mathrm{d}\Omega - l(u) \right\} \tag{3.58}$$

Its solution provides the displacements and indirectly the *spatial* distribution of ϑ over the domain Ω.

3.6.2 Design problems

In the topology design problem that we consider, the design is parametrized by the SIMP model. This is assumed for both the healthy as well as the damaged phase. The minimum potential energy principles governing a fully healthy structure and a damaged structure are thus written as

$$\min_{u_S \in U} \left\{ \tfrac{1}{2} \int_{\Omega} \rho^p E^+_{ijkl}(x) \varepsilon_{ij}(u_S) \varepsilon_{kl}(u_S) \mathrm{d}\Omega - l_S(u_S) \right\} \tag{3.59}$$

$$\min_{u_D \in U} \left\{ \tfrac{1}{2} \int_{\Omega} \rho^p \tilde{\Phi}(\varepsilon(u_D)) \mathrm{d}\Omega - l_D(u_D) \right\} \tag{3.60}$$

Topology design of reinforcement to reduce damage effects In the first problem we consider the design of the reinforcement of a structure so as to minimize the effect of damage on the reinforced structure. The existing structure is part of the ground structure and occupies the domain Ω_G, where we have $\rho(x) = 1,\ x \in \Omega_G$, and the reinforcement can be placed in any part of the remainder $\Omega \setminus \Omega_G$ of the reference domain. The effect of the damage is measured by the compliance of the damaged structure under some damage loads f_D. The design problem thus takes the form

$$\max_{\substack{\rho \\ \rho(x)=1, x\in\Omega_G \\ \int_{\Omega\setminus\Omega_G} \rho \mathrm{d}\Omega \le Vol \\ 0<\rho_{\min}\le\rho\le 1}} \quad \min_{u_D\in U} \left\{ \frac{1}{2}\int_\Omega \rho^p \tilde{\Phi}(\varepsilon(u_D))\mathrm{d}\Omega - \int_\Omega f_D u_D \right\} \tag{3.61}$$

where we maximize the potential energy of the damaged structure, for improved overall stiffness.

Design of structural topology with a constraint on damage effect In the second problem we seek designs that make use of a prescribed amount of material and are of minimum compliance under a set of service loads p_S. In addition, we require that the structure retain a certain amount of stiffness under the action of a separate set of damage loads f_D. The effect of damage is measured by the compliance of the damaged structure under the damage loads p_D. The optimization problem thus reads

$$\begin{aligned} \min_{\substack{\rho \\ \int_\Omega \rho \mathrm{d}\Omega \le V \\ 0<\rho_{\min}\le\rho\le 1}} \quad & \int_\Omega f_S u_S \mathrm{d}\Omega \\ \text{s.t.} \quad & -2 \min_{u_D\in U} \left\{ \frac{1}{2}\int_\Omega \rho^p \tilde{\Phi}(\varepsilon(u_D))\mathrm{d}\Omega - \int_\Omega f_D u_D \right\} \le c_{\max} \end{aligned} \tag{3.62}$$

where u_S is a solution to (3.59) with load f_S. Here the objective function states that the structure (for a given amount V of material) should be as stiff as possible under the service loads, while the constraint is a restriction on the amount of damage allowed under the damage loads, measured in terms of compliance (under the damage load).

Implementation The topology design problems can be solved along the lines described in Chapter 1 (all objectives and constraints are compliance values, simplifying derivative calculations). The extent of damage $\vartheta(x)$ associated with the damage loads is determined by solving a non-linear finite element problem so the process is iterative in the displacements. At each iteration step, the given displacements and associated strains are used to find, within each finite element, ϑ and the details of the local orthotropy and orientation of the rank-2 material that is consistent with the extremal energy expression (3.58). The update of the displacements then consists of a

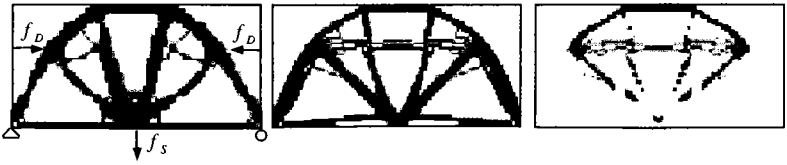

Fig. 3.25. Minimum compliance design. Left: In the absence of damage loads, Mid: With a constraint on the effect of damage loads , and Right: the distribution of damage in this optimal design (from Bendsøe & Díaz 1998).

linear finite element analysis with this material data. A similar scheme was described in Sect. 3.2.2 for the stress-based minimum compliance problem.

4 Topology design of truss structures

Topology optimization of trusses in the form of grid-like continua is a classical subject in structural design. The study of fundamental properties of optimal grid like continua was pioneered by Michell (1904), but this interesting field has only much later developed into what is now the well-established lay-out theory for frames and flexural systems [3], [27]. The application of numerical methods to discrete truss topology problems and similar structural systems has a shorter history with early contributions in, for example, Dorn, Gomory & Greenberg (1964) and Fleron (1964) (see also [32]). The development of computationally efficient methods is not only of great importance for the truss topology problem in itself. It is likewise of interest for solving the reduced problems which arise in the study of simultaneous design of material and structure, as described in Chap. 3.4.

The optimization of the geometry and topology of trusses can conveniently be formulated with the so-called ground structure method. In this approach the layout of a truss structure is found by allowing a certain set of connections between a fixed set of nodal points as potential structural or vanishing members. For the truss topology problem the geometry allows for using the continuously varying cross-sectional bar areas as design variables, including the possibility of zero bar areas. This implies that the truss topology problem can be viewed as a standard sizing problem. This sizing reformulation is possible for the simple reason that the truss as a continuum geometrically is described as one dimensional. Thus for both planar and space trusses there are extra dimensions in physical space that can describe the extension of the truss as a true physical element of space, simplifying the basic modelling for truss topology design as compared to topology design of three dimensional continuum structures.

Truss topology design problems were in early work formulated in terms of member forces, ignoring kinematic compatibility to obtain a linear programming problem in member areas and forces. The resulting topology and force field are then often employed as a starting point for a more complicated design problem formulation, with heuristics, branch and bound techniques, etc. being used to link the two model problems [32]. Alternatively, when displacement formulations are used, then (small) non zero lower bounds on the cross-sectional areas have been imposed in order to have a positive definite

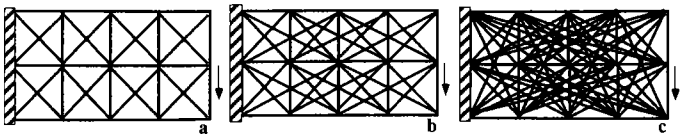

Fig. 4.1. Ground structures for transmitting a vertical force to a vertical line of supports. Truss ground structures of variable complexity in a rectangular domain with a regular 5 by 3 nodal layout. In c) all the connections between the nodal points are included.

stiffness matrix. This means that standard techniques for optimal structural design can be used. Also, it allows for the use of optimality criteria methods for large scale design problems involving compliance, stress, displacement and eigenvalue objectives. In the simultaneous analysis and design approach the design variables and state variables are not distinguished, so the full problem is solved by one unified numerical optimization procedure. However, unless specially developed numerical solution procedures are used, only very small problems can be treated [33]. The use of simulated annealing and genetic algorithm techniques for the topology problems in their original formulation as discrete selection problems, has also been pursued but also these fairly general approaches are with the present technology restricted to fairly small scale problems [33].

In this chapter we will investigate various formulations of truss topology design and outline some options for their numerical processing [32], [33]. We seek specifically to be able to handle problems with a very large number of potential structural elements, using the ground structure approach. For this reason we consider primarily the simplest possible optimal design problem, namely the minimization of compliance (maximization of stiffness) for a given total mass of the structure where a very detailed examination of the properties of the problems is possible. The analysis is general enough to encompass multiple load problems in the worst-case and weighted-average formulation, the case of self-weight loads and the problem of determining the optimal topology of the reinforcement of a structure as for example seen in fail-safe design. Also, variable thickness sheet, sandwich plate and free material problems are covered by the developments. In direct analogy with the continuum setting, these problems can be given in a number of equivalent problem statements, among them problems in the nodal displacements only or in the member forces only. With these reformulations at hand it is possible to devise very efficient algorithms that can handle large scale problems. Also, as we have seen in earlier chapters, the formulations can be obtained through duality principles and the resulting formulations in displacements or stresses correspond to equilibrium problems for an optimally global strain energy and an optimally global complementary energy, respectively.

4.1 Problem formulation for minimum compliance truss design

The ground structure approach allows the truss topology design problem to be viewed as a sizing problem. However, the topology problem is unusual as a structural optimization problem as the number of design variables is typically several magnitudes bigger than the number of state variables describing the equilibrium of the structure. For most structural optimization problems described in the literature the opposite is the case. Also, for truss topology design the stiffness matrix of the full ground structure with certain members at zero gauge can be singular. This implies that most optimal designs have a singular stiffness matrix when described as part of the full ground structuref.

4.1.1 The basic problem statements in displacements

In the ground structure approach for truss topology design a set of n chosen nodal points (N degrees of freedom) and m possible connections are given, and one seeks to find the optimal substructure of this structural universe. In some papers on the ground structure approach, the ground structure is always assumed to be the set of all possible connections between the chosen nodal points, but here we allow the ground structure to be any given set of connections (see Fig. 4.1). This approach may lead to designs that are not the best ones for the chosen set of nodal points, but the approach implicitly allows for restrictions on the possible spectrum of possible member lengths (see Fig. 4.1) as well as for the study of the optimal subset of members of a given truss-layout.

Let a_i, l_i denote the cross-sectional area and length of bar number i, respectively, and we assume that all bars are made of linear elastic materials, with Young's moduli E_i. The volume of the truss is $V = \sum_{i=1}^{m} a_i l_i$. In order to simplify the notation at a later stage, we introduce the bar volumes $t_i = a_i l_i$, $i = 1, . \quad , m$, as the fundamental design variables. Static equilibrium is expressed as

$$\mathbf{Bq} = \mathbf{f}$$

where $\mathbf{q}$ is the member force vector and $\mathbf{f}$ is the nodal force vector of the free degrees of freedom. The ground structure is chosen so that the compatibility matrix $\mathbf{B}$ has full rank and so that $m \geq N$, excluding mechanisms and rigid body motions. The stiffness matrix of the truss is written as

$$\mathbf{K}(\mathbf{t}) = \sum_{i=1}^{m} t_i \mathbf{K}_i$$

where $t_i\mathbf{K}_i$ is the element stiffness matrix for bar number i, written in global coordinates. Note that $\mathbf{K}_i = \frac{E_i}{l_i^2}\mathbf{b}_i\mathbf{b}_i^T$ where $\mathbf{b}_i$ is the i'th column of $\mathbf{B}$.

The problem of finding the minimum compliance truss for a given volume of material (the stiffest truss) has the well-known formulation (cf., the continuum setting Sect. 1.1)

$$\begin{aligned} &\min_{\mathbf{u},\mathbf{t}} \mathbf{f}^T\mathbf{u} \\ &\text{s.t.} \quad \sum_{i=1}^{m} t_i\mathbf{K}_i\mathbf{u} = \mathbf{f}, \quad \sum_{i=1}^{m} t_i = V, \quad t_i \geq 0,\ i = 1,. \quad ,m \end{aligned} \tag{4.1}$$

Problem 4.1 is well studied in the case of an imposed non-negative lower bound on the volumes t_i [32]. In this case the stiffness matrix $\mathbf{K}(\mathbf{t})$ is positive definite for all feasible $\mathbf{t}$ and the displacements can be removed from the problem. The resulting problem in bar volumes turns out to be convex and existence of solutions is assured (cf. Svanberg (1984); see also discussion of the variable thickness sheet problem in Sect. 1.5.2). Allowing for zero lower bounds complicates the analysis, but it also provides valuable insight. The zero lower bound on the variables t_i thus means that bars of the ground structure can be removed and the problem statement thus covers topology design. Problem (4.1) can result in an optimal topology that is a mechanism; this mechanism is in equilibrium under the given load, and infinitesimal bars can be added to obtain a stable structure. Also, if the optimal topology has straight bars with inner nodal points, these nodal points should be ignored. The resulting truss maintains the stiffness and the equilibrium of the original optimal topology.

The zero lower bound in problem 4.1 implies that the stiffness matrix is not necessarily positive definite and the state vector $\mathbf{u}$ cannot be removed by solving $\mathbf{K}(\mathbf{t})\mathbf{u} = \mathbf{f}$. Removing $\mathbf{u}$ from the formulation is not very important for the size of the problem, as, typically, the number m of bars is much greater than the number of degrees of freedom. In the complete ground structure we connect all nodes, having $m = n(n-1)/2$, while the degrees of freedom are only of the order $2n$ or $3n$ (for planar and 3-D trusses). For the complete ground structure we also have a fully populated stiffness matrix lacking any sparsity and bandedness.

Our aim here is to develop methods which can be applied to large scale truss topology problems and for this reason we employ the simplest possible design formulation as stated in problem (4.1). More general problem statements are briefly covered in Sect. 4.4. Nonetheless, a number of extended design settings can be covered within the framework of (4.1). In the case of *multiple loads*, we formulate also for trusses the problem of minimizing a weighted average of the compliances. For a set of M different load cases $\mathbf{f}^k$, $k = 1, \ldots, M$, and weights w^k, $k = 1, \ldots, M$, the multiple load problem reads

$$
\begin{aligned}
&\min_{\mathbf{u},\mathbf{t}} \sum_{k=1}^{M} w^k \mathbf{f}^{k^T} \mathbf{u}^k \\
&\text{s.t.} \quad \sum_{i=1}^{m} t_i \mathbf{K}_i \mathbf{u}^k = \mathbf{f}^k, \quad k = 1, \ldots, M \\
&\qquad \sum_{i=1}^{m} t_i = V, \quad t_i \geq 0, \; i = 1, \ldots, m
\end{aligned}
\tag{4.2}
$$

Note that in problem (4.2) it is possible to refer each load case to a distinct ground sub-structure, and that it thus is possible to cover *fail-safe design* along the lines described in Taylor (1987). Let us introduce an extended displacement vector

$$\hat{\mathbf{u}} = (\mathbf{u}^1, \ldots, \mathbf{u}^M)$$

of all the displacement vectors $\mathbf{u}^k$, $k = 1, \ldots, M$, an extended force vector

$$\hat{\mathbf{f}} = (w^1 \mathbf{f}^1, \ldots, w^M \mathbf{f}^M)$$

of the weighted force vectors $w^k \mathbf{f}^k$, $k = 1, \ldots, M$, and the extended element stiffness matrices as the block diagonal matrices

$$\hat{\mathbf{K}}_i = \begin{pmatrix} w^1 \mathbf{K}_i & & \\ & \ddots & \\ & & w^M \mathbf{K}_i \end{pmatrix}$$

Then problem (4.2) can be written as

$$
\begin{aligned}
&\min_{\hat{\mathbf{u}},\mathbf{t}} \hat{\mathbf{f}}^T \hat{\mathbf{u}} \\
&\text{s.t.} \quad \sum_{i=1}^{m} t_i \hat{\mathbf{K}}_i \hat{\mathbf{u}} = \hat{\mathbf{f}}, \quad \sum_{i=1}^{m} t_i = V, \quad t_i \geq 0, \; i = 1, \ldots, m
\end{aligned}
\tag{4.3}
$$

which is precisely of the same form as problem (4.1).

The problem of *worst case* minimum compliance design for multiple loads $\mathbf{f}^k$, $k = 1, \ldots, M$, reads

$$
\begin{aligned}
&\min_{\mathbf{u}^k,\mathbf{t}} \left\{ \max_{k=1,\ldots,M} \mathbf{f}^{k^T} \mathbf{u}^k = \max_{\substack{\lambda^k \geq 0,\, k=1,\ldots,M \\ \sum_{i=1}^{m} \lambda^k = 1}} \sum_{k=1}^{M} \lambda^k \mathbf{f}^{k^T} \mathbf{u}^k \right\} \\
&\text{s.t.} \quad \sum_{i=1}^{m} t_i \mathbf{K}_i \mathbf{u}^k = \mathbf{f}^k, \quad k = 1, \ldots, M \\
&\qquad \sum_{i=1}^{m} t_i = V, \quad t_i \geq 0, \; i = 1, \ldots, m,
\end{aligned}
\tag{4.4}
$$

where $\mathbf{u}^k$, $k = 1, \quad ., M$ are again the displacements corresponding to the different load cases. Note how the discrete optimization over the compliance values can be converted into a smooth maximization by introducing a convex combination of weighting parameters λ^k, $k = 1, \quad ., M$

We note that the problem formulation (4.1) covers the finite element formulation of the minimum compliance design of continuum problems that exhibit a linear relation between stiffness and the relevant design variable, as exemplified by design of variable thickness sheets, the design of sandwich plates or the free material design (cf. Chap. 3). In these cases the matrices $\mathbf{K}_i$ should be interpreted as the specific element stiffness matrices, and the design variables are the element thicknesses (volumes). For these cases and for the multiple load formulation (4.3), the element stiffness matrices no longer have the form of dyadic products. In order to cover all three cases by one formulation we will write in the following (4.1) in a generalized form

$$\begin{aligned} &\min_{\mathbf{u},\mathbf{t}} \mathbf{f}^T\mathbf{u} \\ &\text{s.t.} \quad \sum_{i=1}^{m} t_i\hat{\mathbf{K}}_i\mathbf{u} = \mathbf{f}, \quad \sum_{i=1}^{m} t_i = V, \quad t_i \geq 0, \; i = 1, . \quad , m \end{aligned} \tag{4.5}$$

where $\hat{\mathbf{K}}_i$ are positive semi-definite, symmetric matrices that satisfy that the matrix $\hat{\mathbf{K}}(\mathbf{t}) = \sum_{i=1}^{m} t_i\hat{\mathbf{K}}_i$ is positive definite if all the design variables t_i's are positive. For trusses this means that the number of bars in the ground structure exceeds the number of degrees of freedom and that the compatibility matrix of this ground structure has full rank.

In analogy to the continuum problems treated earlier in Chaps. 1 and 3, it is also in this discretized case convenient to rewrite the problem statements in terms of a minimum potential energy formulation of the equilibrium constraint. Thus problem (4.5) can be rewritten as a max-min problem in the form[1]

$$\max_{\substack{\mathbf{t}\geq\mathbf{0} \\ \sum_{i=1}^{m} t_i = V}} \; \min_{\mathbf{u}} \left\{ \frac{1}{2}\mathbf{u}^T \left(\sum_{i=1}^{m} t_i\hat{\mathbf{K}}_i \right) \mathbf{u} - \mathbf{f}^T\mathbf{u} \right\} \tag{4.6}$$

This is a saddle point problem for a concave-convex problem, and we shall also for the truss problem in the following use that the max and min operator in (4.6) can be interchanged.

4.1.2 The basic problem statements in member forces

For the continuum formulations of topology design we formulated a stress based minimum compliance problem using the minimum complementary energy principle (cf. problem (1.7) in Sect. 1.1.3). Writing here for the single load truss problem we have the problem

[1] We write $\mathbf{t} \geq \mathbf{0}$ for the condition $t_i \geq 0, \quad \ldots, m$.

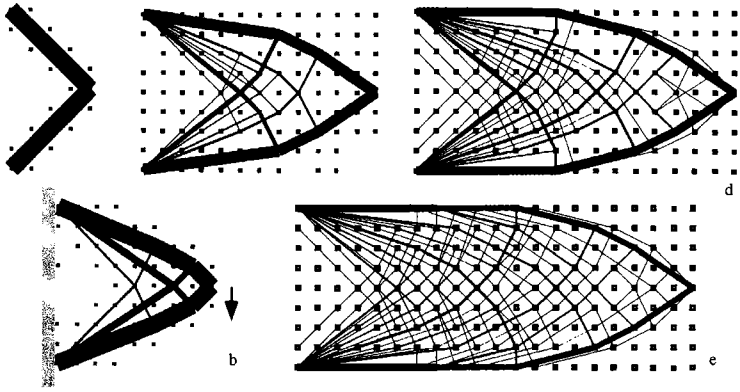

Fig. 4.2. The influence of the ground structure geometry on the optimal topology. Optimal truss topologies for transmitting a single vertical force to a vertical line of supports. The ground structures consist of all possible non-overlapping connections between the nodal points of a regular mesh in rectangles of varying aspect ratios $R = a/b$. a): 632 potential bars for 5 by 9 nodes in a rectangle with $R = 0.5$. Optimal non-dimensional compliance $\Phi = 4.000$. b): 2040 potential bars, 9 by 9 nodes, $R = 1.0$, Φ 5.975. c): 4216 potential bars, 13 by 9 nodes, $R = 1.5$, $\Phi = 9.1676$ d): 7180 potential bars, 17 by 9 nodes, $R = 2.0$, $\Phi = 12.5756$. e): 10940 potential bars, 21 by 9 nodes, $R = 2.5$, $\Phi = 16.4929$ (from Bendsøe, Ben-Tal & Zowe 1994).

$$\begin{aligned} &\inf_{\mathbf{t}} \min_{\mathbf{q}} \frac{1}{2} \sum_{i=1}^{m} \frac{l_i^2}{E_i} \frac{(q_i)^2}{t_i} \\ &\text{s.t.} \quad \mathbf{Bq} = \mathbf{f}, \quad \sum_{i=1}^{m} t_i = V, \quad t_i > 0, \; i = 1, . \quad , m \end{aligned} \tag{4.7}$$

where we have to take the infimum over all positive bar volumes in order to have a well-posed problem. In (4.7), $\mathbf{q}$ is the vector of member forces. For a given $\mathbf{t}$ the solution $\mathbf{q}^*$ to the inner problem of (4.7) satisfies $q_i^* = \frac{E_i}{l_i^2} t_i \mathbf{b}_i^T \mathbf{u}^*$ where $\mathbf{u}^*$ is the displacement of the truss, i.e., $\mathbf{u}^*$ is the solution to the inner problem of (4.6). Note that problem (4.7) is a problem which is *simultaneous convex* in member forces and member volumes.

The traditional formulation of truss topology design in terms of member forces is for single load, *plastic* design [32]. This problem is normally stated as a minimum weight design problem, for all trusses that satisfy static equilibrium within certain constraints on the stresses in the individual bars. With the same stress constraint value $\bar{\sigma}_i$ for both tension and compression, the formulation is in the form of a linear programming problem

$$
\begin{aligned}
&\min_{\mathbf{q},\mathbf{t}} \sum_{i=1}^{m} t_i \\
&\text{s.t.} \quad \mathbf{B}\mathbf{q} = \mathbf{f}\,; \quad -\bar{\sigma}_i t_i \le l_i q_i \le \bar{\sigma}_i t_i, \quad i = 1, \ldots, m \\
&\qquad t_i \ge 0, \quad i = 1, \ldots, m
\end{aligned}
\tag{4.8}
$$

Notice that in problem (4.8) the stress constraints are written in terms of *member forces*. This turns out to be important in order to give a consistent formulation. For some truss problems, the stress in a number of members will converge to a finite non-zero level as the member areas converge to zero, but the member forces will converge to zero, Cheng & Jiang (1992), Kirsch (1990a). This fact should be observed for any truss design problem involving stress constraints (see also Sect. 4.4.4 for further discussion on this issue).

Problem (4.8) is a formulation purely in terms of statics, with no kinematic compatibility included in the formulation. However, a basic solution to this LP problem will automatically satisfy kinematic compatibility, a rather puzzling fact. We note here that (4.8) can be extended to cover cost of supports and to problems involving local stability constraints (buckling etc.) while maintaining the basic properties of (4.8), albeit not the LP form, see Pedersen (1993b), and Pedersen (1993c). This extension will not be discussed here (see Sect. 4.4.4).

With the change of variables $t_i = \frac{l_i}{\bar{\sigma}_i}(q_i^+ + q_i^- \quad \mathbf{q} = (\mathbf{q}^+ - \mathbf{q}^-)$ we can write (4.8) in standard LP form, as

$$
\begin{aligned}
&\min_{\mathbf{q}^+,\mathbf{q}^-} \sum_{i=1}^{m} \frac{l_i}{\bar{\sigma}_i}(q_i^+ + q_i^-) \\
&\text{s.t.} \quad \mathbf{B}(\mathbf{q}^+ - \mathbf{q}^-) = \mathbf{f} \qquad q_i^+ \ge 0,\ q_i^- \ge 0, \quad i = 1, \quad , m
\end{aligned}
\tag{4.9}
$$

Here q_i^+, q_i^- can be interpreted as the member forces tension and compression, respectively. It is easy to see from the necessary conditions of optimality that the problem (4.8) gives rise to fully stressed designs, i.e. designs for which all bars with non-zero bar area have stresses at the maximum allowed level $\bar{\sigma}_i$. Thus one can often in the literature find (4.9) stated directly without reference to (4.8), as for a fully stressed design, the objective function of (4.9) is precisely the weight of the structure. We shall in a later section revert to these formulations and will show that (4.8), (4.7), and (4.1) are all equivalent in a certain sense.

The plastic design formulation can easily be extended to a multiple load situation as

$$
\begin{aligned}
&\min_{\mathbf{q}^k,\mathbf{t}} \sum_{i=1}^{m} t_i \\
&\text{s.t.} \quad \mathbf{B}\mathbf{q}^k = \mathbf{f}^k + \sum_{i=1}^{m} t_i \mathbf{g}_i, \quad k = 1, . \quad , M \\
&\qquad -\bar{\sigma}_i t_i \le l_i q_i^k \le \bar{\sigma}_i t_i, \quad i = 1, \quad , m, \quad k = 1, . \quad , M \\
&\qquad t_i \ge 0, \quad i = 1, \ldots, m \ ,
\end{aligned}
\tag{4.10}
$$

where self-weight loads in the form $\sum_{i=1}^{m} t_i \mathbf{g}_i$ are also considered (see below for details on notation). This problem is also a linear programming problem. However for this case the precise relation between this problem and the minimum compliance problem is not known.

4.1.3 Problem statements including self-weight and reinforcement

The formulations given above in Sect. 4.1.1 lend themselves to natural extensions, such as to the problem of finding the optimal topology of the reinforcement of a given structure and the optimal topology problem with self-weight taken into consideration.

For the reinforcement problem, see, e.g. Olhoff & Taylor (1983), using the ground structure approach, we divide a given ground structure into the set S of bars of fixed size and the set R of possible reinforcing bars. Typically S and R will be chosen as disjoint. We prefer here to allow R to contain (a part of) S as a subset; in this way non-zero lower bounds on the design variables can easily be included in the general problem analysis. The bars (elements) of the given structure have given bar volumes s_i, $i \in S$, and the optimal reinforcement t_i, $i \in R$, is the solution of the minimum compliance problem

$$
\begin{aligned}
&\min_{\mathbf{u},\mathbf{t}} \mathbf{f}^T \mathbf{u} \\
&\text{s.t.} \quad \left[\sum_{i \in R} t_i \hat{\mathbf{K}}_i + \sum_{i \in S} s_i \hat{\mathbf{K}}_i \right] \mathbf{u} = \mathbf{f}, \quad \sum_{i \in R} t_i = V, \quad t_i \ge 0, \ i \in R
\end{aligned}
\tag{4.11}
$$

This problem can be solved by analogous means as can be used for the other topology design problems formulated above. Note that a reinforcement formulation in connection with a multiple load formulation with distinct subground structures of a common ground structure will allow for a very general fail-safe design formulation.

For the important case of optimization where loads due to the weight of the structure are taken into account, we employ the standard assumption that the weight of a bar is carried equally by the joints at its ends, thus neglecting bending effects. With $\mathbf{g}_i$ denoting the specific nodal gravitational force vector due to the self-weight of bar number i the problem of finding the optimal topology with self-weight loads and external loads takes the form

$$\begin{aligned}
&\min_{\mathbf{u},\mathbf{t}} \left[\mathbf{f} + \sum_{i=1}^{m} t_i \mathbf{g}_i\right]^T \mathbf{u} \\
&\text{s.t.} \quad \sum_{i=1}^{m} t_i \hat{\mathbf{K}}_i \mathbf{u} = \mathbf{f} + \sum_{i=1}^{m} t_i \mathbf{g}_i; \ \sum_{i=1}^{m} t_i = V, \ t_i \geq 0, \ i = 1, \quad ., m
\end{aligned} \tag{4.12}$$

Note that for the problem with self-weight, any feasible truss design for which the self-weight load equilibrates the external load is an optimal design with compliance zero and zero displacement field (compliance is non-negative in all cases). Thus to avoid trivial situations, it is natural to assume that such designs are not possible:

$$\left\{ t_i \left| \sum_{i=1}^{m} t_i = V, \quad t_i \geq 0, \quad i = 1, . \quad , m, \quad \mathbf{f} + \sum_{i=1}^{m} t_i \mathbf{g}_i = 0 \right. \right\} = \emptyset$$

We complete this exposition of problem statements by stating the reinforcement problem, with self-weight loads, and general stiffness matrices and loads, so that all cases above are covered as special cases

$$\begin{aligned}
&\min_{\mathbf{u},\mathbf{t}} \left[\mathbf{f} + \sum_{i \in R} t_i \mathbf{g}_i + \sum_{i \in S} s_i \mathbf{g}_i\right]^T \mathbf{u} \\
&\text{s.t.} \quad \sum_{i \in R} t_i \hat{\mathbf{K}}_i \mathbf{u} + \sum_{i \in S} s_i \hat{\mathbf{K}}_i \mathbf{u} = \mathbf{f} + \sum_{i \in R} t_i \mathbf{g}_i + \sum_{i \in S} s_i \mathbf{g}_i \\
&\qquad \sum_{i \in R} t_i = V, \quad t \geq 0, \quad i \in R
\end{aligned} \tag{4.13}$$

Here a max-min formulation as in (4.6) can also be formulated, maintaining the concave-convex nature of the basic problem (4.6).

4.2 Problem equivalence and globally optimized energy functionals

4.2.1 Conditions of optimality

For the sake of completeness of the presentation and as one gains extra information in the truss case, we will in this section derive the optimality conditions also for the minimum compliance truss topology problem (in the formulation (4.12) with self-weight). As for the continuum problems treated earlier, these conditions constitute the basis for the well-known computational scheme named the *optimality criteria method* (cf., Sect. 1.2.1); we will describe this under a general discussion on computational procedures in a later section.

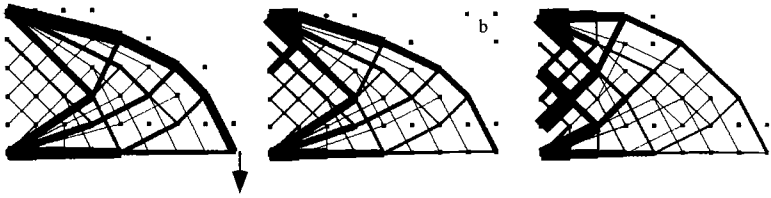

Fig. 4.3. The effect of self-weight loads. Optimal truss topologies for transmitting a single vertical force to a vertical line of supports. The figures show the variation for increasing specific self-weight loads, corresponding to increasing real lengths of the structures. The self-weight is in b) increased by 2 times compared to to the design a). These designs are obtained for a 9 by 6 equidistant nodal lay-out in a rectangular domain of aspect ratio 1.6, and all 919 possible *non-overlapping* connections. If all 1431 possible connections are used, the design b) is modified to the design c). Compare with Fig. 1.8 (from Bendsøe, Ben-Tal & Zowe 1994).

In order to obtain the necessary conditions for optimality for problem (4.12) we introduce Lagrange multipliers $\tilde{\mathbf{u}}, \Lambda, \mu_i$, $i = 1, \ldots, m$, for the equilibrium constraint, the volume constraint and the zero lower bound constraints, respectively. The necessary conditions are thus found as the conditions of stationarity of the Lagrangian

$$\mathcal{L} = (\mathbf{f} + \sum_{i=1}^{m} t_i \mathbf{g}_i)^T \mathbf{u} - \tilde{\mathbf{u}}(\sum_{i=1}^{m} t_i \hat{\mathbf{K}}_i \mathbf{u} - \mathbf{f} - \sum_{i=1}^{m} t_i \mathbf{g}_i)$$
$$+ \Lambda(\sum_{i=1}^{m} t_i - V) + \sum_{i=0}^{m} \mu_i(-t_i)$$

By differentiation we obtain the necessary conditions

$$\sum_{i=1}^{m} t_i \hat{\mathbf{K}}_i \tilde{\mathbf{u}} = \mathbf{f} + \sum_{i=1}^{m} t_i \mathbf{g}_i \qquad \tilde{\mathbf{u}}^T(\hat{\mathbf{K}}_i \mathbf{u} - 2\mathbf{g}_i) = \Lambda - \mu_i$$
$$\mu_i \geq 0 \qquad \mu_i t_i = 0 \qquad i = 1, \ldots, m$$

If we impose a small non-negative lower bound on the areas, the stiffness matrix $\hat{\mathbf{K}}$ is positive definite and thus $\mathbf{u}$ is the unique Lagrange multiplier for the equilibrium constraint, but the situation without a lower bound is not so straightforward.

Now let $\Lambda^*(\mathbf{u})$ denote the maximum of the specific energies $\mathbf{u}^T(\hat{\mathbf{K}}_i \mathbf{u} - 2\mathbf{g}_i)$ (with self-weight) of the individual bars, i.e.

$$\Lambda^*(\mathbf{u}) = \max\left\{\mathbf{u}^T(\hat{\mathbf{K}}_i \mathbf{u} - 2\mathbf{g}_i) \mid i = 1, \ldots, m\right\}$$

and let $J(\mathbf{u})$ denote the set of bars for which the specific energy attains this maximum level

$$J(\mathbf{u}) = \left\{ i \mid \mathbf{u}^T(\hat{\mathbf{K}}_i\mathbf{u} - 2\mathbf{g}_i) = \Lambda^*(\mathbf{u}) \right\}$$

We also define non-dimensional element volumes $\tilde{t}_i = t_i/V$ Then the necessary conditions are satisfied with

$$\begin{aligned} &\tilde{\mathbf{u}} = \mathbf{u};\ t_i = \tilde{t}_i V,\ i \in J(\mathbf{u});\ t_i = 0,\ i \notin J(\mathbf{u});\ \Lambda = \Lambda^*(\mathbf{u}); \\ &\mu_i = 0,\ i \in J(\mathbf{u});\ \mu_i = \Lambda^*(\mathbf{u}) - \mathbf{u}^T(\hat{\mathbf{K}}_i\mathbf{u} - 2\mathbf{g}_i),\ i \notin J(\mathbf{u}) \end{aligned} \tag{4.14}$$

provided that there exist a displacement field $\mathbf{u}$ with corresponding set $J(\mathbf{u})$ and non-dimensional element volumes $\tilde{t}_i$, $i \in J(\mathbf{u})$, such that

$$V \sum_{i \in J(\mathbf{u})} \tilde{t}_i \hat{\mathbf{K}}_i \mathbf{u} = \mathbf{f} + V \sum_{i \in J(\mathbf{u})} \tilde{t}_i \mathbf{g}_i \qquad \sum_{i \in J(\mathbf{u})} \tilde{t}_i = 1 \tag{4.15}$$

The optimality condition (4.15) states that a convex combination of the gradients of the quadratic functions $V(\frac{1}{2}\mathbf{u}^T\hat{\mathbf{K}}_i\mathbf{u} - \mathbf{g}_i^T\mathbf{u})$, $i \in J(\mathbf{u})$, equals the load vector $\mathbf{f}$

It can be shown (see Sect. 4.2.3 below) that there does indeed exist a pair $(\mathbf{u}, \mathbf{t})$ which is a solution to the reduced optimality conditions (4.14, 4.15). This implies that there exists an optimal truss that has bars with constant specific energies and the set $J(\mathbf{u})$ is the set of these active bars. Note that a pair $(\mathbf{u}, \mathbf{t})$ satisfying the necessary conditions (4.14), (4.15) for problem (4.5) is automatically a minimizer for the *non-convex* form (4.12) of the minimum compliance problem. This can be shown by copying the proof of Taylor (1969). For any design $\tilde{s}_i$, $i = 1, \ldots, m$, satisfying the volume constraint and with corresponding displacement field $\mathbf{v}$, we have that

$$\begin{aligned} (\mathbf{f} + \sum_{i=1}^m t_i g_i)^T\mathbf{u} &= 2\mathbf{f}^T\mathbf{u} - \sum_{i=1}^m t_i \mathbf{u}^T(\hat{\mathbf{K}}_i\mathbf{u} - 2g_i) \\ &= 2\mathbf{f}^T\mathbf{u} - \sum_{i=1}^m t_i \Lambda^*(\mathbf{u}) \\ &= 2\mathbf{f}^T\mathbf{u} - V\Lambda^*(\mathbf{u}) = 2\mathbf{f}^T\mathbf{u} - \sum_{i=1}^m \tilde{s}_i \Lambda^*(\mathbf{u}) \\ &\le 2\mathbf{f}^T\mathbf{u} - \sum_{i=1}^m \tilde{s}_i \mathbf{u}^T(\hat{\mathbf{K}}_i\mathbf{u} - 2g_i) \\ &\le 2\max_w \left\{ (\mathbf{f} + \sum_{i=1}^m \tilde{s}_i g_i)^T w - \frac{1}{2}\sum_{i=1}^m \tilde{s}_i w^T \hat{\mathbf{K}}_i w \right\} \\ &= 2(\mathbf{f} + \sum_{i=1}^m \tilde{s}_i g_i)^T\mathbf{u} - \sum_{i=1}^m \tilde{s}_i \mathbf{v}^T\hat{\mathbf{K}}_i\mathbf{v} = (\mathbf{f} + \sum_{i=1}^m \tilde{s}_i g_i)^T\mathbf{v} \end{aligned}$$

where we have invoked the extremum principle for equilibrium. Note that the existence of solutions to the optimality conditions (4.14), (4.15) shows that

there always exists an optimal solution with no more active bars than the degrees of freedom (dimension of $\mathbf{u}$) plus 1; this follows from Caratheodory's theorem on convex combinations (see, e.g. Achtziger et al. (1992); see also McKeown (1997)). Finally we also remark that such a design only has active bars that attain the maximum energy level, as measured by Λ^*, in accordance with what we have seen for the continuum problems as well.

4.2.2 Reduction to problem statements in bar volumes only

It was noted earlier that the truss topology problem is an unusual structural optimization problem, as the acceptance of zero bar volumes implies that the stiffness matrix of the problem can be singular. Thus the standard gradient/adjoint methods of structural optimization which view the problems as optimization problems in the design variables only cannot be invoked directly. However, if we accept to consider the topology optimization problem as a limes inferior problem for a series of optimal design problems with decreasing positive lower bounds on the design variables we can remove the displacements from the formulation (this has consistently been the approach for the continuum structures).

Rewriting (4.5) and imposing positive element volumes as a perturbation of the original problem, we can remove the displacement variables by solving for the now unique displacements

$$\inf_{\substack{t_i>0 \\ \sum_{i=1}^m t_i=V}} \left\{ \Phi(t) \equiv \mathbf{f}^T\hat{\mathbf{K}}(\mathbf{t})^{-1}\mathbf{f} = \max_{\mathbf{u}} \left[2\mathbf{f}^T\mathbf{u} - \mathbf{u}^T \sum_{i=1}^m t_i\hat{\mathbf{K}}_i\mathbf{u} \right] \right\} \tag{4.16}$$

Note that we have exchanged the min-operator with the inf-operator as well as changing the constraint $t_i \geq 0$ to $t_i > 0$. Problem (4.16) is a formulation which, as discussed before, is more standard in structural optimization. Nonetheless, it is still unusual from a computational point of view, as the stiffness matrix in *truss* topology optimization typically will be dense.

It was earlier pointed out that problem (4.16) is convex (see also Svanberg (1984)). This follows from the fact that the compliance function $\Phi(t)$, as a function of the design variables by the second expression in (4.16) is expressed as the supremum (maximum) over a family of convex (linear in this case) functions (cf., Sect. 1.5.2). Note that the gradient of the objective function $\Phi(t)$ is easy to compute and is given as (as seen in Sect. 1.2.3):

$$\frac{\partial\Phi}{\partial t_i} = -\mathbf{u}^T\hat{\mathbf{K}}_i\mathbf{u}, \text{ with } \sum_{i=1}^m t_i\hat{\mathbf{K}}_i\mathbf{u} = \mathbf{f}$$

Note that we for the multiple load problem in its worst-case setting also have a convex formulation in bar volumes only

$$\inf_{\substack{t_i>0,\, i=1,\ldots,m \\ \sum_{i=1}^m t_i=V}} \max_{k=1,\ldots,M} \mathbf{f}^{k\,T}\mathbf{K}(\mathbf{t})^{-1}\mathbf{f}^k \,. \tag{4.17}$$

Semidefinite programs The structure of the minimum compliance *truss* problem also allows for yet another formulation in the displacements only. These fall in a class of mathematical programming problems named *semidefinite programs*, with the acronym SDP. If we rewrite problem (4.16) in terms of a bound variable Φ, which is the value of the compliance, we can write the optimization problem as

$$\begin{aligned} &\min_{\mathbf{u},\mathbf{t},\Phi} \Phi \\ &\text{s.t.} \quad \max_{\mathbf{u}} \left\{ 2\mathbf{f}^T\mathbf{u} - \mathbf{u}^T \sum_{i=1}^{m} t_i \hat{\mathbf{K}}_i \mathbf{u} \right\} \leq \Phi \\ &\qquad \sum_{i=1}^{m} t_i = V, \quad t_i \geq 0,\ i = 1,\ \ldots, m \end{aligned} \tag{4.18}$$

Here the constraint on the potential energy is actually equivalent to a condition that the symmetric matrix

$$\widetilde{\mathbf{A}}(\mathbf{t},\Phi) = \begin{bmatrix} \Phi & \mathbf{f}^T \\ \mathbf{f} & \hat{\mathbf{K}} \end{bmatrix} = \begin{bmatrix} \Phi & \mathbf{f}^T \\ \mathbf{f} & 0 \end{bmatrix} + \sum_{i=1}^{m} t_i \begin{bmatrix} 0 & 0 \\ 0 & \hat{\mathbf{K}}_i \end{bmatrix} \tag{4.19}$$

is positive semidefinite (Ben-Tal & Nemirovski 1994), which we write as $\widetilde{\mathbf{A}} \succeq \mathbf{0}$. The matrix $\widetilde{\mathbf{A}}$ is linear in the variables t_i, and the inequality $\widetilde{\mathbf{A}} \succeq \mathbf{0}$ is then referred to as a *linear matrix inequality*, an LMI (Boyd, Ghaoui, Feron & Balakrishnan 1994). The linearity implies that $\widetilde{\mathbf{A}} \succeq \mathbf{0}$ is a *convex* constraint, which is most directly seen by the definition: $\widetilde{\mathbf{A}} \succeq \mathbf{0}$ if and only if $\widetilde{\mathbf{A}}$ is symmetric and $\mathbf{u}^T\widetilde{\mathbf{A}}\mathbf{u} \geq$ for all $\mathbf{u}$ (this characterization can also be used to show that the condition $\widetilde{\mathbf{A}} \succeq \mathbf{0}$ is equivalent to the condition $2\mathbf{f}^T\mathbf{u} - \mathbf{u}^T\hat{\mathbf{K}}\mathbf{u} \leq \Phi$ for all $\mathbf{u}$, see Ben-Tal & Nemirovski (1994)).

Our optimization problem (4.18) can thus be rewritten as a convex problem in the variables $\mathbf{t}, \Phi$ only (this has now become a standard test problem in mathematical programming, see for example Vandenberghe & Boyd (1996)):

$$\begin{aligned} &\min_{\mathbf{t},\Phi} \Phi \\ &\text{s.t.} \quad \widetilde{\mathbf{A}}(\mathbf{t},\Phi) \succeq \mathbf{0}, \quad \sum_{i=1}^{m} t_i = V, \quad t_i \geq 0,\ i = 1, \ldots, m \end{aligned} \tag{4.20}$$

This reformulation may seem as adding to the complexity of the problem, as initially a constraint like $\widetilde{\mathbf{A}} \succeq \mathbf{0}$ seems difficult to handle. However, this is not the case. Modern interior point algorithms make the solving of SDP's like (4.20) comparable to solving linear programming (LP) problems [33]. As the single load case problem is actually equivalent to an LP problem (see Sect. 4.2.4) this feature is more interesting for the multiple load case which does not have an equivalent LP format. For the worst case situation we actually write the SDP form as:

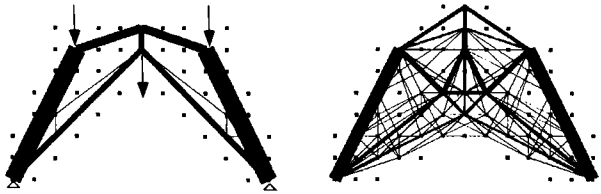

Fig. 4.4. The difference between multiple load and single load case problems. Optimal truss topologies for transmitting three vertical forces to two fixed supports. The truss is optimized with the loads treated as a single load (left) as well as three individual load cases for a min-max, worst case design situation (right). The ground structures consist of all 8744 possible non-overlapping connections between the nodal points of a regular 13 by 13 mesh in a square domain. We do not show the uppermost rows of nodes, as these are not part of the optimal structure (from Bendsøe, Ben-Tal & Zowe 1994).

$$\begin{aligned} &\min_{\mathbf{t},\Phi} \Phi \\ &\text{s.t.} \quad \begin{bmatrix} \Phi & \mathbf{f}^{k^T} \\ \mathbf{f}^k & \hat{\mathbf{K}} \end{bmatrix} \succeq \mathbf{0},\ k = 1, \quad ,M \\ &\qquad \sum_{i=1}^{m} t_i = V, \quad t_i \geq 0,\ i = 1, . \ .,m \end{aligned} \tag{4.21}$$

Also remark that the SDP form can be employed for truss design with bounds $0 \leq t_{\min} \leq t_i \leq t_{\max}$ on the truss volumes; in this situation an LP form is not known either.

If we alternatively consider the compliance $\tilde{\Phi}$ as given and consider the minimum weight design for an upper bound on compliance, an alternative SDP problem can be written as (Brannlund & Svanberg 1997a, Brannlund & Svanberg 1997b):

$$\begin{aligned} &\min_{\mathbf{t}} \sum_{i=1}^{m} t_i \\ &\text{s.t.} \quad \tilde{\Phi} \sum_{i=1}^{m} t_i \mathbf{K}_i - \mathbf{f}^k \mathbf{f}^{k^T} \succeq \mathbf{0},\ k = 1, . \quad ,M \\ &\qquad t_i \geq 0,\ i = 1, \quad ,m \end{aligned} \tag{4.22}$$

4.2.3 Reduction to problem statements in displacements only

We will now use the max-min formulation (4.6) of the truss topology design problem to derive a globally optimal strain energy functional that describes

the energy of the optimal truss. This leads to an alternative, equivalent convex formulation of the problem for which a number of computationally very efficient algorithm can be devised. The derivation is in concept and results similar to the derivation for simultaneous design of structure and material as described in Chap. 3, but the dyadic nature of the stiffness matrix for trusses means that one can go somewhat further, as will be shown in the coming sections.

We will for notational simplicity not cater for the reinforcement situation, so that the version of problem (4.13) that we consider has the form (cf., (4.6))

$$\max_{\substack{\mathbf{t}\geq\mathbf{0}\\ \sum_{i=1}^m t_i=V}} \min_{\mathbf{u}} \left\{ \frac{1}{2}\sum_{i=1}^m t_i \mathbf{u}^T\hat{\mathbf{K}}_i\mathbf{u} - (\mathbf{f}+\sum_{i=1}^m t_i\mathbf{g}_i)^T\mathbf{u} \right\} \tag{4.23}$$

and this problem is linear in the design variable and convex in the displacement variable. Thus the problem is concave-convex (with a convex and compact constraint set in t) and we can interchange the max and the min operators, to obtain

$$\min_{\mathbf{u}} \max_{\substack{\mathbf{t}\geq\mathbf{0}\\ \sum_{i=1}^m t_i=V}} \left\{ \frac{1}{2}\sum_{i=1}^m t_i \mathbf{u}^T\hat{\mathbf{K}}_i\mathbf{u} - (\mathbf{f}+\sum_{i=1}^m t_i\mathbf{g}_i)^T\mathbf{u} \right\}$$

The inner problem is now a linear programming problem in the $\mathbf{t}$ variable. To solve this problem, note that with $t_i \geq 0$, $\sum_{i=1}^m t_i \quad V$ we have the inequality

$$\sum_{i=1}^m t_i(\mathbf{u}^T\hat{\mathbf{K}}_i\mathbf{u} - 2\mathbf{g}_i{}^T\mathbf{u}) \leq V \max_{i=1,\ldots,m} \left\{ \mathbf{u}^T\hat{\mathbf{K}}_i\mathbf{u} - 2\mathbf{g}_i{}^T\mathbf{u} \right\}$$

Here the equality holds if all material is assigned to a bar with maximum specific energy $\mathbf{u}^T\hat{\mathbf{K}}_i\mathbf{u} - 2\mathbf{g}_i^T\mathbf{u}$. Thus we see that the problem (4.23) can be reduced to (Ben-Tal & Bendsøe 1993)

$$\min_{\mathbf{u}} \max_{i=1,\ldots,m} \left\{ \frac{V}{2}\left[\mathbf{u}^T\hat{\mathbf{K}}_i\mathbf{u} - 2\mathbf{g}_i^T\mathbf{u}\right] - \mathbf{f}^T\mathbf{u} \right\} \tag{4.24}$$

This is an *unconstrained*, *convex* and *non-smooth* problem, in the displacement variable $\mathbf{u}$ only, with optimal value minus one half of the optimal value for the problem (4.12). It can equivalently be written as the *smooth*, constrained and convex problem

$$\begin{aligned} &\min_{\mathbf{u},\tau} \{\tau^2 - \mathbf{f}^T\mathbf{u}\} \\ &\text{s.t.} \quad \frac{V}{2}\left[\mathbf{u}^T\hat{\mathbf{K}}_i\mathbf{u} - 2\mathbf{g}_i{}^T\mathbf{u}\right] \leq \tau^2, \quad i = 1,\ldots,m \end{aligned} \tag{4.25}$$

This problem has a large number of constraints, but these can be efficiently handled via interior point methods, see Sect. 4.3.3. For completeness let us

state the equivalent problems for the weighted average, multiple load *truss* case

$$\min_{\mathbf{u}^k}\left[\max_{i=1,\ldots,m}\left\{\sum_{k=1}^{M} w^k(\frac{V}{2}\mathbf{u}^{k^T}\mathbf{K}_i\mathbf{u}^k - \mathbf{f}^{k^T}\mathbf{u}^k)\right\}\right] \tag{4.26}$$

One can think of the resulting displacements only problems shown above as equilibrium problems for a structure with a non-smooth, convex strain energy. Philosophically speaking, this strain energy is the strain energy for a "self-optimized" structure which automatically adjusts its topology and sizing so as to minimize compliance for the applied load(s) (cf. Chap. 3).

It is possible to show existence of solutions to the problems (4.24)-(4.26) and to prove the equivalence between problem statements of the form (4.1)-(4.5) and (4.24)-(4.26) (Ben-Tal & Bendsøe 1993). The solutions are not unique and it is quite well-known that there are normally "many" solutions (actually subspaces of solutions). The equivalence of the problems is understood in the sense that for a solution $\mathbf{u}$ to for example problem (4.24) and the corresponding set $J(\mathbf{u})$ of active bars, there exists a corresponding set of bar volumes $\mathbf{t}$ satisfying the optimality condition

$$\sum_{i\in J(\mathbf{u})} t_i\hat{\mathbf{K}}_i\mathbf{u} = \mathbf{f} + \sum_{i\in J(\mathbf{u})} t_i\mathbf{g}_i \qquad \sum_{i\in J(\mathbf{u})} t_i = V$$
$$t_i = 0,\ i \notin J(\mathbf{u}); \quad t_i \geq 0,\ i = 1,\ldots,m\ ,$$

and these optimality conditions are precisely the optimality conditions for the min-max problem (4.24).

For the worst case multiple load problem it is possible to generate a displacements only formulation in the form (Achtziger 1993, Achtziger 1998)

$$\min_{\substack{\mathbf{u}^k,\,\lambda^k\geq 0\\ \sum_{k=1}^{M}\lambda^k=1}}\left[\max_{i=1,\ldots,m}\left\{\sum_{k=1}^{M}\lambda^k(\frac{V}{2}\mathbf{u}^{k^T}\mathbf{K}_i\mathbf{u}^k - \mathbf{f}^{k^T}\mathbf{u}^k)\right\}\right] \tag{4.27}$$

where we have used weighting parameters $\lambda^k \geq 0$, $k = 1, \quad ,M$ Solutions to this problem can likewise be proved to exist and the optimal value of problem (4.27) equals minus one half the extremal value of problem (4.4) The direct equivalence between the two problems (in the sense discussed for the single load problem) may fail if a multiplier λ^k equals zero in the optimal solution to problem (4.27). In this case we cannot guarantee equilibrium for this load condition, as the equilibrium will not necessarily be enforced by the necessary conditions of optimality. However, a set of bar areas can be identified by considering the loads with non-zero multipliers, and a minimum compliance truss will be generated for these loads. This makes it natural to consider a slightly perturbed version of (4.4) and (4.27), where the multipliers are constrained as $\lambda^k \geq \varepsilon > 0$, $k = 1, \quad ,M$. For the resulting perturbed version of problem (4.27) we can write

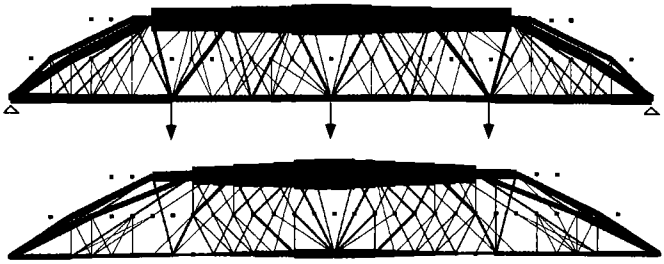

Fig. 4.5. The difference (and similarity) between multiple load case treated in the weighted average formulation (equal weights) (top) and treated in the worst case min-max formulation (below). Optimal truss topologies for transmitting three vertical forces to two fixed supports for a long slender rectangular ground structure of aspect ratio 16 (like a long span bridge), with 33 by 3 equidistant nodes and all 2818 possible non-overlapping connections. In this figure, the vertical scale has been distorted in order to being able to show the results (from Bendsøe, Ben-Tal & Zowe 1994).

$$\min_{\substack{\lambda^k \geq \varepsilon \\ \sum_{k=1}^{M} \lambda^k = 1}} \left(\min_{\mathbf{u}^k} \left[\max_{i=1,\ldots,m} \left\{ \sum_{k=1}^{M} \lambda^k \left(\frac{V}{2} \mathbf{u}^{k^T} \mathbf{K}_i \mathbf{u}^k - \mathbf{f}^{k^T} \mathbf{u}^k \right) \right\} \right] \right) \tag{4.28}$$

indicating that the inner problem in the displacements could be solved using the methods that can be used for the single load case, with the outer problem solved using algorithms for convex non-differentiable optimization problems; this is described in detail in Achtziger (1993) and (1998).

4.2.4 Linear programming problems for single load problems

In the preceding section the minimum compliance truss topology problem was reformulated as a non-smooth, convex problem in the displacements only. This can now be used as a basis for generating a range of other equivalent problem statements.

The starting point is actually the bound formulation (4.25), which for the simpler case of no self-weight becomes, up to a scaling,

$$\begin{aligned} &\min_{\mathbf{u}} \left\{ -\mathbf{f}^T \mathbf{u} \right\} \\ &\text{s.t.} \quad \frac{V}{2} \mathbf{u}^T \hat{\mathbf{K}}_i \mathbf{u} \leq 1, \quad i = 1, . \quad , m \end{aligned} \tag{4.29}$$

i.e. a maximization of compliance, with constraints on the specific strain energies.

For the *single load* truss problem the element stiffness matrices are dyadic products and we get for the specific energies

$$\mathbf{u}^T\mathbf{K}_i\mathbf{u} = \left(\frac{\sqrt{E_i}}{l_i}\mathbf{b}_i{}^T\mathbf{u}\right)^2$$

This special form implies that (4.29) can be written in LP-form as (Achtziger et al. 1992)

$$\begin{aligned} &\min_{\mathbf{u}} \left\{-\mathbf{f}^T\mathbf{u}\right\} \\ &\text{s.t.} \quad -1 \le \sqrt{\frac{VE_i}{2}}\frac{\mathbf{b}_i{}^T\mathbf{u}}{l_i} \le 1, \quad i = 1,. \quad ,m \ , \end{aligned} \tag{4.30}$$

which is a problem of maximizing the compliance with constraints on the strains $\varepsilon_i = l_i{}^{-1}\mathbf{b}_i{}^T\mathbf{u}$ in all bars. For suitable stress constraint values $\bar{\sigma}_i$ it turns out that problem (4.30) is the dual of the force formulation (4.9)

$$\min_{\substack{q_i^+\ge 0,\, q_i^-\ge 0,\\ i=1,\ldots,m\\ \mathbf{B}(\mathbf{q}^+-\mathbf{q}^-)=\mathbf{f}}} \sum_{i=1}^{m} \frac{l_i}{\bar{\sigma}_i}(q_i^+ - q_i^-) \tag{4.31}$$

(cf., Sect. 4.1.2). Here the tension/compression forces q_i^+, q_i^- are the multipliers for the strain inequality constraints of (4.30). As seen in section 4.1.2, problem (4.31) is, after a change of variables, precisely the traditional minimum mass plastic design formulation (4.8). The developments described above show that the minimum compliance design problem for a single load case is equivalent to a minimum mass plastic design formulation, in the sense that for a solution $\mathbf{t}$, $\mathbf{q}$ to the minimum mass plastic design problem with data V, $\bar{\sigma}_i$, there corresponds a solution $\mathbf{t}_C$, $\mathbf{u}_C$ to the minimum compliance problem with data V_C, E_i The precise relations are (cf. Achtziger et al. (1992))

$$\bar{\sigma}_i = \sqrt{E_i}, \quad t_C = \frac{V_C}{V}t, \quad \mathbf{u}_C = \frac{V_C}{V}\tilde{\mathbf{u}}$$

where $\tilde{\mathbf{u}}$ is the dual variable of the minimum mass plastic design problem corresponding to the static equilibrium constraint $\mathbf{Bq} = \mathbf{f}$.

The member force formulations (4.8) and (4.9) are, as described earlier, the traditional formulations for single load truss topology optimization. These are, of course, very efficient formulations and could be solved using *sparse*, primal-dual LP-methods. The force methods are at first glance problems in plastic design, as kinematic compatibility is ignored, and their use in elastic design is justified by the possibility of finding statically determinate solutions. The equivalence between the force methods and the minimum compliance problem for the *single load case* shows that *any* solution to the force LP-formulation leads to a minimum compliance topology design, within the framework of elastic designs. Such designs are uniformly stressed designs, as well as having a constant specific energy in all active bars. The existence of

basic solutions to the linear programming problem (4.9) implies that there exist minimum mass truss topologies with a number of bars not exceeding the degrees of freedom. If there exists such a basic solution with only non-zero forces (areas), this is a statically determinate truss. Otherwise, the truss will have a unique force field for the given load but will be kinematically indeterminate. In other words the truss may have rigid body (mechanism) response to certain loads other than the load for which it is designed; this may be the case even after nodes with no connected bars are removed (see also Kirsch (1989a), Kirsch (1989b) for a discussion on this).

The equivalence between problems (4.8), (4.9) and (4.30) can also be found in Dorn et al. (1964), and the equivalence between problems (4.1) and (4.8) is indicated in Hemp (1973), among other places. In Dorn et al. (1964) one can also find a lengthy discussion on how the force formulations are convenient for studying an eventual static determinacy of the solutions.

The derivation of the linear programming formulations above holds only for the case of pure topology truss design with unconstrained design variables, a single load case and excluding self-weight. Thus, the natural extension of the plastic design situation to problem (4.10) which caters for multiple loads and self-weight loads does not seem to have a natural equivalent statement in terms of displacements and compliances. Also, it is well known that in the case of multiple load plastic design, it is most common that statically indeterminate solutions result, thus imposing a requirement for further redesign if kinematic compatibility is required, as for elastic design (Kirsch 1989b, Kirsch 1993a, Topping 1992).

For the sake of completeness of presentation, note that in the reinforcement case without self-weight, the single load case problem can be reduced to a quadratic optimization problem with linear constraints

$$\begin{aligned} &\min_{\mathbf{u},\mu} \left\{ \frac{1}{2}\mathbf{u}^T \left(\sum_{i\in S} s_i \mathbf{K}_i \right) \mathbf{u} - \mathbf{f}^T\mathbf{u} + \tau^2 \right\} \\ &\text{s.t.} \quad -\tau \leq \sqrt{\frac{VE_i}{2l_i}} {\mathbf{b}_i}^T \mathbf{u} \leq \tau, \quad i \in R \end{aligned} \tag{4.32}$$

Notice here that the matrix $\sum_{i\in s} s_i \mathbf{K}_i$ is positive semi-definite, but usually not positive definite. The problem statement (4.32) also represents a simplification of the minimum compliance problem for a single load case with *lower bounds* on the variables; the vector $\mathbf{s}$ represents the vector of lower bounds on the design variables.

4.2.5 Reduction to problem statements in stresses only

In the following we will base our developments on the worst-case multiple load design formulation (4.28). In order to simplify notation we will refrain from covering the problem of reinforcement and the self-weight problem will also

play a minor role in the following. However, we begin with a general treatment that covers truss, variable thickness sheet and sandwich plate design.

Now returning to problem (4.28) we note that by a change of variables of $\mathbf{u}^k$ to $\frac{1}{\lambda^k}\mathbf{u}^k$ this problem can be stated as

$$\inf_{\substack{\lambda^k>0 \\ \sum_{k=1}^M \lambda^k=1}} \left(\min_{\mathbf{u}^k} \left[\max_{i=1,\ldots,m} \left\{ \sum_{k=1}^M \left(\frac{V}{2}\frac{1}{\lambda^k}\mathbf{u}^{k^T}\mathbf{K}_i\mathbf{u}^k - \mathbf{f}^{k^T}\mathbf{u}^k\right) \right\} \right] \right) \tag{4.33}$$

which is now *jointly* convex on the feasible set in both the multipliers λ^k and the displacements. Here we have used the inf-operator to indicate the use of a decreasing sequence of lower bounds on the multipliers λ^k The presence of the infimum over the multipliers indicates that it is a natural choice to use interior penalty methods for a computational procedure for solving of this problem, as will be described later.

We shall now show that by deriving the dual formulations of (4.33) one can for the *truss* case generate what amounts to stress based min-max minimum compliance formulations. The basis for this derivation is again, as in the earlier development, the dyadic structure of the individual member stiffness matrices. Expressing the maximization over the bar numbers (the inner problem) with a bounding variable and using auxiliary variables $c_i^k = \mathbf{b}_i^T\mathbf{u}^k$ (the member elongations), the equivalent convex dual problem can be derived to have the form

$$\begin{aligned} &\inf_{\mathbf{t}} \min_{\mathbf{q}^k} \left[\max_{k=1,\ldots,m} \left\{ \frac{1}{2}\sum_{i=1}^m \frac{l_i^2}{E_i}\frac{(q_i^k)^2}{t_i} \right\} \right] \\ &\text{s.t.} \quad \mathbf{B}\mathbf{q}^k = \mathbf{f}^k, \quad k=1, \quad ,M \\ &\qquad \sum_{i=1}^m t_i = V, \quad t_i > 0, \quad i=1, \quad ,m \end{aligned} \tag{4.34}$$

With $\bar{\lambda}^k$, $\bar{\mathbf{u}}^k$ denoting the Lagrange multipliers for a bound constraint formulation of the maximization over k and the equilibrium constraint, respectively, we can for an optimum $\mathbf{q}^k$, $\mathbf{t}$ of (4.34) with $\bar{\lambda}^k > 0$, $k = 1, \quad ,M$, identify $\mathbf{u}_k = \bar{\mathbf{u}}^k/\bar{\lambda}^k$, $\mathbf{t}$ as a solution to our original problem statement (4.4) in displacements and bar areas. Also, we can show, from the Karush-Kuhn-Tucker optimality conditions that $q_i^k = \frac{E_i}{l_i^2}t_i\mathbf{b}_i^T\mathbf{u}^k$, i.e. compatibility of stresses and displacements is automatically assured.

The problem (4.34) is actually the minimum compliance problem formulated in terms of the complementary energy, written for the worst-case multiple load situation. For the single load situation, the formulation (4.34) reduces to problem (4.7) which was stated in Sect. 4.1.2.

Finally, we will consider the elimination of the bar volumes from the problem (4.34), by directly solving for these variables. This corresponds to the elimination of bar volumes in the displacements (strain) based formulation

as carried out in the preceding Sect. 4.2.2. Expressing the maximization over load cases by a maximization over a convex combination of weighting factors

$$\min_{\substack{\mathbf{q}^k \\ \mathbf{B}\mathbf{q}^k=\mathbf{f}^k}} \quad \inf_{\substack{\mathbf{t}>\mathbf{0} \\ \sum_{i=1}^m t_i=V}} \quad \max_{\substack{\lambda^k\geq 0 \\ \sum_{k=1}^M \lambda=1}} \left\{ \sum_{k=1}^M \lambda^k \left[\frac{1}{2} \sum_{i=1}^m \frac{l_i^2}{E_i} \frac{(q_i^k)^2}{t_i} \right] \right\} \tag{4.35}$$

we can derive the optimal values of the bar volumes as

$$t_i = V \sqrt{\frac{l_i^2}{E_i} \sum_{k=1}^M \lambda^k (q_i^k)^2} \left[\sum_{i=1}^m \sqrt{\frac{l_i^2}{E_i} \sum_{k=1}^M \lambda^k (q_i^k)^2} \right]^{-} \tag{4.36}$$

Inserting in (4.35) we obtain the following problem in the member forces only

$$\begin{aligned} &\min_{\mathbf{q}^k} \quad \max_{\substack{\lambda^k\geq 0 \\ \sum_{k=1}^M \lambda^k=1}} \left\{ \frac{1}{2V} \left[\sum_{i=1}^m \left(\frac{l_i}{\sqrt{E_i}} \sqrt{\sum_{k=1}^M \lambda^k (q_i^k)^2} \right) \right]^2 \right\} \\ &\text{s.t.} \quad \mathbf{B}\mathbf{q}^k = \mathbf{f}^k, \quad k = 1, \ldots, M \end{aligned} \tag{4.37}$$

For the single load case we recover the traditional linear programming formulation (4.9) in the disguised form

$$\min_{\substack{\mathbf{q} \\ \mathbf{B}\mathbf{q}=\mathbf{f}}} \left\{ \frac{1}{2V} \left[\sum_{i=1}^m \left(\frac{l_i}{\sqrt{E_i}} |q_i| \right) \right]^2 \right\} \tag{4.38}$$

Rescaling the objective function and taking the square root of the objective function results in (4.9). Note that we have again seen that the stress constraint values for the plastic topology problem should be chosen as $\sqrt{E_i}$ Also, as (4.38) was obtained by direct duality without rescaling, one can see that the optimal value Π of the optimal compliance will relate to the optimal value Ψ of the minimum mass plastic design problem as

$$\Psi^2 = \Pi V$$

This relation has also been reported in Rozvany (1993).

Note that (4.38) is the natural formulation for the stress *only* reformulation of the minimum compliance problem stated as a corresponding equilibrium problem for a structure with a non-smooth, convex complementary energy. This is again completely analogous to the situation described for continuum problems in Chap. 3.

4.2.6 Extension to contact problems

The discussion above can be extended to problems involving unilateral contact, as we shall briefly outline in the following (cf., Sect. 3.4.3). Truss

topology design in this context has been studied by Klarbring, Petersson & Rönnqvist (1995), Petersson & Klarbring (1994), Kocvara, Zibulevsky & Zowe (1998). The most natural setting for unilateral contact problems is a displacement based formulation. For an unilateral contact condition of the form $\mathbf{Cu} \leq \mathbf{0}$, the minimum compliance problem (4.6) for contact problems becomes[2]

$$\max_{\substack{\mathbf{t}\geq 0 \\ \sum_{i=1}^{m} t_i = V}} \min_{\substack{\mathbf{u} \\ \mathbf{Cu}\leq \mathbf{0}}} \left\{ \frac{1}{2} \sum_{i=1}^{m} t_i \mathbf{u}^T \mathbf{K}_i \mathbf{u} - \mathbf{f}^T \mathbf{u} \right\} \tag{4.39}$$

where only the inner equilibrium problem is altered. In Klarbring et al. (1995), the problem of finding the stiffest structure among all structures with constant contact pressure is also considered and in this case the unilateral constraint should be of the scalar form $\mathbf{1}_C \mathbf{Cu} \leq \mathbf{0}$, corresponding to a total gap constraint $\mathbf{1}_C \mathbf{d} = 0$, where $\mathbf{d}$ is an initial gap which is designed to achieve constant pressure (see also Klarbring (1992)). This case is also covered by the statement (4.39), by proper choice of $\mathbf{C}$.

The introduction of *design independent* constraints in the inner problem of (4.39) does not change the saddle point property of the problem. As shown in Klarbring et al. (1995), it does not make sense for contact problems to assume that the stiffness matrix is positive definite for at least one design. Instead, one has to assume that the applied force does not give raise to rigid body motions and that the applied force is not entirely applied at the potential contact nodes. With this assumption we have existence of solution and an equivalent displacements only problem in the form

$$\min_{\substack{\mathbf{u} \\ \mathbf{Cu}\leq \mathbf{0}}} \max_{i=1,\ldots,m} \left\{ \frac{V}{2} \mathbf{u}^T \mathbf{K}_i \mathbf{u} - \mathbf{f}^T \mathbf{u} \right\} \tag{4.40}$$

This problem can be solved by equivalent means as (4.25): the extra linear constraints $\mathbf{Cu} \leq \mathbf{0}$ does not influence the efficiency (Kocvara et al. 1998). Consider now the worst-case multiple load problem in the formulation which includes contact

$$\inf_{\substack{\lambda^k > 0 \\ \sum_1^M \lambda^k = 1}} \min_{\substack{\mathbf{u}^k \\ \mathbf{C}^k \mathbf{u}^k \leq \mathbf{0}}} \max_{i=1,\ldots,m} \left\{ \sum_{k=1}^{M} \left(\frac{V}{2} \frac{1}{\lambda^k} \mathbf{u}^{k^T} \mathbf{K}_i \mathbf{u}^k - \mathbf{f}^{k^T} \mathbf{u}^k \right) \right\} \tag{4.41}$$

Here we have related each load case to a potentially different contact condition. Computing the dual of the equilibrium problem, we obtain the complementary energy formulation in the form

[2] The formulation for the reinforcement problem with self-weight is analogous.

$$\inf_{\mathbf{t}} \min_{\mathbf{q}^k, \mathbf{p}^k} \left[\max_{k=1,\ldots,M} \left\{ \frac{1}{2} \sum_{i=1}^{m} \frac{l_i^2}{E_i} \frac{(q_i^k)^2}{t_i} \right\} \right]$$

$$\text{s.t.} \quad \mathbf{B}\mathbf{q}^k = \mathbf{f}^k - \mathbf{C}^{k^T}\mathbf{p}^k, \quad \mathbf{p}^k \geq \mathbf{0}, \quad k = 1, \ldots, M$$

$$\sum_{i=1}^{m} t_i = V, \quad t_i > 0, \quad i = 1, \ldots, m$$

where the contact forces $\mathbf{p}^k$ also enter as variables. As for the non-contact case we can compute the optimal bar volumes (given again by formula (4.36)) and the resulting force-only formulation only change by the addition of the contact forces in the equilibrium constraint. For the single load case we get the disguised linear programming problem

$$\min_{\substack{\mathbf{q}, \mathbf{p} \geq \mathbf{0} \\ \mathbf{B}\mathbf{q} = \mathbf{f} - \mathbf{C}^T\mathbf{p}}} \left\{ \frac{1}{2V} \left[\sum_{i=1}^{m} \left(\frac{l_i}{\sqrt{E_i}} |q_i| \right) \right]^2 \right\}$$

For the displacement formulation one has, likewise, the LP formulation

$$\min_{\mathbf{u}} \left\{ -\mathbf{f}^T\mathbf{u} \right\}$$

$$\text{s.t.} \quad \mathbf{C}\mathbf{u} \leq \mathbf{0}; \qquad -1 \leq \sqrt{\frac{VE_i}{2}} \frac{\mathbf{b}_i^T\mathbf{u}}{l_i} \leq 1, \quad i = 1, \ldots, m$$

taking the development "full circle"

We close this section by remarking that the minimum compliance problem with unilateral contact formulated as a

$$\sup_{\substack{\mathbf{t} > \mathbf{0} \\ \sum_{i=1}^{m} t_i = V}} \left[\Phi(\mathbf{t}) = \min_{\substack{\mathbf{u} \\ \mathbf{C}\mathbf{u} \leq \mathbf{d}}} \left\{ \frac{1}{2} \sum_{i=1}^{m} t_i \mathbf{u}^T \mathbf{K}_i \mathbf{u} - \mathbf{f}^T\mathbf{u} \right\} \right]$$

for positive definite stiffness matrices is actually a C^1-smooth problem in the bar volumes (see also Haslinger & Neittaanmki (1996)). Here we consider that an initial non-zero gap $\mathbf{d}$ is given. The derivatives of the functional $\Phi(t)$ (it is minus one half of the compliance) are given as

$$\frac{\partial}{\partial t_i} \Phi(\mathbf{t}) = \frac{1}{2} \mathbf{u}_*^T \hat{\mathbf{K}}_i \mathbf{u}_*, \text{ with } \mathbf{u}_* = \arg \min_{\substack{\mathbf{u} \\ \mathbf{C}\mathbf{u} \leq \mathbf{d}}} \left\{ \frac{1}{2} \sum_{i=1}^{m} t_i \mathbf{u}^T \hat{\mathbf{K}}_i \mathbf{u} - \mathbf{f}^T\mathbf{u} \right\}$$

Note, however, that the displacements are not differentiable as functions of bar volumes, as the displacements are non-smooth at designs were there are active contact nodes with zero contact forces. This feature means that most other design problems which involves contact conditions are non-smooth problems. Nonetheless, directional derivatives can be computed (Bendsøe, Olhoff & Sokołowski 1985).

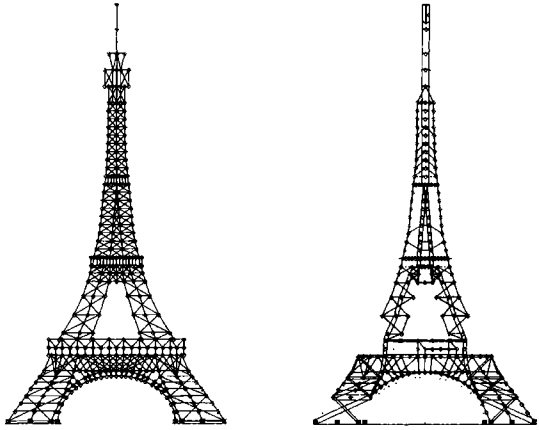

Fig. 4.6. The flexibility in choice of ground structure. Optimal design of a well-known structure. Left hand picture shows the ground structure and the right hand picture the optimal topology for a single downward load at the top of the structure. The example shows that it is crucial to consider multiple load cases for realistic structures. By courtesy of M. Kocvara and J. Zowe.

4.3 Computational procedures and examples

The availability of efficient methods to solve large (sparse) LP problems makes it natural to solve the single load truss topology design problem using the LP formulations. For problems with multiple loads and/or bounded bar areas, for the reinforcement problem as well as for the FEM case, we cannot obtain a linear programming formulation of the minimum compliance problem and we are forced to solve such problems by other means.

Problems of the form (4.1)-(4.5) and (4.11)-(4.13) generalize most easily to more general design situations involving stress and displacement constraints but they are large scale and non-convex. The optimality criterion method is a good and easily programmed option for solving this problem in the minimum compliance setting, if suitable lower bounds on the bar volumes are imposed. Problems (4.24)-(4.28) and (4.25), (4.29) are convex and have the size of the degrees of freedom of the ground structure; the former are non-differentiable and unconstrained and the bound formulations are differentiable, but at the cost of a high number of constraints. Below we shall present a specialized and physically intuitive algorithm for solving problem (4.24); it can be easily implemented to take advantage of the sparsity of the matrices $\hat{\mathbf{K}}_i$, but is actually not efficient compared to other methods based on the smooth formulations. Problem (4.24) has for some time been used as a "difficult" test case for general purpose algorithms for min-max optimiza-

tion or non-differentiable optimization. The most efficient approach (when LP-codes cannot be applied) is to use modern penalty methods for problems (4.25), (4.29) which can be solved by such general purpose algorithms. Alternatively, the SDP format (4.20)-(4.22) can be used. In both cases sparsity and the fact that the number of variables is much lower than the number of constraints should be utilized.

It should be emphasized that the truss topology design problem is a very challenging mathematical programming problem with structure and properties which are a test for even the best of algorithm.

4.3.1 An optimality criteria method

For the continuum problems treated earlier the optimality criteria method is an effective and general mean for solving minimum compliance problems. Also for truss topology design this is a simple computational procedure, but it is not as effective as other approaches based on interior point or SDP techniques. However, it is physically intuitive as the method assigns material to members proportionally to the specific energy of each member in order to reach the situation of constant specific energy in the active bars. Thus each iteration step consists of the following

$$\begin{aligned}
&\text{For } t_i^{K-1} \text{ given, compute } \mathbf{u}_{K-1} \text{ from the equilibrium eqs.}\\
&\text{Find } \Lambda^K \text{ so } \sum_{i=1}^{m} \max\left\{ t_i^{K-1} \frac{\mathbf{u}_{K-1}{}^T \hat{\mathbf{K}}_i \mathbf{u}_{K-1}}{\Lambda^K},\ t_{\min} \right\} = V\\
&\text{Update } t_i^K = \max\left\{ t_i^{K-1} \frac{\mathbf{u}_{K-1}{}^T \hat{\mathbf{K}}_i \mathbf{u}_{K-1}}{\Lambda^K},\ t_{\min} \right\}
\end{aligned} \tag{4.42}$$

The linearity of stiffness and volume in the bar areas implies that the optimality criteria algorithm for the single load case can be viewed as a fully stressed design algorithm, and it is as such a fix point algorithm (Levy 1991). Also, the method can be viewed as an implementation of a sequential quadratic programming technique; this is discussed in detail in Svanberg (1994b), Svanberg (1994a). Also, the similarity to convex approximation techniques as MMA has been outlined in Sect. 1.2.3.

The optimality criteria method involves assembly of the global stiffness matrix as well as solving the equilibrium problem at each iteration step, and this part of the algorithm is the most time consuming. Note, that for $t_{\min} \sim 0.0$ the algorithm can utilize that the volume is linear in the design variables, so that satisfying the volume constraint is just a rescaling of variables. However, the algorithm does not take advantage of the fact that also the stiffness matrix is linear in the design variables. Also for the single load case truss topology problem (4.1) we have that the matrices $\mathbf{K}_i$ are dyadic products and this is not used either.

4.3.2 A non-smooth descent method

One can also devise physically intuitive algorithms that work with the displacements as the primary variables. The basis is then the equivalent problems (4.24)-(4.28). We will here describe an "ϵ-steepest descent" method for these non-smooth problems (Demyanov & Malozemov 1974, Ben-Tal & Bendsøe 1993). The algorithm is actually inefficient, but, as mentioned, it is physically intuitive, and it is closely related to the optimality criteria algorithm. Even though the algorithm solves a problem in the displacement variables it generates the solution $\mathbf{u}$ as well as the bar volumes $\mathbf{t}$. This contrasts to the standard procedure in optimal structural design where one solves for the design variables, with the displacements removed via the state equation and adjoint equation.

We describe the algorithm for the topology design problem with external loads as well as loads due to self-weight. Thus the algorithm for problem (4.24)

$$\min_{\mathbf{u}} \left[F(\mathbf{u}) = \frac{V}{2} \max_{i=1,\ldots,m} \left\{ \mathbf{u}^T \hat{\mathbf{K}}_i \mathbf{u} - 2\mathbf{g}_i^T \mathbf{u} \right\} - \mathbf{f}^T \mathbf{u} \right]$$

consists of the following very intuitive steps (for details consult Ben-Tal & Bendsøe (1993)):

0. Compute an initial guess of displacement field $\mathbf{u}$, for example by solving the equilibrium equations for a feasible set of bar volumes $\mathbf{t}$.
1. For present $\mathbf{u}$, compute $\Lambda^*(\mathbf{u}) = \max_{i \in R} \left\{ \mathbf{u}^T \hat{\mathbf{K}}_i \mathbf{u} - 2\mathbf{g}_i^T \mathbf{u} \right\}$, and indices

$$J(\mathbf{u}) = \left\{ i \in R | \mathbf{u}^T \hat{\mathbf{K}}_i \mathbf{u} - 2\mathbf{g}_i^T \geq \Lambda^*(\mathbf{u}) - \epsilon \right\}$$

2. Compute descent direction $\mathbf{d}$ as $\mathbf{d} = -\sum_{i \in J} t_i \left[\hat{\mathbf{K}}_i \mathbf{u} - \mathbf{g}_i \right] + \mathbf{f}$, where t_i, $i \in J$ are found from

$$\min_{\substack{t_i \geq 0, i \in J \\ \sum_{i \in J} t_i = V}} \left\{ \| \sum_{i \in J} t_i \left[\hat{\mathbf{K}}_i \mathbf{u} - \mathbf{g}_i \right] - \mathbf{f} \|^2 - \sum_{i \in J} t_i \mathbf{u}^T \left[\hat{\mathbf{K}}_i \mathbf{u} - 2\mathbf{g}_i \right] \right\}$$

3. If $\|\mathbf{d}\| \leq \delta$, stop. Else go to 4.
4. Compute a step size α^* for the update $\mathbf{u} := \mathbf{u} + \alpha \mathbf{d}$, by a line search (Golden Section method) with the function

$$\Psi(\alpha) = F(\mathbf{u} + \alpha \mathbf{d}) = \max_{i=1,\ldots,m} \left\{ \bar{a}_i \alpha^2 + \bar{b}_i \alpha + \bar{c}_i \right\}$$

$$\bar{a}_i = \frac{V}{2} \mathbf{d}^T \hat{\mathbf{K}}_i \mathbf{d}, \quad \bar{b}_i = \left[V(\hat{\mathbf{K}}_i \mathbf{u} - \mathbf{g}_i) - \mathbf{f} \right]^T \mathbf{d}$$

$$_i = \left[\frac{V}{2} (\hat{\mathbf{K}}_i \mathbf{u} - 2\mathbf{g}_i) - \mathbf{f} \right]^T \mathbf{u} \, .$$

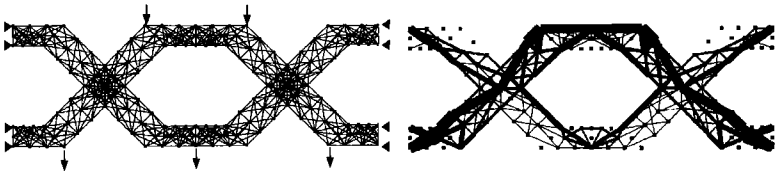

Fig. 4.7. An example of a complicated ground structure geometry, with 156 nodal points and 660 potential bars. The ground structure, supports and five loads are shown at the top. The resulting topology for a weighted average, multiple load problem formulation is shown below. The ground structure was generated by an interactive CAD-based programme, see da Silva Smith (1996) (from Bendsøe, Ben-Tal & Zowe 1994).

5. Update, $\mathbf{u} := \mathbf{u} + \alpha^* \mathbf{d}$, and go to step 1.

Here, ϵ is a relaxation on the activity set J which is crucial to guarantee the convergence of the algorithm, and δ determines the accuracy of the solution (one works with decreasing sequences of these parameters). Each iteration loop of the algorithm consists of first finding the set of almost active bars (Step 1). The descent direction (Step 2) is then found by first finding the bar volumes of these bars which minimizes the error in equilibrium for the given estimate of displacement. The error is measured in a least squares sense and the descent direction is proportional to the residual of the equilibrium for this best fit of bar volumes. The algorithm can be implemented to take full advantage of sparsity, both in storage and in computations. For example one notes that the full stiffness matrix is not required. For a proof of the convergence of the algorithm, we refer to Ben-Tal & Bendsøe (1993). An example of the use of this algorithm for the layout design of aircraft wings can be found in Balabanov & Haftka (1996).

4.3.3 SDP and interior point methods

Methods working with bar volumes It is the provision of a lower bound on the bar volumes that allows for the use of the very effective optimality criterion method. A similar efficiency can be obtained by considering the problem of taking the infimum of the compliances for all truss structures with positive bar volumes

$$\inf_{\substack{t_i \geq 0 \\ \sum_{i=1}^m t_i = V}} \left\{ \Phi(\mathbf{t}) = \mathbf{f}^T \left[\sum_{i=1}^m t_i \hat{\mathbf{K}}_i \right]^{-1} \mathbf{f} \right\} \tag{4.43}$$

As shown earlier this problem is convex and this in combination with the inf-form makes it ideally suited for interior point barrier methods (Ben-Tal

& Nemirovski 1993, Ben-Tal & Nemirovski 1994, Ringertz 1993), as this will imply that the positivity constraint on the bar volumes will be satisfied automatically. Problem (4.43) does not lend itself to the use of sparse techniques, as the Hessian of the objective function $\Phi(t)$ is full. However, the Hessian of the constraint $\sum_{i=1}^{m} t_i \hat{\mathbf{K}}_i u = \mathbf{f}$ is sparse. Sparsity can thus be utilized if the problem (4.5) in both the displacement and design variables is solved using an interior point method. Even though the latter problem is not convex, finding a stationary solution provides also a stationary point for problem (4.43), and thus a minimizer for this convex problem (Ringertz 1993). This approach extends readily to all the problem types described above. The use of an interior barrier method for problem (4.43) involves the use of a suitable sequence of penalty parameters, which in effect corresponds to imposing a constraint of the type $t_i \geq t_{\min} > 0$, $i = 1, \ldots, m$ for a suitable small lower bound value $t_{\min}$. This can make it troublesome to identify precisely which bars are active in the optimal topology. However, convergence of the designs (and relevant displacements) as we take the limit $t_{\min} \to 0$ is guaranteed, see Achtziger (1998).

For the worst-case multiple load problem (4.4), formulated as a smooth problem using a bound formulation with bounding variable α, a possible logarithmic barrier function is of the form

$$\min_{\mathbf{t},\alpha} \left\{ -\sum_{k=1}^{M} \ln(\alpha - \mathbf{f}^{k^T} \left[\sum_{i=1}^{m} t_i \hat{\mathbf{K}}_i \right]^{-1} \mathbf{f}^k) - \sum_{i=1}^{m} \ln(t_i) - \ln(\alpha_{\max} - \alpha) \right\}$$

where $\alpha_{\max}$ is a suitable guaranteed upper bound on the optimal value of the problem. Further details on the use of such interior point methods can be found in for example Ben-Tal & Nemirovski (1994). We also note that the SDP variations of the topology design problem (cf., (4.20) and (4.21)) can be solved by algorithms developed for such problems [33]; such techniques have many common features with the logarithmic barrier approach just outlined.

Methods working with displacements Barrier function methods and especially the so-called "Penalty/Barrier/Multiplier (PBM) Method" can also to great advantage be used for the displacements only formulations of the form (4.24) [33]. This type of algorithms are described briefly in appendix 5.5.

In order to apply the PBM method to for example the min-max multiple load truss topology design problem, the formulation (4.33) is used in a form where the discrete maximization over bar numbers is removed by a bound formulation

$$\begin{aligned} &\inf_{\substack{\lambda^k>0,\,\mathbf{u}^k,\,\tau \\ \sum_{k=1}^M \lambda^k=1}} \left\{ V_\tau - \sum_{k=1}^M \mathbf{f}^{k^T}\mathbf{u}^k \right\} \\ &\quad \text{s.t.} \quad \sum_{k=1}^M \frac{1}{2\lambda^k}\mathbf{u}^{k^T}\mathbf{K}_i\mathbf{u}^k - \tau \le 0, \quad i = 1,\ldots,m \end{aligned} \tag{4.44}$$

Note that (4.44) is a smooth convex optimization problem. It can be shown from the Karush-Kuhn-Tucker conditions of problem (4.44) that the Lagrange multipliers for the constraints on the specific energies are precisely the optimal volumes of the bars in the optimal topology. Hence the optimal bar volumes are approximated directly at each iteration step of the PBM method by the Lagrange multipliers for these constraints. Notice that a further reformulation is handy, namely the formulation

$$\begin{aligned} &\inf_{\substack{s^k,\,\mathbf{x}^k,\,\tau \\ \sum_{k=1}^M (s^k)^2=1}} \left\{ V_\tau - \sum_{k=1}^M s^k\, \mathbf{f}^{k^T}\mathbf{x}^k \right\} \\ &\quad \text{s.t.} \quad \sum_{k=1}^M \mathbf{x}^{k^T}\mathbf{A}_i\, \mathbf{x}^k - 2\tau \le 0, \quad i = 1, \quad ,m \end{aligned} \tag{4.45}$$

which is derived from (4.44) by the transformation $s^k = \sqrt{\lambda^k}$, $\mathbf{x}^k = \mathbf{u}^k/\sqrt{\lambda^k}$ of variables.

For a truss with N degrees of freedom, m potential bars and M load cases, the single load problem (4.29) has N variables and m constraints, while problem (4.45) has $NM + M + 1$ variables and m non-linear constraints. The main computational effort in applying the PBM method is the minimization of the unconstrained penalty/barrier function. This is done using a Newton method, and it is interesting to note that the method does not require an increase in the number of Newton steps as the problem size increases[3] Note that each Newton step corresponds to solving a linear system of equations, which for the single load case is comparable in size to the linear system solved for one full equilibrium analysis step of the "Optimality Criteria Method"

4.3.4 Examples

We have throughout this chapter illustrated some of the features of truss topology design. The main purpose is to illustrate the effect of various modelling choices on the geometry of the lay-outs. Space does not permit an exhaustive discussion on this subject, as many features influence the final

[3] Experiments have shown that up to 70 steps are sufficient for 6 digits of accuracy of the objective function for problems with for example 3 load cases, $m = 16290$ and $N = 458$ [33].

designs, such as the choice of nodal points as well as the geometry and connectivities of the ground structure, the geometry of the loads, the geometry of the supports, etc. Many more examples of large scale truss topology optimization can be found in the literature [32], [33].

For the truss topology problem with a single load case it is possible to generate a catalogue of optimal topologies. Problem (4.1) is made up of expressions that are element wise linear in all variables, except geometric data. Thus, for a specific choice of ground structure geometry and load vector direction, the optimal topology needs only to be computed for one set of assigned values of Young's modulus E, volume V, load size, and one geometric scale; for any other values of these variables, the optimal values of the design variables $\mathbf{t}$, the deformation $\mathbf{u}$, and the compliance $\mathbf{f}^T\mathbf{u}$ can be derived by a simple scaling; the non dimensional parameter

$$\Phi = \frac{(\mathbf{f}^T\mathbf{u})VE}{\|\mathbf{f}\|^2 L^2}$$

is a constant for optimal topologies generated with equivalent topologies of the ground structure, with L being a measure of scale. A similar non-dimensional parameter can be devised for the multiple load case, the case of self-weight loads, etc., but here the catalogue will depend on a further range of parameters, such as the ratios between the sizes of the different applied loads.

A very important feature of the truss topology method is the prediction of Michell frame type lay-outs in certain cases, if such a structure is natures best topology with the given loads, supports and ground structure, as illustrated in Fig. 4.2. This illustrates the varied topologies that can be created for the simple problem of transmitting a single vertical load to a vertical line of supports, through ground structures of rectangular lay-out of different aspect ratios. The range of topologies goes from the optimal two-bar truss with two bars at $\pm 45^o$ to long slender Michell frame lay-outs which at a global scale behaves like a sandwich beam in bending. The transition from "true" trusses to Michell truss continua for this setting has been studied by analytical means in Lewiński, Zhou & Rozvany (1993). Note that we in these examples (as in all cases) clearly see that the topology optimization not only predicts the optimal lay-out of the structures, but also finds the optimal use of the prescribed possible support conditions.

It was mentioned earlier that truss topology compliance optimization under a single load condition leads to statically determinate solutions, but the resultant structures are more often than not mechanisms, which are stable under the applied load. This unfortunate feature can in most cases be avoided by designing the truss for multiple load cases, either in the weighted average formulation or in the worst case, min-max formulation. Figure 4.6 shows that it is important to consider multiple load situations and Fig. 4.4 shows the difference between treating three nodal loads as one, combined load, or as

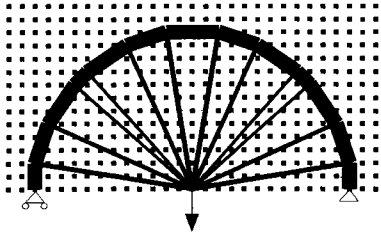

Fig. 4.8. A detailed study of the design of a wheel with a 29 by 15 nodal lay-out with all 57770 possible non-overlapping connections. Compare with Fig. 3.10 (from Bendsøe, Ben-Tal & Zowe 1994).

three independent load cases. Note that we through the multiple load formulation avoid the mechanisms, at the expense of much more complicated topologies. In Fig. 4.5 we show, for a similar load and support condition in a different ground structure the (small) difference between multiple load designs achieved through the weighted average formulation and the min-max formulation. It should be noted that multiple load conditions can also simplify the lay-out of the optimal topology. In all examples with multiple load, worst case design, the nature of the applied loads is here such that all loads have compliance value at the maximal value. This is usually not the case for problems where the optimal structure for one of the applied loads can carry the other loads.

4.4 Extensions of truss topology design

4.4.1 Combined truss topology and geometry optimization

The topology design methods considered so far all employ the basic idea of a ground structure or reference design domain to obtain problem statements that are sizing problems for a fixed geometry. The choice of this reference geometry influences the result of the topology optimization making it important to consider sensitivity analysis of the optimal designs with respect to variation of the reference geometry, and even optimal design of this reference geometry may be fruitful in some situations.

In the ground structure approach to topology design of trusses the positions of nodal points are not used as design variables. This means that a high number of nodal points should be used in the ground structure to obtain efficient topologies. A drawback of the method is that the optimal topologies can be very sensitive to the layout of nodal points, at least if the number of nodal points is relatively low. This makes it natural to consider an extension of the ground structure approach and to include the optimization of the nodal point

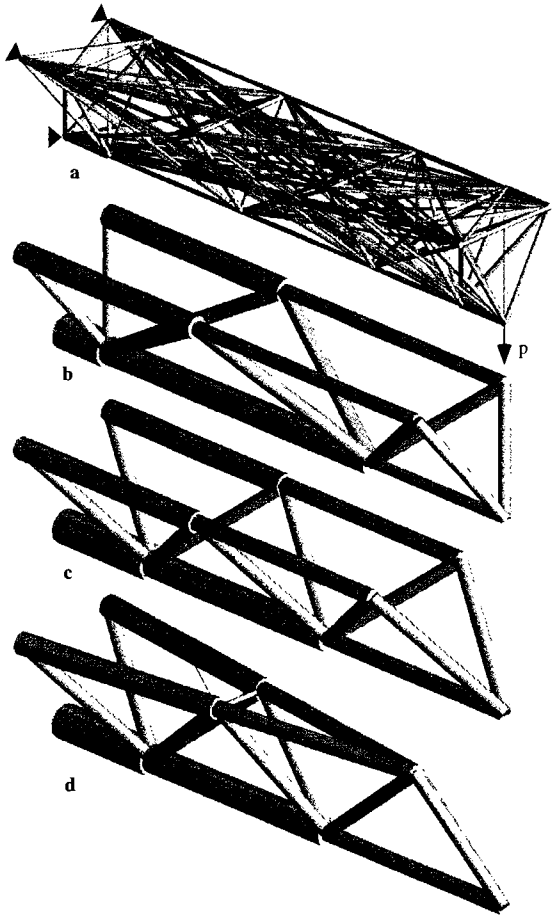

Fig. 4.9. An example of a 3-D topology and geometry optimization for a beam carrying a single load. In a) we show the ground structure of nodal points and potential bars. Note that the ground structure has non-equidistant nodal point positions along the length axis of the "beam" In a) we see the optimal topology for the fixed nodal lay-out of the ground structure, in c) a combined geometry and topology optimization with nodal positions restricted to move along the length axis of the 'beam" Finally, in d) the result of a combined geometry and topology optimization with totally free nodal positions is shown. The (non-dimensional) compliance values of the optimized designs are 1.00, 0.945 and 0.911, respectively (from Bendsøe, Ben-Tal & Zowe 1994).

location for a given number and connectivity of nodal points [32]. With very efficient tools at hand for the topology design with fixed nodal positions it seems natural to treat the variation of nodal positions as an outer optimization in a two-level hierarchical formulation. As the optimal value function of the topology compliance depends on the geometry variables in a non-smooth way, this outer minimization requires non-smooth optimization techniques.

For the combined topology and geometry problem for trusses we have as the simplest formulation

$$\begin{aligned} &\min_{\mathbf{u},\mathbf{a},\mathbf{x}} \ \mathbf{f}^T\mathbf{u} \\ &\text{s.t.} \ \sum_{i=1}^{m} a_i l_i(\mathbf{x})\mathbf{K}_i(\mathbf{x})\mathbf{u} = \mathbf{f} \\ &\qquad \sum_{i=1}^{m} a_i l_i(\mathbf{x}) = V, \quad a_i \geq 0, \ i = 1,\ldots,m \\ &\qquad \bar{x}_j^k \leq x_j^k \leq \hat{x}_j^k, \ j = 1, \quad ,n, \ k = 1,2,(3) \end{aligned} \tag{4.46}$$

which is just problem (4.5) rewritten as a problem depending also on the nodal positions $\mathbf{x}_j$, $j = 1,\ldots,n$. The nodal positions are restricted to lie within certain bounds that should be chosen to make the resultant trusses realizable. As the member volumes are dependent on the nodal positions we have here reverted to the cross-sectional areas of the individual bars as design variables. Problem (4.46) can be solved as a unified problem considering the problem either as a unified analysis and design problem or as a standard structural optimization problem that can be solved through an adjoint method in the areas and nodal positions only (this requires the application of small lower bounds on the cross sectional areas). An alternative solution procedure is to apply a multilevel approach to the combined problem, treating the topology problem as the inner problem. Because of the size of the topology problem, earlier work has usually involved some form of heuristics to speed up the very significant amount of computations involved [32]. Here we consider combining the effective truss topology design methods described earlier with appropriate tools from non-smooth analysis.

For a fixed set of nodal positions we choose here the displacements only form (4.24) of the topology design problem (without self-weight) and thus write (4.46) as a two-level problem

$$\min_{\substack{\mathbf{x} \\ \bar{\mathbf{x}} \leq \mathbf{x} \leq \hat{\mathbf{x}}}} \left(-\min_{\mathbf{u}} \left[\max_{i=1,\ldots,m} \left\{ \frac{V}{2}\mathbf{u}^T\mathbf{K}_i(\mathbf{x})\mathbf{u} - \mathbf{f}^T\mathbf{u} \right\} \right] \right) \tag{4.47}$$

The inner topology problem in the displacements $\mathbf{u}$ can effectively be solved (for fixed $\mathbf{x}$) by one of the computational methods described in Sect. 4.3. The main part remaining is then, of course, the minimization of the so-called master function

$$\mathcal{F}(\mathbf{x}) = -\min_{\mathbf{u}} \left[\max_{i=1,\ldots,m} \left\{ \frac{V}{2} \mathbf{u}^T \mathbf{A}_i(\mathbf{x}) \mathbf{u} - \mathbf{f}^T \mathbf{u} \right\} \right]$$

on the outer level. The number of variables (the nodal positions) in this outer problem will usually be moderate. However, there are two decisive drawbacks. There is no reason for $\mathcal{F}$ to be convex and $\mathcal{F}$ is not differentiable everywhere. Hence we cannot expect to find more than a local minimum of $\mathcal{F}$ and we have to work with codes from non-smooth optimization (e.g., bundle methods (Schramm & Zowe 1992)). These codes require that for each iterate $\mathbf{x}$ we can compute a so-called sub-gradient as a substitute for the gradient. Using tools from non-smooth calculus it is easily seen that this causes no difficulties for the above min-max function $\mathcal{F}$ We add that it is straightforward to show that each local minimizer $\mathbf{x}^*$ of $\mathcal{F}$ together with the associated $\mathbf{t}^*$ and $\mathbf{u}^*$ which solve the topology problem for the fixed nodal positions $\mathbf{x}^*$, gives a local minimizer $[\mathbf{u}^*, \mathbf{a}^*, \mathbf{x}^*]$ (with $a_i^* = t_i^*/l_i(\mathbf{x}^*)$) for problem (4.47).

The two-level approach becomes especially attractive if we consider the single load truss topology problem for which the member stiffness matrices are dyadic products. Then $\mathcal{F}(\mathbf{x})$ reduces to a parametrized linear programming problem (cf., problem (4.30))

$$\mathcal{F}(\mathbf{x}) = \max_{\mathbf{u}} \left\{ \mathbf{f}^T \mathbf{u} \,\middle|\, -1 \le \sqrt{\frac{VE_i}{2}} \frac{\mathbf{b}_i(\mathbf{x})^T \mathbf{u}}{l_i(\mathbf{x})} \le 1, \quad i = 1, \ldots, m \right\}$$

The sub-gradient in this case is basically the derivative with respect to $\mathbf{x}$ of the Lagrange function for this LP-problem. Hence we get a sub-gradient "for free" when solving (4.30) for a given set of nodal positions $\mathbf{x}$. For details we refer to Ben-Tal, Kocvara & Zowe (1993).

4.4.2 Truss design with buckling constraints

In this section[4]we formulate a problem of optimum truss topology design including a constraint on the *global stability* of the structure. We use here the so-called *linear buckling model* as the model of stability. This means that we can express the stability condition as the condition $\mathbf{K}(\mathbf{t}) + \mathbf{G}(\mathbf{u}, \mathbf{t}) \succeq \mathbf{0}$, where $\mathbf{u}$ solves the small-deflection equilibrium equation $\mathbf{K}(\mathbf{t})\mathbf{u} = \mathbf{f}$ and where $\mathbf{G}$ is the standard *geometric matrix* of the truss. Note that *local* buckling constraints require a separate treatment, see Sect. 4.4.4.

Now we can add this stability constraint to the compliance constrained minimum weight truss topology problem to obtain a problem of the form

$$\begin{aligned} \min_{\mathbf{t},\mathbf{u}} \; & \sum_{i=1}^{m} t_i \\ \text{s.t.} \quad & \mathbf{K}(\mathbf{t})\mathbf{u} = \mathbf{f}, \quad \mathbf{f}^T \mathbf{u} \le \tilde{\Phi} \\ & \mathbf{K}(\mathbf{t}) + \mathbf{G}(\mathbf{u}, \mathbf{t}) \succeq \mathbf{0}, \quad t_i \ge 0,, \; i = 1, \quad ,m \end{aligned} \tag{4.48}$$

[4] This and the following section is based on material kindly provided to us by M. Kocvara.

Here $\tilde{\Phi}$ is the given maximal value of the compliance, as in (4.22). Note that we can always find a feasible pair $(\mathbf{t}, \mathbf{u})$ to (4.48), as one can always make the truss stable and also stiff enough by adding enough material to each member (in this sense compliance and stability are not competing objectives).

We have in Sect. 4.2.2 seen that one can use a linear matrix inequality to eliminate the displacement vector from an equilibrium equation that is combined with a compliance constraint. We also here rewrite (4.48) using this idea and arrive at new problem in the variable $\mathbf{t}$ only:

$$\begin{aligned} &\inf_{\mathbf{t}>0} \sum_{i=1}^{m} t_i \\ &\text{s.t.} \quad \widetilde{\mathbf{A}}(\mathbf{t}, \tilde{\Phi}) \succeq \mathbf{0}, \quad \mathbf{A}(\mathbf{t}) + \widetilde{\mathbf{G}}(\mathbf{t}) \succeq \mathbf{0} \\ &\qquad t_i \geq 0, \; i = 1, \ldots, m \end{aligned} \tag{4.49}$$

where $\widetilde{\mathbf{A}}$ is defined in (4.19) and where $\widetilde{\mathbf{G}}(\mathbf{t}) = \mathbf{G}(\mathbf{K}(\mathbf{t})^{-1}\mathbf{f}, \mathbf{t})$. This problem is, due to the buckling constraint, not a standard convex SDP. However, it can still be solved efficiently by a non-convex version of a PBM algorithm for SDP problems (details can be found in Ben-Tal, Jarre, Kocvara, Nemirovski & Zowe (2000), Kocvara (2002)).

An example of what can be achieved with this formulation is illustrated in Fig. 4.10. Here the initial design has $t_i = 1000/m$, $i = 1, \ldots, m$, with a corresponding compliance of 0.177 and a critical force (0.397) that is smaller than one, meaning that the truss is unstable. The standard truss optimization without stability constraint gives a design that is twice as light as the previous one but absolutely unstable. Finally, by truss optimization with stability constraint one can obtain a design that at a volume of 1179.6 is a bit heavier than the first one. However, it is stable under the given load. To see fully the effect of the stability constraint, we have for this example chosen the upper bound for the compliance so that the compliance constraint is not active. For truss (and frame) models *local* buckling of the individual members is also an important aspect to take into consideration

4.4.3 Control of free vibrations

The SDP approach from the previous section can easily be adapted to optimization of trusses with constraints on the free vibration frequencies [33]. Here we formulate the problem of minimizing the weight (volume) of a truss subject to a compliance constraint and such that the lowest eigenfrequency is bigger than or equal to a prescribed value. This latter condition is written as

$$\lambda_i \geq \overline{\lambda}, \qquad i = 1, \ldots, n, \tag{4.50}$$

where λ_i are the eigenvalues of the problem $(\mathbf{K}(\mathbf{t}) - \lambda \mathbf{M}(\mathbf{t}))\mathbf{u} = 0$. Here $\mathbf{M}(\mathbf{t}) = \mathbf{M}_s(\mathbf{t}) + \mathbf{M}_0$ is the mass matrix of the truss; $\mathbf{M}_0$ is the part corre-

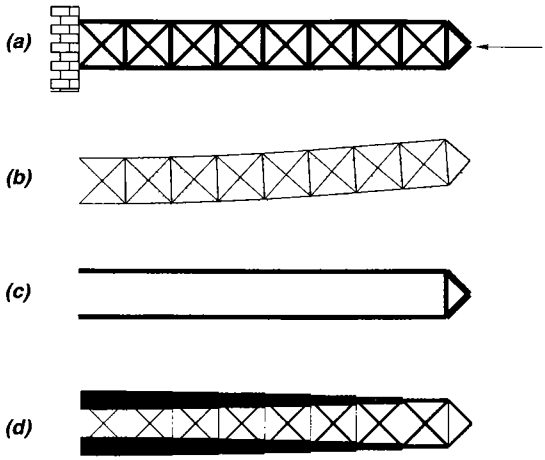

Fig. 4.10. The effect of a constraint on the global buckling load. a) shows the initial truss with its buckling mode in b). c) is the optimal truss without stability constraint and, d) is the optimal truss with a stability constraint. By courtesy of M. Kocvara.

sponding to non-structural mass and the (lumped) structural mass matrix is denoted by $\mathbf{M}_s(\mathbf{t})$.

The condition (4.50) can be written as a matrix inequality $\mathbf{K} - \overline{\lambda}\mathbf{M} \succeq 0$, and, in parallel to problem (4.49), a minimum weight truss design problem with free vibration constraints can be formulated as follows (see also Ohsaki, Fujisawa, Katoh & Kanno (1999)):

$$\begin{aligned} &\min_{\mathbf{t}\geq\mathbf{0}} \sum_{i=1}^{m} t_i \\ &\text{s.t.} \quad \mathbf{K}(\mathbf{t}) - \overline{\lambda}\mathbf{M}(\mathbf{t}) \succeq 0, \quad \widetilde{\mathbf{A}}(\mathbf{t}, \widetilde{\Phi}) \succeq \mathbf{0} \end{aligned} \tag{4.51}$$

This problem includes only linear matrix inequalities (the mass matrix does not depend on $\mathbf{u}$) and is then much easier to solve than the stability problem (4.49). However, note that, in contrast to the stability problem, we may now have problems with feasibility. When $\overline{\lambda}$ is too big one may not be able to find any design $\mathbf{t}$ satisfying the vibration constraint; both of the matrices $\mathbf{A}(\mathbf{t})$ and $\mathbf{M}(\mathbf{t})$ are positive semidefinite and their eigenvalues grow with the same rate for increasing $\mathbf{t}$.

Note that the formulation (4.51) avoids the technicalities of a formulation that directly and explicitly involves the eigenvalues. The non-differentiability

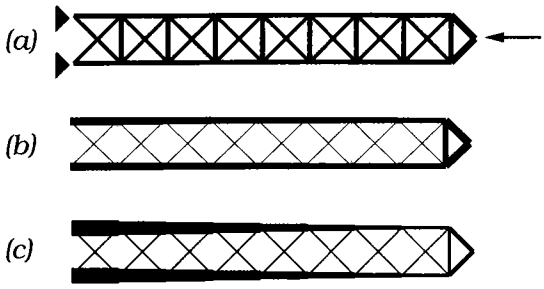

Fig. 4.11. Initial truss (a) and two optimal trusses with respect to free vibration constraint with $\overline{\lambda} = 5.0 \cdot 10^{-5}$ (b) and $\overline{\lambda} = 1.0 \cdot 10^{-4}$ (c). By courtesy of M. Kocvara.

of eigenvalues is circumvented by the application of interior point methods to the matrix-inequality constraint.

As an example we consider again a slender truss fixed on the left-hand side and subject to axial force on the right-hand side; there is a non-structural mass 1.0 at the column tip. The lowest eigenfrequency corresponding to the truss shown in Figure 4.11(a) is $\lambda_{\min} = 5.0 \cdot 10^{-5}$, while $\lambda_{\min}$ corresponding to the optimal truss without vibration constraint is zero (the truss is a mechanism, cf., Fig. 4.10c). If we solve (4.51) with $\overline{\lambda} = 5.0 \cdot 10^{-5}$, the resulting truss weighs 0.5684 (see Figure 4.11(b)). When we try to increase the minimum eigenvalue, setting $\overline{\lambda} = 1.0 \quad 10^{-4}$, we get the truss shown in Figure 4.11(c) that weighs 0.8746.

4.4.4 Variations of the theme

Stress and local buckling constraints The original problem (4.1) can be generalized in a number of ways to cover also local stress and buckling constraints for the truss member. If all members are made of the same material and have the same cross-sectional geometry we can formulate a minimum weight design problem where we include constraints on compliance, displacements, element stresses, slenderness, and local buckling, given by data $\tilde{\Phi}$, $\mathbf{u}_{\min}, \mathbf{u}_{\max}$, $\bar{\sigma}$, $a_{\min}$, and $\bar{s}$, respectively:

$$
\begin{aligned}
\min_{\mathbf{a},\mathbf{q},\mathbf{u}} \quad & \sum_{i=1}^{m} a_i l_i \\
\text{s.t.} \quad & \mathbf{B}\mathbf{q} = \mathbf{f} \\
& q_i = \frac{E}{l_i} a_i \mathbf{b}_i^T \mathbf{u}, \; i = 1, \ldots, m \\
& \mathbf{f}^T \mathbf{u} \leq \tilde{\Phi} \\
& \mathbf{u}_{\min} \leq \mathbf{u} \leq \mathbf{u}_{\max} \\
& -a_i \bar{\sigma} \leq q_i \leq a_i \bar{\sigma}, \; i = 1, \ldots, m \\
& a_i^2 \geq a_{\min} a_i, \; i = 1, \ldots, m \\
& q_i \geq \frac{\bar{s}}{l_i^2} a_i^2, \; i = 1, \ldots, m \\
& 0 \leq a_i \leq a_{\max}, \; i = 1, \ldots, m
\end{aligned}
\tag{4.52}
$$

Here the constraints on stress, slenderness, and buckling should only be enforced if $a_i \neq 0$, but this "unpleasant twist" is easily circumvented here by multiplying the relevant constraints by a_i. Thus the stress and buckling constraints are written in terms of member *forces* rather than member *stresses*.

If kinematic considerations are ignored, simplex like algorithms can be used to generate solutions that operate only with statically determinate designs [32]. In the general situation the same "singularity" problems as noted for the stress constrained continuum problem arises; the techniques outlined in Sect. 2.3 should then be applied here also. However, for a proper model of the local buckling one should take into account the effect of "chains" By this we mean straight connections of several bars, where inner nodes are not connected to any other bars. Such chains appear in most truss topology results. For such chains, the buckling constraint should be evaluated with a different length than the (short) individual bar lengths. This is tricky to formulate and even more tricky to solve – here the perturbation technique for stress constraints does not work (Achtziger 2000) [33].

Discrete optimization In this chapter we have used that the area of a truss bar can be used as a continuous variable for defining the truss topology problem. This means that we accept any cross-sectional area. In may practical situation this is not possible and one would, for example, require that we only can work with discrete values, for example $a_i \in \{0, 1\}$ (in this case problem (4.52) without the slenderness constraint can be written as a mixed, linear 0-1 program, see Stolpe & Svanberg (2002)). An even more complicated situation arises if the design optimization also has to cater for the use of different standard sections, as constraints may then change *form* with the variables (as for buckling) and there is no method to interpolate between the design variables. Thus one is here forced to use algorithms for discrete optimization in their most general form [33].

5 Appendices

5.1 Appendix: Matlab codes

Despite of the apparent complexity of the topology optimization method it can actually be programmed in surprisingly few lines of code. For example, if using a high level programming language like Matlab, the code for solving the basic compliance minimization problem discussed in Chap. 1 may be written in only 99 lines (Sigmund 2001a). In this appendix we first discuss the Matlab implementation of the minimum compliance problem in some detail (based on Sigmund (2001a)). Afterwards, we briefly discuss the extensions of the code to a 105-line compliant mechanism synthesis code and a 91-line code for topology optimization of conductivity problems.

The big advantage of Matlab is that codes can be written very compactly and that, when programming more complex problems, one has direct access to a large number of built-in routines like eigenvalue solvers, complex solvers, optimization routines and graphics libraries. However, this versatility and userfriendliness is obtained on the cost of decreased computational speed. Our experience is that Matlab can be up to five times slower than a low-level programming language like Fortran77 Therefore, Matlab is good for educational purposes and for testing of ideas, but when it comes to practical problems involving tens or hundreds of thousands of elements, one has to program the codes in lower level languages.

5.1.1 A 99 line topology optimization code for compliance minimization

This appendix shows how the code for solving linear compliance minimization problems discussed in Chapter 1 can be written in just 99 lines of Matlab code including optimizer and Finite Element subroutine. The 99 lines are divided into 36 lines for the main program, 12 lines for the Optimality Criteria based optimizer, 16 lines for a mesh-independency filter and 35 lines for the finite element code. In fact, excluding comment lines and lines associated with output and finite element analysis, it is shown that only 49 Matlab input lines are required for solving a well-posed topology optimization problem. By adding three additional lines, the program can solve problems with multiple

load cases. The Matlab code is given in Sec. 5.1.4 and can be down-loaded from the web-site `http://www.topopt.dtu.dk`.[1] Note that the code has been optimized for speed compared to the original code presented in Sigmund (2001a).

5.1.2 Matlab implementation

The Matlab code, is built up as a standard topology optimization code (c.f. Sec 1.2.2 and Fig. 1.5). The main program is called from the Matlab prompt by the line

```
top(nelx,nely,volfrac,penal,rmin)
```

where `nelx` and `nely` are the number of elements in the horizontal and vertical directions, respectively, `volfrac` is the volume fraction, `penal` is the penalization power and `rmin` is the filter size (divided by element size). Other variables as well as boundary conditions are defined in the Matlab code itself and can be edited if needed. For each iteration in the topology optimization loop, the code generates a picture of the current density distribution. Figure 5.1 shows the resulting density distribution obtained by the code when called with the input line

```
top(60,20,0.5,3.0,1.5)
```

The default boundary conditions correspond to half of the 'MBB-beam' (Fig. 5.1). The load is applied vertically in the upper left corner and there is symmetric boundary conditions along the left edge and the structure is supported horizontally in the lower right corner.

Important details of the Matlab code are discussed in the following subsections.

Main program (lines 1–36) The main program (lines 1–36) starts by distributing the material evenly in the design domain (line 4). After some other initializations, the main loop starts with a call to the Finite Element subroutine (line 12) which returns the displacement vector `U`. Since the element stiffness matrix for solid material is the same for all elements, the element stiffness matrix subroutine is called only once (line 14). Following this, a loop over all elements (lines 16–24) determines objective function and sensitivities (1.17). The variables `n1` and `n2` denote upper left and right element node numbers in global node numbers and are used to extract the element displacement vector `Ue` from the global displacement vector `U`. The sensitivity analysis is followed by a call to the mesh-independency filter (line 26) and the Optimality Criteria optimizer (line 28). The current compliance as well as other parameters are printed by lines 30–33 and the resulting density

[1] In the period October 1999 to May 2002, the code has been downloaded by 1230 distinct users.

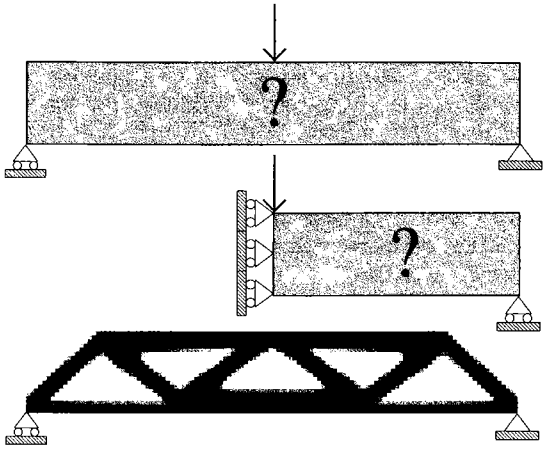

Fig. 5.1. Topology optimization of the MBB-beam. Top: full design domain, middle: half design domain with symmetry boundary conditions and bottom: resulting topology optimized beam (both halves).

distribution is plotted (line 35). The main loop is terminated if the change in design variables (`change` determined in line 30) is less than 1 percent[2] Otherwise above steps are repeated.

Optimality Criteria based optimizer (lines 37–48) The updated design variables are found by the optimizer (lines 37–48). Knowing that the material volume (`sum(sum(xnew))`) is a monotonously decreasing function of the Lagrange multiplier (`lag`), the value of the Lagrangian multiplier that satisfies the volume constraint can be found by a bi-sectioning algorithm (lines 40-48). The bi-sectioning algorithm is initialized by guessing a lower `l1` and an upper `l2` bound for the Lagrangian multiplier (line 39). The interval which bounds the Lagrangian multiplier is repeatedly halved until its size is less than the convergence criteria (line 40).

Mesh-independency filtering (lines 49–64) Lines 49–64 represent the Matlab implementation of Eq. (1.27). Note that not all elements in the design domain are searched in order to find the elements that lie within the radius `rmin` but only those within a square with side lengths two times `round(rmin)` around the considered element. By selecting `rmin` less than one in the call of the routine, the filtered sensitivities will be equal to the original sensitivities making the filter inactive.

[2] This is a rather 'sloppy' convergence criterion and could be decreased if needed

Finite Element code (lines 65–99) The finite Element code is written in lines 65–99. Note that the solver makes use of the sparse option in Matlab. The global stiffness matrix is formed by a loop over all elements (lines 70–77). As was the case in the main program, variables `n1` and `n2` denote upper left and right element node numbers in global node numbers and are used to insert the element stiffness matrix at the right places in the global stiffness matrix.

As mentioned before, both nodes and element are numbered column wise from left to right. Furthermore, each node has two degrees of freedom (horizontal and vertical), thus the command `F(2,1)=-1.` (line 79) applies a vertical unit force force in the upper left corner.

Supports are implemented by eliminating fixed degrees of freedom from the linear equations. Matlab can do this very elegantly with the line

```
84 U(freedofs,:)   K(freedofs,freedofs) \ F(freedofs,:);
```

where `freedofs` indicate the degrees of freedom which are unconstrained. Mostly, it is easier to define the degrees of freedom that are fixed (`fixeddofs`) thereafter the `freedofs` are found automatically using the Matlab operator `setdiff` which finds the free degrees of freedoms as the difference between all degrees of freedom and the fixed degrees of freedom (line 82).

The element stiffness matrix is calculated in lines 86–99. The 8 by 8 matrix for a square bi-linear 4-node element was determined analytically using a symbolic manipulation software. The Young's modulus `E` and the Poisson's ratio `nu` can be altered in lines 88 and 89.

5.1.3 Extensions

The default Matlab code solves the problem of optimizing the material distribution in the MBB-beam (Fig. 5.1) such that its compliance is minimized. A number of extensions and changes in the algorithm can be thought of, a few of which are mentioned in the following.

Other boundary conditions It is very simple to change boundary conditions and support conditions in order to solve other optimization problems. In order to solve the short cantilever example shown in Fig. 5.2, only lines 79 and 80 must be changed to

```
79 F(2*(nelx+1)*(nely+1),1)   -1;
80 fixeddofs      [1:2*(nely+1)];
```

With these changes, the input line for the case shown in Fig. 5.2 is

```
top(32,20,0.4,3.0,1.2)
```

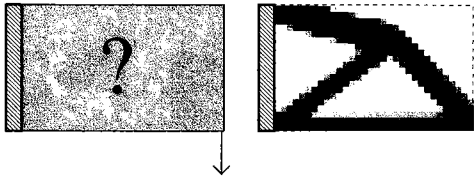

Fig. 5.2. Topology optimization of a cantilever beam. Left: design domain and right: topology optimized beam.

Multiple load cases It is also very simple to extend the algorithm to account for multiple load cases. In fact, this can be done by adding only three additional lines and making minor changes to another 4 lines.

In the case of two load cases, force and displacement vectors must be defined as two-column vectors which means that line 69 is changed to

```
69 F = sparse(2*(nely+1)*(nelx+1),2); U = sparse(2*(nely+1)*(nelx+1),2);
```

The objective function is now the sum of two compliances, i.e.

$$c(\mathbf{x}) = \sum_{i=1}^{2} \mathbf{u}_i^T \mathbf{K} \mathbf{u}_i \tag{5.1}$$

thus lines 20–22 are substituted with the lines

```
19b     dc(ely,elx)
19c     for i = 1:2
20        Ue = U([2*n1-1;2*n1; 2*n2-1;2*n2; 2*n2+1;2*n2+2;2*n1+1;2*n1+2],i);
21        c   c + x(ely,elx)^penal*Ue'*KE*Ue;
22        dc(ely,elx) = dc(ely,elx)   penal*x(ely,elx)^(penal-1)*Ue'*KE*Ue;
22b     end
```

To solve the two-load problem indicated in Fig. 5.3, a unit upward load in the top-right corner is added to line 79, which then becomes

```
79 F(2*(nelx+1)*(nely+1),1)        F(2*(nelx)*(nely+1)+2,2)
```

The input line for Fig. 5.3 is

```
top(30,30,0.4,3.0,1.2)
```

Passive elements In some cases, some of the elements may be required to take the minimum density value (e.g. a hole for a pipe).

An `nely×nelx` array `passive` with zeros at elements free to change and ones at elements fixed to be zero can be defined in the main program and transferred to the OC subroutine (adding `passive` to the call in lines 28 and 38). The added line

```
42b   xnew(find(passive))   0.001;
```

in the OC subroutine looks for passive elements and sets their density equal to the minimum density (0.001).

Figure 5.4 shows the resulting structure obtained with the input

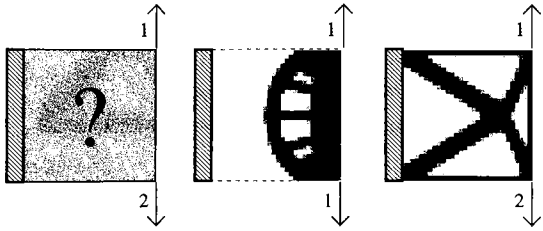

Fig. 5.3. Topology optimization of a cantilever beam with two load-cases. Left: design domain, middle: topology optimized beam using one load case and right: topology optimized beam using two load cases.

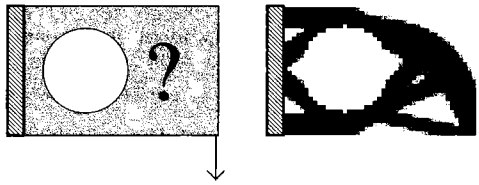

Fig. 5.4. Topology optimization of a cantilever beam with a fixed hole. Left: design domain and right: topology optimized beam.

```
top(45,30,0.5,3.0,1.5),
```

when the following 10 lines were added to the main program (after line 4) in order to find passive elements within a circle with radius `nely/3.` and center (`nely/2.`, `nelx/3.`)

```
for ely   1:nely
  for elx   1:nelx
    if sqrt((ely-nely/2.)^2+(elx-nelx/3.)^2) < nely/3.
      passive(ely,elx)   1;
      x(ely,elx)   0.001;
    else
      passive(ely,elx)   0;
    end
  end
end
```

The MMA optimizer Admittedly, the Optimality Criteria based optimizer implemented here is only good for a single constraint and it is based on a heuristic fixed point type updating scheme. In order to install a better optimizer, one can obtain (free of charge for academic purposes) the Matlab

version of the MMA-algorithm (Svanberg 1987) from Krister Svanberg, KTH, Sweden. The MMA code is called with the following input line

```
mmasub(INPUT-variables,        OUTPUT-variables)
```

where the total number of input/output variables is 20, including objective function, constraints, old and new densities, etc.. Implementing the MMA-optimizer is fairly simple, but requires the definition of several auxiliary variables. However, it allows for the solving of more complex design problems with more than one constraint. The Matlab optimizer will solve the standard topology optimization problem using less iterations at the cost of a slightly increased CPU-time pr. iteration.

5.1.4 Matlab code

The following is a transcript of the Matlab code that can be down-loaded from the web-site `http://www.topopt.dtu.dk`

```
%%%% A 99 LINE TOPOLOGY OPTIMIZATION CODE BY OLE SIGMUND, OCTOBER 1999 %%%
function top(nelx,nely,volfrac,penal,rmin);
% INITIALIZE
x(1:nely,1:nelx)
loop = 0;
change = 1.;
% START ITERATION
while change > 0.01
  loop = loop + 1;
  xold = x;
% FE-ANALYSIS
  [U]=FE(nelx,nely,x,penal);
% OBJECTIVE FUNCTION AND SENSITIVITY ANALYSIS
  [KE]   lk;
  c = 0.
  for ely = 1:nely
    for elx = 1:nelx
      n1   (nely+1)*(elx-1)+ely;
      n2 = (nely+1)* elx   +ely;
      Ue = U([2*n1-1;2*n1; 2*n2-1;2*n2; 2*n2+1;2*n2+2; 2*n1+1;2*n1+2],1);
      c = c + x(ely,elx)^penal*Ue'*KE*Ue;
      dc(ely,elx) = -penal*x(ely,elx)^(penal-1)*Ue'*KE*Ue;
    end
  end
% FILTERING OF SENSITIVITIES
  [dc]     check(nelx,nely,rmin,x,dc);
% DESIGN UPDATE BY THE DPTIMALITY CRITERIA METHOD
  [x]    = OC(nelx,nely,x,volfrac,dc);
% PRINT RESULTS
  change = max(max(abs(x-xold)));
  disp([' It.: ' sprintf('%4i',loop)   Obj.:   sprintf('%10.4f',
       ' Vol.:   sprintf('%6.3f',sum(sum(x))/(nelx*nely))
          ch.:   sprintf('%6.3f',change )])
% PLOT DENSITIES
  colormap(gray); imagesc(-x); axis equal; axis tight; axis off;pause(1e-6);
end
%%%%%%%%%% OPTIMALITY CRITERIA UPDATE %%%%%%%%%%%%%%%%%%
function [xnew]=OC(nelx,nely,x,volfrac,dc)
l1   0; l2   100000; move = 0.2;
while (l2-l1 > 1e-4)
  lmid = 0.5*(l2+l1);
  xnew = max(0.001,max(x-move,min(1.,min(x+move,x.*sqrt(-dc./lmid)))));
```

```
  if sum(sum(xnew))
    l1 = lmid;
  else
    l2 = lmid;
  end
end
%%%%%%%%%% MESH-INDEPENDENCY FILTER %%%%%%%%%%%%%%%%%%%%%%%%%%%%%%%%%%%%%%%%
function [dcn]=check(nelx,nely,rmin,x,dc)
dcn=zeros(nely,nelx);
for i = 1:nelx
  for j   1:nely
    sum=0.0;
    for k = max(i-floor(rmin),1):min(i+floor(rmin),nelx)
      for l = max(j-floor(rmin),1):min(j+floor(rmin),nely)
        fac = rmin-sqrt((i-k)^2+(j-l)^2);
        sum = sum+max(0,fac);
        dcn(j,i) = dcn(j,i) + max(0,fac)*x(l,k)*dc(l,k);
      end
    end
    dcn(j,i) = dcn(j,       ,i)*sum);
  end
end
%%%%%%%%%% FE-ANALYSIS %%%%%%%%%%%%%%%%%%%%%%%%%%%%%%%%%%%%%%%%%%%%%%%%%%%%%
function [U]=FE(nelx,nely,x,penal)
[KE] = lk;
K = sparse(2*(nelx+1)*(nely+1), 2*(nelx+1)*(nely+1));
F = sparse(2*(nely+1)*(nelx+1),1); U = sparse(2*(nely+1)*(nelx+1),1);
for elx = 1:nelx
  for ely = 1:nely
    n1 = (nely+1)*(elx-1)+ely;
    n2 = (nely+1)* elx   +ely;
    edof = [2*n1-1; 2*n1; 2*n2-1; 2*n2; 2*n2+1; 2*n2+2;
    K(edof,edof) = K(edof,edof) + x(ely,elx)^penal*KE;
  end
end
% DEFINE LOADS AND SUPPORTS (HALF MBB-BEAM)
F(2,1) = -1;
fixeddofs   = union([1:2:2*(nely+1)],[2*(nelx+1)*(nely+1)]);
alldofs       [1:2*(nely+1)*(nelx+1)];
freedofs    = setdiff(alldofs,fixeddofs);
% SOLVING
U(freedofs,:) = K(freedofs,freedofs) \ F(freedofs,:
U(fixeddofs,:)= 0;
%%%%%%%%%% ELEMENT STIFFNESS MATRIX %%%%%%%%%%%%%%%%%%%%%%%%%%%%%'
function [KE]=lk
E = 1.;
nu   0.3;
k=[ 1/2-nu/6   1/8+nu/8 -1/4-nu/12 -1/8+3*nu/8
   -1/4+nu/12 -1/8-nu/8  nu/6       1/8-3*nu/8];
KE = E/(1-nu^2)*[ k(1) k(2) k(3) k(4) k(5) k(6) k(7) k(8)
                  k(2) k(1) k(8) k(7) k(6) k(5) k(4) k(3)
                  k(3) k(8) k(1) k(6) k(7) k(4) k(5) k(2)
                  k(4) k(7) k(6) k(1) k(8) k(3) k(2) k(5)
                  k(5) k(6) k(7) k(8) k(1) k(2) k(3) k(4)
                  k(6) k(5) k(4) k(3) k(2) k(1) k(8) k(7)
                  k(7) k(4) k(5) k(2) k(3) k(8) k(1) k(6)
                  k(8) k(3) k(2) k(5) k(4) k(7) k(6) k(1)];
```

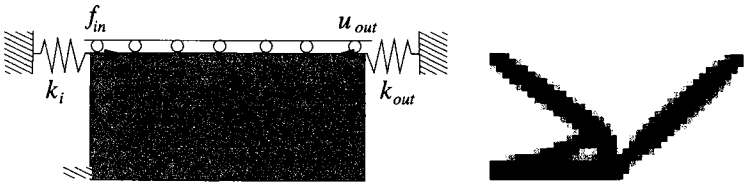

Fig. 5.5. Topology optimization of the inverter. Left: half design domain with symmetry boundary conditions and right: resulting topology.

5.1.5 A 105 line MATLAB code for compliant mechanism synthesis

The Matlab code for compliance minimization described in the previous section can be changed to a code for mechanism synthesis by changing 12 lines and adding 6 new lines of code.[3]

As the default problem, we consider the inverter design problem sketched in Fig. 5.5. The optimization problem for compliant mechanism synthesis was discussed in Sec 2.6. The solution obtained by running the modified code which is named 'topm' with the command line input

```
topm(40,20,0.3,3.0,1.2)
```

is seen in Fig. 5.5(right).

Instead of listing the whole program we just show a list of the changes. This list is obtained by comparing the compliance minimization program 'top.m' with the inverter design program 'topm.m' using the UNIX command 'diff top.m topm.m' This results in output where '<' means lines in 'top.m' and '>' means lines in 'topm.m' In the following we briefly discuss the changes.

First we rename the code from 'top' to 'topm'

```
1,2c1,2
< %%%% A 99 LINE TOPOLOGY OPTIMIZATION CODE BY OLE SIGMUND, OCTOBER 1999 %%%
< function top(nelx,nely,volfrac,penal,rmin);

> %%%% A 105 LINE COMPLIANT MECHANISM DESIGN CODE BY OLE SIGMUND, MAY 2002 %%%
> function topm(nelx,nely,volfrac,penal,rmin);
```

The expression for the sensitivities (2.23) depend on the solution to the adjoint load case (second column of the displacement matrix U)

```
20,22c20,23
<       Ue = U([2*n1-1;2*n1; 2*n2-1;2*n2; 2*n2+1;2*n2+2; 2*n1+1;2*n1+2],1);
<       c = c + x(ely,elx)^penal*Ue'*KE*Ue;
```

[3] Note that the code described uses linear analysis. Therefore, it can only be used to gain insight into compliant mechanism synthesis by topology optimization. For practical problems one should modify the code to include geometrically nonlinear modelling (c.f. Sec. 2.6.5).

```
        dc(ely,elx) = -penal*x(ely,elx)^(penal-1)*Ue'*KE*Ue;

>       Ue1   U([2*n1-1;2*n1; 2*n2-1;2*n2; 2*n2+1;2*n2+2; 2*n1+1;2*n1+2],1);
>       Ue2 = U([2*n1-1;2*n1; 2*n2-1;2*n2; 2*n2+1;2*n2+2; 2*n1+1;2*n1+2],2);
>       c = c + x(ely,elx)^penal*Ue2'*KE*Ue1;
>       dc(ely,elx) = penal*x(ely,elx)^(penal-1)*Ue2'*KE*Ue1;
39,40c40,41
```

We improve the convergence criteria for the bi-sectioning algorithm

```
< l1   0; l2 = 100000; move   0.2;
< while (l2-l1 > 1e-4)

> l1 = 0; l2 = 100000; move = 0.1;
> while (l2-l1)/(l2+l1) > 1e-4 & l2 > 1e-40
```

To stabilize convergence we use a damping factor of 0.3 instead of 0.5 and we take care of the possibility of positive sensitivities

```
42c43
<   xnew = max(0.001,max(x-move,min(1.,min(x+move,x.*sqrt(-dc./lmid)))));

>   xnew = max(0.001,max(x-move,min(1.,min(x+move,x.*(max(1e-10,-
69c70
```

We allocate force and displacement vectors for the real and the adjoint load cases

```
      sparse(2*(nely+1)*(nelx+1),1); U = sparse(2*(nely+1)*(nelx+1),1);

    = sparse(2*(nely+1)*(nelx+1),2); U   sparse(2*(nely+1)*(nelx+1),2);
```

Finally, we define the boundary conditions and the input and output points. Furthermore, we add external springs with stiffness 0.1 to the input and output points.

```
78,80c79,86
< % DEFINE LOADS AND SUPPORTS (HALF MBB-BEAM)
< F(2,1)    1;
< fixeddofs   = union([1:2:2*(nely+1)],[2*(nelx+1)*(nely+1)]);

> % DEFINE LOADS AND SUPPORTS (HALF FORCE INVERTER)
> din=1;
> dout=2*nelx*(nely+1)+1;
> F(din,1)   1;
> F(dout,2)    1;
> K(din,din) = K(din,din) + 0.1;
> K(dout,dout) = K(dout,dout) + 0.1,
> fixeddofs   = union([2:2*(nely+1):                    [2*(nely+1):-1:2*(nely+1)-3]);
```

5.1.6 A 91 line MATLAB code for heat conduction problems

This appendix discusses the modification of the original Matlab code for compliance minimization to heat conduction problems. The FE-solver solves the Laplace differential equation on a plane domain and the code may therefore also be used to model problems such as elastic torsion, electric conduction, magneto statics, potential flow, pressurized membranes and others by changing boundary conditions and loads.

The default problem is sketched in Fig. 5.6. We consider the distribution of two material phases with isotropic conductivities 1 and 0.001, respectively. The square plate is evenly heated (constant source term in all nodes) and

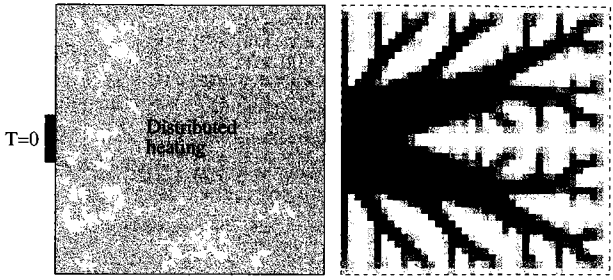

Fig. 5.6. Topology optimization of heat conduction problem. Left: half design domain with symmetry boundary conditions and right: resulting topology.

the center of the left edge is a heat sink, i.e. the temperature is set to zero. Figure 5.6(right) shows the results of running the code with the input line

```
toph(40,40,0.4,3.0,1.2)
```

Below we list the necessary changes to the Matlab code from Sec. 5.1.4 in order to convert it to a code for topology optimization of heat conduction problem. We leave it to the reader to interpret the changes.

```
20,22c20,22
<       Ue = U([2*n1-1;2*n1; 2*n2-1;2*n2; 2*n2+1;2*n2+2; 2*n1+1;2*n1+2],1);
<       c = c + x(ely,elx)^penal*Ue'*KE*Ue;
<       dc(ely,elx) = -penal*x(ely,elx)^(penal-1)*Ue'*KE*Ue;

>       Ue = U([n1; n2; n2+1; n1+1],1);
>       c = c + (0.001+0.999*x(ely,elx)^penal)*Ue'*KE*Ue;
>       dc(ely,elx) = -0.999*penal*x(ely,elx)^(penal-1)*Ue'*KE*Ue;
68,69c68,69
< K = sparse(2*(nelx+1)*(nely+1), 2*(nelx+1)*(nely+1));
< F = sparse(2*(nely+1)*(nelx+1),1); U = sparse(2*(nely+1)*(nelx+1),1);

> K   sparse((nelx+1)*(nely+1), (nelx+1)*(nely+1));
> F = sparse((nely+1)*(nelx+1),1); U = sparse((nely+1)*(nelx+1),1);
74,75c74,75
<     edof   [2*n1-1; 2*n1; 2*n2-1; 2*n2; 2*n2+1; 2*n2+2; 2*n1+1; 2*n1+2];
<     K(edof,edof) = K(edof,edof) + x(ely,elx)^penal*KE;

>     edof = [n1; n2; n2+1; n1+1];
>     K(edof,edof) = K(edof,edof) + (0.001+0.999*x(ely,elx)^penal)*KE;
78,81c78,81
< % DEFINE LOADS AND SUPPORTS (HALF MBB-BEAM)
< F(2,1) = -1;
< fixeddofs   = union([1:2:2*(nely+1)],[2*(nelx+1)*(nely+1)]);
< alldofs       [1:2*(nely+1)*(nelx+1)];

> % DEFINE LOADS AND SUPPORTS (SQUARE PLATE WITH HEAT SINK)
> F(:,1)   0.01;
> fixeddofs   = [nely/2+1-(nely/20):2:nely/2+1+(nely/20)];
> alldofs       [1:(nely+1)*(nelx+1)];
88,99c88,91
< E = 1.;
< nu = 0.3;
< k=[ 1/2-nu/6   1/8+nu/8 -1/4-nu/12 -1/8+3*nu/8 ...
```

```
<    -1/4+nu/12 -1/8-nu/8  nu/6       1/8-3*nu/8];
< KE = E/(1-nu^2)*[ k(1) k(2) k(3) k(4) k(5) k(6) k(7) k(8)
<                   k(2) k(1) k(8) k(7) k(6) k(5) k(4) k(3)
<                   k(3) k(8) k(1) k(6) k(7) k(4) k(5) k(2)
<                   k(4) k(7) k(6) k(1) k(8) k(3) k(2) k(5)
<                   k(5) k(6) k(7) k(8) k(1) k(2) k(3) k(4)
<                   k(6) k(5) k(4) k(3) k(2) k(1) k(8) k(7)
<                   k(7) k(4) k(5) k(2) k(3) k(8) k(1) k(6)
<                   k(8) k(3) k(2) k(5) k(4) k(7) k(6) k(1)];

> KE = [ 2/3 -1/6 -1/3 -1/6
>       -1/6  2/3 -1/6 -1/3
>       -1/3 -1/6  2/3 -1/6
>       -1/6 -1/3 -1/6  2/3];
```

5.2 Appendix: The existence issue

This appendix discusses two fundamental approaches to prove existence of solutions for problems in optimal topology design. The proofs involve fundamental theorems and techniques from functional analysis.

5.2.1 Variable thickness sheet design: Existence

The variable thickness sheet problem reads:

$$\min_{u,h} \quad l(u)$$

$$\text{s.t. } : a_h(u,v) \equiv \int_\Omega h(x) E^0_{ijkl} \varepsilon_{ij}(u) \varepsilon_{kl}(v) \mathrm{d}\Omega = l(v), \text{ for all } v \in U,$$

$$h \in L^\infty(\Omega), \int_\Omega h(x) \mathrm{d}\Omega \leq V, \; 0 < h_{\min} \leq h \leq h_{\max} < \infty$$

Here E^0_{ijkl} is the fixed stiffness tensor for a given linearly elastic material and h is the thickness distribution of the sheet. It is a classical result in the field of distributed optimal control that there exists a solution to this problem (Cea & Malanowski 1970). This follows from the fact that the admissible thickness function h belongs to a closed and bounded and thus weak* compact set in $L^\infty(\Omega)$ and the fact that the compliance, as a function of h given through the equilibrium equation is a lower weak*-semi-continuous function. The latter property is seen by considering the following calculation for a set of feasible thickness functions $h_n, n \in \mathbf{N} \cup \{0\}$ and corresponding displacements $u_n, n \in \mathbf{N} \cup \{0\}$:

$$\begin{aligned} l(u_n) - l(u_0) &= l(u_n) - 2l(u_0) + l(u_0) \\ &= a_{h_n}(u_n, u_n) - 2a_{h_n}(u_n, u_0) + a_{h_0}(u_0, u_0) \\ &= a_{h_n}(u_n - u_0, u_n - u_0) + a_{h_0 - h_n}(u_0, u_0) \end{aligned}$$

As the bilinear forms a_h are uniformly elliptic on our set of admissible designs it follows that: $\liminf \left[l(u_n) - l(u_0) \right] \geq 0$ whenever $\lim_{n\to\infty} \int_\Omega \left[h_n - \right.$

$h_0]\varphi d\Omega = 0$ for all $\varphi \in L^1(\Omega)$, so the compliance is a lower weak*-semi-continuous function of h.

The existence of solutions is easily extended to any problem for which the volume constraint is of the form $\int_\Omega f(h)d\Omega \leq V$ with a convex function $f \quad \mathbf{R} \rightarrow \mathbf{R}$ (such constraints are lower weak*-semi-continuous). Unfortunately, the penalties needed to generate solid-void designs require the use of *concave* functions f However, employing a penalty of intermediate thicknesses via the functional

$$\widetilde{\mathcal{W}}(\rho) = \int_\Omega (h * K)(x)(1 - (h * K)(x))d\Omega$$

is possible, as this functional is weak*-continuous (see Borrvall & Petersson (2001b)) (here one *filters* the thickness h; for notation, see section 1.3.1).

Note that the existence of solutions could also be proved by considering the equivalent formulation (cf. problem (1.6))

$$\max_{\substack{h \in L^\infty(\Omega), \\ 0 \leq h_{\min} \leq h \leq h_{\max} < \infty \\ \int_\Omega h(x)d\Omega \leq Vol}} \min_{v \in U} \left\{ \Psi(h, v) = \frac{1}{2} \int_\Omega h(x) E^0_{ijkl} \varepsilon_{ij}(v) \varepsilon_{kl}(v) d\Omega - l(v) \right\}$$

This problem is a max-min problem for a concave-convex functional $\Psi(h, v)$. The functional and the constraint sets satisfy conditions for the existence of a saddle point, thus proving the existence of solutions to the variable thickness sheet problem. The topologies we invoke on the spaces are here the weak* topology on $L^\infty(\Omega)$ and the standard norm topology on U (i.e., on $H^1(\Omega)$). Then the following conditions for the existence of a saddle point are satisfied:

The set $G = \left\{ h \in L^\infty(\Omega) \middle| 0 \leq h_{\min} \leq h \leq h_{\max} < \infty, \int_\Omega h(x)d\Omega \leq V \right\}$ is convex and compact in $L^\infty(\Omega)$-weak*

$\Psi(\cdot, v)$ is concave and continuous on $L^\infty(\Omega)$-weak*, for all $v \in U$

$\Psi(h, \cdot)$ is convex and continuous on U, for all $h \in G$.

There exists an element $h^0 \in G$, so that $\Psi(h^0, v) \rightarrow \infty$ for $\|v\|_{H^1} \rightarrow \infty$, that is, there exists an admissible thickness distribution for which the potential energy is coercive.

Compared to the proof above we can here accept thickness distributions with vanishing thickness (the uniform coercivity is not required). Also, remark that the saddle point problem considered here is somewhat different from such problems encountered in analysis (in, e.g., mixed finite elements). First, the function $\Psi(h, v)$ in not quadratic and second, we are not working on reflexive spaces. This means that we have to invoke a general minimax theorem (e.g., Moreau (1964), Ekeland & Temam (1976), Lipton (1994c)).

Note that if we do impose the constraint $h \geq h_{\min} > 0$ we have uniqueness of the displacement of the optimal solution (the thickness may not be unique). If $h \geq h_{\min} > 0$, the functions $\Psi(h, \cdot)$ are strictly convex for all h, implying that $\min_{v \in U} \max_{h \in G} \Psi(h, v)$ is a strictly convex problem in the displacements.

This result on existence of solutions for the variable thickness sheet problem is used at several points in this monograph.

5.2.2 Density design with a gradient constraint: Existence

One possible variation of the penalized density design problem with a gradient constraint on the allowable density variations reads:

$$\begin{aligned}
&\min_{u,\rho \in H^1(\Omega)} \quad l(u) \\
&\quad \text{s.t.} : a_\rho(u, v) = l(v), \text{ for all } v \in U \subseteq H^1(\Omega) \\
&\qquad \int_\Omega \rho(x) \mathrm{d}\Omega \leq V \qquad 0 < \rho_{\min} \leq \rho(x) \leq 1,\, x \in \Omega \\
&\qquad \|\rho\|_{H^1} = \left[\int_\Omega (\rho^2 + (\nabla \rho)^2) \mathrm{d}\Omega \right]^{\frac{1}{2}} \leq M
\end{aligned}$$

where $a_\rho(u, v) = \int_\Omega \rho^q(x) E^0_{ijkl} \varepsilon_{ij}(u) \varepsilon_{kl}(v) \mathrm{d}\Omega$, and $1 < q < n/(n-2)$ depending on the spatial dimension n.

Now consider this problem in the following setting. As the objective function does not depend explicitly on the design variable, the problem can be considered as a minimization of a function over a set U^* of displacements arising from each of the admissible designs (as is also the approach used in the computational schemes described in section 1.2):

$$U^* = \left\{ u \in U \middle| \exists \rho \in G_p \quad a_\rho(u, v) = l(v), \text{ for all } v \in U \right\}$$

Here the set of admissible designs is

$$G_P = \left\{ \rho \in H^1(\Omega) \middle| \begin{array}{l} \|\rho\|_{H^1} \leq M;\ \int_\Omega \rho(x) \mathrm{d}\Omega \leq V \cdot \\ 0 < \rho_{\min} \leq \rho(x) \leq 1,\ x \in \Omega \end{array} \right\}$$

From $0 < \rho_{\min} \leq \rho(x)$, it follows that the family $\{a_\rho(\cdot, \cdot) | \rho \in G_p\}$ of forms is uniformly elliptic, that is, there exists a $c > 0$, so

$$a_\rho(u, u) \geq c \|u\|^2_{H^1}, \text{ for all } \rho \in G_P$$

Equilibrium then gives that

$$c\|u\|^2_{H^1} \leq a_\rho(u, u) = l(u) \leq \|f\|_2 \|u\|_2 \quad \text{so } \|u\|_{H^1} \leq c^{-1} \|f\|_2, \text{ for } u \in U^*$$

This means that the set U^* is bounded and thus weakly pre-compact in the reflexive space U. Since the objective function is weakly continuous in the

displacements, existence of solutions to the problem would be assured if the set U^* was weakly closed as well. This is the case here.

That the set U^* is weakly closed follows from the Sobolev embedding theorem, which implies that the bounded set G_P is imbedded as a compact set in $L^{2q}(\Omega)$. As U^* is bounded in U, we thus for any sequence (u_n) of displacements in U^* with corresponding designs (ρ_n) have a subsequence (for convenience denoted by (u_n), (ρ_n) as well), for which

$$\rho_n^q \to \rho_0^q, \text{ in } L^2(\Omega), \text{ strongly; } u_n \to u_0, \text{ in } U, \text{ weakly, as } n \to \infty$$

where ρ_0 is in G_P. From this it follows that

$$a_{\rho_n}(u_n, \varphi) \to a_{\rho_0}(u_0, \varphi) \text{ as } n \to \infty, \text{for all } \varphi \in C_c^\infty(\Omega)$$

Thus $a_{\rho_0}(u_0, \varphi) = l(\varphi)$ for all $\varphi \in C_c^\infty(\Omega)$, and u_0 is in U^*, and we have proved that U^* is weakly closed.

We note that the properties of G_P shown here not only imply existence of solutions for the minimum compliance problem. Existence of solutions holds for a whole range of problems, encompassing minimizing the average deflection, minimizing the average stresses, minimizing the maximum displacement, maximizing the minimum eigenfrequency of free vibrations as well as maximizing the minimum in-plane buckling load (see, e.g., Bendsøe (1983), Bendsøe (1984)).

We remark here that we have obtained existence of solutions by restricting the set of admissible designs. For the 0-1 formulation of shape design, with admissible designs given as in (1.3) the corresponding set of displacements is not closed under weak convergence. This can be seen from taking a sequence of increasingly rapidly varying layered designs, for which the corresponding displacements do converge weakly (follows from homogenization), but where the limiting design is an orthotropic material not covered by the set of admissible designs. As layered designs may be stronger than a macroscopic variation of material and void then means that the existence of solutions is not assured.

Note that we above actually have proved that the set G_P is G-closed (or closed under H-convergence) [5], [25]. Here the G-topology is the topology on designs induced by the weak convergence of solutions to the corresponding equilibrium equations. We thus say that (ρ_n) G-converges to ρ_0 if, for all load linear forms, the solutions

$$a_{\rho_n}(u_n, v) = l(v) \text{ for all } v \in U \qquad a_{\rho_0}(u_0, v) = l(v) \text{ for all } v \in U$$

satisfy $u_n \to u_0$, weakly, as $n \to \infty$. The set of designs (1.3) is not G-closed, and the full description of its G-closure is still not known for elasticity. The existence of solutions for the minimum compliance problem that is obtained through the introduction of finite rank layerings is achieved by extending the set of designs with designs that contain the G-limits of the minimizing

sequences for the *specific* design problem at hand, thus generating only *part of the* G-closure. We mention that the finite rank layerings in the case of the scalar problem of conduction provides a complete description of the G-closure for 0-1 designs [25]. For a complete coverage of the problem of existence of solutions, the relation to G-converge, H-convergence, homogenization and Γ-convergence, we refer the reader to the vast literature on this subject [4], [5], [34] and [25].

5.3 Appendix: Aspects of shape design: The boundary variations method

5.3.1 Design parametrization in shape design

For completeness we will in the this appendix outline the basic concepts required for implementing a boundary variations shape design procedure. But first we shall briefly describe how also this type of problem fits into the general framework for design over a given choice of admissible stiffness tensor, as formulated in section 1.1. To this end, we refer all admissible domains to a reference domain[4] Ω through differentiable one-to-one maps (C^1-diffeomorfisms) $\Phi \quad \Omega \to \Phi(\Omega) \subseteq \mathbf{R}^2$ Thus all domains are of the form $\Phi(\Omega)$, with the volume constraint being expressed as

$$\mathrm{Vol}(\Phi(\Omega)) = \int_{\mathbf{R}^2} 1_{\Phi(\Omega)} \mathrm{d}x \leq V = \int_{\mathbf{R}^2} 1_{\Omega} \mathrm{d}x = \mathrm{Vol}(\Omega)$$

This parametrization means that the topology of *all* admissible domains is given by the choice of reference domain Ω and no change in lay-out is possible. Also, note that in this setting the state variables and the integrals in the problem statements (1.1), (1.6) and (1.7) are all defined on varying domains. For sensitivity analysis and comparison of for example displacements it is crucial to have a formulation on a common domain of reference. The standard technique to obtain this is to use a transformation of coordinates in order to express the equilibrium conditions for the domains $\Phi(\Omega)$ on the reference domain Ω. This results in a formulation (1.1) for which [2]

$$l(u) = \int_{\Omega} pu \,|\det \nabla\varphi^{-1}|\, \mathrm{d}\Omega + \int_{\Gamma_T} tu \,|\mathrm{adj}\nabla\varphi^{-1}|\, \mathrm{d}\Gamma$$

and the stiffness tensors are of the form

$$E_{ijkl} = E^0_{ipkq} (\nabla\varphi^{-1})_{jp} (\nabla\varphi^{-1})_{lq} |\det \nabla\varphi^{-}$$

These formulas express the form of the transformed energy and load expressions. The problem is still basically of the form of (1.1), but now the loads

[4] This is analogous to the approach when using isoparametric elements.

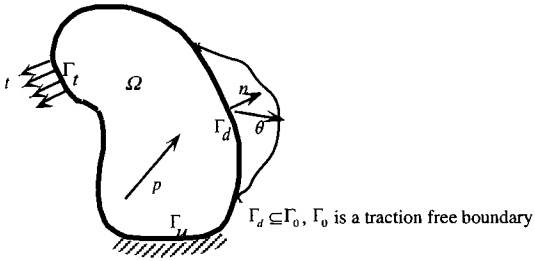

Fig. 5.7. The setting of a boundary shape design problem, indicating a shape perturbation.

are also design dependent. Also, the stiffness tensor depends in an intricate way on the design parametrization. Note that for existence of solutions one can often also in this setting refer to restriction methods (compactness arguments) by restricting the admissible diffeomorfisms to have bounded first and second derivatives [2].

The variation of shape is in implementations of the boundary variations method often controlled via a discrete parametrization of the boundary for example through the control points of splines. The solution of the shape optimization problem using FEM has to be able to handle the changes in shape introduced after each optimization iteration. These changes often require the construction of a new discrete model of the structure after each optimization step. The new mesh should be generated automatically and directly from the design variables used to parametrize the shape. The complications in the boundary shape variations method thus lies almost entirely in the analysis and design sensitivity, while the optimization in itself is simplified by the small number of design variables typically used for these problems. The methodology is, as mentioned, well established and there exist for this type of problem also several commercially available software systems for boundary shape design of structures ([2], [35]).

5.3.2 The basics of a boundary shape design method

In the following we will summarize some aspects of a specific approach to boundary shape design. It contains the generic features of such methods and allows for a comparison with the material distribution method for topology design (generalized shape design). The method that is described is based on standard shape sensitivity analysis and boundary shape variations, with the required precision of local data (including stress values) being obtained with a mixed finite element method (Rodrigues 1988, Bendsøe & Rodrigues 1991). In order to be able to handle moderately large shape variations, a remeshing scheme is also used, in the form of an elliptic mesh generator. For further

literature on boundary shape design and boundary shape design sensitivity analysis, the reader is referred to the vast literature on the subject [2], [[35].

Problem formulation We view here boundary shape optimization as a methodology for post-processing of results from the topology design method. That is, the optimal topology and initial boundary shape are defined and the objective is to refine this initial shape, in this case so that the von Mises equivalent stress in the body is minimized. For a two dimensional linear elastic body the objective is to find, by means of the boundary variation, the shape of the domain $\Omega \subseteq \mathbf{R}^2$ such that the maximum value of the von Mises equivalent stress is minimized subject to a resource constraint and a compliance constraint. We formulate the problem by a bound formulation in order to remove the non-smoothness of the max-stress function (see for example Olhoff (1989) and references therein for other structural optimization applications of this idea). The problem is then

$$
\begin{aligned}
&\min_{\substack{\Omega\in\mathsf{D}\\ \gamma,\sigma,u}} \quad \beta \\
&\text{s.t.} \quad \int_\Omega E_{ijkl}\gamma_{ij}\kappa_{kl}\mathrm{d}\Omega - \int_\Omega \gamma_{ij}\tau_{kl}\mathrm{d}\Omega + \\
&\qquad + \int_\Omega \sigma_{ij}\varepsilon_{ij}(v)\mathrm{d}\Omega + \int_\Omega \tau_{ij}\varepsilon_{ij}(u)\mathrm{d}\Omega - l(u) = 0 \text{ for all } \kappa,\tau,v \\
&\qquad \bar{\sigma}_{eq}(x) \le \beta \text{ for all } x \in \Omega \\
&\qquad l(u) \le \Phi, \quad \int_\Omega \mathrm{d}\Omega \le V
\end{aligned}
\tag{5.2}
$$

Here D denotes the set of admissible shapes, defined through local geometric constraints. The equilibrium is given via the stationarity condition in weak form for the Hu-Washizu variational principle (Washizu 1983), using independent fields γ, σ, u of strains, stresses and displacements. The computational scheme will thus make use of a mixed finite element method to provide for accurate computation of stresses and strains at the element nodes.

The methods which can be used to obtain the set of necessary conditions, to be satisfied at the optimal domain, Ω^* are well documented in the literature and follow the lines of sensitivity analysis already described, so we restrict our presentation to the statement of the type of results that can be obtained [2]. The derivation of the necessary conditions employ the so-called *speed method* for boundary shape variations. This is an infinitesimal version of the mapping method for shape parametrization, as outlined in above. We thus define a perturbation of the optimal domain as

$$\Omega^t = (I + t\theta)(\Omega^*)$$

where θ is the domain perturbation vector field (see Fig. 5.7). The set D_θ of admissible perturbation fields is defined via,

$$\mathsf{D}_\theta = \{\theta | \Omega^t = (I + t\theta)(\Omega^*) \in \mathsf{D}, \text{for } t \text{ small enough}\}$$

The optimality condition associated with this variation of the domain can be stated as a boundary integral condition

$$\int_{\Gamma_d} \left[\sigma_{ij}\bar{\gamma}_{ij} - u \quad f + \Lambda_1 + \Lambda_2 \sigma_{ij}\gamma_{ij}\right](\theta \cdot n)\mathrm{d}\Gamma = 0 \tag{5.3}$$

where $\Lambda_1 \geq 0$, $\Lambda_2 \geq 0$ are Lagrange multipliers for the volume and compliance constraints, respectively. Also, in this equation $\bar{\gamma}_{ij}$ is the adjoint strain field, that is, it is the solution of the adjoint equation, written in mixed variational form as,

$$\int_\Omega E_{ijkl}\bar{\gamma}_{ij}\kappa_{kl}\mathrm{d}\Omega - \int_\Omega \bar{\gamma}_{ij}\tau_{ij}\mathrm{d}\Omega - \int_\Omega \kappa_{ij}\bar{\sigma}_{ij}\mathrm{d}\Omega + \int_\Omega \bar{\sigma}_{ij}\varepsilon_{ij}(v)\mathrm{d}\Omega$$
$$+ \int_\Omega \tau_{ij}\varepsilon_{ij}(\bar{u})\mathrm{d}\Omega + \int_\Omega \eta\left(\frac{\partial \bar{\sigma}_{eq}}{\partial \gamma_{ij}}\kappa_{ij}\right)\mathrm{d}\Omega = 0 \quad \text{for all } \kappa, \tau, v$$

Here $\eta \geq 0$ is the Lagrange multiplier associated with the bound constraint in (5.2) on the von Mises stress (η satisfies $\int_\Omega \eta \mathrm{d}\Omega = 1$). For the case without local geometric constraints on the design domains and without the compliance constraint, the optimality condition becomes

$$\int_{\Gamma_d} \left[\sigma_{ij}\bar{\gamma}_{ij} - \Lambda_1\right](\theta \cdot n)\mathrm{d}\Gamma = 0 \text{ for all } \theta$$

According to this result, the mutual energy $\sigma_{ij}\bar{\lambda}_{ij}$ has constant value along the design boundary Γ_d. We remark here that it may not be convenient to use (5.3) in its boundary integral form, but instead a domain integral should be used. This will depend on the quality of the prediction of the stress at the boundary. Note also that in concrete discretizations, (5.3) should be used in a form that is consistent with the discretization. These aspects are discussed in detail in the literature ([2], [35]).

Numerical model For the example problem at hand (given in (5.2)), the discrete version of the mixed variational formulation can be achieved through a discretization of stress, strain and displacement fields using for example four node isoparametric finite elements. The mixed variational form leads to an indefinite system of equation in the nodal values of the stress, strain and displacement fields. Once this system is solved, the adjoint displacement field can be found from the adjoint equation, discretized using the same finite element interpolation fields as defined for the primal problem. Note that we need the solution of the primal problem to define the force term of the adjoint problem. The Lagrange multiplier $\eta \geq 0$ can be interpolated using bilinear shape functions within each element where stresses are at the maximum level.

The discretization of the design perturbation field θ can be obtained through a range of different approaches. In order to maintain smoothness

of the design, interpolation using splines or global design functions are commonly employed ([2], [35]). The shape of the body is then given through a discrete set of design variables $\{d_i\}$, which for example are the lengths of the position vectors of the respective spline interpolation nodes, expressed with respect to a pre-defined origin. The design perturbation field is expressed through the perturbations $\{\Delta_i\}$ of the lengths of the position vectors.

With these discretizations, the design variables for the optimal boundary shape can be computed iteratively, for example by employing well-known gradient type algorithms, in a scheme that is analogous to that described in section 1.2.3. However, this disguises the need for procedures to update the FE grid during the iterative procedure. Thus, in order to solve numerically the shape optimal design problem, there is for large design changes a need for an automatic grid generator for the finite element model. The choice of an automatic grid generator should relate sensibly to the problem type to be solved. In the case of shape optimal design the sensitivity analysis (and the optimality conditions) require accurate stress and adjoint strain estimates along the design boundary. To minimize the interpolation error of the finite element solution there is a need for grid smoothness and orthogonality. Also, during the domain shape variation, geometric singularities can develop along the design boundaries. The grid generator should minimize the propagation into the domain of mesh non-uniformities, due to these singularities. Finally, we note that the initial shapes can be quite arbitrary. The grid generator should be able to operate on quite general shapes and permit interior boundaries. To cater for these requirements a number of various grid generation techniques for shape design have been used for shape design, and for the methods that have been integrated with topology design, free-mesh, design-element and elliptical mesh generators have been used with good results [10].

5.4 Appendix: Homogenization and layered materials

We shall here discuss various derivations of the effective moduli of layered materials in planar elasticity, mainly to draw a parallel between the homogenization method and the traditional engineering smear-out techniques. Also, we shall see how a specific algebraic form of the formulas of effective moduli leads to a design parametrization that does not involve angles of rotation. These latter formulas were originally derived in the materials science literature as a tool for showing the optimality of bounds on the effective properties of composite materials, but they are also extremely useful for topology design. The reader is referred to [4], [20], [25] for a list of literature on the subject of layering formulas and the relationship to optimal bounds.

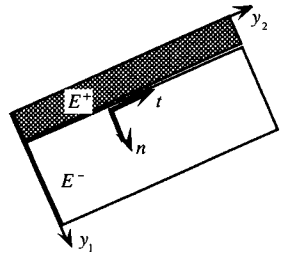

Fig. 5.8. The layered material.

5.4.1 The homogenization formulas

In the following we consider a (single-layer) layered material constructed from two different orthotropic materials with stiffness tensors E^+, E^-, respectively. The layers are in the unit direction $\mathbf{t}$, with the unit normal to the layering direction being denoted by $\mathbf{n}$ (see Fig. 5.8), and the thickness of material E^+ is μ, while the thickness of material E^- is $(1-\mu)$. For the local frame of reference given by $(\mathbf{n}, \mathbf{t})$ we choose coordinates (y_1, y_2), and the unit cell we consider is $[0,1] \times \mathbf{R}$. We assume that the axes of orthotropy of the materials are aligned with the layer directions, so that the only non-zero elements of the stiffness tensors for the materials (and the homogenized material) in the chosen frame are the elements with indices 1111, 2222, 1212 (1221, 2121, 2112) and 1122 (2211).

We will first work directly on the homogenization formulas, using suitable test fields. The homogenization formulas reads

$$\begin{aligned} E^H_{ijkl}(x) &= \min_{\varphi \in U_Y} \frac{1}{|Y|} a_Y(y^{ij} - \varphi, y^{kl} - \varphi) = \frac{1}{|Y|} a_Y(y^{ij} - \chi^{ij}, y^{kl} - \chi^{kl}) \\ &= \frac{1}{|Y|} \int_Y \left[E_{ijkl}(x,y) - E_{ijpq}(x,y) \frac{\partial \chi^{kl}_p}{\partial y_q} \right] \mathrm{d}y \end{aligned} \tag{5.4}$$

with cell problem

$$\left.\begin{aligned} &a_Y(y^{ij} - \chi^{ij}, \varphi) = 0 \text{ or} \\ &\textstyle\int_Y \left[E_{ijpq}(x,y) \frac{\partial \chi^{kl}_p}{\partial y_q} \right] \frac{\partial \varphi_i}{\partial y_j} \mathrm{d}y = \int_Y E_{ijkl}(x,y) \frac{\partial \varphi_i}{\partial y_j} \mathrm{d}y \end{aligned}\right\} \forall \varphi \in U_Y \tag{5.5}$$

where $y^{11} = (y_1, 0)$, $y^{12} = (y_2, 0)$, $y^{21} = (0, y_1)$ and $y^{22} = (0, y_2)$.

Let us now derive the expression for $E^H_{ijkl}(x)$ for the layered material we consider. It is clear that the unit cell fields χ^{kl} are independent of the variable y_2. Also note that in equation (5.4), the term involving the cell deformation

field χ^{kl} is of the form $E_{ijpq}(x,y)\frac{\partial \chi_p^{kl}}{\partial y_q}$, so an explicit expression for χ^{kl} is not needed. Using orthotropy, the homogenization formula for $E^H_{ijkl}(x)$ reads

$$\begin{aligned}
E^H_{1111}(x) &= \int_0^1 (E_{1111} - E_{1111}\tfrac{\partial \chi_1^{11}(y_1)}{\partial y_1})\mathrm{d}y_1 \\
E^H_{2222}(x) &= \int_0^1 (E_{2222} - E_{1122}\tfrac{\partial \chi_1^{22}(y_1)}{\partial y_1})\mathrm{d}y_1 \\
E^H_{1212}(x) &= \int_0^1 (E_{1212} - E_{1212}\tfrac{\partial \chi_2^{12}(y_1)}{\partial y_1})\mathrm{d}y_1 \\
E^H_{1122}(x) &= \int_0^1 (E_{1122} - E_{1111}\tfrac{\partial \chi_1^{22}(y_1)}{\partial y_1})\mathrm{d}y_1
\end{aligned} \tag{5.6}$$

and the corresponding cell problems written with test functions of the form $(\varphi(y_1),0)$ for χ^{11},χ^{22} and test functions of the form $(0,\psi(y_1))$ for χ^{kl}, have the form:

$$\begin{aligned}
\int_0^1 E_{1111}\tfrac{\partial \chi_1^{11}(y_1)}{\partial y_1}\tfrac{\partial \varphi(y_1)}{\partial y_1}\mathrm{d}y_1 &= \int_0^1 E_{1111}\tfrac{\partial \varphi(y_1)}{\partial y_1}\mathrm{d}y_1, \text{ all } \varphi \\
\int_0^1 E_{1111}\tfrac{\partial \chi_1^{22}(y_1)}{\partial y_1}\tfrac{\partial \varphi(y_1)}{\partial y_1}\mathrm{d}y_1 &= \int_0^1 E_{1122}\tfrac{\partial \varphi(y_1)}{\partial y_1}\mathrm{d}y_1, \text{ all } \varphi \\
\int_0^1 E_{1212}\tfrac{\partial \chi_2^{12}(y_1)}{\partial y_1}\tfrac{\partial \Psi(y_1)}{\partial y_1}\mathrm{d}y_1 &= \int_0^1 E_{1212}\tfrac{\partial \Psi(y_1)}{\partial y_1}\mathrm{d}y_1, \text{ all } \psi
\end{aligned}$$

This means that

$$\begin{aligned}
E_{1111}\tfrac{\partial \chi_1^{11}(y_1)}{\partial y_1} &= E_{1111} + c_{11} \\
E_{1111}\tfrac{\partial \chi_1^{22}(y_1)}{\partial y_1} &= E_{1122} + c_{22} \\
E_{1212}\tfrac{\partial \chi_2^{12}(y_1)}{\partial y_1} &= E_{1212} + c_{12}
\end{aligned}$$

and the periodicity condition restricts the constants c_{11}, c_{22}, c_{12} to satisfy:

$$\begin{aligned}
c_{11} &= -\left[M\left(\tfrac{1}{E_{1111}}\right)\right]^{-1} \qquad c_{12} = -\left[M\left(\tfrac{1}{E_{1212}}\right)\right]^{-1} \\
c_{22} &= -\left[M\left(\tfrac{E_{2211}}{E_{1111}}\right)\right]\left[M\left(\tfrac{1}{E_{1111}}\right)\right]^{-1}
\end{aligned}$$

where $M(\,)$ denotes the average over the unit cell.

Inserting these expression in the formulas in (5.6) and using that

$$E_{1122}\tfrac{\partial \chi_1^{22}(y_1)}{\partial y_1} = \tfrac{E_{1122}}{E_{1111}}\left[E_{1111}\tfrac{\partial \chi_1^{22}(y_1)}{\partial y_1}\right] = \tfrac{E_{1122}}{E_{1111}}\left[E_{1122} + c_{22}\right],$$

we obtain the result for E^H (cf., section 3.1.2):

$$E^H_{1111} = \left[M\left(\frac{1}{E_{1111}}\right)\right]^{-1} \quad \left[\frac{\mu}{E^+_{1111}} + \frac{(1-\mu)}{E^-_{1111}}\right]^{-1} = \frac{E^+_{1111}E^-_{1111}}{\mu E^-_{1111}+(1-\mu)E^+_{1111}}$$

$$\begin{aligned}
E^H_{2222} &= M(E_{2222}) - \left[M\left(\frac{E_{1122}{}^2}{E_{1111}}\right)\right] + \left[M\left(\frac{E_{1122}}{E_{1111}}\right)\right]^2 \left[M\left(\frac{1}{E_{1111}}\right)\right]^{-1} \\
&= \mu E^+_{2222} + (1-\mu)E^-_{2222} - \left[\frac{\mu(E^+_{1122})^2}{E^+_{1111}} + \frac{(1-\mu)(E^-_{1122})^2}{E^-_{1111}}\right] + \\
&\quad + \left[\frac{\mu E^+_{1122}}{E^+_{1111}} + \frac{(1-\mu)E^-_{1122}}{E^-_{1111}}\right] \frac{E^+_{1111}E^-_{1111}}{\mu E^-_{1111}+(1-\mu)E^+_{1111}} \\
E^H_{1122} &= \left[M\left(\frac{E_{1122}}{E_{1111}}\right)\right]\left[M\left(\frac{1}{E_{1111}}\right)\right]^{-1} \\
&= \left[\frac{\mu E^+_{1122}}{E^+_{1111}} + \frac{(1-\mu)E^-_{1122}}{E^-_{1111}}\right] \frac{E^+_{1111}E^-_{1111}}{\mu E^-_{1111}+(1-\mu)E^+_{1111}} \\
E^H_{1212} &= \left[M\left(\frac{1}{E_{1212}}\right)\right]^{-1} = \frac{E^+_{1212}E^-_{1212}}{\mu E^-_{1212}+(1-\mu)E^+_{1212}}
\end{aligned}$$

For a layering of two isotropic materials with the same Poisson ratio ν, with different Young's moduli E^+ and E^- respectively, we have that E_{1212} $\frac{1}{2}(1-\nu)E_{1111}$ and E_{1122} νE_{1111} in both materials, so the formulas (in plane stress) reduce to the simple expressions given in (3.7).

5.4.2 The smear-out process

We will now consider a different method for solving the homogenization formulas for the layered case by means that relates directly to more traditional ways of computing effective moduli for such materials. To this end we interpret the homogenization formulas in the following way. Let $\bar{\varepsilon}$ be any macroscopic strain. Then the homogenized material coefficients are defined by the energy relation (with no macroscopically varying parameters)

$$E^H_{ijkl}\bar{\varepsilon}_{ij}\bar{\varepsilon}_{kl} = \min_{\varphi\in U_Y} \frac{1}{|Y|}\int_Y E_{ijkl}(y)\big(\bar{\varepsilon}_{ij} - \varepsilon_{ij}(\varphi)\big)\big(\bar{\varepsilon}_{kl} - \varepsilon_{kl}(\varphi)\big)\mathrm{d}y \tag{5.7}$$

For the minimization over the periodic test fields φ, we have the minimizer φ^* given as a solution to the cell problem

$$\frac{1}{|Y|}\int_Y E_{ijkl}(y)\big(\bar{\varepsilon}_{ij} - \varepsilon_{ij}(\varphi^*)\big)\varepsilon_{kl}(\zeta)\mathrm{d}y, \text{ for all } \zeta \in U_Y \tag{5.8}$$

From this it follows, that

$$E^H_{ijkl}\bar{\varepsilon}_{ij}\bar{\varepsilon}_{kl} = \frac{1}{|Y|}\int_Y E_{ijkl}(y)\big(\bar{\varepsilon}_{ij} - \varepsilon_{ij}(\varphi^*)\big)\bar{\varepsilon}_{kl}\mathrm{d}y, = 0 \text{ for all } \bar{\varepsilon} \tag{5.9}$$

so that the macroscopic stress field defined as $\bar{\sigma}_{ij} = E^H_{ijkl}\bar{\varepsilon}_{kl}$ satisfies

$$\bar{\sigma}_{ij} = E^H_{ijkl}\bar{\varepsilon}_{kl} = \frac{1}{|Y|}\int_Y E_{ijkl}(y)\big(\bar{\varepsilon}_{kl} - \varepsilon_{kl}(\varphi^*)\big)\mathrm{d}y\ . \tag{5.10}$$

We will now show that (5.8) for the layered case is solved by a field φ^*, for which $\big(\bar{\varepsilon}_{ij} - \varepsilon_{ij}(\varphi^*)\big)$ is constant in each material region, that is

$$\big(\bar{\varepsilon}_{ij} - \varepsilon_{ij}(\varphi^*)\big)(y) = \begin{cases} \varepsilon^+ & \text{in material} + \\ \varepsilon^- & \text{in material} - \end{cases} \tag{5.11}$$

where $\varepsilon^+, \varepsilon^-$ are constant fields. Remembering now that we have that

$$E_{ijkl}(y) = \begin{cases} E^+_{ijkl} & \text{in material} + \\ E^-_{ijkl} & \text{in material} - \end{cases} \tag{5.12}$$

together with (5.11) implies that the cell problem is solved for such a field φ^*, provided the interface conditions along the layer interface are satisfied.[5] The natural boundary condition is that the normal component of stress along the interface is continuous. This follows directly from the variational statement (5.8). Moreover, because of regularity of the solution (see, e.g., Escauriaza & Seo (1993)), the tangential component of strain must be continuous (this latter property could also be posed as an ansatz, which is then proven to be true after we have shown that such a condition gives a solution). The continuity conditions are thus:

$$\begin{aligned} &\sigma^+_{ij} n_i n_j = \sigma^-_{ij} n_i n_j \quad \text{or} \quad E^+_{ijkl}\varepsilon^+_{kl} n_i n_j = E^-_{ijkl}\varepsilon^-_{kl} n_i n_j \\ &\sigma^+_{ij} n_i t_j = \sigma^-_{ij} n_i t_j \quad \text{or} \quad E^+_{ijkl}\varepsilon^+_{kl} n_i t_j = E^-_{ijkl}\varepsilon^-_{kl} n_i t_j \\ &\varepsilon^+_{ij} t_i t_j = \varepsilon^-_{ij} t_i t_j \end{aligned} \tag{5.13}$$

Also, remark that from (5.11), (5.12) and (5.10) and from periodicity, follows that

$$\bar{\varepsilon}_{ij} = \frac{1}{|Y|}\int_Y \big(\bar{\varepsilon}_{ij} - \varepsilon_{ij}(\varphi^*)\big)\,\mathrm{d}y = \mu\varepsilon^+_{ij} + (1-\mu)\varepsilon^-_{ij} \tag{5.14}$$

$$\begin{aligned} \bar{\sigma}_{ij} = E^H_{ijkl}\bar{\varepsilon}_{kl} &= \frac{1}{|Y|}\int_Y E_{ijkl}(y)\big(\bar{\varepsilon}_{kl} - \varepsilon_{kl}(\varphi^*)\big)\,\mathrm{d}y \\ &= \mu E^+_{ijkl}\varepsilon^+_{kl} + (1-\mu)E^-_{ijkl}\varepsilon^-_{kl} \end{aligned} \tag{5.15}$$

Here (5.14) and (5.15) express that the homogenized coefficients describe the linear stress-strain relation between the average strain and the average stress, and (5.13) expresses continuity conditions for the stresses and strains in the individual constituents. The equations (5.14), (5.15), and (5.13) are precisely the equations used in standard smear-out calculations, and it is from these equations that we will calculate $\varepsilon^+, \varepsilon^-$ (i.e. prove that we have a solution)

[5] The property of piece-wise constant and compatible strain and stress fields is related to the optimality of the microstructure and is also seen in the analytical derivations of a new class of optimal materials as described in Sect. 2.10.3 (for details see Sigmund (2000b) and Gibiansky & Sigmund (2000)).

and in the process we will also derive the homogenized stiffness tensor E^H_{ijkl}. We can now write the constant tensors $\varepsilon^+, \varepsilon^-$ in terms of the average strain $\bar{\varepsilon}$ and the basis vectors $\mathbf{n}, \mathbf{t}$:

$$\varepsilon^+_{ij} = \bar{\varepsilon}_{ij} + a_1 n_i n_j + \frac{a_2}{2}\left[n_i t_j + t_i n_j\right] + a_3 t_i t_j$$
$$\varepsilon^-_{ij} = \bar{\varepsilon}_{ij} + b_1 n_i n_j + \frac{b_2}{2}\left[n_i t_j + t_i n_j\right] + b_3 t_i t_j$$

In this expression $a_i, b_i,\ i \quad 1,2,3$ are constants to be determined; when determined, we have the solution $\varepsilon^+, \varepsilon^-$ To this end, note that (5.14), (5.15), and (5.13) constitute nine dependent, linear equations, from which we can find $a_i, b_i,\ i = 1,2,3$

First, the continuity of the tangential component of strains imply that $a_3 = b_3 = 0$. Then, from the average strain expression in (5.14) we get

$$\mu a_1 + (1-\mu) b_1 = 0 \quad \text{or} \quad b_1 = -\tfrac{\mu}{1-\mu} a_1$$
$$\mu a_2 + (1-\mu) b_2 = 0 \quad \text{or} \quad b_2 = -\tfrac{\mu}{1-\mu} a_2$$

It is now convenient to introduce the following notation:

$$M(f) = \mu f^+ + (1-\mu) f^-,\ N(f) = (1-\mu) f^+ + \mu f^-$$
$$\text{when } f(y) = \begin{cases} f^+ & \text{in material} + \\ f^- & \text{in material} - \end{cases} \tag{5.16}$$

and also to use the shorter $Ennnn$ for a contraction like $E_{ijkl} n_i n_j n_k n_l$. With this, inserting b_1, b_2 in the conditions of continuity of the normal stress, we get the following two expressions for determining a_1, a_2 (here and in the following we use the symmetry properties of the stiffness tensors):

$$a_1 N(Ennnn) + a_2 N(Ennnt) = (1-\mu)\left[E^-_{ijkl} - E^+_{ijkl}\right] n_i n_j \bar{\varepsilon}_{kl}$$
$$a_1 N(Ennnt) + a_2 N(Entnt) = (1-\mu)\left[E^-_{ijkl} - E^+_{ijkl}\right] n_i t_j \bar{\varepsilon}_{kl}$$

We see that a_1, a_2 and thus the fields $\varepsilon^+, \varepsilon^-$ can be written linearly in terms of $\bar{\varepsilon}$, and in terms of geometric data. To write a_1, a_2 explicitly, we use the additional notation

$$\hat{D} = N(Ennnn) N(Entnt) - N(nnnt)^2$$

so that with $\Delta_{ijkl} = \frac{1-\mu}{\hat{D}}\left[E^-_{ijkl} - E^+_{ijkl}\right]$

$$a_1 = \Delta_{ijkl}\left[N(Entnt) n_i n_j - N(Ennnt) n_i t_j\right] \bar{\varepsilon}_{kl}$$
$$a_2 = \Delta_{ijkl}\left[N(Ennnn) n_i n_j - N(Ennnt) n_i n_j\right] \bar{\varepsilon}_{kl}$$

Now write the average stress in terms of $\varepsilon^+, \varepsilon^-$ and a_1, a_2 (using symmetry)

$$
\begin{aligned}
\bar{\sigma}_{ij} &= \mu E^{+}_{ijkl}\varepsilon^{+}_{kl} + (1-\mu)E^{-}_{ijkl}\varepsilon^{-}_{kl} \\
&= \mu E^{+}_{ijkl}\left[\bar{\varepsilon}_{kl} + a_1 n_k n_l + a_2 n_k t_l\right] + (1-\mu)E^{-}_{ijkl}\left[\bar{\varepsilon}_{kl} + b_1 n_k n_l + b_2 n_k t_l\right] \\
&= M(E_{ijkl})\bar{\varepsilon}_{kl} + \mu\left[E^{+}_{ijpq} - E^{-}_{ijpq}\right]\left[a_1 n_p n_q + a_2 n_p t_q\right] \\
&= \left(M(E_{ijkl}) - \frac{\mu(1-\mu)}{\hat{D}}\left[E^{+}_{ijpq} - E^{-}_{ijpq}\right]\left[E^{+}_{mnkl} - E^{-}_{mnkl}\right]\Xi_{mnpq}\right)\bar{\varepsilon}_{kl}
\end{aligned}
$$

where to achieve symmetry of the homogenized tensor we have set

$$
\begin{aligned}
\Xi_{mnpq} &= N(Entnt)n_m n_n n_p n_q \\
&\quad + \frac{1}{4}N(Ennnn)\left(n_m t_n n_p t_q + t_m n_n n_p t_q + n_m t_n t_p n_q + t_m n_n t_p n_q\right) \\
&\quad - \frac{1}{4}N(Ennnt)\left(t_m n_n n_p n_q + n_m t_n n_p n_q + n_m n_n t_p n_q + n_m n_n n_p t_q\right)
\end{aligned}
$$

From these equations it follows that the homogenized stiffness matrix is given as

$$
E^{H}_{ijkl} = M(E_{ijkl}) - \frac{\mu(1-\mu)}{\hat{D}}\left[E^{+}_{ijpq} - E^{-}_{ijpq}\right]\left[E^{+}_{mnkl} - E^{-}_{mnkl}\right]\Xi_{mnpq}\,, \quad (5.17)
$$

and this holds for anisotropic constituents as well. Equation (5.17) expresses that the effective tensor is given as the average of the stiffnesses of the constituents *plus* some correction terms. For the case of orthotropic constituents which have their axes of orthotropy along the directions $\mathbf{n}, \mathbf{t}$, terms of the form *Ennnt* are all zero, and the effective material parameters can be written somewhat simpler. It can be verified by inspection that (5.17) are equal to the formulas shown earlier.

Let us now perform the same type of operations for the compliance tensor, i.e.

$$
\varepsilon^{+}_{kl} = C^{+}_{ijkl}\sigma^{+}_{ij},\ \varepsilon^{-}_{kl} = C^{-}_{ijkl}\sigma^{-}_{ij},\ \bar{\varepsilon}_{kl} = C^{H}_{ijkl}\bar{\sigma}_{ij}
$$

Here the continuity conditions are, as before

$$
\begin{aligned}
&\sigma^{+}_{ij}n_i n_j = \sigma^{-}_{ij}n_i n_j \\
&\sigma^{+}_{ij}n_i t_j = \sigma^{-}_{ij}n_i t_j \\
&\varepsilon^{+}_{ij}t_i t_j = \varepsilon^{-}_{ij}t_i t_j \text{ or } C^{+}_{ijkl}\sigma^{+}_{ij}t_i t_j = C^{-}_{ijkl}\sigma^{-}_{ij}t_i t_j
\end{aligned}
$$

From this we see that we can write the constant tensors σ^{+}, σ^{-} in terms of the average stress $\bar{\sigma}$ and the basis vectors $\mathbf{n}, \mathbf{t}$:

$$
\sigma^{+}_{ij}n_i n_j = \bar{\sigma}_{ij} + c_3 t_i t_j \qquad \sigma^{-}_{ij}n_i n_j = \bar{\sigma}_{ij} - \frac{\mu}{1-\mu}c_3 t_i t_j \quad (5.18)
$$

where we have used the continuity of the normal component of stress and the average stress expression. Inserting this in the conditions of continuity of the tangential strain, we get the following expression for determining c_3

$$c_3 N(Ctttt) = (1-\mu)\left[C^-_{ijkl} - C^+_{ijkl}\right] t_i t_j \bar{\sigma}_{kl} \tag{5.19}$$

Now write the average strain in terms of σ^+, σ^-, c_3 and $S_{ijpq} = C^+_{ijpq} - C^-_{ijpq}$

$$\begin{aligned}\bar{\varepsilon}_{ij} &= \mu C^+_{ijkl}\sigma^+_{kl} + (1-\mu)C^-_{ijkl}\sigma^-_{kl} \\ &= M(C_{ijkl})\bar{\sigma}_{kl} + S_{ijpq}c_3 t_p t_q \\ &= \left(M(C_{ijkl}) - \frac{\mu(1-\mu)}{N(Ctttt)} S_{ijpq} S_{mnkl} t_m t_n t_p t_q\right)\bar{\sigma}_{kl}\end{aligned}$$

so

$$C^H_{ijkl} = M(C_{ijkl}) - \frac{\mu(1-\mu)}{N(Ctttt)} S_{ijpq} S_{mnkl} t_m t_n t_p t_q \tag{5.20}$$

This is the inverse of the tensor given in (5.17). For the case of orthotropic constituents, the different elements of C^H_{ijkl} are given as

$$\begin{aligned}C^H_{1111} &= M(C_{1111}) - \left[M\left(\frac{C_{1122}{}^2}{C_{2222}}\right)\right] + \left[M\left(\frac{C_{1122}}{C_{2222}}\right)\right]^2 \left[M\left(\frac{1}{C_{2222}}\right)\right]^{-1} \\ C^H_{2222} &= \left[M\left(\frac{1}{C_{2222}}\right)\right]^{-1} \qquad C^H_{1122} = \left[M\left(\frac{C_{1122}}{C_{2222}}\right)\right]\left[M\left(\frac{1}{C_{2222}}\right)\right]^{-1} \\ C^H_{1212} &= M(C_{1212})\end{aligned}$$

Note the similarity with the stiffness case, except for the 1212 term. This plays a role for using plane elasticity results for plate problems, see section 5.4.5 below.

5.4.3 The moment formulation

Let us now write the effective compliance tensor in a different form, which is suitable for iterated homogenization. These formulas have played an important role in the theoretical materials science [25], and were for the elasticity case derived in Francfort & Murat (1986). Here we compute the formulas in the spirit of the smear-out process just carried out. We do, however, proceed in a somewhat different manner.

With the notation of above we have from the average of stresses that

$$\sigma^+_{ij} = \frac{1}{\mu}\left(\bar{\sigma}_{ij} - (1-\mu)\sigma^-_{ij}\right)$$

Now insert this expression in the average over strains, to achieve

$$\begin{aligned}C^H_{ijkl}\bar{\sigma}_{ij} &= \mu C^+_{ijkl}\sigma^+_{ij} + (1-\mu)C^-_{ijkl}\sigma^-_{ij} \\ &= C^+_{ijkl}\bar{\sigma}_{ij} - (1-\mu)C^+_{ijkl}\sigma^-_{ij} + (1-\mu)C^-_{ijkl}\sigma^-_{ij}\end{aligned}$$

Rearranging, we get the equation

$$\left[C^H_{ijkl} - C^+_{ijkl}\right]\bar{\sigma}_{ij} = (1-\mu)\left[C^-_{ijkl} - C^+_{ijkl}\right]\sigma^-_{ij}$$

If $\left[C^-_{ijkl} - C^+_{ijkl}\right]$ is invertible (this is the case if the materials are well-ordered, i.e. if $\left[C^-_{ijkl} - C^+_{ijkl}\right]$ is positive or negative definite), we can write this as

$$\sigma^-_{ij} = \frac{1}{(1-\mu)}\left[C^- - C^+\right]^{-1}_{ijpq}\left[C^H_{pqkl} - C^+_{pqkl}\right]\bar{\sigma}_{kl} \tag{5.21}$$

From the conditions of continuity, we have that

$$\sigma^+_{ij} = \sigma^-_{ij} + \lambda t_i t_j$$
$$C^+_{ijkl}\sigma^+_{ij}t_k t_l = C^+_{ijkl}\left(\sigma^-_{ij} + \lambda t_i t_j\right)t_k t_l = C^-_{ijkl}\sigma^-_{ij}t_k t_l$$

where the constant λ then must be given as

$$\lambda = \tfrac{1}{C^+tttt}\left[C^-_{ijkl} - C^+_{ijkl}\right]\sigma^-_{ij}t_k t_l$$

Now using again the average of stresses we can express $\bar{\sigma}$ as

$$\bar{\sigma}_{ij} = \mu\sigma^+_{ij} + (1-\mu)\sigma^-_{ij} = \sigma^-_{ij} + \mu\frac{1}{C^+tttt}\left[C^-_{pqkl} - C^+_{pqkl}\right]t_k t_l \sigma^-_{pq} t_i t_j$$

Inserting in (5.21) we get that

$$\sigma^-_{ij} = \frac{1}{(1-\mu)}\left[C^- - C^+\right]^{-1}_{ijkl}\left[\sigma^-_{mn} + \frac{\mu}{C^+tttt}\left[C^-_{pqrs} - C^+_{pqrs}\right]t_r t_s \sigma^-_{pq} t_m t_n\right]$$

As this must hold for all stresses σ^- we get after a little rearranging and using index-free notation

$$\left[C^H - C^+\right]^{-1} = \frac{1}{(1-\mu)}\left[\left[C^- - C^+\right]^{-1} + \mu\Gamma^C(\mathbf{t})\right] \tag{5.22}$$

where the tensor $\Gamma^C(\mathbf{t})$ is defined as $\Gamma^C_{ijkl} = \frac{1}{C^+tttt}t_i t_j t_k t_l$. Equation (5.22) can also be written as

$$C^H = C^+ + (1-\mu)\left[\left[C^- - C^+\right]^{-1} + \mu\Gamma^C(\mathbf{t})\right]^{-1} \tag{5.23}$$

We remark here that the form (5.22) is particularly well suited for computing effective moduli for multiple layered materials. To this end let the material indexed as C^- in itself consist of a layering in a direction $\bar{\mathbf{t}}$ of the material C^+ and the material C^0, in proportion γ $(1-\gamma)$. Then from (5.22)

$$\left[C^- - C^+\right]^{-1} = \frac{1}{(1-\gamma)}\left[\left[C^0 - C^+\right]^{-1} + \gamma\Gamma^C(\bar{\mathbf{t}})\right]$$

Now insert this in the formula for C^H to obtain

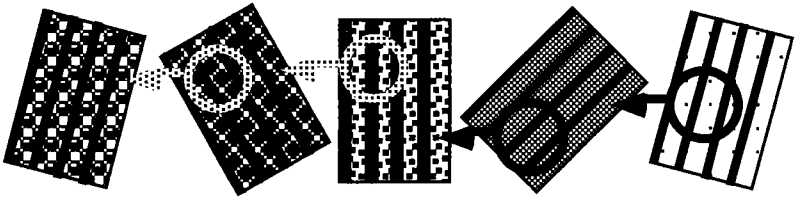

Fig. 5.9. Construction of a rank-5 layered material. The layers of the black C^+ material are the same for each layering in this case.

$$\begin{aligned}\left[C^H - C^+\right]^{-1} &= \frac{1}{(1-\mu)}\left[\frac{1}{(1-\gamma)}\left[\left[C^0 - C^+\right]^{-1} + \gamma\Gamma^C(\bar{\mathrm{t}})\right] + \mu\Gamma^C(\mathrm{t})\right] \\ &= \frac{1}{(1-\mu)(1-\gamma)}\left[\left[C^0 - C^+\right]^{-1} + \gamma\Gamma^C(\bar{\mathrm{t}}) + (1-\gamma)\mu\Gamma^C(\mathrm{t})\right]\end{aligned}$$

This is similar to the expression (5.22), and we note that $\vartheta^0 = (1-\mu)(1-\gamma)$ is the amount of material C^0, while $\vartheta^+ = 1-\vartheta^0 = 1-(1-\mu)(1-\gamma) = \gamma+(1-\mu)\gamma$ is the amount of material C^+ Repeating this process, we see that for any multiple layering constructed from an initial layering of C^0 and C^+ which is then layered consecutively with C^+ the effective parameters can be written as (with $\sum_{r=1}^m \mu_r = 1$)

$$\left[C^H - C^+\right]^{-1} = \frac{1}{(1-\vartheta^+)}\left[\left[C^0 - C^+\right]^{-1} + \vartheta^+\sum_{r=1}^m \mu_r\Gamma^C(t^r)\right] \tag{5.24}$$

for a total density ϑ^+ of C^+ placed in m layers in directions t^r; these layers need not be perpendicular.

Now let us very briefly show how a similar formula is achieved for the stiffness tensors, assuming that the material E^+ is *isotropic*, so that any term of the form E^+nnnt is zero. As above, we get

$$\left[E^H_{ijkl} - E^+_{ijkl}\right]\bar{\varepsilon}_{ij} = (1-\mu)\left[E^-_{ijkl} - E^+_{ijkl}\right]\varepsilon^-_{ij}$$

while we from the conditions of continuity have (using isotropy of E^+)

$$\begin{aligned}&\varepsilon^+_{ij} = \varepsilon^-_{ij} + \lambda_1 n_i n_j + \frac{1}{2}\lambda_2(n_i t_j + t_i n_j) \\ &E^+_{ijkl}\varepsilon^+_{ij}n_k n_l = E^+_{ijkl}(\varepsilon^-_{ij} + \lambda_1 n_i n_j)n_k n_l = E^-_{ijkl}\varepsilon^-_{ij}n_k n_l \\ &E^+_{ijkl}\varepsilon^+_{ij}n_k t_l = E^+_{ijkl}(\varepsilon^-_{ij} + \lambda_1 n_i t_j)n_k t_l = E^-_{ijkl}\varepsilon^-_{ij}n_k t_l\ ,\end{aligned}$$

giving constants λ_1, λ_2 as

$$\lambda_1 = \frac{1}{E^+ nnnn}\left[E^-_{ijkl} - E^+_{ijkl}\right]\varepsilon^-_{ij} n_k n_l, \quad \lambda_2 = \frac{1}{E^+ ntnt}\left[E^-_{ijkl} - E^+_{ijkl}\right]\varepsilon^-_{ij} n_k t_l$$

Repeating the calculations as above, we finally get for the rank-m layering (cf., eq. (5.24)), that

$$\left[E^H - E^+\right]^{-1} = \frac{1}{(1-\vartheta^+)}\left[\left[E^0 - E^+\right]^{-1} + \vartheta^+ \sum_{r=1}^{m} \mu_r \Gamma^E(\mathbf{t}^r)\right] \tag{5.25}$$

with $\sum_{r=1}^{m} \mu_r = 1$. Here the tensor $\Gamma^E(\mathbf{t})$ for symmetry reasons is defined as (E^+ is assumed isotropic) as

$$\Gamma^E_{ijkl} = \frac{1}{E^+_{1111}} n_i n_j n_k n_l + \frac{1}{4E^+_{1212}}\left(n_i t_j n_k t_l + n_i t_j t_k n_l + t_i n_j n_k t_l + t_i n_j t_k n_l\right)$$

From ((5.25) one now have the effective material properties of any rank-m layering given in terms of $2m$ parameters, namely the bulk density ϑ^+ of C^+ material, the m relative layer thicknesses μ_r (of which (m-1) are independent) and the m layer directions given by the angle of rotations of the layers, $\mathbf{n}_r = (\cos\theta_r, \sin\theta_r)$ $\mathbf{t}_r = (-\sin\theta_r, \cos\theta_r)$. We will now see that a reduction in the number of describing parameters is actually possible. To this end notice that every element of the tensors

$$\hat{\Gamma}^E_{ijkl} = \sum_{r=1}^{m} \mu_r \Gamma^E(\mathbf{t}^r), \ \hat{\Gamma}^C_{ijkl} = \sum_{r=1}^{m} \mu_r \Gamma^C(\mathbf{t}^r)$$

are simple affine combinations of parameters (*moments*) of the form

$$\left.\begin{array}{l} m_1 = \sum_{r=1}^{m} \mu_r \cos(2\theta_r), \ m_2 = \sum_{r=1}^{m} \mu_r \cos(4\theta_r) \\ m_3 = \sum_{r=1}^{m} \mu_r \sin(2\theta_r), \ m_4 = \sum_{r=1}^{m} \mu_r \sin(4\theta_r) \end{array}\right\} \text{ with } \sum_{r=1}^{m} \mu_r = 1$$

Moreover, if we consider design over all possible layer combinations as well as layer directions, the tensors $\Gamma^E(\mathbf{t}), \Gamma^C(\mathbf{t})$ will be parametrized by $(m_1, m_2, m_3, m_4) \in \mathbf{R}^4$ belonging to the convex hull $\mathcal{M}$ of the curve

$$(\cos 2\theta, \cos 4\theta, \sin 2\theta, \sin 4\theta), \ \theta \in \mathbf{R} \ ,$$

in 4-space. This convex hull will also encompass the material tensors of rank-2 and rank-3 layerings. However, compared to a rank-3 layering described by 2 relative densities and 3 directions of layerings, by introduction of the *moments* (m_1, m_2, m_3, m_4) we have one less variable to worry about. This is of little importance in an optimization procedure unless an explicit characterization of $\mathcal{M}$ can be given. Fortunately, the solution of the trigonometric moment problem (Krein & Nudelman 1977) let us write the convex set $\mathcal{M}$ as (Avellaneda & Milton 1989)

$$\mathcal{M} = \left\{ (m_1, m_2, m_3, m_4) \in \mathbf{R}^4 \left| \begin{array}{l} m_1^2 + m_3^2 \leq 1, \ -1 \leq m_2 \leq 1, \\ 2m_1^2(1-m_2) + 2m_3^2(1+m_2) + \\ +(m_2^2 + m_4^2) - 4m_1 m_3 m_4 \leq 1 \end{array} \right. \right\}$$

In terms of these moments, the effective compliance tensor for the case of void as the second phase ($E^0 = 0$) can for example be written as (in plane stress)

$$C^H = C^+ + \frac{(1-\rho)}{\rho E}[\hat{\Gamma}^{C0}]^{-1}$$

Here the entries of the tensor $\hat{\Gamma}^{C0}$ are

$$\begin{aligned}
&\hat{\Gamma}^{C0}_{1111} = \tfrac{1}{8}(3 + m_2 - 4m_1), \quad \hat{\Gamma}^{C0}_{2222} = \tfrac{1}{8}(3 + m_2 + 4m_1)\\
&\hat{\Gamma}^{C0}_{1122} = \hat{\Gamma}^{C0}_{2211} = \tfrac{1}{8}(1 - m_2)\\
&\hat{\Gamma}^{C0}_{1112} = \hat{\Gamma}^{C0}_{1121} = \hat{\Gamma}^{C0}_{2111} = \tfrac{1}{8}(m_3 - m_4)\\
&\hat{\Gamma}^{C0}_{1222} = \hat{\Gamma}^{C0}_{2221} = \hat{\Gamma}^{C0}_{2122} = \hat{\Gamma}^{C0}_{2212} = \tfrac{1}{8}(m_3 + m_4)\\
&\hat{\Gamma}^{C0}_{1212} = \hat{\Gamma}^{C0}_{1221} = \hat{\Gamma}^{C0}_{2112} = \hat{\Gamma}^{C0}_{2121} = \tfrac{1}{8}(1 - m_2)
\end{aligned}$$

We keep here the bulk density $\rho = \vartheta^+$, $0 \le \rho \le 1$, of the C^+ material as a suitable design variable (a volume constraint is expressed as $\int_\Omega \rho(x)\mathrm{d}\Omega \le V$).

The moment description used above was first used in Avellaneda & Milton (1989), for studying bounds on effective moduli. In their presentation as well as other similar works [25], one of the moduli above are often removed by introducing the overall rotation of the composite as a variable. As we here seek to avoid periodic functions in the description, all moments are kept throughout.

The moments has, as mentioned, played a significant role for the proof of the optimality of rank-2 and rank-3 materials. It is known that the extreme points of the set $\mathcal{M}$ corresponds to rank-1 materials, and the "surface" of the set corresponds to rank-2 materials, and all interior points can be found by combining these to any rank-3 material. Thus there also exist a direct analytical method for constructing a layered material which achieves a certain moment combination, see for example Lipton (1994a).

5.4.4 Stress criteria for layered composites

For treating stress constraints in topology design it is important to understand how the microlevel stresses depend on the macroscale stress, for intermediate densities [16]. Thus in order to develop a consistent stress criterion for a porous, layered composite material we use the smear-out analysis above to first establish a relationship between the stresses at the micro-level, the macroscopic stresses and the microstructural geometric parameters. Then we limit the maximum of local stress state in the microstructure with a relevant failure criterion. The overall stress criterion (that we also call a "homogenized" macroscopic stress criterion) is finally established as the expression of the local criterion in terms of the macroscopic stresses. Note that this approach generates a stress constraint which ensures that the material at

all macroscopic and microscopic points is in a safe elastic range (like a first failure criterion in laminates).

The developments below are based on a stress based approach, with material properties expressed by the compliance tensor. The results can also be obtained in an analogous way for a formulation in strains and stiffness tensor.

We have seen above that effective elastic properties of layered materials can be written analytically and that the micro-strains and the micro-stresses in each layers of the composite layered materials are *constant*. This means that the micro-stress state of a layered composite can be determined analytically in terms of the layering parameters and in terms of the overall macroscopic stresses $<\sigma_{ij}>$.

We first note that the equations (5.18) and (5.19) make it possible to compute the local stresses in a rank-1 layering, from a given average stress $\bar{\sigma}$. This means that one for a rank-N material can derive the relationship between the local stresses and the averaged stresses in a top to bottom recursive procedure. From average stresses, by going down one scale, it is first possible to determine the stresses in the solid layers and in the layered material, which at this level is considered as a homogenized medium. To its end, the stress of this medium is then the given average stress which is necessary to compute the stresses in the layers at the second level of scale. For our purpose of topology design, we want to deal with rank-2 materials where the second phase is void. Thus one has to deal with the technicality that the compliance tensor of the void is singular. To circumvent this problem, one works with a rank-2 material made of a two isotropic materials with the same Poisson's ratio ν but different Young's moduli: $E^+ = E$ for the solid material under consideration and E^- for a soft material. The porous composite is recovered by passing to the limit $E^- \to 0^+$

Stresses in a rank-2 layered material In the following we work with a rank-2 material, with layers aligned as shown in Fig. 5.8. This means that material "+" is here the solid material, while the material "−" is a rank 1 composite made of layers of the solid material and of the soft material, with layers in the direction parallel to axis y_1. To use the expressions (5.18) and (5.19) we first need the elements of the homogenized compliance tensor of the inner rank-1 composite:

$$C^H_{1111} = K_2 \qquad C^H_{2222} = K_1 + \nu^2 K_2$$

$$C^H_{1212} = \frac{2}{1-\nu} K_1 \qquad C^H_{1122} = -\nu K_2$$

$$K_1 = (1-\nu^2)\frac{\gamma E^- + (1-\gamma)E^+}{E^+ E^-} \qquad K_2 = (\gamma E^+ + (1-\gamma)E^-$$

Since the layering directions are matched with the axes of orthotropy of the constituents, all the shear coupling terms of the compliance tensors are zero and the equations (5.18) and (5.19) for the local stresses take the following simple form:

$$\sigma_{11}^{+} = \bar{\sigma}_{11} \qquad \sigma_{22}^{+} = \bar{\sigma}_{22} + c_3 \qquad \sigma_{12}^{+} = \bar{\sigma}_{12} \tag{5.26}$$

$$\sigma_{11}^{-} = \bar{\sigma}_{11} \qquad \sigma_{22}^{-} = \bar{\sigma}_{22} - \frac{\mu}{1-\mu} c_3 \qquad \sigma_{12}^{-} = \bar{\sigma}_{12} \tag{5.27}$$

with $c_3 = (1-\mu)N(C_{2222})^{-1}\,[C_{22kk}^{-} - C_{22kk}^{+}]\,\bar{\sigma}_{kk}$. The next step is to determine the behaviour of the correction term (given by c_3) of the local stresses when $E^- \to 0^+$ which results in:

$$\left.\begin{array}{l} N(C_{2222})^{-1}\,[C_{2211}^{-} - C_{2211}^{+}]\,\bar{\sigma}_{11} \to 0 \\ N(C_{2222})^{-1}\,[C_{2222}^{-} - C_{2222}^{+}]\,\bar{\sigma}_{22} \to \frac{\bar{\sigma}_{22}}{\mu} \end{array}\right\} \text{when} E^- \to 0^+ \tag{5.28}$$

Introducing this into (5.26) and using that the upper scale average stress is equal to the macroscopic stress (that is, $\bar{\sigma}_{ij} = <\sigma_{ij}>$) we determine the stresses $\sigma^{L2} = \sigma^{+}$ in the solid (outer) layers of the composite as:

$$\sigma_{11}^{L2} = <\sigma_{11}> \qquad \sigma_{22}^{L2} = <\sigma_{22}>/\mu \qquad \sigma_{12}^{L2} = <\sigma_{12}> \tag{5.29}$$

while equation (5.27) gives the average stress in the rank 1 part of the composite:

$$\sigma_{11}^{-} = <\sigma_{11}> \qquad \sigma_{22}^{-} = 0 \qquad \sigma_{12}^{-} = <\sigma_{12}> \tag{5.30}$$

Equation (5.29) shows that the overall stresses are transfered to the local scale with a correction that affects only the σ_{22} term. This is caused by the parallel assemblage of the composite. Seen from direction 1 the assemblage transfers the integral overall stress $<\sigma_{11}>$ from one layer to another. Seen from direction 2 the overall stress $<\sigma_{22}>$ is only withstood by the solid material which increases the local stress by a factor $1/\mu$.

In the next step it is the stress state σ^{-} in the rank 1 composite which is the information that is required to determine the stress state in the layers at the second length scale. The same procedure as used above results here in the the following expression for the microscopic stresses σ^{L1} of the solid layers of the rank 1 region (Duysinx & Bendsøe 1998):

$$\sigma_{11}^{L1} = <\sigma_{11}>/\gamma \qquad \sigma_{22}^{L1} = 0 \qquad \sigma_{12}^{L1} = <\sigma_{12}> \tag{5.31}$$

As the macroscopic stress $<\sigma_{22}>$ is entirely supported by the outer layers of solid of the rank-2 composite, the inner layers are only loaded by $<\sigma_{11}>$ and this stress is supported by fibers with a volume fraction γ. This increases the local stress by a factor $1/\gamma$.

An overall stress criterion for the rank-2 composite For ductile materials we follow the tradition of assuming that local failure can be predicted by a von Mises criterion. To exhibit a criterion in macroscopic stresses, we write the von Mises criterion in terms of local stresses and express these in terms of the macroscopic stresses and layering parameters. At this stage, we also

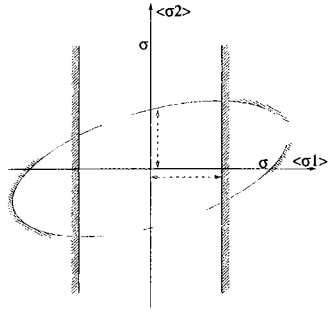

Fig. 5.10. Overall strength domain of a rank-2 layered materials

for simplicity assume that the microstructure is rotated in order to align the two layer directions with the principal directions of the macroscopic stresses.

The stress level in the rank-2 microstructure is thus everywhere under the material elastic limit $\bar{\sigma}_l$ if the two following *macroscopic* stress criteria are satisfied:

$$|<\sigma_{11}>/\gamma| \leq \bar{\sigma}_l \tag{5.32}$$

$$\sqrt{<\sigma_{11}>^2 + <\sigma_{22}>^2/\mu^2 - <\sigma_{11}><\sigma_{22}>/\mu} \leq \bar{\sigma}_l \tag{5.33}$$

The criterion (5.32) for the inner layer is similar to the stress limit of a bar with a hollow cross-section of relative density γ. For the macroscopic observer the overall strength is reduced linearly with the density of the cross-section. Also, the expression (5.33) for the outer layer is similar to a Hill's criterion for orthotropic materials (Hill 1948). Here the stress limit in the direction orthogonal to the layer is $X_1 = \bar{\sigma}_l$, while it, due to the relative thickness of the layers, is reduced to the value $X_2 = \mu\bar{\sigma}_l$ in the direction of the layering. Once again, one observes a macroscopic reduction of the strength. Figure 5.10 illustrates how the strength domain corresponding to the criteria (5.32) and (5.33) shrinks and becomes narrower when the porosity increases. Since there are two levels of layering, one considers the stress limits in the different layers separately and the overall criterion becomes a 'composite' surface which is the inner envelope of the initial strength surfaces in the different layers. This approach is similar to Hashin's failure criterion of unidirectional composites where failure modes of the matrix and of the fibers are distinguished and treated separately (Hashin 1980). It is also identical to the approach adopted in Aboudi (1991) to estimate (by the methods of cells) the initial yield surface of metal matrix composites.

Asymptotic behaviour at zero density The asymptotic behaviour of stresses at zero density plays a key role in the singularity phenomenon in

topology design with stress constraints (see section 2.3). We note here that the macroscopic strains of a composite $<\varepsilon_{ij}>$ in a point retains a *finite* value when the density goes to zero, and the macroscopic stresses are also continuous, but they vanish at zero density since the homogenized stiffness tensor tends to zero. However, the behaviour of the local stresses is completely different. The local stresses tend to finite (non zero) values at zero density. This is shown by expressing the local stresses in terms of the macroscopic strains and the layering parameters only. For the solid, inner layers we have:

$$\lim_{\mu,\gamma\to 0^+} \sigma_{11}^{L1} = E <\varepsilon_{11}^0> \qquad \lim_{\mu,\gamma\to 0^+} \sigma_{22}^{L1} = 0 \ , \qquad \lim_{\mu,\gamma\to 0^+} \sigma_{12}^{L1} = 0 \tag{5.34}$$

while the outer layers have stresses

$$\lim_{\mu,\gamma\to 0^+} \sigma_{11}^{L2} = 0 \ , \qquad \lim_{\mu,\gamma\to 0^+} \sigma_{22}^{L2} = E <\varepsilon_{22}^0> \qquad \lim_{\mu,\gamma\to 0^+} \sigma_{12}^{L2} = 0 \tag{5.35}$$

These stresses are similar to the stresses in a network of fibers intersecting at 90 degrees and in which over-stressing at the intersections is omitted because of a dilute assumption. From the simple analysis above we conclude that topology design with stress constraints for rank-2 materials are subject to the so-called "singularity" phenomenon. This problem is addressed in section 2.3.

5.4.5 Homogenization formulas for Kirchhoff plates

The homogenization formulas for Kirchhoff plates can be derived by an asymptotic expansion approach, as outlined for plane elasticity in section 3.1.2. With D denoting the plate bending stiffness tensor and κ the curvature tensor, the homogenization result is that effective properties D_{ijkl}^H are given as (see Duvaut & Metellus (1976), Duvaut (1976)):

$$\begin{aligned} D_{ijkl}^H &= \min_{\varphi\in U_Y} \frac{1}{|Y|}\int_Y D_{pqrs}(y)\kappa_{pq}(y^{ij}-\varphi)\kappa_{rs}(y^{kl}-\varphi)\mathrm{d}Y \\ &= \frac{1}{|Y|}\int_Y D_{pqrs}(y)\kappa_{pq}(y^{ij}-\chi^{ij})\kappa_{rs}(y^{kl}-\chi^{kl})\mathrm{d}Y \end{aligned} \tag{5.36}$$

Here U_Y denotes the space of Y-periodic virtual displacement fields on the unit cell Y, while χ^{kl} is a microscopic deflection that is given as the Y-periodic solution of the scalar cell-problem

$$\frac{1}{|Y|}\int_Y D_{pqrs}(y)\kappa_{pq}(y^{ij}-\chi^{ij})\kappa_{rs}(\varphi)\mathrm{d}Y = 0 \text{ for all } \varphi \in U_Y \ , \tag{5.37}$$

with reference deflections

$$y^{11} = \frac{1}{2}{y_1}^2, \ y^{12} = y^{21} = y_1 y_2, \text{ and } y^{22} = \frac{1}{2}{y_2}^2 \ ,$$

reflecting that the Kirchhoff plate equation is scalar and of order four. For a plate with one field of *stiffeners*, the effective bending stiffness can be computed from these formulas in a way analogous to the method used for plane elasticity in section 5.4.1. However, it is more instructive to consider the smear-out approach, as described in section 5.4.2. To this end let $D^-_{ijkl} = \frac{h^3}{12} E^0_{ijkl}$ denote the bending stiffness of the solid core of the plate and let $D^+_{ijkl} = \frac{h^3_{\max}}{12} E^0_{ijkl}$ denote the bending stiffness of the stiffened part of the plate, with stiffeners of density μ in the direction $\mathbf{t}$ (coordinate 2) with normal $\mathbf{n}$ (coordinate 1). For the developments it is now important that the plate equation under consideration is a scalar equation and of fourth order in the deflection. This implies that the continuity conditions across the interface holds for the tangential part of the curvature (a regularity condition) and for the normal component of the normal moment (the variational jump condition) (compare with (5.13), section 5.4.3):

$$\kappa^+_{ij} t_i t_j = \kappa^-_{ij} t_i t_j, \quad \kappa^+_{ij} t_i n_j = \kappa^-_{ij} t_i n_i, \quad M^+_{ij} n_i n_j = M^-_{ij} n_i n_j \tag{5.38}$$

Compared to plane elasticity, the *algebraic* form of these interface conditions are such that the moment tensor plays the role of the *strain* tensor, the curvature tensor plays the role of the *stress* tensor and the roles of the vectors $\mathbf{n}$, $\mathbf{t}$ defining the interface are reversed (cf. conjugate beam theory). However, the similar structure allows us to obtain the homogenized stiffness components directly from the results obtained for plane elasticity. Specifically, the homogenized bending *stiffness* can be read off from the homogenized *compliance* tensor as

$$\begin{aligned} D^H_{ijkl} &= M(D_{ijkl}) \\ &\quad - \frac{\mu(1-\mu)}{N(Dnnnn)} \left[D^+_{ijpq} - D^-_{ijpq}\right] \left[D^+_{mnkl} - D^-_{mnkl}\right] n_m n_n n_p n_q \end{aligned}$$

Here we have used the notation defined above in section 5.4.2 (cf., (5.16). For the case of orthotropic constituents, the different elements of D^H_{ijkl} are given as

$$\begin{aligned} D^H_{1111} &= \left[M\left(\tfrac{1}{D_{1111}}\right)\right]^{-1} \qquad D^H_{1122} = \left[M\left(\tfrac{D_{1122}}{D_{1111}}\right)\right]\left[M\left(\tfrac{1}{D_{1111}}\right)\right]^{-1} \\ D^H_{2222} &= M(D_{2222}) - \left[M\left(\tfrac{D^2_{1122}}{D_{1111}}\right)\right] + \left[M\left(\tfrac{D_{1122}}{D_{1111}}\right)\right]^2 \left[M\left(\tfrac{1}{D_{1111}}\right)\right]^{-1} \\ D^H_{1212} &= M(D_{1212}) \end{aligned}$$

These expressions are, except for the 1212 term, exactly the same as for the stiffness tensor in the plane elasticity case (see section 5.4.3).

5.4.6 Hashin-Shtrikman-Walpole (HSW) bounds

The Hashin-Shtrikman upper and lower bounds for electrical and thermal conductivity are given by Hashin & Shtrikman (1963) and Walpole (1966)

$$\sigma_u^{HS} = \begin{cases} \sigma^{(1*)} & \text{for} \quad \sigma^{(1)} \geq \sigma^{(2)} \\ \sigma^{(2*)} & \text{for} \quad \sigma^{(1)} < \sigma^{(2)} \end{cases} \qquad \sigma_l^{HS} = \begin{cases} \sigma^{(2*)} & \text{for} \quad \sigma^{(1)} \geq \sigma^{(2)} \\ \sigma^{(1*)} & \text{for} \quad \sigma^{(1)} < \sigma^{(2)} \end{cases}$$

and for the bulk modulus as

$$\kappa_u^{HS} = \begin{cases} \kappa^{(1*)} & \text{for} \quad \kappa^{(1)} \geq \kappa^{(2)} \\ \kappa^{(2*)} & \text{for} \quad \kappa^{(1)} < \kappa^{(2)} \end{cases} \qquad \kappa_l^{HS} = \begin{cases} \kappa^{(2*)} & \text{for} \quad \kappa^{(1)} \geq \kappa^{(2)} \\ \kappa^{(1*)} & \text{for} \quad \kappa^{(1)} < \kappa^{(2)} \end{cases}$$

and the Hashin-Shtrikman-Walpole bounds for the shear modulus are given by

$$\mu_u^{HSW} = \begin{cases} \mu^{(1*)} & \text{for} \quad \kappa^{(1)} \geq \kappa^{(2)} \quad \text{and} \quad \mu^{(1)} \geq \mu^{(2)} \\ \mu^{(2*)} & \text{for} \quad \kappa^{(1)} < \kappa^{(2)} \quad \text{and} \quad \mu^{(1)} < \mu^{(2)} \\ \mu^{(3*)} & \text{for} \quad \kappa^{(1)} \geq \kappa^{(2)} \quad \text{and} \quad \mu^{(1)} < \mu^{(2)} \\ \mu^{(4*)} & \text{for} \quad \kappa^{(1)} < \kappa^{(2)} \quad \text{and} \quad \mu^{(1)} \geq \mu^{(2)} \end{cases}$$

$$\mu_l^{HSW} = \begin{cases} \mu^{(2*)} & \text{for} \quad \kappa^{(1)} \geq \kappa^{(2)} \quad \text{and} \quad \mu^{(1)} \geq \mu^{(2)} \\ \mu^{(1*)} & \text{for} \quad \kappa^{(1)} < \kappa^{(2)} \quad \text{and} \quad \mu^{(1)} < \mu^{(2)} \\ \mu^{(4*)} & \text{for} \quad \kappa^{(1)} \geq \kappa^{(2)} \quad \text{and} \quad \mu^{(1)} < \mu^{(2)} \\ \mu^{(3*)} & \text{for} \quad \kappa^{(1)} < \kappa^{(2)} \quad \text{and} \quad \mu^{(1)} \geq \mu^{(2)} \end{cases}$$

where

$$\sigma^{(1*)} = \rho_2^e \sigma^{(1)} + (1-\rho_2^e)\,\sigma^{(2)} - \frac{\rho_2^e\,(1-\rho_2^e)\left(\sigma^{(1)}-\sigma^{(2)}\right)^2}{(1-\rho_2^e)\,\sigma^{(1)} + \rho_2^e \sigma^{(2)} + \sigma^{(1)}},$$

$$\sigma^{(2*)} = \rho_2^e \sigma^{(1)} + (1-\rho_2^e)\,\sigma^{(2)} - \frac{\rho_2^e\,(1-\rho_2^e)\left(\sigma^{(1)}-\sigma^{(2)}\right)^2}{(1-\rho_2^e)\,\sigma^{(1)} + \rho_2^e \sigma^{(2)} + \sigma^{(2)}},$$

$$\kappa^{(1*)} = \rho_2^e \kappa^{(1)} + (1-\rho_2^e)\,\kappa^{(2)} - \frac{\rho_2^e\,(1-\rho_2^e)\left(\kappa^{(1)}-\kappa^{(2)}\right)^2}{(1-\rho_2^e)\,\kappa^{(1)} + \rho_2^e \kappa^{(2)} + \mu^{(1)}},$$

$$\kappa^{(2*)} = \rho_2^e \kappa^{(1)} + (1-\rho_2^e)\,\kappa^{(2)} - \frac{\rho_2^e\,(1-\rho_2^e)\left(\kappa^{(1)}-\kappa^{(2)}\right)^2}{(1-\rho_2^e)\,\kappa^{(1)} + \rho_2^e \kappa^{(2)} + \mu^{(2)}},$$

$$\mu^{(1*)} = \rho_2^e \mu^{(1)} + (1-\rho_2^e)\,\mu^{(2)} - \frac{\rho_2^e\,(1-\rho_2^e)\left(\mu^{(1)}-\mu^{(2)}\right)^2}{(1-\rho_2^e)\,\mu^{(1)} + \rho_2^e \mu^{(2)} + \frac{\kappa^{(1)}\,\mu^{(1)}}{\kappa^{(1)}+2\,\mu^{(1)}}},$$

$$\mu^{(2*)} = \rho_2^e \mu^{(1)} + (1-\rho_2^e)\,\mu^{(2)} - \frac{\rho_2^e\,(1-\rho_2^e)\left(\mu^{(1)}-\mu^{(2)}\right)^2}{\left((1-\rho_2^e)\,\mu^{(1)} + \rho_2^e \mu^{(2)} + \frac{\kappa^{(2)}\,\mu^{(2)}}{\kappa^{(2)}+2\,\mu^{(2)}}\right)},$$

$$\mu^{(3*)} = \rho_2^e \mu^{(1)} + (1-\rho_2^e)\,\mu^{(2)} - \frac{\rho_2^e\,(1-\rho_2^e)\left(\mu^{(1)}-\mu^{(2)}\right)^2}{\left((1-\rho_2^e)\,\mu^{(1)} + \rho_2^e \mu^{(2)} + \frac{\kappa^{(2)}\,\mu^{(1)}}{\kappa^{(2)}+2\,\mu^{(1)}}\right)},$$

$$\mu^{(4*)} = \rho_2^e \mu^{(1)} + (1-\rho_2^e)\,\mu^{(2)} - \frac{\rho_2^e\,(1-\rho_2^e)\left(\mu^{(1)}-\mu^{(2)}\right)^2}{\left((1-\rho_2^e)\,\mu^{(1)} + \rho_2^e \mu^{(2)} + \frac{\kappa^{(1)}\,\mu^{(2)}}{\kappa^{(1)}+2\,\mu^{(2)}}\right)}.$$

5.5 Appendix: Barrier methods for topology design

The purpose of this appendix[6] is to give an outline of the principles of one of the most powerful modern methods of numerical optimization, namely barrier methods. Detailed descriptions of the ideas and the theory behind can be found in a vast literature on interior point methods and in several overview papers (see for example Ben-Tal & Nemirovski (2001) and references therein).

5.5.1 Notation

We first introduce a generic convex optimization problem, to fix some notation. Throughout this section we apply standard notation of mathematical programming. The unknown vector in $\mathbf{R}^n$ is denoted by $\mathbf{x} = (x_1, x_2, . \quad , x_n)$, the objective function by f and the constraint functions by g. The gradient of a function (say of f) is denoted by ∇f and the Hessian by $\nabla^2 f$ We consider first a *convex mathematical program*:

$$\min_{\mathbf{x}\in\mathbf{R}^n} f(\mathbf{x}) \quad \text{s.t.:} \quad g_i(\mathbf{x}) \leq 0, \ i \in I \tag{5.39}$$

and assume that

$f \quad \mathbf{R}^n \to \mathbf{R}$ and $g_i \quad \mathbf{R}^n \to \mathbf{R}$, $i \in I$, are twice continuously differentiable convex functions,
- the set of optimal solutions to (5.39) is nonempty and compact,
- there exist a point $\hat{\mathbf{x}}$ such that $g_i(\hat{\mathbf{x}}) < 0$ for all i.

These assumptions are satisfied for a broad range of mathematical programs coming from topology optimization. The reason that this class of problem is particularly attractive is that convex programs are computationally tractable in the sense that there exist numerical methods which efficiently solve every convex program satisfying "mild" additional assumption. In contrast, no efficient universal methods for non-convex mathematical programs are known. Special types of convex programs that arise from structural *analysis* analysis are convex quadratic program (QP):

$$\min_{\mathbf{x}\in\mathbf{R}^n} \left[\tfrac{1}{2}\mathbf{x}^T\mathbf{K}\mathbf{x} - \mathbf{d}^T\mathbf{x}\right] \quad \text{s.t.:} \quad \mathbf{C}\mathbf{x} \leq \mathbf{b}$$

(with a positive definite matrix $\mathbf{K}$). Also, in topology optimization (truss and free material optimization) we have quadratically constrained quadratic programs (QQP):

$$\min_{\mathbf{x}\in\mathbf{R}^n} \mathbf{c}^T\mathbf{x} \quad \text{s.t.:} \quad \mathbf{x}^T\mathbf{A}_i\mathbf{x} \leq \mathbf{b}_i, \quad i \in I$$

with positive definite semidefinite matrices $\mathbf{K}_i$.

[6] This appendix is based on material kindly provided to us by Michal Kocvara.

Newton's method The simplest convex program one can consider is the problem without constraints and with a strongly convex objective function, meaning that the Hessian matrix $\nabla^2 f$ is everywhere positive definite and that $f(\mathbf{x}) \to \infty$ as $\|\mathbf{x}\|_2 \to \infty$. In this case, Newton's method is always the best way to find a solution to $\min f(\mathbf{x})$ It is well known, both from the theory and practice, that Newton's method is extremely fast whenever we are "close enough" to the solution $\mathbf{x}^*$ The theory says that the method is *locally quadratically convergent*. However, it is also well known (mainly from practice) that when we are not "close enough" to $\mathbf{x}^*$, the method may be rather slow and may need many steps to get to a close neighborhood of $\mathbf{x}^*$

5.5.2 Interior-point methods

Interior-point methods are used to transform the "difficult" constrained problem into an "easy" unconstrained one, or into a sequence of unconstrained problems. Once we have an unconstrained problem, we can solve it by Newton's method. The idea is to use a barrier function that sets a barrier against leaving the feasible region. If the optimal solution occurs at the boundary of the feasible region, the procedure moves from the interior to the boundary, hence *interior-point* methods. The barrier function approach was first proposed in the early sixties but the classical barrier approach had its shortcomings. However, new ideas led to the interior-point "revolution" of the nineties.

Classical approach For the constrained convex problem (5.39) we introduce a *barrier function* B that is nonnegative and continuous over the region $\{\mathbf{x} | g_i(\mathbf{x}) < 0\}$, and approaches infinity as the boundary of this region is approached from the interior. One of the most popular barrier functions is the *logarithmic* barrier function

$$B(x) = -\sum_{i=1}^{m} \log(-g_i(x))$$

Instead of (5.39) we now investigate a one-parametric family of functions generated by our objective and the barrier $\Phi(\vartheta; \mathbf{x}) := f(\mathbf{x}) + \vartheta B(\mathbf{x})$ and the corresponding unconstrained convex programs

$$\min_{\mathbf{x}} \Phi(\vartheta; \mathbf{x})$$

Here the *penalty parameter* ϑ is assumed to be nonnegative.

The idea behind the barrier methods is now as follows. We start with some ϑ, say $\vartheta = 1$, and solve the unconstrained auxiliary problem. Then we decrease ϑ by some factor and solve again the auxiliary problem, and so on. We know that, under some mild assumption, the auxiliary problem has a unique $\mathbf{x}(\vartheta)$ for each $\vartheta > 0$, and the *central path*, defined by the solutions

$\mathbf{x}(\vartheta)$, $\vartheta > 0$, is a smooth curve and its limit (for $\vartheta \to 0$) belong to the set of optimal solutions of our original problem. For the solution of the auxiliary problems one applies Newton's method. We know that this method is extremely efficient if we are already close enough to the solution. So assume we solve the auxiliary problem for some initial ϑ. We hope that when we decrease the parameter ϑ "just a bit" the new solution $\mathbf{x}(\vartheta_{\text{new}})$ will be close enough to the old solution $\mathbf{x}(\vartheta_{\text{old}})$. So taking $\mathbf{x}(\vartheta_{\text{old}})$ as a starting point, we can utilize the good convergence behaviour of Newton's method to compute $\mathbf{x}(\vartheta_{\text{new}})$ in just a few iterations, thus following the central path from the interior to the solution $\mathbf{x}^*$ of (5.39) by decreasing ϑ (under some technical assumption $\mathbf{x}(\vartheta) \to \mathbf{x}^*$). Note that we cannot find a solution to (5.39) just in one step by setting ϑ very small. We have no idea where to start the Newton method and with this strategy the Newton method can easily leave the feasible domain (with "catastrophic" consequences as the barrier function may not be defined outside the feasible domain, as happens with the logarithmic barrier).

The idea of barrier methods sounds natural and attractive and it is supported by a solid theory. Nonetheless, in practice, it is disappointing. First, the idea to stay on the central path, and thus to solve the auxiliary problems exactly, is too restrictive. Second, it turns out that the idea of always staying in the region of quadratic convergence of the Newton method may lead to extremely short steps. Third, taking longer steps (i.e. to decrease ϑ more rapidly) makes the Newton method inefficient and we may even leave the feasible region. All these problems come from the freedom in the choice of the penalty function. The "trick" is to restrict our choice to a certain class of functions and to relax the requirement to stay on the central path.

Modern approach The classical barrier methods were developed in the sixties and seventies. After practitioners of nonlinear programming realized the numerical difficulties connected with these methods they slowly but definitely lost interest and switched to SQP-like methods.

In the end of the seventies, an interior-point revolution started in a completely different area of mathematical programming namely linear programming. And it was shown in the mid-eighties that the well-known algorithm by Karmakar can be interpreted as a classical barrier method (Gill, Murray, Sounders, Tomlin & Wright 1986). The present day understanding of modern barrier methods is based heavily on the theoretical work in Nesterov & Nemirovski (1994). Here it is showed that if we restrict the choice of barrier functions to a special class of functions, the so-called *self-concordant* barrier functions, then all the disadvantages of the barrier methods disappear and, when using a proper updating strategy of the penalty parameters ϑ, we get a *polynomial time* method[7] Thus, if B is self-concordant, one can specify

[7] An algorithm for which the maximal number of operations in which we get the solution grows only polynomially with the dimension of the problem.

the notion of "closeness to the central path" and the policy of updating the penalty parameter ϑ in the following way. If an iterate $\mathbf{x}_i$ is close (in the above sense) to the point $\mathbf{x}(\vartheta_i)$ on the central path and we update the parameter ϑ_i to ϑ_{i+1}, then in a *single* Newton step we get a new iterate $\mathbf{x}_{i+1}$ which is close to $\mathbf{x}(\vartheta_{i+1})$. In other words, after every update of ϑ we can perform only one Newton step and stay close to the central path. Moreover, points "close to the central path" belong to the interior of the feasible region. Finally, the penalty updating policy can be defined in terms of problem data: $\vartheta_{i+1} = \vartheta_i/(1 + \frac{0.1}{\sqrt{\theta(B)}})$, where the penalty parameter decreases linearly.

The class of self-concordant function is sufficiently large and contains many popular barriers, in particular the logarithmic barrier function.

There exist today many variations of the basic scheme outlined above. One of these is described below; this has proved to be extremely efficient when solving problems of topology optimization. Strictly speaking it is not a pure "interior-point" method as some of the iterates may be infeasible, but it belongs to the family of modern barrier methods. Another advantage of this method is that it can be naturally generalized to SDP problems.

5.5.3 A barrier method for topology optimization

In this section briefly present the principles of the Penalty/Barrier Multiplier (PBM) method (Ben-Tal & Zibulevsky 1997) which has proved to be a very efficient tool for solving large scale convex programs of the type (4.24) that appear in topology design. The method is based on a choice of a penalty/barrier function $\varphi \quad \mathbf{R} \to \mathbf{R}$ that penalizes the inequality constraints.

For exemplification (the general situation is dealt with in the literature) we consider here the strictly increasing and strictly convex, smooth function

$$\phi_\varrho(s) = \begin{cases} \frac{1}{8\varrho}s^2 + s & \text{if } s \geq -2\varrho \\ -\varrho\left[\log(\frac{s}{-2\varrho}) + \frac{3}{2}\right] & \text{if } s < -2\varrho\,, \end{cases}$$

composed of a logarithmic branch and a quadratic branch (with $0 \leq \varrho \leq 1$). Since $\phi_\varrho(s) \leq 0$ if and only if $s \leq 0$ it follows that the problem (5.39) is equivalent to the problem,

$$\min_{\mathbf{x}} \{f(\mathbf{x}) \mid \phi_\varrho\left[g_i(\mathbf{x})\right] \leq 0,\, i \in I\} \tag{5.40}$$

The Lagrangian corresponding to problem (5.40) is

$$F_\varrho(\mathbf{x}, \vartheta) = f(\mathbf{x}) + \sum_{i \in I} \vartheta_i \phi_\varrho\left[g_i(\mathbf{x})\right] \tag{5.41}$$

and the PBM method consists in minimizing this combined penalty, barrier and multiplier function. Thus the algorithm combines ideas of (exterior) penalty and (interior) barrier methods with the Augmented Lagrangian

method. At the j-th iteration step of the PBM method the penalty parameter $\varrho_j > 0$ and the current estimate of the Lagrange multipliers $\{\vartheta_i^j \quad i \in I\}$ are given. The update of $\mathbf{x}^j$ are computed by a Newton method for the minimization of (5.41), i.e.

$$\mathbf{x}^{j+1} = \arg\min_{\mathbf{x}} F_{\varrho^j}(\mathbf{x}, \vartheta^j)$$

The multipliers are then updated by the rule

$$\vartheta_i^{j+1} = \vartheta_i^j \frac{\mathrm{d}\phi_{\varrho^j}}{\mathrm{d}t}\left[g_i(\mathbf{x}^{j+1})\right], \quad i \in I$$

and the penalty parameter ϱ by the update formula $\varrho_{j+1} = \alpha\varrho_j$ with a parameter α, $0 < \alpha < 1$ For details on motivation, convergence properties and implementation of the PBM method we refer to Ben-Tal & Zibulevsky (1997).

The use of the ϕ_ϱ function combines, in a sense, the advantages of the interior logarithmic penalty function underlying the interior-point polynomial-time algorithms, and those of external penalty, thus allowing to avoid serious computational difficulties arising in pure interior-point methods when they come close to the boundary of the feasible domain. The second derivative ϕ'' is continuous and bounded for all s; this is advantageous when performing the minimization step of the algorithm by for example a modified Newton method with line-search. The choice of the logarithmic-quadratic penalty function ϕ usually reduces the number of Newton steps 2–3 times compared to a use of the pure (shifted) logarithmic penalty, particularly for large-scale problems. Also, the line-search needs much less function and gradient evaluations (typically only 2–3). Moreover, the method is less sensitive to the choice of the initial point $\mathbf{x}^0$

The method described above can also be extended to convex SDP problems and are very efficient for solving such problems from topology optimization. We will not elaborate on this here, but refer to the literature [33].

5.5.4 The free material multiple load case as a SDP problem

It is shown in section 3.4.4 how it is possible to reformulate the single load free material design problem as a convex, quadratically constrained quadratic program. However, the multiple load problem is much more complicated, but it is, however, possible to convert it to a linear SDP problem (as indicated in section 3.4.4). This can, in turn, be efficiently solved by the PBM method (for details, see Ben-Tal, Kocvara, Nemirovski & Zowe (2000)).

In section 3.4.4 it is outlined that the *trace* version of the multiple load problem for minimum compliance for the free parametrization of material can be recast as a problem involving constraints on the eigenvalues of a tensor A that is the sum of dyadic tensors. In FE discretized form with N elements,

we have a problem in the form (for simplicity written for the situation when no bounds on the density are enforced)

$$\begin{aligned} \inf_{\mathbf{u}^k, k=1,\ldots,M} \; & V\tau - 2\sum_{k=1}^{M} (\mathbf{f}^k)^T \mathbf{u}^k \\ \text{s.t.} \quad & \tau\mathbf{I} - \mathbf{A}_e(\mathbf{u}) \succeq 0, \; e = 1, \ldots, N \end{aligned} \tag{5.42}$$

where $\mathbf{A}_e$ are the discretized version of the tensor A

$$\mathbf{A}_e = \sum_{k=1}^{M} \lambda_k \sum_{s=1}^{S} \gamma_{es}^2 \epsilon_{x_{es}}(\mathbf{u}^k) \epsilon_{x_{es}}(\mathbf{u}^k)^T$$

Here x_{es}, $s = 1, \ldots, S$, are points of Gaussian integration in element e, γ_{es}^2 are the the corresponding integration weights, $\epsilon_{x_{es}}$ is the discretized strain vector at x_{es}, and ω_i are the volumes of the elements. Now, with the matrices

$$\begin{aligned} \mathbf{Z}_e &= \left[\gamma_{e1}\epsilon_{x_{e1}}(\mathbf{u}^1), \ldots, \gamma_{es}\epsilon_{x_{es}}(\mathbf{u}^1), \ldots, \gamma_{e1}\epsilon_{x_{e1}}(\mathbf{u}^M), \ldots, \gamma_{es}\epsilon_{x_{es}}(\mathbf{u}^M)\right] \\ \mathbf{L}(\lambda) &= \operatorname{diag}(\lambda_1, \ldots, \lambda_1, \ldots, \lambda_M, \ldots, \lambda_M) \end{aligned}$$

the constraints in (5.42) take the form $\tau\mathbf{I} - \mathbf{Z}_e(\mathbf{u})\mathbf{L}(\lambda)\mathbf{Z}_e(\mathbf{u})^T \succeq 0$ which (by the Shur complement) is equivalent to

$$\begin{bmatrix} \tau\mathbf{I} & \mathbf{Z}_e(\mathbf{u}) \\ \mathbf{Z}_e(\mathbf{u})^T & \mathbf{L}(\lambda)^{-1} \end{bmatrix} \succeq 0.$$

We thus end up with a *semidefinite program* for the discretization of (3.34) in the *trace* case, here written for the weighted average form of the multiple load case. For the min-max variant of this problem a change of variables $\mathbf{v}^k := \lambda_1 \mathbf{u}^k$ allow us also for this case to write a SDP problem in the form:

$$\begin{aligned} \inf_{\substack{\tau,\, \mathbf{v}^k, k=1,\ldots,M \\ \lambda^k > 0, \sum_{k=1}^{M} \lambda^k = 1}} \; & V\tau - 2\sum_{k=1}^{M} (\mathbf{f}^k)^T \mathbf{v}^k \\ \text{s.t.} \quad & \begin{bmatrix} \tau\mathbf{I} & \mathbf{Z}_e(\mathbf{u}) \\ \mathbf{Z}_e(\mathbf{u})^T & \mathbf{L}(\lambda) \end{bmatrix} \succeq 0, \; e = 1, \ldots, N \end{aligned} \tag{5.43}$$

It should be noted here that the optimal elasticity matrices (tensors) E^k can be recovered from the Lagrangian multipliers to the inequality constraints in (5.43). Problem (5.43) is a large scale linear SDP with very many relatively small matrix inequalities. As a result, the Hessian of the Lagrangian associated with this problem is a large and sparse matrix. As such, it can be efficiently solved by the SDP variant of the PBM method mentioned above (Kocvara & Stingl 2001). Note that, when solving the multiple load problems by this method, the limiting factor is not so much the CPU time but rather the CPU memory.

6 Bibliographical notes

The bibliography consists of three parts: bibliographical notes, the list of references at the end of the book, and an author index.

The list of references is concentrated on literature central for the developments described in this monograph, supplemented with background material in order to ease access to work in related fields. The list of references is by no means complete, and should more be seen as a supplement to dedicated survey papers and other monographs.

The purpose of these bibliographical notes is two-fold. The primary purpose is to serve as a guide to the literature in the field of topology design and related subjects. A secondary purpose is to function as a list of references grouped according to subject. In this way long lists of references have been avoided in the main text of the monograph, reference instead being made to these bibliographical notes.

The bibliographical notes cover the various sub-fields of topology design, the groups being largely defined by the structure of the presentation in the main text of the monograph. The entries are divided into books and survey papers and other publications. For the latter category of publications we use a more elaborate division into sub-fields and the emphasis here is on work from within the last decade; for the historical oriented reader we refer to the books and survey papers mentioned below.

The bibliographical notes do not cover all entries of the list of references, as this list also contains specific references used in the main text.

6.1 Books and survey papers

[1] On optimal design in general There exist quite a number of excellent books treating optimal structural design in a broader sense. As textbooks we mention Haftka & Gürdal (1992), Kirsch (1993b), and Eschenauer, Olhoff & Schnell (1997). The monograph Haug, Choi & Komkov (1986) is a classical text that contains detailed information on sensitivity analysis and Lewiński & Telega (2000) covers modelling and design of plate and shells in great detail. A general discussion of optimal designs can be found in Pedersen (2002f). An overview of the developments in the field over the last two decades can be gained by consulting the edited books by Haug & Cea (1981), Morris (1982),

Mota Soares (1987), Rozvany (1993), Pedersen (1993d), Hörnlein & Schittkowski (1993), Haug (1993), Herskovits (1995), Bestle & Schielen (1995), Arora (1997), and by consulting the proceedings of especially the World Congresses of Structural and Multidisciplinary Optimization (WCSMO) Olhoff & Rozvany (1995), Gutkowski & Mróz (1997), Bloebaum (1999), and Cheng, Gu, Liu & Wang (2001). Of books with many analytical results we mention the classical texts Banichuk (1983), Banichuk (1990) and Save & Prager (1985), Save & Prager (1990). Recent survey papers are few, but an overview of issues in structural optimization, encompassing topology, shape and sizing optimization can be found in Maute, Schwarz & Ramm (1999) and Vanderplaats (1999).

Finally, a recent book specializing on design with advanced materials is Kalamkarov & Kolpakov (1997), and the crucial influence of material choice on design is vividly described in the survey papers Ashby (1991) and Lakes (1993).

[2] **On classical shape design methods** Example research monographs are Pironneau (1984), Bennet & Botkin (1986), and Haslinger & Neittaanmki (1996). Sensitivity analysis for shape design problems is treated in detail in Sokołowski & Zolesio (1992). A recent overview of mathematical techniques can be found in Kawohl, Pironneau, Tartar & Zolesio (2000), while one of the most recent monographs in the area is Mohammadi & Pironneau (2001), which spezializes in shape design for fluids. Older survey papers are Ding (1986), Haftka & Gandhi (1986), and Hsu (1994). A recent survey paper dealing with mathematical aspects is Allaire & Henrot (2001).

[3] **On topology design and layout optimization** Classical books on this subject are Hemp (1973), Rozvany (1976), and Rozvany (1989). Following the edited monographs Rozvany (1992) and Bendsøe & Mota Soares (1992), the first text Bendsøe (1995) on topology design based on the material distribution method has been followed by the book Hassani & Hinton (1999), which emphasizes the so-called homogenization method. Recent titles which cover the field in abroad sense are Rozvany (1997b) and Rozvany & Olhoff (2000), with Cherkaev (2000), Allaire (2002) emphasizing more the mathematical aspects of the field. These latter books also cover aspects related to composites and relaxation of functionals (see [4], [5]). Finally, the book Xie & Steven (1997) describes what is called evolutionary methods for topology design. Papers on the close correspondance between bone remodelling schemes and optimal design can be found in Pedersen & Bendsøe (1999).

The most recent survey on topology design, covering the area in great detail, is the very thorough paper (Eschenauer & Olhoff 2001), which contains 425 references. Other example survey papers on classical lay-out theory and topology design are Rozvany (1993), Rozvany, Zhou & Sigmund (1994), Rozvany, Bendsøe & Kirsch (1995), Rozvany (1997a), Sigmund & Petersson (1998), Rozvany (2001a). Surveys of numerical methods for truss-type struc-

tures can be found in for example Topping (1993) and Kirsch (1989a), and Olhoff (1996) and Bendsøe (1997) surveys design with and of materials.

[4] **On homogenization, effective media theory and optimal bounds** A general introduction on the mechanics of composite materials can be found in, e.g., Christensen (1991), Aboudi (1991), Milton (2002), and Torquato (2002). Classical books on the theory of homogenization are Bensoussan, Lions & Papanicolaou (1978), and Sánchez Palencia (1980); a more recent presentation can be found in Cioranescu & Donato (1999). The editied monographs Ericksen, Kinderlehrer, Kohn & Lions (1986), Dal Maso & Dell'Antonio (1991), Bouchitte, Buttazzo & Suquet (1994), Maso & Dell'Antonio (1995), Cioranescu, Damlamian & Donato (1995), and Cherkaev & Kohn (1997) contain papers on this subject and its relations to relaxation and design and represents collections of papers closely related to the contents of the present monograph. Finally, one should note that the recent monographs Cherkaev (2000) and Allaire (2002) on shape and topology optimization covers this subject in detail also.

[5] **On relaxation of functionals in the calculus of variations** Example research monographs are Attouch (1984), Buttazzo (1989), Dacorogna (1989), Lurie (1993), Dal Maso (1993) and Braides & Defranceschi (1998). The book by Dal Maso (1993) contains a very detailed bibliography.

6.2 Papers

[6] **The material distribution method for topology design, basic methodology** The basic idea of finding the topology of a structure by searching for the optimal indicator function of the material set is discussed briefly in for example Cea, Gioan & Michel (1973), and Tartar (1979). The numerical implementation of the material distribution idea (based on homogenized materials) was first described in Bendsøe & Kikuchi (1988), and a closely related idea was pursued in Zochowski (1988). Further early developments of the homogenization idea can be found in Suzuki & Kikuchi (1991), Thomsen (1991); multiple loads were treated in Díaz & Bendsøe (1992), and the close relation between continuum and truss topology design in Díaz & Belding (1993).

The idea of using a penalized variable density approach (SIMP) for numerically approximating the 0-1 design problem was tested in Bendsøe (1989), Rozvany et al. (1994) and Yang & Chuang (1994) and has since been used extensively. That SIMP can be understood as a material based interpolation was shown in Bendsøe & Sigmund (1999). Related to SIMP as well as to the homogenization approach is the use of approximate effective energies (Mlejnek 1992, Mlejnek & Schirrmacher 1993).

[7] **Optimality criteria methods in optimal design** The development of optimality criteria (OC) algorithms for continuum problems can be traced back to for example Wasiutynski (1960), Prager & Taylor (1968), Taylor (1969), Masur (1970). The use of such algorithms for continuum design problems can be found in for example Olhoff (1970), Taylor & Rossow (1977), Cheng & Olhoff (1982), Bendsøe (1986), Bendsøe & Kikuchi (1988), Rozvany & Zhou (1991), Zhou & Rozvany (1991), and Rozvany et al. (1994). Convergence and sufficiency studies and interpretations of OC and the stress ratio method (for trusses) can be found in Levy (1991), Svanberg (1994a), Cheng & Pedersen (1997) and Toader (1997).

For the relation between optimality criteria update schemes, optimal design and models for bone adaptation (adaptive bone-remodelling), see, e.g., Cowin (1990), Weinans, Huiskes & Grootenboer (1992), Cowin (1995), Pettermann, Reiter & Rammerstorfer (1997), Jacobs, Simo, Beaupre & Carter (1997), Huiskes (2000) and Bagge (2000).

[8] **Restriction methods** The perimeter constraint in the basic topology design was first implemented in Haber, Jog & Bendsøe (1996), based on the theory from Ambrosio & Buttazzo (1993) (see also Petersson (1999b)). Implementations in 2D and 3D can be found in Fernandes, Guedes & Rodrigues (1999), Beckers (1999), Borrvall (2001), and Jog (2002b). The anisotropy of approximations is addressed in Petersson (1999b) and Petersson et al. (2000). Related theoretical work involving a so-called capacity constraint can be found in Bucur & Zolesio (1995), Bucur & Zolesio (1996).

Gradient constrained and slope constrained methods are discussed in Borrvall (2001), Petersson & Sigmund (1998), and Zhou et al. (2001). Filters on the density was first used in Bruns & Tortorelli (2001) and analyzed in detail in Bourdin (2001). Minimum length scale control as a constraint was introduced in Poulsen (2001a).

The filtering of sensitivities used extensively in this monograph was introduced in Sigmund (1994a) and Sigmund (1997) (see also Sigmund & Petersson (1998)).

[9] **The checkerboard problem** The control of the checkerboards in topology design was first discussed in Bendsøe, Díaz & Kikuchi (1993), Jog, Haber & Bendsøe (1993), and Rodrigues & Fernandes (1993). Detailed analyses of the problem can be found in Díaz & Sigmund (1995) and Jog & Haber (1996). Direct checkerboard control is discussed in these papers also. More methods are described in Sigmund (1994a), Jang et al. (2001), Poulsen (2001b). The books Hughes (1987), and Brezzi & Fortin (1991) gives relevant background material for saddle point problems in analysis.

[10] **Integration of boundary shape optimization and topology design** Integration of the topology design methods and classical shape design, mainly for 2D problems, received a lot of attention shortly after the material

design method was introduced (Papalambros & Chirehdast 1990, Bendsøe & Rodrigues 1991, Bremicker, Chirehdast, Kikuchi & Papalambros 1992, Olhoff, Bendsøe & Rasmussen 1992b, Olhoff, Lund & Rasmussen 1993, Rasmussen et al. 1993). Newer developments involve adaptation (Maute & Ramm 1997, Bletzinger & Maute 1997, Maute & Ramm 1998) and automatic shape extraction (Marsan & Dutta 1996, Beuzit & Habbal 2001, Lin & Chao 2000, Chang 2001, Tang & Chang 2001, Hsu, Hsu & Chen 2001) in both 2D and3D. Other recent work can be found in Lin & Chou (1999) and Ansola, Canales, Tarrago & Rasmussen (2002). Design of an optimum groundstructure (Chen & Lin 2000) and simultaneous thickness and topology design (Rietz & Petersson 2001) has also been proposed. Finally, Bulman, Sienz & Hinton (2001) has proposed a range of benchmark examples for the field.

[11] Variable thickness sheets, interpolations and design representation The idea of using a variable thickness sheet model to predict topology was first suggested by Rossow & Taylor (1973); see also Didenko (1981), and detailed analyses of this problem (FE convergence, etc.) and the associated contact problem can be found in Petersson (1996), Petersson & Patriksson (1997), Petersson & Haslinger (1998), Petersson (1999a), and Golay & Seppecher (2001).

Other interpolation methods than SIMP are presented in Swan & Kosaka (1997a), Swan & Kosaka (1997b), Stolpe & Svanberg (2001a), and Pedersen (2002e). The application of wavelets for the design description is proposed in Kim & Yoon (2000) and Poulsen (2002), while their use for analysis in topology design is described in DeRose Jr. & Díaz (1999) and DeRose Jr. & Díaz (2000).

[12] Discrete valued optimal topology design problems For continuum structures Anagnostou, Rønquist & Patera (1992) and Ghaddar, Maday & Patera (1995) discussed the use of a pixel-based discrete optimization procedure for part design, as the basis for applying simulated annealing (Shim & Manoochehri 1997) or genetic algorithms (Chapman & Jakiela 1996, Kane & Schoenauer 1996a, Kane & Schoenauer 1996b, Tanie & Kita 1997, Baron, Fisher, Sherlock, Mill & Tuson 1997, Kita & Tanie 1999, Jakiela, Chapman, Duda, Adewuya & Saitou 2000). Dual methods for compliance design has been applied in Beckers (1997), Beckers (1999), and Beckers (2000) for large scale problems.

[13] Alternative approaches to topology design A whole range of methods have been proposed that combine aspects of fully stressed design, OC methods, element removal or structural growth. Typically sensitivity analysis and mathematical programming is not applied. The methods often apply the word "evolutionary", which here should *not* be confused with genetic algorithms. We here mention example papers describing methods that are named as shape (Atrek 1993); evolutionary (Riche &

Cailletaud 1998, Harasaki & Arora 2001); SKO (Baumgartner, Harzheim & Mattheck 1992, Mattheck 1996, Mattheck 1998); self-designing (Christie, Bettess & Bull 1998, Reynolds, McConnachie, Bettess, Christie & Bull 1999); metamorphic (Liu, Parks & Clarkson 2000); self-organising (Payten & Ben-Nissan 1997, Payten, Ben-Nissan & Mercer 1998, Payten & Law 1998); and ESO (Zhao, Steven & Xie 1997, Chu, Xie, Hira & Steven 1997, Kim, Querin, Steven & Xie 2000, Proos, Steven, Querin & Xie 2001, Li, Steven & Xie 2001). See Eschenauer & Olhoff (2001) for an overview.

The bubble method and methods based on topological derivatives are closely related to shape design and are discussed in Eschenauer, Kobelev & Schumacher (1994), Eschenauer & Schumacher (1997), Sokołowski & Zochowski (1999), and Cea, Garreau, Guillaume & Masmoudi (2000). Also here, see Eschenauer & Olhoff (2001) for a detailed overview. Level set methods have also been applied a few times over the last decade (Kumar & Gossard 1992, Kumar & Gossard 1996, Vimawala & Turkiyyah 1995, Hara, Zha & Haegawa 1999, Sethian & Wiegmann 2000) and are in a sense related to the imbedding method of boundary control and the related fictitious domain method (Neittaanmki & Tiba 1995).

[14] Topology design for vibration problems Topology design for improved vibration response of continuum structures using the material design method is described in Díaz & Kikuchi (1992), Soto & Díaz (1993a), Tenek & Hagiwara (1993b) Ma, Kikuchi & Hagiwara (1994), Ma, Kikuchi, Cheng & Hagiwara (1995), Ma, Kikuchi & Cheng (1995), Kawabe & Yoshida (1996), Cox & Lipton (1996), Krog & Olhoff (1999), Min, Kikuchi, Park, Kim & Chang (1999), Min, Nishiwaki & Kikuchi (2000), Kim & Kim (2000a), Pedersen (2000b), Pedersen (2000a), Allaire, Aubry & Jouve (2001), Belblidia & Bulman (2001). Also, design with respect to forced vibrations is described in Ou & Kikuchi (1996a), Ou & Kikuchi (1996b), Jog (2002a) and Tcherniak (2002) and for bandgap structures in Sigmund (2001d), Sigmund & Jensen (2002b), and Sigmund & Jensen (2002a)

The main problem of these types of optimization problems is the non-smoothness of the eigenvalues (see also [15]). Special optimization algorithms to cater for this are described in for example Wardi & Polak (1982) and Overton (1992), with a survey in Lewis & Overton (1996). The non-smoothness problem is addressed in detail in Cox & Overton (1992), Seyranian (1993), Seyranian et al. (1994), and Rodrigues, Guedes & Bendsøe (1995).

[15] Topology design for stability problems Structural design under stability constraints is a vast subject as can be seen by consulting Zyczkowski & Gajewski (1988). For topology design of continuum structures work on structural buckling can be found in Neves et al. (1995), Min & Kikuchi (1997), Folgado & Rodrigues (1998), Sekimoto & Noguchi (2001), Manickarajah, Xie & Steven (1998), and Rahmatalla & Swan (2002), while Neves et al. (2002b) and Neves et al. (2002a) deal with buckling in materials. The related problem

of homogenization of buckling problems is treated in Suquet (1981), and the relation between microscopic and macroscopic buckling is discussed in for example Bendsøe & Triantafyllidis (1990), Geymonat, Müller & Triantafyllidis (1993), and Triantafyllidis & Schnaidt (1993). As for vibration problems, a major obstacle in computations is the non-smoothness of the eigenvalues (see [14]) in the stability problems at multi-modal solutions (such solutions were first discovered by Olhoff & Rasmussen (1977), for columns).

Finally, for work on non-linear buckling problems consult Kemmler, Schwarz & Ramm (2000), Bruns et al. (2002), and Rahmatalla & Swan (2002).

[16] Stress constraints Stress constraints for continuum topology design has only received moderate attention, see Swan & Arora (1997), Duysinx & Bendsøe (1998), Duysinx & Sigmund (1998), Yuge, Iwai & Kikuchi (1999) and Duysinx (2000). The stress constraint developed in Duysinx & Bendsøe (1998) is based on modelling of a simple microstructure; a more general scheme has been developed in Lipton (2001) and Lipton (2002). Note that a similar model is needed in elasto-plastic design (Swan & Kosaka 1997b, Maute, Schwarz & Ramm 1998, Schwarz, Maute & Ramm 2001). The "singularity" problem for stress constraints has mainly been studied for truss structures (Cheng & Jiang 1992, Rozvany & Birker 1994, Cheng 1996, Cheng & Guo 1997, Guo, Cheng & Yamazaki 2001, Guo & Cheng 2000, Rozvany 1996, Rozvany 2001b, Petersson 2001, Stolpe & Svanberg 2001c), but the developments have equal importance for the continuum case.

[17] Geometrically non-linear problems The application of geometrically non-linear analysis has been applied to stiffness design (Jog 1996, Yuge et al. 1999, Kemmler et al. 2000, Buhl et al. 2000, Gea & Luo 2001, Pedersen 2002b, Pedersen 2002c), as well as to mechanism design (Pedersen et al. 2001, Bruns & Tortorelli 2001, Bruns & Tortorelli 2001, Sigmund 2001b, Sigmund 2001c, Sekimoto & Noguchi 2001, Saxena & Ananthasuresh 2001, Buhl 2002). The first approaches to synthesize mechanisms with snap-through or bistable responses have been presented in Sekimoto & Noguchi (2001), Bruns et al. (2002), and Bruns & Sigmund (2001), and problems involving geometrical non-linearity and crashworthiness have been solved in Mayer, Kikuchi & Scott (1996), Soto (2001), Soto & Díaz (1999), and Pedersen (2002b).

[18] Synthesis of compliant mechanisms and MEMS The first applications of topology optimization methods to compliant mechanism synthesis appeared independently in Ananthasuresh, Kota & Gianchandani (1994), Sigmund (1996) and Ananthasuresh, Kota & Kikuchi (1994). Later developments in the area have followed two main directions. One approach initiated in Sigmund (1997) models the output load by a spring which allows full control of the input-output behaviour. Papers following this approach are Larsen et al. (1997), Hetrick, Kikuchi & Kota (2000), Jonsmann, Sigmund & Bouwstra (1999b), Jonsmann, Sigmund & Bouwstra (1999a), Canfield & Frecker

(2000), Tai & Chee (2000), Lau, Du & Lim (2001b), Lau, Du & Lim (2001a), Pedersen et al. (2001), Bruns & Tortorelli (2001), Bruns & Tortorelli (2002), Sigmund (2001a), Sigmund (2001b), Sigmund (2001e) and Yin & Ananthasuresh (2001). Another approach is based on the maximization of the ratio of two mutual energies based on two different finite element problems as initiated in Frecker, Ananthasuresh, Nishiwaki & Kota (1997). Papers following this approach are Nishiwaki, Frecker, Min & Kikuchi (1998), Frecker, Kikuchi & Kota (1999), Kota, Joo, Li, Rodgers & Sniegowski (2001), Ejimi, Nishiwaki, Sekiguchi & Kikuchi (2000) Nishiwaki, Min, Yoo & Kikuchi (2001), Chen, Silva & Kikuchi (2001). It seems that the latter approach provides limited control of the input-output behaviour of the mechanism and as remarked in Hetrick et al. (2000) the objective function is not well bounded. Also there are problems with convergence and dependence on the minimum element density bound, so therefore Hetrick et al. (2000) suggests to use of the spring approach instead.

Mechanisms for shape control of surfaces has been dealt with in Saggere & Kota (1999) and Sigmund (2000b). Since mechanisms intrinsically provide large deflections they should be modelled using large displacement theory, see 17.

Path generating mechanisms have been treated in Pedersen et al. (2001) and Saxena & Ananthasuresh (2001) and design of structures and mechanisms for snap-through and prescribed buckling behavior is seen in Bruns & Sigmund (2001) and Bruns et al. (2002).

Optimization of (linear) dynamic response of mechanisms and actuators has been considered by Du, Lau, Lim & Qui (2000), Nishiwaki, Saitou, Min & Kikuchi (2000) and Tcherniak (2002).

Finally note that the developments on thermal actuators has a counterpart for structures (Rodrigues & Fernandes 1995).

[19] Design of supports Inclusion of the distribution of supports in topology optimization problems has been done in Buhl (2002) for elastic structures and compliant mechanisms using large displacement finite element analysis. Optimization of support distribution for fixed plate topologies was considered in Cox & Uhlig (2001). Similar problems for design of fasteners and position of pin joints in structures are seen in Chickermane & Gea (1997), Jiang & Chirehdast (1997), and Chickermane, Gea, Yang & Chuang (1999), and (indirectly) for fluids in Borrvall & Petersson (2002).

Analytical results for support locations can be found in Rozvany (1974), Mróz & Rozvany (1975) and Prager & Rozvany (1975). Other results are for columns (Rozvany & Mróz 1977, Olhoff & Taylor 1978) and for buckling (Olhoff & Akesson 1991) and vibrations (Åkesson & Olhoff 1988).

[20] Homogenization of periodic media – theory and computations Supplementing the books mentioned above, we mention the recent alternative two-scale convergence theory for the convergence of homogenized functionals

as described in e.g., Allaire (1992). Of interest for design we mention the relation between cell symmetries and symmetries of composite media as described in, e.g. Lene & Duvaut (1981). Computational implementations of the homogenization method for computing effective media characteristics are described in for example Bourgat (1977) and Guedes & Kikuchi (1991). The use of trusses in the inverse homogenization method applies results for homogenization of thin structures as treated in e.g., Cioranescu & Paulin (1999) and Bakhvalov & Panasenko (1989).

[21] **Material design** The technique of inverse homogenization was first developed with truss models (Sigmund 1994a, Sigmund 1994b, Sigmund 1995) and then for continuum elasticity (Sigmund 1994a, Sigmund 1996, Terada & Kikuchi 1996, Swan & Kosaka 1997a, Theocaris & Stavroulakis 1998, Sigmund 2000b, Gibiansky & Sigmund 2000, Hyun & Torquato 2000, Neves, Rodrigues & Guedes 2000, Guedes et al. 2001, Hoppe & Petrova 2001), for conduction (Haslinger & Dvořák 1995), for three phase elastic and thermoelastic properties (Sigmund & Torquato 1996, Sigmund & Torquato 1997, Fujii, Chen & Kikuchi 2001), for piezoelectric transducer design (Silva, Fonseca & Kikuchi 1997, Silva, Fonseca & Kikuchi 1998, Sigmund & Torquato 1999), and for strength (Swan & Arora 1997) and viscoelastic properties (Yi, Park & Youn 2000). The so-called quasiperiodic case has also been considered in Chenais, Mascarenhas & Trabucho (1997) and Ryvkin, Fuchs & Nuller (1999).

Also, we note the different proposals for negative Poisson's ratio materials that can be found in the literature (Kolpakov 1985, Almgren 1985, Lakes 1987, Milton 1992, Rothemburg, Berlin & Bathurst 1991, Sigmund 1994a, Sigmund 1994b, Sigmund 1995)

Design with multiple materials is also found in other areas of topology design, see Thomsen (1992), Olhoff, Thomsen & Rasmussen (1993), Sigmund (2001c) and Selyugin & Chekhov (2001).

[22] **Other areas of applications and variations of the theme** The basic developments of topology design for elasticity have had a parallel (actually slightly preceding) history for problems in conduction, see for example Goodman, Kohn & Reyna (1986), that contains both numerical work and an extensive list of references. Similar design problems arise also in impedance computed tomography as described in, e.g., Kohn & Vogelius (1987), in electromagnetic (and band-gap) problems (Achdou 1993, Dyck & Lowther 1996, Dyck & Lowther 1997, Choi, Lowther & Dyck 1998, Lowther, Mai & Dyck 1998, Byun, Hahn & Park 1999, Cox & Dobson 1999, Cox & Dobson 2000, Byun, Lee, Park, Lee, Choi & Hahn 2000, Chung, Cheon & Hahn 2000, Yoo & Kikuchi 2000, Yoo, Kikuchi & Volakis 2000, Poulton, Movchan, McPhedran, Nicorovici & Antipov 2000, Hoppe, Petrova & Schulz 2001, Korvink, Greiner & Lienemann 2001), and in nuclear physics (Allaire & Castro 2001). Of other subjects not covered here we also men-

tion work on design of cross-sections of beams and shafts (Chirehdast & Ambo 1995, Díaz & Lipton 2000, Kim & Kim 2000b), in biomechaniccal design (Hollister & Kikuchi 1994, Folgado & Rodrigues 1997, Folgado, Fernandes & Rodrigues 2001) (the latter also covers contact conditions), and in civil engineering applications (Mijar, Swan, Arora & Kosaka 1998, Yin & Yang 2000b, Yin & Yang 2000a, Yin, Yang & Guo 2000, Guan, Chen & Loo 2001).

Finally, related to work reported in this monograph we mention design in crashworthiness design (Mayer et al. 1996, Soto & Díaz 1999, Soto 2001, Pedersen 2002b), and the work taking pressure loads into account (Hammer & Olhoff 2000, Hammer & Olhoff 2001, Bing-Chung & Kikuchi 2001, Bourdin & Chambolle 2001) (a related problem for distributed surface loads is treated in Fuchs & Moses (2000)).

[23] Industrial applications Some example papers presenting applications of topology design in an industrial setting covers aerospace applications (Hörnlein et al. 2001, Park, Chang & Youn 2001), machine industry (Magister & Post 1995, Back-Pedersen 1998, Back-Pedersen 1999) and the auto industry (Chirehdast, Sankaranarayanan, Ambo & Johnson 1994, Yang & Chahande 1995, Yang, Chen & Lee 1996, Yang 1997, Schramm 1999, Yang, Chuang, Che & Soto 2000, Ruy & Yang 2001). Many more examples on industrial applications can be found on the Internet, for example at the homepages of the major software companies (NASTRAN, ANSYS, ALTAIR, etc.).

[24] Optimal design with anisotropic materials Optimal design with orthotropic materials and the problem of finding the optimum angle of material rotation is discussed in Rasmussen (1979), Seregin & Troitskii (1982), Banichuk (1983), Fedorov & Cherkaev (1983), Pedersen (1989), Pedersen (1990), Rovati & Taliercio (1991), Pedersen & Bendsøe (1995), and Banichuk & Sharanyuk (1996). Studies on the simultaneous design of thickness and material angle can be found in, e.g, Pedersen (1991), Pedersen (1993a), Pedersen (1995a), and Pedersen (1998).

[25] Relaxation, effective media, optimal bounds and optimal design We refer here to the two recent monographs (Allaire 2002, Cherkaev 2000) that include comprehensive lists of references that covers this subject in great detail. Here we thus just refer to very few papers (see also the main text), with example papers Francfort & Murat (1986), Lurie & Cherkaev (1997) Avellaneda (1987), Francfort, Murat & Tartar (1995) Avellaneda & Milton (1989), Lipton (1994c). Also, the close connection between generalized optimal shape design, relaxation and effective media characteristics is discussed in the example papers and monographs Lurie (1980), Lurie, Cherkaev & Fedorov (1982), Lurie (1993), Kohn & Strang (1986), and Murat & Tartar (1997).

[26] The homogenization method for topology design using optimal energies The explicit derivation of extremal energies for the single load minimum compliance design can be found in Allaire & Kohn (1993) and Jog et al. (1994) for the 2-D case, in Cherkaev & Palais (1997) for the axisymmetric 3-D case and in Allaire (1994) for the full 3-D case. Their use for computations is also treated in these papers. The saddle point and duality principle associated with these calculations is discussed in Lipton (1994c); see also Telega & Lewiński (2000).

The basic idea of working with optimal energies as the basis for computations has since been widely used. One can distinguish between methods that work with explicit expressions (Allaire, Belhachmi & Jouve 1996, Allaire, Bonnetier, Francfort & Jouve 1997, Burns & Cherkaev 1997, Jacobsen, Olhoff & Rønholt 1998, Olhoff, Rønholt & Scheel 1998, Rodrigues, Jacobs, Guedes & Bendsøe 1999), and methods that obtain these energies numerically, as typically required for multiple loads. Here one can use the moment formulations (Díaz & Lipton 1997, Díaz & Lipton 2000) or use inverse homogenization (Theocaris & Stavroulakis 1999, Rodrigues et al. 2002); the latter is also useful for information on bone remodelling (Rodrigues, Jacobs, Guedes & Bendsøe 1999).

[27] Classical layout theory The classical reference here is Michell (1904). Modern lay-out theory was founded by Prager and Rozvany and is described in for example Prager (1985), Prager & Rozvany (1977), as well as in books mentioned above. The mathematical problems involved in lay-out theory is discussed in for example Lagache (1981), and Strang & Kohn (1981), Stavroulakis & Tzaferopoulos (1994), and Lewiński & Telega (2001), with recent computational work to be found in Dewhurst (2001).

[28] Free material design The initial studies on the use of a free parametrization of material was Ringertz (1993), Bendsøe, Guedes, Haber, Pedersen & Taylor (1994), Bendsøe et al. (1995), Bendsøe & Díaz (1993), Bendsøe & Díaz (1994), Bendsøe & Guedes (1994). Generalizations to more general cost measures, as well as the use of penalization schemes for obtaining 0-1 topologies (of anisotropic phases) can be found in Guedes & Taylor (1997), Taylor (1998), Bendsøe, Taylor & Washabaugh (1998), Rodrigues, Soto & Taylor (1999), and Taylor (2000). The development of fast algorithms based on interior point methods is described in Zowe et al. (1997), Ben-Tal, Kocvara, Nemirovski & Zowe (2000), and Kocvara, Zowe & Nemirovski (2000).

[29] The plate problem This is one of the classical problems in structural optimization. Kirchhoff plate design using the thickness only was treated for example by Kozlowski & Mróz (1969), Olhoff (1970). Much of the work related to this area is covered in the recent book Lewiński & Telega (2000), so we will here not try to give a broad background to this vast area. Armand & Lodier (1978) found by numerical means certain numerical instabilities and

this was investigated in detail by Cheng & Olhoff (1981), leading to the use of rib-stiffened plates in design of Kirchhoff plates. Such applications for elastic plates were described in Cheng (1981), Olhoff, Lurie, Cherkaev & Fedorov (1981), Cheng & Olhoff (1982) (for a recent mathematical treatment, see Muńoz & Pedregal (1998)). Multiple load problems and random load problems are studied in for example Lipton (1994b). The use of topology design in general and the homogenization approach in particular for Mindlin plates and shells is discussed in Soto & Díaz (1993b), Fukushima, Suzuki & Kikuchi (1993), Tenek & Hagiwara (1993a), Díaz, Lipton & Soto (1995), Lipton & Díaz (1997), Lee, Bae & Hinton (2000), Pedersen (2001), and Belblidia, Lee, Rechak & Hinton (2001); Olhoff (2000) contains a comparison of the plate model and a 3D model. Finally, stiffener design is the theme of Chung & Lee (1997), Gea & Fu (1997), and Luo & Gea (1998).

Existence of solutions to the plate problem by bounding the variation of the thickness has been discussed in in Litvinov (1980), Niordson (1983), Sokołowski (1981), and Bendsøe (1983). Homogenization of the plate equations and the derivation of models of ribbed plates from 3D elasticity has been dealt with in a huge amount of papers, see Lewiński & Telega (2000).

[30] Laminated plates Lamination parameters as the basis for design of laminates with respect to global criteria has been widely applied (Fukunaga & Vanderplaats 1991, Fukunaga & Sekine 1992, Fukunaga & Sekine 1993, Grenestedt & Gudmundson 1993, Miki & Sugiyama 1993, Fukunaga, Sekine & Sato 1994, Hammer et al. 1996, Hammer 1999b, Autio 2001), where the latter deals with thermal properties as well. To obtain the final design, an inverse procedure a described in Autio, Laitinen & Pramila (1993) and Autio (2000) can produce the final lay-up. Of related work we mention Foldager, Hansen & Olhoff (1998), and Hammer (2000), where damage is considered. In spite of the advantages of using lamination parameters, an important aspect of laminate design remains the handling of discrete variables. Here for example genetic algorithms play an important role, see Haftka (1999).

[31] Material non-linearity and damage problems Topology optimization for problems with elasto-plastic response has been considered in Swan & Kosaka (1997a), Yuge & Kikuchi (1995), Maute et al. (1998), Schwarz et al. (2001), Yuge et al. (1999), and in Mayer et al. (1996), Soto (2001), Soto & Díaz (1999), Pedersen (2002b) Pedersen (2002c) for crashworthiness problems. In the setting of free material design, the study Bendsøe et al. (1996) is based on a unified formulation of elasto-plastic problems and limit analysis described in Plaxton & Taylor (1994).

Damage has been considered in Bendsøe & Díaz (1998); the model used is described in Francfort & Marigo (1993). This is an energy model which in Achtziger & Bendsøe (1995) has been applied for trusses. Finally, an associated degradation model (Achtziger et al. 1998) is in Achtziger & Bendsøe

(1999) used as the basis for design of trusses (the fully stressed design is also here favourable!).

[32] Classical truss topology design by computational methods The classical formulations as LP problems can be found in for example Dorn et al. (1964), Fleron (1964), Pedersen (1970), Hörnlein (1979), Oberndorfer, Achtziger & Hörnlein (1996). In for example Ringertz (1985), such LP solutions are used to produce moderate sized initial designs for more complicated design formulations. And the simplex format is in Pedersen (1993b), Pedersen (1993c), da Silva Smith (1996), da Silva Smith (1997) used to generalize the plastic design setting to include multiple loads and local buckling. More studies can be found in for example Kirsch (1989b), Kirsch (1990b); see also the books and survey papers mentioned above.

For trusses, integrated geometry and topology design is described in for example Pedersen (1970), and Nishino & Duggal (1990), using hierarchical methods. The use of gradient information between the different phases has been considered in Ben-Tal et al. (1993), Bendsøe, Ben-Tal & Zowe (1994).

[33] Reformulations of truss topology design Displacements only formulations of truss topology problems and other reformulations in terms of stresses only have been considered in Achtziger et al. (1992), Ben-Tal & Bendsøe (1993), Bendsøe, Ben-Tal & Zowe (1994), Achtziger (1996), Achtziger (1998), and Muralidhar & Rao (1997), the latter dealing with elastoplastic analysis.

Numerical methods based on interior point algorithms applied on these reformulations have been the theme of Ben-Tal & Nemirovski (1994), Ben-Tal & Nemirovski (1995), and Jarre, Kocvara & Zowe (1998). Extension to contact problems can be found in Petersson & Klarbring (1994), Klarbring et al. (1995), Kocvara et al. (1998), to displacement constraints in Kocvara (1997), to robust design in Ben-Tal & Nemirovski (1997), to vibration problems in Ohsaki et al. (1999), to buckling problems in Ben-Tal, Jarre, Kocvara, Nemirovski & Zowe (2000), Kocvara (2002), and to local buckling in Achtziger (1999a), Achtziger (1999b),

Background material to the PBM method and SDP methods can be found in Vandenberghe & Boyd (1996), Ben-Tal & Roth (1996), Ben-Tal & Zibulevsky (1997), Mosheyev & Zibulevsky (2000).

For trusses with integer design variables a few example references are Ringertz (1986), where truss topology problems are solved by branch and bound, Beckers & Fleury (1997) that use dual methods, and Stolpe & Svanberg (2002) where it is proved that a broad range of problems in 0-1 topology design can be written in mixed integer LP format. Other techniques are genetic algorithms (Hajela & Lee 1995) and simulated annealing (Topping, Khan & Leite 1996).

Finally, topological derivative methods have also been applied to trusses (Bojczuk & Mróz 1999, Mróz & Bojczuk 2001).

[34] Existence of solutions to optimal design problems Of papers addressing in a survey form the problem of non-existence in optimal design problems we mention here Murat (1977), Lurie (1980), Stadler (1986), Cabib & Maso (1988). These papers also discuss the two possibilities of achieving existence of solutions: relaxation or restricting the design space to a compact set. The latter is described in a vast number of papers on for example classical shape design (see books on this subject). A fundamental study on the existence of solution in shape design can be found in Chenais (1975). The crucial notion of G-convergence of elliptic operators is discussed in for example De Giorgi & Spagnolo (1973), Spagnolo (1976), Raĭtum (1978). Explicit calculation of the relaxation of functionals in shape design can be found in for example Buttazzo & Maso (1991), Buttazzo (1993). Consult also the books mentioned above.

[35] On boundary shape design methods The principal introduction to this field can be found in the books and survey papers mentioned above. For some of the original work on shape sensitivity analysis we refer to Murat & Simon (1976), Simon (1980), Rousselet & Haug (1983).

References

Aboudi, J. (1991). *Mechanics of Composite Materials A Unified Micromechanical Approach*, Elsevier Science Publ., Amsterdam.

Achdou, Y (1993). Numerical optimization of a photocell, *Comp. Meth. Appl. Mech. Engng.* **102**: 89–106.

Achtziger, W. (1993). Optimierung von einfach und mehrfach belasteten stabwerken, *Bayreuther Mathematische Schriften, Heft 46.*

Achtziger, W (1996). Truss topology optimization including bar properties different for tension and compression, *Structural Optimization* **12**(1): 63–73.

Achtziger, W (1998). Multiple-load truss topology and sizing optimization: Some properties of minimax compliance, *Journal of Optimization Theory and Applications* **98**(2): 255–280.

Achtziger, W (1999a). Local stability of trusses in the context of topology optimization, part I: Exact modelling, *Structural Optimization* **17**(4): 235–246.

Achtziger, W (1999b). Local stability of trusses in the context of topology optimization, part II: A numerical approach, *Structural Optimization* **17**(4): 247–258.

Achtziger, W (2000). Optimization with variable sets of constraints and an application to truss design, *Computational Optimization and Applications* **15**(1): 69–96.

Achtziger, W & Bendsøe, M. P. (1995). Design for maximal flexibility as a simple computational model of damage, *Structural Optimization* **10**(3-4): 258–268.

Achtziger, W & Bendsøe, M. P. (1999). Optimal topology design of discrete structures resisting degradation effects, *Structural Optimization* **17**(1): 74–78.

Achtziger, W., Bendsøe, M. P., Ben-Tal, A. & Zowe, J. (1992). Equivalent displacement based formulations for maximum strength truss topology design, *Impact of Computing in Science and Engineering* **4**(4): 315–345.

Achtziger, W Bendsøe, M. P. & Taylor, J. E. (1998). Bounds on the effect of progressive structural degradation, *Journal of the Mechanics and Physics of Solids* **46**(6): 1055–1087.

Åkesson, B. & Olhoff, N. (1988). Minimum stiffness of optimally located supports for maximum value of beam eigenfrequencies, *Journal of Sound and Vibration* **120**(3): 457–63.

Allaire, G. (1992). Homogenization and two-scale convergence, *SIAM J. Math. Anal.* **23**: 1482–1518.

Allaire, G. (1994). Explicit lamination parameters for three-dimensional shape optimization, *Control and Cybernetics* **23**: 309–326.

Allaire, G. (2002). *Shape Optimization by the Homogenization Method*, Springer, New York Berlin Heidelberg.

Allaire, G. & Aubry, S. (1999). On optimal microstructures for a plane shape optimization problem, *Structural Optimization* **17**: 86–94.

Allaire, G. Aubry, S. & Jouve, F (1997). Simulation numerique de l'endommagement a l'aide du modele Francfort-Marigo, *Proc. Congres National d'Analyse Numerique, Imbourg, France.*

Allaire, G., Aubry, S. & Jouve, F. (2001). Eigenfrequency optimization in optimal design, *Computer Methods in Applied Mechanics and Engineering* **190**(28): 3565–79.

Allaire, G. Belhachmi, Z. & Jouve, F (1996). The homogenization method for topology and shape optimization. single and multiple loads case, *Rev. Europenne lm. Finis* **5**: 649–672.

Allaire, G., Bonnetier, E., Francfort, G. A. & Jouve, F (1997). Shape optimization by the homogenization method, *Numerische Mathematik* **76**(1): 27–68.

Allaire, G. & Castro, C. (2001). A new approach for the optimal distribution of assemblies in a nuclear reactor, *Numerische Mathematik* **89**(1): 1–29.

Allaire, G. & Francfort, G. A. (1993). A numerical algorithm for topology and shape optimization, *in* M. P. Bendsøe & C. A. Mota Soares (eds), *Topology Optimization of Structures*, Kluwer Academic publishers, pp. 239–248.

Allaire, G. & Henrot, A. (2001). On some recent advances in shape optimization, *Comptes Rendus de l Academie des Sciences Series IIB Mechanics* **329**(5): 383–396.

Allaire, G. & Kohn, R. V (1993). Optimal design for minimum weight and compliance in plane stress using extremal microstructures, *European J. Mech. A.* **12**: 839–878.

Allaire, G. & Kohn, R. V (1994). Optimal lower bounds on the elastic energy of a composite made from two non well-ordered isotropic materials, *Quarterly of Applied Mathematics* **LII**(2): 311–333.

Almgren, R. F (1985). An isotropic three-dimensional structure with Poisson's ratio = -1, *Journal of Elasticity* **12**: 839–878.

Ambrosio, L. & Buttazzo, G. (1993). An optimal design problem with perimeter penalization, *Calculus and Variation* **1**: 55–69.

Anagnostou, G., Rønquist, E. M. & Patera, A. T. (1992). A computational procedure for part design, *Comp. Meth. Appl. Mech. Engng.* **97**: 33–48.

Ananthasuresh, G. K., Kota, S. & Gianchandani, Y (1994). A methodical approach to the design of compliant micromechanisms, *Solid-state sensor and actuator workshop*, pp. 189–192.

Ananthasuresh, G. K., Kota, S. & Kikuchi, N. (1994). Stategies for systematic synthesis of compliant MEMS, *Dynamic Systems and Control* **2**: 677–686.

Ansola, R. Canales, J. Tarrago, J. A. & Rasmussen, J. (2002). An integrated approach for shape and topology optimization of shell structures, *Computers and Structures* **80**(5-6): 449–458.

Armand, J.-L. & Lodier, B. (1978). Optimal design of bending elements, *International Journal of Numerical Methods in Engineering* **13**: 373–384.

Arora, J. S. (ed.) (1997). *Guide to Structural Optimization*, American Society of Civil Engineers, Reston.

Ashby, M. F (1991). Material and shape, *Acta Matell. Mater.* **39**: 1025–1039.

Atrek, E. (1993). SHAPE: A structural shape optimization program, *in* H. R. E. M. Hörnlein & K. Schittkowski (eds), *Software Systems for Structural Optimization*, Birkhauser, Boston, USA, pp. 229–250.

Attouch, H. (1984). *Variational Convergence for Functions and Operators*, Pitman, London, United Kingdom.

Autio, M. (2000). Determining the real lay-up of a laminate corresponding to optimal lamination parameters by genetic search, *Structural and Multidisciplinary Optimization* **20**.

Autio, M. (2001). Optimization of coupled thermal-structural problems of laminated plates with lamination parameters, *Structural and Multidisciplinary Optimization* **21**: 40–51.

Autio, M., Laitinen, M. & Pramila, A. (1993). Systematic creation of composites with prescribed thermomechanical properties, *Computational Engineering* **3**: 249–259.

Avellaneda, M. (1987). Optimal bounds and microgeometries for elastic two-phase composites, *SIAM Journal on Applied Mathematics* **47**(6): 1216–1228.

Avellaneda, M. & Milton, G. W (1989). Bounds on the effective elastic tensor of composites based on two-point correlations, *in* D. Hui & T. J. Kozik (eds), *Composite Material Technology*, ASME, pp. 89–93.

Avellaneda, M. & Swart, P. J. (1998). Calculating the performance of 1-3 piezoelectric composites for hydrophone applications: An effective medium approach, *Journal of the Acoustical Society of America* **103**(3): 1449–67.

Back-Pedersen, A. (1998). Designing an impeler hub using topology optimization, *Proc. 8th Int. ANSYS Conference and Exhibition, Pittsburgh*, Vol. 2, pp. 2.81–2.90.

Back-Pedersen, A. (1999). Taking advanatge of using both topology and shape optimization for practical design, *NAFEMS World Congress '99*, NAFEMS ltd., Glasgow, Newport, Rhode Island, pp. 889–899.

Bagge, M. (2000). A model of bone adaptation as an optimization process, *Journal of Biomechanics* **33**(11): 1349–1357.

Bakhvalov, N. & Panasenko, G. (1989). *Homogenization: Averaging Processes in Periodic Media*, Kluwer Academic Publishers, Dordrecht.

Balabanov, V O. & Haftka, R. T. (1996). Topology optimization of transport wing internal structure, *Journal of Aircraft* **33**(1): 232.

Banichuk, N. V (1983). *Problems and Methods of Optimal Structural Design*, Plenum Press, New-York, USA.

Banichuk, N. V (1990). *Introduction to Optimization of Structures*, Springer Verlag, New-York, USA.

Banichuk, N. V & Sharanyuk, A. V (1996). Optimization of the distribution of anisotropic material in deformable bodies and structures, *Soviet Physics—Doklady* **41**(3): 119–122.

Baron, P., Fisher, R., Sherlock, A., Mill, F. & Tuson, A. (1997). A voxel based approach to evolutionary shape optimisation, *Lecture Notes in Computer Science* **1305**: 253–274.

Baumgartner, A., Harzheim, L. & Mattheck, C. (1992). SKO (Soft Kill Option): The biological way to find an optimum structure topology, *International Journal of Fatigue* **14**: 387–393.

Beckers, M. (1997). Optimisation topologique de structures tridimensionelles en variable discretes, *Technical Report OF-44*, LTAS, University of Liege.

Beckers, M. (1999). Topology optimization using a dual method with discrete variables, *Structural Optimization* **17**(1): 14–24.

Beckers, M. (2000). Dual methods for discrete structual optimization problems, *Int. J. Numer. Meth. Engng* **48**: 1761–1784.

Beckers, M. & Fleury, C. (1997). A primal-dual approach in truss topology optimization, *Computers & Structures* **64**(1-4): 77–88.

Belblidia, F & Bulman, S. (2001). Constrained adaptive topology optimization for vibrating shell structures, *Structural and Multidisciplinary Optimization* **22**: 167–176.

Belblidia, F., Lee, J. E. B., Rechak, S. & Hinton, E. (2001). Topology optimization of plate structures using a single- or three-layered artificial material model, *Advances in Engineering Software* **32**(2): 159–68.

Ben-Tal, A. & Bendsøe, M. P. (1993). A new method for optimal truss topology design, *SIAM J. Optimization* **3**: 322–358.

Ben-Tal, A., Jarre, F Kocvara, M., Nemirovski, A. & Zowe, J. (2000). Optimal design of trusses under a nonconvex global buckling constraint, *Optimization and Engineering* **1**: 189–213.

Ben-Tal, A. Kocvara, M. Nemirovski, A. & Zowe, J. (1999). Free material design via semidefinite programming: The multiload case with contact conditions, *SIAM Journal on Optimization* **9**(4): 813–32.

Ben-Tal, A., Kocvara, M., Nemirovski, A. & Zowe, J. (2000). Free material design via semidefinite programming: the multiload case with contact conditions, *SIAM Review* **42**(4): 695–715.

Ben-Tal, A., Kocvara, M. & Zowe, J. (1993). Two non-smooth methods for simultaneous geometry and topology design of trusses, *in* M. P. Bendsøe & C. A. Mota Soares (eds), *Topology Design of Structures*, Kluwer Academic Publishers, pp. 31–42.

Ben-Tal, A. & Nemirovski, A. (1993). An interior point algorithm for truss topology design, *in* M. P. Bendsøe & C. A. Mota Soares (eds), *Topology Design of Structures, Sesimbra, Portugal*, Kluwer Academic Publishers Group, pp. 55–70.

Ben-Tal, A. & Nemirovski, A. (1994). Potential reduction polynomial time method for truss topology design, *SIAM J. Optimization* **4**: 596–612.

Ben-Tal, A. & Nemirovski, A. (1995). Optimal design of engineering structures. OPTIMA Math. Prog. Soc. Newsletter, No. 47

Ben-Tal, A. & Nemirovski, A. (1997). Robust truss topology design via semidefinite programming, *SIAM Journal on Optimization* **7**(4): 991–1016.

Ben-Tal, A. & Nemirovski, A. (2001). *Lectures on Modern Convex Optimization*, SIAM, Philadelphia. MPS-SIAM Series on Optimization.

Ben-Tal, A. & Roth, G. (1996). Truncated log barrier algorithm for large-scale convex programming and minmax problems: Implementation and computational results, *Optimization Methods and Software* **6**: 283–312.

Ben-Tal, A. & Zibulevsky, M. (1997). Penalty/barrier multiplier methods for convex programming problems, *SIAM Journal on Optimization* **7**(2): 347–366.

Bendsøe, M. P. (1983). *G*-closure and homogenization problems arising in plate optimization, *in* H. A. Eschenauer & N. Olhoff (eds), *Optimization methods in structural design*, Bibliographisches Inst., Mannheim, pp. 270–275.

Bendsøe, M. P (1984). Existence proofs for a class of plate optimization problems, *System modelling and optimization (Copenhagen, 1983)*, Springer-Verlag, Berlin, pp. 773–779.

Bendsøe, M. P. (1986). Generalized plate models and optimal design, *in* J. L. Ericksen, D. Kinderlehrer, R. V Kohn & J.-L. Lions (eds), *Homogenization and Effective Moduli of Materials and Media*, Springer-Verlag, Berlin; New York, pp. 1–26.

Bendsøe, M. P. (1989). Optimal shape design as a material distribution problem, *Structural Optimization* **1**: 193–202.

Bendsøe, M. P. (1995). *Optimization of Structural Topology, Shape and Material*, Springer Verlag, Berlin Heidelberg.

Bendsøe, M. P. (1997). Structural optimization of and with advanced materials, *in* T. Tatsumi, E. Watanabe & T. Kambe (eds), *Theoretical and Applied Mechanics 1996*, Elsevier Science B.V., Amsterdam, pp. 269–284.

Bendsøe, M. P., Ben-Tal, A. & Zowe, J. (1994). Optimization methods for truss geometry and topology design, *Structural Optimization* **7**(3): 141–158.

Bendsøe, M. P. & Díaz, A. R. (1993). Optimization of material properties for Mindlin plate design, *Struct. Optim.* **6**: 268–270.

Bendsøe, M. P. & Díaz, A. R. (1994). Optimization of material properties for improved frequency responce, *Struct. Optim.* **7**: 138–140.

Bendsøe, M. P & Díaz, A. R. (1998). A method for treating damage related criteria in optimal topology design of continuum structures, *Structural Optimization* **16**(2): 108–115.

Bendsøe, M. P., Díaz, A. R. & Kikuchi, N. (1993). Topology and generalized layout optimization of elastic structures, *in* M. P. Bendsøe & C. A. Mota Soares (eds), *Topology Design of Structures*, Kluwer Academic Publishers, pp. 159–206.

Bendsøe, M. P., Díaz, A. R., Lipton, R. & Taylor, J. E. (1995). Optimal design of material properties and material distribution for multiple loading conditions, *International Journal for Numerical Method in Engineering* **38**(7): 1149–1170.

Bendsøe, M. P. & Guedes, J. M. (1994). Some computational aspects of using extremal material properties in the optimal design of shape, topology and material, *Control and Cybernetics* **23**(3): 327–349.

Bendsøe, M. P. Guedes, J. M., Haber, R. B., Pedersen, P. & Taylor, J. E. (1994). An analytical model to predict optimal material properties in the context of optimal structural design, *Transactions of the ASME, Journal of Applied Mechanics* **61**(4): 930–937.

Bendsøe, M. P. Guedes, J. M. Plaxton, S. & Taylor, J. E. (1996). Optimization of structure and material properties for solids composed of softening material, *International Journal of Solids and Structures* **33**(12): 1799–1813.

Bendsøe, M. P. & Haber, R. B. (1993). The Michell layout problem as a low volume fraction limit of the perforated plate optimization problem: An asymptotic study, *Struct. Optim.* **6**: 263–267.

Bendsøe, M. P & Kikuchi, N. (1988). Generating optimal topologies in structural design using a homogenization method, *Computer Methods in Applied Mechanics and Engineering* **71**(2): 197–224.

Bendsøe, M. P. & Mota Soares, C. A. (eds) (1992). *Topology Design of Structures*, Vol. 227 of *NATO ASI series. Series E, Applied sciences*, Kluwer Academic Publishers Group, Dordrecht. Boston. London.

Bendsøe, M. P Olhoff, N. & Sokołowski, J. (1985). Sensitivity analysis of problems of elasticity with unilateral constraints, *Journal of Structural Mechanics* **13**(2): 201–222.

Bendsøe, M. P. & Rodrigues, H. C. (1991). Integrated topology and boundary shape optimization of 2-D solids, *Comp. Meth. Appl. Mech. Engng.* **87**: 15–34.

Bendsøe, M. P. & Sigmund, O. (1999). Material interpolation schemes in topology optimization, *Archives of Applied Mechanics* **69**(9-10): 635–654.

Bendsøe, M. P., Taylor, J. E. & Washabaugh, P. D. (1998). A formulation for optimal continuum structures with a decompositon of material properties into specified and designable parts, *Control and Cybernetics* **27**: 255–264.

Bendsøe, M. P. & Triantafyllidis, N. (1990). Scale effects in the optimal design of a microstructured medium against buckling, *Int. J. Solids Struct.* **26**: 725–741.

Bennet, J. A. & Botkin, M. E. (eds) (1986). *The Optimum Shape: Automated Structural Design*, Plenum Press, New York; London.

Bensoussan, A. Lions, J.-L. & Papanicolaou, G. (1978). *Asymptotic analysis of periodic structures*, North-Holland Publ.

Berlyand, L. V & Kozlov, S. M. (1992). Asymptotics of homogenized moduli for the elastic chess-board composite, *Arch. Rat. Mech. Anal.* **118**: 95–112.

Bestle, D. & Schielen, W (eds) (1995). *IUTAM Symposium on Optimization of Mechanical Systems, Stuttgart, Germany, March 26-31*, Kluwer.

Beuzit, S. & Habbal, A. (2001). Design of an automatic topology/shape optimization software, *in* G. D. Cheng, Y Gu, S. Liu & Y Wang (eds), *WCSMO-4 Proc. Second World Congress of Structural and Multidisciplinary Optimization*, Liaoning Electronic Press, Dalian. CD-rom, ISBN 7-900312-69-2.

Bing-Chung, C. & Kikuchi, N. (2001). Topolgy optimization with design-dependent loads, *Finite Element in Analysis and Design* **37**: 57–70.

Bletzinger, K.-U. & Maute, K. (1997). Towards generalized shape and topology optimization, *Engineering Optimization* **29**(1-4): 201–216.

Bloebaum, C. L. (ed.) (1999). *WCSMO-3 Proc. Second World Congress of Structural and Multidisciplinary Optimization*, Center for Advanced Design, University of Buffalo, Buffalo. CD-rom.

Bojczuk, D. & Mróz, Z. (1999). Optimal topology and configuration design of trusses with stress and buckling constraints, *Structural Optimization* **17**(1): 25–34.

Borrvall, T. (2001). Topology optimization of elastic continua using restriction, *Archives of Computational Methods in Engineering* **8**(4): 351–385.

Borrvall, T. & Petersson, J. (2001a). Large-scale topology optimization in 3D using parallel computing, *Computer Methods in Applied Mechanics and Engineering* **190**(46-47): 6201–29.

Borrvall, T. & Petersson, J. (2001b). Topology optimization using regularized intermediate density control, *Computer Methods in Applied Mechanics and Engineering* **190**: 4911–4928.

Borrvall, T. & Petersson, J. (2002). Topology optimization of fluids in stokes flow, *submitted*

Bouchitte, G. Buttazzo, G. & Suquet, P. (eds) (1994). *Calculus of variations, homogenization and continuum mechanics*, World Scientific, Singapore.

Bourdin, B. (2001). Filters in topology optimization, *International Journal for Numerical Methods in Engineering* **50**(9): 2143–2158.

Bourdin, B. & Chambolle, A. (2001). Design-dependent loads in topology optimization, *Technical report*, Courant Institute, NYU.

Bourgat, J. F (1977). Numerical experiments of the homogenization method for operators with periodic coefficients, *Lecture Notes in Mathematics*, Springer Verlag, Berlin, pp. 330–356.

Boyd, S., Ghaoui, L. E. Feron, E. & Balakrishnan, V (1994). *Linear matrix inequalities in system and control theory*, SIAM, Philadelphia, PA.

Braides, A. & Defranceschi, A. (1998). *Homogenization of Multiple Integrals*, Clarendon Press, Oxford.

Brannlund, U. & Svanberg, K. (1997a). Optimal truss topology, semidefinite programming, and a method based on conservative approximations, *Technical*

Report TRITA/MAT-97-OS7, Department of Mathematics, Royal Institute of Technology, Stockholm.

Brannlund, U. & Svanberg, K. (1997b). Optimization of truss topology by a primal-dual method, *Technical Report TRITA/MAT-97-OS16*, Department of Mathematics, Royal Institute of Technology, Stockholm.

Bremicker, M. Chirehdast, M. Kikuchi, N. & Papalambros, P. Y (1992). Integrated topology and shape optimization in structural design, *Mech. Struct. Mach.* **19**: 551–587.

Brezzi, F & Fortin, M. (1991). *Mixed and Hybrid Finite Element Methods*, Springer Verlag, New York.

Brillouin, L. (1946). *Wave propagation in Periodic Structures*, McGraw-Hill, New York.

Bruns, T. E. & Sigmund, O. (2001). Topology design of bistable mechanisms, *in* G. D. Cheng, Y Gu, S. Liu & Y. Wang (eds), *WCSMO-4 Proc. Second World Congress of Structural and Multidisciplinary Optimization*, Liaoning Electronic Press, Dalian. CD-rom, ISBN 7-900312-69-2.

Bruns, T. E. Sigmund, O. & Tortorelli, D. A. (2002). Numerical methods for the topology optimization of structures that exhibit snap-through, *International Journal for Numerical Methods in Engineering* **55**: 1215–1237.

Bruns, T. E. & Tortorelli, D. A. (2001). Topology optimization of non-linear elastic structures and compliant mechanisms, *Computer Methods in Applied Mechanics and Engineering* **190**(26-27): 3443–3459.

Bruns, T. E. & Tortorelli, D. A. (2002). An element removal and reintroduction strategy for the topology optimization of structures and compliant mechanisms, *International Journal of Numerical Methods in Engineering* To appear.

Bucur, D. & Zolesio, J.-P. (1995). N-dimensional shape optimization under capacitary constraint, *Journal of Differential Equations* **123**(2): 504–522.

Bucur, D. & Zolesio, J.-P. (1996). Existence and stability of the optimum in shape optimization, *ZAMM Zeitschrift fur Angewandte Mathematik und Mechanik* **76**(2): 77–80.

Buhl, T. (2002). Simultaneous topology optimization of structure and supports, *Structural and Multidisciplinary Optimization* **23**(5): 336–346.

Buhl, T. Pedersen, C. B. W & Sigmund, O. (2000). Stiffness design of geometrically non-linear structures using topology optimization, *Structural and Multidisciplinary Optimization* **19**(2): 93–104.

Bulman, S. Sienz, J. & Hinton, E. (2001). Comparisons between algorithms for structural topology optimization using a series of benchmark studies, *Computers and Structures* **79**(12): 1203–1218.

Burns, T. & Cherkaev, A. V (1997). Optimal distribution of multimaterial composites for torsional beams, *Structural Optimization* **13**(1): 14–23.

Buttazzo, G. (1989). *Semicontinuity, relaxation and integral representation in the calculus of variations*, Longman Scientific and Technical, Harlow, Essex, UK.

Buttazzo, G. (1993). Existence via relaxation for some domain optimization problems, *in* M. P. Bendsøe & C. A. Mota Soares (eds), *Topology Design of Structures*, Kluwer Academic Publishers, pp. 337–344.

Buttazzo, G. & Maso, G. D. (1991). Shape optimization for Dirichlet problems: Relaxed solutions and optimality conditions, *Appl Math. Optim.* **23**: 17–49.

Byun, J.-K., Hahn, S.-Y & Park, I.-H. (1999). Topology optimization of electrical devices using mutual energy and sensitivity, *Magnetics, IEEE Transactions on* **35**(52): 3718–3720.

Byun, J.-K., Lee, J.-H., Park, I.-H., Lee, H.-B. Choi, K. & Hahn, S.-Y (2000). Inverse problem application of topology optimization method with mutual energy concept and design sensitivity, *Magnetics, IEEE Transactions on* **36**(41): 1144–1147.

Cabib, E. & Maso, G. D. (1988). On a class of optimum problems in structural design, *J. Optim. Th. Appl.* **56**: 39–65.

Canfield, S. & Frecker, M. I. (2000). Topology optimization of compliant mechanical amplifiers for piezoelectric actuators, *Structural and Multidisciplinary Optimization* **20**: 269–279.

Cea, J., Garreau, S. Guillaume, P & Masmoudi, M. (2000). The shape and topological optimizations connection, *Comput. Methods Appl. Mech. Engrg.* **188**: 713–726.

Cea, J. Gioan, A. & Michel, J. (1973). Quelques resultat sur l'identification de domaines, *Calcolo III / IV*

Cea, J. & Malanowski, K. (1970). An example of a max-min problem in partial differential equations, *SIAM J. Control* **8**: 305–316.

Chambolle, A. (1995). Image segmentation by variational methods: Mumford and Shah functional and the discrete approximations, *SIAM Journal on Applied Mathematics* **55**(3): 827–863.

Chang, K.-H. (2001). Structural shape optimization – from concept to manufacturing, *in* G. D. Cheng, Y Gu, S. Liu & Y Wang (eds), *WCSMO-4 Proc. Second World Congress of Structural and Multidisciplinary Optimization*, Liaoning Electronic Press, Dalian. CD-rom, ISBN 7-900312-69-2.

Chapman, C. D. & Jakiela, M. J. (1996). Genetic algorithm-based structural topology design with compliance and topology simplification considerations, *Transactions of the ASME R Journal of Mechanical Design* **188**(1): 89–97.

Chen, B.-C. Silva, E. C. N. & Kikuchi, N. (2001). Advances in computational design and optimization with application to MEMS, *International Journal for Numerical Methods in Engineering* **52**: 23–62.

Chen, T.-Y & Lin, C.-Y (2000). Determination of optimum design spaces for topology optimization, *Finite Elements in Analysis and Design* **36**: 1–16.

Chenais, D. (1975). On the existence of a solution in a domain identification problem, *J. Math. Anal. Appl.* **52**: 189–289.

Chenais, D. Mascarenhas, M. L. & Trabucho, L. (1997). On the optimization of non periodic homogenized microstructures, *RAIRO - M2AN Mathem. Modell. Numerical Analysis* **31**(5): 559–598.

Cheng, G. D. (1981). On non-smoothness in optimal design of solid, elastic plates, *Int. J. Solids Struct.* **17**: 795–810.

Cheng, G. D. (1996). Some interesting developments of structural optimization, *in* T. Tatsumi, E. Watanabe & T. Kambe (eds), *Proc. ICTAM Kyoto, 1996, XIXth International Congress of Theoretical and Applied Mechanics*, Elsevier Science B.V

Cheng, G. D., Gu, Y. Liu, S. & Wang, Y (eds) (2001). *WCSMO-4 Proc. Second World Congress of Structural and Multidisciplinary Optimization*, Liaoning Electronic Press, Dalian. CD-rom, ISBN 7-900312-69-2.

Cheng, G. D. & Guo, X. (1997). ϵ-relaxed approach in topology optimization, *Structural Optimization* **13**: 258–266.

Cheng, G. D. & Jiang, Z. (1992). Study on topology optimization with stress constraints, *Engineering Optimization* **20**: 129–148.

Cheng, G. D. & Olhoff, N. (1981). An investigation concerning optimal design of solid elastic plates, *International Journal of Solids and Structures* **17**: 305–323.

Cheng, G. D. & Olhoff, N. (1982). Regularized formulation for optimal design of axisymmetric plates, *International Journal of Solids and Structures* **18**(2): 153–169.

Cheng, G. D. & Pedersen, P. (1997). On sufficiency conditions for optimal design based on extremum principles of mechanics, *Journal of the Mechanics and Physics of Solids* **45**(1): 135–150.

Cherkaev, A. V (1993). Stability of optimal structures of elastic composites, *Topology design of structures (Sesimbra, 1992)*,, Vol. 227 of *NATO Adv. Sci. Inst. Ser. E Appl. Sci.*, Kluwer Academic Publishers Group, Dordrecht, pp. 547–558.

Cherkaev, A. V (2000). *Variational Methods for Structural Optimization*, Springer, New York Berlin Heidelberg.

Cherkaev, A. V & Gibiansky, L. V (1993). Coupled esimates for the bulk and shear moduli of a two-dimensional isotropic elastic composite, *Journal of the Mechanics and Physics of Solids* **41**(5): 937–980.

Cherkaev, A. V & Kohn, R. V (eds) (1997). *Topics in the mathematical modelling of composite materials*, Birkhäuser Boston Inc. Cambridge, MA.

Cherkaev, A. V., Krog, L. A. & Kucuk, I. (1998). Stable optimal design of two-component elastic structures, *Control and Cybernetics* **27**(2): 265–282.

Cherkaev, A. V & Palais, R. (1997). Optimal design of three-dimensional axisymmetric structures, *Structural Optimization* **13**(1): 10–23.

Chickermane, H. & Gea, H. C. (1997). Design of multi-component structural systems for optimal layout topology and joint locations, *Eng. Comput.* **13**: 235–243.

Chickermane, H., Gea, H. C. Yang, R. J. & Chuang, C.-H. (1999). Optimal fastener pattern design considering bearing loads, *Structural Optimization* **17**(2-3): 140–146.

Chirehdast, M. & Ambo, S. D. (1995). Topology optimization of planar cross-sections, *Structural Optimization* **9**(3-4): 266.

Chirehdast, M. Sankaranarayanan, S. Ambo, S. D. & Johnson, R. (1994). Validation of topology optimization for component design, *In Proc. 5th AIAA/USAF/NASA/ISSMO Symposium on Multidisciplinary Analysis and Optimization*, Panama City, F, pp. 132–137

Choi, S. H. E., Lowther, D. A. & Dyck, D. N. (1998). OPITIMIZATION determining boundary shapes from the optimized material distribution system, *IEEE Transactions on Magnetics* **34**(5 Part.1): 2833–2836.

Christensen, R. M. (1991). *Mechanics of Composite Materials*, Krieger, Amsterdam.

Christie, W C., Bettess, P. & Bull, J. W. (1998). Self-designing structures: A practical approach, *Engineering Computations* **15**: 35–48. 1.

Chu, D. N. Xie, Y M. Hira, A. & Steven, G. P. (1997). On various aspects of evolutionary structural optimization for problems with stiffness constraints, *Finite Element in Analysis and Design* **24**: 197–212.

Chung, J. & Lee, K. (1997). Optimal design of rib structures using the topology optimization technique, *Proc. Instn. Mech. Engrs.* **211**: 425–437. Part C.

Chung, Y.-S. Cheon, C. & Hahn, S.-Y (2000). Reconstruction of dielectric cylinders using FDTD and topology optimization technique, *IEEE Transactions on Magnetics* **36**(4): 956–959.

Cioranescu, D. Damlamian, A. & Donato, P. (eds) (1995). *Homogenization and applications to material sciences*, Gakkōtosho Co., Tokyo.

Cioranescu, D. & Donato, P. (1999). *An introduction to homogenization*, The Clarendon Press Oxford University Press, New York.

Cioranescu, D. & Paulin, J. S. J. (1979). Homogenization in open sets with holes, *J. Math. Anal. Appl.* **71**: 590–607.

Cioranescu, D. & Paulin, J. S. J. (1999). *Homogenization of reticulated structures*, Springer-Verlag, New York.

Cowin, S. C. (1990). Structural adaptation of bones, *Appl. Mech. Rev.* **43**: 127–133.

Cowin, S. C. (1995). On the minimization and maximization of the strain energy density in cortical bone tissue, *Journal of Biomechanics* **28**(4): 445–447.

Cox, S. J. & Dobson, D. C. (1999). Maximizing band gaps in two-dimensional photonic crystals, *SIAM Journal for Applied Mathematics* **59**(6): 2108–2120.

Cox, S. J. & Dobson, D. C. (2000). Band structure optimization of two-dimensional photonic crystals in h-polarization, *Journal of Computational Physics* **158**(2): 214–224.

Cox, S. J. & Lipton, R. (1996). Extremal eigenvalue problems for two-phase conductors, *Archive for Rational Mechanics and Analysis* **136**(2): 101–117.

Cox, S. J. & Overton, M. L. (1992). On the optimal design of columns against buckling, *SIAM Journal on Mathematical Analysis* **23**(2): 287–325.

Cox, S. J. & Uhlig, P. X. (2001). Minimal compliance fastening of elastic bodies, *Structural and Multidisciplinary Optimization* **22**(2): 139–148.

Crisfield, M. A. (1997). *Non-linear finite element analysis of solids and structure*, Vol. 1–2, John Wiley and Sons, Ltd., England.

da Silva Smith, O. (1996). An interactive system for truss topology design, *Advances in Engineering Software* **27**(1-2): 167–178.

da Silva Smith, O. (1997). Topology optimization of trusses with local stability constraints and multiple loading conditions - a heuristic approach, *Structural Optimization* **13**(2-3): 155–166.

Dacorogna, B. (1989). *Direct methods in the calculus of variations*, Springer-Verlag, Berlin; Heidelberg; London; etc.

Dal Maso, G. (1993). *An introduction to Γ-convergence*, Birkhäuser Boston Inc. Cambridge, MA.

Dal Maso, G. & Dell'Antonio, G. F (eds) (1991). *Composite Media and Homogenization Theory*, Birkhuser, Boston.

De Giorgi, E. & Spagnolo, S. (1973). Sulla convergenza degli integrali dell'energia per operatori ellittici del secondo ordine, *Boll. U. M. I.* **8**: 391–411.

Demyanov, V F & Malozemov, V N. (1974). *Introduction to Minimax*, John Wiley and Sons, New York.

DeRose Jr., G. C. A. & Díaz, A. R. (1999). Single scale wavelet approximations in layout optimization, *Structural Optimization* **18**(1): 1–11.

DeRose Jr. G. C. A. & Díaz, A. R. (2000). Solving three-dimensional layout optimization problems using fixed scale wavelets, *Computational Mechanics* **25**: 274–285.

Dewhurst, P. (2001). Analytical solutions and numerical procedures for minimum-weight Michell structures, *Journal of the Mechanics and Physics of Solids* **49**: 445–467.

Díaz, A. R. & Belding, B. (1993). On optimum truss layout by a homogenization method, *Journal of Mechanical Design, Transactions Of the ASME* **115**: 367–373.

Díaz, A. R. & Bendsøe, M. P. (1992). Shape optimization of structures for multiple loading situations using a homogenization method, *Structural Optimization* **4**: 17–22.

Díaz, A. R. & Kikuchi, N. (1992). Solution to shape and topology eigenvalue optimization problems using a homogenization method, *International Journal for Numerical Methods in Engineering* **35**: 1487–1502.

Díaz, A. R. & Lipton, R. (1997). Optimal material layout for 3D elastic structures, *Structural Optimization* **13**(1): 60–64.

Díaz, A. R. & Lipton, R. (2000). Optimal material layout in 3D elastic structures subjected to multiple loads, *Mech. Struch and Mach* **28**: 219–236.

Díaz, A. R. Lipton, R. & Soto, C. A. (1995). A new formulation of the problem of optimum reinforcement of Reissner-Mindlin plates, *Computer Methods in Applied Mechanics and Engineering* **123**(1-4): 121–139.

Díaz, A. R. & Sigmund, O. (1995). Checkerboard patterns in layout optimization, *Structural Optimization* **10**(1): 40–45.

Didenko, N. I. (1981). Optimal distribution of bending stiffness of an elastic freely supported plate, *Mech. Solids (MTT)* **16**: 133–143.

Ding, Y (1986). Shape optimization of structures: A literature survey, *Computers and Structures* **24**(6): 985–1004.

Dorn, W., Gomory, R. & Greenberg, M. (1964). Automatic design of optimal structures, *J. de Mecanique* **3**: 25–52.

Du, H., Lau, G. K., Lim, M. K. & Qui, J. (2000). Topological optimization of mechanical amplifiers for piezoelectric actuators under dynamic motion, *Smart Mater. Struct* **9**: 788–800.

Duvaut, G. (1976). Analyse fonctionnelle et mecanique des milieux continus. application l'etude des materiaux composites elastiques a structure periodique - homogeneisation, *Proc. 14the IUTAM Congress, Delft*, The Netherlands, North-Holland Publ.,Amsterdam, pp. 119–132.

Duvaut, G. & Metellus, A.-M. (1976). Homognisation d'une plaque mince en flexion de structure priodique et symtrique, *C.R. Acad. Sc. Paris, t. 283, Serie A* pp. 947–950.

Duysinx, P. (1997). Layout optimization: A mathematical programming approach, Danish Center for Applied Mathematics and Mechanics, DCAMM Report No. 540.

Duysinx, P. (2000). Topology optimization with different stress limits in tension and compression, *in* C. L. Bloebaum (ed.), *WCSMO-3 Proc. Third World Congress of Structural and Multidisciplinary Optimization*, University of New York at Buffalo. CD rom.

Duysinx, P. & Bendsøe, M. P. (1998). Topology optimization of continuum structures with local stress coinstraints, *International Journal for Numerical Methods in Engineering* **43**(8): 1453–1478.

Duysinx, P. & Sigmund, O. (1998). New developments in handling stress constraints in optimal material distributions, *7th Symposium on Multidiciplinary Analysis and Optimization*, AIAA/USAF/NASA/ISSMO, AIAA-98-4906, pp. 1501–1509.

Dyck, D. N. & Lowther, D. A. (1996). Automated design of magnetic devices by optimizing material distribution, *IEEE Transactions on Magnetics* **32**(3 Part.1): 1188–1193.

Dyck, D. N. & Lowther, D. A. (1997). Composite microstructure of permeable material for the optimized material distribution method of automated design, *IEEE Transactions on Magnetics* **33**(2 Part.2): 1828–1831.

Ejimi, S. Nishiwaki, S. Sekiguchi, M. & Kikuchi, N. (2000). Optimal structural design of compliant mechanisms, *JSME International Journal* **43**(2): 130–137.

Ekeland, I. & Temam, R. (1976). *Convex analysis and variational problems*, North-Holland, Amsterdam.

Ericksen, J. L., Kinderlehrer, D., Kohn, R. V & Lions, J.-L. (eds) (1986). *Homogenization and Effective Moduli of Materials and Media.*, Springer, Berlin.

Escauriaza, L. & Seo, J. K. (1993). Regularity properties of solutions to transmission problems, *Trans. AMS.* **338**: 405–430.

Eschenauer, H. A., Kobelev, V V & Schumacher, A. (1994). Bubble method for topology and shape optimization of structures, *Structural Optimization* **8**: 42–51.

Eschenauer, H. A. & Olhoff, N. (2001). Topology optimization of continuum structures: A review, *Appl Mech Rev* **54**(4): 331–390.

Eschenauer, H. A. Olhoff, N. & Schnell, W (1997). *Applied Structural Mechanics Fundamentals of Elasticity, Load-Bearing Structures, Structural Optimization*, Springer, Berlin.

Eschenauer, H. A. & Schumacher, A. (1997). Topology and shape optimization procedures using hole positioning criteria – theory and applications, *in* G. I. N. Rozvany (ed.), *Topology Optimization in Structural Mechanics, CISM Courses and Lectures*, Vol. 374, Springer, Vienna, pp. 135–196.

Fedorov, A. V & Cherkaev, A. V (1983). Choosing of optimal orientation of axes of elastic symmetry of orthotropic plate, *Mechanics of Solids* **3**: 135–142.

Fernandes, P., Guedes, J. M. & Rodrigues, H. C. (1999). Topology optimization of three-dimensional linear elastic structures with a constraint on perimeter, *Computers & Structures* **73**(6): 583–594.

Fleron, P. (1964). The minimum weight of trusses, *Bygnings statiske Meddelelser* **35**: 81–96.

Fleury, C. (1993). Mathematical programming methods for constrained optimization: Dual methods, *in* M. P. Kamat (ed.), *Structural Optimization Status and Promise*, Vol. 150 of *Progress in Astronautics and Aeronautics*, AIAA, pp. 123–150.

Foldager, J., Hansen, J. S. & Olhoff, N. (1998). A general approach forcing convexity of ply angle optimization in composite laminates, *Structural Optimization* **16**(2): 201–211.

Folgado, J., Fernandes, P. & Rodrigues, H. C. (2001). Topology optimization of three-dimensional structures under contact conditions, *in* G. D. Cheng, Y Gu, S. Liu & Y. Wang (eds), *WCSMO-4 Proc. Second World Congress of Structural and Multidisciplinary Optimization*, Liaoning Electronic Press, Dalian. CD-rom, ISBN 7-900312-69-2.

Folgado, J. & Rodrigues, H. C. (1997). Topology optimization methods applied to the design of orthopaedics implants, *in* Z. Gutkowski & Z. Mróz (eds), *Proc. Second World Congress of Structural and Multidisciplinary Optimization*, Inst. of Fundamental Technological Research, Warsaw, pp. 563–568.

Folgado, J. & Rodrigues, H. C. (1998). Structural optimization with a non-smooth buckling load criterion, *Control and Cybernetics* **27**: 235–254.

Francfort, G. A. & Marigo, J. (1993). Stable damage evolution in a brittle continuous medium, *European Journal of Mechanics, A, Solids.* **12**: 149–189.

Francfort, G. A. & Murat, F (1986). Homogenization and optimal bounds in linear elasticity, *Archive for Rational Mechanics and Analysis* **94**(4): 307–334.

Francfort, G. A. Murat, F. & Tartar, L. (1995). Fourth-order moments of non-negative measures on S^2 and applications, *Archive for Rational Mechanics and Analysis* **131**(4): 305–333.

Frecker, M. I., Ananthasuresh, G. K., Nishiwaki, S. & Kota, S. (1997). Topological synthesis of compliant mechanisms using multi-criteria optimization, *Transactions of the ASME* **119**(2): 238–245.

Frecker, M. I. Kikuchi, N. & Kota, S. (1999). Topology optimization of compliant mechanisms with multiple outputs, *Structural Optimization* **17**(4): 269–278.

Fuchs, M. B. & Moses, E. (2000). Optimal structural topologies with transmissible loads, *Structural and Multidisciplinary Optimization* **19**.

Fujii, D. Chen, B.-C. & Kikuchi, N. (2001). Composite material design of two-dimensional structures using the homogenization design method, *International Journal for Numerical Methods in Engineering* **50**: 2032–2051.

Fukunaga, H. & Sekine, H. (1992). Stiffness design method of symmetric laminates using lamination parameters, *AIAA J.* **30**: 2791–2793.

Fukunaga, H. & Sekine, H. (1993). Optimum design of composite structures for shape, layer angle and layer thickness distributions, *J. Comp. Mat.* **28**: 708–731.

Fukunaga, H., Sekine, H. & Sato, M. (1994). Optimal design of symmetric laminated plates for fundamental frequency, *Journal of Sound and Vibration* **171**(2): 219–229.

Fukunaga, H. & Vanderplaats, G. N. (1991). Stiffness optimization of orthotropic laminated composites using lamination parameters, *AIAA J* **29**: 641–646.

Fukushima, J., Suzuki, K. & Kikuchi, N. (1993). Applications to car bodies: Generalized layout design of three-dimensional shells, *in* G. I. N. Rozvany (ed.), *Optimization of Large Structural Systems*, Kluwer Academic Publishers,, Dordrecht, pp. 177–191.

Gea, G. H. & Fu, Y (1997). Optimal 3D stiffener design with frequency considerations, *Advances in Engineering Software* **28**(8): 525–531.

Gea, H. C. & Luo, J. H. (2001). Topology optimization of structures with geometrical non-linearities, *Computers and Structures* **79**: 1977–1985.

Geymonat, G. Müller, S. & Triantafyllidis, N. (1993). Homogenization of non-linearly elastic materials, microscopic bifurcation and macroscopic loss of rank-one convexity, *Archive for Rational Mechanics and Analysis* **122**(3): 231–290.

Ghaddar, C., Maday, Y. & Patera, A. T. (1995). Analysis of a part design procedure, *Numerische Mathematik* **71**(4): 465–510.

Gibiansky, L. V & Sigmund, O. (2000). Multiphase elastic composites with extremal bulk modulus, *Journal of the Mechanics and Physics of Solids* **48**(3): 461–498.

Gibiansky, L. V & Torquato, S. (1997). Thermal expansion of isotropic multiphase composites and polycrystals, *Journal of the Mechanics and Physics of Solids* **45**(7): 1223–1252.

Gibson, L. J. & Ashby, M. F (1988). *Cellular Solids, Structure and Properties*, Pergamon Press, Oxford, England.

Gill, P. E., Murray, W., Sounders, M. A., Tomlin, J. A. & Wright, M. (1986). On projected Newton barrier methods for linear programming and an equivalence to Karmakar's projective method, *Mathematical Programming* **36**: 183–209.

Golay, F & Seppecher, P. (2001). Locking materials and the topology of optimal shapes, *European Journal of Mechanics, A/Solids* **20**: 631–644.

Goodman, J., Kohn, R. V & Reyna, L. (1986). Numerical study of a relaxed variational problem from optimal design, *Computer Methods in Applied Mechanics and Engineering* **57**: 107–127.

Grabovsky, Y & Kohn, R. V (1995). Microstructures minimizing the energy of a two phase elastic composite in two space dimensions. II: The Vigdergauz microstructure, *Journal of the Mechanics and Physics of Solids* **43**(6): 949–972.

Grenestedt, J. L. & Gudmundson, P. (1993). Layup optimization of composite material structures, *in* P. Pedersen (ed.), *Optimal Design with Advanced Materials*, Elsevier Science Publ. B.V Amsterdam, pp. 311–336.

Guan, H., Chen, A. Y.-J. & Loo, Y.-C. (2001). Topology optimization of bridge type structures with stress and displacement constraints, *International Journal of Computational Engineering Science* **2**(2): 199–221.

Guedes, J. M. & Kikuchi, N. (1991). Preprocessing and postprocessing for materials based on the homogenization method with adaptive finite element methods, *Computer Methods in Applied Mechanical Engineering* **83**: 143–198.

Guedes, J. M. Rodrigues, H. C. & Bendsøe, M. P. (2001). On the computational approximation of energy bounds for multiload cases with one level of microstructure, *in* G. D. Cheng, Y Gu, S. Liu & Y. Wang (eds), *WCSMO-4 Proc. Second World Congress of Structural and Multidisciplinary Optimization*, Liaoning Electronic Press, Dalian. CD-rom, ISBN 7-900312-69-2.

Guedes, J. M. & Taylor, J. E. (1997). On the prediction of material properties and topology for optimal continuum structures, *Structural Optimization* **14**(2-3): 193–199.

Guo, X. & Cheng, G. D. (2000). Extrapolation approach for the solution of singular optima, *Structural and Multidisciplinary Optimization* **19**.

Guo, X. Cheng, G. D. & Yamazaki, K. (2001). A new approach for the solution of singular optima in truss topology optimization with stress and local buckling constraints, *Structural and Multidisciplinary Optimization* **22**(5): 364–373.

Gutkowski, Z. & Mróz, Z. (eds) (1997). *WCSMO-2 Proc. Second World Congress of Structural and Multidisciplinary Optimization*, Inst. of Fundamental Technological Research, Warsaw.

Haber, R. B. Jog, C. S. & Bendsøe, M. P. (1996). A new approach to variable-topology shape design using a constraint on the perimeter, *Structural Optimization* **11**(1): 1–11.

Haftka, R. T. (1999). Genetic algorithms for optimization of composite laminates, *NATO ASI Series E Applied Sciences Advanced Study Institute* **361**: 431–442.

Haftka, R. T. & Gandhi, R. V (1986). Structural shape optimization A survey, *Computer Methods in Applied Mechanics and Engineering* **57**: 91–106.

Haftka, R. T. & Gürdal, Z. (1992). *Elements of structural optimization*, third edn, Kluwer Academic Publishers Group, Dordrecht.

Hajela, P. & Lee, E. (1995). Genetic algorithms in truss topological optimization, *International Journal of Solids and Structures* **32**(22): 3341–3357.

Hammer, V B. (1999a). Optimal laminate design subject to single membrane loads, *Structural Optimization* **17**(1): 65–73.

Hammer, V B. (1999b). Optimal laminate design subject to single membrane loads, *Structural Optimization* **17**(1): 65–73.

Hammer, V B. (2000). Optimization of fibrous laminates undergoing progressive damage, *International Journal for Numerical Methods in Engineering* **48**(9): 1265–1284.

Hammer, V B. (2001). Checkmate? - Nodal densities in topology optimization, *in* M. P. Bendsøe, N. Olhoff & J. Rasmussen (eds), *Proc. 2nd Max Planck Workshop on Engineering Design Optimization*, Dept. of Mathematics, Technical University of Denmark, Lyngby.

Hammer, V B., Bendsøe, M. P., Lipton, R. & Pedersen, P. (1996). Parametrization in laminate design for optimal compliance, *International Journal of Solids and Structures* **34**(4): 415–434.

Hammer, V B. & Olhoff, N. (2000). Topology optimization of continuum structures subjected to pressure loading, *Structural and Multidisciplinary Optimization* **19**: 85–92.

Hammer, V B. & Olhoff, N. (2001). Topology optimization of 3D structures with design dependent loads, *in* G. D. Cheng, Y. Gu, S. Liu & Y Wang (eds), *WCSMO-4 Proc. Second World Congress of Structural and Multidisciplinary Optimization*, Liaoning Electronic Press, Dalian. CD-rom, ISBN 7-900312-69-2.

Hara, K. Zha, H. & Haegawa, T. (1999). Topology-adaptive modelling of objects by a level set method with multi-level stopping conditions, *Proc. IEEE Int. Conf. Image Proces.*, Vol. 4, IEEE, pp. 371–375.

Harasaki, H. & Arora, J. S. (2001). A new class of evolutionary methods based on the concept of transferred force for structural design, *Structural and Multidisciplinary Optimization* **22**: 35–56.

Hashin, Z. (1980). Failure criteria for unidirectional fiber composites, *Journal of Applied Mechanics* **47**: 329–334.

Hashin, Z. & Shtrikman, S. (1963). A variational approach to the theory of the elastic behaviour of multiphase materials, *Journal of the Mechanics and Physics of Solids* **11**: 127–140.

Haslinger, J. & Dvořák, J. (1995). Optimum composite material design, *RAIRO-Mathematical Modelling and Numerical Analysis-Modelisation* **29**(6): 657–686.

Haslinger, J. & Neittaanmki, P. (1996). *Finite Element Approximation for Optimal Shape Design Material and Topology Design*, John Wiley & Sons, Chichester, GB.

Hassani, B. & Hinton, E. (1999). *Homogenization and Structural Topology Optimization Theory, Practice and Software*, Springer, New York Berlin Heidelberg.

Haug, E. J. & Cea, J. (eds) (1981). *Optimization of Distributed Paramter Structures, Vols. 1 and 2*, Sijthoff and Noordhoff, Alphen aan den Rijn.

Haug, E. J., Choi, K. K. & Komkov, V (1986). *Design Sensitivity Analysis of Structural System*, Mathematics in Science and Engineering. Volume 177, Academic Press, New York.

Haug, E. J. (ed.) (1993). *Concurrent Engineering: Tools and Technologies for Mechanical Systems Design*, Vol. 108 of *NATO ASI series. Series F, Computer and systems sciences*, Springer-Verlag, Berlin; Heidelberg; London; etc.

Hemp, W (1973). *Optimum structures*, Clarendon Press, Oxford.

Herskovits, J. (ed.) (1995). *Advances in Structural Optimization*, Kluwer Academic Publishers, Dordrecht.

Hetrick, J. A., Kikuchi, N. & Kota, S. (2000). Robustness of compliant mechanism topology optimization formulations, *SPIE* **3667**

Hill, R. (1948). A theory of the yielding and plastic flow of anisotropic materials, *Proceedings of the Royal Society of London A* **193**: 58.

Hollister, S. J. & Kikuchi, N. (1994). Implant design synthesis using topology optimization and digital imaging, *Advances in Bioengineering and American Society of Mechanical Engineers, Bioengineering Division (Publication) BED* **28**: 403–404.

Hoppe, R. H. W & Petrova, S. I. (2001). VI large-scale computations for mechanical engineering problems - structural optimization of biomorphic microcellular ceramics by homogenization approach, *Lecture Notes in Computer Science* **2179**: 353–360.

Hoppe, R. H. W., Petrova, S. I. & Schulz, V H. (2001). Numerical analysis and its applications topology optimization of conductive media described by Maxwell's equations, *Lecture Notes in Computer Science* **1988**: 414–422.

Hörnlein, H. R. E. M. (1979). Ein Algorithmus zur Strukturoptimierung von Fachwerkkonstruktionen. Diplomarbeit, Ludwig-Maximillians-Universit¨at Munchen.

Hörnlein, H. R. E. M., Kocvara, M. & Werner, R. (2001). Material optimization: Bridging the gap between conceptual and preliminary design, *Aerospace Science and Technology* **5**(8): 541–554.

Hörnlein, H. R. E. M. & Schittkowski, K. (1993). *Software Systems for Structural Optimization*, Birkhuser, Boston, USA.

Hsu, Y.-L. (1994). A review of structural shape optimization, *Computers in Industry* **25**(1): 3–14.

Hsu, Y.-L., Hsu, M.-S. & Chen, C.-T. (2001). Interpreting results from topology optimization using density contours, *Computers and Structures* **79**: 1049–1058.

Huang, J., Walsh, T. Mancini, L., Wlotkowski, M. Yang, R. J. & Chuang, C.-H. (1993). A new approach for weight reduction in truck frame design, *Journal of Commercial Vehicles* pp. 959–967.

Hughes, T. J. R. (1987). *The Finite Element Method*, Prentice-Hall, Englewood Cliffs, New Jersey.

Huiskes, R. (2000). If bone is the answer, then what is the question?, *J. Anat.* **197**: 145–156.

Hyun, S. & Torquato, S. (2000). Designng composite microstructures with tageted properties, *Materials Research Society* **16**(1): 280–285.

Jacobs, C. R., Simo, J. C., Beaupre, G. S. & Carter, D. R. (1997). Adaptive bone remodeling incorporating simultaneous density and anisotropy considerations, *Journal of Biomechanics* **30**(6): 603–613.

Jacobsen, J. B. Olhoff, N. & Rønholt, E. (1998). Generalized shape optimization of three-dimensional structures using materials with optimum microstructures, *Mechanics of Materials* **28**(1-4): 207–225.

Jakiela, M. J., Chapman, C. D., Duda, J., Adewuya, A. & Saitou, K. (2000). Continuum structural topology design with genetic algorithms, *Comput. Methods Appl. Mech. Eng.* **186**: 339–356.

Jang, G.-W., Kim, T. S., Kim, Y Y., Kim, M., Park, C. & Shin, D. (2001). Nonconforming finite element for checkerboard-free topology optimization, *in* G. D. Cheng, Y Gu, S. Liu & Y. Wang (eds), *WCSMO-4 Proc. Second World Congress of Structural and Multidisciplinary Optimization*, Liaoning Electronic Press, Dalian. CD-rom, ISBN 7-900312-69-2.

Jarre, F., Kocvara, M. & Zowe, J. (1998). Optimal truss design by interior-point methods, *SIAM Journal on Optimization* **8**(4): 1084–1107.

Jiang, T. & Chirehdast, M. (1997). A systems approach to structural topology optimization: Designing optimal connections, *Transactions of the ASME - R Journal of Mechanical Design* **119**(1): 40–46.

Jog, C. S. (1996). Distributed-parameter optimization and topology design for nonlinear thermoelasticity, *Computer Methods in Applied Mechanics and Engineering* **132**(1-2): 117–134.

Jog, C. S. (2002a). Topology design of structures subjected to periodic loading, *J. of Sound and Vibration* **253**: 687–709.

Jog, C. S. (2002b). Topology design of structures using a dual algorithm and a constraint on the perimeter, *International Journal for Numerical Methods in Engineering* **54**(7): 1007–1019.

Jog, C. S. & Haber, R. B. (1996). Stability of finite element models for distributed-parameter optimization and topology design, *Computer Methods in Applied Mechanics and Engineering* **130**(3-4): 203–226.

Jog, C. S. Haber, R. B. & Bendsøe, M. P. (1993). A displacement based topology design with self-adaptive materials, *in* M. P. Bendsøe & C. A. Mota Soares (eds), *Topology Design of Structures*, Kluwer Academic Publishers Group, Amsterdam, pp. 219–238.

Jog, C. S., Haber, R. B. & Bendsøe, M. P. (1994). Topology design with optimized self-adaptive materials, *International Journal for Numerical Methods in Engineering* **37**(8): 1323–1350.

Johnson, C. & Pitkäranta, J. (1982). Analysis of some mixed finite element methods related to reduced integration, *Mathematics of Computations* **38**(158): 375–400.

Jonsmann, J. Sigmund, O. & Bouwstra, S. (1999a). Compliant electro-thermal microactuators, *MEMS'99*, pp. 588–593.

Jonsmann, J., Sigmund, O. & Bouwstra, S. (1999b). Compliant thermal microactuators, *Sensors and Actuators A: Physical* **76**(1-3): 463–469.

Jonsmann, J., Sigmund, O. & Bouwstra, S. (1999c). Multi degrees of freedom electro-thermal microactuators, *TRANSDUCERS'99*, pp. 1372–1375.

Kalamkarov, A. L. & Kolpakov, A. G. (1997). *Analysis, Design and Optimization of Composite Structures*, John Wiley & Sons, New York; London; Sydney.

Kane, C. & Schoenauer, M. (1996a). Genetic operators for two-dimensional shape optimization, *Lecture Notes in Computer Science* **1063**: 355–369.

Kane, C. & Schoenauer, M. (1996b). Topological optimum design using genetic algorithms, *Control Cybern* **25**: 1059–1087.

Kawabe, Y & Yoshida, S. (1996). Structural optimization by density distribution for maximization of natural frequency, *Transactions of the ASME - R - Journal of Mechanical Design* **118**(1): 157–159.

Kawohl, B., Pironneau, O. Tartar, L. & Zolesio, J.-P. (eds) (2000). *Optimal Shape Design*, Lecture Notes in Mathematics, Vol. 1740, Springer, Berlin New York Heidelberg.

Kemmler, R., Schwarz, S. & Ramm, E. (2000). Topology optimization including geometrically nonlinear response, *in* C. L. Bloebaum (ed.), *WCSMO-3 Proc. Third World Congress of Structural and Multidisciplinary Optimization*, University of New York at Buffalo. CD rom.

Kim, H. Querin, O. M. Steven, G. P. & Xie, Y. M. (2000). Method for varying the number of cavities in an optimized topology using evolutionary structural optimization, *Structural and Multidisciplinary Optimization* **19**.

Kim, T. S. & Kim, Y Y (2000a). Mac-based mode-tracking in structual topology optimization, *Computers and Structures* **74**: 357–383.

Kim, Y Y & Kim, T. S. (2000b). Topology optimization of beam cross sections, *International Journal of Solids and Structures* **37**: 477–493.

Kim, Y Y & Yoon, G. H. (2000). Multi-resolution multi-scale topology optimization- a new paradigm, *International Journal of Solids and Structures* **37**: 5529–5559.

Kirsch, U. (1989a). Optimal topologies of structures, *Appl. Mech. Rev.* **42**: 223–239.

Kirsch, U. (1989b). Optimal topologies of truss structures, *Comp. Meth. Engrg.* **72**: 15–28.

Kirsch, U. (1990a). On singular topologies in optimum structural design, *Structural Optimization* **2**: 133–142.

Kirsch, U. (1990b). On the relationship between optimum structural topologies and geometries, *Struct. Optim.* **2**: 39–45.

Kirsch, U. (1993a). Fundamental properties of optimal topologies, *in* M. P. Bendsøe & C. A. Mota Soares (eds), *Topology Design of Structures*, Kluwer Academic Publishers, pp. 3–18.

Kirsch, U. (1993b). *Structural Optimization: Fundamentals and Applications*, Springer, New York Berlin Heidelberg.

Kita, E. & Tanie, H. (1999). Topology and shape optimization of continuum structures using GA and BEM, *Structural Optimization* **17**(2-3): 130–139.

Kittel, C. (1986). *Solid State Physics*, John Wiley & Sons, New York.

Klarbring, A. (1992). On the problem of optimizing contact force distributions, *JOTA* **74**: 131–150.

Klarbring, A., Petersson, J. & Rönnqvist, M. (1995). Truss topology optimization involving unilateral contact, *J. Optim. Theory Appl.* pp. 1–31.

Kocvara, M. (1997). Topology optimization with displacement constraints: A bilevel programming approach, *Structural Optimization* **14**(4): 256–263.

Kocvara, M. (2002). On the modelling and solving of the truss design problem with global stability constraints, *Struct. Multidisc. Optimization* In print.

Kocvara, M. & Stingl, M. (2001). PENNON —A generalized augmented Lagrangian method for semidefinite programming, *Preprint 286*, Institute of Applied Mathematics, University of Erlangen.

Kocvara, M., Zibulevsky, M. & Zowe, J. (1998). Mechanical design problems with unilateral contact, *RAIRO Mathematical Modelling and Numerical Analysis* **32**(3): 255–282.

Kocvara, M., Zowe, J. & Nemirovski, A. (2000). Cascading - an approach to robust material optimization, *Computers & Structures* **76**(1-3): 431–442.

Kohn, R. V & Strang, G. (1986). Optimal design and relaxation of variational problems, *Communications on Pure and Applied Mathematics (New York)* **39**: 1–25 (part I), 139–182 (part II) and 353–357 (part III).

Kohn, R. V & Vogelius, M. (1987). Relaxation of a variational method for impedance computed tomography, *Comm. Pure Appl. Math.* **40**: 745–777.

Kolpakov, A. G. (1985). Determination of the average characteristics of elastic frameworks, *PMM Journal of applied Mathematics and Mechanics, U.S.S.R.* **49**: 739–745.

Korvink, J. G. Greiner, A. & Lienemann, J. (2001). Numerical offset optimization of magnetic field sensor microsystems, *Technisches Messen tm* **68**(6): 298–308.

Kosaka, I. & Swan, C. C. (1999). A symmetry reduction method for continuum structural topology optimization, *Computers and Structures* **70**(1): 47–61.

Kota, S., Joo, J., Li, Z., Rodgers, S. M. & Sniegowski, J. (2001). Design of compliant mechanisms: Applications to MEMS, *Analog Integrated Circuits and Signal Processing* **29**: 7–15.

Kozlowski, W & Mróz, Z. (1969). Optimal design of solid plates, *Int. J. Solids Struct.* **5**: 781–794.

Krajcinovic, D. (1996). *Damage Mechanics*, Elsevier Science B.V., Amsterdam.

Krein, M. G. & Nudelman, A. A. (1977). The Markov moment problem and extremal problems, *Translations of Math. Monographs, 50*, American Mathematical Society, Providence, USA.

Krog, L. A. & Olhoff, N. (1999). Optimum topology and reinforcement design of disk and plate structures with multiple stiffness and eigenfrequency objectives, *Computers and Structures* **72**: 535–563.

Kumar, A. V & Gossard, D. C. (1992). Geometric modeling for shape and topology optimization, *IFIP Transactions B (Applications in Technology); Geometric Modeling for Product Realization*, Vol. B-8, pp. 81–94.

Kumar, A. V & Gossard, D. C. (1996). Synthesis of optimal shape and topology of structures, *Trans. ASME Journal of Mechanical Design* **118**(1): 68–74.

Lagache, J.-M. (1981). Treillis de volume minimal dans une region donne, *J. de Mcanique* **20**: 415–448.

Lakes, R. (1987). Foam structures with negative Poisson's ratio, *Science* **235**: 1038.

Lakes, R. (1993). Materials with structural hierarchy, *Nature* **361**: 511–515.

Larsen, U. D. Sigmund, O. & Bouwstra, S. (1997). Design and fabrication of compliant micromechanisms and structures with negative poisson's ratio, *IEEE Journal of Microelectromechanical Systems* **6**(2): 99–106.

Lau, G. K., Du, H. & Lim, M. K. (2001a). Techniques to suppress intermediate density in topology optimization of compliant mechanisms, *Computational Mechanics* **27**: 426–435.

Lau, G. K. Du, H. & Lim, M. K. (2001b). Use of functional specifications as objective functions in topology optimization of compliant mechanism, *Comput. Methods Appl. Mech. Engrg* **190**: 4421–4433.

Leblond, J. B., Perrin, G. & Deveaux, J. (1994). Bifurcation effects in ductile metals with damage delocalization, *Journal of Applied Mechanics* **61**: 236–242.

Lee, S. J. Bae, J. E. & Hinton, E. (2000). Shell topology optimization using the layered artificial material model, *International Journal for Numerical Methods in Engineering* **47**(4): 843–868.

Lemaitre, J. (1996). *A Course on Damage Mechanics, 2nd edition*, Springer-Verlag, Berlin Heidelberg.

Lene, F & Duvaut, G. (1981). Resultats d'isotropie pour des milieux homogeneises, *C.R. Acad. Sc. Paris Serie II* **7 293**: 477–480.

Levin, V M. (1967). Thermal expansion coefficients of heterogeneous materials, *Mekhanika Tverdoga Tela* **2**: 88–94.

Levy, R. (1991). Fixed point theory and structural optimization, *Eng. Opt.* **17**: 251–261.

Lewiński, T. & Telega, J. J. (2000). *Plates, laminates and shells Asymptotic analysis and homogenization*, World Scientific Publishing Co. Inc., River Edge, NJ.

Lewiński, T. & Telega, J. J. (2001). Michell-like grillages and structures with locking, *Arch. Mech.* **53**(3): 303–331.

Lewiński, T., Zhou, M. & Rozvany, G. I. N. (1993). Exact least-weight truss layouts for rectangular domains with various support conditions, *Structural Optimization* **6**: 65–67.

Lewis, A. S. & Overton, M. L. (1996). Eigenvalue optimization, *Acta Numerica* **5**: 149–90.

Li, Q., Steven, G. P. & Xie, Y M. (2001). A simple checkerboard suppression algorithm for evolutionary structural optimization, *Structural and Multidisciplinary Optimization* **22**(3): 230–47.

Lin, C.-Y & Chao, L.-S. (2000). Automated image interpretation for integrated topology and shape optimization, *Structural and Multidisciplinary Optimization* **20**.

Lin, C.-Y & Chou, J.-N. (1999). A two-stage approach for structural topology optimization, *Advances in Engineering Software* **30**(4): 261–271.

Lipton, R. (1994a). On optimal reinforcement of plates and choice of design parameters., *Control and Cybernetics* **23**: 481–493.

Lipton, R. (1994b). Optimal design and relaxation for reinforced plates subject to random transverse loads, *J. Prob. Engng. Mech.* **9**: 167–177.

Lipton, R. (1994c). Saddle-point theorem with application to structural optimization, *JOTA* **81**: 549–568.

Lipton, R. (2001). Optimal inequalities for gradients of solutions of elliptic equations occurring in two-phase heat conductors, *SIAM J. Math. Anal.* **32**(5): 1081–1093.

Lipton, R. (2002). Design of functionally graded composite structures in the presence of stress constraints, *International Journal of Solids and Structures* **39**(9): 2575–2586.

Lipton, R. & Díaz, A. R. (1997). Reinforced Mindlin plates with extremal stiffness, *International Journal of Solids and Structures* **24**(28): 3691–3704.

Litvinov, V G. (1980). Optimal control of the natural frequency of a plate of variable thickness, *U.S.S.R. Comp. Maths. Math. Phys.* **19**: 70–86.

Liu, J. S., Parks, G. T. & Clarkson, P. J. (2000). Metamorphic development: A new topology optimization method for continuum structures, *Structural and Multidisciplinary Optimization* **20**.

Lowther, D. A. Mai, W & Dyck, D. N. (1998). OPTIMIZATION A comparison of MRI magnet design using a Hopfield network and the optimized material distribution method, *IEEE Transactions on Magnetics* **34**(5): 2885–2888.

Luo, J. H. & Gea, H. C. (1998). Optimal bead orientation of 3D shell/plate structures, *Finite Elements in Analysis and Design* **31**(1): 55–71.

Lurie, K. A. (1980). Optimal design of elastic bodies and the problem of regularization, *Wissenschaftliche Zeitschrift, Techn. Hochschule Leipzig* **4**: 339–347

Lurie, K. A. (1993). *Applied Optimal Control Theory of Distributed Systems*, Plenum Press, New York; London.

Lurie, K. A. & Cherkaev, A. V (1997). Effective characteristics of composite materials and the optimal design of structural elements [partial translation of MR 88e:73019], *in* A. V Cherkaev & R. V Kohn (eds), *Topics in the mathematical modelling of composite materials*, Vol. 31 of *Progress in nonlinear differential equations and their applications*, Birkhäuser, Boston, MA, pp. 175–258.

Lurie, K. A. Cherkaev, A. V & Fedorov, A. V (1982). Regularization of optimal design problems for bars and plates. I, II, *Journal of Optimization Theory and Applications* **37**(4): 499–522, 523–543.

Ma, Z.-D. Kikuchi, N. & Cheng, H.-C. (1995). Topological design for vibrating structures, *Computer Methods in Applied Mechanics and Engineering* **121**(1-4): 259–280.

Ma, Z.-D., Kikuchi, N. Cheng, H.-C. & Hagiwara, I. (1995). Topological optimization technique for free vibration problems, *Transactions of the ASME E Journal of Applied Mechanics* **62**(1): 200–207.

Ma, Z.-D. Kikuchi, N. & Hagiwara, I. (1994). Structural topology and shape optimization for a frequency response problem, *Comp. Mech.* **13**: 157–174.

Maar, B. & Schulz, V H. (2000). Interior point multigrid methods for topology optimization, *Structural and Multidisciplinary Optimization* **19**(3): 214–224.

Magister, R. & Post, P. U. (1995). Use of structural optimization in the development of pneumatic components, *in* G. I. N. Rozvany & N. Olhoff (eds), *Proc. First World Congress of Structural and Multidisciplinary Optimization*, Pergamon Press, Oxford, pp. 445–452.

Manickarajah, D. Xie, Y M. & Steven, G. P. (1998). An evolutionary method for optimization of plate buckling resistance, *Finite elements in analysis and design* **29**: 205–230.

Marsan, A. L. & Dutta, D. (1996). Construction of a surface model and layered manufacturing data from 3D homogenization output, *Transactions of the ASME R Journal of Mechanical Design* **118**(3): 412–418.

Maso, G. D. & Dell'Antonio, G. F (eds) (1995). *Composite Media and Homogenization Theory*, World Scientific, Singapore.

Masur, E. F (1970). Optimum stiffness and strength of elastic structures, *Journal of Engineering Mechanics* **96**: 621–640.

Mathews, J. & Walker, R. (1964). *Mathematical Methods of Physics*, Addison-Wesley, Redwood City, Calif.

Mattheck, C. (1996). Design in nature, *Structural Engineering International* **6**(3): 177–180.

Mattheck, C. (1998). Design in nature: Learning from trees, *Nature* **392**(6673): 0–242. Springer Verlag, Berlin/Heidelberg.

Maute, K. & Ramm, E. (1997). Adaptive topology optimization of shell structures, *AIAA Journal American Institute of Aeronautics and Astronautics* **35**(11): 1767–177.

Maute, K. & Ramm, E. (1998). Adaptive topology optimization, *Structural Optimization* **10**(2): 100–112.

Maute, K., Schwarz, S. & Ramm, E. (1998). Adaptive topology optimization of elastoplastic structures, *Structural Optimization* **15**(2): 81–90.

Maute, K. Schwarz, S. & Ramm, E. (1999). Structural optimization the interaction between form and mechanics, *ZAMM Zeitschrift fur Angewandte Mathematik und Mechanik* **79**(10): 651–673.

Mayer, R. R. Kikuchi, N. & Scott, R. A. (1996). Application of topological optimization techniques to structural crashworthiness, *International Journal for Numerical Methods in Engineering* **39**(8): 1383–1404.

McKeown, J. J. (1997). Upper limits on the number of elements in elastic structures of minimum weight, *Structural Optimization* **13**(2-3): 128–133.

Michell, A. G. M. (1904). The limit of economy of material in frame structures, *Philosophical Magazine* **8**(6): 589–597.

Mijar, A. R. Swan, C. C. Arora, J. S. & Kosaka, I. (1998). Continuum topology optimization for concept design of frame bracing systems, *Journal of Structural Engineering - Reston* **124**(5): 541–550.

Miki, M. & Sugiyama, Y (1993). Optimum design of laminated composite plates using lamination parameters, *AIAA J* **31**: 921–922.

Milton, G. (2002). *The Theory of Composites*, Cambridge University Press, Cambridge.

Milton, G. W (1990). On characterizing the set of possible effective tensors of composites: The variational method and the translation method, *Communications on Pure and Applied Mathematics (New York)* **43**(1): 63–125.

Milton, G. W (1992). Composite materials with Poisson's ratios close to − *Journal of the Mechanics and Physics of Solids* **40**(5): 1105–1137.

Milton, G. W & Cherkaev, A. V (1995). Which elasticity tensors are realizable?, *Transactions of the ASME H Journal of Engineering Materials and Technology* **117**(4): 483–493.

Min, S. J. & Kikuchi, N. (1997). Optimal reinforcement design of structures under the buckling load using the homogenization design method, *Struct. Eng. Mech.* **5**: 565–576.

Min, S. J., Kikuchi, N., Park, Y C., Kim, S. & Chang, S. (1999). Optimal topology design of structures under dynamic loads, *Structural Optimization.* **17**(2-3): 208–21.

Min, S. J., Nishiwaki, S. & Kikuchi, N. (2000). Unified topology design of static and vibrating structures using multiobjective optimization, *Computers and Structers* **75**: 93–116.

Mirsky, L. (1959). On the trace of matrix products, *Math. Nach.* **20**: 171–174.

Mlejnek, H. P. (1992). Some aspects of the genesis of structures, *Structural Optimization* **5**: 64–69.

Mlejnek, H. P. & Schirrmacher, R. (1993). An engineering approach to optimal material distribution and shape finding, *Computational Methods in Applied Mechanics and Engineering* **106**: 1–26.

Mohammadi, B. & Pironneau, O. (2001). *Applied Shape Optimization for Fluids*, Oxford University Press, Oxford.

Moreau, J.-J. (1964). Théorèmes "inf-sup", *C. R. Acad. Sci. Paris* **258**: 2720–2722.

Morris, A. J. (ed.) (1982). *Foundations of Structural Optimization: A Unified Approach*, John Wiley & Sons, Chichester.

Mosheyev, L. & Zibulevsky, M. (2000). Penalty/barrier multiplier algorithm for semidefinite programming, *Optimization Methods and Software* **13**: 235–261.

Mota Soares, C. A. (ed.) (1987). *Computer Aided Optimal Design: Structural and Mechanical Systems*, Vol. 27 of *NATO ASI series. Series F*, Springer-Verlag, Berlin; Heidelberg; London; etc.

Mróz, Z. & Bojczuk, D. (2001). Optimal design evolution with finite topology variations, *in* G. D. Cheng, Y Gu, S. Liu & Y Wang (eds), *WCSMO-4 Proc. Second World Congress of Structural and Multidisciplinary Optimization*, Liaoning Electronic Press, Dalian. CD-rom, ISBN 7-900312-69-2.

Mróz, Z. & Rozvany, G. I. N. (1975). Optimal design of structures with variable support conditions, *Journal of Optimization Theory and Applications* **15**(1): 85–101.

Mullender, M. G., Huiskes, R. & Weinans. H. (1994). A physiological approach to the simulation of bone remodelling as a self-organizational controll process, *Journal of Biomechanics* **11**: 1389–1394.

Muńoz, J. & Pedregal, P. (1998). On the relaxation of an optimal design problem for plates, *Asymptotic Analysis* **16**: 125–140.

Muralidhar, R. & Rao, J. R. (1997). New models for optimal truss topology in limit design based on unified elastic/plastic analysis, *Computer Methods in Applied Mechanics and Engineering* **140**(1-2): 109–138.

Murat, F (1977). Contre-examples pour divers problèmes où le contrôle intervient dans les coefficients, *Annali di Matematica Pura ed Applicata. Series 4* pp. 49–68.

Murat, F & Simon, J. (1976). *Studies on Optimal Shape Design Problems*, Lectures Notes in Computer Science, 41, Springer Verlag, Berlin.

Murat, F & Tartar, L. (1997). Calculus of variations and homogenization, *in* A. V Cherkaev & R. V Kohn (eds), *Topics in the mathematical modeling of composite materials*, Vol. 31 of *Progress in nonlinear differential equations and their applications*, Birkhäuser, Boston, pp. 139–173.

Neittaanmki, P. & Tiba, D. (1995). An embedding of domains approach in free boundary problems and optimal shape design, *SIAM J. Control Optim.* **33**: 1587–1602.

Nesterov, J. E. & Nemirovski, A. (1994). *Interior Point Polynomial Methods in Convex Programming: Theory and Applications*, SIAM, Philadelphia.

Neves, M. M., Rodrigues, H. C. & Guedes, J. M. (1995). Generalized topology design of structures with a buckling load criterion, *Structural Optimization* **10**(2): 71–78.

Neves, M. M., Rodrigues, H. C. & Guedes, J. M. (2000). Optimal design of periodic linear elastic microstructures, *Computers & Structures* **76**: 421–429.

Neves, M. M. Sigmund, O. & Bendsøe, M. P. (2002a). Topology optimization of periodic microstructures with a buckling criteria, *in* H. A. Mang, F G. Rammerstorfer & J. Eberhardsteiner (eds), *Proceedings of the Fifth World Congress on Computational Mechanics*, Vienna University of Technology, Austria, p. http://wccm.tuwien.ac.at.

Neves, M. M. Sigmund, O. & Bendsøe, M. P. (2002b). Topology optimization of periodic microstructures with a penalization of highly localized buckling modes, *International Journal of Numerical Methods on Engineering* **54**(6): 809–834.

Niordson, F I. (1983). Optimal design of plates with a constraint on the slope of the thickness function, *International Journal of Solids and Structures* **19**: 141–151.

Nishino, F & Duggal, R. (1990). Shape optimum design of trusses under multiple loading, *Int. J. Solids Struct.* **26**: 17–27.

Nishiwaki, S. Frecker, M. I. Min, S. J. & Kikuchi, N. (1998). Topology optimization of compliant mechanisms using the homogenization method, *International Journal of Numerical Methods in Engineering* **42**(3): 535–560.

Nishiwaki, S., Min, S. J. Yoo, J. & Kikuchi, N. (2001). Optimal structural design considering flexibility, *Comput. Methods Appl. Mech. Engrg.* **190**: 4457–4504.

Nishiwaki, S. Saitou, K., Min, S. J. & Kikuchi, N. (2000). Topological design considering flexibility under periodic loads, *Structural and Multidisciplinary Optimization* **19**.

Oberndorfer, J. M., Achtziger, W & Hörnlein, H. R. E. M. (1996). Two approaches for truss topology optimization: A comparison for practical use, *Structural Optimization* **11**(3-4): 137–144.

Ohsaki, M., Fujisawa, K., Katoh, N. & Kanno, Y (1999). Semi-definite programming for topology optimization of trusses under miltiple eigenvalue constraints, *Comput. Methods. Appl. Mech. Engrg.* **180**: 203–217.

Olhoff, N. (1970). Optimal design of vibrating circular plates, *Int. J. Solids Struct.* **6**: 139–156.

Olhoff, N. (1989). Multicriterion structural optimization via bound formulation and mathematical programming, *Struct. Optim.* **1**: 11–17.

Olhoff, N. (1996). On optimum design of structures and materials, *Meccanica* **31**: 143–161.

Olhoff, N. (2000). Comparative study of optimizing the topology of plate-like structures via plate theory and 3-D elasticity, *in* G. I. N. Rozvany & N. Olhoff (eds), *Topology Optimization of Structures and Composite Continua*, Kluwer Academic Publishers, Dordrecht, pp. 37–48.

Olhoff, N. & Akesson, B. (1991). Minimum stiffness of optimally located supports for maximum value of column buckling loads, *Structural Optimization* **3**(3): 163–75.

Olhoff, N. Bendsøe, M. P. & Rasmussen, J. (1992a). CAD-integrated structural topology and design optimization, *Shape and layout optimization of structural systems and optimality criteria methods*, Springer-Verlag, Vienna, pp. 171–197.

Olhoff, N., Bendsøe, M. P. & Rasmussen, J. (1992b). On CAD-integrated structural topology and design optimization, *Computer Methods in Applied Mechanics and Engineering* **89**: 259–279.

Olhoff, N., Lund, E. & Rasmussen, J. (1993). Concurrent engineering: Tools and technologies for mechanical system design, *in* E. J. Haug (ed.), *Concurrent engineering design optimization in a CAD environment*, Springer-Verlag, pp. 523–86.

Olhoff, N., Lurie, K. A., Cherkaev, A. V & Fedorov, A. V (1981). Sliding regimes and anisotropy in optimal design of vibrating axisymmetric plates, *International Journal of Solids and Structures* **17**(10): 931–948.

Olhoff, N. & Rasmussen, S. H. (1977). On bimodal optimum loads of clamped columns, *International Journal of Solids and Structures* **13**: 605–514.

Olhoff, N. Rønholt, E. & Scheel, J. (1998). Topology optimization of three-dimensional structures using optimum microstructures, *Structural Optimization* **16**(1): 1–18.

Olhoff, N. & Rozvany, G. I. N. (eds) (1995). *Proceedings of the First World Congress of Structural and Multidisciplinary Optimization: 28 May–2 June 1995, Goslar, Germany: WCSMO-1*, Pergamon, New York.

Olhoff, N. & Taylor, J. E. (1978). Designing continuous colmns for minimum total cost of material and interior supports, *Journal of Structural Mechanics* **6**: 367–382.

Olhoff, N. & Taylor, J. E. (1979). On optimal structural remodeling, *JOTA* **27**: 571–582.

Olhoff, N. & Taylor, J. E. (1983). On structural optimization, *Journal of Applied Mechanics* **50**(4): 1139–1151.

Olhoff, N. Thomsen, J. & Rasmussen, J. (1993). Topology optimization of bimaterial structures, *in* P. Pedersen (ed.), *Optimal Design with Advanced Materials*, Elsevier, Amsterdam, The Netherlands, pp. 191–206.

Ou, J. S. & Kikuchi, N. (1996a). Integrated optimal structural and vibration control design, *Structural Optimization* **12**(4): 209–216.

Ou, J. S. & Kikuchi, N. (1996b). Optimal design of controlled structures, *Structural Optimization* **11**: 19–28.

Overton, M. L. (1992). Large-scale optimization of eigenvalues, *SIAM J. Optimization* **2**: 88–120.

Papalambros, P. Y & Chirehdast, M. (1990). An integrated environment for structural configuration design, *J. Engrg. Design* **1**: 73–96.

Park, K.-S. Chang, S.-Y & Youn, S.-K. (2001). Topology optimization of the primary mirror of a multi-spectral camera, *in* G. D. Cheng, Y Gu, S. Liu & Y Wang (eds), *WCSMO-4 Proc. Second World Congress of Structural and Multidisciplinary Optimization*, Liaoning Electronic Press, Dalian. CD-rom, ISBN 7-900312-69-2.

Payten, W. M. & Ben-Nissan, B. (1997). Optimal structure formation using a chaotic self-organisational algorithm, *Comput. & Graphics* **21**: 685–688.

Payten, W M., Ben-Nissan, B. & Mercer, D. J. (1998). Optimal topology design using a global self-organisational approach, *International Journal of Solids and Structures* **35**(3-4): 219–237.

Payten, W M. & Law, M. (1998). Generalized shape optimization using stress constraints under multiple load cases, *Structural Optimization* **15**(3-4): 269–274.

Pedersen, C. B. W (2002a). *On Topology Design of Frame Structures for Crashworthiness*, PhD thesis, Department of Mechanical Engineering, Solid Mechanics, Technical University of Denmark.

Pedersen, C. B. W (2002b). Topology optimization design of crushed 2D-frames for desired energy absorption history, *Submitted* also appeared as DCAMM-report 666, Danish Center for Applied Mathematics and Mechanics.

Pedersen, C. B. W (2002c). Topology optimization of 2D-frame structures with path dependent response, *International Journal for Numerical Methods in Engineering (accepted)*

Pedersen, C. B. W (2002d). Topology optimization of energy absorbing frames, *in* H. A. Mang, F G. Rammerstorfer & J. Eberhardsteiner (eds), *Proceedings of the Fifth World Congress on Computational Mechanics*, Vienna University of Technology, Austria, p. http://wccm.tuwien.ac.at.

Pedersen, C. B. W Buhl, T. & Sigmund, O. (2001). Topology synthesis of large-displacement compliant mechanisms, *International Journal of Numerical Methods in Engineering* **50**(12): 2683–2705.

Pedersen, N. L. (2000a). Design of cantilever probes for atomic force microscopy (AFM), *Engineering Optimization* **32**(3): 373–392.

Pedersen, N. L. (2000b). Maximization of eigenvalues using topology optimization, *Structural and Multidisciplinary Optimization* **20**(1): 2–11.

Pedersen, N. L. (2001). On topology optimization of plates with prestress, *International Journal of Numerical Methods in Engineering* **51**(2): 225–240.

Pedersen, N. L. (2002e). Topology optimization of laminated plates with prestress, *Computers & Structures* **80**(7-8): 559–70.

Pedersen, P. (1970). On the minimum mass layout of trusses, *AGARD Conference Proceedings No. 36, Symposium on Structural Optimization*, pp. 189–192.

Pedersen, P. (1989). On optimal orientation of orthotropic materials, *Structural Optimization* **1**: 101–106.

Pedersen, P (1990). Bounds on elastic energy in solids of orthotropic materials, *Structural Optimization* **2**: 55–63.

Pedersen, P. (1991). On thickness and orientational design with orthotropic materials, *Structural Optimization* **3**: 69–78.

Pedersen, P. (1993a). Concurrent engineering design with and of advanced materials, *in* E. J. Haug (ed.), *Concurrent Engineering Tools and Technologies for Mechanical Systems Design*, Springer Verlag, New York, USA, pp. 627–670.

Pedersen, P. (1993b). Topology optimization of three dimensional trusses, *in* M. P Bendsøe & C. A. Mota Soares (eds), *Topology Design of Structures*, Kluwer Academic Publishers, pp. 19–30.

Pedersen, P. (1993c). Topology optimization of three dimensional trusses with cost of supports, *in* J. Herskovits (ed.), *Structural Optimization 1993, The World Congress on Optimal Design of Structural Systems. Proceedings VOL. X*, Mech. Engng. Program, COPPE/Federal University of Rio de Janeiro, Rio de Janeiro, Brazil., pp. 11–20.

Pedersen, P. (1995a). Material optimization - an engineering view, *in* J. Herskovits (ed.), *Advances in Structural Optimization*, Kluwer Academic Publishers, Dordrecht, pp. 223–261.

Pedersen, P. (1995b). Simple transformations by proper contracted forms: can we change the usual practice?, *Communications in Numerical Methods in Engineering* **11**(10): 821–829.

Pedersen, P. (1998). Some general optimal design results using anisotropic, nonlinear materials, *Structural Optimization* **15**: 73–80.

Pedersen, P. (2002f). *Optimal Designs and Identifications for Structures and Materials Problems and Tools*, Dept. Mech. Engng., Technical University of Denmark, Lyngby, Denmark.

Pedersen, P. & Bendsøe, M. P (1995). On strain-stress fields resulting from optimal orientation, *in* G. I. N. Rozvany & N. Olhoff (eds), *Proc. First World Congress of Structural and Multidisciplinary Optimization*, Pergamon Press, Oxford, pp. 243–250.

Pedersen, P. & Bendsøe, M. P. (eds) (1999). *Synthesis in Bio Solid Mechanics*, Kluwer Academic Publishers, Dordrecht.

Pedersen, P. (ed.) (1993d). *Optimal Design with Advanced Materials*, Elsevier, Amsterdam, The Netherlands.

Petersen, K. E. (1982). Silicon as a mechanical material, *Proc. IEEE* **70**(5): 420–457

Petersson, J. (1996). On stiffness maximization of variable thickness sheet with unilateral contact, *Quarterly of Applied Mathematics* **54**(3): 541–550.

Petersson, J. (1999a). A finite element analysis of optimal variable thickness sheets, *SIAM J. Num. Anal.* **36**: 1759–1778.

Petersson, J. (1999b). Some convergence results in perimeter-controlled topology optimization, *Computer Methods in Applied Mechanics and Engineering* **171**(1-2): 123–140.

Petersson, J. (2001). On continuity of the design-to-state mappings for trusses with variable topology, *International Journal of Engineering Science* **39**(10): 1119–1141.

Petersson, J. Beckers, M. & Duysinx, P. (2000). Almost isotropic perimeters in topology optimization, *in* C. L. Bloebaum (ed.), *WCSMO-3 Proc. Third World Congress of Structural and Multidisciplinary Optimization*, University of New York at Buffalo. CD rom.

Petersson, J. & Haslinger, J. (1998). An approximation theory for optimum sheets in unilateral contact, *Quarterly of Applied Mathematics* **56**(2): 309–32.

Petersson, J. & Klarbring, A. (1994). Saddle point approach to stiffness optimization of discrete structures including unilateral contact, *Control and Cybernetics* **23**: 461–479.

Petersson, J. & Patriksson, M. (1997). Topology optimization of sheets in contact by a subgradient method, *International Journal for Numerical Methods in Engineering* **40**(7): 1295–321.

Petersson, J. & Sigmund, O. (1998). Slope constrained topology optimization, *International Journal for Numerical Methods in Engineering* **41**(8): 1417–1434.

Pettermann, H. E. Reiter, T. J. & Rammerstorfer, F G. (1997). Computational simulation of internal bone remodeling, *Archives of Computational Methods in Engineering, State of the art reviews* **4**(4): 295–323.

Pironneau, O. (1973). On optimal profiles in Stokes flow, *Journal of Fluid Mechanics* **59**: 117–128.

Pironneau, O. (1984). *Optimal Shape Design for Elliptic Systems*, Springer-Verlag.

Plaxton, S. & Taylor, J. E. (1994). Applications of a generalized complementary energy principle for the equilibrium analysis of softening material, *Comp. Meth. Appl. Mech. Engng.* **117**: 91–104.

Poulsen, T. A. (2001a). A new scheme for imposing a minimum length scale in topology optimization, Danish Center for Applied Mathematics and Mechanics, DCAMM Report No. 663.

Poulsen, T. A. (2001b). A simple scheme to prevent checkerboard patterns and one-node connected hinges in topology optimization, submitted.

Poulsen, T. A. (2002). Topology optimization in wavelet space, *Int. Journal Numerical Methods in Engineering* **53**: 567–582.

Poulton, C. G., Movchan, A. B., McPhedran, R. C., Nicorovici, N. A. & Antipov, Y A. (2000). Eigenvalue problems for doubly periodic elastic structures and phononic band gaps, *Proceedings of the Royal Society of London, Series A (Mathematical, Physical and Engineering Sciences)* **456**(2002): 2543–59.

Prager, W (1985). Optimal design of grillages, *in* M. Save & W Prager (eds), *Structural Optimization*, Plenum Press, New York, USA, pp. 153–200.

Prager, W & Rozvany, G. I. N. (1975). Plastic design of beams: Optimal locations of supports and steps in yield moment, *International Journal of Mechanical Sciences* **17**(10): 627–631.

Prager, W. & Rozvany, G. I. N. (1977). Optimization of structural geometry, *in* A. Bednarek & L. Cesari (eds), *Dynamical Systems*, Academic Press, New York.

Prager, W. & Taylor, J. E. (1968). Problems of optimal structural design, *J. Applied Mechs.* **35**: 102–106.

Proos, K. A., Steven, G. P., Querin, O. M. & Xie, Y M. (2001). Multicriterion evolutionary structural optimization using the weighting and the global criterion methods, *AIAA Journal* **39**(10): 2006–2012.

Rahmatalla, S. & Swan, C. C. (2002). Continuum topology optimization of buckling-sensitivie structures, *submitted*

Raĭtum, U. E. (1978). The extension of extremal problems connected with a linear elliptic equation, *Soviet Math.* **19**: 1342–1345.

Rasmussen, J., Lund, E. Birker, T. & Olhoff, N. (1993). The CAOS system, *in* H. R. E. M. Hörnlein & K. Schittkowski (eds), *Software Systems for Structural Optimization*, Birkhuser, Boston, USA, pp. 75–96.

Rasmussen, S. H. (1979). *Optimization of Fiber-Reinforced Structures (in Danish). DCAMM Report No. S12*, PhD thesis, The Danish Center for Applied Mathematics and Mechanics, The Technical University of Denmark, DK-2800 Lyngby.

Reynolds, D., McConnachie, J. Bettess, P. Christie, W C. & Bull, J. W (1999). Reverse adaptivity – A new evolutionary tool for structural optimization, *International Journal for Numerical Methods in Engineering* **45**: 529–552. 5.

Riche, R. L. & Cailletaud, G. (1998). A mixed evolutionary/heuristic approach to shape optimization, *International Journal for Numerical Methods in Engineering* **41**(8): 1463–1484.

Rietz, A. (2001). Sufficiency of a finite exponent in SIMP (power law) methods, *Structural and Multidisciplinary Optimization* **21**: 159–163.

Rietz, A. & Petersson, J. (2001). Simultaneous shape and thickness optimization, *Structural and Multidisciplinary Optimization* **23**(1): 14–23.

Ringertz, U. (1985). On topology optimization of trusses, *Engrg. Optim.* **9**: 21–36.

Ringertz, U. (1986). A branch and bound algorithm for topology optimization of truss structures, *Engrg. Optim.* **10**: 111–124.

Ringertz, U. (1993). On finding the optimal distribution of material properties, *Struct. Optim.* **5**: 265–267.

Rodrigues, H. C. (1988). Shape optimal design of elastic bodies using a mixed variational formulation, *Comp. Meth. Appl. Mech. Engng.* **69**: 29–44.

Rodrigues, H. C. & Fernandes, P. (1993). Topology optimization of linear elastic structures subjected to thermal loads, *in* M. P. Bendsøe & C. A. Mota Soares (eds), *Topology Design of Structures*, Kluwer Academic Publishers, pp. 437–450.

Rodrigues, H. C. & Fernandes, P. (1995). A material based model for topology optimization of thermoelastic structures, *International Journal for Numerical Methods in Engineering* **38**(12): 1951–1965.

Rodrigues, H. C., Guedes, J. M. & Bendsøe, M. P. (1995). Necessary conditions for optimal design of structures with a non-smooth eigenvalue based criterion, *Structural Optimization* **9**(1): 52–56.

Rodrigues, H. C., Jacobs, C., Guedes, J. M. & Bendsøe, M. P. (1999). Global and local material optimization models applied to anisotropic bone adaption, *in* P. Pedersen & M. P. Bendsøe (eds), *Synthesis in bio solid mechanics*, IUTAM, Kluwer, Dordrecht.

Rodrigues, H. C., Soto, C. A. & Taylor, J. E. (1999). A design model to predict optimal two-material composite structure, *Structural Optimization* **17**(2-3): 186–198.

Rodrigues, H., Guedes, J. M. & Bendsøe, M. P. (2002). Hierarchical optimization of material and structure, *Structural and Multidisciplinary Optimization* **24**(1): 1–10.

Rosen, B. W & Hashin, Z. (1970). Effective thermal expansion and specific heat of composite materials, *International Journal of Engineering Science* **8**: 157–173.

Rossow, M. P. & Taylor, J. E. (1973). A finite element method for the optimal design of variable thickness sheets, *AIAA J.* **11**: 1566–1569.

Rothemburg, L. Berlin, A. A. & Bathurst, J. (1991). Microstructures of isotropic materials with negative poisson's ratio, *Nature* **354**: 470–472.

Rousselet, B. & Haug, E. J. (1983). Design sensitivity analysis in structural mechanics, III. effects of shape variation, *J. Struct. Mech.* **10**: 273–310.

Rovati, M. & Taliercio, A. (1991). Optimal orientation of the symmetry axes of orthotropic 3-D materials, *in* H. A. Eschenauer, C. Mattheck & N. Olhoff (eds), *Int. Conf. Engng. Optimization in Design Processes, Karlsruhe*, Vol. 63, Springer Verlag, Berlin, FRG, pp. 127–134. Lecture Notes in Engineering.

Rozvany, G. I. N. (1974). Optimization of unspecified generalized forces in structural design, *Journal Appl. Mech. ASME* **41**: 1143–1145.

Rozvany, G. I. N. (1976). *Optimal Design of Flexural Systems*, Pergamon Press, Oxford.

Rozvany, G. I. N. (1989). *Structural design via optimality criteria*, Kluwer Academic Publishers Group, Dordrecht. Boston. London.

Rozvany, G. I. N. (1996). Difficulties in truss topology optimization with stress, local buckling and system stability constraints, *Structural Optimization* **11**(3-4): 213–217.

Rozvany, G. I. N. (1997a). Aims, scope, basic concepts and methods of topology optimization, *in* G. I. N. Rozvany (ed.), *Topology Optimization in Structural Mechanics*, Springer, Vienna, pp. 1–55. CISM Courses and Lectures, 374.

Rozvany, G. I. N. (2001a). Aims, scope, methods, history and unified terminology of computer-aided topology optimization in structural mechanics, *Structural and Multidisciplinary Optimization* **21**: 90–108.

Rozvany, G. I. N. (2001b). On design-dependent constraints and singular topologies, *Structural and Multidisciplinary Optimization* **21**: 164–172.

Rozvany, G. I. N. Bendsøe, M. P. & Kirsch, U. (1995). Layout optimization of structures, *Applied Mechanics Reviews* **48**(2): 41–119.

Rozvany, G. I. N. & Birker, T. (1994). On singular topologies in exact layout optimization, *Structural Optimization* **8**: 228–235.

Rozvany, G. I. N. (ed.) (1992). *Shape and Lay-Out Optimization of Structural Systems and Optimality Criteria Methods*, Springer Verlag, Wien. CISM Lecture Notes No. 325.

Rozvany, G. I. N. (ed.) (1993). *Optimization of Large Structural Systems*, Kluwer Academic Publishers, Dordrecht, The Netherlands.

Rozvany, G. I. N. (ed.) (1997b). *Topology optimization in structural mechanics*, Springer-Verlag, Vienna.

Rozvany, G. I. N. & Mróz, Z. (1977). Column design: Optimization of support conditions and segmentation, *Journal of Structural Mechanics* **5**(3): 279–290.

Rozvany, G. I. N. & Olhoff, N. (eds) (2000). *Topology Optimization of Structures and Composite Continua*, Kluwer Academic Publishers, Dordrecht.

Rozvany, G. I. N. & Zhou, M. (1991). The COC algorithm, part I: Cross-section optimization or sizing, *Computer Methods in Applied Mechanics and Engineering* **89**: 281–308.

Rozvany, G. I. N., Zhou, M. & Sigmund, O. (1994). Topology optimization in structural design, *in* H. Adeli (ed.), *Advances in Design Optimization*, Chapman and Hall, London, chapter 10, pp. 340–399.

Ruy, W.-S. & Yang, Y.-S. (2001). Selection strategies in a structural design support system, *Structural and Multidisciplinary Optimization* **21**: 69–79.

Ryvkin, M., Fuchs, M. B. & Nuller, B. (1999). Optimal design of infinite repetitive structures, *Structural Optimization* **18**(2-3): 202–209.

Saggere, L. & Kota, S. (1999). Static shape control of smart structures using compliant mechanisms, *AIAA Journal* **37**(5): 572–579.

Sánchez Palencia, E. (1980). *Nonhomogeneous media and vibration theory*, Springer-Verlag, Berlin.

Save, M. & Prager, W (eds) (1985). *Structural Optimization, Vol. Optimality Criteria*, Plenum Press, New York.

Save, M. & Prager, W (eds) (1990). *Structural Optimization, Vol. 2, Mathematical Optimization*, Plenum Press, New York.

Saxena, A. & Ananthasuresh, G. K. (2001). Topology synthesis of compliant mechanisms for nonlinear force-deflection and curved path specifications, *Transactions of the ASME R Journal of Mechanical Design* **123**(1): 33–42.

Schapery, R. A. (1968). Thermal expansion coefficients of composite materials based on energy principles, *Journal of Composite Materials* **2**(3): 380–404.

Schittkowski, K. (1985). NLPQL: A FORTRAN subroutine solving constrained nonlinear programming problems, *Annals Oper. Res.* **5**: 485–500.

Schramm, H. & Zowe, J. (1992). A version of the bundle idea for minimizing a nonsmooth function: Conceptual idea, convergence analysis, numerical results, *SIAM J. Optimization* **1**: 121–152.

Schramm, U. (1999). The use of structural optimization in automotive design state of the art and vision, *in* C. L. Bloebaum (ed.), *Third World Congress of Structural and Multidisciplinary Optimization*, pp. 200–202. University of New York at Buffalo.

Schwarz, S., Maute, K. & Ramm, E. (2001). Topology optimization for elastoplastic structural response, *Computational Methods in Applied Engineering* **190**: 2135–2155.

Sekimoto, T. & Noguchi, H. (2001). Homologous topology optimization in large displacement and buckling problems, *JSME International Journal* **44**(4): 616–622. Series A.

Selyugin, S. V & Chekhov, V V (2001). Multimaterial design of physically nonlinear structures, *Structural and Multidisciplinary Optimization* **21**: 209–217.

Seregin, G. A. & Troitskii, V A. (1982). On the best position of elastic symmetry planes in an orthotropic body, *PMM USSR* **45**: 139–142.

Sethian, J. A. & Wiegmann, A. (2000). Structural boundary design via level set and immersed interface methods, *Journal of Computational Physics* **163**(2): 489–528.

Seyranian, A. P. (1993). Sensitivity analysis of multiple eigenvalues, *Mech. Struct. Mach.* **21**: 261–284.

Seyranian, A. P., Lund, E. & Olhoff, N. (1994). Multiple eigenvalues in structural optimization problems, *Structural Optimization* **8**(4): 207–227.

Shim, P. Y & Manoochehri, S. (1997). Generating optimal configurations in structural design using simulated annealing, *International Journal for Numerical Methods in Engineering* **40**(6): 1053–1069.

Sigmund, O. (1994a). *Design of material structures using topology optimization*, PhD thesis, Department of Solid Mechanics, Technical University of Denmark.

Sigmund, O. (1994b). Materials with prescribed constitutive parameters: an inverse homogenization problem, *International Journal of Solids and Structures* **31**(17): 2313–2329.

Sigmund, O. (1995). Tailoring materials with prescribed elastic properties, *Mechanics of Materials* **20**: 351–368.

Sigmund, O. (1996). Some inverse problems in topology design of materials and mechanisms, *in* D. Bestle & W Schielen (eds), *Symposium on optimization of mechanical systems*, IUTAM, Kluwer, Netherlands, pp. 277–284.

Sigmund, O. (1997). On the design of compliant mechanisms using topology optimization, *Mechanics of Structures and Machines* **25**(4): 495–526.

Sigmund, O. (1999). On the optimality of bone microstructure, *in* P Pedersen & M. P. Bendsøe (eds), *Synthesis in Bio Solid Mechanics*, IUTAM, Kluwer, pp. 221–234.

Sigmund, O. (2000a). Mechanics of solids and fluids topology optimization: A tool for the tailoring of structures and materials, *Philosophical Transactions Mathematical Physical and Engineering Sciences* **358**(1765): 211–228.

Sigmund, O. (2000b). A new class of extremal composites, *Journal of the Mechanics and Physics of Solids* **48**(2): 397–428.

Sigmund, O. (2001a). A 99 line topology optimization code written in MATLAB, *Structural and Multidisciplinary Optimization* **21**: 120–127.

Sigmund, O. (2001b). Design of multiphysics actuators using topology optimization - Part I: One-material structures, *Computer Methods in Applied Mechanics and Engineering* **190**(49-50): 6577–6604.

Sigmund, O. (2001c). Design of multiphysics actuators using topology optimization Part II: Two-material structures, *Computer Methods in Applied Mechanics and Engineering* **190**(49-50): 6605–6627.

Sigmund, O. (2001d). Microstructural design of elastic band gap structures, *in* G. D. Cheng, Y Gu, S. Liu & Y Wang (eds), *WCSMO-4 Proc. Second World Congress of Structural and Multidisciplinary Optimization*, Liaoning Electronic Press, Dalian. CD-rom, ISBN 7-900312-69-2.

Sigmund, O. (2001e). Recent developments in extremal material design, *in* W A. Wall, K.-U. Bletzinger & K. Schweizerhof (eds), *Trend in computational Mechanics*, CIMNE, pp. 228–232.

Sigmund, O. & Jensen, J. S. (2002a). Systematic design of phononic band gap materials and structures, *Submitted*

Sigmund, O. & Jensen, J. S. (2002b). Topology optimization of elastic band gap structures and waveguides, *in* H. A. Mang, F G. Rammerstorfer & J. Eberhardsteiner (eds), *Proceedings of the Fifth World Congress on Computational Mechanics*, Vienna University of Technology, Austria, p. http://wccm.tuwien.ac.at.

Sigmund, O. & Petersson, J. (1998). Numerical instabilities in topology optimization: A survey on procedures dealing with checkerboards, mesh-dependencies and local minima, *Structural Optimization* **16**(1): 68–75.

Sigmund, O. & Torquato, S. (1996). Composites with extremal thermal expansion coefficients, *Applied Physics Letters* **69**(21): 3203–3205.

Sigmund, O. & Torquato, S. (1997). Design of materials with extreme thermal expansion using a three-phase topology optimization method, *Journal of the Mechanics and Physics of Solids* **45**(6): 1037–1067.

Sigmund, O. & Torquato, S. (1999). Design of smart composite materials using topology optimization, *Smart Materials and Structures* **8**(3): 365–379.

Sigmund, O. Torquato, S. & Aksay, I. A. (1998). On the design of 1-3 piezocomposites using topology optimization, *Journal of Materials Research* **13**(4): 1038–1048.

Silva, E. C. N. Fonseca, J. S. O. & Kikuchi, N. (1997). Optimal design of piezoelectric microstructures, *Computational Mechanics* **19**(5): 397–410.

Silva, E. C. N., Fonseca, J. S. O. & Kikuchi, N. (1998). Optimal design of periodic piezocomposites, *Computer Methods in Applied Mechanics and Engineering* **159**(2): 49–77.

Simon, J. (1980). Differentiation with respect to the domain in boundary value problems, *Num. Funct. Anal. Opt.* **2**: 649–687.

Sokołowski, J. (1981). Optimal control in coefficients for weak variational problems in Hilbert space, *Appl. Math. Optim.* **7**: 283–293.

Sokołowski, J. & Zochowski, A. (1999). On the topological derivative in shape optimization, *SIAM J. Control Opt.* **37**: 1251–1272.

Sokołowski, J. & Zolesio, J.-P. (1992). *Introduction to Shape Optimization. Shape Sensitivity Analysis.*, Springer-Verlag.

Soto, C. A. (2001). Structural topology optimization: from minimizing compliance to maximizing energy absorption, *International Journal of Vehicle Design* **25**(1/2): 142–163.

Soto, C. A. (2002). Applications of structural topology optimization in the automotive industry: Past, present and future, *in* H. A. Mang, F G. Rammerstorfer & J. Eberhardsteiner (eds), *Proceedings of the Fifth World Congress on Computational Mechanics*, Vienna University of Technology, Austria, p. http://wccm.tuwien.ac.at.

Soto, C. A. & Díaz, A. R. (1993a). Layout of plate structures for improved dynamic responce using a homogenization method, *in* Gilmore et al. (eds), *Advances in Design Automatization*, ASME, Albuquerque, NM, pp. 667–674.

Soto, C. A. & Díaz, A. R. (1993b). On modelling of ribbed plates for shape optimization, *Structural Optimization* **6**: 175–188.

Soto, C. A. & Díaz, A. R. (1999). Basic models for topology design optimization in crashworthiness problems, *Procedding of DETC 99*, ASME.

Soto, C. A. & Yang, R. J. (1999). Optimum layout of embossed ribs to maximize natural frequencies in plates, *Design Optimization: International Journal for Product and Process improvement* **1**(1): 44–54.

Soto, C. A., Yang, R. J. & DeVries, R. (1996). Structural topology optimization for forced frequency vibrations, *1996 ASME Design Engineering Technical COnferences*, DETC/DAC-1477, Irvine, California.

Spagnolo, S. (1976). Convergence in energy for elliptic operators, *in* B. Hubbard (ed.), *Numerical Solution of Partial Differential Equations*, Vol. 3, Academic Press, New York, pp. 469–498.

Stadler, W (1986). Non-existence of solutions in optimal structural design, *Opt. Control Appl. Meth.* **7**: 243–258.

Stavroulakis, G. E. & Tzaferopoulos, M. A. (1994). A variational inequality approach to optimal plastic design of structures via the Prager-Rozvany theory, *Struct. Optim.* **7**: 160–169.

Stolpe, M. & Svanberg, K. (2001a). An alternative interpolation scheme for minimum compliance optimization, *Structural and Multidisciplinary Optimization* **22**: 116–124.

Stolpe, M. & Svanberg, K. (2001b). On the trajectories of penalization methods for topology optimization, *Structural and Multidisciplinary Optimization* **21**: 128–139.

Stolpe, M. & Svanberg, K. (2001c). On the trajectories of the epsilon-relaxation approach for stress-constrained truss topology optimization, *Structural and Multidisciplinary Optimization* **21**: 140–151.

Stolpe, M. & Svanberg, K. (2002). Modeling topology optimization problems as mixed linear 0-1 programs, *International Journal of Numerical Methods in Engineering* To appear.

Strang, G. & Kohn, R. V (1981). Hencky-prandtl nets and constrained Michell trusses, *In Proc. Int. Symposium on Optimum Structural Design*, Pineridge Press Ltd., Swansea, pp. 4–17 to 4–22. Tucson, Arizona.

Suquet, P. (1981). Prevision par homogneisation du flambement de plaques elastiques renforcees, *Rech. Aerosp.* pp. 99–107.

Suzuki, K. & Kikuchi, N. (1991). A homogenization method for shape and topology optimization, *Comp. Meth. Appl. Mechs. Engng.* **93**(3): 291–318.

Svanberg, K. (1984). On local and global minima in structural optimization, *in* E. Atrek, R. H. Gallagher, K. M. Ragsdell & O. C. Zienkiewicz (eds), *New Directions in Optimum Structural Design*, Wiley, New York, pp. 327–341.

Svanberg, K. (1987). The method of moving asymptotes A new method for structural optimization, *International Journal for Numerical Methods in Engineering* **24**: 359–373.

Svanberg, K. (1994a). Global convergence of the stress ratio method for truss sizing, *Struct. Optim.* **8**: 60–68.

Svanberg, K. (1994b). On the convexity and concavity of compliances, *Struct. Optim.* **7**: 42–46.

Svanberg, K. (2002). A class of globally convergent optimization methods based on conservative convex separable approximations, *SIAM Journal on Optimization* **12**(2): 555–573.

Swan, C. C. & Arora, J. S. (1997). Topology design of material layout in structured composites of high stiffness and strength, *Structural Optimization* **13**(1): 45–59.

Swan, C. C. & Kosaka, I. (1997a). Voigt-Reuss topology optimization for structures with linear elastic material behaviours, *International Journal for Numerical Methods in Engineering* **40**(16): 3033–3058.

Swan, C. C. & Kosaka, I. (1997b). Voigt-Reuss topology optimization for structures with non-linear material behaviors, *International journal for numerical methods in engineering* **40**: 3785–3814.

Tai, K. & Chee, T. H. (2000). Design of structures and compliant mechanisms by evolutionary optimization of morphological representations of topology, *Transactions of the ASME* **122**: 560566.

Tang, P.-S. & Chang, K.-H. (2001). Integration of topology and shape optimization for design of structural components, *Structural and Multidisciplinary Optimization* **22**: 65–82.

Tanie, H. & Kita, E. (1997). Topology optimization of continuum structures by using GA and BEM, *Structural Optimization* **16**(2-3): 218–225.

Tartar, L. (1979). Estimation de coefficients homogénéisés, *Computing methods in applied sciences and engineering (Proc. Third Internat. Sympos., Versailles, 1977), I,*, Vol. 704 of *Lecture Notes in Mathematics*, Springer-Verlag, Berlin; Heidelberg; London; etc., pp. 364–373.

Taylor, J. E. (1969). Maximum strength elastic structural design, *Proc. ASCE* **95**: 653–663.

Taylor, J. E. (1987). Distributed parameter optimal structural design: Some basic problem formulations and their applications, *in* C. A. Mota Soares (ed.), *Computer Aided Optimal Design: Structural and Mechanical Systems*, Springer-Verlag, Berlin, pp. 3–85.

Taylor, J. E. (1993). A global extremum principle for the analysis of solids composed of softening material, *International Journal of Solids and Structures* **30**(15): 2057–2069.

Taylor, J. E. (1994). A global extremum principle in mixed form for equilibrium analysis with elastic/stiffening materials (a generalized minimum potential energy principle), *Journal of Applied Mechanics* **61**(4): 914–918.

Taylor, J. E. (1998). An energy model for the optimal design of linear continuum structures, *Structural Optimization* **16**: 116–127.

Taylor, J. E. (2000). A formulation for optimal structural desig with optimal materials, *in* G. I. N. Rozvany & N. Olhoff (eds), *Topology Optimization of Structures and Composite Continua*, Kluwer Academic Publishers, Dordrecht, pp. 49–59.

Taylor, J. E. & Rossow, M. P. (1977). Optimal truss design based on an algorithm using optimality criteria, *Int. J. Solids Struct.* **13**: 913–923.

Tcherniak, D. (2002). Topology optimization of resonating structures using SIMP method, *International Journal for Numerical Methods in Engineering* **54**(11): 1605–1622.

Tcherniak, D. & Sigmund, O. (2001). A web-based topology optimization program, *Structural and Multidisciplinary Optimization* **22**(3): 179–87.

Telega, J. J. & Lewiński, T. (2000). On a saddle-point theorem in minimum compliance design, *J. Optim. Theory Appl.* **106**(2): 441–450.

Tenek, L. H. & Hagiwara, I. (1993a). Optimization of material distribution within isotropic and anisotropic plates using homogenization, *Computer Methods in Applied Mechanics and Engineering* **109**(1-2): 155–167.

Tenek, L. H. & Hagiwara, I. (1993b). Static and vibrational shape and topology optimization using homogenization and mathematical programming, *Computer Methods in Applied Mechanics and Engineering* **109**(1-2): 143–154.

Terada, K. & Kikuchi, N. (1996). Microstructural design of composites using the homogenization method and digital images, *Mat. Sci. Res. Int.* **2**: 65–72.

Theocaris, P. S. & Stavroulakis, G. E. (1998). Multilevel optimal design of composite structures including materials with negative Poisson's ratio, *Structural Optimization* **15**(1): 8–15.

Theocaris, P. S. & Stavroulakis, G. E. (1999). Optimal material design in composites: An iterative approach based on homogenized cells, *Computer Methods in Applied Mechanics and Engineering* **169**(1-2): 31–42.

Thomas, H. L., Zhou, M. & Schramm, U. (2002). Issues of commercial optimization software development, *Structural and Multidisciplinary Optimization* **23**(2): 97–110.

Thomsen, J. (1991). Optimization of composite discs, *Struct. Optim.* **3**: 89–98.

Thomsen, J. (1992). Topology optimization of structures composed of one or two materials, *Struct. Optim.* **5**: 108–115.

Toader, A. M. (1997). Convergence of an algorithm in optimal design, *Structural Optimization* **13**(2-3): 195–198.

Topping, B. M. V (1992). Mathematical programming techniques for shape optimization of skeletal structures, *in* G. I. N. Rozvany (ed.), *Optimization of Large Structural Systems*, Kluwer Academic Publishers, Dordrecht, The Netherlands, pp. 349–276.

Topping, B. M. V (1993). Topology design of discrete structures, *in* M. P. Bendsøe & C. A. Mota Soares (eds), *Topology Design of Structures*, Kluwer Academic Publishers, pp. 517–534.

Topping, B. M. V Khan, A. I. & Leite, J. P. D. B. (1996). Topological design of truss structures using simulated annealing, *Structural Engineering Review* **8**(2-3): 301–314.

Torquato, S. (2002). *Random heterogeneous materials Microstructure and macroscopic properties*, Springer, New York.

Triantafyllidis, N. & Schnaidt, W. C. (1993). Comparison of microscopic and macroscopic instabilities in a class of two-dimensional periodic composites, *Journal of the Mechanics and Physics of Solids* **41**(9): 1533–65.

Tsai, S. W & Hahn, H. T. (1980). *Introduction to Composite Materials*, Technomic Publ. Co. Inc.

Vandenberghe, L. & Boyd, S. (1996). Semidefinite programming, *SIAM Review* **38**(1): 49–95.

Vanderplaats, G. N. (1999). Structural design optimization status and direction, *Journal of Aircraft* **36**(1): 11–20.

Vasseur, J. O. Deymier, P. A., Frantziskonis, G. Hong, G., Djafari-Rouhani, B. & Dobrzynski, L. (1998). Experimental evidence for the existence of absolute acoustic band gaps in two-dimensional periodic composite media, *Journal of Physics: Condensed Matter* **10**(27): 6051–64.

Vigdergauz, S. B. (1989). Regular structures with extremal elastic properties, *Mechanics of Solids* **24**: 57–63.

Vigdergauz, S. B. (1994). Two-dimensional grained composites of extreme rigidity, *Journal of Applied Mechanics* **61**(2): 390–394.

Vigdergauz, S. B. (1999). Energy-minimizing inclusions in a planar elastic structure with macroisotropy, *Structural Optimization* **17**(2-3): 104–112.

Vimawala, M. S. & Turkiyyah, G. M. (1995). Computational procedures for topological shape design, *Computer Methods in Applied Mechanics and Engineering* **125**(1-4): 257–285.

Walpole, L. J. (1966). On bounds for the overall elastic moduli of inhomogeneous systems, *Journal of the Mechanics and Physics of Solids* **14**: 151–162.

Wardi, Y Y & Polak, E. (1982). A nondifferentiable optimization algorithm for structural problems with eigenvalue inequality constraints, *J. Struct. Mech.* **11**: 561–577.

Washizu, K. (1983). *Variational Methods in Elasticity and Plasticity*, Pergamon, Oxford, Great Britain.

Wasiutynski, Z. (1960). On the congruency of the forming according to the minimum potential energy with that according to equal strength, *Bull. de L'Academie Polonaise des Sciences, Serie des Sciences Techniques* **8**: 259–268.

Weinans, H., Huiskes, R. & Grootenboer, H. J. (1992). The behavior of adaptive bone-remodeling simulation models, *J. Biomechanics* **25**: 1425–1441.

Xie, Y M. & Steven, G. P. (1997). *Evolutionary Structural Optimisation*, Springer Verlag, Berlin.

Yang, R. J. (1997). Multidiscipline topology optimization, *Computers and Structures* **63**(6): 1205–1212.

Yang, R. J. & Chahande, A. I. (1995). Automotive applications of topology optimization, *Structural Optimization* **9**(3-4): 245–249.

Yang, R. J., Chen, C. J. & Lee, C. H. (1996). Bead pattern optimization, *Structural Optimization* **12**(1-4): 217–221.

Yang, R. J. & Chuang, C.-H. (1994). Optimal topology design using linear programming, *Computers and Structures* **52**(2): 265–276.

Yang, R. J. Chuang, C.-H. Che, X. & Soto, C. A. (2000). New applications of topology optimization in automotive industry, *International Journal of Vehicle Design* **23**(1): 1–15.

Yi, Y Park, S. & Youn, S.-K. (2000). Design of microstructures of viscoelastic composites for optimal damping characteristics, *International Journal of Solids and Structures* **37**: 4791–4810.

Yin, L. & Ananthasuresh, G. K. (2001). Topology optimization of compliant mechanisms with multiple materials using a peak function material interpolation scheme, *Structural and Multidisciplinary Optimization* **23**(1): 49–62.

Yin, L. & Yang, W (2000a). Topology optimization for tunnel support in layered geological structures, *International Journal for Numerical Methods in Engineering* **47**(12): 1983–1996.

Yin, L. & Yang, W (2000b). Topology optimization to prevent tunnel heaves under different stress biaxialities, *International Journal for Numerical and Analytical Methods in Geomechanics* **24**(9): 783–792.

Yin, L., Yang, W. & Guo, T. (2000). Tunnel reinforcement via topology optimization, *International Journal for Numerical and Analytical Methods in Geomechanics* **24**(2): 201–214.

Yoo, J. & Kikuchi, N. (2000). Topology optimization in magnetic fields using the homogenization design method, *Int. J. Numer. Meth. Engng* **48**: 1463–1479.

Yoo, J., Kikuchi, N. & Volakis, J. L. (2000). Structural optimazation in magnetic devices by the homogenization design method, *IEEE Transactions on Magnetics* **36**(3): 574–580.

Yuge, K., Iwai, N. & Kikuchi, N. (1999). Optimization of 2-D structures subjected to nonlinear deformations using the homogenization method, *Structural Optimization* **17**(4): 286–298.

Yuge, K. & Kikuchi, N. (1995). Optimization of a frame structure subjected to a plastic deformation, *Structural Optimization* **10**(3-4): 197–208.

Zhao, C. Steven, G. P. & Xie, Y M. (1997). Evolutionary optimization of maximizing the difference between two natural frequencies of a vibrating structure, *Structural Optimization* **13**(2-3): 148–154.

Zhou, M. & Rozvany, G. I. N. (1991). The COC algorithm, part II: Topological, geometry and generalized shape optimization, *Computer Methods in Applied Mechanics and Engineering* **89**.

Zhou, M. & Rozvany, G. I. N. (2001). On the validity of ESO type methods in topology optimization, *Structural and Multidisciplinary Optimization* **21**: 80–83.

Zhou, M., Shyy, Y K. & Thomas, H. L. (2001). Checkerboard and minimum member size control in topology optimization, *Structural and Multidisciplinary Optimization* **21**: 152–158.

Zienkiewicz, O. C. & Taylor, R. L. (2000). *The Finite Element Method (Parts 1-3)*, Butterworth Heinemann, Oxford.

Zochowski, A. (1988). The design of a two-dimensional domain, *J. Struc. Mech.* **16**: 17–34.

Zowe, J., Kocvara, M. & Bendsøe, M. P. (1997). Free material optimization via mathematical programming, *Mathematical Programming* **79**(1–3, Ser. B): 445–466.

Zyczkowski, M. & Gajewski, A. (1988). *Optimal Structural Design under Stability Constraints*, Kluwer Academic Press, Dordrecht.

Author index

Index

Printing: Mercedes-Druck, Berlin
Binding: Buchbinderei Lüderitz & Bauer, Berlin

ERATA

Topology Optimization – Theory, Methods and Applications

Main changes in the 2nd printing

Martin P. Bendsøe and Ole Sigmund

October 7, 2003

In the following we write the changes that were done in the second printing of our book (due late fall 2003). A number of references have also been updated.

p. 34, Eq. (1.26) changed to

$$
\begin{aligned}
&E_{ijkl}(x) = ((\rho * K)(x))^p \, E^0_{ijkl}, \;\; \rho \in L^\infty(\Omega) \; , \\
&(\rho * K)(x) = \frac{1}{< K >} \int_\Omega \rho(y) K(x-y) \, \mathrm{d}y \; , \quad < K > = \int_{R^n} K(y) \, \mathrm{d}y \; , \\
&\int_\Omega \rho(x) \mathrm{d}\Omega \leq V; \quad 0 \leq \rho(x) \leq 1, \quad x \in \Omega \; ,
\end{aligned}
$$

p. 53, Eq. (1.35) index on C changed:

$$
\min_{E \in \mathsf{E}_{\mathrm{ad}}} \; \min_{\substack{\mathrm{div}\sigma^k + f^k = 0 \text{ in } \Omega, \\ \sigma^k \cdot n = t^k \text{ on } \Gamma^k_T \\ k=1,\ldots,M}} \left\{ \frac{1}{2} \int_\Omega \sum_{k=1}^M w^k C_{ijpq} \sigma^k_{ij} \sigma^k_{pq} \mathrm{d}\Omega \right\} .
$$

p. 54, index on E^0 changed:

$$
B_K = \Lambda_K^{-1} p \rho(x)^{(p-1)} E^0_{ijnm} \sum_{k=1}^M w^k \varepsilon_{ij}(u^k_K) \varepsilon_{nm}(u^k_K) \; .
$$

p. 55, Eq. (1.36) ρ corrected to h:

$$\begin{aligned}
&\min_{u,h} \quad l(u) \\
&\text{s.t.}: a_h(u,v) \equiv \int_\Omega h(x) E^0_{ijkl} \varepsilon_{ij}(u) \varepsilon_{kl}(v) \mathrm{d}\Omega = l(v), \ \text{for all}\, v \in U \ , \\
&\qquad \int_\Omega h(x) \mathrm{d}\Omega \le V, \ h_{\min} \le h \le h_{\max} < \infty \ .
\end{aligned}$$

p. 55, Eq. (1.37) changed to

$$\begin{aligned}
&\min_{\substack{h \in L^\infty(\Omega), \\ h_{\min} \le h \le h_{\max} < \infty \\ \int_\Omega h(x) \mathrm{d}\Omega \le V}} \quad c(h) \\
&c(h) = \max_{v \in U} \left\{ 2l(v) - \int_\Omega h(x) E^0_{ijkl} \varepsilon_{ij}(v) \varepsilon_{kl}(v) \mathrm{d}\Omega \right\} .
\end{aligned}$$

p. 80, last line in figure text:
"lower" changed to "higher"

p. 81, 3rd line in figure text:
added "hatched area"

p. 188, Fig. 3.14 corrected to:

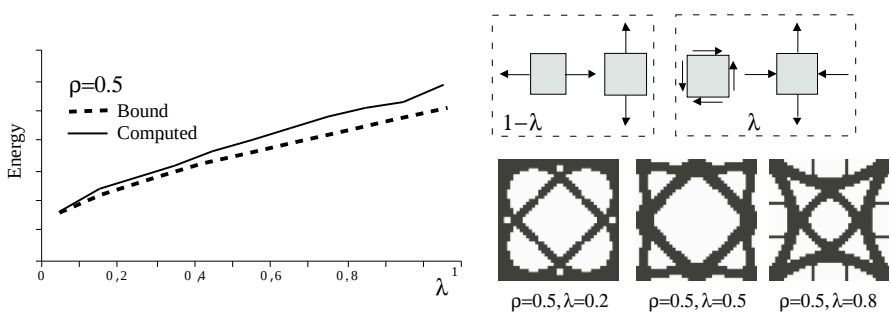

p. 234, l. 14:
"$\mathbf{u}^T \widetilde{\mathbf{A}} \mathbf{u} \ge$" corrected to "$\mathbf{u}^T \widetilde{\mathbf{A}} \mathbf{u} \ge 0$"

p. 234, 3rd line of last paragraph:
"Modern interior ...." changed to "Modern interior point algorithms solve SDP's like (4.20) in polynomial time [33]."

p. 236, Eq. (4.25) τ^2 changed to τ:

$$\min_{\mathbf{u},\,\tau} \left\{\tau - \mathbf{f}^T\mathbf{u}\right\}$$
$$\text{s.t.}: \frac{V}{2}\left[\mathbf{u}^T\hat{\mathbf{K}}_i\mathbf{u} - 2\mathbf{g}_i{}^T\mathbf{u}\right] \leq \tau, \quad i = 1, \ldots, m\ .$$

p. 239, Eq. (4.31) changed to:

$$\min_{\substack{q_i^+ \geq 0,\, q_i^- \geq 0,\\ i=1,\ldots,m\\ \mathbf{B}(\mathbf{q}^+ - \mathbf{q}^-) = \mathbf{f}}} \sum_{i=1}^{m} \frac{l_i}{\bar{\sigma}_i}(q_i^+ + q_i^-)\ .$$

p. 239, l. 4 of last paragraph:
"... primal-dual LP-methods" changed to "primal-dual interior point LP-methods or the simplex algorithm"

p. 240, Eq. (4.32) changed to:

$$\min_{\mathbf{u},\,\tau} \left\{\frac{1}{2}\mathbf{u}^T\left(\sum_{i\in S} s_i\mathbf{K}_i\right)\mathbf{u} - \mathbf{f}^T\mathbf{u} + \tau^2\right\}$$
$$\text{s.t.}: -\tau \leq \sqrt{\frac{VE_i}{2}}\frac{\mathbf{b}_i{}^T\mathbf{u}}{l_i} \leq \tau, \quad i \in R\ .$$

p. 250, Eq. (4.44) V_τ changed to $V\tau$:

$$\inf_{\substack{\lambda^k > 0,\, \mathbf{u}^k,\, \tau\\ \sum_{k=1}^M \lambda^k = 1}} \left\{V\tau - \sum_{k=1}^{M} \mathbf{f}^{k\,T}\mathbf{u}^k\right\}$$
$$\text{s.t.}: \sum_{k=1}^{M} \frac{1}{2\lambda^k}\mathbf{u}^{k\,T}\mathbf{K}_i\mathbf{u}^k - \tau \leq 0, \quad i = 1, \ldots, m\ .$$

p. 250, Eq. (4.45) V_τ changed to $V\tau$ and $\mathbf{A}_i$ changed to $\mathbf{K}_i$:

$$\inf_{\substack{s^k,\, \mathbf{x}^k, \tau\\ \sum_{k=1}^M (s^k)^2 = 1}} \left\{V\tau - \sum_{k=1}^{M} s^k\ \mathbf{f}^{k\,T}\mathbf{x}^k\right\}$$
$$\text{s.t.}: \sum_{k=1}^{M} \mathbf{x}^{k\,T}\mathbf{K}_i\ \mathbf{x}^k - 2\tau \leq 0, \quad i = 1, \ldots, m\ .$$

p. 255, first equation, $\mathbf{A}_i$ changed to $\mathbf{K}_i$:

$$\mathcal{F}(\mathbf{x}) = -\min_{\mathbf{u}}\left[\max_{i=1,\ldots,m}\left\{\frac{V}{2}\mathbf{u}^T\mathbf{K}_i(\mathbf{x})\mathbf{u} - \mathbf{f}^T\mathbf{u}\right\}\right]\ ,$$

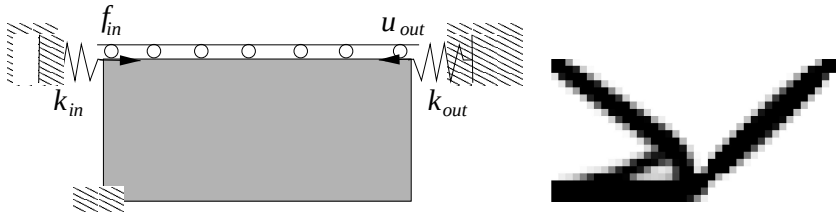

Figure 1: Topology optimization of the inverter. Left: half design domain with symmetry boundary conditions and right: resulting topology.

p. 271, 6th to last line changed to:

```
> fixeddofs   = [nely/2+1-(nely/20):nely/2+1+(nely/20)];
```

The Matlab code and description for mechanism synthesis in Appendix 5.1.5 on page 269 has been updated and improved to:

5.1.5 A 104 line MATLAB code for compliant mechanism synthesis

The Matlab code for compliance minimization described in the previous section can be changed to a code for mechanism synthesis by changing 13 lines, deleting one and adding 6 new lines of code.[1]

As the default problem, we consider the inverter design problem sketched in Fig. 5.5. The optimization problem for compliant mechanism synthesis was discussed in Sec 2.6. The solution obtained by running the modified code which is named 'topm' with the command line input

```
topm(40,20,0.3,3.0,1.2)
```

is seen in Fig. 1(right).

Instead of listing the whole program we just show a list of the changes. This list is obtained by comparing the compliance minimization program 'top.m' with the inverter design program 'topm.m' using the UNIX command 'diff top.m topm.m'. This results in output where '<' means lines in 'top.m' and '>' means lines in 'topm.m'. In the following we briefly discuss the changes.

First we rename the code from 'top' to 'topm'

```
1,2c1,2
< %%%% A 99 LINE TOPOLOGY OPTIMIZATION CODE BY OLE SIGMUND, OCTOBER 1999 %%%
```

[1]Note that the code described uses linear analysis. Therefore, it can only be used to gain insight into compliant mechanism synthesis by topology optimization. For practical problems one should modify the code to include geometrically non-linear modelling (c.f. Sec. 2.6.5).

```
< function top(nelx,nely,volfrac,penal,rmin);
---
> %%%% A 104 LINE COMPLIANT MECHANISM DESIGN CODE BY OLE SIGMUND, MAY 2002 %%%
> function topm(nelx,nely,volfrac,penal,rmin);
```

Instead of calculating the output displacement (objective funtion) in the main program we return it from the FE subroutine and we remove its initialization

```
12c12
<   [U]=FE(nelx,nely,x,penal);
---
>   [U,c]=FE(nelx,nely,x,penal);
15d14
<   c = 0.;
```

The expression for the sensitivities (2.23) depends on the solution to the adjoint load case (second column of the displacement matrix `U`)

```
20,22c19,21
<       Ue = U([2*n1-1;2*n1; 2*n2-1;2*n2; 2*n2+1;2*n2+2; 2*n1+1;2*n1+2],1);
<       c = c + x(ely,elx)^penal*Ue'*KE*Ue;
<       dc(ely,elx) = -penal*x(ely,elx)^(penal-1)*Ue'*KE*Ue;
---
>       Ue1 = U([2*n1-1;2*n1; 2*n2-1;2*n2; 2*n2+1;2*n2+2; 2*n1+1;2*n1+2],1);
>       Ue2 = U([2*n1-1;2*n1; 2*n2-1;2*n2; 2*n2+1;2*n2+2; 2*n1+1;2*n1+2],2);
>       dc(ely,elx) = penal*x(ely,elx)^(penal-1)*Ue1'*KE*Ue2;
```

We improve the convergence criteria for the bi-sectioning algorithm

```
39,40c38,39
< l1 = 0; l2 = 100000; move = 0.2;
< while (l2-l1 > 1e-4)
---
> l1 = 0; l2 = 100000; move = 0.1;
> while (l2-l1)/(l2+l1) > 1e-4 & l2 > 1e-40
```

To stabilize convergence we use a damping factor of 0.3 instead of 0.5 and we take care of the possibility of positive sensitivities

```
42c41
<   xnew = max(0.001,max(x-move,min(1.,min(x+move,x.*sqrt(-dc./lmid)))));
---
>   xnew = max(0.001,max(x-move,min(1.,min(x+move,x.*(max(1e-10,-dc./lmid)).^0.3))));
```

We return the output displacement to the main program

```
66c65
< function [U]=FE(nelx,nely,x,penal)
---
> function [U,Uout]=FE(nelx,nely,x,penal)
```

We allocate force and displacement vectors for the real and the adjoint load cases

```
69c68
< F = sparse(2*(nely+1)*(nelx+1),1); U = zeros(2*(nely+1)*(nelx+1),1);
---
> F = sparse(2*(nely+1)*(nelx+1),2); U = sparse(2*(nely+1)*(nelx+1),2);
```

Finally, we define the boundary conditions and the input and output points. Furthermore, we add external springs with stiffness 0.1 to the input and output points and we save the value of the output displacement to be returned to the main program.

```
78,80c77,84
< % DEFINE LOADS AND SUPPORTS (HALF MBB-BEAM)
< F(2,1) = -1;
< fixeddofs   = union([1:2:2*(nely+1)],[2*(nelx+1)*(nely+1)]);
---
> % DEFINE LOADS AND SUPPORTS (HALF FORCE INVERTER)
> din=1;
> dout=2*nelx*(nely+1)+1;
> F(din,1) = 1;
> F(dout,2) =  -1;
> K(din,din) = K(din,din) + 0.1;
> K(dout,dout) = K(dout,dout) + 0.1;
> fixeddofs   = union([2:2*(nely+1):2*(nely+1)*(nelx+1)], [2*(nely+1):-1:2*(nely+1)-3]);
85a90
> Uout = U(dout,1);
100,119d104
```

The topology optimization method solves the basic engineering problem of distributing a limited amount of material in a design space. The first edition of this book has become the standard text on optimal design which is concerned with the optimization of structural topology, shape and material. This edition has been substantially revised and updated to reflect progress made in modelling and computational procedures. It also encompasses a comprehensive and unified description of the state-of-the-art of the so-called material distribution method, based on the use of mathematical programming and finite elements. Applications treated include not only structures but also MEMS and materials

ISBN 3-540-42992-1

9 783540 429920

http://www.springer.de